

The background of the entire page features a stylized brain shape composed of numerous interconnected nodes and lines, creating a network-like structure. The brain is divided into several color-coded regions: yellow, orange, red, purple, and blue. The top half of the brain is set against a solid blue background, while the bottom half is on a white background.

DECIPHERING THE BIOMARKERS OF ALZHEIMER'S DISEASE

EDITED BY: Yu Chen, Kin Ying Mok and Jie Tu
PUBLISHED IN: Frontiers in Neuroscience



frontiers

Frontiers eBook Copyright Statement

The copyright in the text of individual articles in this eBook is the property of their respective authors or their respective institutions or funders. The copyright in graphics and images within each article may be subject to copyright of other parties. In both cases this is subject to a license granted to Frontiers.

The compilation of articles constituting this eBook is the property of Frontiers.

Each article within this eBook, and the eBook itself, are published under the most recent version of the Creative Commons CC-BY licence.

The version current at the date of publication of this eBook is CC-BY 4.0. If the CC-BY licence is updated, the licence granted by Frontiers is automatically updated to the new version.

When exercising any right under the CC-BY licence, Frontiers must be attributed as the original publisher of the article or eBook, as applicable.

Authors have the responsibility of ensuring that any graphics or other materials which are the property of others may be included in the CC-BY licence, but this should be checked before relying on the CC-BY licence to reproduce those materials. Any copyright notices relating to those materials must be complied with.

Copyright and source acknowledgement notices may not be removed and must be displayed in any copy, derivative work or partial copy which includes the elements in question.

All copyright, and all rights therein, are protected by national and international copyright laws. The above represents a summary only. For further information please read Frontiers' Conditions for Website Use and Copyright Statement, and the applicable CC-BY licence.

ISSN 1664-8714

ISBN 978-2-88974-383-4

DOI 10.3389/978-2-88974-383-4

About Frontiers

Frontiers is more than just an open-access publisher of scholarly articles: it is a pioneering approach to the world of academia, radically improving the way scholarly research is managed. The grand vision of Frontiers is a world where all people have an equal opportunity to seek, share and generate knowledge. Frontiers provides immediate and permanent online open access to all its publications, but this alone is not enough to realize our grand goals.

Frontiers Journal Series

The Frontiers Journal Series is a multi-tier and interdisciplinary set of open-access, online journals, promising a paradigm shift from the current review, selection and dissemination processes in academic publishing. All Frontiers journals are driven by researchers for researchers; therefore, they constitute a service to the scholarly community. At the same time, the Frontiers Journal Series operates on a revolutionary invention, the tiered publishing system, initially addressing specific communities of scholars, and gradually climbing up to broader public understanding, thus serving the interests of the lay society, too.

Dedication to Quality

Each Frontiers article is a landmark of the highest quality, thanks to genuinely collaborative interactions between authors and review editors, who include some of the world's best academicians. Research must be certified by peers before entering a stream of knowledge that may eventually reach the public - and shape society; therefore, Frontiers only applies the most rigorous and unbiased reviews.

Frontiers revolutionizes research publishing by freely delivering the most outstanding research, evaluated with no bias from both the academic and social point of view. By applying the most advanced information technologies, Frontiers is catapulting scholarly publishing into a new generation.

What are Frontiers Research Topics?

Frontiers Research Topics are very popular trademarks of the Frontiers Journals Series: they are collections of at least ten articles, all centered on a particular subject. With their unique mix of varied contributions from Original Research to Review Articles, Frontiers Research Topics unify the most influential researchers, the latest key findings and historical advances in a hot research area! Find out more on how to host your own Frontiers Research Topic or contribute to one as an author by contacting the Frontiers Editorial Office: frontiersin.org/about/contact

DECIPHERING THE BIOMARKERS OF ALZHEIMER'S DISEASE

Topic Editors:

Yu Chen, Chinese Academy of Sciences (CAS), China

Kin Ying Mok, University College London, United Kingdom

Jie Tu, Chinese Academy of Sciences (CAS), China

Citation: Chen, Y., Mok, K. Y., Tu, J., eds. (2022). Deciphering the Biomarkers of Alzheimer's Disease. Lausanne: Frontiers Media SA.
doi: 10.3389/978-2-88974-383-4

Table of Contents

- 05 *Entorhinal and Transentorhinal Atrophy in Preclinical Alzheimer's Disease***
Sue Kulason, Eileen Xu, Daniel J. Tward, Arnold Bakker, Marilyn Albert, Laurent Younes and Michael I. Miller for the Alzheimer's Disease Neuroimaging Initiative
- 17 *miRNA Alterations Elicit Pathways Involved in Memory Decline and Synaptic Function in the Hippocampus of Aged Tg4-42 Mice***
Yvonne Bouter, Tim Kacprowski, Fanny Rößler, Lars R. Jensen, Andreas W. Kuss and Thomas A. Bayer
- 37 *Investigation on the Alteration of Brain Functional Network and Its Role in the Identification of Mild Cognitive Impairment***
Lulu Zhang, Huangjing Ni, Zhinan Yu, Jun Wang, Jiaolong Qin, Fengzhen Hou and Albert Yang for the Alzheimer's Disease Neuroimaging Initiative (ADNI)
- 50 *Neuroprotective Effect of Optogenetics Varies With Distance From Channelrhodopsin-2 Expression in an Amyloid- β -Injected Mouse Model of Alzheimer's Disease***
Xiaorui Cui, Feng Zhang, Hui Zhang, Xi Huang, Kewei Wang, Ting Huang, Xifei Yang and Liangyu Zou
- 58 *microRNA-Based Biomarkers in Alzheimer's Disease (AD)***
Yuhai Zhao, Vivian Jaber, Peter N. Alexandrov, Andrea Vergallo, Simone Lista, Harald Hampel and Walter J. Lukiw
- 74 *Association of Odor Identification Ability With Amyloid- β and Tau Burden: A Systematic Review and Meta-Analysis***
Lihui Tu, Xiaozhen Lv, Zili Fan, Ming Zhang, Huali Wang and Xin Yu
- 85 *Progranulin Adsorbs to Polypropylene Tubes and Disrupts Functional Assays: Implications for Research, Biomarker Studies, and Therapeutics***
Sushmitha Gururaj, Paul J. Sampognaro, Andrea R. Argouarch and Aimee W. Kao
- 95 *Network Diffusion Modeling Explains Longitudinal Tau PET Data***
Amelie Schäfer, Elizabeth C. Mormino and Ellen Kuhl for the Alzheimer's Disease Neuroimaging Initiative
- 110 *The Correlations Between Plasma Fibrinogen With Amyloid-Beta and Tau Levels in Patients With Alzheimer's Disease***
Dong-Yu Fan, Hao-Lun Sun, Pu-Yang Sun, Jie-Ming Jian, Wei-Wei Li, Ying-Ying Shen, Fan Zeng, Yan-Jiang Wang and Xian-Le Bu
- 117 *Association Study of Alcohol Dehydrogenase and Aldehyde Dehydrogenase Polymorphism With Alzheimer Disease in the Taiwanese Population***
Yah-Yuan Wu, Yun-Shien Lee, Yu-Li Liu, Wen-Chuin Hsu, Wei-Min Ho, Yu-Hua Huang, Shih-Jen Tsai, Po-Hsiu Kuo and Yi-Chun Chen
- 126 *Tau Deletion Prevents Cognitive Impairment and Mitochondrial Dysfunction Age Associated by a Mechanism Dependent on Cyclophilin-D***
Claudia Jara, Waldo Cerpa, Cheril Tapia-Rojas and Rodrigo A. Quintanilla

- 142** *Dysregulation of Phosphoinositide 5-Phosphatases and Phosphoinositides in Alzheimer's Disease*
Kunie Ando, Christophe Erneux, Mégane Homa, Sarah Houben, Marie-Ange de Fisenne, Jean-Pierre Brion and Karelle Leroy
- 148** *Quantitative Methods for the Detection of Tau Seeding Activity in Human Biofluids*
Aurelien Lathuiliere and Bradley T. Hyman
- 155** *Polygenic Score Models for Alzheimer's Disease: From Research to Clinical Applications*
Xiaopu Zhou, Yolanda Y. T. Li, Amy K. Y. Fu and Nancy Y. Ip
- 165** *Machine Learning Driven Profiling of Cerebrospinal Fluid Core Biomarkers in Alzheimer's Disease and Other Neurological Disorders*
Giovanni Bellomo, Antonio Indaco, Davide Chiasserini, Emanuela Maderna, Federico Paolini Paoletti, Lorenzo Gaetani, Silvia Paciotti, Maya Petricciuolo, Fabrizio Tagliavini, Giorgio Giaccone, Lucilla Parnetti and Giuseppe Di Fede
- 174** *Changes of Regional Neural Activity Homogeneity in Preclinical Alzheimer's Disease: Compensation and Dysfunction*
Zhen Zhang, Liang Cui, Yanlu Huang, Yu Chen, Yuehua Li and Qihao Guo
- 187** *Parametric Estimation of Reference Signal Intensity for Semi-Quantification of Tau Deposition: A Flortaucipir and [¹⁸F]-APN-1607 Study*
Huiwei Zhang, Min Wang, Jiaying Lu, Weiqi Bao, Ling Li, Jiehui Jiang, Chuantao Zuo and Alzheimer's Disease Neuroimaging Initiative
- 196** *Identification of Electroencephalogram Signals in Alzheimer's Disease by Multifractal and Multiscale Entropy Analysis*
Momo Ando, Sou Nobukawa, Mitsuru Kikuchi and Tetsuya Takahashi
- 207** *Differences in Multimodal Electroencephalogram and Clinical Correlations Between Early-Onset Alzheimer's Disease and Frontotemporal Dementia*
Nan Lin, Jing Gao, Chenhui Mao, Heyang Sun, Qiang Lu and Liying Cui
- 218** *Blood–Brain Barrier Breakdown: An Emerging Biomarker of Cognitive Impairment in Normal Aging and Dementia*
Basharat Hussain, Cheng Fang and Junlei Chang



Entorhinal and Transentorhinal Atrophy in Preclinical Alzheimer's Disease

Sue Kulason^{1,2,3*}, Eileen Xu¹, Daniel J. Tward^{4,5}, Arnold Bakker^{6,7}, Marilyn Albert⁷, Laurent Younes^{1,2,8} and Michael I. Miller^{1,2,3,9} for the Alzheimer's Disease Neuroimaging Initiative

¹ Center for Imaging Science, Johns Hopkins University, Baltimore, MD, United States, ² Institute for Computational Medicine, Johns Hopkins University, Baltimore, MD, United States, ³ Department of Biomedical Engineering, Johns Hopkins University, Baltimore, MD, United States, ⁴ Department of Computational Medicine, University of California, Los Angeles, Los Angeles, CA, United States, ⁵ Department of Neurology, Ahmanson-Lovelace Brain Mapping Center, University of California, Los Angeles, Los Angeles, CA, United States, ⁶ Department of Psychiatry and Behavioral Sciences, Johns Hopkins University, Baltimore, MD, United States, ⁷ Department of Neurology, Johns Hopkins University, Baltimore, MD, United States, ⁸ Department of Applied Mathematics and Statistics, Johns Hopkins University, Baltimore, MD, United States, ⁹ Kavli Neuroscience Discovery Institute, Johns Hopkins University, Baltimore, MD, United States

OPEN ACCESS

Edited by:

Jie Tu,
Chinese Academy of Sciences, China

Reviewed by:

Ricardo Insausti,
University of Castilla-La Mancha,
Spain
José Luna-Muñoz,
Universidad Nacional Autónoma de
México, Mexico

*Correspondence:

Sue Kulason
skulaso1@jhu.edu

Specialty section:

This article was submitted to
Neurodegeneration,
a section of the journal
Frontiers in Neuroscience

Received: 14 April 2020

Accepted: 09 July 2020

Published: 21 August 2020

Citation:

Kulason S, Xu E, Tward DJ, Bakker A, Albert M, Younes L and Miller MI (2020) Entorhinal and Transentorhinal Atrophy in Preclinical Alzheimer's Disease. *Front. Neurosci.* 14:804. doi: 10.3389/fnins.2020.00804

This study examines the atrophy patterns in the entorhinal and transentorhinal cortices of subjects that converted from normal cognition to mild cognitive impairment. The regions were manually segmented from 3T MRI, then corrected for variability in boundary definition over time using an automated approach called longitudinal diffeomorphometry. Cortical thickness was calculated by deforming the gray matter-white matter boundary surface to the pial surface using an approach called normal geodesic flow. The surface was parcellated based on four atlases using large deformation diffeomorphic metric mapping. Average cortical thickness was calculated for (1) manually-defined entorhinal cortex, and (2) manually-defined transentorhinal cortex. Group-wise difference analysis was applied to determine where atrophy occurred, and change point analysis was applied to determine when atrophy started to occur. The results showed that by the time a diagnosis of mild cognitive impairment is made, the transentorhinal cortex and entorhinal cortex was up to 0.6 mm thinner than a control with normal cognition. A change point in atrophy rate was detected in the transentorhinal cortex 9–14 years prior to a diagnosis of mild cognitive impairment, and in the entorhinal cortex 8–11 years prior. The findings are consistent with autopsy findings that demonstrate neuronal changes in the transentorhinal cortex before the entorhinal cortex.

Keywords: transentorhinal, entorhinal, preclinical, cortical thickness, change point, diffeomorphometry

1. BACKGROUND

Evidence suggests that neuropathological changes of Alzheimer's disease (AD) begin years before the onset of clinical symptoms (Sperling et al., 2011). Accumulation of these neuropathological changes is associated with neuronal injury, which can be measured indirectly by structural magnetic resonance imaging (MRI) (Atiya et al., 2003; Kantarci and Jack, 2004). A number of MRI studies have detected atrophy in the entorhinal cortex (ERC), hippocampus and amygdala associated with clinical disease severity (Devanand et al., 2007; La Joie et al., 2012; Miller et al., 2015b) and years

to AD dementia conversion (Atiya et al., 2003; Kantarci and Jack, 2003). More recent MRI studies have focused on evidence of atrophy that precede clinical symptoms (Jack et al., 2004; Csernansky et al., 2005; den Heijer et al., 2006; Apostolova et al., 2010; Dickerson et al., 2011; Miller et al., 2013; Soldan et al., 2015; Pettigrew et al., 2016), often detecting these smaller changes using time-series data analysis (Durrleman et al., 2012) and survival analysis. These MRI biomarkers of AD-related atrophy prior to manifestation of clinical symptoms are of interest because (1) they may aid in assessing efficacy of therapeutic interventions and (2) they may aid in the identification of populations that can benefit from therapeutic intervention prior to clinical symptoms.

Braak's staging of AD suggests that cortical accumulation of neurofibrillary tangles starts in the transentorhinal cortex (TEC), spreads medially to the ERC, and then involves the hippocampus and amygdala (Braak and Braak, 1991; Braak et al., 2006). Accumulation of tau pathology has been correlated with changes in cognitive status in the presence of β -amyloid plaques (Nelson et al., 2012), as well as with TEC atrophy as detected in MRI (Xie et al., 2018). While relatively few MRI studies exist on AD-related TEC changes (Tward et al., 2017b; Wolk et al., 2017), our recent work demonstrated that subjects with mild cognitive impairment (MCI) have increased baseline atrophy and increased rate of atrophy compared to cognitively normal controls, and that changes in the TEC had greater magnitude than changes in the ERC, hippocampus, and amygdala (Kulason et al., 2019). In addition, our group's work on change point analysis has demonstrated MRI-based shape metrics can detect atrophy in the ERC earlier than hippocampal and amygdalar atrophy (Younes et al., 2014). These changes precede clinical symptoms by up to 10 years.

The evidence of MRI biomarkers that precede clinical symptoms taken together with evidence of cortical AD-related changes selectively occurring first in the TEC motivate a close look at TEC atrophy over the preclinical stage of AD progression. In this study, we aim to localize, both spatially and temporally, MRI-based atrophy detection within the TEC and ERC by examining subjects from two diagnostic groups: stable normal cognition (NC), and NC to MCI converters.

2. METHODS

2.1. Data Collection

Subjects were selected from the ADNI database (adni.loni.usc.edu). The criteria for stable NC included the absence of a diagnosis of MCI or AD on all baseline and follow-up visits, a CDR score of 0 on all baseline and follow-up visits, evidence of performance within the normal range on the Logical Memory Subtest of the Wechsler Memory Scale on all baseline and follow-up visits (based on education adjusted norms), and negative results for elevated amyloid β levels on the baseline visit (greater than a cut off of 192 pg/mL from CSF as established by the ADNI Biospecimen Core).

The criteria for NC to MCI converters included evidence of performance within the normal range on the Logical Memory Subtest of the Wechsler Memory Scale at baseline (based on education adjusted norms), a CDR score of 0 on the baseline

TABLE 1 | Demographics (mean \pm standard deviation where applicable).

Diagnostic group	Stable NC	NC to MCI
Sample size (n)	33	17
Baseline age (years)	72.3 \pm 5.5	74.9 \pm 5.3
Sex (% Female)	45.5	70.6
# of scans (years)	4.5 \pm 0.6	4.6 \pm 1.1
Scan period (years)	3.4 \pm 1.1	2.9 \pm 1.0
Clinical evaluation period (years)	5.3 \pm 2.4	6.4 \pm 3.7

exam, a diagnosis of NC at baseline, and a diagnosis of MCI or dementia at a subsequent follow-up visit. Estimated MCI age-of-onset was established based on annual assessment of diagnosis. Note that subjects missing a diagnostic evaluation more than a year prior to MCI diagnosis were excluded, and one subject with an MCI diagnosis was also excluded due to a stable, high score on the Logical Memory Subtest of the Wechsler Memory Scale 5 years after diagnosis.

In addition, subjects had to have a minimum of three 3T MRI scans over 2 or more years. Out of the 30 subjects that met all criteria for NC to MCI converters, all subjects were examined and 17 had a continuous collateral sulcus (CoS) and were included in this study (see section 2.2 for detailed explanation). We examined a subset of available stable NC subjects to reach a total sample size of 50. Out of the 84 subjects that met all criteria for stable NC, 68 were examined and 33 had a continuous collateral sulcus and were included in this study. The demographics of subjects included in this study are summarized in **Table 1**. Two-sample t-tests showed no significant diagnostic group differences by age, number of scans, scan period, or clinical evaluation period. Pearson chi-squared test showed no significant diagnostic group difference by sex. Note that the clinical evaluation period is longer than the scan period because the scan protocol was updated in the ADNI 3 cohort to an accelerated scan sequence. These accelerated scans were not included in this analysis.

2.2. Manual Segmentation and Surface-Based Morphometry

As in previous projects (Tward et al., 2017b; Kulason et al., 2019), we restricted the analysis to the left hemisphere and excluded subjects with a discontinuous CoS in the defined region of interest. There are several variants of the CoS to consider, illustrated in **Figure 1**. The first variant is a deep, continuous sulcus where the rhinal sulcus shares a sulcal bed with the collateral sulcus proper. This variant has been referred to as Type I CoS (Ding and Van Hoesen, 2010) and Type II/Type III rhinal sulcus (Huntgeburth and Petrides, 2012). The second variant is a discontinuous CoS where the collateral sulcus proper begins posterior to the GI. This variant has been referred to as a Type IIa CoS (Ding and Van Hoesen, 2010) and Type I rhinal sulcus (Huntgeburth and Petrides, 2012). Finally, there is a variant with a discontinuous CoS where the collateral sulcus proper begins anterior to the GI, and therefore is excluded for this study. This variant has been referred to as a Type IIb CoS

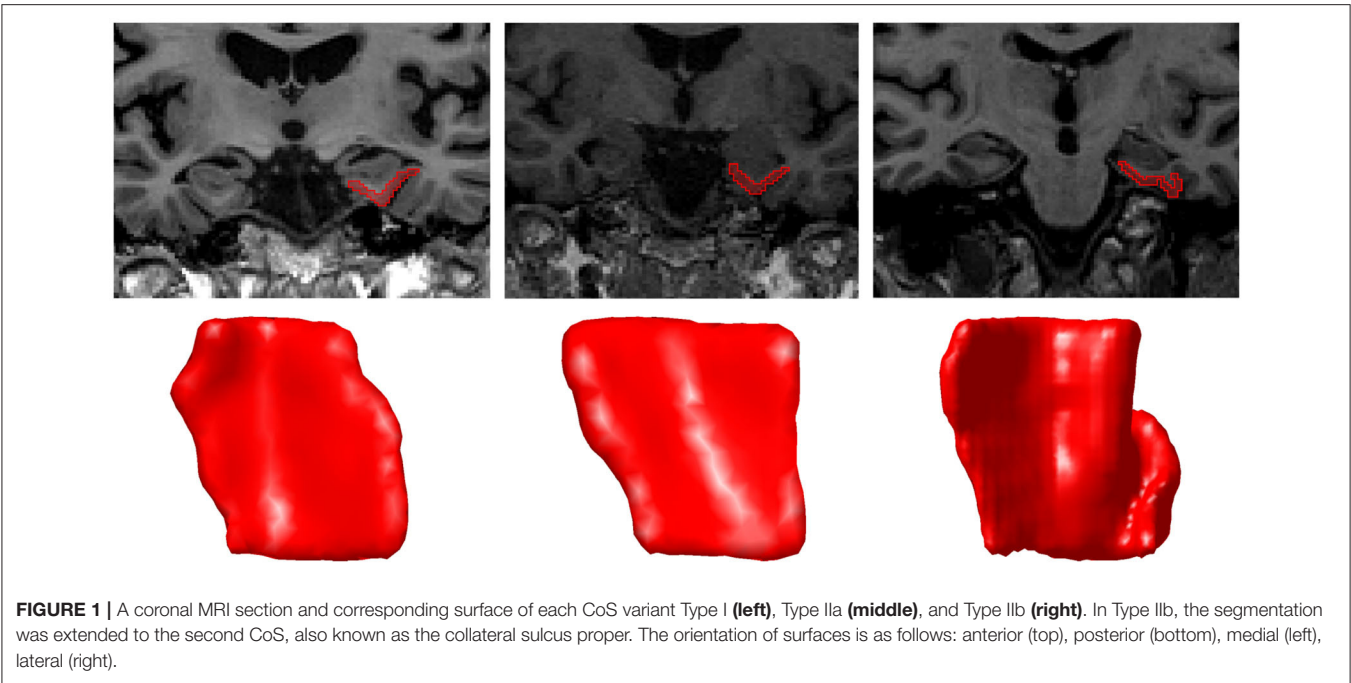


TABLE 2 | Distribution of collateral sulcus variants.

	Type I (continuous CoS)	Type IIa (discontinuous posterior CoS)	Type IIb (discontinuous anterior CoS)
NC (n = 68)	21 (31%)	12 (18%)	35 (51%)
NC to MCI (n = 30)	13 (43%)	4 (13%)	13 (43%)
Total (n = 98)	34 (35%)	16 (16%)	48 (49%)

Type IIb CoS were excluded from this analysis.

(Ding and Van Hoesen, 2010) and also falls into the category for Type I rhinal sulcus (Huntgeburth and Petrides, 2012). **Table 2** categorizes the proportion of CoS variants prior to exclusion of Type IIb. Previous work has shown there is a relationship between CoS depth and the boundaries of the ERC and TEC with respect to anatomical markers (Insausti et al., 1998). Briefly, in a shallow CoS (< 1cm) the ERC extends to the deepest extent of the CoS. In a regular CoS (between 1 and 1.5 cm), the ERC extends to the midpoint of the medial bank of the CoS. In a deep CoS (> 1.5cm) the ERC extends up to the CoS. In this subject set we found that excluded Type IIb CoS subjects most often had a shallow CoS, while the Type I and Type IIa variants included in this study were of a regular to deep CoS type.

226 3T T1 MRI scans were used in this study. ERC and TEC were segmented manually using Seg3D software (Center for Integrative Biomedical Computing, 2016). We followed an established procedure for segmentation and delineation of the ERC and TEC (Tward et al., 2017b) that was based on anatomical landmarks described near cytoarchitectonically-defined ERC boundaries (Insausti et al., 1998; Ding and Van Hoesen, 2010).

The anterior boundary of the ERC and TEC were defined 4mm anterior to the hippocampal head. Delineation of the ERC and TEC anterior to this boundary is more complex and excluded from this study. Earlier works suggest that the area anterior to this region is a mix of ERC and perirhinal cortex (Insausti et al., 1998), or olfactory cortex (Krimer et al., 1997), whereas a more recent work suggests that this area is, in fact, part of the ERC (Ding and Van Hoesen, 2010). The posterior boundary for ERC and TEC was defined 2 mm posterior to the gyrus intralimbicus (GI) (Insausti et al., 1998). The medial extent of the ERC was defined as far as the gray/white boundary was visible. This delineation excludes a small dorsal medial aspect of the ERC that rests against the amygdala, and is similar to how other T1 MRI protocols delineate the ERC (Desikan et al., 2006; Maass et al., 2015). The lateral extent of the ERC and medial extent of the TEC was defined at the medial extent of the collateral sulcus (CoS), as is found in a deep CoS (Insausti et al., 1998). The lateral extent of the TEC was defined as being at the deepest extent of the CoS, as is also found in a deep CoS (Ding and Van Hoesen, 2010).

Figure 2 shows a sample of ERC plus TEC surfaces generated from manual segmentations. A population template for the ERC plus TEC surface was calculated from these surfaces by taking the average (Fréchet mean) diffeomorphism in a Bayesian setting (Ma et al., 2008). Then, the segmentations were adjusted for variability in boundaries over time by mapping the population template simultaneously onto each scan of a time series (Tward et al., 2017a). The result is a set of surfaces of the ERC plus TEC.

2.3. Surface Parcellation

Studies of this region have tended to use inconsistent nomenclature. We mapped four atlases with commonly used

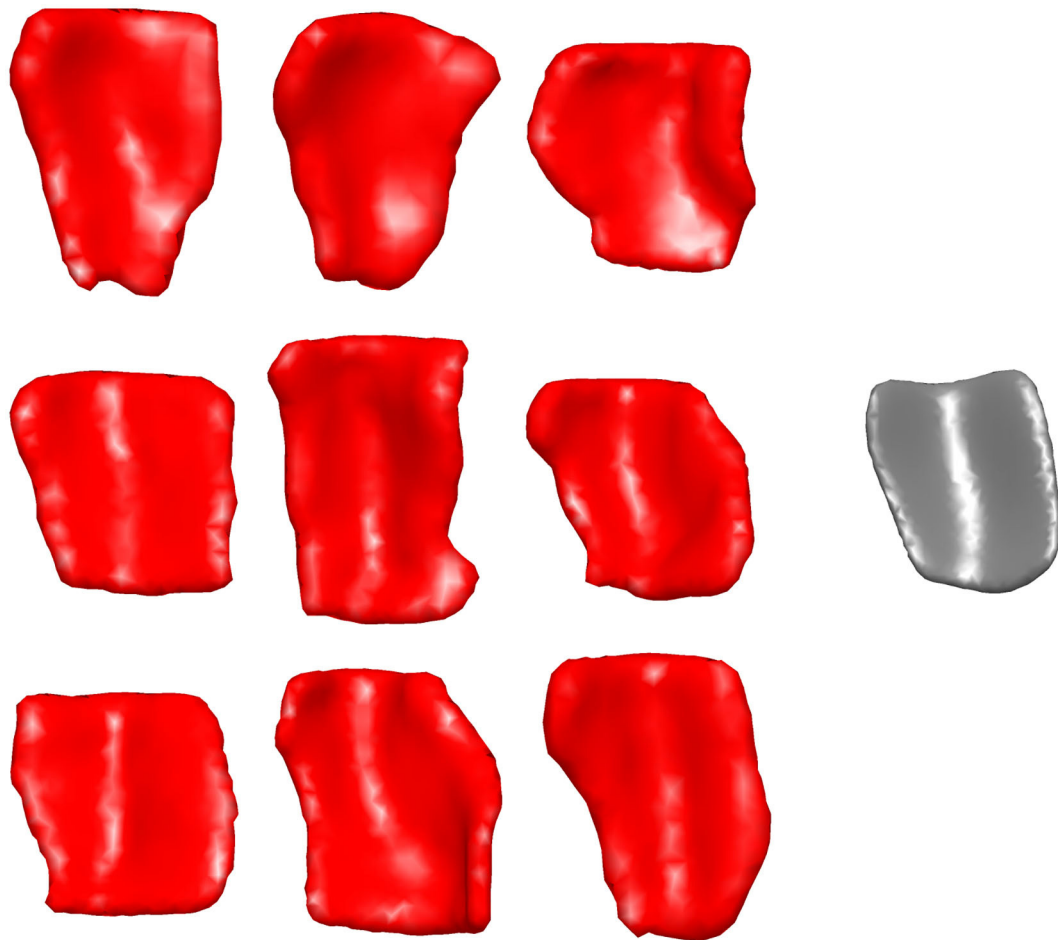


FIGURE 2 | Sample of ERC plus TEC surfaces generated from manual segmentations (**left**) and the resultant population template (**right**). The orientation is as follows: anterior (top), posterior (bottom), medial (left), lateral (right).

sub-regional labels onto our ERC plus TEC population template: (1) manual labels of ERC and TEC based on cortical folding seen in structural MRI (Tward et al., 2017b), (2) automated labels of ERC and parahippocampal gyrus (PHG) based on cortical folding seen in structural MRI (Desikan et al., 2006), (3) labels of posterior medial ERC (pmERC), anterior lateral ERC (alERC), and perirhinal cortex (PRC) based on connectivity patterns seen in functional MRI after manual segmentation of ERC in structural 7T MRI (Maass et al., 2015), and (4) histological labels of intermediate superior ERC, intermediate rostral ERC, intermediate caudal ERC, prorhinal ERC, medial rostral ERC, medial caudal ERC, lateral ERC, sulcal ERC and TEC as identified in an 11T *ex vivo* MRI (Krimer et al., 1997; Miller et al., 2015a).

Manual segmentation of ERC and TEC was performed on an scan with a Type IIa CoS variant of regular depth (1.30 cm). To generate labels from the Desikan-Killiany atlas, FreeSurfer 6.0 was run on the same scan. The functional MRI atlas was provided on a subject with Type IIa CoS variant of regular depth (1.20 cm) (Maass et al., 2015). The *ex vivo* MRI atlas was provided on a subject with a Type IIb CoS variant of shallow depth (0.75

cm). For each atlas, we manually segmented the ERC plus TEC from the structural MRI following the same protocol as for our subjects. In the *ex vivo* case, since the CoS was shallow, the TEC was extended to the lateral bank of the CoS, as seen in histology (Insausti et al., 1998; Ding and Van Hoesen, 2010). We then mapped the atlas labels to the manually-defined ERC plus TEC surface by linear interpolation. Finally, we mapped these surfaces and their labels to the population template surface following the LDDMM framework (Beg et al., 2005). The result was four sets of labels, one from each atlas, on each vertex of the population template surface.

The Desikan-Killiany atlas defined the anterior boundary of ERC at the rostral end of the CoS; this was approximately 6 mm anterior to the boundary defined in our protocol. The functional MRI atlas defined the anterior boundary at the rostral end of the amygdala, which coincided with our protocol's boundary. The anterior boundary on the *ex vivo* MRI atlas was 0.5 mm posterior to our protocol's boundary.

The Desikan-Killiany atlas defined the posterior boundary at the caudal end of the amygdala. This excludes a posterior portion

of the ERC that runs lateral to the hippocampal formation (Krimer et al., 1997; Insausti et al., 1998; Ding and Van Hoesen, 2010). The functional MRI atlas defined the posterior boundary as extending to the caudal end of the CoS. Since this atlas was a Type IIa CoS variant, the caudal extent of the CoS coincided with 1.2 mm posterior to the GI, or one 0.6 mm slice anterior to our protocol's boundary. The posterior boundary of the *ex vivo* atlas was 1.0 mm anterior to our protocol's boundary.

The Desikan-Killiany atlas, functional MRI atlas, and our protocol defined the medial boundary at the furthest extent where gray/white boundary was visible. The *ex vivo* atlas included the dorsal medial aspect of the ERC that borders the amygdala, a border that is not always visible on 3T T1 MRI. An overlay of the *ex vivo* atlas ERC partition and our protocol's ERC plus TEC partition highlights this difference as shown in **Figure 3**.

Finally, the Desikan-Killiany atlas defined the lateral extent of entorhinal cortex as the most lateral extent of the CoS. This boundary definition most closely followed that of a shallow CoS variant (Insausti et al., 1998), often seen in Type IIb CoS that were excluded from this study. The functional MRI atlas delineated the ERC ending at the shoulder of the CoS, a definition that most closely followed the boundary of a deep CoS variant (Insausti et al., 1998). Our protocol also followed the delineation that matches a deep CoS variant. Since the subjects included in this study range from regular CoS depth (1.0–1.5 cm) to deep CoS depth (> 1.5 cm), it is likely that our protocol may include a small portion of the ERC within the TEC label.

2.4. Cortical Thickness

To calculate vertex-wise cortical thickness, we followed an established procedure based on LDDMM (Ratnanather et al., 2019). The ERC plus TEC surface was cut into two surfaces: the pial surface and the gray matter-white matter boundary surface. The gray matter-white matter boundary surface was deformed to the pial surface within the LDDMM framework, with an additional imposed constraint that the surface must flow in the direction normal to its evolving surface. Cortical thickness was then estimated as the distance along these trajectories. Average ERC thickness and average TEC thickness were calculated as the mean thickness across vertex labeled ERC and TEC, respectively, as mapped from the manual structural MRI atlas.

2.5. Group Difference Analysis

We tested where there were differences in shape measures by diagnostic group. The log-linear mixed effects model under the null hypothesis can be written as Equation (1) given a subject i , scan j , and vertex k .

$$\log(\text{thickness})_{i,j,k} = a_k + b_k \text{age}_{i,j} + c_k \text{sex}_i + e_{i,k} + \epsilon_{i,j,k} \quad (1)$$

The constants a , b , c , and the variance of 0-mean Gaussians e and ϵ are estimated by maximum likelihood. e is the subject-specific random effect, while age and sex (a binary indicator variable) are fixed effects.

The log-linear mixed effects model under the alternative hypothesis can be written as Equation (2).

$$\begin{aligned} \log(\text{thickness})_{i,j,k} = & a_k + b_k \text{age}_{i,j} \\ & + \left(a'_k + b'_k (\text{age}_{i,j} - \text{age_MCIonset}_i) \right) \text{isMCI}_i \\ & + c \text{sex}_i + e_{i,k} + \epsilon_{i,j,k} \end{aligned} \quad (2)$$

isMCI is a binary indicator variable for whether a subject belongs to the group that converted from NC to MCI, and age_MCIonset is the age of MCI diagnosis. a' is the mean difference in log thickness at the time of MCI diagnosis for subjects that converted from NC to MCI. b' corresponds to the disease-related rate of change in this group.

We tested whether the model under the alternative hypothesis significantly fit the data better than the model under the null hypothesis by using the likelihood ratio as a test statistic and bootstrap resampling 10,000 samples. The bootstrapped samples were constructed by sampling from whitened residuals under the null hypothesis. We compared the likelihood ratio to the distribution of likelihood ratios of the bootstrapped samples. We corrected for multiple comparisons over the vertices by using the maximum test statistic over all vertices for each set of bootstrapped samples (Nichols and Hayasaka, 2003). We rejected the null hypothesis when the true likelihood ratio was greater than 95% of the bootstrapped likelihood ratios.

2.6. Change Point Analysis

We tested when a change in atrophy rate occurred with respect to MCI diagnosis. Details for constructing and testing this change point model are described in another work (Tang et al., 2017). Here we provide a brief summary of the approach.

The log-linear mixed effects model under the null hypothesis can be written as Equation (3) given a subject i , scan j , and location k .

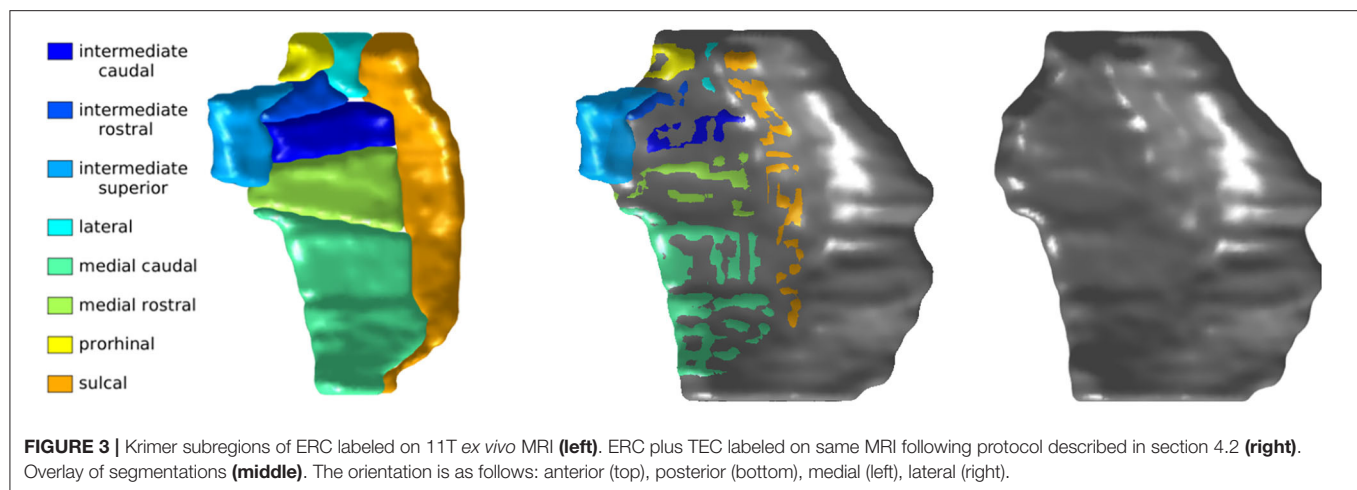
$$\begin{aligned} \log(\text{thickness})_{i,j,k} = & a_k + b_k \text{age}_{i,j} + c_k \text{sex}_i \\ & + d_k \text{age_MCIonset}_i + e_{i,k} + \epsilon_{i,j,k} \end{aligned} \quad (3)$$

The constants a , b , c , d , and the variance of 0-mean Gaussians e and ϵ are estimated by maximum likelihood. e is the subject-specific random effect, while age and sex (a binary indicator variable) are fixed effects. Unlike in the group-wise difference analysis, this model has only two locations in order to reduce computational complexity: one for average ERC thickness, and the other for average TEC thickness.

The model under the alternative hypothesis can be written as Equation (4).

$$\begin{aligned} \log(\text{thickness})_{i,j,k} = & a_k + b_k \text{age}_{i,j} \\ & + b'_k (\text{age}_{i,j} - (\text{age_MCIonset}_i + \Delta))^+ \\ & + c_k \text{sex}_i + d_k \text{age_MCIonset}_i + e_{i,k} + \epsilon_{i,j,k} \end{aligned} \quad (4)$$

Δ is the number of years from a diagnosis of MCI to the change point in atrophy rate, and $(\text{age_MCIonset}_i + \Delta)^+ =$



$\max(\text{age_MCIonset}_i + \Delta, 0)$ is the number of years past the change point. The constants a, b, c, d , and the variance of 0-mean Gaussians e and ϵ are estimated by maximum likelihood over a fixed Δ with yearly increments of Δ between -50 and 50 years. The best candidate Δ is calculated from the posterior mean.

For stable NC subjects, we estimated MCI diagnosis from a conditional probability distribution where the age of onset was constrained to be after the last diagnostic evaluation, and drawn from a Gaussian distribution with mean age of $\mu_1 = 93$ years and standard deviation of $\sigma_1 = 14.5$ years. This distribution of MCI diagnosis was estimated (Tang et al., 2017) using a set of 1,000 subjects enrolled with normal cognition and a family history of Alzheimer's disease.

Since the subjects in this study were selected to meet diagnostic group criteria and do not represent a random sample over the progression of the disease, we re-weighted the likelihood function by the distribution of stable NC and NC to MCI converters expected if the subjects were selected blind to diagnostic group. The subjects in the ADNI database were enrolled to meet a set number of subjects per diagnostic group, and as such, cannot be used to estimate this distribution. Instead, we examined the BIOCARD database, where subjects were enrolled cognitively normal and followed for up to 22 years at time we examined this database (biocard-se.org). This distribution was calculated from a subset of subjects over 65 years of age at their most recent follow-up visit. Specifically, the proportion was 184/260 stable NC and 44/260 NC to MCI converters.

We tested whether the model under the alternative hypothesis significantly fit the data better than the model under the null hypothesis using the likelihood ratio as a test statistic and bootstrap resampling 1,000 samples. The bootstrapped samples are constructed by sampling from whitened residuals under the null hypothesis, with imputed values for age_MCIonset for stable NC subjects. We compared the likelihood ratio to the distribution of likelihood ratios of the bootstrapped samples and rejected the null hypothesis when the likelihood ratio was greater than 95% of the bootstrapped likelihood ratios. We used the maximum

test statistic over pairs of ERC and TEC statistics to control family-wise error rate (Nichols and Hayasaka, 2003).

In the case where the null hypothesis was rejected, we then determined the confidence interval for Δ , b and b' by bootstrap resampling under the alternative hypothesis 1,000 times. The bootstrapped samples were constructed by sampling from whitened residuals under the alternative hypothesis, with imputed values for age_MCIonset for NC subjects. In the case where the null hypothesis was rejected for both ERC and TEC measures, we then calculated the probability that the change point for TEC occurred before the change point for ERC based on the change point Δ of each pair of bootstrapped samples under the alternative hypothesis. This one-sided test was selected based on histological evidence that changes occurred in the TEC before the ERC (Braak et al., 2006).

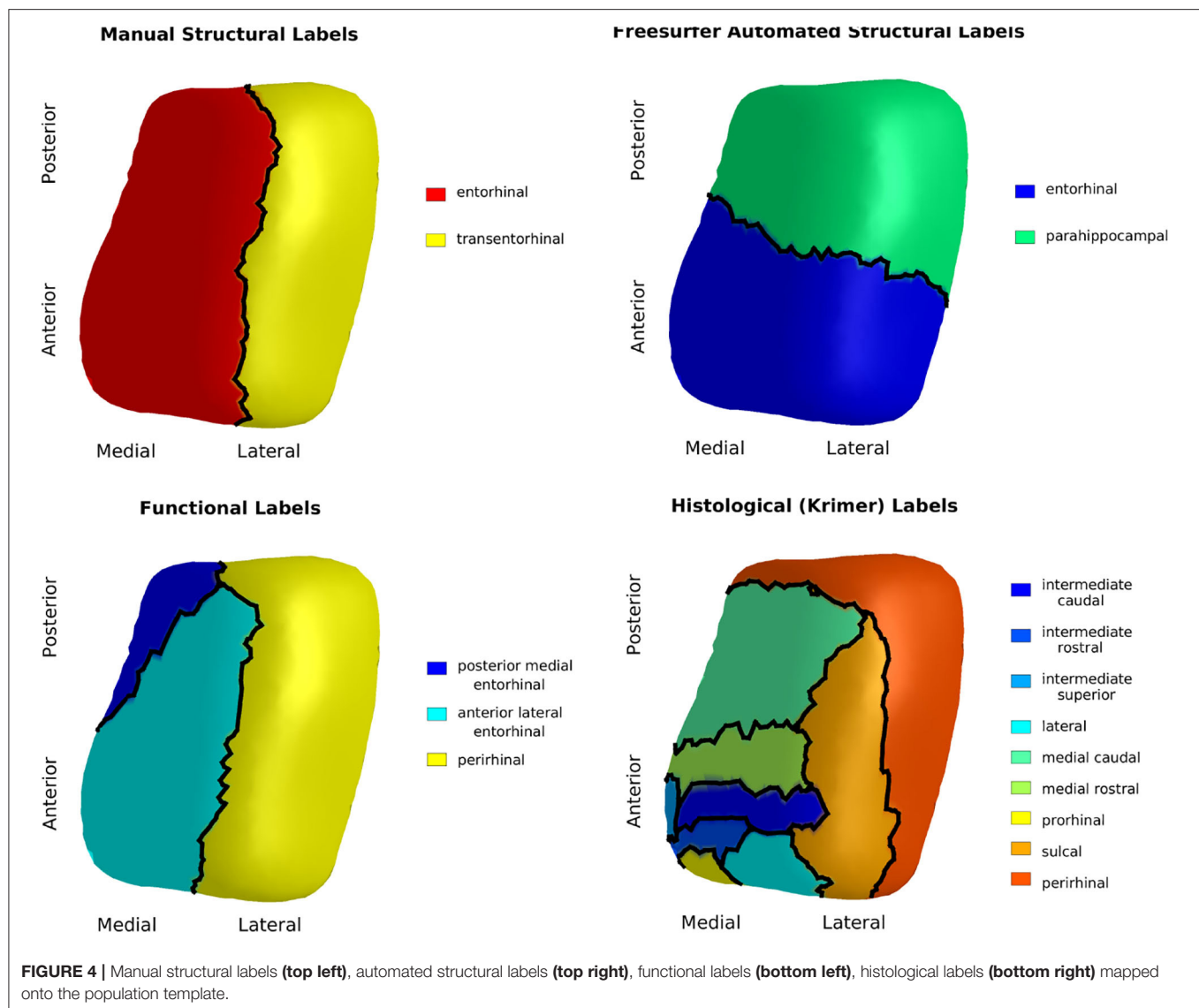
3. RESULTS

3.1. Surface Parcellation

The results of the four atlas mappings onto the population template surface are shown in **Figure 4**. Comparison of the atlases highlight inconsistencies introduced by varying nomenclature and CoS variant. The automated labels based on cortical folding used by Desikan-Killany defined the ERC extending into the CoS, a definition that matches a shallow CoS variant. The atlas also excluded the posterior extent of the ERC. In contrast, the functional MRI atlas defined the perirhinal cortex (PRC), an area that includes the TEC, and separated this structure from the ERC using a definition that matches a deep CoS variant. Histologically-defined subregions of the ERC show yet another popular parcellation of this region on a regular depth (1–1.5 cm) CoS variant. Note how in this definition, the sulcal ERC extends into the shoulder of the CoS. In this study, average ERC and average TEC metrics were calculated based on the labels shown in the manual structural labels (top left).

3.2. Cortical Thickness

Average cortical thickness of TEC and average cortical thickness of ERC are plotted in **Figure 5**. The TEC is slightly thicker than



the ERC, which is in agreement with previous work (Kulason et al., 2019). In both regions, organization by MCI diagnosis date show cortical thickness measures decrease with progression of the disease, and that the rate of cortical thinning is noticeably steeper in NC to MCI converters than in stable NC subjects.

3.3. Diagnostic Group Difference Analysis

We rejected the null hypothesis with global $p < 0.0001$ and concluded that there was a difference in cortical thickness between diagnostic groups. **Figure 6** shows the difference in atrophy and atrophy rate across all vertices. A summary of average and maximum atrophy/atrophy rates is shown in **Table 3**. As the data demonstrates, at the time of MCI diagnosis, individuals who had progressed to a diagnosis of MCI were as much as 0.58 mm thinner in the ERC and 0.60 mm thinner in the TEC. The additional atrophy rate in the participants who progressed from NC to MCI was 2.96% per year in the ERC

on average and 2.43% per year in the TEC on average. This is a notable increase from age-related atrophy which was, on average, 0.68% per year in the TEC and 0.66% per year in the ERC. In other words, the average total atrophy rate in NC to MCI converters was 5.35 times greater in the ERC and 4.68 times greater in the TEC compared to stable NC subjects.

3.4. Change Point Analysis

We rejected the null hypothesis and concluded that there was a change point 9.02 years before MCI onset for the ERC ($p < 0.001$) and 10.69 years before MCI diagnosis for the TEC ($p < 0.001$). Prior to the change point, the atrophy rate was 0.35%/year for the ERC and 0.34%/year for the TEC. After the change point, the additional atrophy was 3.75%/year for the ERC and 2.58%/year for the TEC. The 95% confidence interval for the parameters of interest are shown in **Table 4**. The ERC change point in thickness occurred at or before the TEC change point

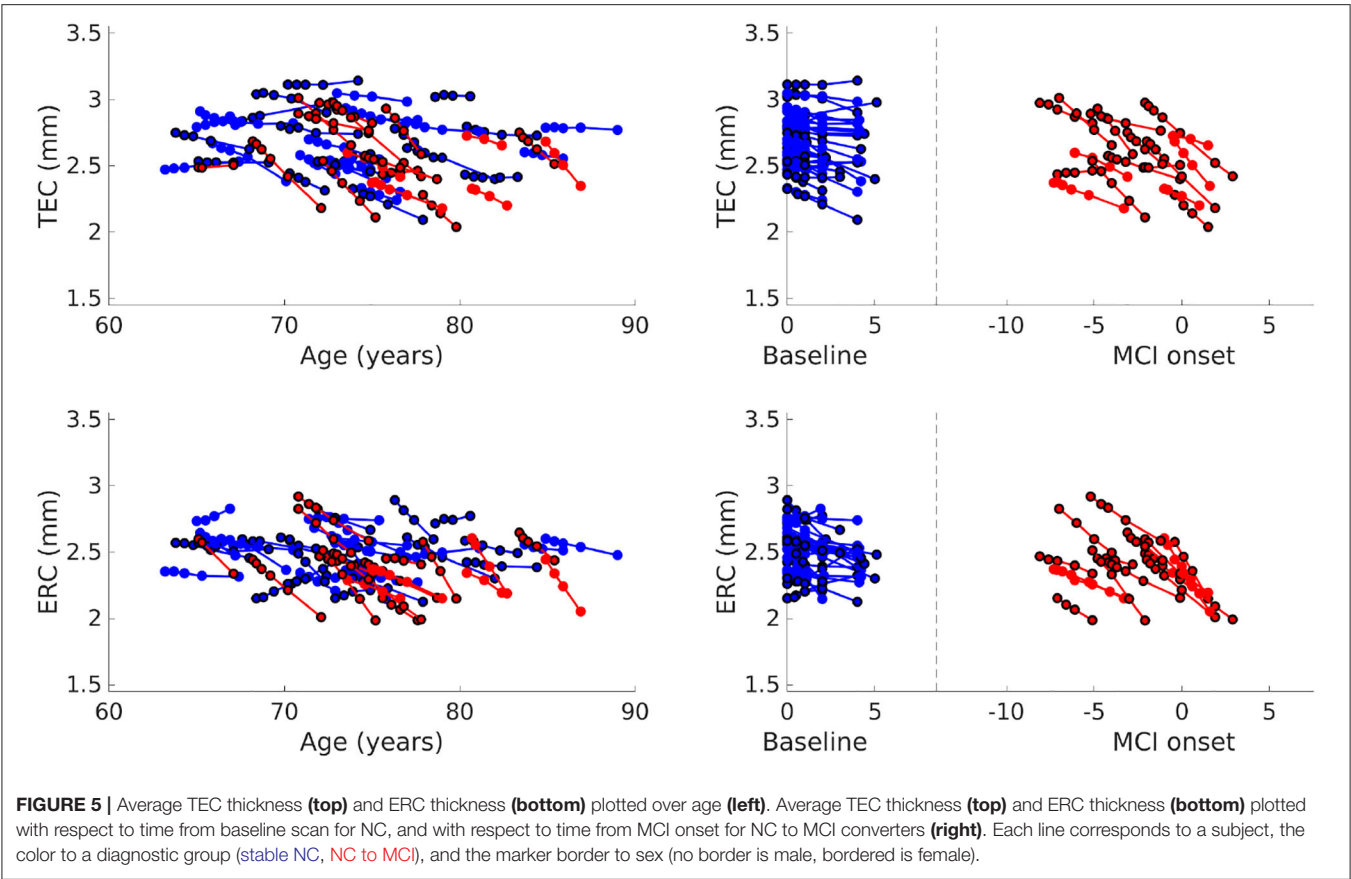


TABLE 3 | Summary of group-wise difference analysis by region.

	ERC average	ERC max	TEC average	TEC max
Atrophy at MCI diagnosis	0.25 mm (8.46%)	0.58 mm (16.54%)	0.23 mm (7.63%)	0.60 mm (17.34%)
MCI-related Atrophy rate	2.96 %/year	4.23 %/year	2.43 %/year	4.11 %/year
age-related Atrophy rate	0.68 %/year	2.08 %/year	0.66 %/year	1.61 %/year

in 3.75% of bootstrapped samples. We concluded that the TEC change point preceded the ERC change point.

4. DISCUSSION

The first major finding of this study is that anterior regions of the ERC and TEC were more than half a millimeter thinner (up to 17% thinner) in NC to MCI converters at the time of MCI diagnosis, and that disease-related atrophy was roughly 3% per year. The evidence suggests that disease-related atrophy begins prior to an MCI diagnosis in the anterior lateral region of ERC and anterior region of TEC. This is in line with our previous study

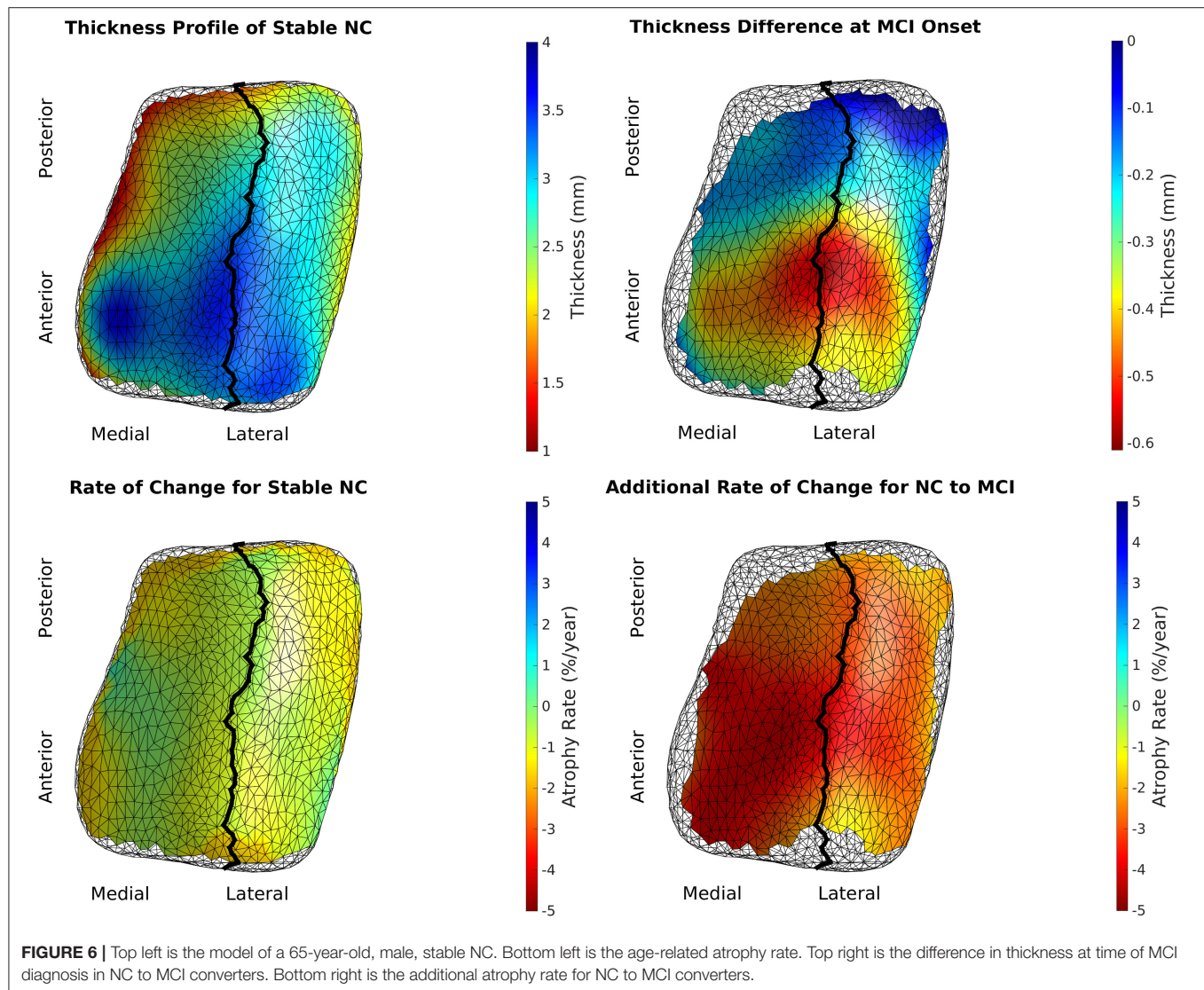
TABLE 4 | 95% confidence interval (min, max).

	Change point (years before MCI)	Age-related rate (%/year atrophy)	Disease-related rate (%/year atrophy)
ERC thickness	(7.63, 11.31)	(0.07, 0.65)	(3.03, 4.41)
TEC thickness	(8.92, 13.80)	(0.10, 0.56)	(2.11, 3.08)

Change point, age-related rate, and disease-related rate correspond to the variables $-\Delta$, $-b$, and $-b'$, respectively. The disease-related rate is the additional rate seen post change point.

that examined subjects after an MCI diagnosis, where we found disease-related thickness atrophy was 5% atrophy per year in the TEC and that MCI subjects were on average 23% thinner than NC (Kulason et al., 2019). The 3% atrophy per year in NC to MCI converters vs. 5% atrophy per year in subjects after MCI diagnosis may suggest that the atrophy rate increases with progression of the disease from the preclinical to clinical stage.

The second major finding of this study is that there was a change in the rate of ERC thickness atrophy 8–11 years prior to MCI diagnosis, and a change in the rate of TEC thickness atrophy 9–14 years before the diagnosis of MCI. The order of the change points, TEC before ERC, is consistent with histological report of neurofibrillary tau accumulation in this region (Braak et al., 2006). The time of change point is consistent with a



previous study, which found changes in surface area of the FreeSurfer-defined ERC 8–10 years prior to symptom onset (Younes et al., 2014).

These findings emphasize the discrepancies in nomenclature pertaining to the TEC and ERC. We showed how the Desikan-Killiany atlas defined ERC beginning anterior to our protocol and ending anterior to our protocol. Our protocol closely matched the anterior and posterior boundaries defined in the function MRI atlas and *ex vivo* atlases. The Desikan-Killiany ERC extended laterally into the CoS, which is accurate for shallow CoS common variant in Type IIb CoS, and not as accurate for the regular and deep CoS variants that were included in this study. The *ex vivo* atlas, a subject with Type IIa CoS variant of regular depth, marked the sulcal ERC lateral boundary shortly past the shoulder of the CoS, which is consistent with cytoarchitectonically-defined ERC in previous studies (Krimer et al., 1997; Insausti et al., 1998; Ding and Van Hoesen, 2010). The functional MRI atlas and Desikan-Killiany atlas chose not to define the TEC separate from

perirhinal cortex and fusiform gyrus, respectively. The 4 surface parcellations mapped to the same coordinate system highlight the need for a standardized nomenclature of this region, much like the work being done to standardize sub-regional boundaries of the hippocampus (Adler et al., 2018; Olsen et al., 2019).

There are a number of strengths to this study. The subjects were carefully selected to (1) follow a strict set of inclusion criteria for diagnostic grouping, and (2) exclude subjects with a discontinuous CoS within the region of interest. This was done to reduce confounding factors introduced by other medical conditions and natural variability in cortical folding. In addition, scans were manually segmented to avoid errors introduced by automated segmentation methods. Finally, the results were put in the context of several atlases for broader interpretation of findings.

There are also a few limitations to this study, the first being a relatively small sample size. Accurate segmentations, which have been performed manually for this study, are extremely

time consuming. The ERC is particularly difficult to segment automatically due to its proximity with the meninges and oculomotor nerve. These neighboring structures are a similar intensity to gray matter voxels in T1 scans. Some recent work has been done to address this issue using automatic parcellation (Xie et al., 2017); a future direction is to determine whether this type of automated approach to segmentation affects ERC and TEC metrics produced in this analysis.

Another limitation of this study is that the distribution of samples is biased by diagnostic grouping. It is difficult to estimate the true distribution of diagnostic groups because the ADNI protocol selected subjects based on diagnosis and the follow-up time varies. This is mitigated by the use of distribution estimates calculated from the BIOCARD database.

In the future, this study can be extended to include shallow, discontinuous CoS variants for detecting Alzheimer's-related changes. It is of interest to develop metrics of disease progression that are robust to this natural variation in folding. Autopsy studies have shown that subjects with a shallow, discontinuous CoS have a TEC that begins at the deepest extent of the CoS and extends out laterally, whereas deep, continuous CoS have a TEC that begins at the shoulder of the CoS and extends only to the deepest extent of the CoS (Insausti et al., 1998; Ding and Van Hoesen, 2010). Therefore, a multi-atlas approach with CoS variant-specific atlases may be desirable to delineate the ERC and TEC accurately for a full population of subjects.

Finally, given the localization of tau to CA1 after initial deposits along the boundary of TEC and ERC (Braak and Braak, 1991), it is of interest to extend thickness analysis to this region. Unfortunately, the CA1 subfield cannot be segmented separately from the hippocampal formation in 3T T1 MRI. Previous volumetric analysis of the hippocampus has shown 9% atrophy in MCI subjects, compared to 27% volumetric atrophy of ERC plus TEC in MCI subjects (Kulason et al., 2019). Previous change point analysis of surface expansion/contraction metrics have shown a hippocampal change point 2–4 years prior to symptom onset, compared to 8–10 years prior to symptom onset for a Desikan-Killiany defined ERC (Younes et al., 2014). As more high resolution T2 MRI data become available, such as with data being collected in the more recent ADNI 3 protocol, it will be of interest to extend this thickness analysis to the CA1 subfield.

This study provides strong evidence that TEC and ERC thickness is a sensitive measure to progression to the symptomatic phase of Alzheimer's disease and that disease-related atrophy begins to occur at least 9 years prior to a clinical diagnosis of MCI.

DATA AVAILABILITY STATEMENT

The data analyzed in this study is subject to the following licenses/restrictions: Individuals need to register with ADNI and agree to the conditions in the "ADNI Data Use Agreement" and undergo limited screening by the DPC before accessing data. Requests to access these datasets should be directed to <http://adni.loni.usc.edu/data-samples/access-data/>.

ETHICS STATEMENT

The studies involving human participants were reviewed and approved by Good Clinical Practice guidelines, the Declaration of Helsinki, and the US 21 CFR Part 50-Protection of Human Subjects, and Part 56-Institutional Review Boards (IRB). The patients/participants provided their written informed consent to participate in this study.

AUTHOR CONTRIBUTIONS

SK and EX processed the data. SK performed the analysis, drafted the manuscript, and designed the figures. DT, MA, LY, and MM contributed to the design and implementation of the research and to the analysis of the results. All authors contributed to the editing of the manuscript.

FUNDING

This work was supported by the National Institutes of Health (P41-EB015909 and R01-EB020062); and the Kavli Neuroscience Discovery Institute. MM reports personal fees from AnatomyWorks, LLC, outside the submitted work, and jointly owns AnatomyWorks. Dr. Miller's relationship with AnatomyWorks is being handled under full disclosure by the Johns Hopkins University.

ACKNOWLEDGMENTS

A special thank you to Kanami Mori for her work on manually segmenting the 11T *ex vivo* MRI atlas and to Anthony Kolasny for maintaining the Center for Imaging Science server on which much of this analysis was run.

Data used in the preparation of this article were obtained from the Alzheimer's Disease Neuroimaging Initiative (ADNI) database (adni.loni.usc.edu). As such, the investigators within the ADNI contributed to the design and implementation of ADNI and/or provided data but did not participate in the analysis or writing of this report. A complete listing of ADNI investigators can be found at http://adni.loni.usc.edu/wp-content/uploads/how_to_apply/ADNI_Acknowledgement_List.pdf. Data collection and sharing for this project was funded by the Alzheimer's Disease Neuroimaging Initiative (ADNI) (National Institutes of Health Grant U01 AG024904) and DODADNI (Department of Defense award number W81XWH-12-2-0012). ADNI is funded by the National Institute on Aging, the National Institute of Biomedical Imaging and Bioengineering, and through generous contributions from the following: AbbVie, Alzheimer's Association; Alzheimer's Drug Discovery Foundation; Araclon Biotech; BioClinica, Inc.; Biogen; Bristol-Myers Squibb Company; CereSpir, Inc.; Cogstate; Eisai Inc.; Elan Pharmaceuticals, Inc.; Eli Lilly and Company; EuroImmun; F. Hoffmann-La Roche Ltd. and its affiliated company Genentech, Inc.; Fujirebio; GE Healthcare; IXICO Ltd.; Janssen Alzheimer Immunotherapy Research & Development, LLC; Johnson & Johnson Pharmaceutical Research & Development LLC; Lumosity; Lundbeck; Merck & Co, Inc.; Meso Scale Diagnostics,

LLC; NeuroRx Research; Neurotrack Technologies; Novartis Pharmaceuticals Corporation; Pfizer Inc.; Piramal Imaging; Servier; Takeda Pharmaceutical Company; and Transition Therapeutics. The Canadian Institutes of Health Research is providing funds to support ADNI clinical sites in Canada. Private sector contributions are facilitated by the Foundation for the National Institutes of Health (www.fnih.org). The grantee organization is the Northern California Institute for Research and Education, and the study is coordinated by the Alzheimer's Therapeutic Research Institute at the University of Southern California. ADNI data are disseminated by the Laboratory for Neuroimaging at the University of Southern California.

Data from the BIOCARD study are supported by grant U19 AG033655 from the National Institute on Aging. The BIOCARD Study consists of 7 Cores with the following members: (1) The Administrative Core (MA, Barbara Rodzon), (2) the Clinical Core (MA, Anja Soldan, Rebecca Gottesman, Ned Sacktor, Corinne Pettigrew, Scott Turner, Leonie Farrington, Maura Grega, Jules, Gilles, Gay Rudow, Rostislav Brichko, Scott Rudow), (3) the Imaging Core (MM, Susumu Mori, Tilak Ratnanather, Anthony Kolasny, Hanzhang Lu, Kenichi Oishi, LY), (4) the Biospecimen Core (Abhay Moghekar, Jacqueline Darrow, Richard O'Brien), (5) the Informatics Core (Roberta

Scherer, David Shade, Ann Ervin, Jennifer Jones, Hamadou Coulibaly, Kathy Moser), the (6) Biostatistics Core (Mei-Cheng Wang, Yuxin Zhu, Jiangxia Wang), and (7) the Neuropathology Core (Juan Troncoso, Olga Pletnikova, Karen Fisher). We would also like to acknowledge the members of the BIOCARD Scientific Advisory Board who provide oversight and guidance regarding the conduct of the study including: Drs. John Csernansky, David Holtzman, David Knopman, Walter Kukull and Kevin Duff, as well as Drs. Laurie Ryan and John Hsiao, who provide oversight on behalf of the NIA. Additionally, we recognize the members of the BIOCARD Resource Allocation Committee who provide ongoing guidance regarding the use of the biospecimens collected as part of the study, including: Drs. Constantine Lyketsos, Carlos Pardo, Gerard Schellenberg, Leslie Shaw, Madhav Thambisetty, and John Trojanowski. We would like to acknowledge the contributions of the Geriatric Psychiatry Branch (GPB) of the intramural program of the NIMH who initiated this study (PI: Dr. Trey Sunderland). Dr. Karen Putnam provided documentation of the GPB study procedures and the datafiles received from NIMH. We acknowledge the altruism of the participants and their families and contributions of the BIOCARD research and support staff for their contributions to this study.

REFERENCES

- Adler, D. H., Wisse, L. E., Ittyerah, R., Pluta, J. B., Ding, S.-L., Xie, L., et al. (2018). Characterizing the human hippocampus in aging and Alzheimer's disease using a computational atlas derived from *ex vivo* MRI and histology. *Proc. Natl. Acad. Sci. U.S.A.* 115, 4252–4257. doi: 10.1073/pnas.1801093115
- Apostolova, L. G., Mosconi, L., Thompson, P. M., Green, A. E., Hwang, K. S., Ramirez, A., et al. (2010). Subregional hippocampal atrophy predicts Alzheimer's dementia in the cognitively normal. *Neurobiol. Aging* 31, 1077–1088. doi: 10.1016/j.neurobiolaging.2008.08.008
- Atiya, M., Hyman, B. T., Albert, M. S., and Killiany, R. (2003). Structural magnetic resonance imaging in established and prodromal Alzheimer disease: a review. *Alzheimer Dis. Assoc. Disord.* 17, 177–195. doi: 10.1097/00002093-200307000-00010
- Beg, M. F., Miller, M. I., Trounev, A., and Younes, L. (2005). Computing large deformation metric mappings via geodesic flows of diffeomorphisms. *Int. J. Comput. Vis.* 61, 139–157. doi: 10.1023/B:VISI.0000043755.93987.a
- Braak, H., Alafuzoff, I., Arzberger, T., Kretschmar, H., and Del Tredici, K. (2006). Staging of Alzheimer disease-associated neurofibrillary pathology using paraffin sections and immunocytochemistry. *Acta Neuropathol.* 112, 389–404. doi: 10.1007/s00401-006-0127-z
- Braak, H., and Braak, E. (1991). Neuropathological staging of Alzheimer-related changes. *Acta Neuropathol.* 4, 239–259. doi: 10.1007/BF00308809
- Center for Integrative Biomedical Computing (2016). *Seg3D: Volumetric Image Segmentation and Visualization*. Scientific Computing and Imaging Institute (SCI). Available online at: <http://www.seg3d.org>
- Csernansky, J. G., Wang, L., Swank, J., Miller, J. P., Gado, M., McKeel, D., et al. (2005). Preclinical detection of Alzheimer's disease: hippocampal shape and volume predict dementia onset in the elderly. *Neuroimage* 25, 783–792. doi: 10.1016/j.neuroimage.2004.12.036
- den Heijer, T., Geerlings, M. I., Hoebeek, F. E., Hofman, A., Koudstaal, P. J., and Breteler, M. M. (2006). Use of hippocampal and amygdalar volumes on magnetic resonance imaging to predict dementia in cognitively intact elderly people. *Arch. Gen. Psychiatry* 63, 57–62. doi: 10.1001/archpsyc.63.1.57
- Desikan, R. S., Ségonne, F., Fischl, B., Quinn, B. T., Dickerson, B. C., Blacker, D., et al. (2006). An automated labeling system for subdividing the human cerebral cortex on MRI scans into gyral based regions of interest. *Neuroimage* 31, 968–980. doi: 10.1016/j.neuroimage.2006.01.021
- Devanand, D. P., Pradhaban, G., Liu, X., Khandji, A., De Santi, S., Segal, S., et al. (2007). Hippocampal and entorhinal atrophy in mild cognitive impairment prediction of Alzheimer disease. *Neurology* 68, 828–836. doi: 10.1212/01.wnl.0000256697.20968.d7
- Dickerson, B., Stoub, T., Shah, R., Sperling, R., Killiany, R., Albert, M., et al. (2011). Alzheimer-signature MRI biomarker predicts AD dementia in cognitively normal adults. *Neurology* 76, 1395–1402. doi: 10.1212/WNL.0b013e3182166e96
- Ding, S.-L., and Van Hoesen, G. W. (2010). Borders, extent, and topography of human perirhinal cortex as revealed using multiple modern neuroanatomical and pathological markers. *Hum. Brain Mapp.* 31, 1359–1379. doi: 10.1002/hbm.20940
- Durrleman, S., Fletcher, T., Gerig, G., and Niethammer, M. (2012). "Spatio-temporal image analysis for longitudinal and time-series image data," in *Second International Workshop, STIA 2012, Held in Conjunction with MICCAI 2012* (Nice: Springer). doi: 10.1007/978-3-642-33555-6
- Huntgeburth, S. C., and Petrides, M. (2012). Morphological patterns of the collateral sulcus in the human brain. *Eur. J. Neurosci.* 35, 1295–1311. doi: 10.1111/j.1460-9568.2012.08031.x
- Insausti, R., Juottonen, K., Soininen, H., Insausti, A. M., Partanen, K., Vainio, P., et al. (1998). MR volumetric analysis of the human entorhinal, perirhinal, and temporopolar cortices. *Am. J. Neuroradiol.* 19, 659–671. doi: 10.1016/S0197-4580(98)00007-4
- Jack, C. R., Shiung, M. M., Gunter, J. L., O'Brien, P. C., Weigand, S. D., Knopman, D. S., et al. (2004). Comparison of different MRI brain atrophy rate measures with clinical disease progression in AD. *Neurology* 62, 591–600. doi: 10.1212/01.WNL.0000110315.26026.EF
- Kantarci, K., and Jack, C. R. (2003). Neuroimaging in Alzheimer disease: an evidence-based review. *Neuroimaging Clin.* 13, 197–209. doi: 10.1016/S1052-5149(03)00025-X
- Kantarci, K., and Jack, C. R. (2004). Quantitative magnetic resonance techniques as surrogate markers of Alzheimer's disease. *NeuroRx* 1, 196–205. doi: 10.1602/neurorx.1.2.196

- Krimer, L. S., Hyde, T. M., Herman, M. M., and Saunders, R. C. (1997). The entorhinal cortex: an examination of cyto- and myeloarchitectonic organization in humans. *Cereb. Cortex* 7, 722–731. doi: 10.1093/cercor/7.8.722
- Kulason, S., Tward, D. J., Brown, T., Sicat, C. S., Liu, C.-F., Ratnanather, J. T., et al. (2019). Cortical thickness atrophy in the transentorhinal cortex in mild cognitive impairment. *Neuroimage Clin.* 21:101617. doi: 10.1016/j.nicl.2018.101617
- La Joie, R., Perrotin, A., Barré, L., Hommet, C., Mézenge, F., Ibazizene, M., et al. (2012). Region-specific hierarchy between atrophy, hypometabolism, and β -amyloid (A β) load in Alzheimer's disease dementia. *J. Neurosci.* 32, 16265–16273. doi: 10.1523/JNEUROSCI.2170-12.2012
- Ma, J., Miller, M. I., Trouné, A., and Younes, L. (2008). Bayesian template estimation in computational anatomy. *Neuroimage* 42, 252–261. doi: 10.1016/j.neuroimage.2008.03.056
- Maass, A., Berron, D., Libby, L. A., Ranganath, C., and Düzel, E. (2015). Functional subregions of the human entorhinal cortex. *eLife* 4:e06426. doi: 10.7554/eLife.06426
- Miller, M. I., Ratnanather, J. T., Tward, D. J., Brown, T., Lee, D. S., Ketcha, M., et al. (2015a). Network neurodegeneration in Alzheimer's disease via MRI based shape diffeomorphometry and high-field atlas. *Front. Bioeng. Biotechnol.* 3:54. doi: 10.3389/fbioe.2015.00054
- Miller, M. I., Younes, L., Ratnanather, J. T., Brown, T., Trinh, H., Lee, D. S., et al. (2015b). Amygdalar atrophy in symptomatic Alzheimer's disease based on diffeomorphometry: the BIOCARD cohort. *Neurobiol. Aging* 36:S3–S10. doi: 10.1016/j.neurobiolaging.2014.06.032
- Miller, M. I., Younes, L., Ratnanather, J. T., Brown, T., Trinh, H., Postell, E., et al. (2013). The diffeomorphometry of temporal lobe structures in preclinical Alzheimer's disease. *Neuroimage Clin.* 3, 352–360. doi: 10.1016/j.nicl.2013.09.001
- Nelson, P. T., Alafuzoff, I., Bigio, E. H., Bouras, C., Braak, H., Cairns, N. J., et al. (2012). Correlation of Alzheimer disease neuropathologic changes with cognitive status: a review of the literature. *J. Neuropathol. Exp. Neurol.* 71, 362–381. doi: 10.1097/NEN.0b013e31825018f7
- Nichols, T., and Hayasaka, S. (2003). Controlling the familywise error rate in functional neuroimaging: a comparative review. *Stat. Methods Med. Res.* 12, 419–446. doi: 10.1191/0962280203sm341ra
- Olsen, R. K., Carr, V. A., Daugherty, A. M., La Joie, R., Amaral, R. S., Amunts, K., et al. (2019). Progress update from the hippocampal subfields group. *Alzheimers Dement. Diagn. Assess. Dis. Monitor.* 11, 439–449. doi: 10.1016/j.dadm.2019.04.001
- Pettigrew, C., Soldan, A., Zhu, Y., Wang, M.-C., Moghekar, A., Brown, T., et al. (2016). Cortical thickness in relation to clinical symptom onset in preclinical AD. *Neuroimage Clin.* 12, 116–122. doi: 10.1016/j.nicl.2016.06.010
- Ratnanather, J. T., Arguillere, S., Kuttan, K. S., Hubka, P., Kral, A., and Younes, L. (2019). "Chapter 7: 3D normal coordinate systems for cortical areas," in *Mathematics of Shapes and Applications*, Vol. 37 (Singapore: World Scientific), 167–180. doi: 10.1142/9789811200137_0007
- Soldan, A., Pettigrew, C., Lu, Y., Wang, M.-C., Selnes, O., Albert, M., et al. (2015). Relationship of medial temporal lobe atrophy, APOE genotype, and cognitive reserve in preclinical Alzheimer's disease. *Hum. Brain Mapp.* 36, 2826–2841. doi: 10.1002/hbm.22810
- Sperling, R. A., Aisen, P. S., Beckett, L. A., Bennett, D. A., Craft, S., Fagan, A. M., et al. (2011). Toward defining the preclinical stages of Alzheimer's disease: recommendations from the National Institute on Aging-Alzheimer's Association workgroups on diagnostic guidelines for Alzheimer's disease. *Alzheimers Dement.* 7, 280–292. doi: 10.1016/j.jalz.2011.03.003
- Tang, X., Miller, M. I., and Younes, L. (2017). Biomarker change-point estimation with right censoring in longitudinal studies. *Ann. Appl. Stat.* 11:1738. doi: 10.1214/17-AOAS1056
- Tward, D., Miller, M., Alzheimer's Disease Neuroimaging Initiative (2017a). "Unbiased diffeomorphic mapping of longitudinal data with simultaneous subject specific template estimation," in *Graphs in Biomedical Image Analysis, Computational Anatomy and Imaging Genetics* (Cham: Springer), 125–136. doi: 10.1007/978-3-319-67675-3_12
- Tward, D. J., Sicat, C. S., Brown, T., Bakker, A., Gallagher, M., Albert, M., et al. (2017b). Entorhinal and transentorhinal atrophy in mild cognitive impairment using longitudinal diffeomorphometry. *Alzheimers Dement.* 9, 41–50. doi: 10.1016/j.dadm.2017.07.005
- Wolk, D. A., Das, S. R., Mueller, S. G., Weiner, M. W., Yushkevich, P. A., Initiative, A. D. N., et al. (2017). Medial temporal lobe subregional morphometry using high resolution MRI in Alzheimer's disease. *Neurobiol. Aging* 49, 204–213. doi: 10.1016/j.neurobiolaging.2016.09.011
- Xie, L., Das, S. R., Wisse, L. E., Ittyerah, R., Yushkevich, P. A., Wolk, D. A., et al. (2018). Early tau burden correlates with higher rate of atrophy in transentorhinal cortex. *J. Alzheimers Dis.* 62, 85–92. doi: 10.3233/JAD-170945
- Xie, L., Pluta, J. B., Das, S. R., Wisse, L. E., Wang, H., Mancuso, L., et al. (2017). Multi-template analysis of human perirhinal cortex in brain MRI: explicitly accounting for anatomical variability. *Neuroimage* 144, 183–202. doi: 10.1016/j.neuroimage.2016.09.070
- Younes, L., Albert, M., Miller, M. I., BIOCARD Research Team (2014). Inferring changepoint times of medial temporal lobe morphometric change in preclinical Alzheimer's disease. *Neuroimage Clin.* 5, 178–187. doi: 10.1016/j.nicl.2014.04.009

Conflict of Interest: The authors declare that the research was conducted in the absence of any commercial or financial relationships that could be construed as a potential conflict of interest.

Copyright © 2020 Kulason, Xu, Tward, Bakker, Albert, Younes, and Miller. This is an open-access article distributed under the terms of the Creative Commons Attribution License (CC BY). The use, distribution or reproduction in other forums is permitted, provided the original author(s) and the copyright owner(s) are credited and that the original publication in this journal is cited, in accordance with accepted academic practice. No use, distribution or reproduction is permitted which does not comply with these terms.



miRNA Alterations Elicit Pathways Involved in Memory Decline and Synaptic Function in the Hippocampus of Aged Tg4-42 Mice

Yvonne Bouter¹, Tim Kacprowski², Fanny Rößler², Lars R. Jensen³, Andreas W. Kuss^{3*} and Thomas A. Bayer^{1*}

¹ Division of Molecular Psychiatry, Department of Psychiatry and Psychotherapy, University Medical Center Göttingen (UMG), Georg-August-University, Göttingen, Germany, ² Research Group Computational Systems Medicine, Chair of Experimental Bioinformatics, TUM School of Life Sciences Weihenstephan (WZW), Technical University of Munich (TUM), Weihenstephan, Germany, ³ Human Molecular Genetics Group, Department of Functional Genomics, Interfaculty Institute for Genetics and Functional Genomics, University Medicine Greifswald, Greifswald, Germany

OPEN ACCESS

Edited by:

Jie Tu,
Chinese Academy of Sciences (CAS),
China

Reviewed by:

Wang-Xia Wang,
University of Kentucky, United States
Nataliya G. Kolosova,
Russian Academy of Sciences, Russia

*Correspondence:

Andreas W. Kuss
kussa@uni-greifswald.de
Thomas A. Bayer
tbayer@gwdg.de

Specialty section:

This article was submitted to
Neurodegeneration,
a section of the journal
Frontiers in Neuroscience

Received: 06 July 2020

Accepted: 18 August 2020

Published: 10 September 2020

Citation:

Bouter Y, Kacprowski T, Rößler F,
Jensen LR, Kuss AW and Bayer TA
(2020) miRNA Alterations Elicit
Pathways Involved in Memory Decline
and Synaptic Function
in the Hippocampus of Aged Tg4-42
Mice. *Front. Neurosci.* 14:580524.
doi: 10.3389/fnins.2020.580524

The transcriptome of non-coding RNA (ncRNA) species is increasingly focused in Alzheimer's disease (AD) research. NcRNAs comprise, among others, transfer RNAs, long non-coding RNAs and microRNAs (miRs), each with their own specific biological function. We used smallRNASeq to assess miR expression in the hippocampus of young (3 month old) and aged (8 month old) Tg4-42 mice, a model system for sporadic AD, as well as age-matched wildtype controls. Tg4-42 mice express N-truncated A β ₄₋₄₂, develop age-related neuron loss, reduced neurogenesis and behavioral deficits. Our results do not only confirm known miR-AD associations in Tg4-42 mice, but more importantly pinpoint 22 additional miRs associated to the disease. Twenty-five miRs were differentially expressed in both aged Tg4-42 and aged wildtype mice while eight miRs were differentially expressed only in aged wildtype mice, and 33 only in aged Tg4-42 mice. No significant alteration in the miRNome was detected in young mice, which indicates that the changes observed in aged mice are down-stream effects of A β -induced pathology in the Tg4-42 mouse model for AD. Targets of those miRs were predicted using miRWalk. For miRs that were differentially expressed only in the Tg4-42 model, 128 targets could be identified, whereas 18 genes were targeted by miRs only differentially expressed in wildtype mice and 85 genes were targeted by miRs differentially expressed in both mouse models. Genes targeted by differentially expressed miRs in the Tg4-42 model were enriched for negative regulation of long-term synaptic potentiation, learning or memory, regulation of *trans*-synaptic signaling and modulation of chemical synaptic transmission obtained. This untargeted miR sequencing approach supports previous reports on the Tg4-42 mice as a valuable model for AD. Furthermore, it revealed miRs involved in AD, which can serve as biomarkers or therapeutic targets.

Keywords: miRNA transcriptome, miRNA-Seq, NGS, transgenic mouse model, Tg4-42, Alzheimer

INTRODUCTION

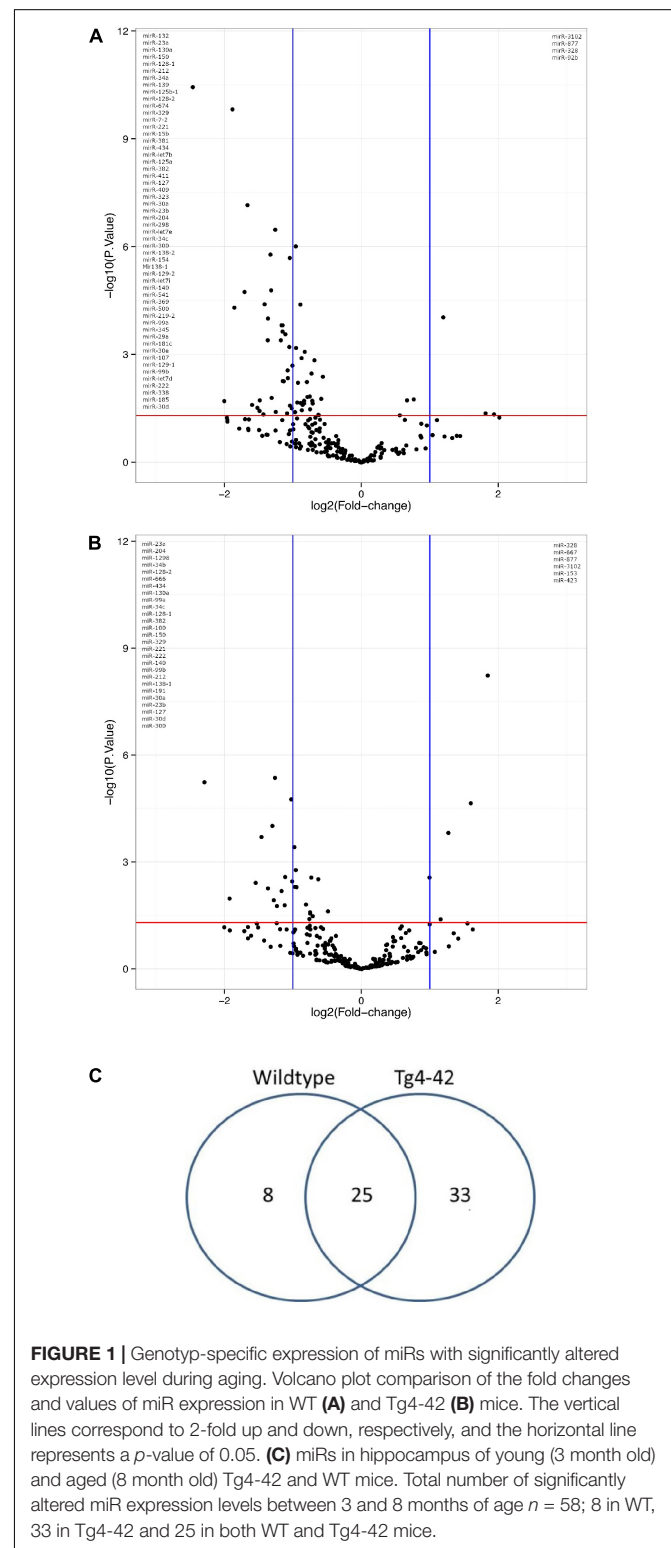
MiRs are short non-coding RNAs that are heavily involved in post-transcriptional regulation of gene expression through targeting specific mRNAs (Bartel, 2004). The miR transcriptome (miRNome) includes all miR species and renders a profile of gene regulation at the studied time point and location. Altered miR expression profiles therefore provide information not only about the miRs themselves, but also about their target genes and, hence, the regulated processes. As miRs have already been implicated in neurodevelopment and brain aging, as well as in synapse function and cognitive performance, in both, health and disease (Salta and De Strooper, 2012, 2017b), this information can pinpoint mechanisms involved in the molecular pathogenesis of Alzheimer's disease (AD). Furthermore, miRs can easily be targeted by artificial oligonucleotides to influence gene regulation for therapeutic processes (Roshan et al., 2009). Hence, miRNome profiling ultimately promotes the search for new biomarkers and therapeutics.

Next-generation sequencing (NGS) of the miR pool offers an unbiased technical approach to identify the miR signature of cells, tissues or organs. Previous reports have demonstrated the power of NGS to unravel the molecular profile of pathological alterations in neurodegenerative diseases like AD (Twine et al., 2011). Differentially expressed genes (DEGs) were identified by RNASeq of young, and aged Tg4-42 mice in comparison with 5XFAD mice, another AD mouse model (Bouter et al., 2014). Many of the DEGs specifically found in the 5XFAD model belong to neuroinflammatory processes typically associated with plaques. Other DEGs were found in both AD mouse models indicating common disease pathways associated with behavioral deficits and neuron loss. The 5XFAD model develops early plaque formation, intraneuronal A β aggregation, neuron loss, and behavioral deficits (Oakley et al., 2006; Jawhar et al., 2012). As such the 5XFAD model is widely used in the AD field. High-throughput RNASeq analysis of young 5XFAD mice, e.g., identified DEGs in the frontal cortex mainly associated with cardiovascular disease and DEGs in the cerebellum mainly associated with mitochondrial dysfunction (Kim et al., 2012).

A plethora of previous publications discuss miRs as potentially involved in the pathogenesis of AD and/or as putative biomarkers for AD including several systematic assessments of the importance of miRs in this disorder [reviewed for example by Salta and De Strooper (2012, 2017b), Angelucci et al. (2019), Wang et al. (2019)]. Notably, the expression of miR-338-5p was significantly down-regulated in the hippocampus of patients with AD and 5XFAD transgenic mice (Qian et al., 2019). The expression of miR-146a correlated with plaque load and synaptic pathology in Tg2576 and in 5XFAD mice (Li et al., 2011).

We have performed NGS of the miRNome of the hippocampus of young (3 month old) and aged (8 month old) Tg4-42 mice, which represent a unique model for sporadic AD. The Tg4-42 model expresses only wildtype non-mutant A β 4-42 and develops at the age of 8 months, severe neuron loss and hippocampus-related behavioral deficits (Bouter et al., 2013). At 3 months of age, Tg4-42 mice show reduced neurogenesis (Gerberding et al., 2019) and synaptic hyperexcitability

(Dietrich et al., 2018), which represents an early sign of AD-typical alteration. Reduced glucose metabolism detected by FDG-PET *in vivo* imaging (Bouter et al., 2019) correlates well with the observed neuron loss and neurological deficits at



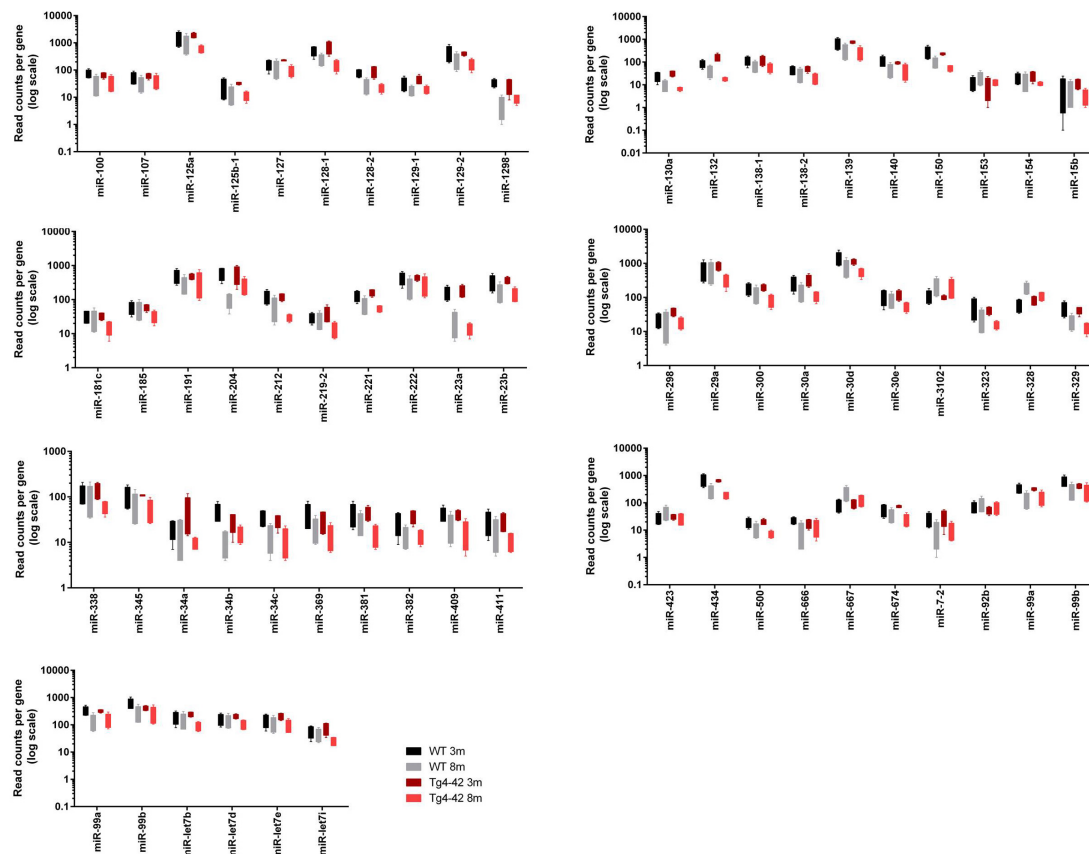


FIGURE 2 | Box plots of significantly altered miRNAs in hippocampus of young (3 month old; 3m) and aged (8 month old; 8m) Tg4-42 and WT.

8 months of age (Bouter et al., 2013). The aim of the current study was to identify miRNAs and their targets to unravel molecules and processes triggered by AD-typical memory deficits and hippocampal neuron death. Therefore, we compared the age of 3 months (prior to neuron loss and neurological alterations) with the age of 8 months (after onset of neuron loss and neurological alterations).

MATERIALS AND METHODS

Transgenic Mice

We used the transgenic mouse lines Tg4-42 kept on the C57BL/6J genetic background. Tg4-42 mice express human A β_{4-42} fused to the murine TRH signal peptide under the control of the neuronal Thy-1 promoter (Bouter et al., 2013). Young (3 month) and aged (8 month) Tg4-42 and age-matched wildtype control mice (WT, C57BL/6J) were studied. All animals were handled according to the German guidelines for animal care. All efforts were made to minimize suffering and the number of animals used for this study.

Tissue Harvesting

Mice were sacrificed via CO₂ anaesthetization followed by cervical dislocation. Brain hemispheres were carefully dissected

and the hippocampus removed, frozen on dry ice and stored at -80°C for subsequent use.

Small RNA Next-Generation Sequencing

Small RNA-isolation was performed using the miRvana miRNA Isolation Kit (Life Technologies) according to the manufacturer's instructions. For library preparation, we used the Ion Total RNA-Seq Kit v2 for Small RNA Libraries (Life Technologies) for sequencing on an Ion PGM system (Thermo Fisher Scientific) running Torrent Suite software 5.12.1., again following the instructions of the manufacturer. STAR v2.6.0a with default parameters was used to map the reads to the GRCm38 (mm10) mouse assembly (Dobin et al., 2013). Afterward, read counts per feature were determined with HTSeq v0.10.0 (Anders et al., 2015). Bam files were submitted to the European Nucleotide Archive¹ with the accession identification number of the project PRJEB39314.

Differential Expression Analysis

During quality control of the mapped data, RNAs with less than 10 readcounts across all samples were excluded and

¹<https://www.ebi.ac.uk/ena>

TABLE 1 | MiRs significantly altered in hippocampus between 3 and 8 month-old exclusively in Tg4-42 mice.

	Expression	References
miR-107	−0.7	Wang W.X. et al., 2011; Shu et al., 2018
miR-125a	−1.2	Ifrim et al., 2015
miR-125b-1	−1.4	Banzhaf-Strathmann et al., 2014; Lardenoije et al., 2015; Lu et al., 2017; Salta and De Strooper, 2017b; Elliott et al., 2018; Jin et al., 2018; Ottaviani et al., 2019
miR-129-1	−0.7	
miR-129-2	−0.9	Strickland et al., 2011
miR-132	−2.5	Majer et al., 2012; Freischmidt et al., 2013; Bicker et al., 2014; Essandoh et al., 2016; Tasaki et al., 2018
miR-138-2	−1.0	Boscher et al., 2019
miR-139	−1.4	Noh et al., 2014; Lardenoije et al., 2015; Salta and De Strooper, 2017b
miR-154	−0.9	
miR-15b	−1.2	
miR-181c	−0.8	Lardenoije et al., 2015; Villela et al., 2016
miR-185	−0.6	Forstner et al., 2013; Wen et al., 2018
miR-219-2	−0.8	
miR-298	−1.0	
miR-29a	−0.8	Bettens et al., 2009
miR-30e	−0.7	Margis et al., 2011; Lardenoije et al., 2015; Salta and De Strooper, 2017b
miR-323	−1.1	Che et al., 2019
miR-338	−0.6	Chun et al., 2017
miR-345	−0.8	Freiesleben et al., 2016; Wei et al., 2020
miR-34a	−1.5	Sun et al., 2018
miR-369	−0.9	Serpente et al., 2011
miR-381	−1.2	Li et al., 2020
miR-409	−1.1	Liu et al., 2019
miR-411	−1.1	
miR-500	−0.8	
miR-541	−0.9	Zhang et al., 2011
miR-674	−1.3	Lardenoije et al., 2015; Salta and De Strooper, 2017b
miR-7-2	−1.3	
miR-92b	+0.6	
miR-let7b	−1.2	Lehmann et al., 2012; Derkow et al., 2018
miR-let7d	−0.7	Singh et al., 2018
miR-let7e	−1.0	Derkow et al., 2018
miR-let7i	−0.9	

References are given for known links to Alzheimer's disease, other neurodegenerative disorders and/or brain function. **Supplementary Table S1** shows the entire list of miRs level changes. Decreased expression level at 8 month of age, −; increased expression level at 8 month of age, +.

technical replicates were collapsed after heatmap inspection (**Supplementary Figure S1**). Transcripts with less than 10 reads across all remaining samples were discarded. The heatmap in **Supplementary Figure S1** was compiled with variance-stabilized data, while the differential expression analyses were conducted on the raw count data, due to DESeq2's statistical model (Love et al., 2014). The comparisons were done across contrasts corresponding to the age groups or the genotypes, respectively. Correction for multiple testing was done via independent hypothesis weighting as implemented in DESeq2 (Love et al., 2014), and a result was deemed significant if FDR < 0.05."

MiR Target and Overrepresentation Analysis

For the target mining of differentially expressed miRs (FDR < 0.05) we used miRWalk version 3 (Sticht et al., 2018),

which uses a random forest based algorithm, and TarPmiR (Ding et al., 2016), to predict possible miR targets. It also allows to compare the results with the predictions of other target mining algorithms such as TargetScan (Agarwal et al., 2015) and miRDB (Chen and Wang, 2020), as well as validated interactions from miRTarBase (Chou et al., 2018). Only gene targets that were confirmed by at least two of these databases were considered for the further analysis to minimize false positives. The analysis required unique miR names mapped to the specific strand. Hence, we used both miR-3p and miR-5p, if available. The identified targets were then used to conduct a Gene Ontology (GO) (Rigden and Fernandez, 2018) overrepresentation analysis with the PANTHER algorithm (Mi et al., 2019) relying on the GO release of December 9th, 2019, to check for biological processes that are targeted by the differentially expressed miRs.

RESULTS

NGS of Non-coding RNAs in Mouse Hippocampus

Small RNASeq yielded 761,373 and 1,054,109 raw sequence reads for young and old wildtype (WT) mouse hippocampi, respectively. For young WT mice on average 160,723 reads ($n = 4$; on average 84% of raw reads) and for old WT mice 213,338 reads ($n = 4$; on average 81% of raw reads) per animal were mapped.

For Tg4-42 mice a total of 758,968 (4 young animals) and 2,252,799 (4 old animals, each sequenced twice) raw reads were produced. In young Tg4-42 mice, mapping was successful for on average 160,808 reads per sample (on average 85% of raw reads) and for old Tg4-42 mice on average 449,797 mapped reads per animal (224,899 reads per sample; on average 80% of raw reads) were obtained.

Analyses of miRs at 3 and 8 Months of Age in Tg4-42 and Wildtype Mice

In order to demonstrate the expression and significant distribution of identified miRs volcano plots were created (Figures 1A,B). In total, 237 miRs were detected. There was a significant change in expression of 58 miRs observed between young and aged Tg4-42, as well as between young and aged WT mice (Figure 1C). No significant differences were observed across genotypes within an age group (data not shown). Of 33 differentially expressed miRs exclusively found in aged Tg4-42 mice, some were reported to be associated with AD. The remaining miRs could now be associated with an AD-typical mouse model for the first time. Figure 2 demonstrates the levels of all miRs with a significantly altered expression level between 3 and 8 months of age either in Tg4-42, WT or in both. In aged Tg4-42 mice, mostly decreased levels of miRs have been observed.

Table 1 lists references for known links to AD, other neurodegenerative disorders and/or brain function. Five miRs

TABLE 2 | MiRs significantly altered in hippocampus between 3 and 8 month-old exclusively in wildtype mice.

	Expression	References
miR-100	−1.1	Lu et al., 2017; Elliott et al., 2018; Ottaviani et al., 2019
miR-1298	−1.9	
miR-153	+1.2	Gui et al., 2015
miR-191	−0.7	Smith et al., 2010
miR-34b	−1.5	
miR-423	+1.0	
miR-666	−1.4	
miR-667	+1.6	

References are given for known links to Alzheimer's disease, other neurodegenerative disorders and/or brain function. **Supplementary Table S1** shows the entire list of miRs level changes. Decreased expression level at 8 month of age, −; increased expression level at 8 month of age, +.

identified in aged WT mouse brain were increased and four decreased during aging (Table 2). MiRs found in both Tg4-42 and WT hippocampi were decreased during aging, only one was increased (Table 3). The GO annotation analysis of predicted miR targets in Tg4-42 revealed that reduced long-term synaptic potentiation, learning or memory, regulation of *trans*-synaptic signaling and modulation of chemical synaptic transmission obtained top scores (Figure 3A). None of these annotations were overrepresented in WT mice (Figure 3B). The GO analysis of predicted miR targets in either Tg4-42 or WT mice or both elicited also other cellular components (Table 4), molecular functions (Table 5) and biological processes (Table 6).

DISCUSSION

We performed NGS of the miRNome of the hippocampus of Tg4-42 mice, a model for sporadic AD. We assessed the pool of miRs before and after onset of AD-typical changes like gliosis, reduced glucose uptake into the brain, neuron

TABLE 3 | MiRs significantly altered in hippocampus between 3 and 8 month-old wildtype mice and Tg4-42 mice.

	Expression In WT mice	Expression In Tg4-42 mice	References
miR-127	−1.1	−0.7	Essandoh et al., 2016
miR-128-1	−1.7	↓ 1.2	Tiribuzi et al., 2014
miR-128-2	−1.4	−1.5	
miR-130a	−1.9	−1.3	Zhao et al., 2014
miR-138-1	−0.9	−0.8	Lin et al., 2018
miR-140	−0.9	−1.0	
miR-150	−1.8	−1.0	Punga et al., 2015
miR-204	−1.0	−2.3	Cammaerts et al., 2015
miR-212	−1.7	−0.8	Wang W.X. et al., 2011
miR-221	−1.3	−1.0	Seeley et al., 2018
miR-222	−0.6	−1.0	Wang et al., 2015; Seeley et al., 2018
miR-23a	−1.9	−2.6	Fenoglio et al., 2016
miR-23b	−1.0	−0.7	
miR-300	−1.0	−0.5	Li et al., 2018
miR-30a	−1.1	−0.7	Sun et al., 2016
miR-30d	−0.6	−0.6	
miR-3102	+1.2	+1.3	
miR-328	+0.7	+1.8	
miR-329	−1.3	−1.0	Urdinguio et al., 2010
miR-34c	−1.0	−1.2	Haramati et al., 2011
miR-382	−1.1	−1.1	Song et al., 2017
miR-434	−1.2	−1.3	
miR-877	+0.8	+1.5	Zhao et al., 2020
miR-99a	−0.8	−1.3	Bras et al., 2018
miR-99b	−0.7	−0.9	Cao et al., 2017

References are given for known links to Alzheimer's disease, other neurodegenerative disorders and/or brain function. **Supplementary Table S1** shows the entire list of miRs level changes. Decreased expression level at 8 month of age, −; increased expression level at 8 month of age, +.

TABLE 4 | GO annotation and pathway enrichment analysis of predicted miR targets on Cellular Components.

			Tg4-42			WT		
Gene ontology	Label		FDR	No. genes	No. miRs	FDR	No. genes	No. miRs
Significant in Tg4-42 and WT								
1	GO:0000785	Chromatin	2.24E-02	16	13	3.17E-02	11	9
2	GO:0005622	Intracellular	1.08E-04	161	34	8.21E-03	82	18
3	GO:0043231	Intracellular membrane-bounded organelle	3.51E-03	125	31	2.96E-02	66	18
4	GO:0043229	Intracellular organelle	1.18E-02	137	33	3.75E-02	73	18
5	GO:0005634	Nucleus	8.52E-03	89	30	1.56E-02	52	17
6	GO:0043226	Organelle	4.61E-03	142	33	8.78E-03	76	18
Significant in Tg4-42 only								
1	GO:0110165	Cellular anatomical entity	1.11E-02	189	35	2.87E-01	93	19
2	GO:0005694	Chromosome	4.53E-02	23	15	2.32E-01	13	9
3	GO:0043227	Membrane-bounded organelle	3.42E-03	132	32	7.72E-02	68	19
4	GO:0098794	Postsynapse	2.73E-02	18	10	9.06E-01	8	7
5	GO:0032991	Protein-containing complex	9.02E-03	76	26	1.00E+0	34	12
6	GO:0045202	Synapse	4.25E-03	31	15	1.00E+0	12	7
7	GO:0097060	Synaptic membrane	2.43E-02	14	7	1.00E+0	5	4
Significant in WT only								
1	GO:0031981	Nuclear lumen	1.65E-01	54	24	3.20E-02	35	13

Benjamini–Hochberg False Discovery Rate (FDR).

loss and loss of reference memory (Bouter et al., 2013, 2019; Dietrich et al., 2018; Gerberding et al., 2019). The Tg4-42 mouse model is one of few mouse models developing neuron death in the CA1 region of the hippocampus (Bayer and Wirths, 2014), as such it might provide a powerful tool for preclinical drug testing and identification of the underlying molecular pathways driving AD pathology. The difference of diverse miR levels between 3 and 8 months of age in Tg4-42 elicits the AD-typical effects after onset of neuron loss and behavioral deficits. We cannot draw any conclusion on the difference in miR levels in aged mice, as the normal lifespan is at least 24 months.

At least 1% of the human genome encodes miR and every miR can regulate up to 200 mRNAs suggesting that dysregulation of miR expression could be associated with several human pathological conditions including central neurological disorders (Angelucci et al., 2019). In addition to NGS of the miRs, we have performed a search for the targets of identified miRs using state-of-the-art bioinformatics and addressed the question whether the affected processes are meaningful in the context of known AD-typical changes in the Tg4-42 mouse model.

MiRs Identified in the Hippocampus of 8 Month Old Tg4-42 Mice

A total of 33 miRs were altered in the hippocampus between 3 and 8 month-old exclusively found in Tg4-42 mice. All but one was significantly decreased at the age of 8 months. Some of the miRs identified were already linked to AD pathology, while others could be associated to AD for the first time. In gray matter of the brain of patients with AD, down-regulation

of a set of miRs (including several miR-15/107 genes and miR-29 paralogs) correlated strongly with the density of amyloid plaques. MiR-212 was found decreased in white matter, whereas miR-424 was upregulated in AD (Wang A. et al., 2011). Expression of miR-107 and BACE1 mRNA correlated with alterations in brain pathology in individuals with mild cognitive impairment (Wang et al., 2016). MiR-107 reversed the impairments of spatial memory and long-term potentiation caused by intraventricular injection of A β _{1–42} (Shu et al., 2018). MiR-125a may have a role in regulating the translation of PSD-95 mRNA. Impairments in the local synthesis of PSD-95, important for synaptic structure and function, may affect dendritic spine development and synaptic plasticity in fragile X syndrome (Ifrim et al., 2015). MiR-125b-1 induced tau hyperphosphorylation and cognitive deficits in AD (Banzhaf-Strathmann et al., 2014), may be involved in the regulation of inflammatory factors and oxidative stress by SphK1 (Jin et al., 2018). It has been found to be associated with other neurodegenerative diseases as well (Lardenoije et al., 2015; Salta and De Strooper, 2017b). TGF- β induced miR-100 and miR-125b (Ottaviani et al., 2019). MiR-100 and miR-125b coordinately suppress Wnt/b-catenin negative regulators, thereby increasing Wnt signaling (Lu et al., 2017). A pathogenic-positive feedback loop has been identified in which A β induced Dickkopf-1 expression activating non-canonical Wnt signaling, promoting synapse loss and enhancing A β production (Elliott et al., 2018). MiR-129-2 was reported to be down-regulated in spinal cord (Strickland et al., 2011). MiR-132 is involved in synaptic plasticity (Bicker et al., 2014) and may be associated with TDP-43 binding in amyotrophic lateral sclerosis (Freischmidt et al., 2013). Prion-infected hippocampal neurons elicited altered expression of miR-132 (Majer et al., 2012) and have been discussed to play an important role in inflammation control

TABLE 5 | GO annotation and pathway enrichment analysis of predicted miR targets on Molecular Function.

Gene ontology	Label	Tg4-42			WT			
		FDR	No. genes	No. miRs	FDR	No. genes	No. miRs	
Significant in Tg4-42 and WT								
1	GO:0005488	Binding	9.51E-05	159	36	1.22E-02	79	20
2	GO:0035326	cis-regulatory region binding	1.46E-03	20	15	2.17E-02	12	10
3	GO:0000987	cis-regulatory region sequence-specific DNA binding	1.35E-03	20	15	2.16E-02	12	10
4	GO:0003677	DNA binding	2.45E-04	42	21	1.69E-02	24	14
5	GO:0000981	DNA-binding transcription factor activity, RNA polymerase II-specific	2.35E-04	25	17	1.56E-02	14	11
6	GO:1901363	Heterocyclic compound binding	1.10E-03	75	28	2.48E-02	39	16
7	GO:0003676	Nucleic acid binding	1.08E-03	53	24	2.41E-02	29	16
8	GO:0097159	organic cyclic compound binding	1.62E-03	75	28	3.45E-02	39	16
9	GO:0005515	Protein binding	4.25E-06	128	33	3.60E-04	67	16
10	GO:0001067	regulatory region nucleic acid binding	5.16E-04	26	19	1.45E-02	15	12
11	GO:0000978	RNA polymerase II cis-regulatory region sequence-specific DNA binding	1.15E-03	20	15	2.09E-02	12	10
12	GO:0001012	RNA polymerase II regulatory region DNA binding	4.73E-04	25	18	2.00E-02	14	11
13	GO:0000977	RNA polymerase II regulatory region sequence-specific DNA binding	4.59E-04	25	18	1.99E-02	14	11
14	GO:0043565	sequence-specific DNA binding	1.03E-03	29	18	1.47E-02	18	12
15	GO:1990837	sequence-specific double-stranded DNA binding	1.24E-03	25	18	2.95E-02	14	11
16	GO:0008134	Transcription factor binding	1.06E-02	19	11	3.04E-02	12	6
17	GO:0140110	Transcription regulator activity	1.25E-04	36	20	1.77E-02	19	12
18	GO:0044212	Transcription regulatory region DNA binding	5.32E-04	26	19	1.73E-02	15	12
19	GO:0000976	Transcription regulatory region sequence-specific DNA binding	6.36E-04	25	18	2.27E-02	14	11
Significant in Tg4-42 only								
1	GO:0001216	DNA-binding transcription activator activity	3.00E-02	14	10	7.50E-02	9	7
2	GO:0001228	DNA-binding transcription activator activity, RNA polymerase II-specific	2.92E-02	14	10	7.85E-02	9	7
3	GO:0003700	DNA-binding transcription factor activity	1.06E-04	30	18	7.46E-02	14	11
4	GO:0140297	DNA-binding transcription factor binding	1.14E-02	13	8	7.67E-02	8	5
5	GO:0001217	DNA-binding transcription repressor activity	1.10E-02	11	8	1.00E+0	4	4
6	GO:0001227	DNA-binding transcription repressor activity, RNA polymerase II-specific	1.14E-02	11	8	1.00E+0	4	4
7	GO:0003690	Double-stranded DNA binding	1.30E-03	26	18	6.18E-02	14	11
8	GO:0043167	Ion binding	1.17E-02	77	30	8.46E-01	37	16
9	GO:0019904	Protein domain specific binding	4.26E-03	21	14	1.00E+0	6	4

Benjamini–Hochberg False Discovery Rate (FDR).

(Essandoh et al., 2016). MiR profiling in the human brain has revealed miR-132 as one of the most severely down-regulated miRs at the intermediate and late Braak stages of AD, as well as in other neurodegenerative disorders (Salta and De Strooper, 2017a). MiR-132 has been implicated in synaptic plasticity together with miR-134 and miR-138 (Bicker et al., 2014). Duplication of the miR-138-2 locus was observed exclusively in early onset AD cases and miR-138 overexpression *in vitro* induced A β production and tau phosphorylation (Boscher et al., 2019). Interestingly, levels of miR-132 and miR-138-2 were significantly decreased in aged Tg4-42 mice indicating that dendritic mRNA transport and local translation in the postsynaptic compartment play an important role in synaptic plasticity, learning and memory (Bicker et al., 2014) in this model system for AD. *In vitro* A β treatment increased the expression of miR-139 targets (Noh et al., 2014), and has been found to be associated with other neurodegenerative diseases (Lardenoije et al., 2015; Salta and De Strooper, 2017b). MiR-181c correlated with genome-wide DNA methylation changes

of ncRNAs in patients with AD (Villela et al., 2016), and is involved in epigenetics of aging and neurodegeneration (Lardenoije et al., 2015). Overexpression of miR-185 inhibits autophagy and apoptosis of dopaminergic neurons by regulating the AMPK/mTOR signaling pathway in Parkinson's disease (Bicker et al., 2014). The 22q11.2 deletion is a known genetic risk factor for schizophrenia and mouse models of 22q11.2DS have demonstrated down-regulation of miR-185 in key brain areas of affected individuals. This reduction was associated with dendritic and spine development deficits in hippocampal neurons (Freischmidt et al., 2013). Association studies in the 3'UTR of BACE1 and the miR-29 gene cluster did not identify an association with AD. A weak statistical interaction was observed between rs535860 (BACE1 3'UTR) and rs34772568 (near miR-29a). The authors concluded a major contribution of this miR (Bettens et al., 2009). MiR-30a has been found to be associated with Parkinson disease (Margis et al., 2011) as well as Huntington disease (Lardenoije et al., 2015; Salta and De Strooper, 2017b). MiR-338-3p depletion has been shown to be important for

TABLE 6 | GO annotation and pathway enrichment analysis of predicted miR targets on Biological Process.

			Tg4-42			WT		
Gene ontology		Label	FDR	No. genes	No. miRs	FDR	No. genes	No. miRs
Significant in Tg4-42 and WT								
1	GO:0048856	Anatomical structure development	1.05E-05	85	32	2.28E-02	42	14
2	GO:0048646	Anatomical structure formation involved in morphogenesis	1.83E-02	21	11	2.61E-03	16	8
3	GO:0009653	Anatomical structure morphogenesis	8.34E-05	46	22	4.24E-05	30	12
4	GO:0048513	Animal organ development	1.22E-03	53	24	5.78E-03	31	12
5	GO:0007420	Brain development	1.59E-03	19	11	2.81E-03	13	6
6	GO:0000902	Cell morphogenesis	4.41E-02	17	11	3.64E-02	12	7
7	GO:0032989	Cellular component morphogenesis	3.30E-02	19	12	1.17E-02	14	8
8	GO:0016043	Cellular component organization	8.48E-05	80	24	5.23E-03	43	11
9	GO:0071840	Cellular component organization or biogenesis	1.67E-04	81	24	6.33E-03	44	11
10	GO:0007417	Central nervous system development	1.44E-02	20	12	3.08E-02	13	6
11	GO:0048598	Embryonic morphogenesis	2.44E-02	16	12	2.65E-03	13	8
12	GO:0007167	Enzyme linked receptor protein signaling pathway	2.72E-03	17	12	3.38E-03	12	6
13	GO:0060322	Head development	3.91E-03	19	11	5.83E-03	13	6
14	GO:0007275	Multicellular organism development	1.30E-04	77	29	4.27E-03	42	14
15	GO:0009890	Negative regulation of biosynthetic process	3.09E-05	37	23	4.01E-02	18	12
16	GO:2000113	Negative regulation of cellular macromolecule biosynthetic process	3.14E-05	35	22	4.08E-02	17	12
17	GO:0010629	Negative regulation of gene expression	1.15E-05	39	23	1.61E-02	20	13
18	GO:0010605	Negative regulation of macromolecule metabolic process	2.61E-05	50	23	4.26E-02	25	13
19	GO:0051172	Negative regulation of nitrogen compound metabolic process	2.58E-05	48	22	4.97E-02	23	12
20	GO:1903507	Negative regulation of nucleic acid-templated transcription	8.74E-05	31	20	2.82E-02	16	11
21	GO:0045934	Negative regulation of nucleobase-containing compound metabolic process	3.80E-05	35	20	1.84E-02	18	11
22	GO:1902679	Negative regulation of RNA biosynthetic process	8.73E-05	31	20	2.80E-02	16	11
23	GO:0051253	Negative regulation of RNA metabolic process	5.03E-05	33	20	2.14E-02	17	11
24	GO:0045892	Negative regulation of transcription, DNA-templated	8.63E-05	31	20	2.76E-02	16	11
25	GO:0007399	Nervous system development	1.52E-03	43	20	2.46E-02	24	10
26	GO:0048518	Positive regulation of biological process	9.98E-07	97	30	7.35E-05	52	15
27	GO:0009891	Positive regulation of biosynthetic process	4.06E-05	42	22	4.52E-05	27	12
28	GO:0031328	Positive regulation of cellular biosynthetic process	2.76E-05	42	22	3.37E-05	27	12
29	GO:0031325	Positive regulation of cellular metabolic process	9.67E-07	64	28	1.12E-05	38	14
30	GO:0048522	Positive regulation of cellular process	7.16E-07	90	28	1.78E-05	50	14
31	GO:0010628	Positive regulation of gene expression	9.37E-08	49	22	2.74E-05	28	12

(Continued)

TABLE 6 | Continued

	Gene ontology	Label	Tg4-42			WT		
			FDR	No. genes	No. miRs	FDR	No. genes	No. miRs
32	GO:0010557	Positive regulation of macromolecule biosynthetic process	7.11E-06	42	22	4.21E-05	26	12
33	GO:0010604	Positive regulation of macromolecule metabolic process	1.33E-07	66	28	2.40E-05	37	14
34	GO:0009893	Positive regulation of metabolic process	7.36E-07	68	29	2.64E-05	38	14
35	GO:0051173	Positive regulation of nitrogen compound metabolic process	2.30E-06	61	28	1.51E-05	37	14
36	GO:1903508	Positive regulation of nucleic acid-templated transcription	3.00E-06	39	22	1.58E-05	25	12
37	GO:0045935	Positive regulation of nucleobase-containing compound metabolic process	1.21E-07	46	25	9.54E-06	28	13
38	GO:1902680	Positive regulation of RNA biosynthetic process	2.83E-06	39	22	1.37E-05	25	12
39	GO:0051254	Positive regulation of RNA metabolic process	2.66E-08	45	25	1.64E-05	27	13
40	GO:0045944	Positive regulation of transcription by RNA polymerase II	1.07E-03	28	16	4.64E-04	19	10
41	GO:0045893	Positive regulation of transcription, DNA-templated	7.21E-06	38	21	1.80E-05	25	12
42	GO:0022603	Regulation of anatomical structure morphogenesis	9.88E-04	27	16	3.42E-02	15	9
43	GO:0009889	Regulation of biosynthetic process	1.03E-08	73	28	6.46E-04	35	14
44	GO:0031326	Regulation of cellular biosynthetic process	9.92E-09	73	28	5.24E-04	35	14
45	GO:2000112	Regulation of cellular macromolecule biosynthetic process	1.02E-08	69	27	3.29E-04	34	14
46	GO:0031323	Regulation of cellular metabolic process	1.18E-08	96	30	3.35E-04	46	15
47	GO:0010468	regulation of gene expression	5.80E-09	78	27	6.35E-04	36	14
48	GO:0010556	Regulation of macromolecule biosynthetic process	9.78E-09	71	28	4.07E-04	34	14
49	GO:0060255	Regulation of macromolecule metabolic process	1.05E-08	96	30	1.33E-03	45	15
50	GO:0019222	regulation of metabolic process	1.26E-08	100	31	2.53E-03	46	15
51	GO:0051171	Regulation of nitrogen compound metabolic process	1.03E-08	92	30	3.23E-04	45	15
52	GO:1903506	Regulation of nucleic acid-templated transcription	3.18E-08	62	26	3.24E-04	31	13
53	GO:0019219	Regulation of nucleobase-containing compound metabolic process	2.72E-08	69	29	2.01E-04	35	14
54	GO:0080090	Regulation of primary metabolic process	9.49E-09	95	30	3.46E-04	45	15
55	GO:2001141	Regulation of RNA biosynthetic process	3.06E-08	62	26	3.16E-04	31	13
56	GO:0051252	Regulation of RNA metabolic process	9.26E-09	67	29	3.19E-04	33	14
57	GO:0006357	Regulation of transcription by RNA polymerase II	8.21E-07	46	23	5.09E-04	24	13
58	GO:0006355	Regulation of transcription, DNA-templated	6.53E-08	61	25	3.38E-04	31	13
59	GO:0048731	System development	3.77E-05	72	28	2.69E-03	39	13
60	GO:0009888	Tissue development	3.53E-02	30	17	3.96E-02	19	11
61	GO:0035239	Tube morphogenesis	2.66E-03	20	10	2.96E-02	12	7

(Continued)

TABLE 6 | Continued

			Tg4-42			WT		
Gene ontology		Label	FDR	No. genes	No. miRs	FDR	No. genes	No. miRs
Significant in Tg4-42 only								
1	GO:0009887	Animal organ morphogenesis	2.48E-02	22	15	2.10E-01	12	9
2	GO:0008306	Associative learning	4.10E-02	6	5	1.00E+00	2	1
3	GO:0007610	Behavior	1.71E-03	20	12	9.40E-01	7	5
4	GO:0065007	Biological regulation	7.24E-04	143	35	3.44E-01	67	16
5	GO:0048514	Blood vessel morphogenesis	2.02E-02	13	8	9.93E-01	5	4
6	GO:0048468	Cell development	1.12E-04	39	19	4.83E-01	16	9
7	GO:0030154	Cell differentiation	1.09E-03	61	26	4.39E-01	28	13
8	GO:0034330	Cell junction organization	5.87E-03	15	11	3.88E-01	7	4
9	GO:0048667	Cell morphogenesis involved in neuron differentiation	2.35E-02	13	9	1.14E-01	8	6
10	GO:0032990	Cell part morphogenesis	1.22E-02	15	11	8.20E-02	9	7
11	GO:0048858	Cell projection morphogenesis	7.70E-03	15	11	6.72E-02	9	7
12	GO:0048869	cellular developmental process	1.78E-03	61	26	4.59E-01	28	13
13	GO:0044260	Cellular macromolecule metabolic process	5.72E-04	63	24	5.02E-01	29	8
14	GO:0044237	Cellular metabolic process	4.38E-02	80	28	1.00E+00	33	9
15	GO:0009987	Cellular process	1.28E-02	155	37	1.00E+00	69	16
16	GO:0044267	Cellular protein metabolic process	2.83E-02	45	20	5.60E-01	22	8
17	GO:0006464	cellular protein modification process	8.05E-03	40	19	9.41E-02	22	8
18	GO:0070887	Cellular response to chemical stimulus	1.47E-03	44	19	2.56E-01	21	8
19	GO:0006974	Cellular response to DNA damage stimulus	2.24E-02	16	9	1.00E+00	3	3
20	GO:0071495	Cellular response to endogenous stimulus	3.29E-03	23	14	2.78E-01	11	6
21	GO:0071363	Cellular response to growth factor stimulus	1.19E-02	13	11	2.08E-01	7	5
22	GO:0071310	Cellular response to organic substance	1.70E-03	37	18	1.68E-01	18	8
23	GO:0033554	Cellular response to stress	2.60E-02	27	15	1.00E+00	8	6
24	GO:0050890	Cognition	8.16E-04	14	11	6.99E-01	5	4
25	GO:1904888	Cranial skeletal system development	4.16E-02	5	5	3.06E-01	3	3
26	GO:0007010	Cytoskeleton organization	1.23E-02	24	15	2.90E-01	12	5
27	GO:0048589	Developmental growth	2.96E-02	13	7	1.34E-01	8	6
28	GO:0032502	Developmental process	4.12E-05	87	32	6.05E-02	42	14
29	GO:0009790	Embryo development	3.48E-02	24	15	5.95E-02	15	9
30	GO:0060429	Epithelium development	2.60E-02	22	14	1.05E-01	13	10
31	GO:0007186	G protein-coupled receptor signaling pathway	1.82E-02	4	3	9.95E-01	3	2
32	GO:0035195	Gene silencing by miRNA	7.35E-03	5	5	6.48E-01	2	2
33	GO:0048699	Generation of neurons	1.40E-03	35	17	1.12E-01	18	10
34	GO:0040007	Growth	3.84E-02	13	7	1.51E-01	8	6
35	GO:0035556	Intracellular signal transduction	3.13E-03	30	15	8.90E-01	12	7

(Continued)

TABLE 6 | Continued

	<i>Gene ontology</i>	<i>Label</i>	Tg4-42			WT		
			<i>FDR</i>	<i>No. genes</i>	<i>No. miRs</i>	<i>FDR</i>	<i>No. genes</i>	<i>No. miRs</i>
36	GO:0070059	Intrinsic apoptotic signaling pathway in response to endoplasmic reticulum stress	4.26E-02	4	4	6.05E-01	2	2
37	GO:0007612	Learning	6.44E-03	9	8	9.88E-01	3	2
38	GO:0007611	Learning or memory	2.69E-04	14	11	5.76E-01	5	4
39	GO:0007616	Long-term memory	6.81E-03	5	5	1.15E-01	3	3
40	GO:0043170	Macromolecule metabolic process	3.88E-04	76	28	9.76E-01	32	9
41	GO:0043412	Macromolecule modification	1.78E-02	41	19	1.84E-01	22	8
42	GO:0007613	Memory	2.35E-03	9	8	3.43E-01	4	4
43	GO:0035278	miRNA mediated inhibition of translation	2.69E-02	3	3	1.00E+00	1	1
44	GO:0050804	Modulation of chemical synaptic transmission	2.01E-04	19	12	8.98E-01	6	5
45	GO:0032501	Multicellular organismal process	1.82E-02	94	31	7.10E-01	45	14
46	GO:0061061	muscle structure development	2.24E-02	14	10	4.53E-01	7	5
47	GO:0048519	Negative regulation of biological process	7.27E-04	77	27	1.49E-01	38	13
48	GO:0009895	Negative regulation of catabolic process	4.44E-02	10	7	1.00E+00	3	3
49	GO:0010648	Negative regulation of cell communication	4.37E-02	26	12	1.00E+00	10	7
50	GO:0010721	Negative regulation of cell development	9.76E-03	13	8	1.00E+00	3	2
51	GO:0045596	Negative regulation of cell differentiation	1.89E-03	21	12	1.00E+00	6	5
52	GO:0034249	Negative regulation of cellular amide metabolic process	4.37E-02	7	7	1.00E+00	1	1
53	GO:0031327	Negative regulation of cellular biosynthetic process	1.75E-05	37	23	6.36E-02	17	12
54	GO:0031330	Negative regulation of cellular catabolic process	4.05E-02	9	6	1.00E+00	2	2
55	GO:0031324	Negative regulation of cellular metabolic process	3.16E-06	53	23	6.26E-02	24	12
56	GO:0048523	Negative regulation of cellular process	4.26E-04	72	25	1.06E-01	36	12
57	GO:0032269	Negative regulation of cellular protein metabolic process	4.24E-02	21	12	1.00E+00	8	6
58	GO:0051093	Negative regulation of developmental process	2.57E-03	25	14	7.96E-01	10	7
59	GO:1902532	Negative regulation of intracellular signal transduction	2.94E-02	14	8	8.35E-01	6	6
60	GO:0010558	Negative regulation of macromolecule biosynthetic process	4.95E-05	35	22	5.11E-02	17	12
61	GO:0051045	Negative regulation of membrane protein ectodomain proteolysis	1.03E-02	3	3	9.48E-02	2	2
62	GO:0009892	Negative regulation of metabolic process	3.02E-06	56	25	6.65E-02	26	13
63	GO:0051241	Negative regulation of multicellular organismal process	1.50E-02	27	16	5.08E-01	13	8
64	GO:0051961	Negative regulation of nervous system development	4.69E-02	11	7	1.00E+00	2	1
65	GO:0050768	Negative regulation of neurogenesis	3.01E-02	11	7	1.00E+00	2	1
66	GO:0043524	Negative regulation of neuron apoptotic process	2.88E-02	8	7	1.55E-01	5	5
67	GO:1901215	Negative regulation of neuron death	1.51E-02	10	9	1.29E-01	6	6
68	GO:0045665	Negative regulation of neuron differentiation	1.82E-02	10	7	1.00E+00	1	1
69	GO:2000635	Negative regulation of primary miRNA processing	3.82E-02	2	2	6.20E-01	1	1
70	GO:0048585	Negative regulation of response to stimulus	4.16E-02	29	13	1.00E+00	10	7

(Continued)

TABLE 6 | Continued

	<i>Gene ontology</i>	<i>Label</i>	Tg4-42			WT		
			<i>FDR</i>	<i>No. genes</i>	<i>No. miRs</i>	<i>FDR</i>	<i>No. genes</i>	<i>No. miRs</i>
71	GO:0023057	Negative regulation of signaling	4.42E-02	26	12	1.00E+00	10	7
72	GO:0000122	Negative regulation of transcription by RNA polymerase II	3.74E-03	22	15	4.21E-01	10	8
73	GO:0017148	Negative regulation of translation	2.46E-02	7	7	1.00E+00	1	1
74	GO:0040033	negative regulation of translation, ncRNA-mediated	2.70E-02	3	3	1.00E+00	1	1
75	GO:0022008	Neurogenesis	8.64E-04	37	19	1.45E-01	18	10
76	GO:0048666	Neuron development	2.70E-03	22	13	1.69E-01	11	7
77	GO:0030182	Neuron differentiation	2.64E-03	25	15	5.69E-02	14	9
78	GO:0031175	neuron projection development	1.78E-03	20	13	1.46E-01	10	7
79	GO:0048812	Neuron projection morphogenesis	6.34E-03	15	11	6.01E-02	9	7
80	GO:0006807	Nitrogen compound metabolic process	4.11E-02	74	27	1.00E+00	32	9
81	GO:0006996	Organelle organization	3.94E-03	51	21	5.06E-02	28	9
82	GO:0016310	Phosphorylation	4.05E-02	21	14	1.00E+00	9	6
83	GO:0120039	Plasma membrane bounded cell projection morphogenesis	6.89E-03	15	11	6.34E-02	9	7
84	GO:0045597	Positive regulation of cell differentiation	1.50E-02	24	13	8.00E-02	14	8
85	GO:0030307	Positive regulation of cell growth	3.58E-02	8	6	5.61E-01	4	4
86	GO:0048639	Positive regulation of developmental growth	1.63E-03	11	8	6.76E-01	4	4
87	GO:0051094	Positive regulation of developmental process	1.57E-02	30	15	2.09E-01	16	9
88	GO:0045927	Positive regulation of growth	1.40E-03	13	9	1.00E+00	4	4
89	GO:1900273	positive regulation of long-term synaptic potentiation	1.60E-02	4	3	1.00E+00	1	1
90	GO:0061014	Positive regulation of mRNA catabolic process	1.56E-02	5	5	1.00E+00	1	1
91	GO:0048636	Positive regulation of muscle organ development	1.57E-02	6	4	1.00E+00	1	1
92	GO:1901863	Positive regulation of muscle tissue development	2.84E-03	7	5	1.00E+00	2	2
93	GO:0050769	Positive regulation of neurogenesis	3.52E-02	15	8	1.56E-01	9	5
94	GO:0045666	Positive regulation of neuron differentiation	1.66E-02	14	8	6.05E-02	9	5
95	GO:0010976	Positive regulation of neuron projection development	2.09E-02	12	8	6.07E-02	8	5
96	GO:1900153	Positive regulation of nuclear-transcribed mRNA catabolic process, deadenylation-dependent decay	6.12E-03	4	4	1.00E+00	1	1
97	GO:0060213	Positive regulation of nuclear-transcribed mRNA poly(A) tail shortening	1.98E-03	4	4	1.00E+00	1	1
98	GO:0045844	Positive regulation of striated muscle tissue development	1.56E-02	6	4	1.00E+00	1	1
99	GO:0050806	Positive regulation of synaptic transmission	8.45E-03	9	8	1.00E+00	3	3
100	GO:0009791	Post-embryonic development	2.00E-02	7	7	7.25E-01	3	3
101	GO:0016441	Posttranscriptional gene silencing	1.38E-02	5	5	7.50E-01	2	2
102	GO:0035194	Posttranscriptional gene silencing by RNA	1.29E-02	5	5	7.29E-01	2	2
103	GO:0019538	Protein metabolic process	4.44E-02	51	23	1.00E+00	22	8
104	GO:0036211	Protein modification process	7.99E-03	40	19	9.33E-02	22	8

(Continued)

TABLE 6 | Continued

	<i>Gene ontology</i>	<i>Label</i>	Tg4-42			WT		
			<i>FDR</i>	<i>No. genes</i>	<i>No. miRs</i>	<i>FDR</i>	<i>No. genes</i>	<i>No. miRs</i>
105	GO:0006468	Protein phosphorylation	4.16E-02	17	11	4.21E-01	9	6
106	GO:0042981	Regulation of apoptotic process	2.00E-02	29	16	3.06E-01	15	9
107	GO:0050770	Regulation of axonogenesis	1.82E-02	9	6	6.59E-02	6	5
108	GO:0050789	regulation of biological process	1.53E-04	141	35	9.13E-02	67	16
109	GO:0065008	Regulation of biological quality	1.90E-05	69	23	1.68E-01	31	8
110	GO:0009894	Regulation of catabolic process	2.68E-03	22	15	3.68E-01	10	6
111	GO:0010646	Regulation of cell communication	1.14E-04	60	22	3.45E-01	26	12
112	GO:0060284	Regulation of cell development	2.47E-02	23	11	8.90E-01	10	5
113	GO:0045595	Regulation of cell differentiation	1.35E-03	38	17	6.79E-02	20	9
114	GO:0022604	Regulation of cell morphogenesis	4.39E-02	14	10	5.97E-01	7	5
115	GO:0042127	Regulation of cell population proliferation	2.30E-02	31	17	1.00E+00	10	7
116	GO:0034248	Regulation of cellular amide metabolic process	2.68E-02	12	9	1.00E+00	2	2
117	GO:0031329	Regulation of cellular catabolic process	1.96E-03	20	14	6.40E-01	8	5
118	GO:0051128	Regulation of cellular component organization	1.65E-03	46	23	1.50E-01	23	11
119	GO:0060341	Regulation of cellular localization	1.04E-03	23	11	6.31E-01	9	5
120	GO:0050794	Regulation of cellular process	8.35E-05	136	34	5.79E-02	65	15
121	GO:0032268	Regulation of cellular protein metabolic process	7.75E-03	44	23	4.38E-01	21	12
122	GO:0048638	Regulation of developmental growth	1.25E-02	13	9	8.77E-01	5	5
123	GO:0050793	Regulation of developmental process	5.53E-03	46	21	1.33E-01	24	10
124	GO:0040029	Regulation of gene expression, epigenetic	1.92E-02	9	7	1.00E+00	3	2
125	GO:0060968	Regulation of gene silencing	1.81E-02	6	6	1.00E+00	1	1
126	GO:0060964	Regulation of gene silencing by miRNA	7.93E-03	5	5	1.00E+00	1	1
127	GO:0060966	Regulation of gene silencing by RNA	1.02E-02	5	5	1.00E+00	1	1
128	GO:0040008	Regulation of growth	5.38E-03	19	12	1.00E+00	6	6
129	GO:0032879	Regulation of localization	5.41E-04	52	17	5.64E-02	27	8
130	GO:1900271	Regulation of long-term synaptic potentiation	2.85E-04	7	6	7.69E-01	2	2
131	GO:0042391	Regulation of membrane potential	2.93E-02	12	7	3.32E-01	7	3
132	GO:0065009	Regulation of molecular function	4.38E-02	41	20	3.15E-01	22	10
133	GO:2000026	Regulation of multicellular organismal development	6.79E-03	39	19	5.69E-02	22	10
134	GO:0051239	Regulation of multicellular organismal process	1.52E-02	51	23	8.43E-02	28	11
135	GO:0048634	Regulation of muscle organ development	1.89E-02	8	5	9.31E-01	3	3
136	GO:1901861	Regulation of muscle tissue development	4.60E-03	9	6	4.39E-01	4	4
137	GO:0051960	Regulation of nervous system development	3.96E-03	25	12	2.89E-01	12	6

(Continued)

TABLE 6 | Continued

	<i>Gene ontology</i>	<i>Label</i>	Tg4-42			WT		
			<i>FDR</i>	<i>No. genes</i>	<i>No. miRs</i>	<i>FDR</i>	<i>No. genes</i>	<i>No. miRs</i>
138	GO:0050767	Regulation of neurogenesis	5.14E-03	23	11	5.93E-01	10	5
139	GO:0043523	Regulation of neuron apoptotic process	7.20E-03	11	9	1.56E-01	6	6
140	GO:1901214	Regulation of neuron death	7.69E-03	13	11	4.55E-01	6	6
141	GO:0045664	Regulation of neuron differentiation	2.62E-03	21	10	5.01E-01	9	5
142	GO:0010975	Regulation of neuron projection development	2.13E-02	16	9	4.40E-01	8	5
143	GO:0099601	Regulation of neurotransmitter receptor activity	3.27E-02	5	5	9.02E-01	2	2
144	GO:1900151	Regulation of nuclear-transcribed mRNA catabolic process, deadenylation-dependent decay	7.94E-03	4	4	1.00E+00	1	1
145	GO:0060211	Regulation of nuclear-transcribed mRNA poly(A) tail shortening	2.94E-03	4	4	1.00E+00	1	1
146	GO:0060147	Regulation of posttranscriptional gene silencing	1.03E-02	5	5	1.00E+00	1	1
147	GO:2000634	Regulation of primary miRNA processing	3.80E-02	2	2	6.19E-01	1	1
148	GO:0043067	Regulation of programmed cell death	2.26E-02	29	16	2.02E-01	16	9
149	GO:0032880	Regulation of protein localization	4.11E-02	22	13	2.95E-01	12	7
150	GO:0051246	Regulation of protein metabolic process	1.28E-02	45	23	5.12E-01	22	12
151	GO:0023051	Regulation of signaling	4.97E-05	61	22	3.54E-01	26	12
152	GO:0016202	Regulation of striated muscle tissue development	1.70E-02	8	5	9.25E-01	3	3
153	GO:0051963	Regulation of synapse assembly	1.86E-02	7	5	5.64E-02	5	3
154	GO:0050807	Regulation of synapse organization	2.61E-02	10	8	1.69E-01	6	4
155	GO:0050803	Regulation of synapse structure or activity	3.38E-02	10	8	1.98E-01	6	4
156	GO:0048167	Regulation of synaptic plasticity	2.92E-06	15	12	7.00E-01	4	4
157	GO:0045974	Regulation of translation, ncRNA-mediated	2.67E-02	3	3	1.00E+00	1	1
158	GO:0051049	Regulation of transport	1.26E-02	36	14	3.17E-01	18	6
159	GO:0099177	Regulation of <i>trans</i> -synaptic signaling	2.04E-04	19	12	8.99E-01	6	5
160	GO:0060627	Regulation of vesicle-mediated transport	4.23E-02	15	8	7.31E-01	7	2
161	GO:0042221	Response to chemical	1.26E-02	54	22	9.38E-01	24	8
162	GO:0009719	Response to endogenous stimulus	1.53E-03	27	15	1.87E-01	13	7
163	GO:0032354	Response to follicle-stimulating hormone	1.91E-02	3	3	1.45E-01	2	2
164	GO:0034698	Response to gonadotropin	4.15E-02	3	3	2.28E-01	2	2
165	GO:0070848	Response to growth factor	1.52E-02	13	11	2.37E-01	7	5
166	GO:0009725	Response to hormone	2.19E-02	16	11	4.43E-01	8	5
167	GO:0010033	Response to organic substance	4.12E-02	40	19	5.53E-01	20	8
168	GO:0050779	RNA destabilization	3.48E-02	4	4	1.00E+00	1	1
169	GO:0060021	Roof of mouth development	1.41E-04	9	8	5.24E-01	3	3
170	GO:0050808	Synapse organization	1.49E-02	11	9	1.00E+00	4	3
171	GO:0035295	Tube development	1.45E-03	24	12	6.01E-02	13	8

(Continued)

TABLE 6 | Continued

	Gene ontology	Label	Tg4-42			WT		
			FDR	No. genes	No. miRs	FDR	No. genes	No. miRs
Significant in WT only								
1	GO:0016477	Cell migration	6.09E-01	14	7	1.15E-02	14	7
2	GO:0000904	Cell morphogenesis involved in differentiation	6.51E-02	14	9	1.90E-02	11	6
3	GO:0048870	Cell motility	4.92E-01	16	7	1.18E-02	15	7
4	GO:0051674	Localization of cell	4.93E-01	16	7	1.20E-02	15	7
5	GO:0040011	Locomotion	1.65E-01	21	10	8.95E-03	17	7
6	GO:0060485	Mesenchyme development	6.24E-02	8	6	1.82E-02	7	6
7	GO:0006928	Movement of cell or subcellular component	1.46E-01	24	11	1.84E-02	18	7
8	GO:0001843	Neural tube closure	4.55E-01	4	4	4.21E-02	5	5
9	GO:0051169	Nuclear transport	1.39E-01	7	4	1.54E-02	7	4
10	GO:0006913	Nucleocytoplasmic transport	1.39E-01	7	4	1.57E-02	7	4
11	GO:0050772	Positive regulation of axonogenesis	1.42E-01	5	4	4.71E-03	6	5
12	GO:0010770	Positive regulation of cell morphogenesis involved in differentiation	2.79E-01	6	4	1.12E-02	7	5
13	GO:0048729	Tissue morphogenesis	1.15E-01	14	10	3.68E-02	11	9
14	GO:0060606	Tube closure	4.63E-01	4	4	4.27E-02	5	5

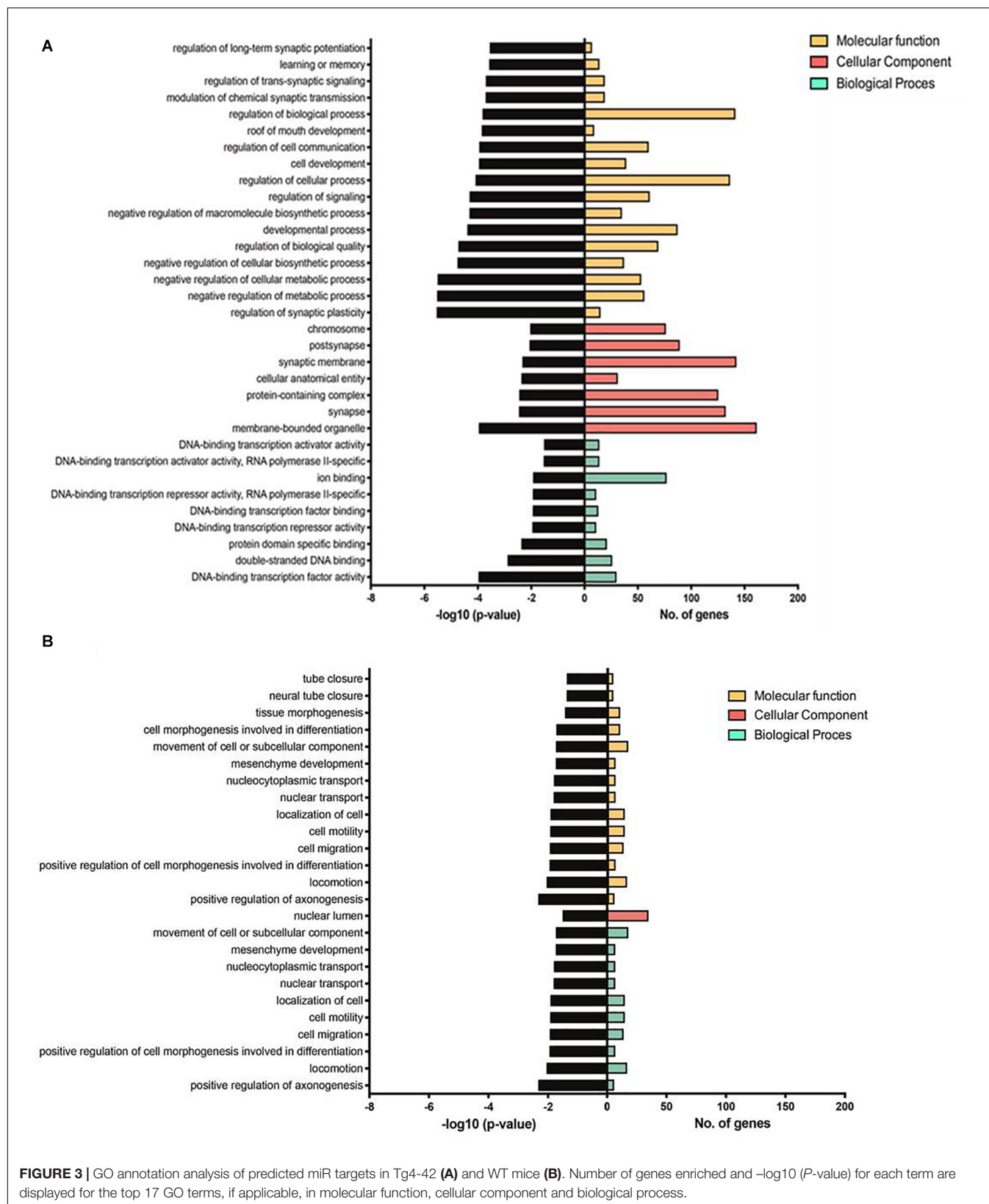
Benjamini-Hochberg False Discovery Rate (FDR).

auditory thalamo-cortical signaling in 22q11DS mice, and may trigger the pathogenic mechanism of 22q11DS-related psychosis (Chun et al., 2017). MiR-345-5p may act as blood biomarker in multiple sclerosis (Freiesleben et al., 2016), and miR-345-3p attenuated apoptosis and inflammation caused by oxidized low-density lipoprotein by targeting TRAF6 via TAK1/p38/NF-kB signaling (Wei et al., 2020). An *in vitro* study indicated that miR-34a may inhibit Aβ clearance by targeting endophilin-3 including uptake and autophagy-mediated degradation (Sun et al., 2018). The rs1050283 SNP likely acts as a risk factor for sporadic AD. It is associated with a decreased expression of oxidized LDL receptor 1 mRNA in the absence of miR-369-3p de-regulation and may affect the binding of miR-369-3p to its 3'UTR consensus sequence (Bettens et al., 2009). MiR-381 showed a protective effect against inflammatory damage (Li et al., 2020). MiR-409 was reported in IL-17-induced inflammatory cytokine production in astrocytes by targeting the SOCS3/STAT3 signaling pathway in EAE mice (Liu et al., 2019). MiR-541 acts on neurite outgrowth and differentiation via nerve growth factor and synapsin I in neuronal precursor cells (Chun et al., 2017). MiR-674 demonstrated an association with Parkinson disease and Huntington (Lardenoije et al., 2015; Salta and De Strooper, 2017b). CSF from individuals with AD contained increased amounts of miR-let7b, and intrathecal injection of miR-let7b in wild-type mice induced neurodegeneration (Lehmann et al., 2012). Elevated levels of miR-let7b and miR-let7e were found in CSF of patients with AD and major depressive symptoms, but not in patients with fronto-temporal disorder (Derkow et al., 2018). MiR-let7d is a key regulator of bi-directionally transcribed genes mediating epigenetic silencing and nucleolar organization (Singh et al., 2018). For miRs miR-129-1, miR-154, miR-15b, miR-219-2, miR-298, miR-323, miR-411, miR-500, miR-7-2, miR-92b, miR-let7i this study is the first to describe deregulation in an AD mouse model. Interestingly, GO-Annotation analysis ("Cellular Components") revealed that only miRs, which were exclusively deregulated in the Tg4-42 model showed an enrichment of targets in connection with the synapse. Such and similar annotations were completely absent among the targets of miRs that were deregulated in both aged mutant and WT mice. With respect to the "Molecular Function" and "Biological Process" annotation, this difference is even more pronounced.

As the Tg4-42 model shows reduced neurogenesis, synaptic hyperexcitability and develops neuron loss as well as behavioral deficits without plaque formation, the newly found deregulated miRs in this model could be involved in plaque-independent pathological pathways. Taken together these observations strongly support our conclusion that the identified miRs play a role in the etiology of AD and thus deserve further investigation as putative biomarkers or therapeutics.

MiRs Identified in the Hippocampus of 8 Month Old Wildtype Mice

Eight miRs were exclusively altered in the hippocampus between 3 and 8 month-old in WT mice. TGF-β induced an lncRNA with its encoded miRs, miR-100 and miR-125b



(Ottaviani et al., 2019). MiR-100 and miR-125b coordinately suppressed Wnt/ β -catenin negative regulators thereby increased Wnt signaling (Lu et al., 2017). MiR-153 was over-expressed in CSF exosomes from patients with Parkinson disease (Serpente et al., 2011). There is evidence that miR-191 and miR-222 are co-regulated and are important for neurodevelopment (Li et al., 2020). MiR-1298, miR-34b, miR-423, miR-666 and miR-667 have not been previously reported to be associated to AD, neurodegenerative disorders or brain function.

MiRs Identified in the Hippocampus of 8 Month Old Tg4-42 and Wildtype Mice

25 miRs were differentially expressed between 3 and 8 month-old Tg4-42 as well as WT mice. All but three of them were significantly decreased at 8 months of age. MiR-127 has been reported to modulate macrophage polarization and therefore may have a crucial role in inflammation (Essandoh et al., 2016). MiR-128-1 up-regulation correlated with A β degradation in monocytes from patients with sporadic AD (Tiribuzi et al., 2014). MiR-130a was involved in inflammatory processes by targeting the transforming growth factor- β 1 and interleukin 18 genes (Zhao et al., 2014). MiR-132 expression levels were found to be associated with hippocampal sclerosis in a subgroup of AD patients (Tasaki et al., 2018). MiR-138-1 was transcriptionally up-regulated during myelination and downregulated upon nerve injury (Lin et al., 2018). miR-150-5p may act as a circulating biomarker for patients with the autoimmune neuromuscular disorder myasthenia gravis (Punga et al., 2015). A genetic variant located near the miR-204 gene was significantly associated with schizophrenia resulting in reduced expression of miR-204 in neuronal-like SH-SY5Y cells (Cammaerts et al., 2015). MiR-212 was down-regulated in white matter of patients with AD (Wang W.X. et al., 2011). MiR-222 was down-regulated in the AD mouse model APPswe/PS Δ E9 (Wang et al., 2015). Lipopolysaccharide stimulation in mice led to increased expression of miR-221 and miR-222, thereby causing transcriptional silencing of a subset of inflammatory genes, which depend on chromatin remodeling. In patients with sepsis, increased expression of miR-221 and miR-222 correlated with immunoparalysis and increased organ damage (Seeley et al., 2018). Preliminary results indicated that aberrant levels of circulating miR-23a are recovered in fingolimod-treated multiple sclerosis patients representing a potential biomarker (Fenoglio et al., 2016). MiR-300 was involved in the inflammatory response in endothelial cells and enhanced autophagy by activation of the AMPK/mTOR signaling pathway (Li et al., 2018). MiR-323 suppressed neuron death via the transforming growth factor- β 1/SMAD3 signaling pathway (Che et al., 2019). The expression of miR-30a was associated as a prediction serum marker in epilepsy (Lin et al., 2018). MiR-34c has been shown to have a physiological role in regulating the central stress response (Cammaerts et al., 2015). MiR-329 was upregulated in a mouse model for Rett syndrome, which is a complex neurological disorder that has been associated with mutations in the gene coding for Mecp2

(Urduingio et al., 2010). MiR-382 inhibited cell proliferation and invasion of retinoblastoma by targeting BDNF-mediated PI3K/AKT signaling pathway (Song et al., 2017). MiR-877-3P regulated vascular endothelial cell autophagy and apoptosis under the high-glucose condition (Zhao et al., 2020). MiR-99a was found overexpressed in the brain of patients with Down syndrome (Bras et al., 2018). MiR-99b may have a role in spinal cord injury via the regulation of mTOR (Cao et al., 2017). Again, several miRs, namely, miR-128-2, miR-140, miR-23b, miR-30d, miR-3102, miR-328 and miR-434 could be linked to an AD mouse model for the first time in this study.

Annotation Analysis of miR Targets

The analyses of the GO annotation of predicted miR targets in Tg4-42 and WT mice revealed diverse cellular component, molecular functions and biological processes similar to our previous study of the mRNome of the whole brain of Tg4-42 and 5XFAD mice (Bouter et al., 2014). The GO annotations in Tg4-42 hippocampus demonstrated that the most enriched pathways belong to synaptic signaling and transmission involved in memory processes, which was not found in WT mice. Hence, these pathways appear specific for the AD-typical mental decline and neurodegenerative events.

CONCLUSION

We were able to validate the Tg4-42 as a valuable model for sporadic AD. We could confirm previously reported AD-associations of several miRs. Importantly, the untargeted small RNAseq approach also allowed us to link several additional miRs to a mouse model for AD. The identified miRs have a role in the age-dependent deficits in learning and memory as well as neuron loss in the hippocampus in Tg4-42 mice. The annotation of miR target genes supported these strong reductions in synaptic processes involved in learning and memory.

DATA AVAILABILITY STATEMENT

The datasets for this study have been uploaded to the European Nucleotide Archive (<https://www.ebi.ac.uk/ena>) with the accession identification number of the project PRJEB39314.

ETHICS STATEMENT

The animal study was reviewed and approved by the Niedersächsisches Landesamt für Verbraucherschutz und Lebensmittelsicherheit, Röverskamp 5, 26203 Oldenburg, Germany and Landesamt für Gesundheit und Soziales LAGe So Darwinstr. 15, 10589 Berlin, Germany.

AUTHOR CONTRIBUTIONS

YB contributed to the experimental design and analyzed the data. TK and FR analyzed the data. AK and LJ contributed

to the experimental design and were responsible for NGS-data generation and primary data analysis. TB wrote the manuscript, analyzed the data, and supervised the experimental design and the entire project. All authors read, reviewed, and approved the final manuscript.

ACKNOWLEDGMENTS

We thank Robert Weissman and Stefan Weiss for bioinformatics support in primary data analysis and Corina Jensen and Christian Sperling for excellent technical assistance.

REFERENCES

- Agarwal, V., Bell, G. W., Nam, J. W., and Bartel, D. P. (2015). Predicting effective microRNA target sites in mammalian mRNAs. *eLife* 4:5. doi: 10.7554/eLife.05005
- Anders, S., Pyl, P. T., and Huber, W. (2015). HTSeq—a Python framework to work with high-throughput sequencing data. *Bioinformatics* 31, 166–169. doi: 10.1093/bioinformatics/btu638
- Angelucci, F., Cechova, K., Valis, M., Kuca, K., Zhang, B., and Hort, J. (2019). MicroRNAs in Alzheimer's disease: diagnostic markers or therapeutic agents? *Front. Pharmacol.* 10:665. doi: 10.3389/fphar.2019.00665
- Banzhaf-Strathmann, J., Benito, E., May, S., Arzberger, T., Tahirovic, S., Kretschmar, H., et al. (2014). MicroRNA-125b induces tau hyperphosphorylation and cognitive deficits in Alzheimer's disease. *EMBO J.* 33, 1667–1680. doi: 10.15252/embj.201387576
- Bartel, D. P. (2004). MicroRNAs: genomics, biogenesis, mechanism, and function. *Cell* 116, 281–297.
- Bayer, T., and Wirths, O. (2014). Focusing the amyloid cascade hypothesis on N-truncated Abeta peptides as drug targets against Alzheimer's disease. *Acta Neuropathol.* 127, 787–801. doi: 10.1007/s00401-014-1287-x
- Bettens, K., Brouwers, N., Engelborghs, S., Van Mieghem, H., De Deyn, P. P., Theuns, J., et al. (2009). APP and BACE1 miR genetic variability has no major role in risk for Alzheimer disease. *Hum. Mutat.* 30, 1207–1213. doi: 10.1002/humu.21027
- Bicker, S., Lackinger, M., Weiss, K., and Schratz, G. (2014). MicroRNA-132, -134, and -138: a microRNA triad rules in neuronal dendrites. *Cell Mol. Life Sci.* 71, 3987–4005. doi: 10.1007/s00018-014-1671-7
- Boscher, E., Husson, T., Quenez, O., Laquerriere, A., Marguet, F., Cassinari, K., et al. (2019). Copy number variants in miR-138 as a potential risk factor for early-onset Alzheimer's disease. *J. Alzheimers Dis.* 68, 1243–1255. doi: 10.3233/jad-180940
- Bouter, C., Henniges, P., Franke, T. N., Irwin, C., Sahlmann, C. O., Sichler, M. E., et al. (2019). 18F-FDG-PET detects drastic changes in brain metabolism in the Tg4-42 model of Alzheimer's disease. *Front. Aging Neurosci.* 10:425. doi: 10.3389/fnagi.2018.00425
- Bouter, Y., Dietrich, K., Wittmann, J. L., Rezaei-Ghaleh, N., Pillot, T., Papot-Couturier, S., et al. (2013). N-truncated amyloid beta (Aβeta) 4–42 forms stable aggregates and induces acute and long-lasting behavioral deficits. *Acta Neuropathol.* 126, 189–205. doi: 10.1007/s00401-013-1129-2
- Bouter, Y., Kacprowski, T., Weissmann, R., Dietrich, K., Borgers, H., Brauß, A., et al. (2014). Deciphering the molecular profile of plaques, memory decline and neuron-loss in two mouse models for Alzheimer's disease by deep sequencing. *Front. Aging Neurosci.* 6:75. doi: 10.3389/fnagi.2014.00075
- Bras, A., Rodrigues, A. S., Gomes, B., and Rueff, J. (2018). Down syndrome and microRNAs. *Biomed. Rep.* 8, 11–16.
- Cammaerts, S., Strazisar, M., Smets, B., Weckhuysen, S., Nordin, A., De Jonghe, P., et al. (2015). Schizophrenia-associated MIR204 Regulates Noncoding RNAs and affects neurotransmitter and ion channel gene sets. *PLoS One* 10:e0144428. doi: 10.1371/journal.pone.0144428

SUPPLEMENTARY MATERIAL

The Supplementary Material for this article can be found online at: <https://www.frontiersin.org/articles/10.3389/fnins.2020.580524/full#supplementary-material>

FIGURE S1 | Heatmap of most variable genes for quality control. Individual sample after collapsing replicates with DESeq2. S1–20 represent individual sample labels.

TABLE S1 | Analysis of hippocampal miR between young and aged Tg4-42 and wildtype mice. Plus log 2-fold change means higher levels at 8 months of age. Minus log 2-fold change means lower levels at 8 months of age. *P*-values are only shown if significant (<0.05). Abbreviations: 3M, 3 month old; 8M, 8 month old.

- Cao, F., Liu, T., Sun, S., and Feng, S. (2017). The role of the miR-99b-5p/mTOR signaling pathway in neuroregeneration in mice following spinal cord injury. *Mol. Med. Rep.* 16, 9355–9360. doi: 10.3892/mmr.2017.7816
- Che, F., Du, H., Wei, J., Zhang, W., Cheng, Z., and Tong, Y. (2019). MicroRNA-323 suppresses nerve cell toxicity in cerebral infarction via the transforming growth factor-beta1/SMAD3 signaling pathway. *Int. J. Mol. Med.* 43, 993–1002.
- Chen, Y., and Wang, X. (2020). miRDB: an online database for prediction of functional microRNA targets. *Nucleic Acids Res.* 48, D127–D131.
- Chou, C. H., Shrestha, S., Yang, C. D., Chang, N. W., Lin, Y. L., Liao, K. W., et al. (2018). miRTarBase update 2018: a resource for experimentally validated microRNA-target interactions. *Nucleic Acids Res.* 46, D296–D302.
- Chun, S., Du, F., Westmoreland, J. J., Han, S. B., Wang, Y. D., Eddins, D., et al. (2017). Thalamic miR-338-3p mediates auditory thalamocortical disruption and its late onset in models of 22q11.2 microdeletion. *Nat. Med.* 23, 39–48. doi: 10.1038/nm.4240
- Derkow, K., Rossling, R., Schipke, C., Kruger, C., Bauer, J., Fahling, M., et al. (2018). Distinct expression of the neurotoxic microRNA family let-7 in the cerebrospinal fluid of patients with Alzheimer's disease. *PLoS One* 13:e0200602. doi: 10.1371/journal.pone.0200602
- Dietrich, K., Bouter, Y., Muller, M., and Bayer, T. A. (2018). Synaptic alterations in mouse models for Alzheimer disease—a special focus on N-truncated Abeta 4–42. *Molecules* 23:718. doi: 10.3390/molecules23040718
- Ding, J., Li, X., and Hu, H. (2016). TarPmiR: a new approach for microRNA target site prediction. *Bioinformatics* 32, 2768–2775. doi: 10.1093/bioinformatics/btw318
- Dobin, A., Davis, C. A., Schlesinger, F., Drenkow, J., Zaleski, C., Jha, S., et al. (2013). STAR: ultrafast universal RNA-seq aligner. *Bioinformatics* 29, 15–21. doi: 10.1093/bioinformatics/bts635
- Elliott, C., Rojo, A. I., Ribe, E., Broadstock, M., Xia, W., Morin, P., et al. (2018). A role for APP in Wnt signalling links synapse loss with beta-amyloid production. *Transl. Psychiatry* 8:179. doi: 10.1038/s41398-018-0231-6
- Essandoh, K., Li, Y., Huo, J., and Fan, G. C. (2016). MiR-mediated macrophage polarization and its potential role in the regulation of inflammatory response. *Shock* 46, 122–131. doi: 10.1097/shk.0000000000000604
- Fenoglio, C., De Riz, M., Pietroboni, A. M., Calvi, A., Serpente, M., Cioffi, S. M., et al. (2016). Effect of fingolimod treatment on circulating miR-15b, miR23a and miR-223 levels in patients with multiple sclerosis. *J. Neuroimmunol.* 299, 81–83. doi: 10.1016/j.jneuroim.2016.08.017
- Forstner, A. J., Degenhardt, F., Schratz, G., and Nothen, M. M. (2013). MicroRNAs as the cause of schizophrenia in 22q11.2 deletion carriers, and possible implications for idiopathic disease: a mini-review. *Front. Mol. Neurosci.* 6:47. doi: 10.3389/fnfmol.2013.00047
- Freiesleben, S., Hecker, M., Zettl, U. K., Fuellen, G., and Taher, L. (2016). Analysis of microRNA and gene expression profiles in multiple sclerosis: integrating interaction data to uncover regulatory mechanisms. *Sci. Rep.* 6:34512. doi: 10.1038/srep34512
- Freischmidt, A., Muller, K., Ludolph, A. C., and Weishaupt, J. H. (2013). Systemic dysregulation of TDP-43 binding microRNAs in amyotrophic lateral sclerosis. *Acta Neuropathol. Commun.* 1:42. doi: 10.1186/2051-5960-1-42

- Gerberding, A. L., Zampar, S., Stazi, M., Liebetanz, D., and Wirths, O. (2019). Physical activity ameliorates impaired hippocampal neurogenesis in the Tg4-42 mouse model of Alzheimer's disease. *ASN Neurol.* 11:692. doi: 10.1177/1759091419892692
- Gui, Y., Liu, H., Zhang, L., Lv, W., and Hu, X. (2015). Altered microRNA profiles in cerebrospinal fluid exosome in Parkinson disease and Alzheimer disease. *Oncotarget* 6, 37043–37053. doi: 10.18632/oncotarget.6158
- Haramati, S., Navon, I., Issler, O., Ezra-Nevo, G., Gil, S., Zwang, R., et al. (2011). MicroRNA as repressors of stress-induced anxiety: the case of amygdalar miR-34. *J. Neurosci.* 31, 14191–14203. doi: 10.1523/jneurosci.1673-11.2011
- Ifrim, M. F., Williams, K. R., and Bassell, G. J. (2015). Single-molecule imaging of PSD-95 mRNA translation in dendrites and its dysregulation in a mouse model of fragile X syndrome. *J. Neurosci.* 35, 7116–7130. doi: 10.1523/jneurosci.2802-14.2015
- Jawhar, S., Trawicka, A., Jenneckens, C., Bayer, T. A., and Wirths, O. (2012). Motor deficits, neuron loss, and reduced anxiety coinciding with axonal degeneration and intraneuronal Abeta aggregation in the 5XFAD mouse model of Alzheimer's disease. *Neurobiol. Aging* 33, 196.e29–196.e40.
- Jin, Y., Tu, Q., and Liu, M. (2018). MicroRNA125b regulates Alzheimer's disease through SphK1 regulation. *Mol. Med. Rep.* 18, 2373–2380.
- Kim, K. H., Moon, M., Yu, S. B., Mook-Jung, I., and Kim, J. I. (2012). RNA-Seq analysis of frontal cortex and cerebellum from 5XFAD mice at early stage of disease pathology. *J. Alzheimers Dis.* 29, 793–808. doi: 10.3233/jad-2012-111793
- Lardenoije, R., Iatrou, A., Kenis, G., Kompotis, K., Steinbusch, H. W., Mastroeni, D., et al. (2015). The epigenetics of aging and neurodegeneration. *Prog. Neurobiol.* 131, 21–64.
- Lehmann, S. M., Kruger, C., Park, B., Derkow, K., Rosenberger, K., Baumgart, J., et al. (2012). An unconventional role for miR: let-7 activates Toll-like receptor 7 and causes neurodegeneration. *Nat. Neurosci.* 15, 827–835. doi: 10.1038/nn.3113
- Li, Y., Huang, J., Yan, H., Li, X., Ding, C., Wang, Q., et al. (2020). Protective effect of microRNA381 against inflammatory damage of endothelial cells during coronary heart disease by targeting CXCR4. *Mol. Med. Rep.* 21, 1439–1448.
- Li, Y., Ke, J., Peng, C., Wu, F., and Song, Y. (2018). microRNA-300/NAMPT regulates inflammatory responses through activation of AMPK/mTOR signaling pathway in neonatal sepsis. *Biomed. Pharmacother.* 108, 271–279. doi: 10.1016/j.biopha.2018.08.064
- Li, Y. Y., Cui, J. G., Hill, J. M., Bhattacharjee, S., Zhao, Y., and Lukiw, W. J. (2011). Increased expression of miR-146a in Alzheimer's disease transgenic mouse models. *Neurosci. Lett.* 487, 94–98. doi: 10.1016/j.neulet.2010.09.079
- Lin, H. P., Oksuz, I., Svaren, J., and Awatramani, R. (2018). Egr2-dependent microRNA-138 is dispensable for peripheral nerve myelination. *Sci. Rep.* 8:3817. doi: 10.1038/s41598-018-22010-8
- Liu, X., Zhou, F., Yang, Y., Wang, W., Niu, L., Zuo, D., et al. (2019). MiR-409-3p and MiR-1896 co-operatively participate in IL-17-induced inflammatory cytokine production in astrocytes and pathogenesis of EAE mice via targeting SOCS3/STAT3 signaling. *Glia* 67, 101–112. doi: 10.1002/glia.23530
- Love, M. I., Huber, W., and Anders, S. (2014). Moderated estimation of fold change and dispersion for RNA-seq data with DESeq2. *Genome Biol.* 15:550.
- Lu, Y., Zhao, X., Liu, Q., Li, C., Graves-Deal, R., Cao, Z., et al. (2017). lncRNA MIR100HG-derived miR-100 and miR-125b mediate cetuximab resistance via Wnt/beta-catenin signaling. *Nat. Med.* 23, 1331–1341. doi: 10.1038/nm.4424
- Majer, A., Medina, S. J., Niu, Y., Abrenica, B., Manguiat, K. J., Frost, K. L., et al. (2012). Early mechanisms of pathobiology are revealed by transcriptional temporal dynamics in hippocampal CA1 neurons of prion infected mice. *PLoS Pathog.* 8:e1003002. doi: 10.1371/journal.ppat.1003002
- Margis, R., Margis, R., and Rieder, C. R. M. (2011). Identification of blood microRNAs associated to Parkinson's disease. *J. Biotechnol.* 152, 96–101. doi: 10.1016/j.jbiotec.2011.01.023
- Mi, H., Muruganujan, A., Ebert, D., Huang, X., and Thomas, P. D. (2019). PANTHER version 14: more genomes, a new PANTHER GO-slim and improvements in enrichment analysis tools. *Nucleic Acids Res.* 47, D419–D426.
- Noh, H., Park, C., Park, S., Lee, Y. S., Cho, S. Y., and Seo, H. (2014). Prediction of miR-mRNA associations in Alzheimer's disease mice using network topology. *BMC Genom.* 15:644. doi: 10.1186/1471-2164-15-644
- Oakley, H., Cole, S. L., Logan, S., Maus, E., Shao, P., Craft, J., et al. (2006). Intraneuronal beta-amyloid aggregates, neurodegeneration, and neuron loss in transgenic mice with five familial Alzheimer's disease mutations: potential factors in amyloid plaque formation. *J. Neurosci.* 26, 10129–10140. doi: 10.1523/jneurosci.1202-06.2006
- Ottaviani, S., Stebbing, J., Frampton, A. E., Zagorac, S., Krell, J., De Giorgio, A., et al. (2019). Author correction: TGF-beta induces miR-100 and miR-125b but blocks let-7a through LIN28B controlling PDAC progression. *Nat. Commun.* 10:3738. doi: 10.1038/s41467-019-11752-2
- Punga, A. R., Andersson, M., Alimohammadi, M., and Punga, T. (2015). Disease specific signature of circulating miR-150-5p and miR-21-5p in myasthenia gravis patients. *J. Neurol. Sci.* 356, 90–96. doi: 10.1016/j.jns.2015.06.019
- Qian, Q., Zhang, J., He, F. P., Bao, W. X., Zheng, T. T., Zhou, D. M., et al. (2019). Down-regulated expression of microRNA-338-5p contributes to neuropathology in Alzheimer's disease. *FASEB J.* 33, 4404–4417. doi: 10.1096/fj.201801846r
- Rigden, D. J., and Fernandez, X. M. (2018). The 2018 Nucleic acids research database issue and the online molecular biology database collection. *Nucleic Acids Res.* 46, D1–D7.
- Roshan, R., Ghosh, T., Scaria, V., and Pillai, B. (2009). MicroRNAs: novel therapeutic targets in neurodegenerative diseases. *Drug Discov. Today* 14, 1123–1129. doi: 10.1016/j.drudis.2009.09.009
- Salta, E., and De Strooper, B. (2012). Non-coding RNAs with essential roles in neurodegenerative disorders. *Lancet Neurol.* 11, 189–200. doi: 10.1016/s1474-4422(11)70286-1
- Salta, E., and De Strooper, B. (2017a). microRNA-132: a key noncoding RNA operating in the cellular phase of Alzheimer's disease. *FASEB J.* 31, 424–433. doi: 10.1096/fj.201601308
- Salta, E., and De Strooper, B. (2017b). Noncoding RNAs in neurodegeneration. *Nat. Rev. Neurosci.* 18, 627–640. doi: 10.1038/nrn.2017.90
- Seeley, J. J., Baker, R. G., Mohamed, G., Bruns, T., Hayden, M. S., Deshmukh, S. D., et al. (2018). Induction of innate immune memory via microRNA targeting of chromatin remodelling factors. *Nature* 559, 114–119. doi: 10.1038/s41586-018-0253-5
- Serpente, M., Fenoglio, C., Villa, C., Cortini, F., Cantoni, C., Ridolfi, E., et al. (2011). Role of OLR1 and its regulating hsa-miR369-3p in Alzheimer's disease: genetics and expression analysis. *J. Alzheimers Dis.* 26, 787–793. doi: 10.3233/jad-2011-110074
- Shu, B., Zhang, X., Du, G., Fu, Q., and Huang, L. (2018). MicroRNA-107 prevents amyloid-beta-induced neurotoxicity and memory impairment in mice. *Int. J. Mol. Med.* 41, 1665–1672.
- Singh, I., Contreras, A., Cordero, J., Rubio, K., Dobersch, S., Gunther, S., et al. (2018). MiCEE is a ncRNA-protein complex that mediates epigenetic silencing and nucleolar organization. *Nat. Genet.* 50, 990–1001. doi: 10.1038/s41588-018-0139-3
- Smith, B., Treadwell, J., Zhang, D., Ly, D., Mckinnell, I., Walker, P. R., et al. (2010). Large-scale expression analysis reveals distinct microRNA profiles at different stages of human neurodevelopment. *PLoS One* 5:e11109. doi: 10.1371/journal.pone.0011109
- Song, D., Diao, J., Yang, Y., and Chen, Y. (2017). MicroRNA382 inhibits cell proliferation and invasion of retinoblastoma by targeting BDNF-mediated PI3K/AKT signalling pathway. *Mol. Med. Rep.* 16, 6428–6436. doi: 10.3892/mmr.2017.7396
- Sticht, C., De La Torre, C., Parveen, A., and Gretz, N. (2018). miRWalk: An online resource for prediction of microRNA binding sites. *PLoS One* 13:e0206239. doi: 10.1371/journal.pone.0206239
- Strickland, E. R., Hook, M. A., Balaraman, S., Huie, J. R., Grau, J. W., and Miranda, R. C. (2011). MicroRNA dysregulation following spinal cord contusion: implications for neural plasticity and repair. *Neuroscience* 186, 146–160. doi: 10.1016/j.neuroscience.2011.03.063
- Sun, B., Fan, P., Liao, M., and Zhang, Y. (2018). Modeling endophilin-mediated Abeta disposal in glioma cells. *Biochim. Biophys. Acta Mol. Cell Res.* 1865, 1385–1396. doi: 10.1016/j.bbamcr.2018.06.015
- Sun, J., Cheng, W., Liu, L., Tao, S., Xia, Z., Qi, L., et al. (2016). Identification of serum miRs differentially expressed in human epilepsy at seizure onset and post-seizure. *Mol. Med. Rep.* 14, 5318–5324. doi: 10.3892/mmr.2016.5906

- Tasaki, S., Gaiteri, C., Mostafavi, S., De Jager, P. L., and Bennett, D. A. (2018). The molecular and neuropathological consequences of genetic risk for Alzheimer's dementia. *Front. Neurosci.* 12:699. doi: 10.3389/fnins.2018.00699
- Tiribuzi, R., Crispoltoni, L., Porcellati, S., Di Lullo, M., Florenzano, F., Pirro, M., et al. (2014). miR128 up-regulation correlates with impaired amyloid beta(1-42) degradation in monocytes from patients with sporadic Alzheimer's disease. *Neurobiol. Aging* 35, 345–356. doi: 10.1016/j.neurobiolaging.2013.08.003
- Twine, N. A., Janitz, K., Wilkins, M. R., and Janitz, M. (2011). Whole transcriptome sequencing reveals gene expression and splicing differences in brain regions affected by Alzheimer's disease. *PLoS One* 6:e16266. doi: 10.1371/journal.pone.016266
- Urdinguio, R. G., Fernandez, A. F., Lopez-Nieva, P., Rossi, S., Huertas, D., Kulis, M., et al. (2010). Disrupted microRNA expression caused by Mecp2 loss in a mouse model of Rett syndrome. *Epigenetics* 5, 656–663. doi: 10.4161/epi.5.7.13055
- Villela, D., Ramalho, R. F., Silva, A. R., Brentani, H., Suemoto, C. K., Pasqualucci, C. A., et al. (2016). Differential DNA methylation of MicroRNA genes in temporal cortex from Alzheimer's disease individuals. *Neural Plast.* 2016:2584940. doi: 10.1155/2016/2584940
- Wang, A., Das, P., Switzer, R. C. III, Golde, T. E., and Jankowsky, J. L. (2011). Robust amyloid clearance in a mouse model of Alzheimer's disease provides novel insights into the mechanism of amyloid-beta immunotherapy. *J. Neurosci.* 31, 4124–4136. doi: 10.1523/jneurosci.5077-10.2011
- Wang, M., Qin, L., and Tang, B. (2019). MicroRNAs in Alzheimer's disease. *Front. Genet.* 10:153. doi: 10.3389/fgene.2019.00153
- Wang, T., Shi, F., Jin, Y., Jiang, W., Shen, D., and Xiao, S. (2016). Abnormal changes of brain cortical anatomy and the association with plasma MicroRNA107 level in amnesic mild cognitive impairment. *Front. Aging Neurosci.* 8:112. doi: 10.3389/fnagi.2016.00112
- Wang, W. X., Huang, Q., Hu, Y., Stromberg, A. J., and Nelson, P. T. (2011). Patterns of microRNA expression in normal and early Alzheimer's disease human temporal cortex: white matter versus gray matter. *Acta Neuropathol.* 121, 193–205. doi: 10.1007/s00401-010-0756-0
- Wang, X., Xu, Y., Zhu, H., Ma, C., Dai, X., and Qin, C. (2015). Downregulated microRNA-222 is correlated with increased p27Kip(1) expression in a double transgenic mouse model of Alzheimer's disease. *Mol. Med. Rep.* 12, 7687–7692. doi: 10.3892/mmr.2015.4339
- Wei, Q., Tu, Y., Zuo, L., Zhao, J., Chang, Z., Zou, Y., et al. (2020). MiR-345-3p attenuates apoptosis and inflammation caused by oxidized low-density lipoprotein by targeting TRAF6 via TAK1/p38/NF- κ B signaling in endothelial cells. *Life Sci.* 241:117142. doi: 10.1016/j.lfs.2019.117142
- Wen, Z., Zhang, J., Tang, P., Tu, N., Wang, K., and Wu, G. (2018). Overexpression of miR185 inhibits autophagy and apoptosis of dopaminergic neurons by regulating the AMPK/mTOR signaling pathway in Parkinson's disease. *Mol. Med. Rep.* 17, 131–137.
- Zhang, J., Liu, L. H., Zhou, Y., Li, Y. P., Shao, Z. H., Wu, Y. J., et al. (2011). Effects of miR-541 on neurite outgrowth during neuronal differentiation. *Cell Biochem. Funct.* 29, 279–286. doi: 10.1002/cbf.1747
- Zhao, H., Li, H., Du, W., Zhang, D., Ge, J., Xue, F., et al. (2014). Reduced MIR130A is involved in primary immune thrombocytopenia via targeting TGF β 1 and IL18. *Br. J. Haematol.* 166, 767–773. doi: 10.1111/bjh.12934
- Zhao, X., Su, L., He, X., Zhao, B., and Miao, J. (2020). Long noncoding RNA CA7-4 promotes autophagy and apoptosis via sponging MIR877-3P and MIR5680 in high glucose-induced vascular endothelial cells. *Autophagy* 16, 70–85. doi: 10.1080/15548627.2019.1598750

Conflict of Interest: The University Medicine Göttingen holds a patent on the Tg4-42 mouse model for Alzheimer's disease.

Copyright © 2020 Bouter, Kacprowski, Rößler, Jensen, Kuss and Bayer. This is an open-access article distributed under the terms of the Creative Commons Attribution License (CC BY). The use, distribution or reproduction in other forums is permitted, provided the original author(s) and the copyright owner(s) are credited and that the original publication in this journal is cited, in accordance with accepted academic practice. No use, distribution or reproduction is permitted which does not comply with these terms.



Investigation on the Alteration of Brain Functional Network and Its Role in the Identification of Mild Cognitive Impairment

Lulu Zhang^{1†}, Huangjing Ni^{2†}, Zhinan Yu¹, Jun Wang², Jiaolong Qin³, Fengzhen Hou^{1*} and Albert Yang⁴ for the Alzheimer's Disease Neuroimaging Initiative (ADNI)

OPEN ACCESS

Edited by:

Kin Ying Mok,
University College London,
United Kingdom

Reviewed by:

Kewei Chen,
Banner Alzheimer's Institute,
United States
Can Martin Zhang,
Massachusetts General Hospital and
Harvard Medical School, United
States
Jie Xiang,
Taiyuan University of Technology,
China

*Correspondence:

Fengzhen Hou
houfz@cpu.edu.cn

[†]These authors have contributed
equally to this work

Specialty section:

This article was submitted to
Neurodegeneration,
a section of the journal
Frontiers in Neuroscience

Received: 02 May 2020

Accepted: 04 September 2020

Published: 30 September 2020

Citation:

Zhang L, Ni H, Yu Z, Wang J,
Qin J, Hou F and Yang A
for the Alzheimer's Disease
Neuroimaging Initiative (ADNI) (2020)
Investigation on the Alteration of Brain
Functional Network and Its Role
in the Identification of Mild Cognitive
Impairment.
Front. Neurosci. 14:558434.
doi: 10.3389/fnins.2020.558434

¹ Key Laboratory of Biomedical Functional Materials, School of Science, China Pharmaceutical University, Nanjing, China, ² Smart Health Big Data Analysis and Location Services Engineering Lab of Jiangsu Province, School of Geographic and Biologic Information, Nanjing University of Posts and Telecommunications, Nanjing, China, ³ Key Laboratory of Intelligent Perception and Systems for High-Dimensional Information of Ministry of Education, School of Computer Science and Engineering, Nanjing University of Science and Technology, Nanjing, China, ⁴ Division of Interdisciplinary Medicine and Biotechnology, Department of Medicine, Beth Israel Deaconess Medical Center/Harvard Medical School, Boston, MA, United States

Mild cognitive impairment (MCI) is generally regarded as a prodromal stage of Alzheimer's disease (AD). In coping with the challenges caused by AD, we analyzed resting-state functional magnetic resonance imaging data of 82 MCI subjects and 93 normal controls (NCs). The alteration of brain functional network in MCI was investigated on three scales, including global metrics, nodal characteristics, and modular properties. The results supported the existence of small worldness, hubs, and community structure in the brain functional networks of both groups. Compared with NCs, the network altered in MCI over all the three scales. In scale I, we found significantly decreased characteristic path length and increased global efficiency in MCI. Moreover, altered global network metrics were associated with cognitive level evaluated by neuropsychological assessments. In scale II, the nodal betweenness centrality of some global hubs, such as the right Crus II of cerebellar hemisphere (CERCRU2.R) and fusiform gyrus (FFG.R), changed significantly and associated with the severity and cognitive impairment in MCI. In scale III, although anatomically adjacent regions tended to be clustered into the same module regardless of group, discrepancies existed in the composition of modules in both groups, with a prominent separation of the cerebellum and a less localized organization of community structure in MCI compared with NC. Taking advantages of random forest approach, we achieved an accuracy of 91.4% to discriminate MCI patients from NCs by integrating cognitive assessments and network analysis. The importance of the used features fed into the classifier further validated the nodal characteristics of CERCRU2.R and FFG.R could be potential biomarkers in the identification of MCI. In conclusion, the present study demonstrated that the brain functional connectome data altered at the stage of MCI and could assist the automatic diagnosis of MCI patients.

Keywords: Alzheimer's disease, mild cognitive impairment, resting-state functional MRI, modular structure, graph theory, machine learning

INTRODUCTION

Alzheimer's disease (AD), a neurodegenerative disease, represents the most common type of dementia (Ahmadlou et al., 2010; Li et al., 2011). The prevalence of AD is a tremendous burden to individuals, families, and society. The treatment for AD remains unavailable and no way can prevent or reverse the progression of AD; only the early intervention of AD may influence its onset and deterioration (Al-Shoukry et al., 2020). Mild cognitive impairment (MCI) is generally regarded as a prodromal stage of AD since patients with MCI convert to AD at a rate of approximately 15% per year (Davatzikos et al., 2011). Hence, it is important to explore the neuropathological alteration in MCI, discover potential target for neuromodulation in treating MCI, and prompt effective method for the early diagnosis of MCI.

Theoretically, the human brain can be represented as a "connectome," a large-scale network of interconnected regions that provides the anatomical substrate for neural communication, functional processing, and information integration (Fornito et al., 2013). Brain connectivity has been widely analyzed based on the graph theory by regarding neural elements (e.g., neurons and brain regions) as nodes and some measures of structural, functional, or causal interaction between nodes as edges (Fornito et al., 2013; Onias et al., 2014; Khazaei et al., 2015; Fang et al., 2017). Numerous studies have demonstrated its effectiveness in investigating the altered brain network pattern with MCI (Yao et al., 2010, 2018; Zhao et al., 2012; Seo et al., 2013; Xiang et al., 2013; Son et al., 2015; Deng et al., 2016; Pereira et al., 2016; Sánchez-Catasús et al., 2018). One of the shortcomings in most related studies is that only the cerebral regions were considered. However, recent studies have demonstrated that the cerebellum may play a vital role in neurodegenerative processes like AD. Evidences from functional imaging studies have reported the involvement of the cerebellum in various cognitive tasks besides the traditional motor ones (Stoodley, 2012), and cerebellar abnormality has also been reported in AD/MCI patients recently (Tabatabaei-Jafari et al., 2017; Pagen et al., 2020). Therefore, exploring the whole-brain functional network, including both cerebral and cerebellar regions, can disclose more comprehensive information of the abnormal brain connectome in MCI patients.

Graph metrics of the functional brain network are found to be informative to characterize MCI patients (Khazaei et al., 2016; Xu et al., 2020). In practice, in a brain functional network, a region can be deemed as a node, and the edges can be determined by the functional interaction of nodes. Various metrics have been proposed in the literature to quantify the topological characteristics of such a network and can be generally classified into three distinct scales. Measures from the three scales variously focus on characterizing aspects of function integration and segregation, quantifying importance of individual brain regions, and detecting patterns of local anatomical circuitry (Rubinov and Sporns, 2010; Tijms et al., 2013).

Moreover, the past decades witness the increasing growth in clinical use of artificial intelligence. Machine learning approaches are found to be quite useful for discriminating MCI patients

from normal controls (NCs) (Tanveer et al., 2020). Some researchers made use of linguistic and/or acoustic features (Gosztolya et al., 2019; Orimaye et al., 2020; Calzà et al., 2021), while the overwhelming majority of previous studies focused on utilizing the neuroimaging biomarkers for the identification of MCI (Tanveer et al., 2020). Growing functional magnetic resonance imaging (fMRI) studies have been devoted to the classification task between MCI patients and NCs (Chen et al., 2011; Jie et al., 2013, 2014; Suk et al., 2013; Wang et al., 2013; Wee et al., 2013a,b; Cui et al., 2018; Xu et al., 2020). Most recently, Xu et al. (2020) utilized a combination of information in the functional brain connectome for the discrimination of MCI and NC. When the functional connections, global metrics, and nodal metrics were combined, an accuracy of 92.9% was achieved on 105 participants (41 MCI patients and 60 NCs). However, accuracy dramatically dropped to 66.0% when testing the pretrained model with an independent dataset from the AD Neuroimaging Initiative (ADNI) database (Xu et al., 2020).

In this study, we retrospectively analyzed resting-state fMRI (rs-fMRI) data derived from 82 MCI patients and 93 NCs from ADNI. Brain functional networks were constructed from rs-fMRI data, and the network metrics were analyzed from three scales. Both cerebral and cerebellar regions were covered in the construction of the graph. A weighted network was used in order to keep the information in the functional connectivity (FC). Furthermore, graph metrics were then combined to train and validate an automatic model on MCI and NC subjects. Our primary goal was to investigate the alterations of network properties that occurred at the stage of MCI and to find out whether the analysis of functional network can assist the accurate diagnosis of MCI patients.

PARTICIPANTS

In this study, rs-fMRI data derived from 82 MCI patients and 93 NCs were obtained from the ADNI database.¹ Participants in ADNI were included in the present study if they met the following criteria: (i) ages between 55.0 and 80.0; (ii) scanning with parameters of repetition time of 3,000 ms, echo time of 30 ms, flip angle of 80° or 90°, slices of 48, and voxel size of 3.31 mm × 3.31 mm × 3.31 or 3.44 mm × 3.44 mm × 3.40 mm; (iii) available records of their cognitive and behavioral assessments, comprising scores from the 13-item AD assessment scale (ADAS13), clinical dementia rating scale sum of boxes (CDRSB), Mini-Mental State Examination (MMSE), and frequently asked questions (FAQ); (iv) head motions <1.5 mm and 1.5°; (v) mean fractional displacement head motion values <0.2 mm; and (vi) satisfying MRI quality control and excluding unclear spatial normalization pictures. The demographics and clinical characteristics of the participants are illustrated in **Table 1**. Cross-sectional comparisons indicated a significant group effect on ADAS13, CDRSB, MMSE, or FAQ scores.

¹<http://adni.loni.usc.edu/>

TABLE 1 | Demographic and clinical characteristics of MCI and NC.

Information	NC	MCI	p-value
Number of participants	93	82	
Age (years)	70.47 ± 5.91	71.61 ± 5.1	0.176
Gender (male/female)	46/36	36/57	0.024*
ADAS13 score	14.92 ± 6.81	11.62 ± 5.3	0.001*
CDRSB score	1.38 ± 1.26	0.13 ± 0.6	<0.001*
MMSE score	27.89 ± 1.82	28.88 ± 1.46	<0.001*
FAQ total score	3.15 ± 4.53	0.4 ± 1.93	<0.001*

NC, normal controls; MCI, mild cognitive impairment; ADAS13, 13-item Alzheimer's Disease Assessment Scale; CDRSB, Clinical Dementia Rating sum of boxes score; MMSE, Mini-Mental State Examination; FAQ, frequently asked questions; plus-minus score values are mean ± SD. *Significant difference between the two groups ($p < 0.05$).

Data Preprocessing

In this study, after discarding the first several volumes (five and seven for the data acquired before and after year 2014, respectively), data preprocessing was conducted with the help of Data Processing Assistant for Resting-State fMRI Advanced Edition (version 4.3), which is based on Statistical Parametric Mapping (SPM,²) and the toolbox for Data Processing and Analysis of Brain Imaging (DPABI³) (Yan and Zang, 2010; Yan et al., 2016). First, slice timing, motion correction, and normalization to the Montreal Neurological Institute space were conducted using T1 image unified segmentation. Then, nuisance covariates including six head motion parameters, white matter signal, cerebral spinal fluid signal, and global signal were regressed. In order to remove the spiking influence caused by motion artifacts (Power et al., 2012; Burgess et al., 2016; Ciric et al., 2017, 2018), a despiking step (Parkes et al., 2017) was adopted. Next, the temporal filtering (0.01–0.1 Hz) step was performed. Like general fMRI data using the echo-planar imaging sequence, artifacts could be caused by the distortion and loss of signal in the anterior temporal and orbitofrontal regions in ADNI, which might influence the connectivity between these regions and the others. To reduce the variability due to susceptibility artifacts, temporal signal-to-noise ratio (TSNR) (Murphy et al., 2007) map on the whole brain was calculated for each subject. A binary TSNR mask was obtained when a threshold of 20 was set on the averaged TSNR map (Zhuo et al., 2016) and further intersected with the Automated Anatomical Labeling (AAL) atlas to generate the final mask. Finally, based on the TSNR-thresholded AAL atlas, the preprocessed images were parcellated into 116 regions of interest (ROIs) and the regional mean time series of blood oxygenation level-dependent signals with the first 135 time points were extracted from each ROI for the further analysis.

From ROI Time Series to Weighted and Undirected Network

Time series derived from the i th and j th ROIs were denoted as X_i and X_j , respectively. The absolute Pearson correlation coefficient

between X_i and X_j , denoted as r_{ij} and calculated by Formula (1), was used in the present study to evaluate the FC between the two ROIs.

$$r_{ij} = \left| \frac{\sum (X_i - \bar{X}_i)(X_j - \bar{X}_j)}{\sqrt{\sum (X_i - \bar{X}_i)^2} \sqrt{\sum (X_j - \bar{X}_j)^2}} \right| \quad (1)$$

Here, \bar{X}_i and \bar{X}_j represent the mean of time series X_i and X_j , respectively. Given a total of N ROIs, a symmetric matrix \mathbf{w} with $N \times N$ elements can be obtained by evaluating the FC values over all the possible ROI pairs, as shown in Formula (2):

$$w_{ij} = \begin{cases} 1, & i = j \\ r_{ij}, & i, j \in [1, N], \text{ and } i \neq j \end{cases} \quad (2)$$

In order to exclude the self-connections, values in the diagonal line of matrix \mathbf{w} were then set to 0. In this way, for each individual, a fully connected, undirected, and weighted network was obtained by regarding each ROI as a node and \mathbf{w} as the adjacent matrix. We also constructed group-level networks based on the individual adjacent matrix for MCI patients and NCs, respectively. That is, the element w_{ij} of the group-level network is the average value of w_{ij} in each individual graph within a certain group. Such a group-level network summarizes FC maps on average over all subjects within the group and captures the connectivity backbone of the group (Meunier et al., 2009; Sun et al., 2014).

Topological Metrics in Three Scales

The topological characteristics of a fully connected network might be contaminated by the presence of numerous weak connections among ROIs. Generally, a threshold is used, and only the supra-threshold FCs are retained, leading to a sparse network for analysis. The term network sparsity or density was proposed to represent the proportion of supra-threshold connections relative to all possible connections. As most graph theoretic measures are contingent on the number of nodes and the connection density, it is common to prescribe a shared network sparsity for all the networks compared (Fornito et al., 2013). However, there is no unified rule for the determination of network sparsity. Therefore, we used a wide range of sparsities, i.e., from 5 to 50% with steps of 1%, to analyze graphical properties of brain functional network. When a certain sparsity was used, each full-connected network (estimated for either an individual or a group) was thresholded by keeping the corresponding number of edges with the strongest FCs.

For each participant, based on the individual network thresholded by a certain sparsity, classical network metrics for scale I, such as the clustering coefficient (C), characteristic path length (L), global efficiency (GE), and small worldness (SW , random number was set as 1,000) were investigated in this study. In scale II, the regional nodal characteristics regarding the global hubs were assessed qualitatively on the group-level networks obtained across the sparsities ranging from 5 to 50%. The betweenness centrality of a node i (denoted as bc_i) in the group-level network was calculated and normalized as $BC_i = bc_i / \langle bc_i \rangle$, where $\langle bc_i \rangle$ is the average betweenness of all

²<http://www.fil.ion.ucl.ac.uk/spm>

³<http://rfmri.org/DPABI>

nodes. BC_i measures the importance of node i over information flow between other nodes throughout the network, and the regions with high values of BC_i are usually identified as hubs. Some studies identified hubs as nodes with BC_i larger than 1.5 (He et al., 2008) or 2 (Yao et al., 2010), and in this study, we used a stricter threshold for the definition of hubs as 2.5. To be noted, nodal bc_i was also calculated for each subject on the individual network and the group difference was evaluated.

In scale III, we investigated the modular structure quantitatively via the group-level networks. The modular organization has been thought to be one of the most fundamental principles in complex systems and demonstrated to exist in human brain networks in previous studies (Deng et al., 2016; Pereira et al., 2016; Jalili, 2017). Modularity (denoted as Q in the following), a measure for the quality of the community structure in a network (Newman, 2006), was computed on the group-level networks for a qualitative assessment when network sparsity ranged from 5 to 50%, with steps of 1%. Meanwhile, modules were detected as subsets of nodes in the network that are more densely connected to the other nodes in the same module than to nodes outside the module (Radicchi et al., 2004).

Definitions and brief descriptions of the network metrics used are given in the Supplementary Material (**Supplementary Table S1**). More details can be found in a previous report (Rubinov and Sporns, 2010). The calculation of those metrics were implemented in MATLAB (version R2014a, Mathworks Inc., Natick, MA, United States) software with Brain Connectivity Toolbox (Rubinov and Sporns, 2010).

Statistical Analysis

Statistical evaluations were conducted using R program (version 4.0.2). For cross-sectional comparisons of demographic and clinical characteristics between the MCI and NC groups, the normality of the data was first evaluated by Lilliefors test. The Fisher's exact test was applied to categorical variables (only gender here), and Wilcoxon rank sum test or t -test was used to compare the continuous variables in the case of violating the normality or not. Logistic regression analysis, which considered group as dependent variable and network metrics (both global and nodal measures, i.e., C , L , GE , SW , and nodal bc_i) as independent variables, was used to evaluate whether there is significant difference of network metrics between both groups. Moreover, gender was controlled as concomitant variable in the logistic regression analysis. $p < 0.05$ was considered as an indicator for significant difference.

Classification of MCI and NC

In this study, in addition to four scores of cognitive assessments, there are four global and 116 nodal (i.e., bc) network metrics for each subject, resulting in 124 features under each sparsity. Considering the classification scenario with high-dimensional features and low-size samples, we hereby proposed a two-layer random forest approach for the task, with the first layer for feature selection and the second for classification. Such an approach was implemented on Python 3.7 with the widely used scikit-learn library (Pedregosa et al., 2011).

The importance of the used features can be measured by the out-of-bag (OOB) error (Genuer et al., 2010). In the random forest approach, under each sparsity, all the 124 features were fed into the first-layer forest and ranked according to the OOB error provided by scikit-learn. Afterward, the top N important features of the first layer were selected and fed into the second layer to train a model. A wide range of N from 5 to 30 was considered in this study.

For the second layer, two hyperparameters of the random forest, i.e., the number of trees in the forest and the maximum depth of the tree, were fine-tuned. Specifically, a five-fold grid search was embedded in an outer loop to fulfill a 10-fold nested cross-validation (CV) for evaluating the performance of the classifier, i.e., the accuracy, sensitivity, specificity, and area under receiver operating characteristic curve (AUC). Nested CV was demonstrated to produce robust and unbiased performance estimates regardless of sample size (Vabalas et al., 2019).

RESULTS

Global Network Metrics of Scale I

Global network properties including C , L , GE , and SW were calculated and compared for the MCI and NC groups across sparsities ranging from 5 to 50%, with steps of 1%. The results are illustrated in **Figure 1**. In both groups, all the global network metrics altered rapidly along with small sparsities and gradually converged toward a sparsity of 50%. No significant group difference of C was found at any sparsities (**Figure 1A**). Compared to NC, a significant decrease (or increase) of L (or GE) was observed in MCI across almost all the sparsities (**Figures 1B,C**). As shown in **Figure 1D**, the SW values were larger than one for both groups under all the calculated sparsities, suggesting the existence of small-world properties in the functional networks. However, significant group difference of SW can only be observed with the sparsity of 16–20%.

Moreover, partial correlation analysis (controlling gender) was used to evaluate the association between global network metrics (C , L , GE , and SW) and clinical characteristics (ADAS13, CDRSB, MMSE, and FAQ scores) by pooling all participants together. The values of C were shown to be associated negatively with MMSE and positively with CDRSB, ADAS13, or FAQ scores (**Figure 2A**), indicating a stable association between C and clinical symptoms of MCI regardless of network sparsity. Similarly, significant correlation was found between other global network metrics and the cognitive scores.

In **Figures 1, 2**, rapid alterations can be observed on both the values of the global network metrics and the correlation coefficients between them and the clinical scores when the used network sparsity was small (about <13%). Such an observation may be attributed to the isolated ROIs in the individual networks, which has a percentage >5% when sparsity <9% for NC and 12% for MCI group (shown in **Supplementary Figure S1**).

Nodal Characteristics of Scale II

The global hubs of the functional brain network were detected in both groups across all the considered sparsities. As shown in

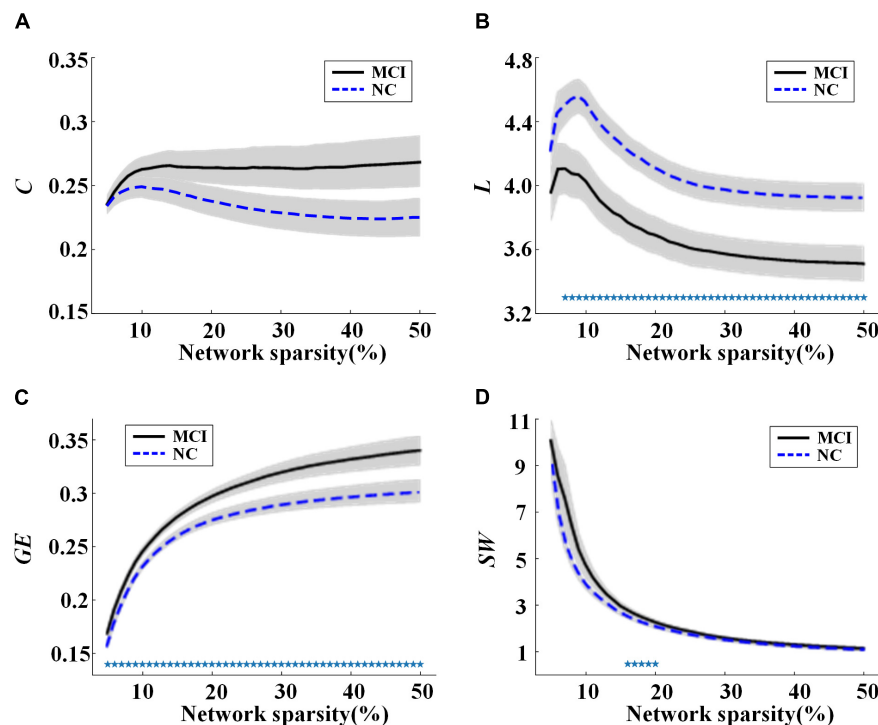


FIGURE 1 | Values of global network metrics (the central line represents the group mean and the envelopes represents mean \pm standard error) for normal controls (NC) and mild cognitive impairment (MCI) patients: **(A)** clustering coefficient, **(B)** characteristic path length, **(C)** global efficiency, and **(D)** small worldness. The symbol “*” represents a significant group difference of the network metric in the corresponding sparsity ($p < 0.05$, logistic regression analysis, controlling gender).

Figure 3, the right lobule VIII of cerebellar hemisphere (CER8.R) and the left insula (INS.L) were identified as global hubs across almost all the sparsities in both groups. Additionally, global hubs also occur frequently on regions including the left lobule VIII of the cerebellar hemisphere (CER8.L), the right lobule IV–V of the cerebellar hemisphere (CER4–5.R), the right superior frontal gyrus of the medial orbital surface (ORBsup.med.R), and the right middle frontal gyrus (MFG.R) in MCI (**Figure 3A**), as well as the right lobule VI of the cerebellar hemisphere (CER6.R), the left lobule IV–V of the cerebellar hemisphere (CER4–5.L), the bilateral Crus II of the cerebellar hemisphere (CERCERU2), and the left temporal pole of the superior temporal gyrus (TPOsup.L) in NC (**Figure 3B**). Moreover, regions in MCI, including the left rolandic operculum (ROL.L), the right superior temporal gyrus (STG.R), the right inferior occipital gyrus (IOG.R), and right caudate nucleus (CAU.R), and regions in NC, such as the right putamen (PUT.R), the left superior temporal gyrus (STG.L), the right temporal pole of superior temporal gyrus (TPOsup.R), and bilateral fusiform gyrus (FFG) were also identified as global hubs at about one third (or more) sparsities.

Significant differences of nodal bc between MCI patients and NCs were found in many ROIs, which were also identified as global hubs and altered across the groups, such as CER8.L, CERCERU2.R, bilateral FFG, IOG.R, and CAU.R (**Figure 4**). **Figure 5** further illustrates the values of bc in those regions, demonstrating an agreement with the quantitative information provided by the hubs of the group-level network.

The Modular Structure of Scale III

Figure 6A shows the modularity Q achieved for group-level networks and the corresponding randomized networks across the sparsities from 5 to 50%. The value of Q decreased with the increasing network sparsity for both groups. The result of permutation tests demonstrated that Q is significantly larger than those obtained by the randomly shuffled networks, indicating that the modular structure obtained is non-random across all the sparsities (**Figure 6A**) (see **Supplementary Material** for the details of permutation tests). The number of modules detected for each group also alters with the sparsities (**Figure 6B**). When there are no isolated nodes in the group-level network (i.e., sparsity larger than 7%), there would be two to five modules in each group.

Table 2 and **Figure 7** illustrated the modular structures detected in both groups at a sparsity of 16% where we obtained highest performance to discriminate MCI patients from NCs (introduced below). Four functionally oriented modules were uncovered for both groups. For the modular structure of NC, anatomically adjacent ROIs tended to be clustered into the same module. The first module, represented as Module I, contains the thalamus, basal ganglia, and all the ROIs in the cerebellar regions. Module II of NC covers the entire parietal lobe and the majority of frontal lobe. Moreover, the right anterior cingulate and paracingulate gyri, the bilateral precentral gyrus, and the bilateral posterior cingulate gyrus also joined in this module. The left middle frontal gyrus and all the ROIs located in the occipital lobe constitute a new module, named as Module III. All the rest

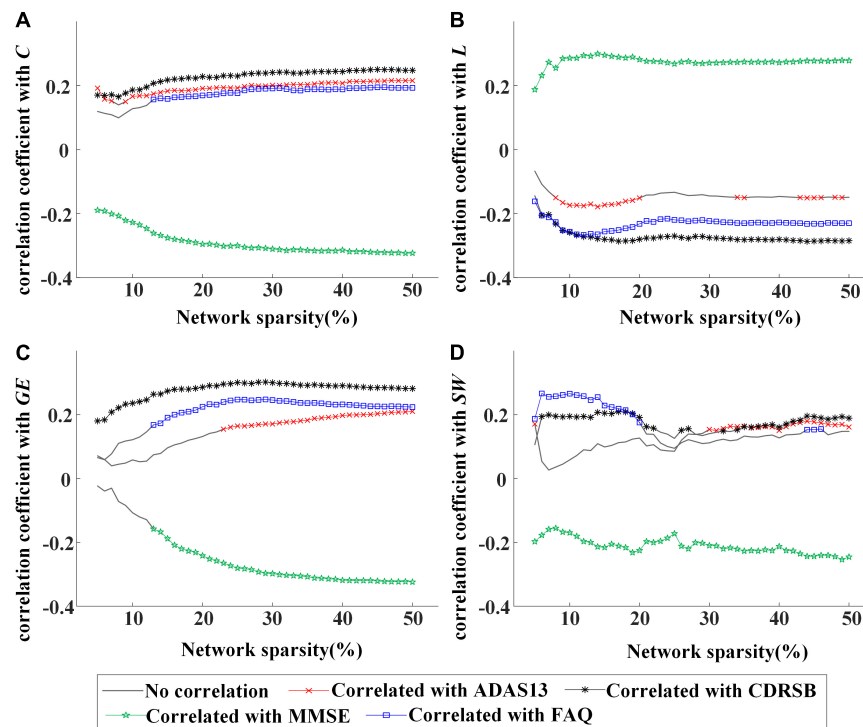


FIGURE 2 | Values of correlation coefficient between global network metrics and clinical assessments [13-item Alzheimer's disease assessment scale (ADAS13), clinical dementia rating scale sum of boxes (CDRSB), Mini-Mental State Examination (MMSE), and frequently asked questions (FAQ) scores]: **(A)** clustering coefficient, **(B)** characteristic path length, **(C)** global efficiency, and **(D)** small worldness. The symbol "x", "*", "♦", or "◻" represents a significant correlation ($p < 0.05$, partial correlation analysis, controlling gender) between the network metric and cognitive score in the corresponding sparsity.

of the ROIs were included in Module IV for NC group. For the MCI group, although anatomically adjacent regions are still likely to be included in the same module, alterations occur in its composition of modules, with a less localized organization of community structure compared with NC. For example, the ROIs of the cerebellum are separated into two modules, whereas they stay in the same module in the NC group. Moreover, the orbital surface of the frontal lobe distributed in two modules and exhibited a denser connection with ROIs such as the bilateral insula, hippocampus, and amygdala.

Classification of MCI and NC

Using the proposed two-layer random forest approach, we performed the classification of MCI patients and NCs. An accuracy of 86.3% was obtained by merely using the clinical assessments (scores of MMSE, CDRSB, ADAS13, and FAQ). However, when integrated with network metrics, improved accuracies can be achieved across all the sparsities (as shown in **Figure 8**), with highest accuracy of 91.4% obtained at the sparsity of 16%. The results suggested that the network metrics could provide additional useful information to assist the diagnosis of MCI patients.

The highest accuracy (91.4%) was achieved when we used the top 10 discriminative features (as shown in **Figure 9**). The CDRSB was found to be the most informative feature for the classification of MCI patients and NCs, with an overwhelming

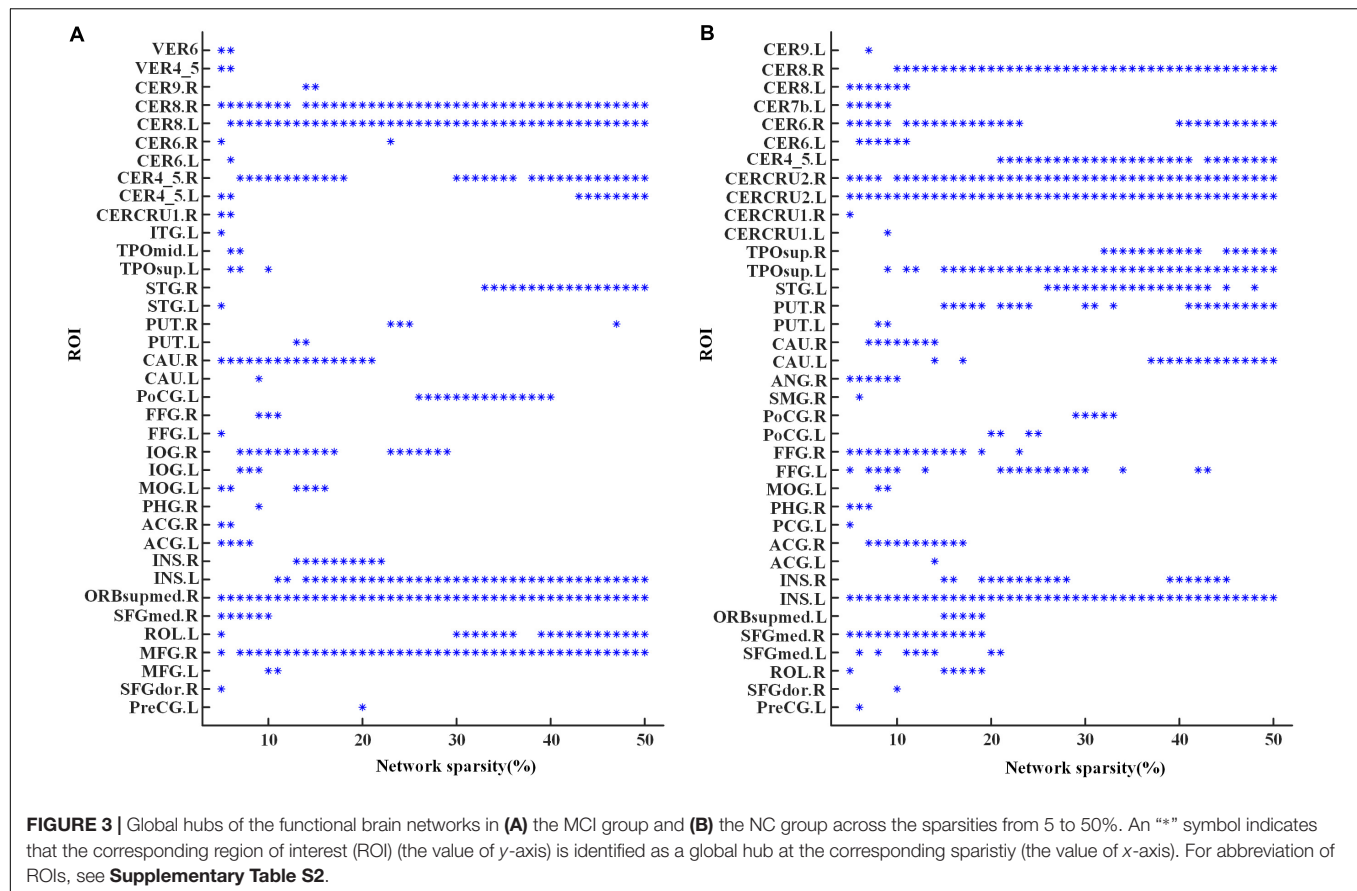
importance compared with the other features. Other cognitive assessments, FAQ, ADAS13, and MMSE, ranked at the second, fourth, and fifth positions, respectively. As for the network properties, nodal bc of CERCRU2.R also ranked in the top 5 important features. Moreover, the top 10 discriminative features included global metric L and nodal bc of another four regions, i.e., FFG.R, the right supramarginal gyrus (SMG.R), the right lobule VIIB of the cerebellar hemisphere (CERE7b.R), and IOG.R.

DISCUSSION

In the present work, we investigated the alteration of brain functional network in MCI patients. The network measures were explored on three scales, concerning its global metrics, nodal characteristics, and modular properties. Furthermore, the application of network metrics for patient's identification was performed and evaluated on a two-layer random forest approach. The results showed significant alterations of network metrics in MCI and suggested that the analysis of brain functional network could provide assistant information for the diagnosis of MCI with neuropsychological assessments.

Alterations in Global Network Metrics

The global network properties of scale I have been widely investigated in previous studies (Stam and Reijneveld, 2007;



Jalili, 2016). However, discrepancies exist in previous studies regarding the alteration of C , L , and GE of the human brain network in MCI. Taking L for example, some researchers found no significant difference between MCI and NC (Yao et al., 2010), while others reported a significant increase (Yao et al., 2018) or a significant decrease (Son et al., 2015) of L in MCI compared with NC. Here, significantly decreased L and increased GE were found in MCI compared with NC under almost all the considered sparsities, suggesting that an enhanced functional integration of brain network might occur at the prodromal stage of AD. Such an observation might be indicative of a possible compensatory mechanism in the early stage of AD (Zhou and Lui, 2013). Moreover, existing studies have demonstrated that the clinical symptoms of AD, such as impairments of memory, language, and other cognitive functions, were associated with abnormal structural and functional brain networks (Liu et al., 2017). In this study, we also observed a significant correlation between global network metrics and the clinical cognitive evaluations, suggesting that graph theory analysis could act as a strategy to differentiate MCI patients from NC subjects.

Alterations in Nodal Characteristics of Scale II

The existence of global hubs in human brain networks was supported by the present study. Although in this study, the global

hubs were identified on the group-level network, it provided informative findings that might be associated with the underlying pathological mechanism of MCI.

The most informative observation for the global hubs is its distribution in the cerebellum. For both groups, stable hubs were mainly distributed in cerebellar lobules IV–VI, VII, and VIII. Studies on cerebellar functional topography have shown that activity in sensorimotor regions were related to the contralateral cerebellar lobules IV–VI and VIII, whereas more cognitively demanding tasks engaged prefrontal and parietal cortices along with cerebellar lobules VI and VII (Stoodley et al., 2012). In the present study, CER8.R and CER4_5.L or CER4_5.R were identified as global hubs in both groups, which might suggest a maintained motor function in the MCI group. However, prominent alteration has been revealed within cerebellar lobules VI and VII since bilateral CERCRU2 (a part of lobule VII) and CER6.L were found to be stable hubs in the NC group but not in the MCI group (except for a few sparsities). Furthermore, the nodal bc of CERCRU2.R decreased significantly ($p < 0.05$, uncorrected) in MCI patients. We further observed positive correlation (partial correlation analysis, $p < 0.05$, controlling for gender) between nodal bc of CERCRU2.L and MMSE score across 40 out of 46 sparsities (average correlation coefficient over these sparsities was 0.19), and negative correlation between nodal bc of CERCRU2.R and ADAS13 scores (32 sparsities, average correlation coefficient was -0.18). The MMSE is the

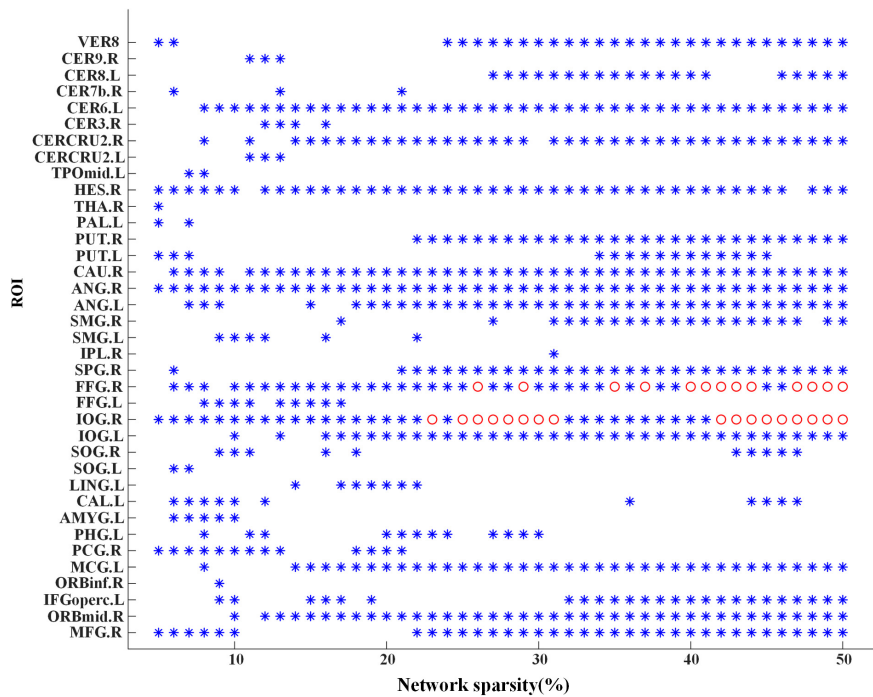


FIGURE 4 | Group difference of nodal betweenness centrality of the individual brain networks across the sparsities from 5 to 50%. A symbol of “**” indicates a significant difference ($p < 0.05$, logistic regression analysis, controlling gender) of bc in the corresponding region of interest (ROI) (the value of y-axis) at the corresponding sparsity (the value of x-axis). Additionally, the “o” symbol is employed for a significant difference at the level of $p < 0.05/116$ (logistic regression analysis, controlling gender). For abbreviation of ROIs, see **Supplementary Table S2**.

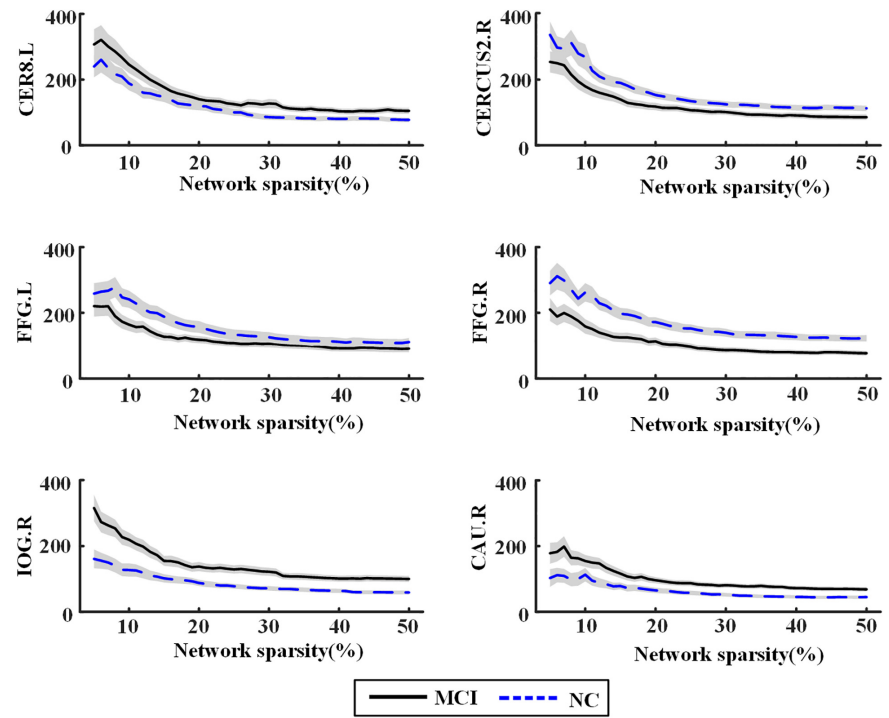


FIGURE 5 | Nodal betweenness centrality of the individual brain networks for normal control (NC) and mild cognitive impairment (MCI) in six regions of interest (ROIs). The central line represents the group mean and the envelopes represents mean \pm standard error. For abbreviation of ROIs, see **Supplementary Table S2**.

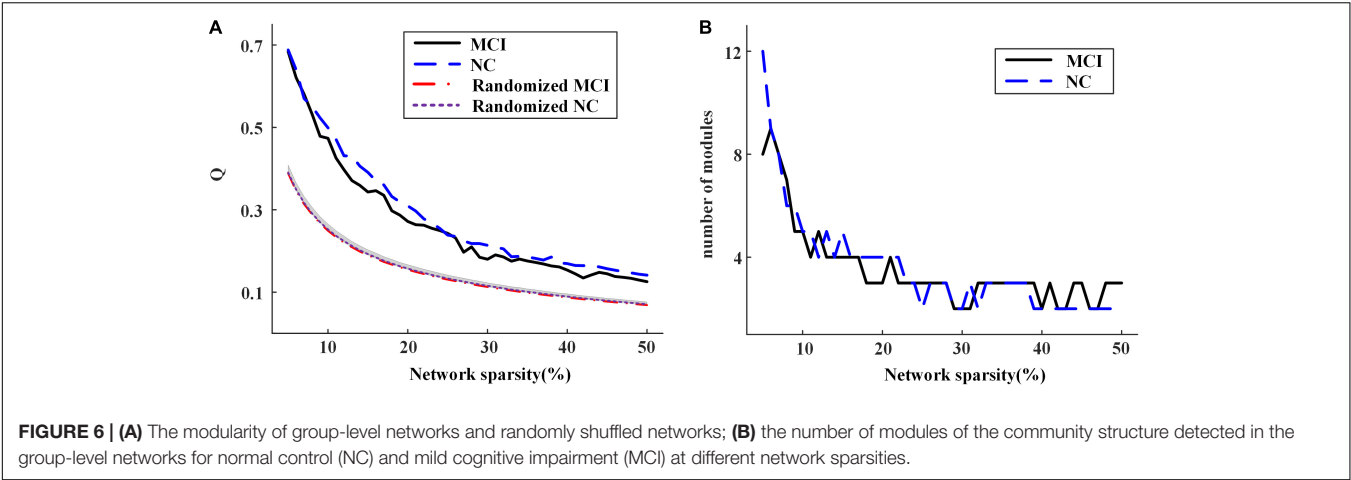


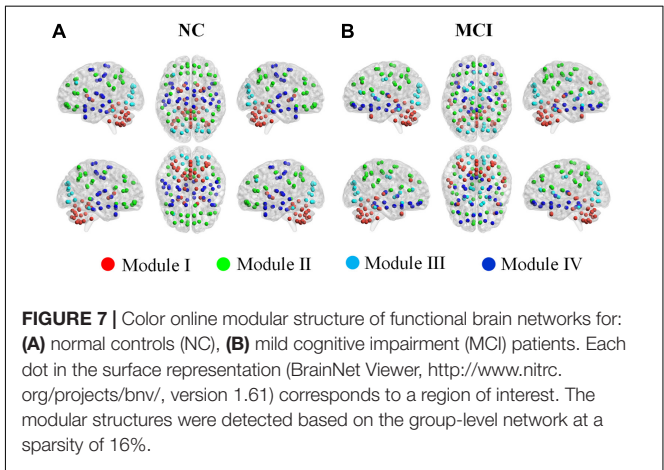
TABLE 2 | Alterations of modular composition in MCI group relative to NC.

Module in NC	Anatomical classification (abbreviation) of ROIs	Module in MCI
I (34)	CERCRU1.L, CERCRU1.R, CERCRU2.L, CERCRU2.R, CER4_5.R, CER6.L, CER6.R, CER7b.L, CER7b.R, CER8.L, CER8.R, CER9.L, CER9.R, CER10.L, CER10.R, VER4_5, VER6, VER7, VER8, VER9, VER10 CER3.L, CER3.R, CER4_5.L, VER1_2, VER3 CAU.L, CAU.R, PUT.L, PUT.R, PAL.L, PAL.R, THA.L, THA.R	I (21) IV (5) III (8)
II (37)	PreCG.L, PreCG.R, SFGdor.L, SFGdor.R, IFGoperc.L, IFGoperc.R, IFGtriang.L, IFGtriang.R, SFGmed.L, SFGmed.R, ORBsupmed.L, ORBsupmed.R, PCG.L, PCG.R, SPG.L, SPG.R, IPL.L, IPL.R, SMG.L, SMG.R, ANG.L, ANG.R, PCUN.L, PCUN.R MFG.R, MTG.R ORBsup.L, ORBsup.R, ORBmid.L, ORBmid.R, ORBinf.L, ORBinf.R, REC.L, REC.R OLF.R, ACG.L, ACG.R	II (24) I (2) IV (8) III (3)
III (15)	CAL.L, CAL.R, CUN.L, CUN.R, LING.L, LING.R, SOG.L, SOG.R, MOG.L, MOG.R, IOG.L, IOG.R, FFG.L, FFG.R MFG.L	III (14) II (1)
IV (30)	STG.L, STG.R, MTG.L, TPOmid.L, TPOmid.R, ITG.L, ITG.R ROL.L, ROL.R, SMA.L, SMA.R, PoCG.L, PoCG.R, PCL.L, PCL.R OLF.L, INS.L, INS.R, HIP.L, HIP.R, PHG.L, PHG.R, AMYG.L, AMYG.R, HES.L, HES.R, TPOsup.L, TPOsup.R MCG.L, MCG.R	I (7) II (8) IV (13) III (2)

NC, normal controls; MCI, mild cognitive impairment subjects. For the description of the AAL-atlas abbreviations, see **Supplementary Table S2**.

best known and the most common used short screening tool of AD for providing an overall measure of cognitive impairment in clinical, research, and community settings (Arevalo-Rodriguez et al., 2015), where ADAS13 is another widely used cognitive assessment with a higher value indicating poorer cognitive performance (Mohs et al., 1997; Sano et al., 2011). In this study, cognitive impairment of the MCI patients was reflected by both MMSE and ADAS13 scores (**Table 1**). A previous study demonstrated that cognitive impairments may occur when posterior lobe lesions affect cerebellar lobules VI and VII, which would disrupt cerebellar modulation of cognitive loops with cerebral association cortices (Stoodley et al., 2012). Therefore, our findings suggested that alteration of FC in the cerebellum (especially in the CERCRU2) be associated with the cognitive impairment in MCI, and the cerebellum may be a potential target for neuromodulation in treating MCI.

Significant changes of the network metrics of scale II were also in found the bilateral FFG (especially FFG.R) and IOG.R. FFG is thought to be a key structure for functionally specialized computations of high-level vision such



as face perception, object recognition, and reading (Weiner and Zilles, 2016). Katja Weibert and Timothy J. Andrews demonstrated that the activity in FFG.R predicts the behavioral

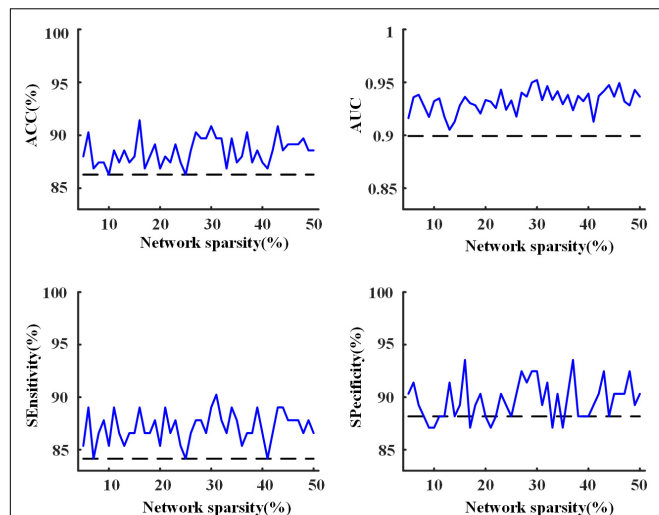


FIGURE 8 | The accuracy, area under receiver operating characteristic curve (AUC), sensitivity, and specificity of the 10-fold cross-validation (CV) for the classification of mild cognitive impairment (MCI) and normal control (NC) with the proposed two-layer random forest approach. The dashed line was achieved by using only the scores of clinical assessments while the solid line represents the model performance obtained after the combination of clinical assessments and network analysis.

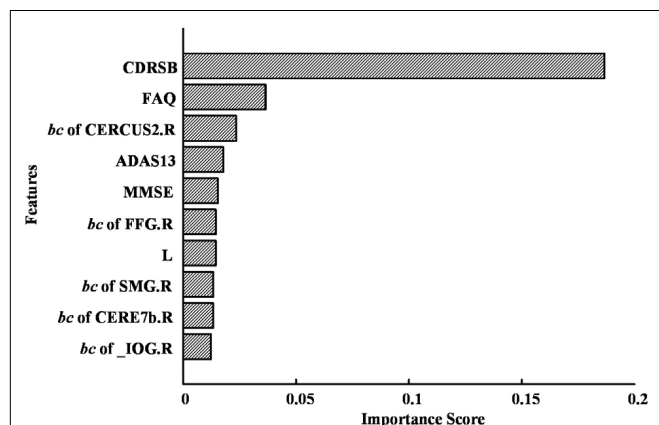


FIGURE 9 | The top 10 discriminative features and their feature importance in the first-layer random forest for the classification of mild cognitive impairment (MCI) and normal control (NC) at a sparsity of 16%. For abbreviation of regions of interest (ROIs), see **Supplementary Table S2**.

advantage for the perception of familiar faces (Weibert and Andrews, 2015). Based on a study of rs-fMRI, Cai et al. (2015) reported altered FC of FFG in patients suffering from amnesic MCI. IOG is also important for the visual function during face processing, since it is connected to the amygdala via white matter connectivity and forms a network for facial recognition with the amygdala (Sato et al., 2017). Previous studies demonstrated activation in bilateral FFG and IOG.R revealed by a face localizer contrast (faces–objects) (Rossion et al., 2003). In the present study, we found that both FFG.R and FFG.L are frequently present as

global hubs in NC but absent in MCI, while IOG.R turns out in MCI but not in NC. Furthermore, the nodal *bc* of FFG.R decreased significantly in MCI while that of IOG.R significantly increased. We thus speculated that MCI patients might have an affected function of FFG.R, leading to a compensatory role in IOG.R.

Alterations in Modular Structure of Scale III

The present study confirms the existence of modular organization in human brain networks, even in MCI patients. We detected four modules for each group. For both groups, although discrepancies existed in their composition of modules, some common features can be found in the modular structure. Such features might throw light on the basis of two fundamental aspects of the human functional brain network, i.e., the functional segmentation and integration. On the one hand, anatomically adjacent ROIs tend to be clustered into the same module, which might be the foundation of the functional segmentation of the brain network. On the other hand, those ROIs, whose anatomical neighbors were involved into a different module, are likely to act as bridges to connect different modules and to be identified as global hubs in the whole network. Such a phenomenon should contribute to the functional integration and the existence of small-worldness property of the brain network.

The prominent alteration of the modular structure in MCI (compared with NC) occurs in the cerebellum, with its ROIs grouped into two modules. Another obvious change in the modular structure in MCI occurs in the medial prefrontal cortex, especially the orbitofrontal cortex (OFC). In previous studies, the OFC has been found to be involved in sensory integration, in representing the affective value of reinforcers, and in decision making and expectation (Kringelbach, 2005). In the present study, six out of eight OFC ROIs are shifted to Module IV and clustered with the hippocampus and parahippocampal regions in MCI. As structural abnormalities in the OFC have been revealed by neuroimaging studies in MCI patients (Wang et al., 2020), in the future, it would be of interest to investigate whether our findings related to the OFC is the cause or effect of its structural abnormalities in MCI.

The Classification of MCI and NC

In clinical practice, the MCI diagnosis mainly depended on concerns of the cognition changes from the patient, knowledgeable informant, or according to a skilled clinician's observation (Langa and Levine, 2014). Neuropsychological assessments, such as CDRSB and MMSE, are often used in clinical trial for objective evidence of cognitive impairment (Langa and Levine, 2014). In the present study, with the combination of MMSE, CDRSB, ADAS13, and FAQ scores, we found an accuracy of 86.3% for the classification of MCI and NC, confirming the effectiveness of neuropsychological assessments in the diagnosis of MCI. Improved performances with highest accuracy of 91.4%

can be achieved by combining neuropsychological assessments and network analysis after feature selection implemented via random forest approach. Furthermore, we found that the CDRSB score played a vital role in discriminating MCI, in line with a previous study which demonstrated that the CDRSB score could be used to accurately stage severity of AD and MCI (O'bryant et al., 2008). In addition, our results of feature selection further indicated the importance to investigate the role of CERCRU2.R, FFG.R, and IOG.R in MCI.

CONCLUSION AND LIMITATION

In this study, we investigated the alterations of brain functional network in MCI. Although small-world properties, global hubs, and modular structures were observed in both groups, network metrics significantly changed in MCI when compared with NC. The role of cerebellar regions, especially the Crus II of cerebellar hemisphere, were found to be associated with the cognitive impairment in MCI patients and discriminative in the identification of MCI. Although network metrics were demonstrated to provide useful information to assist the diagnosis of MCI in clinical practice, future investigation is required to clarify the association between these alterations and the underlying pathological mechanism of MCI.

Moreover, the sex factor was controlled in the statistical analysis to evaluate the group difference of network metrics or their association with clinical characteristics in scales I and II. Because the modular structure of each group was computed at group level, the findings in scale III are hereby descriptive, which suggests that we cannot statistically assess whether they are partly contributed by sex difference. Given our observation that sex contribution to scales I and II is trivial, we speculate that the descriptive modular structure is not contributed by sex difference. Future study on a larger sample is thus in favor of the validation of our findings, especially those in scale III.

DATA AVAILABILITY STATEMENT

Publicly available datasets were analyzed in this study, which can be found at: <http://adni.loni.usc.edu/>.

ETHICS STATEMENT

The studies involving human participants were reviewed and approved by the institutional review board of each participating center in the ADNI study. Each participant provided signed

informed consent before the study. All methods were carried out in accordance with relevant guidelines and regulations. The current study analyzed de-identified data from the ADNI database, and did not involve a research protocol requiring approval by the relevant institutional review board or ethics committee.

AUTHOR CONTRIBUTIONS

FH, JW, JQ, and AY designed this study. LZ and ZY analyzed the data. LZ, FH, and HN wrote the article. All authors contributed to the article and approved the submitted version.

FUNDING

This research was funded by the National Natural Science Foundation of China (Grant Nos. 61401518 and 81701346), the Natural Science Foundation of Jiangsu Province (Grant No. BK20190736), Jiangsu Provincial Key R&D Program (Social Development) (Grant No. BE2015700), Natural Science Research Major Program in Universities of Jiangsu Province (Grant No. 16KJA310002), NUPTSF (Grant No. NY218138), and the Double First-Class University project.

ACKNOWLEDGMENTS

The authors acknowledge the support team of the AD Neuroimaging Initiative (ADNI) for their detailed explanations and assistance in our use of the dataset. ADNI was launched in 2003 as a \$60 million, 5-year public-private partnership by the National Institute on Aging, the National Institute of Biomedical Imaging and Bioengineering, the Food and Drug Administration, private pharmaceutical companies, and non-profit organizations (Podhorna et al., 2016). The primary goal of ADNI was to test whether a combination of clinical and neuropsychological assessment, serial MRI, positron emission tomography, and examination of other biological markers could indicate progression from MCI to AD.

SUPPLEMENTARY MATERIAL

The Supplementary Material for this article can be found online at: <https://www.frontiersin.org/articles/10.3389/fnins.2020.558434/full#supplementary-material>

REFERENCES

- Ahmadlou, M., Adeli, H., and Adeli, A. (2010). New diagnostic EEG markers of the Alzheimer's disease using visibility graph. *J. Neural Transm.* 117, 1099–1109. doi: 10.1007/s00702-010-0450-3
- Al-Shoukry, S., Rassem, T. H., and Makbol, N. M. (2020). Alzheimer's diseases detection by using deep learning algorithms: a mini-review. *IEEE Access* 8, 77131–77141. doi: 10.1109/access.2020.2989396
- Arevalo-Rodriguez, I., Smailagic, N., Roqué I Figuls, M., Ciapponi, A., Sanchez-Perez, E., Giannakou, A., et al. (2015). Mini-Mental State Examination (MMSE) for the detection of Alzheimer's disease and other dementias in people with mild cognitive impairment (MCI). *Cochrane Database Systematic Rev.* 2015:CD010783. doi: 10.1002/14651858.CD010783.pub2
- Burgess, G. C., Kandala, S., Dan, N., Laumann, T. O., Power, J. D., Adeyemo, B., et al. (2016). Evaluation of denoising strategies to address motion-correlated

- artifact in resting state fmri data from the human connectome project. *Brain Connect.* 6, 669–680. doi: 10.1089/brain.2016.0435
- Cai, S., Chong, T., Zhang, Y., Li, J., von Deneen, K. M., Ren, J., et al. (2015). Altered functional connectivity of fusiform gyrus in subjects with amnesic mild cognitive impairment: a resting-state fMRI study. *Front. Hum. Neurosci.* 9:471. doi: 10.3389/fnhum.2015.00471
- Calzà, L., Gagliardi, G., Rossini Favretti, R., and Tamburini, F. (2021). Linguistic features and automatic classifiers for identifying mild cognitive impairment and dementia. *Comp. Speech Lang.* 65:101113. doi: 10.1016/j.csl.2020.101113
- Chen, G., Ward, B. D., and Xie, C. (2011). Classification of Alzheimer disease, mild cognitive impairment, and normal cognitive status with large-scale network analysis based on resting-state functional MR imaging. *Radiology* 259, 213–221. doi: 10.1148/radiol.10100734
- Ciric, R., Rosen, A., Erus, G., Cieslak, M., Adebimpe, A., Cook, P. A., et al. (2018). Mitigating head motion artifact in functional connectivity MRI. *Nat. Protocols* 13, 2801–2826. doi: 10.1038/s41596-018-0065-y
- Ciric, R., Wolf, D. H., Power, J. D., Roalf, D. R., Baum, G. L., Ruparel, K., et al. (2017). Benchmarking of participant-level confound regression strategies for the control of motion artifact in studies of functional connectivity. *Neuroimage* 154, 174–187. doi: 10.1016/j.neuroimage.2017.03.020
- Cui, X., Xiang, J., Guo, H., Yin, G., Zhang, H., Lan, F., et al. (2018). Classification of Alzheimer's disease, mild cognitive impairment, and normal controls with subnetwork selection and graph kernel principal component analysis based on minimum spanning tree brain functional network. *Front. Comput. Neurosci.* 12:31. doi: 10.3389/fncom.2018.00031
- Davatzikos, C., Bhatt, P., Shaw, L. M., Batmanghelich, K. N., and Trojanowski, J. Q. (2011). Prediction of MCI to AD conversion, via MRI, CSF biomarkers, and pattern classification. *Neurobiol. Aging* 32:2322.e19–27. doi: 10.1016/j.neurobiolaging.2010.05.023
- Deng, Y., Shi, L., Lei, Y., Wang, D., Alzheimer's Disease, and Neuroimaging Initiative. (2016). Altered topological organization of high-level visual networks in Alzheimer's disease and mild cognitive impairment patients. *Neurosci. Lett.* 630, 147–153. doi: 10.1016/j.neulet.2016.07.043
- Fang, J., Chen, H., Cao, Z., Jiang, Y., Ma, L., Ma, H., et al. (2017). Impaired brain network architecture in newly diagnosed parkinson's disease based on graph theoretical analysis. *Neurosci. Lett.* 14, 151–158. doi: 10.1016/j.neulet.2017.08.002
- Fornito, A., Zalesky, A., and Breakspear, M. (2013). Graph analysis of the human connectome: Promise, progress, and pitfalls. *Neuroimage* 80, 426–444. doi: 10.1016/j.neuroimage.2013.04.087
- Genuer, R., Poggi, J. M., and Tuleau-Malot, C. (2010). *Variable Selection Using Random Forests*. Amsterdam: Elsevier Science Inc. doi: 10.1016/j.patrec.2010.03.014
- Gosztolya, G., Vincze, V., Tóth, L., Pákási, M., Kálmán, J., Hoffmann, I., et al. (2019). Identifying mild cognitive impairment and mild Alzheimer's disease based on spontaneous speech using ASR and linguistic features. *Comp. Speech Lang.* 53, 181–197. doi: 10.1016/j.csl.2018.07.007
- He, Y., Chen, Z., and Evans, A. (2008). Structural insights into aberrant topological patterns of large-scale cortical networks in Alzheimer's disease. *J. Neurosci.* 28, 4756–4766. doi: 10.1523/jneurosci.0141-08.2008
- Jalili, M. (2016). Functional brain networks: does the choice of dependency estimator and binarization method matter? *Sci. Rep.* 6:29780. doi: 10.1038/srep29780
- Jalili, M. (2017). Graph theoretical analysis of Alzheimer's disease: discrimination of AD patients from healthy subjects. *Inform. Sci.* 384, 145–156. doi: 10.1016/j.ins.2016.08.047
- Jie, B., Zhang, D., Gao, W., Wang, Q., Wee, C. Y., Shen, D., et al. (2013). Integration of network topological and connectivity properties for neuroimaging classification. *IEEE Transact. Bio-med. Eng.* 61, 576–589. doi: 10.1109/tbme.2013.2284195
- Jie, B., Zhang, D., and Wee, C.-Y. (2014). Topological graph kernel on multiple thresholded functional connectivity networks for mild cognitive impairment classification. *Hum. Brain Mapp.* 35, 2876–2897. doi: 10.1002/hbm.22353
- Khazaei, A., Ebrahimzadeh, A., and Babajani-Feremi, A. (2015). Identifying patients with Alzheimer's disease using resting-state fMRI and graph theory. *Clin. Neurophysiol.* 126, 2132–2141. doi: 10.1016/j.clinph.2015.02.060
- Khazaei, A., Ebrahimzadeh, A., and Babajani-Feremi, A. (2016). Application of advanced machine learning methods on resting-state fMRI network for identification of mild cognitive impairment and Alzheimer's disease. *Brain Imag. Behav.* 10, 799–817. doi: 10.1007/s11682-015-9448-7
- Kringelbach, M. L. (2005). The human orbitofrontal cortex: linking reward to hedonic experience. *Nat. Rev. Neurosci.* 6, 691–702. doi: 10.1038/nrn1747
- Langa, K. M., and Levine, D. A. (2014). The diagnosis and management of mild cognitive impairment: a clinical review. *JAMA* 312, 2551–2561. doi: 10.1001/jama.2014.13806
- Li, Y., Wang, Y., Wu, G., Shi, F., Zhou, L., Lin, W., et al. (2011). Discriminant analysis of longitudinal cortical thickness changes in Alzheimer's disease using dynamic and network features. *Neurobiol. Aging* 33, 427.415–430. doi: 10.1016/j.neurobiolaging.2010.11.008
- Liu, J., Li, M., Pan, Y., Lan, W., Zheng, R., Wu, F.-X., et al. (2017). Complex brain network analysis and its applications to brain disorders: a survey. *Complexity* 2017:27. doi: 10.1017/9781316882610.003
- Meunier, D., Achard, S., Morcom, A., and Bullmore, E. (2009). Age-related changes in modular organization of human brain functional networks. *Neuroimage* 44, 715–723. doi: 10.1016/j.neuroimage.2008.09.062
- Mohs, R. C., Knopman, D., Petersen, R. C., Ferris, S. H., Ernesto, C., Grundman, M., et al. (1997). Development of cognitive instruments for use in clinical trials of antidementia drugs: additions to the Alzheimer's disease assessment scale that broaden its scope. the Alzheimer's disease cooperative study. *Alzheimer Dis. Assoc. Disord* 11(Suppl. 2), S13–S21. doi: 10.1097/00002093-199700112-00003
- Murphy, K., Bodurka, J., and Bandettini, P. (2007). How long to scan? the relationship between fmri temporal signal to noise ratio and necessary scan duration. *NeuroImage* 34, 565–574. doi: 10.1016/j.neuroimage.2006.09.032
- Newman, M. E. J. (2006). Modularity and community structure in networks. *Proc. Natl. Acad. Sci. U.S.A.* 103, 8577–8582. doi: 10.1073/pnas.0601602103
- O'bryant, S. E., Waring, S. C., Cullum, C. M., Hall, J., Lacritz, L., Massman, P. J., et al. (2008). Staging dementia using clinical dementia rating scale sum of boxes scores: a texas Alzheimer's research consortium study. *Arch. Neurol.* 65, 1091–1095. doi: 10.1001/archneur.65.8.1091
- Onias, H., Viol, A., Palhano-Fontes, F., Andrade, K. C., Sturzbecher, M., Viswanathan, G., et al. (2014). Brain complex network analysis by means of resting state fMRI and graph analysis: will it be helpful in clinical epilepsy? *Epilepsy Behav.* 38, 71–80. doi: 10.1016/j.yebeh.2013.11.019
- Orimaye, S. O., Goodkin, K., Riaz, O. A., Salcedo, J. M., Al-Khateeb, T., Awujoola, A. O., et al. (2020). A machine learning-based linguistic battery for diagnosing mild cognitive impairment due to Alzheimer's disease. *PLoS One* 15:e0229460. doi: 10.1371/journal.pone.0229460
- Pagen, L. H. G., Van De Ven, V. G., Gronenschild, E. H. B. M., Priovoulos, N., Verhey, F. R. J., Jacobs, H. I. L., et al. (2020). Contributions of cerebro-cerebellar default mode connectivity patterns to memory performance in mild cognitive impairment. *J. Alzheimer's Dis.* 75, 633–647. doi: 10.3233/jad-191127
- Parkes, L., Fulcher, B., Yücel, M., and Fornito, A. (2017). An evaluation of the efficacy, reliability, and sensitivity of motion correction strategies for resting-state functional MRI. *Neuroimage* 171, 415–436. doi: 10.1016/j.neuroimage.2017.12.073
- Pedregosa, F., Varoquaux, G., Gramfort, A., Michel, V., and Thirion, B. (2011). Scikit-learn: machine learning in python. *J. Mach. Learn. Res.* 12, 2825–2830.
- Pereira, J. B., Mijalkov, M., and Kakaei, E. (2016). Disrupted network topology in patients with stable and progressive mild cognitive impairment and Alzheimer's disease. *Cereb. Cortex* 26, 3476–3493. doi: 10.1093/cercor/bhw128
- Podhorna, J., Krahne, T., Shear, M., Harrison, J. E., Alzheimer's Disease, and Neuroimaging Initiative. (2016). Alzheimer's disease assessment scale-cognitive subscale variants in mild cognitive impairment and mild Alzheimer's disease: change over time and the effect of enrichment strategies. *Alzheimers Res. Ther.* 8:8. doi: 10.1186/s13195-016-0170-5
- Power, J. D., Barnes, K. A., Snyder, A. Z., Schlaggar, B. L., and Petersen, S. E. (2012). Spurious but systematic correlations in functional connectivity MRI networks arise from subject motion. *NeuroImage* 59, 2142–2154. doi: 10.1016/j.neuroimage.2011.10.018
- Radicchi, F., Castellano, C., Cecconi, F., Loreto, V., and Parisi, D. (2004). Defining and identifying communities in networks. *Proc. Natl. Acad. Sci. U.S.A.* 101, 2658–2663. doi: 10.1073/pnas.0400054101
- Rossion, B., Schiltz, C., and Crommelinck, M. (2003). The functionally defined right occipital and fusiform "face areas" discriminate novel from visually familiar faces. *Neuroimage* 19, 877–883. doi: 10.1016/S1053-8119(03)00105-8

- Rubinov, M., and Sporns, O. (2010). Complex network measures of brain connectivity: uses and interpretations. *NeuroImage* 52, 1059–1069. doi: 10.1016/j.neuroimage.2009.10.003
- Sánchez-Catasús, C. A., Willemsen, A., Boellaard, R., Juárez-Orozco, L. E., Samper-Noa, J., Aguila-Ruiz, A., et al. (2018). Episodic memory in mild cognitive impairment inversely correlates with the global modularity of the cerebral blood flow network. *Psychiatry Res. Neuroimag.* 282, 73–81. doi: 10.1016/j.psychres.2018.11.003
- Sano, M., Raman, R., Emond, J., Juárez-Orozco, L. E., Samper-Noa, J., Aguila-Ruiz, A., et al. (2011). Adding delayed recall to the Alzheimer disease assessment scale is useful in studies of mild cognitive impairment but not Alzheimer disease. *Alzheimer Dis. Assoc. Disord.* 25, 122–127. doi: 10.1097/wad.0b013e3181f883b7
- Sato, W., Kochiyama, T., Uono, S., Matsuda, K., Usui, K., Usui, N., et al. (2017). Bidirectional electric communication between the inferior occipital gyrus and the amygdala during face processing. *Hum. Brain Mapp.* 38, 4511–4524. doi: 10.1002/hbm.23678
- Seo, E. H., Lee, D. Y., Lee, J.-M., Park, J. S., Sohn, B. K., Lee, D. S., et al. (2013). Whole-brain functional networks in cognitively normal, mild cognitive impairment, and Alzheimer's disease. *PLoS One* 8:e53922. doi: 10.1371/journal.pone.0053922
- Son, S.-J., Kim, J., Seo, J., Lee, J. M., Park, H., Alzheimer's Disease, et al. (2015). Connectivity analysis of normal and mild cognitive impairment patients based on FDG and PiB-PET images. *Neurosci. Res.* 98, 50–58. doi: 10.1016/j.neures.2015.04.002
- Stam, C. J., and Reijneveld, J. C. (2007). Graph theoretical analysis of complex networks in the brain. *Nonlinear Biomed. Phys.* 1:3. doi: 10.1186/1753-4631-1-3
- Stoodley, C. J. (2012). The cerebellum and cognition: evidence from functional imaging studies. *Cerebellum* 11, 352–365. doi: 10.1007/s12311-011-0260-7
- Stoodley, C. J., Valera, E. M., and Schmahmann, J. D. (2012). Functional topography of the cerebellum for motor and cognitive tasks: an fMRI study. *NeuroImage* 59, 1560–1570. doi: 10.1016/j.neuroimage.2011.08.065
- Suk, H.-I., Wee, C.-Y., and Shen, D. (2013). Discriminative group sparse representation for mild cognitive impairment classification. *Mach. Learn. Med. Imag.* 2013, 131–138. doi: 10.1007/978-3-319-02267-3_17
- Sun, Y., Yin, Q., Fang, R., Yan, X., Wang, Y., Bezerianos, A., et al. (2014). Disrupted functional brain connectivity and its association to structural connectivity in amnesic mild cognitive impairment and Alzheimer's disease. *PLoS One* 9:e96505. doi: 10.1371/journal.pone.0096505
- Tabatabaei-Jafari, H., Walsh, E., Shaw, M. E., Cherbuin, N., Alzheimer's Disease, and Neuroimaging Initiative. (2017). The cerebellum shrinks faster than normal ageing in Alzheimer's disease but not in mild cognitive impairment. *Hum. Brain Mapp.* 38, 3141–3150. doi: 10.1002/hbm.23580
- Tanveer, M., Richhariya, B., Khan, R. U., Rashid, A. H., Khanna, P., Prasad, M., et al. (2020). Machine learning techniques for the diagnosis of Alzheimer's disease: a review. *ACM Trans. Multimedia Comput. Commun. Appl.* 16, 1–35. doi: 10.1145/3344998
- Tijms, B. M., Wink, A. M., De Haan, W., van der Flier, W. M., Stam, C. J., Scheltens, P., et al. (2013). Alzheimer's disease: connecting findings from graph theoretical studies of brain networks. *Neurobiol. Aging* 34, 2023–2036. doi: 10.1016/j.neurobiolaging.2013.02.020
- Vabalas, A., Gowen, E., Poliakoff, E., and Casson, A. J. (2019). Machine learning algorithm validation with a limited sample size. *PLoS One* 14:e0224365. doi: 10.1371/journal.pone.0224365
- Wang, J., Zuo, X., and Dai, Z. (2013). Disrupted functional brain connectome in individuals at risk for Alzheimer's disease. *Biol. Psychiatry* 73, 472–481. doi: 10.1016/j.biopsych.2012.03.026
- Wang, Z., Zhang, X., Liu, R., Wang, Y., Qing, Z., Lu, J., et al. (2020). Altered sulcogyral patterns of orbitofrontal cortex in patients with mild cognitive impairment. *Psychiatry Res. Neuroimag.* 302:111108. doi: 10.1016/j.psychres.2020.111108
- Wee, C.-Y., Li, Y., Jie, B., Peng, Z. W., and Shen, D. (2013a). Identification of MCI using optimal sparse MAR modeled effective connectivity networks. *Med. Image Comput. Comp. Ass. Intervent. – MICCAI* 2013, 319–327. doi: 10.1007/978-3-642-40763-5_40
- Wee, C.-Y., Yap, P.-T., Zhang, D., Wang, L., and Shen, D. (2013b). Group-constrained sparse fMRI connectivity modeling for mild cognitive impairment identification. *Brain Struct. Funct.* 219, 641–656. doi: 10.1007/s00429-013-0524-8
- Weibert, K., and Andrews, T. J. (2015). Activity in the right fusiform face area predicts the behavioural advantage for the perception of familiar faces. *Neuropsychologia* 75, 588–596. doi: 10.1016/j.neuropsychologia.2015.07.015
- Weiner, K. S., and Zilles, K. (2016). The anatomical and functional specialization of the fusiform gyrus. *Neuropsychologia* 83, 48–62. doi: 10.1016/j.neuropsychologia.2015.06.033
- Xiang, J., Guo, H., Cao, R., Liang, H., and Chen, J. (2013). An abnormal resting-state functional brain network indicates progression towards Alzheimer's disease. *Neural Regenerat. Res.* 8:2789.
- Xu, X., Li, W., Mei, J., Tao, M., Wang, X., Zhao, Q., et al. (2020). Feature selection and combination of information in the functional brain connectome for discrimination of mild cognitive impairment and analyses of altered brain patterns. *Front. Aging Neurosci.* 12:28. doi: 10.3389/fnagi.2020.00028
- Yan, C., and Zang, Y. (2010). DPARSF: a MATLAB toolbox for “pipeline” data analysis of resting-state fMRI. *Front. Systems Neurosci.* 4:13. doi: 10.3389/fnsys.2010.00013
- Yan, C. G., Wang, X. D., Zuo, X. N., and Zang, Y. F. (2016). DPABI: data processing & analysis for (Resting-State) brain imaging. *Neuroinformatics* 14, 339–351. doi: 10.1007/s12021-016-9299-4
- Yao, Z., Hu, B., Chen, X., Xie, Y., Gutknecht, J., Majoe, D., et al. (2018). Learning metabolic brain networks in MCI and AD by robustness and leave-one-out analysis: an FDG-PET study. *Am. J. Alzheimer's Dis. Other Dementias* 33, 42–54. doi: 10.1177/1533317517731535
- Yao, Z., Zhang, Y., Lin, L., Zhou, Y., Xu, C., Jiang, T., et al. (2010). Abnormal cortical networks in mild cognitive impairment and Alzheimer's disease. *PLoS Comput. Biol.* 6:e1001006. doi: 10.1371/journal.pcbi.1001006
- Zhao, X., Liu, Y., Wang, X., Liu, B., Xi, Q., Guo, Q., et al. (2012). Disrupted small-world brain networks in moderate Alzheimer's disease: a resting-state fMRI study. *PLoS One* 7:e33540. doi: 10.1371/journal.pone.0033540
- Zhou, Y., and Lui, Y. W. (2013). Small-world properties in mild cognitive impairment and early Alzheimer's disease: a cortical thickness MRI study. *ISRN Geriatrics* 2013:542080. doi: 10.1155/2013/542080
- Zhuo, J., Fan, L., Liu, Y., Zhang, Y., Yu, C., and Jiang, T. (2016). Connectivity profiles reveal a transition subarea in the parahippocampal region that integrates the anterior temporal-posterior medial systems. *J. Neurosci.* 36, 2782–2795. doi: 10.1523/jneurosci.1975-15.2016

Conflict of Interest: The authors declare that the research was conducted in the absence of any commercial or financial relationships that could be construed as a potential conflict of interest.

Copyright © 2020 Zhang, Ni, Yu, Wang, Qin, Hou and Yang for the Alzheimer's Disease Neuroimaging Initiative (ADNI). This is an open-access article distributed under the terms of the Creative Commons Attribution License (CC BY). The use, distribution or reproduction in other forums is permitted, provided the original author(s) and the copyright owner(s) are credited and that the original publication in this journal is cited, in accordance with accepted academic practice. No use, distribution or reproduction is permitted which does not comply with these terms.



Neuroprotective Effect of Optogenetics Varies With Distance From Channelrhodopsin-2 Expression in an Amyloid- β -Injected Mouse Model of Alzheimer's Disease

Xiaorui Cui^{1,2†}, Feng Zhang^{3†}, Hui Zhang⁴, Xi Huang⁴, Kewei Wang⁵, Ting Huang⁶, Xifei Yang^{7*} and Liangyu Zou^{4*}

OPEN ACCESS

Edited by:

Kin Ying Mok,
University College London,
United Kingdom

Reviewed by:

Harun Noristani,
Temple University, United States
Xingchun Gou,
Xi'an Medical University, China

*Correspondence:

Liangyu Zou
zouliangyu@yahoo.com
Xifei Yang
xifeiyang@gmail.com

[†] These authors have contributed
equally to this work

Specialty section:

This article was submitted to
Neurodegeneration,
a section of the journal
Frontiers in Neuroscience

Received: 15 July 2020

Accepted: 14 September 2020

Published: 09 October 2020

Citation:

Cui X, Zhang F, Zhang H,
Huang X, Wang K, Huang T, Yang X
and Zou L (2020) Neuroprotective
Effect of Optogenetics Varies With
Distance From Channelrhodopsin-2
Expression in an Amyloid- β -Injected
Mouse Model of Alzheimer's Disease.
Front. Neurosci. 14:583628.
doi: 10.3389/fnins.2020.583628

¹ Department of Neurology, Second Clinical Medical College of Jinan University, Shenzhen People's Hospital, Shenzhen, China, ² Department of Neurology, Affiliated Hospital of Xiangnan University, Chenzhou, China, ³ Intensive Care Unit, The First Affiliated Hospital, Jinan University, Guangzhou, China, ⁴ Department of Neurology, Shenzhen People's Hospital (First Affiliated Hospital of Southern University of Science and Technology), Second Clinical College, Jinan University, Shenzhen, China, ⁵ Department of Neurology, Longgang District People's Hospital of Shenzhen, Shenzhen, China, ⁶ Department of Cerebrovascular Disease, People's Hospital of Yuxi, The Sixth Affiliated Hospital of Kunming Medical University, Yuxi, China, ⁷ Key Laboratory of Modern Toxicology of Shenzhen, Shenzhen Center for Disease Control and Prevention, Shenzhen, China

Background: Alzheimer's disease (AD) is a progressive neurodegenerative disease that is the most common cause of dementia. Optogenetics uses a combination of genetic engineering and light to activate or inhibit specific neurons in the brain.

Objective: The objective of the study was to examine the effect of activation of glutamatergic neurons in the hippocampus of mice injected with A β 1-42 on memory function and biomarkers of neuroinflammation and neuroprotection in the brain to elucidate the clinical utility of optogenetic neuromodulation in AD.

Methods: AAV5–CaMKII–channelrhodopsin-2 (CHR2)–mCherry (A β -CHR2 mice) or AAV5–CaMKII–mCherry (A β -non-CHR2 mice) was injected into the dentate gyrus (DG) of the bilateral hippocampus of an A β 1-42-injected mouse model of AD. The novel object recognition test was used to investigate working memory (M1), short-term memory (M2), and long-term memory (M3) after A β 1-42 injection. Hippocampus tissues were collected for immunohistochemical analysis.

Results: Compared to controls, M1 and M2 were significantly higher in A β -CHR2 mice, but there was no significant difference in M3; NeuN and synapsin expression were significantly increased in the DG of A β -CHR2 mice, but not in CA1, CA3, the subventricular zone (SVZ), or the entorhinal cortex (ENT); GluR2 and IL-10 expressions were significantly increased, and GFAP expression was significantly decreased, in CA1, CA3, the DG, and the SVZ of A β -CHR2 mice, but not in the ENT.

Conclusion: Activation of glutamatergic neurons by optogenetics in the bilateral DG of an A β -injected mouse model of AD improved M1 and M2, but not M3. A single-target optogenetics strategy has spatial limitations; therefore, a multiple targeted optogenetics approach to AD therapy should be explored.

Keywords: Alzheimer's disease, amyloid-1-42, channelrhodopsin-2, memory, novel object recognition, neuroprotection, neuro-inflammation

INTRODUCTION

Alzheimer's disease (AD) is a progressive neurodegenerative disease that is the most common cause of dementia (Aravanis et al., 2007). AD is characterized by pathological changes that include amyloid- β (A β) deposition, marked neuronal loss, and tau hyperphosphorylation (Gomez-Isla et al., 1996; Scheff et al., 2006; Crews and Masliah, 2010). Increasingly, evidence suggests that soluble low-molecular-weight A β oligomers are associated with neurotoxicity (Lambert et al., 1998; Lesne et al., 2006; Ono et al., 2009). In a novel mouse model, small, soluble A β_{1-42} oligomers induced extensive neuronal loss *in vivo*, and initiated a cascade of events that mimicked key neuropathological events in AD (Brouillette et al., 2012).

Optogenetics uses a combination of genetic engineering and light to activate or inhibit specific neurons in the brain and explore the functions associated with those neurons (Deisseroth, 2011). Optogenetics has been used to investigate the pathophysiology of Parkinson's disease and epilepsy, but studies applying optogenetics to AD are scarce.

AAV5–CaMKII–Chr2–mCherry is an adeno-associated virus (AAV) expressing channelrhodopsin-2 (Chr2)–mCherry under the control of the glutamatergic neuron promoter, CamKII (Aravanis et al., 2007). The objective of the present study was to examine the effect of activation of glutamatergic neurons in the hippocampus of mice injected with soluble low-molecular-weight A β_{1-42} on memory function and biomarkers of neuroinflammation and neuroprotection in the brain to elucidate the clinical utility of optogenetic neuromodulation in AD.

MATERIALS AND METHODS

Study Design

All experiments were approved by the Animal Resources Committee, Jinan University, China (No. LL-KT-2011134) and performed according to the Guide for the Care and Use of Laboratory Animals (NIH publication No. 8523, revised 1985).

A flow chart of the study design is shown in **Figure 1**. A total of 36 8-month-old female C57BL/6 mice were purchased from Guangdong Medical Laboratory Animal Center, China [license No. SCXK (Yue) 2008-0002]. Mice were housed at $20 \pm 2^\circ\text{C}$ and $55 \pm 5\%$ humidity, with free access to food and water, under a 12/12 h light/dark cycle. The mice were randomly allocated into three groups: A β mice ($n = 6$), A β -non-CHR2 mice ($n = 6$),

and A β -CHR2 mice ($n = 6$). AAV5–CaMKII–CHR2–mCherry (A β -CHR2 mice) or AAV5–CaMKII–mCherry (A β -non-CHR2 mice) was injected into the dentate gyrus (DG) of the mouse bilateral hippocampus. Fourteen days later, $0.2 \mu\text{g}$ of soluble low-molecular-weight A β_{1-42} was injected, and light stimulation with an optical fiber was performed at the same site. Low-molecular-weight A β_{1-42} injection and light stimulation were repeated once a day for 7 days. Behavioral tests were performed on Day 0 and Days 1–6 after A β_{1-42} injection. Mice were sacrificed on Day 7, and tissues were collected for immunochemical analysis.

Soluble Low-Molecular-Weight A β_{1-42}

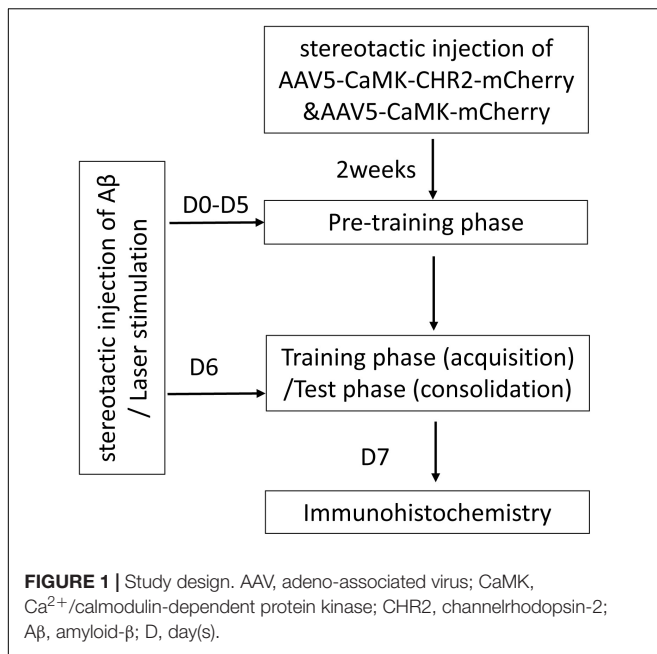
A β_{1-42} peptide solution was prepared according to a previously published protocol (Kuperstein et al., 2010; Brouillette et al., 2012). Briefly, A β_{1-42} peptide (Sigma A9810) was dissolved in 99% hexafluoroisopropanol (HFIP) (Sigma-Aldrich) to a concentration of 1 mg/ml. After evaporation under nitrogen gas, the peptide film was dissolved in dimethylsulfoxide (DMSO; Sigma-Aldrich) to a concentration of 1 mg/ml and eluted on a 5 ml HiTrap desalting column (GE Healthcare) with 50 mM Tris, 1 mM EDTA buffer, and pH 7.5. A β_{1-42} concentration was measured with a BCA protein assay kit (Pierce, Rockford, IL, United States). A β_{1-42} was stored on ice and used within 30 min.

Surgical Procedures

AAV5–CaMKII–CHR2–mCherry and AAV5–CaMKII–mCherry were provided by Shenzhen Institutes of Advanced Technology, Chinese Academy of Sciences. All surgeries were performed under stereotaxic guidance.

Mice were anesthetized with 500 mg/kg of avertin. Bilateral cannulae (328OPD-2.8/Spc with a removable dummy wire; Plastics One) were stereotaxically implanted into the DG of the hippocampus [coordinates with respect to bregma: -2.2 mm anteroposterior (AP), $\pm 1.4 \text{ mm}$ mediolateral (ML), -2.1 mm dorsoventral (DV)], as previously described (Paxinos and Watson, 2005; Brouillette et al., 2012). AAV5–CaMKII–CHR2–mCherry or AAV5–CaMKII–mCherry were injected at 100 nl/min for 10 min to a total of $1 \mu\text{l}$ through a microelectrode holder (MPH6S; WPI) using a glass micropipette and a $10 \mu\text{l}$ Hamilton microsyringe (701LT; Hamilton). The needle was retained for 5 min following completion of the injection. Expression of AAV5–CaMKII–CHR2–mCherry and AAV5–CaMKII–mCherry were histologically confirmed 14 days after surgery. Subsequently, A β_{1-42} $0.2 \mu\text{g}/\mu\text{l}$ was injected into the DG at 100 nl/min for 10 min to a total of $1 \mu\text{l}$, as previously described. Next, a fiber optic patchcord optical fiber (200 mm core diameter; Doric Lenses) was implanted at

Abbreviations: AD, Alzheimer's disease; DG, dentate gyrus; ENT, entorhinal cortex; GFAP, glial fibrillary acidic protein; GluR2, glutamate receptors; IL, interleukin; NeuN, neuronal nuclei; SVZ, subventricular zone.



the site of the A β_{1-42} injection, and optical stimulation was generated by a laser (473 nm, 1–3 ms, 10 Hz) (Changchun New Industries) for 5 min.

Behavioral Test

The novel object recognition test was used to assess the ability of mice to recognize a novel object in their environment. The novel object recognition test was conducted in three phases: (1) Pre-training, mice were allowed to explore an arena without objects for 5 min daily on Day 0 and Days 1–5 after A β_{1-42} injection. (2) Training phase (acquisition): on Day 6 after A β_{1-42} injection, the mice were placed in the arena with two identical sample objects (A1 and A2) positioned in two adjacent corners 10 cm from the walls. The mice were placed against the center of the opposite wall with their back to the objects. The mice were allowed to explore the objects for 3 min and were then placed in their home cage. A memory index (M0) was calculated as follows: $M0 (\%) = (\text{exploration time devoted to object A2} / \text{exploration time devoted to object A1} + \text{exploration time devoted to object A2}) \times 100$. (3) Test phase (consolidation): mice were placed in the arena with two objects in the same position, one was identical to the sample objects, and the other was novel (A1 and B). The mice were allowed to explore the objects 5 min, 2 h, or 24 h after the training phase to measure working memory (M1), short-term memory (M2), or long-term memory (M3). The memory indices were calculated as follows: $M1, M2, M3 (\%) = \text{exploration time devoted to object B} / (\text{exploration time devoted to object A1} + \text{exploration time devoted to object B}) \times 100$. A higher memory index implied a better ability to recognize a familiar object.

Immunohistochemistry

Mouse brain was embedded in paraffin. Brain tissue was sectioned to 30 μm in the coronal plane at the target area

and temporarily stored in a 12-well plate in PBS. Sections were treated with xylene and rehydrated in graded ethanol (Fachim et al., 2016). Sections were blocked in 3% BSA at room temperature for 1 h and incubated in 0.3% Triton X-100/PBS with primary antibody overnight at 4°C. Primary antibodies were mouse anti-gial fibrillary acidic protein (GFAP, 5 $\mu\text{g}/\text{ml}$, Cat. No. MAB3402, Chemicon), monoclonal mouse anti-NeuN (1:500, Cat. No. MAB377, Millipore), monoclonal mouse anti-synapsin Ia/b (A-1, 1:100, Cat. NO. sc-398849, Santa Cruz), rabbit anti-glutamate receptor 2 (GluR-2, 1:4,000 Cat. No. AB1768, Millipore), or mouse anti-interleukin (IL)-10 (A-2, 1:100 Cat. No. sc-365858, Santa Cruz). After washing, sections were incubated with secondary antibody in the dark for 1 h at room temperature. Secondary antibodies were goat anti-mouse IgG (H&L, 1:2,000 Cat. No. ab7067; Abcam) or goat anti-rabbit IgG (H&L, HRP, 1:2,000 Cat. No. ab6721; Abcam). Images of CA1, CA3, the DG, the subventricular zone (SVZ), and the entorhinal cortex (ENT) were visualized with a light microscope (DMI 3000 B; Leica, Buffalo Grove, IL, United States). The number of immunostained-positive cells was counted using Image J software (NIH, Bethesda, MD, United States) in a double-blind manner and was expressed as a percentage of the A β mice.

Statistical Analysis

Statistical analyses were performed using SPSS19.0 and Prism 6 (GraphPad). Data are presented as mean \pm SEM. Data from the behavioral tests were compared using repeated measures analysis of variance. Data from immunohistochemical analysis were compared with one-way analysis of variance. $P < 0.05$ was considered statistically significant.

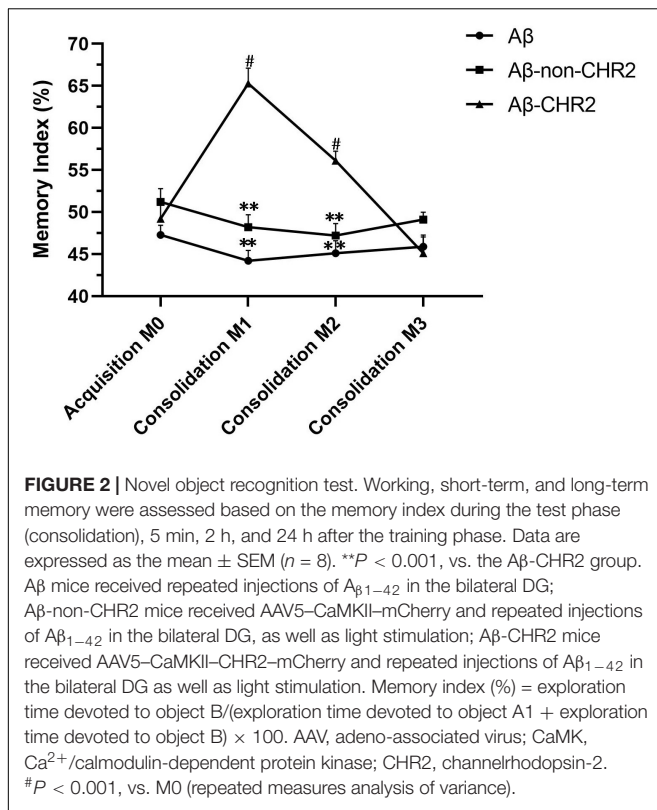
RESULTS

Effect of AAV5–CaMK–CHR2–mCherry on Memory Function in Mice

M1 and M2 were significantly increased compared to M0 in A β -CHR2 mice ($F = 25.12$, $P < 0.0001$), but there was no significant difference between M0 and M3 ($P > 0.05$). There were no significant differences between M0, M1, M2, and M3 in A β -non-CHR2 mice and A β mice (A β -non-CHR2 mice, $F = 1.524$, $P > 0.05$; A β mice, $F = 1.099$, $P > 0.05$). M1 and M2 were significantly higher in A β -CHR2 mice compared to A β -non-CHR2 mice and A β mice ($F = 53.93$, $P < 0.001$ for M1; $F = 18.31$, $P < 0.001$ for M2). There were no significant differences in M3 in A β -CHR2 mice, A β -non-CHR2 mice, and A β mice ($F = 2.002$, $P > 0.05$) (Figure 2). These results suggest that working memory and short-term memory, but not long-term memory, were rescued by optogenetic treatment.

Effect of AAV5–CaMKII–CHR2–mCherry on NeuN and Synapsin Expression in CA1, CA3, the DG, the SVZ, and the ENT

NeuN and synapsin expressions were significantly increased in the DG of A β -CHR2 mice compared to that of A β -non-CHR2 mice and A β mice ($P < 0.05$). There were no significant



differences in NeuN and synapsin expression in CA1, CA3, the SVZ, or the ENT of A β -CHR2 mice, A β -non-CHR2 mice, and A β mice ($P > 0.05$) (Figure 3).

Effect of AAV5-CaMKII-CHR2-mCherry on GluR2, IL-10, and GFAP Expression in CA1, CA3, the DG, the SVZ, and the ENT

GluR2 and IL-10 expressions were significantly increased, and GFAP expression was significantly decreased in CA1, CA3, the DG, and the SVZ of A β -CHR2 mice compared to A β -non-CHR2 mice and A β mice ($P < 0.05$). There were no significant differences in GluR2, IL-10, and GFAP expression in the ENT of A β -CHR2 mice, A β -non-CHR2 mice, and A β mice ($P > 0.05$) (Figure 4).

DISCUSSION

This study used optogenetics and investigated the effect of stimulating CaMK-CHR2-expressing neurons in the DG of the bilateral hippocampus on memory function and biomarkers of neuroinflammation and neuroprotection in the brain of an A β -injected mouse model of AD. Findings showed: (1) optogenetics improved working memory and short-term memory, but not long-term memory, in A β -CHR2 mice, and (2) optogenetics activated GluR2, attenuated neuroinflammation, and exerted neuroprotective effects in the core but not the peripheral areas of CHR2 expression.

Optogenetics enables precise temporal control of neuronal activity and has been used in a number of contexts (Gradinaru et al., 2009; Tye et al., 2011). Bi et al. (2006) proposed the expression of microbial-type channelrhodopsins, such as ChR2, in surviving inner retinal neurons as a potential strategy for the restoration of vision after rod and cone degeneration. Van den Oever et al. (2013) used optogenetics to explore the involvement of ventromedial prefrontal cortex (vmPFC) pyramidal cells in recent and remote conditioned cocaine memory in mice. Activation of pyramidal cells resulted in the loss of remote memory, without affecting recent memory, and inhibition of pyramidal cells impaired recall of recent memory, without affecting remote memory (Van den Oever et al., 2013).

Cognitive impairment in AD is characterized by memory disorders, mental and behavioral changes, insomnia, and autonomic dysfunction (Greene et al., 1996). Memory is a complex phenomenon, and memory impairment is the most prominent symptom of AD. In the present study, a novel object recognition test was used to assess memory function in an A β -injected mouse model of AD. The novel object recognition test has been used to evaluate the ability of mice to recognize a novel object in familiar surroundings (Ennaceur and Delacour, 1988) and to recognize an object after administration of bilateral lidocaine (Hammond et al., 2004), providing information on working memory, short-term memory, and long-term memory. The present study demonstrated that M1 and M2 were significantly higher in A β -CHR2 mice compared to A β -non-CHR2 mice and A β mice, and there were no significant differences in M3 in A β -CHR2 mice, A β -non-CHR2 mice, and A β mice. This implies that optogenetics improved working memory and short-term memory, but not long-term memory, in A β -CHR2 mice.

The hippocampus is severely affected early in the AD process (Hyman et al., 1984; Hyman et al., 1994). The hippocampus proper, which is defined by CA1-CA3 and the dentate gyrus, is the core structure within a larger hippocampal formation, which includes the adjacent subicular and rhinal cortices. The entorhinal cortex is among the first of the medial temporal lobe regions to exhibit dysfunction in early AD (Khan et al., 2014). Therefore, the neurobiological mechanisms underlying the improvement in memory function after optogenetic activation in the A β -injected mouse model of AD were investigated using histological studies of the neurons and synapses in the mouse hippocampus and entorhinal cortex.

NeuN and synapsin have neuroprotective effects. NeuN is a biomarker for arcuate neurons, and synapsins are involved in synaptogenesis and plasticity of mature synapses and play a major role in maintaining brain physiology (Meunier et al., 2015). Synapsins I and II are the major synapsin isoforms in neurons; both can be recognized by anti-synapsin Ia/b. Synapsin I is associated with elongation of axons and regulation of synaptic vesicle fusion. Synapsin II is essential for the synaptic vesicle cycle through its involvement in vesicle docking (Mirza and Zahid, 2018). In the present study, NeuN and synapsin expression in the core area of CHR2 injection was significantly increased, while there was no difference in NeuN and synapsin expression in the peripheral areas of CHR2 expression, including CA1, CA3,

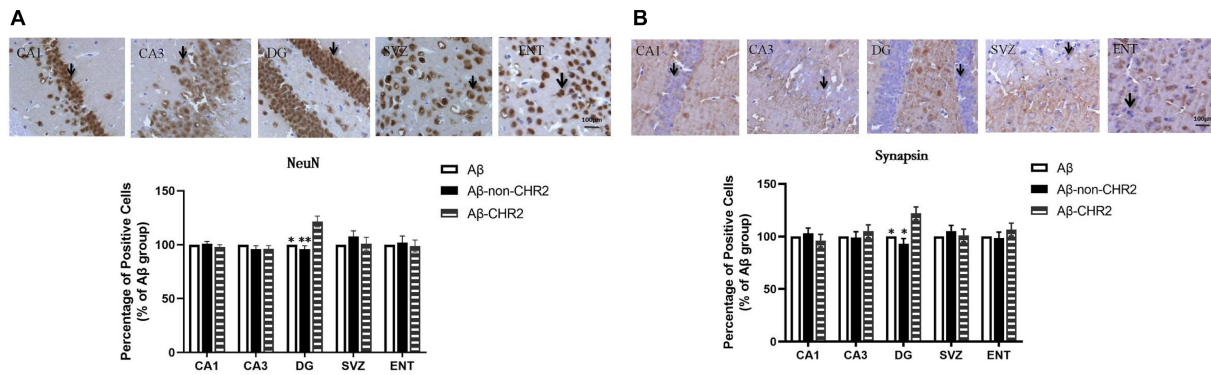


FIGURE 3 | Effect of CHR2 on NeuN (A) and synapsin (B) expression in CA1, CA3, the DG, the SVZ and the ENT ($n = 6$). Arrows show the positive cells, 400 \times . * $P < 0.05$, ** $P < 0.01$ vs. the A β -CHR2 mice. A β mice received repeated injections of A β_{1-42} in the bilateral DG; A β -non-CHR2 mice received AAV5-CaMKII-mCherry and repeated injections of A β_{1-42} in the bilateral DG, as well as light stimulation; A β -CHR2 mice received AAV5-CaMKII-CHR2-mCherry and repeated injections of A β_{1-42} in the bilateral DG as well as light stimulation. DG, dentate gyrus; ENT, entorhinal cortex; NeuN, neuronal nuclei; SVZ, subventricular zone.

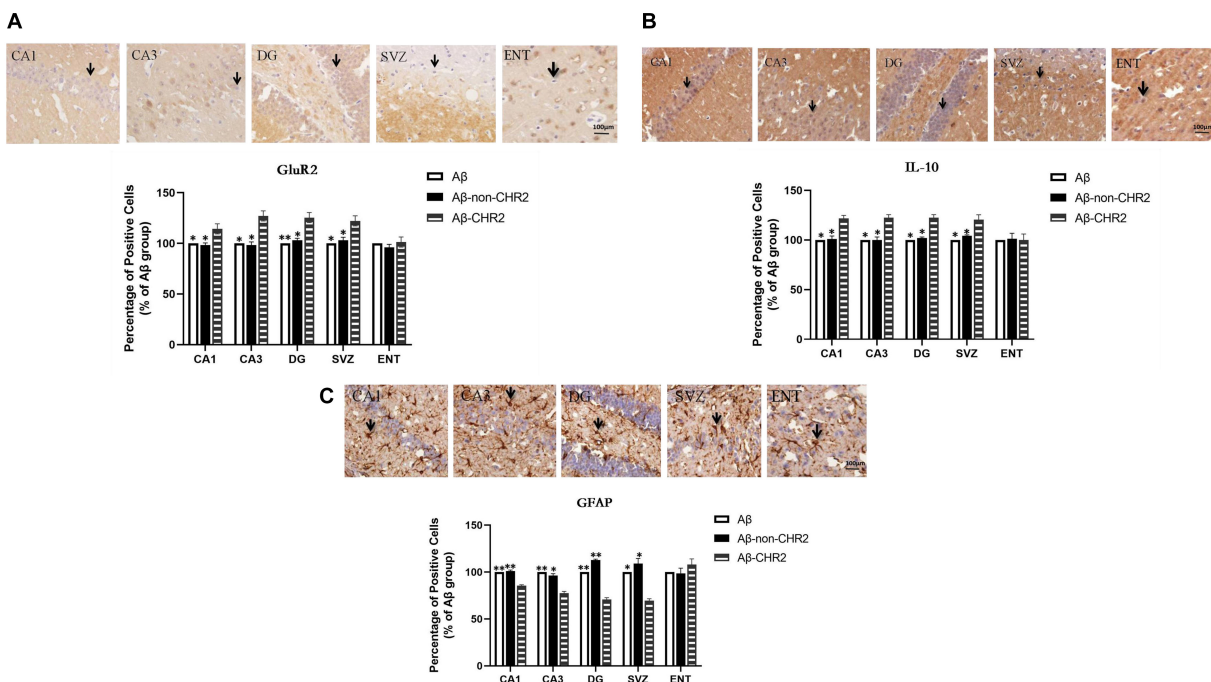


FIGURE 4 | Effect of CHR2 on GluR2 (A), IL-10 (B), and GFAP (C), expression in CA1, CA3, DG, the SVZ, and the ENT ($n = 6$). Arrows show positive cells, 400 \times . * $P < 0.05$, ** $P < 0.01$ vs. A β -CHR2 mice. A β mice received repeated injections of A β_{1-42} in the bilateral DG; A β -non-CHR2 mice received AAV5-CaMKII-mCherry and repeated injections of A β_{1-42} in the bilateral DG, as well as light stimulation; A β -CHR2 mice received AAV5-CaMKII-CHR2-mCherry and repeated injections of A β_{1-42} in the bilateral DG as well as light stimulation. DG, dentate gyrus; ENT, entorhinal cortex; GFAP, glial fibrillary acidic protein; GluR2, glutamate receptors; IL, interleukin; NeuN, neuronal nuclei; SVZ, subventricular zone.

the SVZ, and the more distant ENT, compared to controls. This suggests that optogenetic activation of glutamatergic neurons in the DG exerted neuroprotective effects locally, but the effects of optogenetics declined or disappeared with distance from CHR2 expression.

Various regions of the brain are involved in executive memory. The medial temporal lobe (hippocampal system), prefrontal cortex, diencephalon (papillary body and thalamus),

and amygdala are reciprocally connected and associated with learning and memory (Naya et al., 2017; Shirayama et al., 2017; Guo et al., 2019). Short-term memory (including working memory) and long-term memory are separate systems. The neural basis of short-term memory and long-term memory are located in the hippocampus and multiple cortical regions, respectively (Matthews, 2015; Hampson et al., 2018). In the present study, the neuroprotective effect of optogenetics was

limited to the DG and may have been one mechanism underlying the observed improvement in working memory and short-term memory in A β -CHR2 mice. As optogenetic activation of neurons in the DG did not extend to the cortex, there was no obvious enhancement of long-term memory.

Optogenetics combines optics and genetics to control well-defined events in tissues or behaviors in animals (Duebel et al., 2015). It drives physiological changes in a tissue by influencing neurons or synapses via cytokines or neurotransmitters (Van den Oever et al., 2013). A β is a pathological hallmark of AD, and A β -injected mouse models of AD show AD-like behavioral abnormalities and A β pathology. Here, optogenetics was used to activate glutamatergic neurons in the brain of an A β -injected mouse model of AD.

The glutamate family of receptors includes the ionotropic receptors [e.g., α -amino-3-hydroxy-5-methyl-4-isoxazolepropionate (AMPA)] and metabotropic receptors (mGluR; G-protein coupled). AMPA receptors are comprised of different combinations of GluR1–GluR4 subunits. RNA editing at the Q/R site of the GluR2 subunit confers Ca²⁺ impermeability to AMPA receptors. The edited form represents nearly 100% of GluR2 subunits expressed in the adult mammals' brain (Burnashev et al., 1992; Borges and Dingledine, 1998). Thus, the presence of the edited GluR2 subunit plays a key role in determining a neuron's vulnerability to glutamate toxicity (Palmer and Gershon, 1990). In the present study, optogenetics increased GluR2 expression in CA1, CA3, the DG, and the SVZ, but not in the ENT.

Glutamate is the most abundant free amino acid in the brain and is the major excitatory neurotransmitter in the mammalian central nervous system (Meldrum, 2000; Reiner and Levitz, 2018). Evidence suggests that AD is characterized by impaired glutamate uptake, alterations in the glutamate–glutamine cycle (Walton and Dodd, 2007), and glutamatergic excitotoxicity (Palmer and Gershon, 1990; Lau and Tymianski, 2010), whereby the neurotoxic action of glutamate follows the overactivation of Ca²⁺-permeable ionotropic glutamate receptors (Choi, 1992).

The maintenance of normal glutamatergic neurotransmission and glutamate clearance depends on active glutamate uptake into glial cells and neurons as glutamate released by neuronal cells is not subsequently metabolized in the extracellular space (Malik and Willnow, 2019). Excitatory amino acid transporters (EAATs) are needed to maintain a low glutamate concentration in the extracellular space and prevent excitotoxicity (Logan and Snyder, 1971; Tanaka et al., 1997). Activation of mGluR2/3 increases the levels of EAAT1 and 2 proteins (Aronica et al., 2003; Lyon et al., 2008; Lin et al., 2014), and mice deficient in mGluR2 have decreased levels of EAAT3 mRNA (Lyon et al., 2008). In the present study, an increase in GluR2 may have upregulated the expression of the EAATs, causing bulk glutamate uptake from the extracellular space and preventing excitotoxicity. This may be one mechanism by which optogenetics with CaMKII targeting glutamatergic neurons exerts a neuroprotective effect.

Findings regarding the associations between AD and inflammatory cytokines, including interleukin (IL)-1 β , IL-2, IL-4, IL-6, IL-8, IL-12, IL-18, tumor necrosis factor (TNF)- α ,

transforming growth factor (TGF)- β , interferon (IFN)- γ , and the C-reactive protein are controversial (Julian et al., 2015). However, IL-10, a cytokine with anti-inflammatory properties, may be a main cytokine associated with the pathogenesis of AD (Swardfager et al., 2010; Sardi et al., 2011; Kiyota et al., 2012). IL-10 limits the immune response to pathogens and microbial flora. AAV serotype 2/1 hybrid-mediated neuronal expression of the mouse IL-10 gene in hippocampal neurons of amyloid precursor protein + presenilin-1 bigenic mice resulted in sustained expression of IL-10, reduced astro/microgliosis, enhanced plasma A β levels, and enhanced neurogenesis.

Glial fibrillary acidic protein (GFAP) is a commonly used marker for astrocytes (Sofroniew and Vinters, 2010). A β increases GFAP levels in the hippocampus (Meunier et al., 2015), and GFAP is upregulated in astrocytes of patients with AD (Perez-Nievas and Serrano-Pozo, 2018), which initiates neuroinflammation and cellular damage. AAV vectors containing the astrocyte-specific Gfa2 promoter to target hippocampal astrocytes and interfere with the biochemical cascades leading to astrocyte activation in APP/PS1 mice confirmed a deleterious role for activated astrocytes in AD.

In the present study, increased GluR2 expression may have alleviated excitotoxicity, upregulated IL-10, and downregulated GFAP. Thus, diminished neuroinflammation induced by optogenetics may have protected neurons and synapses from the neurotoxicity of A β . It was noteworthy that there was increased expression of glutamate receptors (GluR2) and IL-10 and decreased expression of GFAP in CA1, CA3, the DG, and the SVZ, but not the ENT, which is distant to the injection site. Neuroprotection induced by optogenetics was limited to the core area of AAV5–CaMKII–CHR2–mCherry injection. In addition, activation of glutamatergic neurons by AAV5–CaMKII–CHR2–mCherry injection increased NeuN and synapsin expression in the core area (DG) of CHR2 injection, while there were significant changes in the expression of GluR2, IL-10, and GFAP in the core and peripheral areas of CHR2 expression, including CA1, CA3, and the SVZ. This suggests that optogenetic activation of glutamatergic neurons with the CaMKII–CHR2 gene has an extensive effect on astrocytes, although the interaction and mechanism need to be investigated in future studies.

The neuronal–glial network is a potential target for intervention in AD. Consistent with this, our optogenetic technique that selectively stimulated CaMKII–CHR2-expressing neurons in the DG of the bilateral hippocampus improved working memory and short-term memory, altered neuroinflammation, attenuated excitotoxicity induced by A β , and exerted neuroprotective effects in our mouse model of AD. This effect was likely mediated by the neuronal–glial network and activation of glutamate receptors.

While optogenetics has temporal precision, spatial resolution, and neuronal specificity, it has inevitable limitations. In the present study, increased NeuN and synapsin expression were only found in the DG, and increased IL-10 and GluR2 expression and decreased GFAP expression were not found in the ENT of the A β -injected mouse model of AD. This implies that activation of glutamatergic neurons in the DG modulated neuroinflammation in local and peripheral areas and exerted neuroprotective effects

locally, and the effects of optogenetics varied with the distance from CHR2 expression.

Thus, although optogenetics has a potential as an effective treatment for AD, a single-target strategy has spatial limitations. AD has a wide range of injuries, and a multiple targeted optogenetics approach may be a more effective therapy.

CONCLUSION

In conclusion, activation of glutamatergic neurons by optogenetics in the bilateral DG of an A β -injected mouse model of AD improved working memory and short-term memory and downregulated biomarkers of neuroinflammation in the core and peripheral areas of CHR2 expression and upregulated biomarkers of neuroprotection in the core area of CHR2 expression. Due to the spatial constraints of optogenetics, a multiple targeted approach may be needed to address the heterogeneous clinical presentation and pathology of AD.

DATA AVAILABILITY STATEMENT

The raw data supporting the conclusions of this article will be made available by the authors, without undue reservation.

REFERENCES

- Aravanis, A. M., Wang, L. P., Zhang, F., Meltzer, L. A., Mogri, M. Z., Schneider, M. B., et al. (2007). An optical neural interface: in vivo control of rodent motor cortex with integrated fiberoptic and optogenetic technology. *J. Neural Eng.* 4, S143–S156. doi: 10.1088/1741-2560/4/3/S02
- Aronica, E., Gorter, J. A., Ijlst-Keizers, H., Rozemuller, A. J., Yankaya, B., Leenstra, S., et al. (2003). Expression and functional role of mGluR3 and mGluR5 in human astrocytes and glioma cells: opposite regulation of glutamate transporter proteins. *Eur. J. Neurosci.* 17, 2106–2118. doi: 10.1046/j.1460-9568.2003.02657.x
- Bi, A., Cui, J., Ma, Y. P., Olshevskaya, E., Pu, M., Dizhoor, A. M., et al. (2006). Ectopic expression of a microbial-type rhodopsin restores visual responses in mice with photoreceptor degeneration. *Neuron* 50, 23–33. doi: 10.1016/j.neuron.2006.02.026
- Borges, K., and Dingledine, R. (1998). AMPA receptors: molecular and functional diversity. *Prog. Brain Res.* 116, 153–170. doi: 10.1016/s0079-6123(08)60436-7
- Brouillette, J., Caillierez, R., Zommer, N., Alves-Pires, C., Benilova, I., Blum, D., et al. (2012). Neurotoxicity and memory deficits induced by soluble low-molecular-weight amyloid- β 1-42 oligomers are revealed in vivo by using a novel animal model. *J. Neurosci.* 32, 7852–7861. doi: 10.1523/jneurosci.5901-11.2012
- Burnashev, N., Monyer, H., Seeburg, P. H., and Sakmann, B. (1992). Divalent ion permeability of AMPA receptor channels is dominated by the edited form of a single subunit. *Neuron* 8, 189–198. doi: 10.1016/0896-6273(92)90120-3
- Choi, D. W. (1992). Bench to bedside: the glutamate connection. *Science* 258, 241–243. doi: 10.1126/science.1357748
- Crews, L., and Masliah, E. (2010). Molecular mechanisms of neurodegeneration in Alzheimer's disease. *Hum. Mol. Genet.* 19, R12–R20. doi: 10.1093/hmg/ddq160
- Deisseroth, K. (2011). Optogenetics. *Nat. Methods* 8, 26–29. doi: 10.1038/nmeth.f.324
- Duebel, J., Marazova, K., and Sahel, J. A. (2015). Optogenetics. *Curr. Opin. Ophthalmol.* 26, 226–232. doi: 10.1097/ico.0000000000000140
- Ennaceur, A., and Delacour, J. (1988). A new one-trial test for neurobiological studies of memory in rats. 1: behavioral data. *Behav. Brain Res.* 31, 47–59. doi: 10.1016/0166-4328(88)90157-x

ETHICS STATEMENT

All experiments were performed following approval by the Jinan University Animal Resources Committee and according to recommended standards for the care and use of laboratory animals.

AUTHOR CONTRIBUTIONS

LZ and XY contributed to the conception and design of the study. XC, FZ, and HZ performed the novel object recognition test and immunohistochemical analyses. XC, FZ, and LZ performed the statistical analysis. XC wrote the first draft of the manuscript. XH, KW, and TH wrote sections of the manuscript. All authors contributed to manuscript revision, and read and approved the submitted version.

FUNDING

This study was supported by the National Natural Science Foundation of China, No. 81171191 to LZ and the Guangdong Province Key Areas Research and Development Program 2018–2019 “Brain Science and Brain-like Research” Major Science and Technology Special Project, No. 2018B 030336001 to LZ.

- Fachim, H. A., Pereira, A. C., Iyomasa-Pilon, M. M., and Rosa, M. L. (2016). Differential expression of AMPA subunits induced by NMDA intrahippocampal injection in rats. *Front. Neurosci.* 10:32. doi: 10.3389/fnins.2016.00032
- Gomez-Isla, T., Price, J. L., McKeel, D. W. Jr., Morris, J. C., and Growdon, J. H. (1996). Profound loss of layer II entorhinal cortex neurons occurs in very mild Alzheimer's disease. *J. Neurosci.* 16, 4491–4500. doi: 10.1523/jneurosci.16-14-04491.1996
- Gradinaru, V., Mogri, M., Thompson, K. R., Henderson, J. M., and Deisseroth, K. (2009). Optical deconstruction of parkinsonian neural circuitry. *Science* 324, 354–359. doi: 10.1126/science.1167093
- Greene, J. D., Patterson, K., Xuereb, J., and Hodges, J. R. (1996). Alzheimer disease and nonfluent progressive aphasia. *Arch. Neurol.* 53, 1072–1078. doi: 10.1001/archneur.1996.00550100158027
- Guo, J. Y., Ragland, J. D., and Carter, C. S. (2019). Memory and cognition in schizophrenia. *Mol. Psychiatry* 24, 633–642. doi: 10.1038/s41380-018-0231-1
- Hammond, R. S., Tull, L. E., and Stackman, R. W. (2004). On the delay-dependent involvement of the hippocampus in object recognition memory. *Neurobiol. Learn. Mem.* 82, 26–34. doi: 10.1016/j.nlm.2004.03.005
- Hampson, R. E., Song, D., Robinson, B. S., Fetterhoff, D., Dakos, A. S., Roeder, B. M., et al. (2018). Developing a hippocampal neural prosthetic to facilitate human memory encoding and recall. *J. Neural Eng.* 15:036014. doi: 10.1088/1741-2552/aaad7
- Hyman, B. T., Penney, J. B. Jr., Blackstone, C. D., and Young, A. B. (1994). Localization of non-N-methyl-D-aspartate glutamate receptors in normal and Alzheimer hippocampal formation. *Ann. Neurol.* 35, 31–37. doi: 10.1002/ana.410350106
- Hyman, B. T., Van Hoesen, G. W., Damasio, A. R., and Barnes, C. L. (1984). Alzheimer's disease: cell-specific pathology isolates the hippocampal formation. *Science* 225, 1168–1170. doi: 10.1126/science.6474172
- Julian, A., Dugast, E., Ragot, S., Krolak-Salmon, P., Berrut, G., Dantoine, T., et al. (2015). There is no correlation between peripheral inflammation and cognitive status at diagnosis in Alzheimer's disease. *Aging Clin. Exp. Res.* 27, 589–594. doi: 10.1007/s40520-015-0332-5

- Khan, U. A., Liu, L., Provenzano, F. A., Berman, D. E., Profaci, C. P., Sloan, R., et al. (2014). Molecular drivers and cortical spread of lateral entorhinal cortex dysfunction in preclinical Alzheimer's disease. *Nat. Neurosci.* 17, 304–311. doi: 10.1038/nn.3606
- Kiyota, T., Ingraham, K. L., Swan, R. J., Jacobsen, M. T., Andrews, S. J., and Ikezu, T. (2012). AAV serotype 2/1-mediated gene delivery of anti-inflammatory interleukin-10 enhances neurogenesis and cognitive function in APP+PS1 mice. *Gene Ther.* 19, 724–733. doi: 10.1038/gt.2011.126
- Kuperstein, I., Broersen, K., Benilova, I., Rozenski, J., Jonckheere, W., Debulpaep, M., et al. (2010). Neurotoxicity of Alzheimer's disease A β peptides is induced by small changes in the A β 42 to A β 40 ratio. *EMBO J.* 29, 3408–3420. doi: 10.1038/emboj.2010.211
- Lambert, M. P., Barlow, A. K., Chromy, B. A., Edwards, C., Freed, R., Liosatos, M., et al. (1998). Diffusible, nonfibrillar ligands derived from A β 1–42 are potent central nervous system neurotoxins. *Proc. Natl. Acad. Sci. U.S.A.* 95, 6448–6453. doi: 10.1073/pnas.95.11.6448
- Lau, A., and Tymianski, M. (2010). Glutamate receptors, neurotoxicity and neurodegeneration. *Pflugers Arch.* 460, 525–542. doi: 10.1007/s00424-010-0809-1
- Lesne, S., Koh, M. T., Kotilinek, L., Kaye, R., Glabe, C. G., Yang, A., et al. (2006). A specific amyloid-beta protein assembly in the brain impairs memory. *Nature* 440, 352–357. doi: 10.1038/nature04533
- Lin, C. H., You, J. R., Wei, K. C., and Gean, P. W. (2014). Stimulating ERK/PI3K/NF κ B signaling pathways upon activation of mGluR2/3 restores OGD-induced impairment in glutamate clearance in astrocytes. *Eur. J. Neurosci.* 39, 83–96. doi: 10.1111/ejn.12383
- Logan, W. J., and Snyder, S. H. (1971). Unique high affinity uptake systems for glycine, glutamic and aspartic acids in central nervous tissue of the rat. *Nature* 234, 297–299. doi: 10.1038/234297b0
- Lyon, L., Kew, J. N., Corti, C., Harrison, P. J., and Burnet, P. W. (2008). Altered hippocampal expression of glutamate receptors and transporters in GRM2 and GRM3 knockout mice. *Synapse* 62, 842–850. doi: 10.1002/syn.20553
- Malik, A. R., and Willnow, T. E. (2019). Excitatory amino acid transporters in physiology and disorders of the central nervous system. *Int. J. Mol. Sci.* 20:5671. doi: 10.3390/ijms20225671
- Matthews, B. R. (2015). Memory dysfunction. *Behav. Neurol. Neuropsychiatry* 21, 613–626. doi: 10.1212/01.Con.0000466656.59413.29
- Meldrum, B. S. (2000). Glutamate as a neurotransmitter in the brain: review of physiology and pathology. *J. Nutr.* 130(4S Suppl.), 1007s–1015s. doi: 10.1093/jn/130.4.1007S
- Meunier, J., Borjini, N., Gillis, C., Villard, V., and Maurice, T. (2015). Brain toxicity and inflammation induced in vivo in mice by the amyloid- β forty-two inducer aptin-4, a roscovitine derivative. *J. Alzheimers. Dis.* 44, 507–524. doi: 10.3233/jad-140711
- Mirza, F. J., and Zahid, S. (2018). The role of synapsins in neurological disorders. *Neurosci. Bull.* 34, 349–358. doi: 10.1007/s12264-017-0201-7
- Naya, Y., Chen, H., Yang, C., and Suzuki, W. A. (2017). Contributions of primate prefrontal cortex and medial temporal lobe to temporal-order memory. *Proc. Natl. Acad. Sci. U.S.A.* 114, 13555–13560. doi: 10.1073/pnas.1712711114
- Ono, K., Condrón, M. M., and Teplow, D. B. (2009). Structure-neurotoxicity relationships of amyloid beta-protein oligomers. *Proc. Natl. Acad. Sci. U.S.A.* 106, 14745–14750. doi: 10.1073/pnas.0905127106
- Palmer, A. M., and Gershon, S. (1990). Is the neuronal basis of Alzheimer's disease cholinergic or glutamatergic? *FASEB J.* 4, 2745–2752. doi: 10.1096/fasebj.4.10.2165009
- Paxinos, G., and Watson, C. (2005). *The Rat Brain in Stereotaxic Coordinates*, Ed 5 Edn. Burlington: Elsevier.
- Perez-Nievas, B. G., and Serrano-Pozo, A. (2018). Deciphering the astrocyte reaction in Alzheimer's disease. *Front. Aging Neurosci.* 10:114. doi: 10.3389/fnagi.2018.00114
- Reiner, A., and Levitz, J. (2018). Glutamatergic signaling in the central nervous system: ionotropic and metabotropic receptors in concert. *Neuron* 98, 1080–1098. doi: 10.1016/j.neuron.2018.05.018
- Sardi, F., Fassina, L., Venturini, L., Inguscio, M., Guerriero, F., Rolfo, E., et al. (2011). Alzheimer's disease, autoimmunity and inflammation. The good, the bad and the ugly. *Autoimmun. Rev.* 11, 149–153. doi: 10.1016/j.autrev.2011.09.005
- Scheff, S. W., Price, D. A., Schmitt, F. A., and Mufson, E. J. (2006). Hippocampal synaptic loss in early Alzheimer's disease and mild cognitive impairment. *Neurobiol. Aging* 27, 1372–1384. doi: 10.1016/j.neurobiolaging.2005.09.012
- Shirayama, Y., Takahashi, M., Osone, F., Hara, A., and Okubo, T. (2017). Myo-inositol, glutamate, and glutamine in the prefrontal cortex, hippocampus, and amygdala in major depression. *Biol. Psychiatry Cogn. Neurosci. Neuroimaging* 2, 196–204. doi: 10.1016/j.bpsc.2016.11.006
- Sofroniew, M. V., and Vinters, H. V. (2010). Astrocytes: biology and pathology. *Acta Neuropathol.* 119, 7–35. doi: 10.1007/s00401-009-0619-8
- Swardfager, W., Lanctôt, K., Rothenburg, L., Wong, A., Cappell, J., and Herrmann, N. (2010). A meta-analysis of cytokines in Alzheimer's disease. *Biol. Psychiatry* 68, 930–941. doi: 10.1016/j.biopsych.2010.06.012
- Tanaka, K., Watase, K., Manabe, T., Yamada, K., Watanabe, M., Takahashi, K., et al. (1997). Epilepsy and exacerbation of brain injury in mice lacking the glutamate transporter GLT-1. *Science* 276, 1699–1702. doi: 10.1126/science.276.5319.1699
- Tye, K. M., Prakash, R., Kim, S. Y., Fenno, L. E., Grosenick, L., Zarabi, H., et al. (2011). Amygdala circuitry mediating reversible and bidirectional control of anxiety. *Nature* 471, 358–362. doi: 10.1038/nature09820
- Van den Oever, M. C., Rotaru, D. C., Heinsbroek, J. A., Gouwensberg, Y., Deisseroth, K., Stuber, G. D., et al. (2013). Ventromedial prefrontal cortex pyramidal cells have a temporal dynamic role in recall and extinction of cocaine-associated memory. *J. Neurosci.* 33, 18225–18233. doi: 10.1523/jneurosci.2412-13.2013
- Walton, H. S., and Dodd, P. R. (2007). Glutamate-glutamine cycling in Alzheimer's disease. *Neurochem. Int.* 50, 1052–1066. doi: 10.1016/j.neuint.2006.10.007

Conflict of Interest: The authors declare that the research was conducted in the absence of any commercial or financial relationships that could be construed as a potential conflict of interest.

Copyright © 2020 Cui, Zhang, Zhang, Huang, Wang, Huang, Yang and Zou. This is an open-access article distributed under the terms of the Creative Commons Attribution License (CC BY). The use, distribution or reproduction in other forums is permitted, provided the original author(s) and the copyright owner(s) are credited and that the original publication in this journal is cited, in accordance with accepted academic practice. No use, distribution or reproduction is permitted which does not comply with these terms.



microRNA-Based Biomarkers in Alzheimer's Disease (AD)

Yuhai Zhao^{1,2}, Vivian Jaber¹, Peter N. Alexandrov^{3†}, Andrea Vergallo⁴, Simone Lista^{4,5,6}, Harald Hampel⁴ and Walter J. Lukiw^{1,3,7,8*}

¹ LSU Neuroscience Center, Louisiana State University Health Sciences Center, New Orleans, LA, United States,

² Department of Cell Biology and Anatomy, Louisiana State University Health Science Center, New Orleans, LA, United States, ³ Russian Academy of Medical Sciences, Moscow, Russia, ⁴ Sorbonne University, GRC n° 21, Alzheimer Precision Medicine (APM), AP-HP, Pitié-Salpêtrière Hospital, Paris, France, ⁵ Brain & Spine Institute (ICM), INSERM U 1127, CNRS UMR 7225, Boulevard de l'Hôpital, Paris, France, ⁶ Institute of Memory and Alzheimer's Disease (IM2A), Department of Neurology, Pitié-Salpêtrière Hospital, AP-HP, Boulevard de l'hôpital, Paris, France, ⁷ Department of Ophthalmology, LSU Neuroscience Center Louisiana State University Health Science Center, New Orleans, LA, United States, ⁸ Department of Neurology, LSU Neuroscience Center Louisiana State University Health Science Center, New Orleans, LA, United States

OPEN ACCESS

Edited by:

Yu Chen,
Shenzhen Institutes of Advanced
Technology (CAS), China

Reviewed by:

Subodh Kumar,
Texas Tech University Health
Sciences Center, United States
Wang-Xia Wang,
University of Kentucky, United States

*Correspondence:

Walter J. Lukiw
wlukiw@lsuhsc.edu

†Deceased

Specialty section:

This article was submitted to
Neurodegeneration,
a section of the journal
Frontiers in Neuroscience

Received: 20 July 2020

Accepted: 04 September 2020

Published: 30 October 2020

Citation:

Zhao Y, Jaber V, Alexandrov PN, Vergallo A, Lista S, Hampel H and Lukiw WJ (2020) microRNA-Based Biomarkers in Alzheimer's Disease (AD). *Front. Neurosci.* 14:585432. doi: 10.3389/fnins.2020.585432

Alzheimer's disease (AD) is a multifactorial, age-related neurological disease characterized by complex pathophysiological dynamics taking place at multiple biological levels, including molecular, genetic, epigenetic, cellular and large-scale brain networks. These alterations account for multiple pathophysiological mechanisms such as brain protein accumulation, neuroinflammatory/neuro-immune processes, synaptic dysfunction, and neurodegeneration that eventually lead to cognitive and behavioral decline. Alterations in microRNA (miRNA) signaling have been implicated in the epigenetics and molecular genetics of all neurobiological processes associated with AD pathophysiology. These changes encompass altered miRNA abundance, speciation and complexity in anatomical regions of the CNS targeted by the disease, including modified miRNA expression patterns in brain tissues, the systemic circulation, the extracellular fluid (ECF) and the cerebrospinal fluid (CSF). miRNAs have been investigated as candidate biomarkers for AD diagnosis, disease prediction, prognosis and therapeutic purposes because of their involvement in multiple brain signaling pathways in both health and disease. In this review we will: (i) highlight the significantly heterogeneous nature of miRNA expression and complexity in AD tissues and biofluids; (ii) address how information may be extracted from these data to be used as a diagnostic, prognostic and/or screening tools across the entire continuum of AD, from the preclinical stage, through the prodromal, i.e., mild cognitive impairment (MCI) phase all the way to clinically overt dementia; and (iii) consider how specific miRNA expression patterns could be categorized using miRNA reporters that span AD pathophysiological initiation and disease progression.

Keywords: aging, Alzheimer's disease, AD biomarkers, AD diagnostics, AD heterogeneity, human biochemical individuality, inflammatory neurodegeneration, microRNA (miRNA)

Abbreviations: AD, Alzheimer's disease; AD biomarkers; AD diagnostics; AD heterogeneity; human biochemical individuality; inflammatory neurodegeneration; microRNA (miRNA).

OVERVIEW

Alzheimer's disease (AD) represents a complex, multifactorial, age- and gender-related, progressive neurological degeneration of the human brain and central nervous system (CNS) whose clinical course is highly variable, heterogeneous, extremely insidious, and ultimately lethal. Final outcomes involve complex and irreversible alterations in behavior, inability to conduct daily activities, visual, visuospatial and perceptive disruption, and escalating deficits in cognition and impairment of recent memories in the AD patient, while older memories are often retained. Symptomology for AD is also highly variable, interactive and progressive to the extent of daily to weekly changes in the AD patient's psychiatric condition. Clinically, toward the termination of the AD process there is usually progressive forfeiture of the swallowing reflex (dysphagia) and the onset of inspirational pneumonia to which most AD patients succumb over a clinical course averaging about ~5–12 years (Dinsmore, 1999; Ahluwalia and Vellas, 2003; DeTure and Dickson, 2019; von Arnim et al., 2019; Cao et al., 2020^{1,2,3}; last accessed 26 August 2020). The definitive diagnosis of AD is one of the most difficult and challenging in neurology (Arvanitakis et al., 2019; Fierini, 2020; Ghaffari et al., 2020; Guest et al., 2020; Habes et al., 2020; Turner et al., 2020). AD is more often than not accompanied by other multimodal dementing neuropathologies including neurovascular and/or cardiovascular disease involving vascular-based dementia, multiple infarct dementia (MID) and/or strokes or “mini-strokes,” frontotemporal dementia (FTD), hippocampal sclerosis, Lewy body disease, and several other dementing illnesses and comorbidities such as Down's syndrome (trisomy 21), epilepsy and prion disease [including bovine spongiform encephalopathy (BSE; mad cow disease), Creutzfeldt–Jakob disease, Gerstmann–Sträussler–Scheinker syndrome, and other relatively rare human prion disorders] and other rare AD subtypes (Dinsmore, 1999; Lemcke and David, 2018; DeTure and Dickson, 2019; Checksfield, 2020; Fierini, 2020; Emrani et al., 2020; Habes et al., 2020; Williams et al., 2020⁴; last accessed 26 August 2020). The accurate identification of AD is exacerbated by the global lack of routine diagnostic tools for identifying patients early enough in their disease course, i.e., the “prodromal” period, for designing a suitable intervention or prospective treatment regimen. *Of equal concern is our lack of basic understanding of the underlying root causes of AD and the widely observed variability in the clinical presentation of AD once the onset of the disease process is clinically recognized* (Ashford et al., 1992; Hudon et al., 2020; Patnode et al., 2020). For AD only symptomatic treatments that suppress the clinical manifestations are currently available (Lukiw et al., 2012; Hampel and Lista, 2013; Lukiw, 2013a,b; Praticò, 2013; Hampel et al., 2014; Kim et al., 2014; Yanagida et al., 2017; Blennow

and Zetterberg, 2018; Cole and Seabrook, 2020). Increasing stratification and categorization of AD, comorbidities and inter-current illness that may have contributed to the clinical diagnosis and outcome of AD may be required to develop the most efficacious treatments (see below).

CLINICAL ASPECTS OF AD HETEROGENEITY

With regard to the overall general classification of AD, affected patients are broadly categorized as having either an early onset (EOAD, under ~65 years of age), or late onset (LOAD, over ~65 years of age); about ~5% of all AD cases appear to have a genetic component (see below) while the remaining ~95% of all AD cases are of an idiopathic or sporadic nature, or are of an unknown origin (Guerreiro et al., 2012; Jiang et al., 2013; Barnes et al., 2015; Cao et al., 2020; Dumurgier and Tzourio, 2020). Over 50 susceptibility genes and gene loci have been associated with LOAD (Sims et al., 2020). The transmissibility of AD amongst *Homo sapiens* by casual or iatrogenic routes and involving self-propagating amyloidogenic prion-like lipoprotein aggregates or free or microvesicle-encapsulated pathogenic miRNAs has not been completely ruled out (Lukiw et al., 2012; Burwinkel et al., 2018; Lemcke and David, 2018; Caghey and Kraus, 2019; Hampton, 2019; Lukiw, 2020a,b; Lukiw and Pogue, 2020).

The clinical analysis and categorization of presenile dementia in the elderly typically incorporates semi-structured interviews with AD patients, their care-givers and other informants to obtain information necessary to rate the individual's cognitive performance in six domains of cognitive and functional performance: memory skills, orientation, judgment and problem solving, community affairs, home and hobbies, and personal care; the clinical dementia rating (CDR; a five point scale ranging from 0 or normal to 3 for severe dementia) protocol has evolved as a condensed, useful, reliable and valid global assessment measure for AD (Morris, 1997; Verhulsdonk et al., 2015⁵). There are in addition several other widely used psychiatric and diagnostic tests including the mini-mental status exam (MMSE; Arvanitakis et al., 2019; Alzheimer's Association, 2020). While the diagnostic criteria for AD vary globally systematic review and meta-analysis of AD incidence and prevalence have repeatedly revealed several globalized trends (Zhu et al., 2019; Dumurgier and Tzourio, 2020). These include the significantly higher occurrence of AD in aged human females (about ~2 times greater than that in males) and strong association with aging (Guerreiro et al., 2012; Bhattacharjee and Lukiw, 2013; Jiang et al., 2013; Cao et al., 2020; Dumurgier and Tzourio, 2020; Lukiw, 2020a,b). The wide variety of behavioral disorders, extreme heterogeneity in neurological disturbances, mnemonic and cognitive deficits including significant age- and gender-based differences, combined with supplementary neurological diseases such as neurovascular disease and ischemic and/or hemorrhagic stroke are extremely common, especially in the most elderly of LOAD patients (Dinsmore, 1999; Fierini, 2020;

¹<https://www.alzinfo.org/articles/when-patients-with-advanced-alzheimers-get-pneumonia/>

²<https://www.medicalnewstoday.com/articles/315123>

³<https://www.alz.org/alzheimers-dementia/stages>

⁴<https://www.j-alz.com/editors-blog/posts/is-there-alzheimers-disease>

⁵<https://knightadrc.wustl.edu/cdr/cdr.htm>

Emrani et al., 2020; Habes et al., 2020). Environmental factors and life style triggers such as occupational exposures to pesticides, organic solvents, environmental neurotoxins such as aluminum and mercury, anesthetics and/or food additives, education, smoking, increased body-mass index (BMI), obesity, metabolic syndrome and diabetes, microbial and gastrointestinal (GI) tract microbiome contributions such as highly proinflammatory *Bacteroides fragilis* lipopolysaccharides (BF-LPS) to the onset and development of AD are being increasingly recognized but their mechanism of pathological contribution are in most cases not well understood, and are currently under intense research investigation (Hill et al., 2014a,b; Altveş et al., 2020; Lukiw, 2020a,b; Rahman et al., 2020). *A priori* this strongly suggests: (i) that a considerable array of factors have been evidenced to contribute to the onset and propagation of AD; and (ii) that a very wide range of molecular-genetic, neurophysiological and neurobiological mechanisms, pathways and signaling processes are affected in the AD brain (Figure 1).

TRADITIONAL PATHOPHYSIOLOGICAL BIOMARKERS FOR AD ARE NON-SPECIFIC

Alzheimer's disease neuropathology encompasses several interrelated features: (i) the progressive disorganization and dropout of neocortical synapses that involve loss of selective synaptic components, synaptic atrophy, "pruning" and synaptic loss; (ii) neuronal atrophy, cytoarchitectural deficits and neurite retraction and degeneration, neuronal cell death and loss of inter-neuronal communication; (iii) the progressive deposition and accumulation of amyloid-beta ($A\beta$) peptides and other insoluble end-stage oxidized lipoproteins into dense, pro-inflammatory senile plaque (SP) aggregates; (iv) the accumulation and aggregation of hyper-phosphorylated tau proteins into neurofibrillary tangles (NFT) that disrupt the normal neural cell cytoarchitecture; (v) neurovascular pathology; (vi) dysfunctional autophagy; (vii) progressive inflammatory neurodegeneration and anatomical targeting of specific anatomical regions of the brain and primarily the association neocortex and hippocampal CA1 regions; (viii) alterations in the innate-immune response and other immunological biomarkers; (ix) changes in the gastrointestinal tract (GI-tract) microbiome; (x) dysfunction and alterations in the glymphatic system of the CNS; (xi) multiple functional associations with diet, obesity, metabolic disease and diabetes; and (xii) blood lipoprotein composition and blood type (Lukiw et al., 1992; Lukiw, 2007; Cogswell et al., 2008; Lukiw, 2013a,b; Praticò, 2013; Hampel and Lista, 2013; Kim et al., 2014; Sherva et al., 2014; Canobbio et al., 2015; De Marco and Venneri, 2015; Jin et al., 2015; Verhulsdonk et al., 2015; Wang et al., 2015; Zhao et al., 2015; Blennow and Zetterberg, 2018; Hampel et al., 2018a,b,c; Arvanitakis et al., 2019; von Arnim et al., 2019; Cole and Seabrook, 2020; Dumurgier and Tzourio, 2020; Hampel et al., 2020a,b; Khoury and Grossberg, 2020; Lewczuk et al., 2020; McGurran et al., 2020; Rodriguez and Lachmann, 2020; Rossini et al., 2020; Stanciu et al., 2020; Turner et al., 2020).

These highly interactive characteristics once again collectively underscore the participation of multiple pathogenic pathways, and the involvement of multiple deficits in the expression of CNS genes and genetic regulatory mechanisms in AD (Colangelo et al., 2002; Jaber et al., 2019; Sims et al., 2020). Importantly, the magnitude of each of these neuropathological biomarkers varies widely amongst the prodromal, moderate, and severe states of AD and not one of these multiple features of AD change are either characteristic or distinguishing for the AD phenotype. Put another way many of these attributes are in part typical of other incapacitating age-related neurological disorders of the human CNS. Accordingly, this culminates in a remarkably heterogeneous neuropathological framework for AD, with significant variations in disease initiation, onset, progression, severity of neuropathology, extent of behavioral disruption, cognitive deficits and memory loss, visual and visuospatial impairment, time course and other temporal aspects, CDR or MMSE ratings in individual AD patients and the frequent contribution of inter-current illness, and particularly with other kinds of age-related neurological disease (Verhulsdonk et al., 2015; Rossini et al., 2020; Tetreault et al., 2020). Given the enormous complexity of traditional biomarkers and their compartmentalization in AD onset, course and diagnosis, it is clear that the most informative molecular biomarkers for AD will be those which are involved in multiple regulatory aspects of brain function and neuropathological signaling. The participation of small families of pathology-implicated miRNAs are emerging as prime candidates that help define the molecular genetics and epigenetics of AD.

microRNA (miRNA) - Definitions and Actions

microRNAs (miRNA) represent a class of ~19–23 nucleotide (nt) single-stranded non-coding RNA (sncRNA) that are important epigenetic, posttranscriptional regulators of messenger RNA (mRNA) complexity. Their diminutive size, amphipathic nature, high solubility make them extremely mobile, omnipresent throughout the brain and CNS and the smallest information-carrying nucleic acid signaling molecules in eukaryotes yet described (Hill et al., 2014a,b; Pogue et al., 2014; Lemcke and David, 2018; Zhao et al., 2018; Lukiw, 2020a,b; van den Berg et al., 2020). To date about ~2650 individual human miRNAs have been cataloged and characterized, however, the abundance of miRNAs in the human brain and retina number only about ~20–35 individual, high abundance, neurologically functional species which exhibit both tissue and cell type-specific expression patterns (Burmistrova et al., 2007; Lukiw, 2007; Hill and Lukiw, 2016; Konovalova et al., 2019; Singh and Yadav, 2020; Wu and Kuo, 2020; miRBase release 22.1; October 2018⁶; last accessed 26 August 2020). The major mode of action of these sncRNAs is to interact, via base-pair complementarity, with the 3'-untranslated region (3'-UTR) of their target messenger RNAs (mRNAs), and in doing so degrade that mRNA, and hence decrease the potential for that specific mRNA to be expressed (Roshan et al., 2009; De Smaele et al., 2010; McGeary et al., 2019; Eisen et al., 2020;

⁶www.mirbase.org

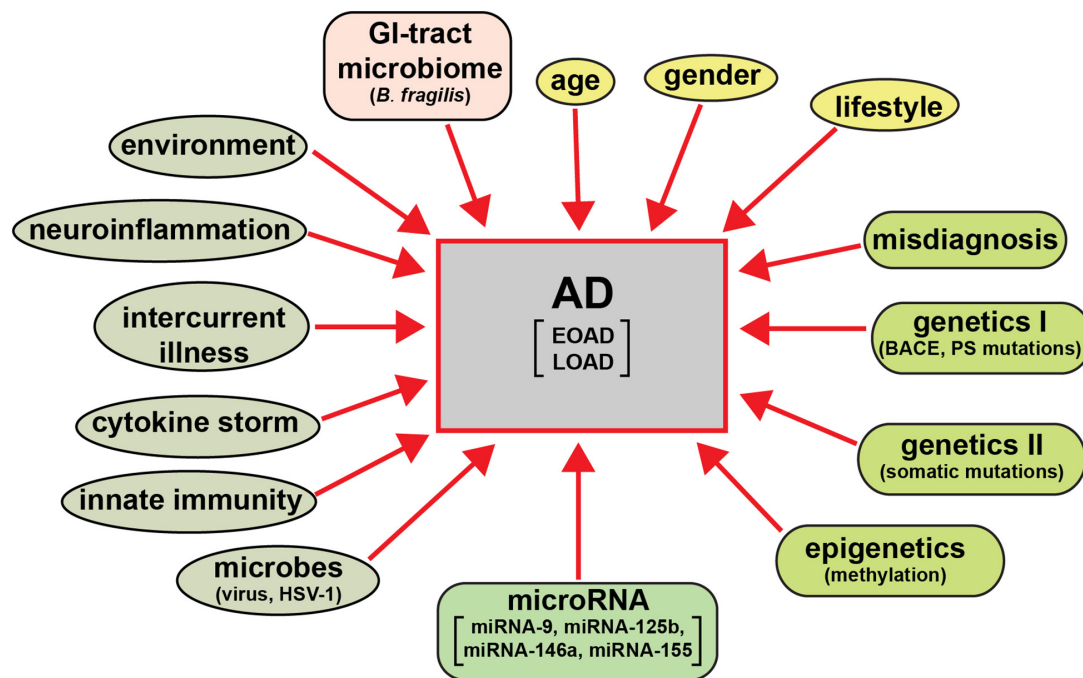


FIGURE 1 | AD is an extremely heterogeneous neurological disorder. Just as there are multiple factors that have significant potential to contribute to AD type and AD symptomatic and molecular-genetic heterogeneity, the neuropathological pathways and pathway biomarkers encompassing these factors can be intercepted and interrogated to obtain extremely useful diagnostic information which more clearly define the prodrome, onset and course of AD as well as related progressive neurodegenerative disorders. The pervasive and modulatory nature of miRNAs in both brain tissues and multiple biofluid compartments (such as the ECF, CSF, and blood serum) make miRNAs ideal candidates to expand our understanding of the diagnosis of temporal aspects of the AD pathophysiology.

Pawlica et al., 2020). The most widely observed mechanism in the mammalian brain is for an inducible and up-regulated miRNA to down-regulate their polyA⁺ mRNA targets and thereby reduce the expression of mRNA-encoded genetic information. The mechanism of action of miRNAs has been described and schematized in some detail (see Hobert, 2008; Eichhorn et al., 2014; Kleaveland et al., 2018; McGeary et al., 2019; Eisen et al., 2020; **Figure 2**).

Interestingly, single mRNA 3'-UTRs in the mammalian brain and retina can have multiple miRNA binding site targets, and single miRNAs may have more than one mRNA target making them strong potential candidates for addressing the multiple complexities of the disruption of mRNA-based gene expression in AD (Colangelo et al., 2002; Lukiw and Alexandrov, 2012; Eichhorn et al., 2014; Eisen et al., 2020). These findings support the strengthening contention: (i) that brain-enriched miRNAs operate as fundamental components of an epigenetically controlled post-transcriptional signaling network in the mammalian CNS (Lukiw and Alexandrov, 2012; Kleaveland et al., 2018; Jaber et al., 2019; Eisen et al., 2020); and (ii) that miRNAs have an established capability to act independently, coordinately and/or cooperatively to create a highly sophisticated and interactive regulatory miRNA-mRNA network for families of brain genes that regulate many essential brain functions that are specifically altered in AD brain (Jaber et al., 2017; Kleaveland et al., 2018; Eisen et al., 2020; Lukiw, 2020a,b). Importantly, information-carrying ribonucleic acids

such as highly soluble and mobile, single-stranded non-coding RNAs (sncRNAs) including microRNAs (miRNAs) can affect the operation of a large number of highly interactive pathogenic signaling pathways in the CNS, and represent strategic candidates for promoting AD onset, and for modulating or maintaining AD propagation and disease spread (Alexandrov et al., 2012; Lukiw et al., 2012; Chandrasekaran and Bonchev, 2016; Clement et al., 2016; Kleaveland et al., 2018; Lemcke and David, 2018; Hill, 2019; Jaber et al., 2019; Konvalova et al., 2019; Condrat et al., 2020; Fan et al., 2020; Kou et al., 2020).

microRNA (miRNA) SIGNALING IN AD

The multi-system, multi-pathway and sometimes overlapping regulatory roles for potentially pathogenic miRNA gene families in the neocortex, hippocampus, the limbic system and the CNS in general make miRNA prime candidates for modulating the expression of many mRNA targets in complex, progressive and ultimately lethal neurological disorders of the CNS that include AD (Lukiw, 2007; Zhao et al., 2016a,b; Jaber et al., 2017, 2019; **Figure 2**). It is for this reason there has been much recent interest in vesicle-encapsulated and/or biofluid-enriched monomeric miRNAs as potential ribonucleic acid indicators which are predictive and/or diagnostic biomarkers for the onset and development of AD (Bahlakeh et al., 2020; Krammes et al., 2020; Serpente et al., 2020; Wang et al., 2020). Indeed homeostatic

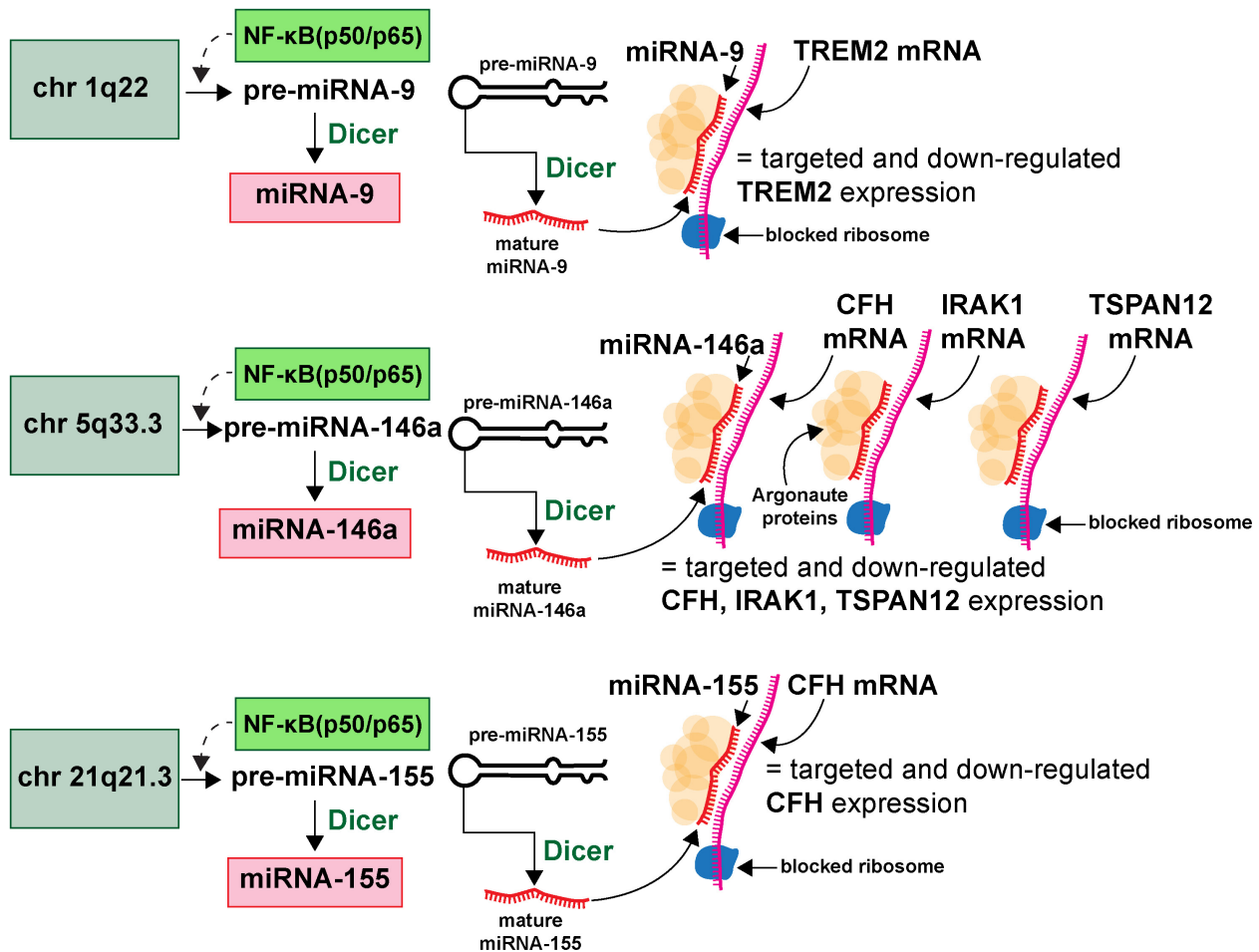


FIGURE 2 | Highly simplified schematic of an AD-relevant microRNA-messenger RNA (miRNA-mRNA) regulatory network involving 3 different miRNAs and 4 different mRNAs; this drawing graphically illustrates the molecular-genetic mechanism of microRNA (miRNA) generation and targeted miRNA-mRNA interaction; selective pathogenic families of miRNAs (for example miRNA-9, miRNA-146a and miRNA-155), transcribed from genes located on 3 different chromosomes (chr 1q22, chr 5q33.3, chr 21q21.3) generate precursor miRNAs (pre-miRNAs) which are subsequently processed into neurologically active mature miRNAs (miRNA-9, miRNA-146a and miRNA-155 shown as an example); many more chromosomes, miRNAs and mRNAs and miRNA-mRNA signaling networks are probably involved; many AD-relevant miRNA encoding genes are under transcriptional control by the pro-inflammatory transcription factor NF- κ B (p50/p65); mature miRNAs subsequently find their target mRNAs (TREM2, CFH, IRAK-1, and TSPAN12 shown) and the miRNA-mRNA double-stranded RNA complex is blocked at the entrance to the ribosome (blue spherical complex on mRNA stand) and the miRNA-mRNA complex is degraded; the major mode of miRNA action in the mammalian brain is pathologically up-regulated miRNAs driving the down-regulation of AD-relevant genes (see text); single miRNAs can target multiple mRNAs and multiple miRNAs can target a single mRNA (see also **Figure 3**); miRNAs have established roles in recognizing multiple mRNA sequences (genetic pleiotropy), combinatorial and cooperativity in gene regulation, template accessibility (mediated by various RNA binding proteins; in this diagram orange spheres at the miRNA-mRNA interface called “Argonaute proteins”) and post-transcriptional regulation of the transcriptome (Hobert, 2008; Jaber et al., 2019; Eisen et al., 2020; Lukiw, 2020a,b). Combined with other metrics, the precise quantitation of miRNA abundance, speciation and complexity in various AD biofluids has strong potential for increasing the accuracy of AD diagnostics; recent preliminary *in vitro* studies further indicate that anti-miRNA (antimiR, antagomir, AM)-based therapies may be effective in quenching the excessive miRNA-mediated downregulation of critical mRNA-driven gene expression in AD (Zhao et al., 2016a,b; Jaber et al., 2019; Fan et al., 2020; Ghaffari et al., 2020).

levels of all 2650 miRNAs are an excellent indicator of normal brain operation and of homeostatic brain function in health and in aging, the development of dyshomeostasis, and the onset of disease. The nature of miRNAs epigenetic and post-transcriptional regulation of about ~27,000 messenger RNA (mRNAs), participation in a complex miRNA-mRNA linked network defining the brain cell's transcriptome, and the shaping of this transcriptome over time under many neurophysiological conditions is both highly informative in understanding the

molecular-genetics of human brain function and has been useful in the field of diagnostic and prognostic biomarkers for AD and other progressive inflammatory neurodegeneration of the human CNS (Jaber et al., 2017, 2019; Sims et al., 2020). Patterns of miRNA expression are complex – for example natural miRNA abundance has been shown to fluctuate during neural development and differentiation of the human brain and in the aging CNS (Giorgi Silveira et al., 2020; Ma et al., 2020; Wu and Kuo, 2020). Emerging data continue to support the concept

that the analysis and characterization of specific miRNAs may be especially useful in the prodromal and pre-clinical phases of AD in which a very subtle pro-inflammatory neuropathology develops and molecular changes begin to accumulate even in the absence of the full-blown clinical symptoms as shown by the moderate and more advanced phases of AD (Hill and Lukiw, 2016; Bahlakeh et al., 2020; Fan et al., 2020; Ma et al., 2020; Wu and Kuo, 2020).

microRNA (miRNA) AND PROGRESSIVE INFLAMMATORY NEURODEGENERATION

In general, up-regulated miRNAs and down-regulation of essential neural signaling components (via down-regulation of key mRNAs) have been proposed by many independent groups to be a highly active process in the initiation and propagation of progressive inflammatory neurodegenerative diseases such as AD, amyotrophic lateral sclerosis (ALS), Huntington's disease (HD), Parkinson's disease (PD), trisomy 21 (T21; DS; Down's syndrome), motor neuron disease, neurovascular disease, prion disease and several other terminal neuropathies (Holohan et al., 2013; Christoforidou et al., 2020; Singh and Yadav, 2020; Wang and Zhang, 2020; Wu and Kuo, 2020). It is interesting that to date no single newly generated *de novo* miRNA has been associated with AD – that is, miRNA alterations in AD reflect significant and absolute differences in abundance, speciation and perhaps stoichiometric relationships of existing miRNA species. Put another way, no specific miRNA “suddenly appears” at the onset, or propagation of AD, and it is a matter of up-regulation or down-regulation of an already existing miRNA species in a specific anatomical region that has been the most consistently observed in the AD brain. Interestingly, very recent molecular-genetic studies have indicated that even when derived from cell and tissue sources that are homogenous, such as pluripotent stem cells, individual cells in these unique populations often exhibit significant differences in miRNA abundance and complexity, gene expression, protein abundance and phenotypic output; here individual families of miRNAs appear to have a deterministic role in reconfiguring the “*pluripotency network*” and miRNA-mRNA linking patterns in individual cells with important downstream functional consequences (Li et al., 2015; Liu et al., 2015; Atlasi et al., 2020; Chakraborty et al., 2020; Kumar and Reddy, 2020).

Since a general down-regulation in gene expression in AD brain, especially for AD relevant components such as synaptic and cyto-architectural elements, deficits in the clearance of pro-inflammatory components and amyloid aggregates, and the consistent catabolic nature of the neurodegenerative disease process, has been repeatedly reported by multiple independent research groups, it follows that miRNAs that control gene expression in various AD tissues and biofluids could be indicative for AD-type change and perhaps diagnostic for prodromal aspects of the AD. Further, understanding of miRNA biogenesis and the signaling pathways in which groups of miRNAs participate either cooperatively or synergistically might aid the discovery of diagnostic biomarkers or development of effective

therapeutics for progressive and lethal neurodegenerative disorders (Zhao et al., 2016a,b; Cole and Seabrook, 2020).

OVERVIEW OF miRNA ABUNDANCE IN AD TISSUES AND BIOFLUID COMPARTMENTS

One important limitation of the analysis of miRNAs in human CNS tissues, extracellular fluid (ECF) and CSF is that, apart from CNS biopsies, brain tissue samples must be obtained post-mortem, and miRNAs have a relatively short post-mortem half-life in both human brain and retina, on the range of about ~1 to 3 h for a typical 22 nucleotide (nt) single-stranded miRNA (~45% G + T) in the human neocortical and hippocampal compartments that have been analyzed and for which there is experimental data (Sethi and Lukiw, 2009; Rügger and Großhans, 2012; Pogue et al., 2014; Tudek et al., 2019). Very few studies have addressed miRNA half-life *in vitro* or *in vivo* but currently both miRNA and mRNA decay kinetics have been shown: (i) to follow the same AU-enrichment rules of single-stranded miRNA and mRNA stability that is, the more AU-enriched elements (AREs) in the sncRNA, miRNA or mRNA, the shorter the half-life (Sethi and Lukiw, 2009; Rügger and Großhans, 2012; Clement et al., 2016; Van Meter et al., 2020); (ii) to be stabilized in part by miRNA binding proteins (Zang et al., 2020); (iii) to be further stabilized by circularization (circRNA; Lukiw, 2013a,b; Zhao et al., 2016a,b; Xie et al., 2017; Kondo et al., 2020) and/or (iv) by their inclusion into exosomes or intracellular or extracellular micro-vesicles (Badhwar and Haqqani, 2020; Bitetto and Di Fonzo, 2020; Groot and Lee, 2020; Upadhyay et al., 2020). Another indication of the usefulness of post-mortem material for molecular-genetic studies is that nuclei extracted from human brain biopsies or post-mortem brain tissues are able to fully support *in vitro* run-on transcription for up to ~3–4 h after which there is a precipitous decline in polymerization activity (Cui et al., 2005; Rügger and Großhans, 2012; Clement et al., 2016). It is important to appreciate the fact that microRNAs (miRNAs) with a mass of just ~7628 Da (for a typical 22 nt sncRNA like miRNA-146a) are the *smallest and most abundant ribonucleic acid information-carrying components of tissues*, the ECF, the CSF and blood serum compartments. The miRNA abundance in tissues, ECF, CSF or blood serum provides valuable insight and “current snapshot” of soluble pathogenic sncRNA biomarkers that may be diagnostic for human neurological disease types. These miRNA “*information packages*” have recently been shown to be sequestered into extracellular, lipophilic microvesicles or exosomes that shuttle between cells and tissues and/or amongst ECF, CSF and blood serum compartments (Alexandrov et al., 2013; Jaber et al., 2017, 2019; Badhwar and Haqqani, 2020; Bitetto and Di Fonzo, 2020; Upadhyay et al., 2020; Vanherle et al., 2020). Extracellularly secreted miRNAs circulating in the peripheral blood are referred to as “*circulating miRNAs*”; they are either encapsulated by extracellular vesicles such as exosomes and microvesicles, or bound to molecules such as the Argonaute protein, or HDL cholesterol (Zernecke et al., 2009; Arroyo et al., 2011; Vickers et al., 2011; Ishibe et al.,

2018; Groot and Lee, 2020; Upadhyaya et al., 2020). In addition, miRNAs that leak from destroyed cells and apoptotic bodies are also found among circulating serum miRNAs and have been implicated in the spreading of AD neuropathology (Zernecke et al., 2009; Lukiw et al., 2012). It is also noteworthy to point out that while the ECF, CSF and blood serum can be considered as relatively contiguous biofluids, there may be selective biophysical barrier-mediated effects on miRNA permeability, translocation and *trans*-membrane transport of microRNAs which ends up as having the ECF, CSF, and blood serum compartments essentially distinct in their miRNA content and stoichiometric abundance (Blennow et al., 2010; Alexandrov et al., 2013; Hampel et al., 2018a,b,c; Ishibe et al., 2018; see below).

As the name suggests ECFs have been shown as being representative of the saline-based biofluids surrounding individual brain cell types (Alexandrov et al., 2012; Pogue et al., 2014; Shetty and Zanirati, 2020). ECF, sometimes referred to as interstitial fluid (ISF), drains through very narrow intercellular spaces within gray matter into bulk flow perivascular channels that surround penetrating arteries and then flows to the surface of the brain to join the CSF that drains into cervical lymph nodes (Shetty and Zanirati, 2020; Upadhyaya et al., 2020; Weller, 2020). Human brain CSF, produced by the choroid plexus and secreted into the brain ventricles and subarachnoid space, plays critical roles in the biophysical and immune protection of the brain and provides intra-cerebral transport of nutrients, cofactors and hormones, as well as small signaling molecules such as sncRNAs and miRNAs. Since ECF and CSF circulates throughout and within the entire CNS: (i) ECF and CSF composition is representative of the biofluids surrounding both brain cells and multiple anatomical regions of the brain and spinal cord; and (ii) provides valuable insight into soluble pathogenic bio-markers that bathe CNS cells and tissues, including soluble miRNAs that have diagnostic value for human brain health, disease or injury (Hampel et al., 2018a,b,c; Shetty and Zanirati, 2020; Weller, 2020). Human peripheral blood serum is defined as the clear-yellowish fluid that remains from blood plasma after clotting factors (such as fibrinogen and prothrombin) have been removed after clot formation and whole blood centrifugation, and contains the same components as plasma such as fatty acids, hormones, cytokines, chemokines, carbohydrates, growth factors, and miRNAs (both free miRNAs and those packaged into extracellular vesicles) and is the circulating carrier of exogenous and endogenous fatty acids, free lipids and lipoproteins in the systemic circulation (Hill, 2019; Penner et al., 2019; Lukiw and Pogue, 2020; Shetty and Zanirati, 2020⁷; last accessed 26 August 2020). The ease and relative non-invasiveness of blood serum and CSF accessibility, and acquisition in large human populations, makes it one of the most studied of all biofluid compartments in diagnostic medicine for AD and other neurological disorders.

Regarding the presence and persistence of the same miRNAs in multiple AD brain tissues and biofluids, we are aware of only one relevant peer-reviewed research report concerning miRNAs in the extracellular fluid (ECF) obtained from highly purified AD brain tissue supernatants, and parallel studies on

encapsulated miRNAs packaged into extracellular vesicles in ECF and CSF (Alexandrov et al., 2012; Lukiw and Pogue, 2020). The purpose of the Alexandrov et al. (2012) paper was to ascertain if the increased miRNAs found in AD brain tissues were contiguous with up-regulated miRNAs found in AD ECF and CSF. Based on extensive fluorescent miRNA-array and RNA sequencing analysis, the results indicated significant common increases in miRNA-9, miRNA-34a, miRNA-125b, miRNA-146a, miRNA-155 that were shared by AD brain tissues, ECF and CSF. Transcription from each of these inducible miRNA genes are known to be under NF- κ B (p50/p65)-regulated genetic control (Zhao et al., 2015; Lukiw, 2020a,b). Interestingly in miRNA abundance analysis of A β -peptide stressed human neuronal-glia (HNG) cell primary co-cultures, ECF displayed an up-regulation of these same miRNAs, an effect that was quenched using anti-NF- κ B agents CAPE and CAY10512. Overall the results indicated that these same microRNAs including miRNA-9, miRNA-34a, miRNA-125b, miRNA-146a, and miRNA-155 are brain tissue-, CSF- and ECF-abundant, NF- κ B-sensitive pro-inflammatory miRNAs, and their enrichment in both tissues and circulating AD biofluids suggest that they may be involved in the modulation or proliferation of miRNA-triggered pathogenic signaling throughout the human brain and CNS (Alexandrov et al., 2012; Hill, 2019; Lukiw and Pogue, 2020; Shetty and Zanirati, 2020).

In related studies and using different sources of AD samples including blood serum, post-mortem brain tissues, AD fibroblasts, AD β -lymphocytes, AD cell lines, transgenic AD (TgAD) mouse models and AD CSF all confirmed the increased presence (and biomarker potential) of miRNA-455-3p. This miRNA was found to reduce A β peptide toxicity, while enhancing mitochondrial biogenesis and synaptic activity and maintaining healthy mitochondrial dynamics (Kumar and Reddy, 2019; Kumar et al., 2019; Kumar and Reddy, 2020). These findings further underscore the concept that these independently documented differences may: (i) be just another example of the high levels in heterogeneity of miRNA expression in different human populations from different AD brains and patients; (ii) serve as an example of the considerable miRNA redundancy and complexity in the AD process; and (iii) indicate that multiple miRNAs are involved in the regulation of multiple gene expression pathways and patterns whose abundances are highly sensitive to alterations in the biochemical, neurochemical, neuropathological, and/or cellular environment (Alexandrov et al., 2012; Lukiw, 2013a,b; Kumar and Reddy, 2019; Kumar et al., 2019; Kumar and Reddy, 2020; Lukiw and Pogue, 2020).

INFORMATIVE miRNAS IN AD

As previously discussed, the decidedly heterogeneous nature of AD appears to pervade through all molecular, genetic and epigenetic, neuropathological and behavioral, mnemonic and cognitive aspects of the disease, including the pre-clinical symptomology, initiation, disease course and presentation. Indeed in depth summaries of hundreds of peer-reviewed scientific reports to date has provided no general consensus

⁷<https://www.innov-research.com/blogs/news/the-importance-of-human-serum>

of what single specific miRNAs are up-or-down regulated in any tissue or biofluid compartment in many thousands of AD patients, but rather a “trend” or “pattern” in certain miRNA abundance and speciation. This is perhaps not too surprising because of the manifold symptoms typically presented by AD patients, their often complicated and non-uniform drug history, the insidious nature and progressiveness of the disease, the age and gender of the AD patient, and other disease-related aspects including inter-current illness and the genetic make-up of individual AD patients.

Concerning the potential for contribution of specific miRNAs to AD, we recently surveyed the number of published papers on “miRNA biomarkers for AD” using the National Institutes of Health National Library of Medicine website MedLine at PubMed Central (⁸last accessed 26 August 2020). Using the keywords “Alzheimer's disease” and “miRNA” indicates that there are just under ~13,000 publications on this topic since the original publication on selective miRNA alterations in AD brain about ~14 years ago (Lukiw, 2007). Inspection of several of these recent reports continues to support the contention of extensive miRNA heterogeneity in both AD tissues and biofluids (ECF, CSF, and blood serum) and continues to *provide no general consensus of any single miRNA that defines causation for the onset or duration of the AD pathophysiology* (Moradifard et al., 2018; Peña-Bautista et al., 2019; Silvestro et al., 2019; Swarbrick et al., 2019; Condrat et al., 2020; Giorgi Silveira et al., 2020; van den Berg et al., 2020). It is becoming clear, however, that a panel of multiple AD-relevant “pro-inflammatory” or “pro-pathology” miRNAs may be useful in contributing to the diagnosis of AD at any stage of the disease. For example one extremely thorough systematic review was recently conducted to quantify significantly deregulated miRNAs in the peripheral blood of AD patients, and these deregulated miRNAs were cross-referenced against the miRNAs known to be deregulated in limbic regions of brain tissues, such as the hippocampus, in moderate-to-advanced stages of AD (Swarbrick et al., 2019). These analyses resulted in a panel of at least 11 miRNAs (in numerical ascendancy) - miRNA-26b, miRNA-30e, miRNA-34a, miRNA-34c, miRNA-107, miRNA-125b, miRNA-146a, miRNA-151, miRNA-200c, miRNA-210, and hsa-miRNA-485, hypothesized to be both deregulated early in AD and up to nearly ~20 years before the onset of any clinical symptomatology. Network analysis of these 11 miRNAs indicated that they were found to be associated with the cell cycle and cell surface receptor (Wnt/ β -catenin) signaling, cellular response to stress, cellular senescence, gene expression regulation, and nerve growth factor and Rho GTPase signaling. Another in depth study had previously indicated that just five miRNAs - miRNA-9, miRNA-34a, miRNA-125b, miRNA-146a, and miRNA-155 - are significantly abundant in AD neocortical brain tissues as well as the ECF and CSF and each miRNA was found to interactively contribute to the AD pathophysiology (Figure 2). Interestingly, each of these five miRNAs have been shown to contain strong binding sites for the inflammatory transcription factor NF- κ B in their immediate promoters, are therefore said to be under NF- κ B (p50/p65) control and are referred to as “pro-inflammatory miRNAs” (Pogue and Lukiw,

2018; Gong and Sun, 2020; Zamani et al., 2020). The contiguous presence of specific pro-inflammatory miRNAs in AD tissue, ECF and CSF may be the result of their *trans*-compartmental solubility or may be part of a RNA-based signaling system between neocortical brain tissues and the ECF and/or CSF that is reflective or diagnostic for the neurodegenerative disease state (Alexandrov et al., 2012; Jaber et al., 2019; Veitch et al., 2019; Wang et al., 2020).

miRNA FOR PRECISION MEDICINE-BASED DIAGNOSTICS AND THERAPEUTICS

Extensive demographic analysis tells us that human neurodegenerative diseases such as AD are among the fastest growing neurologically incapacitating diseases of aging human populations in Westernized societies (⁹last accessed 26 August 2020). Despite the significant medical and scientific advances made in our understanding of the AD pathophysiological mechanisms on a global scale, there is currently no effective cure for this rapidly expanding form of age related and terminally lethal senile dementia. AD is the leading cause of dementia and globally about ~50 million people have some form of dementia, and someone in the world develops dementia every 3 s (¹⁰last accessed 26 August 2020). The repeated failures of pharmacological strategies and clinical trials over the last decade in the development of novel and efficacious treatments and disease-modifying therapeutics for AD is due in part to the fact that AD is a singularly heterogeneous disorder caused by “human genetic and biochemical heterogeneity,” considerably different genetic and epigenetic profiles, age, gender and lifestyle factors, prodromal and more advanced phases of the disease, environmental triggers, misdiagnosis and/or importantly, the presence of other “inter-current illness” (Figure 1; Lukiw, 2013a,b; Blennow and Zetterberg, 2018; Cole and Seabrook, 2020; Lewczuk et al., 2020). The majority of clinical trials have focused on the immunological modulation of amyloid- β peptide (A β 40 and A β 42) signaling in AD, including therapeutic drugs targeted against A β 42 peptide accumulation, inhibition of β -secretase and γ -secretase cleavage enzymes, and anti-A β peptide monoclonal antibody approaches, however, in most of the clinical trials for patients with mild-to-moderate AD these drugs did not meet the expected endpoints. While A β peptides have long been proposed to play a central role in AD, and the A β pathway remains a valuable therapeutic target, the accuracy, importance, and even the correctness of the “amyloidocentric hypothesis” in driving AD neuropathology has been recently questioned (Ricciarelli and Fedele, 2017; Mullane and Williams, 2018; Cole and Seabrook, 2020). In addition, most AD patients are diagnosed in the middle-to-late-stages of this disorder when irreversible damage to the brain has already occurred, and the “pre-clinical” or “prodromal” phase has already passed. More recently therapeutic approaches and disease

⁸www.ncbi.nlm.nih.gov

⁹<https://www.alz.org/alzheimers-dementia/facts-figures>

¹⁰<https://www.usaginstalzheimers.org/learn/alzheimers-crisis?gclid=EAIaIQobChMI287jSPG96QIVDdbACh0HjAm0EAAAYBCAAEgILDvDBWc>

modification strategies directed against other AD-implicated pathological mechanisms, including alterations in tau signaling, the cholinergic system, anti-microbial and anti-viral approaches and hormone replacement therapies, to name a few, may provide improved clinical efficacy (Bhute et al., 2020; Habes et al., 2020; Hampel et al., 2020a,b; Iqbal et al., 2020; Zhou et al., 2020).

Using data-driven studies in the identification of the earliest signs of AD and the implementation of biomarker testing and PET and/or MRI neuroimaging during the prodromal or earliest stages of the disease is an urgent contemporary quest in AD diagnostics (Zhao et al., 2015; Fierini, 2020; Emrani et al., 2020; Habes et al., 2020). This current void may be in part filled by precise miRNA profiling of miRNA-containing biofluids along the course of AD. The use of novel molecular-genetic, multimodal neuroimaging techniques and their integration under the systems biology approach should: (i) allow clinicians and researchers to better understand miRNA-based factors involved in AD initiation and trajectory; and (ii) to deliver targeted interventions tailored to the molecular-genetic and miRNA-signaling profiles of the individual AD patient, according to the precision medicine paradigm (Hampel et al., 2016, 2017, 2018a,b,c, 2019; Lista et al., 2016; Castrillo et al., 2018; Veitch et al., 2019). Such a precision medicine-based framework is now increasingly facing the clinical and biological/genetic complexity and heterogeneity of AD. This is the field where miRNA neurobiology involving both stabilized miRNAs and anti-miRNA strategies may play a significant and to date yet unexploited role (Zhao et al., 2016a,b; Jaber et al., 2019; Ghaffari et al., 2020).

It is also clear that given the complexity of AD onset, disease course and diagnosis effective future therapeutic approaches including miRNA and anti-miRNA (antimiR, antagomir, AM) strategies: (i) will need to be concurrent and multidimensional, targeting the multiple disease pathways and neurological symptoms that will both inhibit both primary disease pathogenesis and minimize ancillary off-target effects; (ii) will be integrated with advancement in the development of specific and sensitive neuroimaging and biofluid-based diagnostic tools for miRNA and other AD-relevant biomarkers; (iii) will involve *precision medicine and individualized therapies* developed within the systems biology and systems neurophysiology approaches; and (iv) will be utilized in parallel with primary medical care for screening and in a second level diagnostic work-up for specialist diagnosis and clinical management (see below; Gurland et al., 1995; Galvin et al., 2010; Hampel et al., 2016, 2019; Lista et al., 2016; Castrillo et al., 2018; Jaber et al., 2019; Penner et al., 2019; Turner et al., 2020).

microRNA, “HUMAN BIOCHEMICAL INDIVIDUALITY” AND THERAPEUTIC STRATEGIES

If high-density Gene-chip-based microarray analysis, LED-Northern analysis and current RNA sequencing strategies are of any indication of AD variability, then there are real and significant human population differences in miRNA abundance,

speciation and complexity throughout the course of AD. For example one study has demonstrated variability in miRNA abundance, speciation and complexity amongst different human populations with specific reference to AD incidence amongst Caucasians and African Americans (Lukiw, 2013a,b). There continues to be an urgent requirement to identify novel protein, proteolipid and ribonucleic acid biomarkers, advanced high-resolution MRI- and PET-based neuroimaging techniques and related diagnostic methodologies for the early detection of AD in different populations. Together these will be potentially useful as a multidimensional screening technology yielding data whose integration will allow the determination, and gauge the potential risk to develop cognitive decline and/or impending neurological disruption in AD compared to healthy aging cognitively normal individuals from different population groups.

While the characterization of miRNA in neurodegenerative disease is highly informative, this information alone cannot easily discriminate between closely related neurodegenerative conditions. Many miRNA signals appear to be non-specific biomarkers of brain cell atrophy, injury or death and inflammatory neurodegeneration, response to psychoactive medications or they may be associated with other non-AD pathologies that have gone undiagnosed or misdiagnosed (**Figure 1**). However, in combination with other specific biomarkers or diagnostic tools, the quantification of multiple species of miRNAs might be a useful part of the diagnostic puzzle to assist in the detection and discrimination of certain specific neurodegenerative disorders even though they may possess significant clinical overlap (Jużwik et al., 2019; Kou et al., 2020; Lukiw and Pogue, 2020; Ma et al., 2020). The analysis of miRNAs over time, such as in integrated studies of neurodevelopment in humans and in experimental transgenic animal models of AD (TgAD), have already been shown: (i) to be a promising tracer and prognostic biomarker for homeostatic brain function during normal brain development and neuronal differentiation from the embryonic period to adulthood (Giorgi Silveira et al., 2020); and (ii) in conjunction with extensive neuropsychological testing, may be further useful to monitor and predict the incidence of onset, the rate of progression of disease activity and its trajectory, and to further evaluate in detail both therapeutic responses and clinical efficacy (Peña-Bautista et al., 2019). Significant heterogeneity in AD symptomology, large variation in clinical disease presentation, progression and patterns of neural system disconnection and degeneration, and molecular, genetic and epigenetic biomarkers at various stages of AD progression make this disease: (i) perhaps the preeminent example of what Linus Pauling originally referred to as “*human biochemical individuality*” – that each human individual represents a remarkably and biochemically unique case with regard to their health and susceptibility to develop disease (Pauling, 1976; reviewed in the context of AD by Lukiw, 2013a,b); and (ii) a target of both highly precise interventional treatment and the best example yet described for the potential application of “*personalized medicine*.” As previously pointed out, the strong heterogeneity in AD neuropathology, course and miRNA profiles of individuals with AD versus age- and gender matched

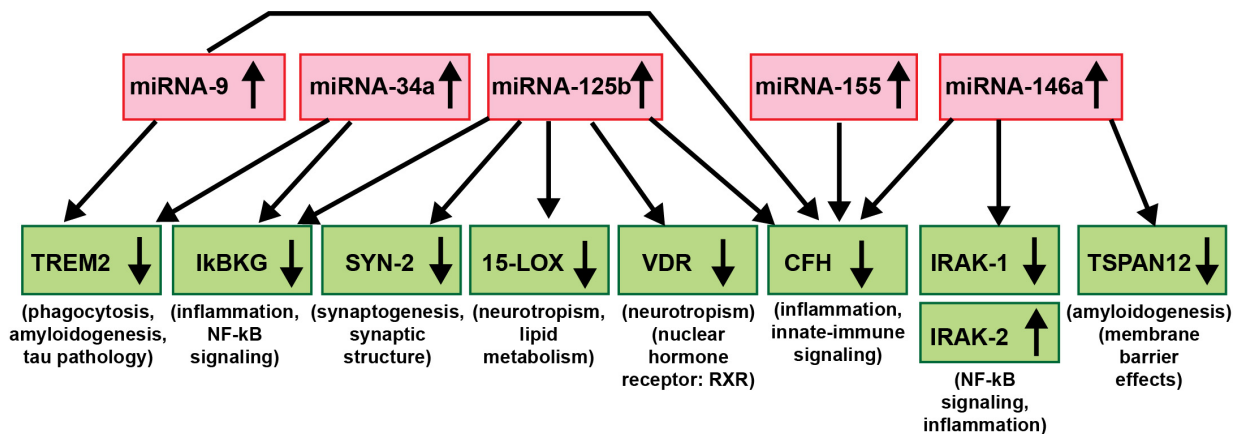


FIGURE 3 | An example of a highly interactive miRNA-mRNA regulatory network involving 5 miRNAs and 9 mRNAs; there is a significant contribution of up-regulated miRNA signaling (red boxes) to specific aspects of the down-regulated mRNA-mediated expression of key AD-relevant genes (green boxes) and AD neuropathology (Chandrasekaran and Bonchev, 2016; Clement et al., 2016; Hill and Lukiw, 2016; Jaber et al., 2017, 2019; Lukiw, 2020a,b). Just 5 significantly up-regulated miRNAs – miRNA-9, miRNA-34a, miRNA-125b, miRNA-146a, and miRNA-155 (all reported to be up-regulated in AD and/or TgAD models) – can account for the down-regulation of 8 mRNA targets critically involved in multiple aspects of AD neuropathology (IRAK-2 is up-regulated due to a compensatory mechanism as described in Cui et al., 2010). Briefly, these miRNAs down-regulate miRNA-directed mRNA target degradation involved in phagocytosis deficits, amyloidogenesis and tau pathology (TREM2, TSPAN12), inflammation, NF-kB- and innate-immune signaling (IkbKG, CFH, IRAK1; with a compensatory increase in IRAK-2), neurotropism (15-LOX, VDR), synaptic maintenance and synaptogenesis (SYN-2), all of which are distinguishing pathological features characteristic of AD neuropathology. Using DNA and RNA sequencing, microfluidic-based GeneChip microarray analysis and advanced LED-Northern dot blot analysis it has been recently reported that: (i) miRNA-9, miRNA-34a, miRNA-125b, miRNA-146a and miRNA-155 are easily detected in the human brain neocortex and retina; (ii) all have NF-kB-recognition features in their immediate upstream promoters; (iii) these same miRNAs are induced by increases in NF-kB due to reactive-oxygen species (ROS) induced stress; and (iv) these 5 miRNAs form a pro-inflammatory gene family up-regulated in AD brain neocortex and hippocampal CA1 (Colangelo et al., 2002; Cogswell et al., 2008; Zhao et al., 2015; Fan et al., 2020; Lukiw, 2020a,b). This diagram is based on studies from our laboratories in which each AD and age- and gender-matched control sample (N~135) were interrogated for 2,650 human miRNAs and 27,000 human mRNAs using RNA sequencing, microarray analysis and/or advanced LED-Northern dot blotting technologies in a single experiment and miRNA-mRNA linkage analysis and bioinformatics were subsequently analyzed (Jaber et al., 2019; Fan et al., 2020; Lukiw and Pogue, 2020; manuscript in preparation).

controls strongly support this concept. The integration of multiple pharmacogenomic strategies for a personalized medical treatment in AD is now currently the most effective choice to optimize our existing therapeutic tools while reducing unwanted off-target effects. These include a significant dedication of medical personnel to individual AD patients in cooperation with family and caregivers, multiple combinatorial approaches including extensive clinical assessment, intermittent brain neuroimaging over the onset and course of AD and a host of multiple molecular, genetic, epigenetic, neurophysiological, and neurobiological strategies with focus on CSF, serum biomarkers, miRNA and perhaps other sncRNA abundance in these biofluid compartments. While significant progress is being made: it is important to point out that: (i) combinatorial diagnostic methodologies incorporating molecular genetic markers such as miRNA screening combined with DNA-based gene mutation analysis, advanced MRI- or PET-neuroimaging techniques and conscientious clinical evaluations, still have difficulty in the diagnosis of AD, often requiring the stratification of AD into complex subgroups and post-mortem verification (Guerreiro et al., 2012; Pogue and Lukiw, 2018; Penner et al., 2019; Peña-Bautista et al., 2019; Guest et al., 2020; Habes et al., 2020; Hampel et al., 2020a,b; Hudon et al., 2020; Khoury and Grossberg, 2020; Sherva et al., 2014; Rossini et al., 2020; Serpente et al., 2020; Sims et al., 2020; Singh and Yadav, 2020; Swarbrick et al., 2019; Turner et al., 2020; van den Berg et al., 2020;

Wang et al., 2020; Weller, 2020); and (ii) currently available pharmacology and strategic treatments (including targeted drug delivery) based on these diagnostic tools, in the majority of cases, still do not directly address the primary underlying cause of either EOAD or LOAD but are sadly limited to the temporary alleviation of clinical symptoms (Di Resta and Ferrari, 2019; Veitch et al., 2019; Guest et al., 2020; Khoury and Grossberg, 2020; Lewczuk et al., 2020; Patnode et al., 2020; Rahman et al., 2020).

CONCLUDING REMARKS

As critical modulators of the brain and CNS transcriptome across neurodevelopment, aging and in neurological health and disease, both in human studies and in TgAD models, research evidence continues to implicate miRNAs as major epigenetic contributors to AD onset, incidence, neuropathology, epidemiology, disease course, severity and progression (Sethi and Lukiw, 2009; Lukiw, 2013a,b; Jaber et al., 2017, 2019; Wang et al., 2017; Condrat et al., 2020; Cole and Seabrook, 2020; Lukiw and Pogue, 2020; Moradifard et al., 2018; Wang and Zhang, 2020; Wang et al., 2020; **Figure 3**). Importantly, to date no single miRNA has been found that is diagnostic for the “prodromal” or “MCI” phase of AD or for any particular defined stage of the disease and this is likely to

remain the case in future miRNA abundance studies. The most recent findings underscore the idea that *it is very unlikely that any single miRNA in brain tissues, the ECF, CSF, blood serum, urine or any other biofluid compartments from multiple human populations will be predictive for AD at any stage of the disease*. What might be particularly useful for significantly improved AD diagnostics, however, would be a selective, high-density panel of a “*pathogenic and inflammatory neurodegeneration-associated miRNA family*” that along with other molecular-based, gene expression-based or neuroimaging-related biometrics could more accurately identify and predict the onset and course of AD-type change (Wang et al., 2017; Wang and Zhang, 2020; Wang et al., 2020; see **Figure 3**). According to the systems biology approach, one of the pillars of precision medicine, a comprehensive evaluation, encompassing multiple pathophysiological mechanisms at different biological levels is needed to fully untangle the dynamics of AD and inform therapeutic decision-making at the individual level. miRNA-, mRNA- and protein-based gene expression alterations and patterns, AD-relevant DNA mutations, pro-inflammatory biomarkers, such as the novel flood of inflammatory cytokines contributing to the cytokine storm in AD, A β 40- and A β 42-peptide load in the ECF, CSF and blood serum, combined with data from MRI- and PET-based neuroimaging, familial and clinical history and lifestyle factors could be extremely useful in improving diagnosis and prognosis of AD onset and development and perhaps, even the susceptibility to AD initiation and/or development (Zhao et al., 2015; Wang et al., 2017; Frost et al., 2019; Hampel et al., 2019; Jużwik et al., 2019; Swarbrick et al., 2019; Adams et al., 2020; Condrat et al., 2020; Hampel et al., 2020a,b; Serpente et al., 2020; Turner et al., 2020; Wang and Zhang, 2020; Wang et al., 2020).

One may argue that the heterogeneity of miRNAs in AD tissues and biofluids may make these ribonucleic acid-based biomarkers too variable in reflecting a pathological condition, however, of the known ~2650 currently identified human miRNAs only about ~35 miRNA species are known to be abundant in the brain, retina and CNS (see above; ¹¹Lukiw, 2007; Zhao et al., 2015; Jaber et al., 2017). If miRNA abundance is any reflection of its importance, this appears to significantly restrict the total number of expressed miRNAs that may be mis-regulated in AD brain. Moreover the basis of “*individualized prevention, precise and personalized*” treatment strategies using a systems biology approach requires an input from a very large number of independent data sources. While miRNA abundance, speciation and complexity is a very important one of these data sources, it is the information that may be extracted from all of these data sources together that should be the most effective as a diagnostic, prognostic and/or screening tool across the entire continuum of AD (Wang et al., 2015, 2017; Jaber et al., 2017, 2019; Lukiw and Pogue, 2020; Wang and Zhang, 2020; Wang et al., 2020).

Lastly, multiple analytical molecular-genetic approaches, geriatric, and clinical evaluation, current neuroimaging

methods and resulting integrated diagnostic and predictive strategies are currently within the capabilities of contemporary clinical and medical neurology. Improved clinical data acquisition, coordination, interpretation and integration of clinical, laboratory and healthcare resources will be required to obtain a more accurate diagnostic profile of the “*provisional AD patient*.” miRNA-mRNA linkage or association mapping for AD-relevant neurological pathways should be additionally useful as a diagnostic approach because miRNA-mediated regulatory mechanisms appear to involve a large number of pathogenic and highly integrated gene expression pathways in the CNS. An equally wide variety of “*individualized prevention, precise and personalized*” treatment strategies will also be required to more effectively address AD and other insidious, age-related neurological disorders, including the application of novel and highly customized, personalized and/or combinatorial miRNA modulatory and/or anti-miRNA-based pharmacological strategies whose therapeutic design and implementation have yet to be considered.

DISCLOSURE

HH is an employee of Eisai Inc. and serves as Senior Associate Editor for the Journal Alzheimer's and Dementia and does not receive any fees or honoraria since May 2019; before May 2019 he had received lecture fees from Servier, Biogen and Roche, research grants from Pfizer, Avid, and MSD Avenir (paid to the institution), travel funding from Functional Neuromodulation, Axovant, Eli Lilly and company, Takeda and Zinfandel, GE Healthcare and Oryzon Genomics, consultancy fees from Qynapse, Jung Diagnostics, Cytox Ltd., Axovant, Anavex, Takeda and Zinfandel, GE Healthcare and Oryzon Genomics, and Functional Neuromodulation, and participated in scientific advisory boards of Functional Neuromodulation, Axovant, Eisai, Eli Lilly and company, Cytox Ltd., GE Healthcare, Takeda and Zinfandel, Oryzon Genomics and Roche Diagnostics. HH is co-inventor in the following patents as a scientific expert and has received no royalties:

In vitro Multiparameter Determination Method for The Diagnosis and Early Diagnosis of Neurodegenerative Disorders Patent Number: 8916388;

In vitro Procedure for Diagnosis and Early Diagnosis of Neurodegenerative Diseases Patent Number: 8298784;

Neurodegenerative Markers for Psychiatric Conditions Publication Number: 20120196300;

In vitro Multiparameter Determination Method for The Diagnosis and Early Diagnosis of Neurodegenerative Disorders Publication Number: 20100062463;

In vitro Method for The Diagnosis and Early Diagnosis of Neurodegenerative Disorders Publication Number: 20100035286;

¹¹<http://www.mirbase.org/>

In vitro Procedure for Diagnosis and Early Diagnosis of Neurodegenerative Diseases Publication Number: 20090263822;

In vitro Method for The Diagnosis of Neurodegenerative Diseases Patent Number: 7547553;

CSF Diagnostic *in Vitro* Method for Diagnosis of Dementias and Neuroinflammatory Diseases Publication Number: 20080206797;

In vitro Method for The Diagnosis of Neurodegenerative Diseases Publication Number: 20080199966;

Neurodegenerative Markers for Psychiatric Conditions Publication Number: 20080131921;

AV is an employee of Eisai Inc. He does not receive any fees or honoraria since November 2019. Before November 2019 he had received lecture honoraria from Roche, MagQu LLC, and Servier.

SL has received lecture honoraria from Roche and Servier.

WL serves on 36 journal editorial boards and study sections and is senior academic editor for the journals *Frontiers in Genetics*, *Molecular Neurobiology* and *PLOS One*. Research on miRNA and mRNA in the Lukiw laboratory involving biomarkers in AD and in other forms of neurological or retinal disease, amyloidogenesis, synaptogenesis and neuroinflammation was supported through an unrestricted grant to the LSU Eye Center from Research to Prevent Blindness (RPB); the Louisiana Biotechnology Research Network (LBRN) and NIH grants NEI EY006311, NIA AG18031 and NIA AG038834 (WL).

AUTHOR CONTRIBUTIONS

YZ, VJ, PA, AV, SL, HH, and WL researched the manuscript. WL assembled all data and wrote the manuscript. All authors contributed to the article and approved the submitted version.

REFERENCES

- Adams, S. H., Anthony, J. C., Carvajal, R., Chae, L., Khoo, C. S. H., Latulippe, M. E., et al. (2020). Perspective: guiding principles for the implementation of personalized nutrition approaches that benefit health and function. *Adv. Nutr.* 11, 25–34. doi: 10.1093/advances/nmz086
- Ahluwalia, N., and Vellas, B. (2003). Immunologic and inflammatory mediators and cognitive decline in Alzheimer's disease. *Immunol. Allergy Clin. North Am.* 23, 103–115. doi: 10.1016/s0889-8561(02)00048-6
- Alexandrov, P. N., Dua, P., Hill, J. M., Bhattacharjee, S., Zhao, Y., and Lukiw, W. J. (2012). microRNA (miRNA) speciation in Alzheimer's disease (AD) cerebrospinal fluid (CSF) and extracellular fluid (ECF). *Int. J. Biochem. Mol. Biol.* 3, 365–373.
- Alexandrov, P. N., Zhao, Y., Jones, B. M., Bhattacharjee, S., and Lukiw, W. J. (2013). Expression of the phagocytosis-essential protein TREM2 is down-regulated by an aluminum-induced miRNA-34a in a murine microglial cell line. *J. Inorg. Biochem.* 128, 267–269. doi: 10.1016/j.jinorgbio.2013.05.010
- Altveß, S., Yildiz, H. K., and Vural, H. C. (2020). Interaction of the microbiota with the human body in health and diseases. *Biosci. Microb. Food Health* 39, 23–32. doi: 10.12938/bmfh.19-023

FUNDING

AV and HH are employees of Eisai Inc. This work has been performed during his previous position at Sorbonne University, Paris, France. At Sorbonne University he was supported by the AXA Research Fund, the “Fondation partenariale Sorbonne Université” and the “Fondation pour la Recherche sur Alzheimer,” Paris, France. This work was presented in part at the Society for Neuroscience (SFN) Annual Meeting 19–23 October 2019 Chicago IL, United States. WL is the Bollinger Professor of Alzheimer's disease (AD) at the LSU School of Medicine and Health Sciences Center. He serves on 36 journal editorial boards and study sections and is senior academic editor for the journals *Frontiers in Genetics*, *Neurochemical Research*, *Folia Neuropathologica* and *PLoS One*. Research on miRNA and mRNA in the Lukiw laboratory involving biomarkers in AD and in other forms of neurological or retinal disease, prion disease, amyloidogenesis, synaptogenesis, neuro-inflammation and environmental neurotoxicology was supported through an unrestricted grant to the LSU Eye Center from Research to Prevent Blindness (RPB); the Louisiana Biotechnology Research Network (LBRN) and NIH grants NEI EY006311, NIA AG18031, and NIA AG038834 (WL).

ACKNOWLEDGMENTS

Sincere thanks are extended to Drs. L. Carver, E. Head, W. Poon, H. LeBlanc, F. Culicchia, C. Eicken, and C. Hebel for short post-mortem interval (PMI) human brain and/or retinal tissues or extracts, miRNA array work and initial data interpretation, and to D Guillot and AI Pogue for expert technical assistance. Thanks are also extended to the many neuropathologists, physicians and researchers of Canada and the United States who have provided high quality, short PMI, human CNS, retinal tissues or extracted total brain and retinal RNA and biofluids (ECF, CSF, and blood serum sample) for scientific study.

- Alzheimer's Association (2020). *Alzheimer's Disease Facts and Figures March 2020*. Chicago, IL: Alzheimer's Association.
- Arroyo, J. D., Chevillet, J. R., and Kroh, E. M. (2011). Argonaute2 complexes carry a population of circulating microRNAs independent of vesicles in human plasma. *Proc. Natl. Acad. Sci. U.S.A.* 108, 5003–5008. doi: 10.1073/pnas.1019055108
- Arvanitakis, Z., Shah, R. C., and Bennett, D. A. (2019). Diagnosis and management of dementia: review. *JAMA* 322, 1589–1599. doi: 10.1001/jama.2019.4782
- Ashford, J. W., Kumar, V., Barringer, M., Becker, M., Bice, J., Ryan, N., et al. (1992). Assessing Alzheimer severity with a global clinical scale. *Int. Psychogeriatr.* 4, 55–74. doi: 10.1017/s1041610292000905
- Atlasi, Y., Jafarnejad, S. M., Gkogkas, C. G., Vermeulen, M., Sonenberg, N., and Stunnenberg, H. G. (2020). The translational landscape of ground state pluripotency. *Nat. Commun.* 11:1617. doi: 10.1038/s41467-020-15449-9
- Badhwar, A., and Haqqani, A. S. (2020). Biomarker potential of brain-secreted extracellular vesicles in blood in Alzheimer's disease. *Alzheimers Dement.* 12:e12001. doi: 10.1002/dad2.12001
- Bahlakeh, G., Gorji, A., Soltani, H., and Ghadiri, T. (2020). MicroRNA alterations in neuropathologic cognitive disorders with an emphasis on dementia: lessons from animal models. *J. Cell Physiol.* doi: 10.1002/jcp.29908 [Epub ahead of print].

- Barnes, J., Dickerson, B., Frost, C., Jiskoot, L. C., Wolk, D., and van der Flier, W. M. (2015). Alzheimer's disease first symptoms are age dependent: evidence from the NACC data set. *Alzheimers Dement.* 11, 1349–1357. doi: 10.1016/j.jalz.2014.12.007
- Bhattacharjee, S., and Lukiw, W. J. (2013). Alzheimer's disease and the microbiome. *Front. Cell Neurosci.* 7:153. doi: 10.3389/fncel.2013.00153
- Bhute, S., Sarmah, D., Datta, A., Rane, P., Shard, A., Goswami, A., et al. (2020). Molecular pathogenesis and interventional strategies for Alzheimer's disease: promises and pitfalls. *ACS Pharmacol. Transl. Sci.* 3, 472–488. doi: 10.1021/acspsci.9b00104
- Bitetto, G., and Di Fonzo, A. (2020). Nucleo-cytoplasmic transport defects and protein aggregates in neurodegeneration. *Transl. Neurodegener.* 9:25. doi: 10.1186/s40035020-00205-2
- Blennow, K., Hampel, H., Weiner, M., and Zetterberg, H. (2010). Cerebrospinal fluid, and plasma biomarkers in Alzheimer disease. *Nat. Rev. Neurol.* 6, 131–144. doi: 10.1038/nrneurol.2010.4
- Blennow, K., and Zetterberg, H. (2018). Biomarkers for Alzheimer's disease: current status and prospects for the future. *J. Intern. Med.* 284, 643–663. doi: 10.1111/joim.12816
- Burmistrova, O. A., Goltsov, A. Y., Abramova, L. I., Kaleda, V. G., Orlova, V. A., and Rogaev, E. I. (2007). MicroRNA in schizophrenia: genetic and expression analysis of miR-130b (22q11). *Biochemistry* 72, 578–582. doi: 10.1134/s0006297907050161
- Burwink, M., Lutzenberger, M., Heppner, F. L., Schulz-Schaeffer, W., and Baier, M. (2018). Intravenous injection of beta-amyloid seeds promotes cerebral amyloid angiopathy (CAA). *Acta Neuropathol. Commun.* 6:23. doi: 10.1186/s40478-018-0511-7
- Canobbio, I., Abubaker, A. A., Visconte, C., Torti, M., and Pula, G. (2015). Role of amyloid peptides in vascular dysfunction and platelet dysregulation in Alzheimer's disease. *Front. Cell Neurosci.* 9:65. doi: 10.3389/fncel.2015.00065
- Cao, Q., Tan, C. C., Xu, W., Hu, H., Cao, X. P., Dong, Q., et al. (2020). The prevalence of dementia: a systematic review and meta-analysis. *J. Alzheimers. Dis.* 73, 1157–1166. doi: 10.3233/JAD-191092
- Castrillo, J. I., Lista, S., Hampel, H., and Ritchie, C. W. (2018). Systems biology methods for Alzheimer's disease research toward molecular signatures, subtypes, and stages and precision medicine: application in cohort studies and trials. *Methods Mol. Biol.* 1750, 31–66. doi: 10.1007/978-1-4939-7704-8_3
- Caughey, B., and Kraus, A. (2019). Transmissibility versus pathogenicity of self-propagating protein aggregates. *Viruses* 11:E1044. doi: 10.3390/v11111044
- Chakraborty, M., Hu, S., Visness, E., Del Giudice, M., De Martino, A., Bosia, C., et al. (2020). MicroRNAs organize intrinsic variation into stem cell states. *Proc. Natl. Acad. Sci. U.S.A.* 117, 6942–6950. doi: 10.1073/pn1073as.1920695117
- Chandrasekaran, S., and Bonchev, D. (2016). Network topology analysis of post-mortem brain microarrays identifies more Alzheimer's related genes and microRNAs and points to novel routes for fighting with the disease. *PLoS One* 11:e0144052. doi: 10.1371/journal.pone.0144052
- Checksfield, M. (ed.) (2020). "National Academies of Sciences, Engineering, and Medicine; Division of Behavioral and Social Sciences and Education; Board on Behavioral, Cognitive, and Sensory Sciences; Committee on Developing a Behavioral and Social Science Research Agenda on Alzheimer's Disease and Alzheimer's Disease-Related Dementias," in *Proceedings of the a Workshop*, (Washington (DC): National Academies Press (USA)).
- Christoforidou, E., Joilin, G., and Hafezparast, M. (2020). Potential of activated microglia as a source of dysregulated extracellular microRNAs contributing to neurodegeneration in amyotrophic lateral sclerosis. *J. Neuroinflamm.* 17:135. doi: 10.1186/s12974-020-01822-4
- Clement, C., Hill, J. M., Dua, P., Culicchia, F., and Lukiw, W. J. (2016). Analysis of RNA from Alzheimer's disease post-mortem brain tissues. *Mol. Neurobiol.* 53, 1322–1328. doi: 10.1007/s12035-015-9105-6
- Cogswell, J. P., Ward, J., Taylor, I. A., Waters, M., Shi, Y., Cannon, B., et al. (2008). Identification of miRNA changes in Alzheimer's brain and CSF yields putative biomarkers and insights into disease pathways. *J. Alzheimers. Dis.* 14, 27–41. doi: 10.3233/jad-2008-14103
- Colangelo, V., Schurr, J., Ball, M. J., Pelaez, R. P., Bazan, N. G., and Lukiw, W. J. (2002). Gene expression profiling of 12633 genes in Alzheimer hippocampal CA1: transcription and neurotrophic factor down-regulation and up-regulation of apoptotic and pro-inflammatory signaling. *J. Neurosci. Res.* 70, 462–473. doi: 10.1002/jnr.10351
- Cole, M. A., and Seabrook, G. R. (2020). On the horizon-the value and promise of the global pipeline of Alzheimer's disease therapeutics. *Alzheimers Dement.* 6:e12009. doi: 10.1002/trc2.12009
- Condrat, C. E., Thompson, D. C., Barbu, M. G., Bugnar, O. L., Boboc, A., Cretoiu, D., et al. (2020). miRNAs as biomarkers in disease: latest findings regarding their role in diagnosis and prognosis. *Cells* 9:276. doi: 10.3390/cells9020276
- Cui, J. G., Li, Y. Y., Zhao, Y., Bhattacharjee, S., and Lukiw, W. J. (2010). Differential regulation of interleukin-1 receptor-associated kinase-1 (IRAK-1) and IRAK-2 by miRNA-146a and NF- κ B in stressed human astroglial cells and in Alzheimer disease. *J. Biol. Chem.* 285, 38951–38960. doi: 10.1074/jbc.M110.178848
- Cui, J. G., Zhao, Y., and Lukiw, W. J. (2005). Isolation of high spectral quality RNA using run-on gene transcription; application to gene expression profiling of human brain. *Cell Mol. Neurobiol.* 25, 789–794. doi: 10.1007/s10571-005-4035-x
- De Marco, M., and Venneri, A. (2015). 'O' blood type is associated with larger grey-matter volumes in the cerebellum. *Brain Res. Bull.* 116, 1–6. doi: 10.1016/j.brainresbull.2015.05.005
- De Smaele, E., Ferretti, E., and Gulino, A. (2010). MicroRNAs as biomarkers for CNS cancer and other disorders. *Brain Res.* 1338, 100–111. doi: 10.1016/j.brainres.2010.03.103
- DeTure, M. A., and Dickson, D. W. (2019). The neuropathological diagnosis of Alzheimer's disease. *Mol. Neurodegener.* 14:32. doi: 10.1186/s13024-019-0333-5
- Di Resta, C., and Ferrari, M. (2019). New molecular approaches to Alzheimer's disease. *Clin. Biochem.* 72, 81–86. doi: 10.1016/j.clinbiochem.2019.04.010
- Dinsmore, S. T. (1999). Alzheimer's disease diagnosis. *J. Am. Osteopath. Assoc.* 99, S1–S6. doi: 10.7556/jaoa.1999.99.9.s1
- Dumurgier, J., and Tzourio, C. (2020). Epidemiology of neurological diseases in older adults. *Rev. Neurol.* 4, S0035–S3787. doi: 10.1016/j.neurol.2020.01.356
- Eichhorn, S. W., Guo, H., and McGeary, S. E. (2014). mRNA destabilization is the dominant effect of mammalian microRNAs by the time substantial repression ensues. *Mol. Cell* 56, 104–115. doi: 10.1016/j.molcel.2014.08.028
- Eisen, T. J., Eichhorn, S. W., Subtelny, A. O., Lin, K. S., McGeary, S. E., Gupta, S., et al. (2020). The dynamics of cytoplasmic mRNA metabolism. *Mol. Cell* 77, 786–799.e10. doi: 10.1016/j.molcel.2019.12.005
- Emrani, S., Lamar, M., Price, C. C., Wasserman, V., Matusz, E., Au, R., et al. (2020). Alzheimer's/vascular spectrum dementia: classification in addition to diagnosis. *J. Alzheimers. Dis.* 73, 63–71. doi: 10.3233/JAD-190654
- Fan, W., Liang, C., and Ou, M. (2020). MicroRNA-146a is a wide-reaching neuroinflammatory regulator and potential treatment target in neurological diseases. *Front. Mol. Neurosci.* 13:90. doi: 10.3389/fnmol.2020.00090
- Fierini, F. (2020). Mixed dementia: neglected clinical entity or nosographic artifice? *J. Neurol. Sci.* 15:116662. doi: 10.1016/j.jns.2019.116662
- Frost, G. R., Jonas, L. A., and Li, Y. M. (2019). Friend, foe or both? immune activity in Alzheimer's disease. *Front. Aging Neurosci.* 11:337. doi: 10.3389/fnagi.2019.00337
- Galvin, J. E., Fagan, A. M., Holtzman, D. M., Mintun, M. A., and Morris, J. C. (2010). Relationship of dementia screening tests with biomarkers of Alzheimer's disease. *Brain* 133, 3290–3300. doi: 10.1093/brain/awq204
- Ghaffari, M., Sanadgol, N., and Abdollahi, M. (2020). A systematic review of current progresses in the nucleic acid-based therapies for neurodegeneration with implications for Alzheimer's Mini. *Rev. Med. Chem.* doi: 10.2174/1389557520666200513122357 [Online ahead of print]
- Giorgi, S., Perelló Ferrua, C., do Amaral, C. C., Fernandez Garcia, T., de Souza, K. B., and Nedel, F. (2020). microRNAs expressed in neuronal differentiation and their associated pathways: systematic review and bioinformatics analysis. *Brain Res. Bull.* 157, 140–148.
- Gong, J., and Sun, D. (2020). Study on the mechanism of curcumin to reduce the inflammatory response of temporal lobe in Alzheimer's disease by regulating miRNA-146a. *Minerva Med.* doi: 10.23736/S0026-4806.20.06463-0
- Groot, M., and Lee, H. (2020). Sorting Mechanisms for MicroRNAs into Extracellular Vesicles, and Their Associated Diseases. *Cells* 9:1044. doi: 10.3390/cells9041044
- Guerreiro, R. J., Gustafson, D. R., and Hardy, J. (2012). The genetic architecture of Alzheimer's disease: beyond APP, PSENs and APOE. *Neurobiol. Aging* 33, 437–456. doi: 10.1016/j.neurobiolaging.2010.03.025

- Guest, F. L., Rahmoune, H., and Guest, P. C. (2020). Early diagnosis and targeted treatment strategy for improved therapeutic outcomes in Alzheimer's disease. *Adv. Exp. Med. Biol.* 1260, 175–191. doi: 10.1007/978-3-030-426675_8
- Gurland, B. J., Wilder, D. E., Chen, J., Lantigua, R., Mayeux, R., and Van Nostrand, J. (1995). A flexible system of detection for Alzheimer's disease and related dementias. *Aging* 7, 165–172. doi: 10.1007/BF03324308
- Habes, M., Grothe, M. J., Tunc, B., McMillan, C., Wolk, D. A., and Davatzikos, C. (2020). Disentangling heterogeneity in Alzheimer's disease and related dementias using data-driven methods. *Biol. Psychiatry* 88, 70–82. doi: 10.1016/j.biopsych.2020.01.016
- Hampel, H., Caraci, F., Cuello, A. C., Caruso, G., Nisticò, R., Corbo, M., et al. (2020a). A path toward precision medicine for neuroinflammatory mechanisms in Alzheimer's disease. *Front. Immunol.* 11:456. doi: 10.3389/fimmu.2020.00456
- Hampel, H., Vergallo, A., Caraci, F., Cuello, A. C., Lemercier, P., Vellas, B., et al. (2020b). Alzheimer Precision Medicine Initiative (APMI). Future avenues for Alzheimer's disease detection and therapy: liquid biopsy, intracellular signaling modulation, systems pharmacology drug discovery. *Neuropharmacology* 2020:108081. doi: 10.1016/j.neuropharm.2020.108081
- Hampel, H., and Lista, S. (2013). Use of biomarkers and imaging to assess pathophysiology, mechanisms of action and target engagement. *J. Nutr. Health Aging* 17, 54–63. doi: 10.1007/s12603-013-0003-1
- Hampel, H., Lista, S., Teipel, S. J., Garaci, F., Nisticò, R., Blennow, K., et al. (2014). Perspective on future role of biological markers in clinical therapy trials of Alzheimer's disease: a long-range point of view beyond 2020. *Biochem. Pharmacol.* 88, 426–449. doi: 10.1016/j.bcp.2013.11.009
- Hampel, H., O'Bryant, S. E., Castrillo, J. I., Ritchie, C., Rojkova, K., Broich, K., et al. (2016). Precision Medicine - The golden gate for detection, treatment and prevention of Alzheimer's disease. *J. Prev. Alzheimers Dis.* 3, 243–259. doi: 10.14283/jpad.2016.112
- Hampel, H., O'Bryant, S. E., Durrleman, S., Younesi, E., Rojkova, K., Escott-Price, V., et al. (2017). A precision medicine initiative for Alzheimer's disease: the road ahead to biomarker-guided integrative disease modeling. *Climacteric* 20, 107–118. doi: 10.1080/13697137.2017.1287866
- Hampel, H., O'Bryant, S. E., Molinuevo, J. L., Zetterberg, H., Masters, C. L., Lista, S., et al. (2018a). Blood-based biomarkers for Alzheimer disease: mapping the road to the clinic. *Nat. Rev. Neurol.* 14, 639–652. doi: 10.1038/s41582-018-0079-7
- Hampel, H., Toschi, N., Babiloni, C., Baldacci, F., Black, K. L., Bokde, A. L. W., et al. (2018b). Revolution of Alzheimer precision neurology. Passageway of systems biology and neurophysiology. *J. Alzheimers Dis.* 64, S47–S105. doi: 10.3233/JAD-179932
- Hampel, H., Vergallo, A., Aguilar, L. F., Benda, N., Broich, K., Cuello, A. C., et al. (2018c). Precision pharmacology for Alzheimer's disease. *Pharmacol. Res.* 130, 331–365. doi: 10.1016/j.phrs.2018.02.014
- Hampel, H., Vergallo, A., Perry, G., and Lista, S. (2019). Alzheimer precision medicine initiative (APMI). The Alzheimer precision medicine initiative. *J. Alzheimers Dis.* 68, 1–24. doi: 10.3233/JAD-181121
- Hampton, T. (2019). Studies further support transmissibility of Alzheimer disease-associated proteins. *JAMA* 321, 1243–1244. doi: 10.1001/jama.2019.2650.xx28
- Hill, A. F. (2019). Extracellular vesicles and neurodegenerative diseases. *J. Neurosci.* 39, 9269–9273. doi: 10.1523/JNEUROSCI.0147-18.2019
- Hill, J. M., Bhattacharjee, S., Pogue, A. I., and Lukiw, W. J. (2014a). The gastrointestinal tract microbiome and potential link to Alzheimer's disease. *Front. Neurol.* 5:43. doi: 10.3389/fneur.2014.00043
- Hill, J. M., Zhao, Y., Bhattacharjee, S., and Lukiw, W. J. (2014b). miRNAs and viroids utilize common strategies in genetic signal transfer. *Front. Mol. Neurosci.* 7:10. doi: 10.3389/fnmol.2014.00010
- Hill, J. M., and Lukiw, W. J. (2016). microRNA (miRNA)-mediated pathogenetic signaling in Alzheimer's disease (AD). *Neurochem. Res.* 41, 96–100. doi: 10.1007/s11064-015-1734-7
- Hoibert, O. (2008). Gene regulation by transcription factors and microRNAs. *Science* 319, 1785–1786. doi: 10.1126/science.1151651
- Holohan, K. N., Lahiri, D. K., Schneider, B. P., Foroud, T., and Saykin, A. J. (2013). Functional microRNAs in Alzheimer's disease and cancer: differential regulation of common mechanisms and pathways. *Front. Genet.* 3:323. doi: 10.3389/fgenet.2012.00323
- Hudon, C., Escudier, F., De Roy, J., Croteau, J., Cross, N., Dang-Vu, T. T., et al. (2020). Behavioral and psychological symptoms that predict cognitive decline or impairment in cognitively normal middle-aged or older adults: a meta-analysis. *Neuropsychol. Rev.* doi: 10.1007/s11065-020-09437-5 [Online ahead of print].
- Iqbal, U. H., Zeng, E., and Pasinetti, G. M. (2020). The use of antimicrobial and antiviral drugs in Alzheimer's Disease. *Int. J. Mol. Sci.* 21:E4920. doi: 10.3390/ijms21144920
- Ishibe, Y., Kusaoi, M., Murayama, G., Nemoto, T., Kon, T., Ogasawara, M., et al. (2018). Changes in the expression of circulating miRNAs in systemic lupus erythematosus patient blood plasma after passing through a plasma adsorption membrane. *Ther. Apher. Dial.* 22, 278–289. doi: 10.1111/1744-9987.12695
- Jaber, V., Zhao, Y., and Lukiw, W. J. (2017). Alterations in micro RNA-messenger RNA (miRNA-mRNA) coupled signaling networks in sporadic Alzheimer's disease (AD) hippocampal CA1. *J. Alzheimers. Dis. Parkinsonism* 7:312. doi: 10.4172/2161-0460.1000312
- Jaber, V. R., Zhao, Y., Sharfman, N. M., Li, W., and Lukiw, W. J. (2019). Addressing Alzheimer's disease (AD) neuropathology using anti-microRNA (AM) strategies. *Mol. Neurobiol.* 56, 8101–8108. doi: 10.1007/s12035-019-1632-0
- Jiang, T., Yu, J. T., Tian, Y., and Tan, L. (2013). Epidemiology and etiology of Alzheimer's disease: from genetic to non-genetic factors. *Curr. Alzheimer Res.* 10, 852–867. doi: 10.2174/15672050113109990155
- Jin, S. C., Carrasquillo, M. M., Benitez, B. A., Skorupa, T., Carrell, D., and Patel, D. (2015). TREM2 is associated with increased risk for Alzheimer's disease in African Americans. *Mol. Neurodegener.* 10, 19–26.
- Jużwik, C. A., Drake, S., Zhang, Y., Paradis-Isler, N., Sylvester, A., Amar-Zifkin, A., et al. (2019). microRNA dysregulation in neurodegenerative diseases: a systematic review. *Prog. Neurobiol.* 182:101664. doi: 10.1016/j.pneurobio.2019.101664
- Khoury, R., and Grossberg, G. T. (2020). Deciphering Alzheimer's disease: predicting new therapeutic strategies via improved understanding of biology and pathogenesis [published online ahead of print, 2020 Jun 30]. *Expert. Opin. Ther. Targets* 2020:1790530. doi: 10.1080/14728222.2020.1790530
- Kim, D. H., Yeo, S. H., Park, J. M., Choi, J. Y., Lee, T. H., Park, S. Y., et al. (2014). Genetic markers for diagnosis and pathogenesis of Alzheimer's disease. *Gene* 545, 185–193.
- Kleaveland, B., Shi, C. Y., Stefano, J., and Bartel, D. P. (2018). A network of noncoding regulatory RNAs acts in the mammalian brain. *Cell* 174, 350–362.e17. doi: 10.1016/j.cell.2018.05.022
- Kondo, M. A., Mohan, A., and Mather, K. A. (2020). Going around in circles: deciphering the role of circular RNAs in neurodegenerative disease. *Curr. Opin. Psychiatry* 33, 141–147. doi: 10.1097/ycp.0000000000000582
- Konolova, J., Gerasymchuk, D., Parkkinen, I., Chmielarz, P., and Domanskyi, A. (2019). Interplay between microRNAs and oxidative stress in neurodegenerative diseases. *Int. J. Mol. Sci.* 20:E6055. doi: 10.3390/ijms20236055
- Kou, X., Chen, D., and Chen, N. (2020). The regulation of microRNAs in Alzheimer's disease. *Front. Neurol.* 11:288. doi: 10.3389/fneur.2020.00288
- Krammes, L., Hart, M., Rheinheimer, S., Diener, C., Menegatti, J., Grässer, F., et al. (2020). Induction of the endoplasmic-reticulum-stress response: microRNA34a targeting of the IRE1 α -branch. *Cells* 9:E1442. doi: 10.3390/cells9061442
- Kumar, S., Reddy, A. P., Yin, X., and Reddy, P. H. (2019). Novel MicroRNA-455-3p and its protective effects against abnormal APP processing and amyloid beta toxicity in Alzheimer's disease. *Biochim. Biophys. Acta Mol. Basis Dis.* 1865, 2428–2440. doi: 10.1016/j.bbdis.2019.06.006
- Kumar, S., and Reddy, P. H. (2019). A new discovery of microRNA-455-3p in Alzheimer's disease. *J. Alzheimers. Dis.* 72, S117–S130. doi: 10.3233/JAD-190583
- Kumar, S., and Reddy, P. H. (2020). The role of synaptic microRNAs in Alzheimer's disease. *Biochim. Biophys. Acta Mol. Basis Dis.* 2020:165937. doi: 10.1016/j.bbdis.2020.165937
- Lemcke, H., and David, R. (2018). Potential mechanisms of microRNA mobility. *Traffic* 19, 910–917. doi: 10.1111/tra.12606
- Lewczuk, P., Łukaszewicz-Zajac, M., Mroczko, P., and Kornhuber, J. (2020). Clinical significance of fluid biomarkers in Alzheimer's disease. *Pharmacol. Rep.* 72, 528–542. doi: 10.1007/s43440-020-00107-0
- Li, J. Q., Tan, L., Wang, H. F., Tan, M. S., Tan, L., Xu, W., et al. (2015). Risk factors for predicting progression from mild cognitive impairment to Alzheimer's disease: a systematic review and meta-analysis of cohort studies.

- J. *Neurol. Neurosurg. Psychiatry* 87, 476–484. doi: 10.1136/jnnp-2014-310095
- Lista, S., Khachaturian, Z. S., Rujescu, D., Garaci, F., Dubois, B., and Hampel, H. (2016). Application of systems theory in longitudinal studies on the origin and progression of Alzheimer's disease. *Methods Mol. Biol.* 1303, 49–67. doi: 10.1007/978-1-4939-2627-5_2
- Liu, Z., Skamagki, M., Kim, K., and Zhao, R. (2015). Canonical microRNA activity facilitates but may be dispensable for transcription factor-mediated reprogramming. *Stem Cell Reports* 5, 1119–1127. doi: 10.1016/j.stemcr.2015.11.002
- Lukiw, W. J. (2007). Micro-RNA speciation in fetal, adult and Alzheimer's disease hippocampus. *Neuroreport* 18, 297–300. doi: 10.1097/wnr.0b013e3280148e8b
- Lukiw, W. J. (2013a). Circular RNA (circRNA) in Alzheimer's disease (AD). *Front. Genet.* 4:307. doi: 10.3389/fgene.2013.00307
- Lukiw, W. J. (2013b). Variability in micro RNA (miRNA) abundance, speciation and complexity amongst different human populations and potential relevance to Alzheimer's disease (AD). *Front. Cell Neurosci.* 7:133. doi: 10.3389/fncel.2013.00133
- Lukiw, W. J. (2020a). Gastrointestinal (GI) tract microbiome-derived neurotoxins-potent neuro-inflammatory signals from the GI tract via the systemic circulation into the brain. *Front. Cell Infect. Microbiol.* 10:22. doi: 10.3389/fcimb.2020.00022
- Lukiw, W. J. (2020b). microRNA-146a signaling in Alzheimer's disease (AD) and prion disease (PrD). *Front. Neurol.* 11:462. doi: 10.3389/fneur.2020.00462
- Lukiw, W. J., and Alexandrov, P. N. (2012). Regulation of complement factor H (CFH) by multiple miRNAs in Alzheimer's disease (AD) brain. *Mol. Neurobiol.* 46, 11–19. doi: 10.1007/s12035-012-8234-4
- Lukiw, W. J., Alexandrov, P. N., Zhao, Y., Hill, J. M., and Bhattacharjee, S. (2012). Spreading of Alzheimer's disease inflammatory signaling through soluble micro-RNA. *Neuroreport* 23, 621–626. doi: 10.1097/00001756-201207110-00009
- Lukiw, W. J., Handley, P., Wong, L., Crapper, and McLachlan, D. R. (1992). BC200 RNA in normal human neocortex, non-Alzheimer dementia, and senile dementia of the Alzheimer type (AD). *Neurochem. Res.* 17, 591–597. doi: 10.1007/bf00968788
- Lukiw, W. J., and Pogue, A. I. (2020). Vesicular transport of encapsulated microRNA between glial and neuronal cells. *Int. J. Mol. Sci.* 21:5078. doi: 10.3390/ijms21145078
- Ma, F., Zhang, X., and Yin, K. J. (2020). microRNAs in central nervous system diseases: a prospective role in regulating blood-brain barrier integrity. *Exp. Neurol.* 323:113094. doi: 10.1016/j.expneurol.2019.113094
- McGeary, S. E., Lin, K. S., Shi, C. Y., Pham, T. M., Bisaria, N., Kelly, G. M., et al. (2019). The biochemical basis of microRNA targeting efficacy. *Science* 366:eaav1741. doi: 10.1126/science.aav1741
- McGurran, H., Glenn, J., Madero, E., and Bott, N. (2020). Risk reduction and prevention of Alzheimer's disease: biological mechanisms of diet. *Curr. Alzheimer Res.* 17, 407–427. doi: 10.2174/1567205017666200624200651
- Moradifard, S., Hoseinbeyki, M., Ganji, S. M., and Minucheher, Z. (2018). Analysis of microRNA and gene expression profiles in Alzheimer's disease: a meta-analysis approach. *Sci. Rep.* 8:4767. doi: 10.1038/s41598-018-20959-0
- Morris, J. C. (1997). Clinical dementia rating: a reliable and valid diagnostic and staging measure for dementia of the Alzheimer type. *Int. Psychogeriatr.* 9, 173–176. doi: 10.1017/s1041610297004870
- Mullane, K., and Williams, M. (2018). Alzheimer's disease (AD) therapeutics: repeated clinical failures continue to question the amyloid hypothesis of AD and the current understanding of AD causality. *Biochem. Pharmacol.* 158, 359–375. doi: 10.1016/j.bcp.2018.09.026
- Patnode, C. D., Perdue, L. A., Rossom, R. C., Rushkin, M. C., Redmond, N., Thomas, R. G., et al. (2020). *Screening for Cognitive Impairment in Older Adults [An Evidence Update for the US Preventive Services Task Force]*. Rockville, MD: Agency for Healthcare Research and Quality (US).
- Pauling, L. (1976). *Vitamin C and the Common Cold*, ed. W. H. Freeman (San Francisco CA: WH Freeman Press).
- Pawlica, P., Sheu-Gruttadauria, J., MacRae, I. J., and Steitz, J. A. (2020). How complementary targets expose the microRNA 3' end for tailing and trimming during target-directed microRNA degradation. *Cold Spring Harb. Symp. Quant. Biol.* 2019:039321. doi: 10.1101/sqb.2019.84.039321
- Peña-Bautista, C., Baquero, M., Vento, M., and Cháfer-Pericás, C. (2019). Omics-based biomarkers for the early Alzheimer disease diagnosis and reliable therapeutic targets development. *Curr. Neuropharmacol.* 17:630647. doi: 10.2174/1570159X16666180926123722
- Penner, G., Lecocq, S., Chopin, A., Vedoya, X., Lista, S., Vergallo, A., et al. (2019). Blood-based diagnostics of Alzheimer's disease. *Expert Rev. Mol. Diagn.* 19, 613–621. doi: 10.1080/14737159.2019.1626719
- Pogue, A. I., Hill, J. M., and Lukiw, W. J. (2014). microRNA (miRNA): sequence and stability, viroid-like properties, and disease association in the CNS. *Brain Res.* 1584, 73–79. doi: 10.1016/j.brainres.2014.03.042
- Pogue, A. I., and Lukiw, W. J. (2018). Up-regulated Pro-inflammatory microRNAs (miRNAs) in Alzheimer's disease (AD) and age-related macular degeneration (AMD). *Cell Mol. Neurobiol.* 38, 1021–1031. doi: 10.1007/s10571017-0572-3
- Praticò, D. (2013). Alzheimer's disease and the quest for its biological measures. *J. Alzheimers. Dis.* 33, S237–S241. doi: 10.3233/JAD-2012-129023
- Rahman, M. A., Rahman, M. S., Uddin, M. J., Mamun-Or-Rashid, A. N. M., Pang, M. G., and Rhim, H. (2020). Emerging risk of environmental factors: insight mechanisms of Alzheimer's diseases. *Environ. Sci. Pollut. Res. Int.* doi: 10.1007/s11356-020-08243-z [Online ahead of print]
- Ricciarelli, R., and Fedele, E. (2017). The amyloid cascade hypothesis in Alzheimer's disease: it's time to change our mind. *Curr. Neuropharmacol.* 15, 926–935. doi: 10.2174/1570159X15666170116143743
- Rodriguez, F. S., and Lachmann, T. (2020). Systematic review on the impact of intelligence on cognitive decline, and dementia risk. *Front. Psychiatry* 11:658. doi: 10.3389/fpsyt.2020.00658
- Roshan, R., Ghosh, T., Scaria, V., and Pillai, B. (2009). MicroRNAs: novel therapeutic targets in neurodegenerative diseases. *Drug Discov. Today* 14, 1123–1129. doi: 10.1016/j.drudis.2009.09.009
- Rossini, P. M., Di Iorio, R., Vecchio, F., Anfossi, M., Babiloni, C., Bozzali, M., et al. (2020). Early diagnosis of Alzheimer's disease: the role of biomarkers including advanced EEG signal analysis. *Clin. Neurophysiol.* 131, 1287–1310. doi: 10.1016/j.clinph.2020.03.003
- Rüegger, S., and Großhans, H. (2012). MicroRNA turnover: when, how, and why. *Trends Biochem. Sci.* 37:43646. doi: 10.1016/j.tibs.2012.07.002
- Serpente, M., Fenoglio, C., D'Anca, M., Arcaro, M., Sorrentino, S., Visconte, C., et al. (2020). MiRNA profiling in plasma neural-derived small extracellular vesicles from patients with Alzheimer's disease. *Cells* 9:E1443. doi: 10.3390/cells9061443
- Sethi, P., and Lukiw, W. J. (2009). Micro-RNA abundance and stability in human brain: specific alterations in Alzheimer's disease temporal lobe neocortex. *Neurosci. Lett.* 459, 100–104. doi: 10.1016/j.neulet.2009.04.052
- Sherva, R., Tripodis, Y., Bennett, D. A., Chibnik, L. B., Crane, P. K., de Jager, P. L., et al. (2014). GENAROAD Consortium: Alzheimer's disease neuroimaging initiative; Alzheimer's disease genetics consortium. Genome-wide association study of the rate of cognitive decline in Alzheimer's disease. *Alzheimers Dement.* 10, 45–52. doi: 10.1016/j.jalz.2013.01.008
- Shetty, A. K., and Zanirati, G. (2020). The interstitial system of the brain in health and disease. *Aging Dis.* 11, 200–211. doi: 10.14336/AD.2020.0103
- Silvestro, S., Bramanti, P., and Mazzon, E. (2019). Role of miRNAs in Alzheimer's disease and possible fields of application. *Int. J. Mol. Sci.* 20:E3979. doi: 10.3390/ijms20163979
- Sims, R., Hill, M., and Williams, J. (2020). The multiplex model of the genetics of Alzheimer's disease. *Nat. Neurosci.* 23, 311–322. doi: 10.1038/s41593-020-0599-5
- Singh, T., and Yadav, S. (2020). Role of microRNAs in neurodegeneration induced by environmental neurotoxins and aging. *Ageing Res. Rev.* 60:101068. doi: 10.1016/j.arr.2020.101068
- Stanciu, G. D., Bild, V., Ababei, D. C., Rusu, R. N., Cobzaru, A., Padurar, L., et al. (2020). Link between diabetes and Alzheimer's disease due to the shared amyloid aggregation and deposition involving both neurodegenerative changes and neurovascular damages. *J. Clin. Med.* 9:E1713. doi: 10.3390/jcm9061713
- Swarbrick, S., Wrang, N., Ghosh, S., and Stolz, A. (2019). Systematic review of miRNA as biomarkers in Alzheimer's disease. *Mol. Neurobiol.* 56, 6156–6167. doi: 10.1007/s12035-019-1500-y
- Tetreault, A. M., Phan, T., Orlando, D., Lyu, I., Kang, H., Landman, B., et al. (2020). Alzheimer's disease neuroimaging initiative. network localization of clinical, cognitive, and neuropsychiatric symptoms in alzheimer's disease. *Brain* 143, 1249–1260. doi: 10.1093/brain/awaa058

- Tudek, A., Schmid, M., and Jensen, T. H. (2019). Escaping nuclear decay: the significance of mRNA export for gene expression. *Curr. Genet.* 65, 473–476. doi: 10.1007/s00294-018-0913-x
- Turner, R. S., Stubbs, T., Davies, D. A., and Albeni, B. C. (2020). Potential new approaches for diagnosis of Alzheimer's disease and related dementias. *Front. Neurol.* 11:496. doi: 10.3389/fneur.2020.00496
- Upadhyay, R., Zingg, W., Shetty, S., and Shetty, A. K. (2020). Astrocyte-derived extracellular vesicles: neuroreparative properties and role in the pathogenesis of neurodegenerative disorders. *J. Control. Release* 323, 225–239. doi: 10.1016/j.jconrel.2020.04.017
- van den Berg, M. M. J., Krauskopf, J., Ramaekers, J. G., Kleinjans, J. C. S., Prickaerts, J., and Briedé, J. J. (2020). Circulating microRNAs as potential biomarkers for psychiatric and neurodegenerative disorders. *Prog. Neurobiol.* 185:101732. doi: 10.1016/j.pneurobio.2019.101732
- Van Meter, E. N., Onyango, J. A., and Teske, K. A. (2020). A review of currently identified small molecule modulators of microRNA function. *Eur. J. Med. Chem.* 188:112008. doi: 10.1016/j.ejmech.2019.112008
- Vanherle, S., Haidar, M., Irobi, J., Bogie, J. F. J., and Hendriks, J. J. A. (2020). Extracellular vesicle-associated lipids in central nervous system disorders. *Adv. Drug Deliv. Rev.* doi: 10.1016/j.addr.2020.04.011 [Epub ahead of print].
- Veitch, D. P., Weiner, M. W., Aisen, P. S., Beckett, L. A., Cairns, N. J., Green, R. C., et al. (2019). Alzheimer's Disease Neuroimaging Initiative. Understanding disease progression and improving Alzheimer's disease clinical trials: recent highlights from the Alzheimer's Disease Neuroimaging Initiative. *Alzheimers Dement.* 15:106152. doi: 10.1016/j.jalz.2018.08.005
- Verhulsdonk, S., Hellen, F., Höft, B., Supprian, T., and Lange-Asschenfeldt, C. (2015). Attention and CERAD test performances in cognitively impaired elderly subjects. *Acta Neurol. Scand.* 131, 364–371. doi: 10.1111/ane.12346
- Vickers, K. C., Palmisano, B. T., Shoucri, B. M., Shamburek, R. D., and Remaley, A. T. (2011). microRNAs are transported in plasma and delivered to recipient cells by high-density lipoproteins. *Nat. Cell Biol.* 13, 423–433. doi: 10.1038/ncb2210
- von Arnim, C. A. F., Bartsch, T., Jacobs, A. H., Holbrook, J., Bergmann, P., Zieschang, T., et al. (2019). Diagnosis and treatment of cognitive impairment. *Z. Gerontol. Geriatr.* 52, 309–315. doi: 10.1007/s00391019-01560-0
- Wang, L., and Zhang, L. (2020). Circulating microRNAs as diagnostic biomarkers for motor neuron disease. *Front. Neurosci.* 14:354. doi: 10.3389/fnins.2020.00354
- Wang, W. X., Fardo, D. W., Jicha, G. A., and Nelson, P. T. (2017). A customized quantitative PCR microRNA panel provides a technically robust context for studying neurodegenerative disease biomarkers and indicates a high correlation between cerebrospinal fluid and choroid plexus microRNA expression. *Mol. Neurobiol.* 54, 8191–8202. doi: 10.1007/s12035-016-0316-2
- Wang, Z., Shen, L., Wang, Y., and Huang, S. (2020). Integrated analysis of miRNA and mRNA expression in the blood of patients with Alzheimer's disease. *Mol. Med. Rep.* 22, 1053–1062. doi: 10.3892/mmr.2020.11162
- Wang, Z., Wang, J., Zhang, H., Mchugh, R., Sun, X., Li, K., et al. (2015). Interhemispheric functional and structural disconnection in Alzheimer's disease: a combined resting-state fMRI and DTI Study. *PLoS One* 10:e0126310. doi: 10.1371/journal.pone.0126310
- Weller, R. O. (2020). How well does the CSF inform upon pathology in the brain in Creutzfeldt-Jakob and Alzheimer's diseases? *J. Pathol.* 194:1. doi: 10.1002/1096-9896(200105)194:1<1::aid-path871>3.0.co;2-m
- Williams, O. A., An, Y., Armstrong, N. M., Kitner-Triolo, M., Ferrucci, L., and Resnick, S. M. (2020). Profiles of cognitive change in preclinical and prodromal Alzheimer's disease using change-point analysis. *J. Alzheimers Dis.* 75, 1169–1180. doi: 10.3233/JAD-191268
- Wu, Y. Y., and Kuo, H. C. (2020). Functional roles and networks of non-coding RNAs in the pathogenesis of neurodegenerative diseases. *J. Biomed. Sci.* 7:49. doi: 10.1186/s12929-020-00636-z
- Xie, L., Mao, M., Xiong, K., and Jiang, B. (2017). Circular RNAs: a novel player in development and disease of the central nervous system. *Front. Cell Neurosci.* 11:354. doi: 10.3389/fncel.2017.00354
- Yanagida, K., Tagami, S., and Okochi, M. (2017). Cerebrospinal fluid and blood biomarkers in Alzheimer's disease. *Brain Nerve.* 69, 825–833. doi: 10.11477/mf.1416200826
- Zamani, P., Oskuee, R. K., Atkin, S. L., Navashenaq, J. G., and Sahebkar, A. (2020). MicroRNAs as important regulators of the NLRP3 inflammasome. *Prog. Biophys. Mol. Biol.* 150, 50–61. doi: 10.1016/j.pbiomolbio.2019.05.004
- Zang, J., Lu, D., and Xu, A. (2020). The interaction of circRNAs, and RNA binding proteins: an important part of circRNA maintenance, and function. *J. Neurosci. Res.* 98, 87–97. doi: 10.1002/jnr.24356
- Zernecke, A., Bidzhikov, K., Noels, H., Shagdarsuren, E., Gan, L., Denecke, B., et al. (2009). Delivery of microRNA-126 by apoptotic bodies induces CXCL12-dependent vascular protection. *Sci. Signal.* 2:ra81. doi: 10.1126/scisignal.2000610
- Zhao, Y., Alexandrov, P. N., Jaber, V., and Lukiw, W. J. (2016a). Deficiency in the ubiquitin conjugating enzyme UBE2A in Alzheimer's disease (AD) is linked to deficits in a natural circular miRNA-7 sponge (circRNA; ciRS-7). *Genes* 7:E116.
- Zhao, Y., Alexandrov, P. N., and Lukiw, W. J. (2016b). Anti-microRNAs as novel therapeutic agents in the clinical management of Alzheimer's disease. *Front. Neurosci.* 10:59. doi: 10.3389/fnins.2016.00059
- Zhao, Y., Bhattacharjee, S., Dua, P., Alexandrov, P. N., and Lukiw, W. J. (2015). microRNA-based biomarkers and the diagnosis of Alzheimer's disease. *Front. Neurol.* 6:162. doi: 10.3389/fneur.2015.00162
- Zhao, Y., Cong, L., and Lukiw, W. J. (2018). Plant and animal microRNAs (miRNAs) and their potential for inter-kingdom communication. *Cell Mol. Neurobiol.* 38, 133–140. doi: 10.1007/s10571-017-0547-4
- Zhou, C., Wu, Q., Wang, Z., Wang, Q., Liang, Y., and Liu, S. (2020). The effect of hormone replacement therapy on cognitive function in female patients with alzheimer's disease: a meta-analysis. *Am. J. Alzheimers Dis. Other Dement.* 35:1533317520938585. doi: 10.1177/1533317520938585
- Zhu, Y., Liu, H., Lu, X. L., Zhang, B., Weng, W., Yang, J., et al. (2019). Prevalence of dementia in the People's Republic of China from 1985 to 2015: a systematic review and meta-regression analysis. *BMC Public Health* 19:578. doi: 10.1186/s12889-019-6840-z

Conflict of Interest: The authors declare that the research was conducted in the absence of any commercial or financial relationships that could be construed as a potential conflict of interest.

Copyright © 2020 Zhao, Jaber, Alexandrov, Vergallo, Lista, Hampel and Lukiw. This is an open-access article distributed under the terms of the Creative Commons Attribution License (CC BY). The use, distribution or reproduction in other forums is permitted, provided the original author(s) and the copyright owner(s) are credited and that the original publication in this journal is cited, in accordance with accepted academic practice. No use, distribution or reproduction is permitted which does not comply with these terms.



Association of Odor Identification Ability With Amyloid- β and Tau Burden: A Systematic Review and Meta-Analysis

Lihui Tu^{1,2}, Xiaozhen Lv^{1,2}, Zili Fan^{1,2}, Ming Zhang^{1,2,3}, Huali Wang^{1,2*} and Xin Yu^{1,2*}

¹ Dementia Care and Research Center, Clinical Research Division, Peking University Institute of Mental Health (Sixth Hospital), Beijing, China, ² Beijing Dementia Key Lab, National Clinical Research Center for Mental Disorders, Key Laboratory of Mental Health, Ministry of Health Peking University, Beijing, China, ³ Department of Psychiatry, The Third Affiliated Hospital of Sun Yat-sen University, Guangzhou, China

OPEN ACCESS

Edited by:

Kin Ying Mok,
University College London,
United Kingdom

Reviewed by:

Andrea Vergallo,
Sorbonne Universités, France
Cristian Ripoli,
Catholic University of the Sacred
Heart, Italy

*Correspondence:

Huali Wang
huali_wang@bjmu.edu.cn
Xin Yu
yuxin@bjmu.edu.cn

Specialty section:

This article was submitted to
Neurodegeneration,
a section of the journal
Frontiers in Neuroscience

Received: 23 July 2020

Accepted: 27 October 2020

Published: 26 November 2020

Citation:

Tu L, Lv X, Fan Z, Zhang M, Wang H
and Yu X (2020) Association of Odor
Identification Ability With Amyloid- β
and Tau Burden: A Systematic Review
and Meta-Analysis.
Front. Neurosci. 14:586330.
doi: 10.3389/fnins.2020.586330

Background: The associations between olfactory identification (OI) ability and the Alzheimer's disease biomarkers were not clear.

Objective: This meta-analysis aimed to examine the associations between OI and A β and tau burden.

Methods: Electronic databases (PubMed, Embase, PsycINFO, and Google Scholar) were searched until June 2019 to identify studies that reported correlation coefficients or regression coefficients between OI and A β or tau levels measured by positron emission tomography (PET) or cerebrospinal fluid (CSF). Pooled Pearson correlation coefficients were computed for the PET imaging and CSF biomarkers, with subgroup analysis for subjects classified into different groups.

Results: Nine studies met the inclusion criteria. Of these, five studies ($N = 494$) involved A β PET, one involved tau PET ($N = 26$), and four involved CSF A β or tau ($N = 345$). OI was negatively associated with A β PET in the mixed ($r = -0.25$, $P = 0.008$) and cognitively normal groups ($r = -0.15$, $P = 0.004$) but not in the mild cognitive impairment group. A similar association with CSF total tau in the mixed group was also observed. No association was found between OI and CSF phosphorylated tau or A β_{42} in the subgroup analysis of the CSF biomarkers. Due to a lack of data, no pooled r value could be computed for the association between the OI and tau PET.

Conclusion: The associations between OI ability and A β and CSF tau burden in older adults are negligible. While current evidence does not support the association, further studies using PET tau imaging are warranted.

Keywords: olfaction, Alzheimer's disease, amyloid- β , tau, positron emission tomography, cerebrospinal fluid

INTRODUCTION

Amyloid- β (A β) aggregates and tau neurofibrillary tangles are known as the two neuropathological hallmarks of Alzheimer's disease (AD) (Villemagne et al., 2018). The importance of the two biomarkers, whether for clinical or research use, is obvious in the biologically oriented effort to tackle the worldwide AD issue (Jansen et al., 2015; Alzheimer's Association, 2020). This is especially true when the National Institute on Aging and Alzheimer's Association (NIA-AA) proposed the A β /tau/neurodegeneration (AT(N)) classification system to update the diagnostic criteria for AD recommended in 2011 (Jack et al., 2018). This biomarker-driven research framework has shown potential to improve the predictive accuracy for memory decline among non-demented elderly individuals and thereby provide prognostic values for clinical change and progression (Jack et al., 2019; Yu et al., 2019).

In the evolving biomarker research field of AD, olfactory function has been frequently seen in studies related to neurodegenerative diseases (Marin et al., 2018; Dintica et al., 2019; Tu et al., 2020) since its first association with dementia was claimed in 1974 (Waldton, 1974). Impaired olfaction, olfactory identification (OI) ability in particular, has been reported in AD and prodromal AD ailments, such as mild cognitive impairment (MCI) (Roalf et al., 2017; Marin et al., 2018; Jung et al., 2019). Moreover, several lines of evidence have indicated that OI impairment is valuable in predicting cognitive decline in cognitively intact participants and progression from MCI to AD dementia, and it might suggest neurodegeneration in the brain among non-demented older adults (Devanand et al., 2015; Roberts et al., 2016; Dintica et al., 2019). OI, the ability to identify and name specific odorants, is therefore considered a potential early biomarker of cognitive decline and AD dementia.

Due to the well-known disadvantages of current standard measures of AD biomarkers, namely, their expensive cost and invasiveness, a convenient, inexpensive, and easily accessible test that predicts amyloid and tau status would therefore reduce the burden and cost of clinical AD trials. Studies have attempted to identify correlations of OI ability with amyloid and tau burden both *in vitro* and *in vivo*. Postmortem studies (Kovacs et al., 1999; Attems et al., 2005; Attems and Jellinger, 2006; Wilson et al., 2007, 2009; Franks et al., 2015) have linked OI ability with the pathologic manifestations of AD, A β , and neurofibrillary tangles. Studies involving *in vivo* positron emission tomography (PET) imaging scans or cerebrospinal fluid (CSF) measures also showed interesting results. But the results are inconsistent and inconclusive; the aim of this systematic review was therefore to provide a comprehensive overview of OI ability associated with the A β and tau burden in older adults.

METHODS

Selection Criteria

This systematic review was conducted according to the PRISMA guidelines (Moher et al., 2015) and followed a predetermined protocol (PROSPERO No. CRD42019138642). The selection criteria of the studies were as follows: (1) reported associations

between OI test scores and A β or tau levels (measured via PET imaging or CSF); (2) evaluated OI by common smell tests, such as the University of Pennsylvania Smell Identification Test (UPSIT), the "Sniffin' Sticks" OI test, and the Odor Stick Identification Test for Japanese (OSIT-J); (3) included older adults (mean age of sample ≥ 60 years); and (4) made data available in the publication or via contact with the authors to allow computation of correlation coefficients.

Search Strategy

Systematic electronic databases (PubMed, Embase, PsycINFO, and Google Scholar) were searched for articles published in English from their inception until June 2019 with the following search items: "olfaction" OR "smell" OR "odor" OR "olfactory" AND "amyloid" OR "tau" OR "cerebrospinal fluid" OR "positron emission tomography." Filters were applied to limit searches to human studies in the English language. The reference lists and similar articles of the eligible publications were searched manually for additional studies.

Amyloid and Tau Assessment

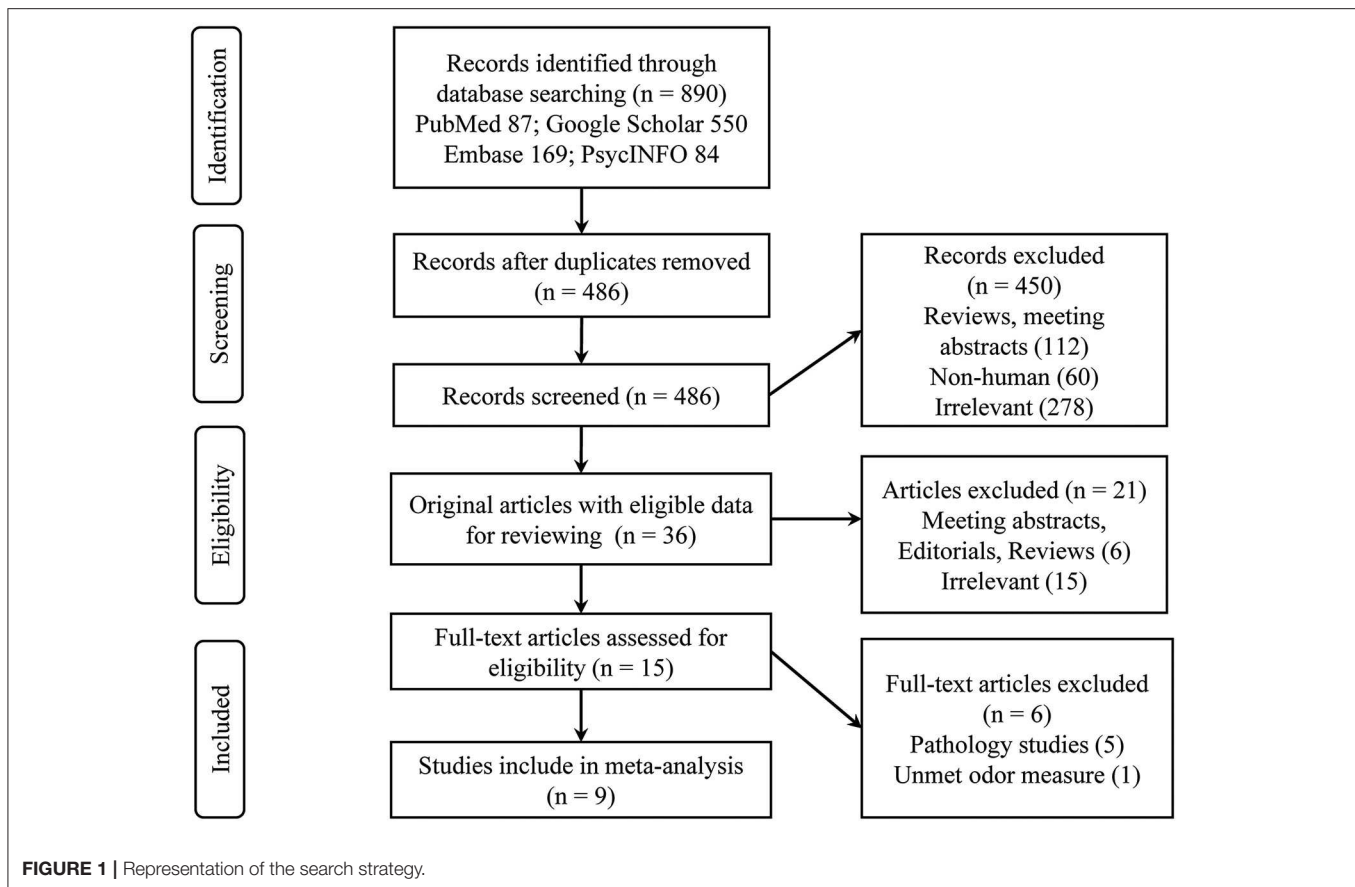
PET amyloid imaging agents included Pittsburgh Compound B (PIB), florbetapir, and florbetaben. PET tau imaging agents included tau-specific ligands, such as flortaucipir. Estimates of amyloid and tau binding in PET studies were used from the global cortex or cortical regions via standardized uptake value ratios (SUVs) or distribution volume ratios (DVRs). The CSF method included measurement of A β 1-42 (A β ₄₂), *p*-tau₁₈₁, and *t*-tau levels.

Odor Identification Test

OI was tested with the UPSIT, Sniffin' Sticks, OSIT-J, or other commercially available tests. The shorter versions of the UPSIT and Sniffin' Sticks test were also eligible. Homemade tests and tests that also assessed other olfactory functions (e.g., olfactory threshold or discrimination) were excluded.

Data Extraction and Study Quality Assessment

Data were independently extracted by two investigators (LT and XL) from cross-sectional cohort studies and baseline measurements of longitudinal studies with clinical follow-up. For the studies with different groups of subjects, i.e., cognitively normal (CN), MCI, AD, and mixed (whole sample) groups, the correlation coefficient values were extracted separately for the subgroup comparisons when data were available. The following information was extracted from each included study: the sample size, the study design, the country and cohort name, the methodology used to measure AD biomarkers, the odor tests, the sample demographic characteristics, and the bivariate correlations (or related statistical information) between the AD biomarkers and the OI score. The methodologic quality of each included study was assessed using the Quality Assessment of Diagnostic Accuracy Studies (QUADAS-2) tool (Whiting et al., 2011).



Effect Size Computation and Statistical Analysis

The cross-sectional associations between OI test scores and A β or tau levels were evaluated using Pearson correlation coefficients (r). A preadjusted r was used in all studies when available. In cases where r values were not reported, they were calculated from the scatter plot graph of the OI score vs. A β or tau levels. Two studies (Körtvélyessy et al., 2015; Risacher et al., 2017) reported a non-significant association between the OI score and A β or tau levels, but no data were available. In this case, $z = 0.00$ was assigned as a conservative estimate. The other three studies reported an unstandardized regression coefficient (b) (Growdon et al., 2015; Reijts et al., 2017; Vassilaki et al., 2017), with which we calculated r according to previous methods (Kim et al., 2019). Specifically, the following formulas were used:

$$(\text{Estimated } r)^2 = t^2 / (t^2 + n - 2)$$

$$t = b / \text{the standard error of } b$$

$$\text{Estimated } r \times b \geq 0.$$

We used the Comprehensive Meta-Analysis (CMA), version 3 software (Biostat, NJ) to compute the r values and calculate the pooled mean r values for the PET imaging and CSF biomarkers, with subgroup analysis for subjects classified into different groups. As random-effects models incorporate between-study heterogeneity and give wider (i.e., more conservative) confidence

intervals (CIs) when heterogeneity is suspected, all analyses and plots were reported using a random-effects model. The presence of publication bias with a funnel plot was not assessed because very few studies were included in our meta-analysis (Sterne et al., 2011). To examine between-study heterogeneity, in addition to Cochran's Q (to determine whether the between-study variability was greater than the sampling error) and τ (to quantify the between-study variance of the true effect sizes), the I^2 statistic was also used.

Post hoc subgroup analyses were conducted to determine the source of the heterogeneity when statistically significant heterogeneity was identified. The analyses examined the degree to which heterogeneity resulted from variance due to moderators such as (a) the type of OI test (e.g., UPSIT edition), (b) the PET imaging method (PIB or non-PIB) and the measurements (SUVR or DVR), (c) the code of the SUVR/DVR (continuous or categorical), (d) adjustments for covariates (e.g., age, sex) or lack thereof, (e) the sample size, and (f) the method r was obtained.

RESULTS

Description of Studies

A total of nine eligible studies were included in the final systematic review and meta-analysis (see **Figure 1** for flowchart),

with five studies pertaining to A β PET and four about CSF A β or tau. The characteristics of the included studies are shown in **Table 1**. The selected studies were published between 2010 and 2018. Seven studies were cross-sectional, and two were longitudinal. The median number of subjects per study was 93 (range, 22–215), with a total number of 839 (56% female) subjects. Three studies with a relatively large sample (over 100) focused on CN older adults, two of which utilized the PET imaging method (Growdon et al., 2015; Vassilaki et al., 2017). For the PET method, the included total sample sizes of CN, MCI, and AD individuals were 392, 75, and 20, respectively, with seven subjective cognitive decline (regarded as CN in our analysis) individuals. The sample sizes for the studies using the CSF method were 161, 63, and 95 individuals, respectively, with 26 non-AD dementia patients. The mean sample age was 71.8 years (SD = 6.8).

Demographic variables such as age, sex, and education were adjusted statistically in a few studies. The inclusion criteria for individuals with MCI were mostly according to Petersen's criteria, while for AD, it was the NINCDS-ADRDA criteria. The methodologic quality assessment showed that only the patient selection domain had the high risk of bias, mostly due to inappropriate exclusions (**Table 2**).

AD Biomarkers

Five studies applied A β PET imaging [four used ^{11}C PIB (Bahar-Fuchs et al., 2010; Growdon et al., 2015; Vassilaki et al., 2017; Kreisl et al., 2018); one used ^{18}F -florbetapir/florbetaben (Risacher et al., 2017)], and only one study utilized tau PET imaging [^{18}F -flortaucipir (Risacher et al., 2017)]. For the majority of studies, the PET SUVR was used as a continuous variable to explore the association between the A β burden and OI score. Four studies measured CSF levels, two of which examined A β_{42} , p -tau, and t -tau (Körtvélyessy et al., 2015; Lafaille-Magnan et al., 2017), whereas one study measured A β_{42} and p -tau (Kouzuki et al., 2018), and the other one measured A β_{42} and t -tau (Reijs et al., 2017).

Odor Identification Score

The OI score was obtained mostly (seven studies) from the UPSIT, with 40 odors used by four studies and a short edition (6–12 odors) used by three studies. The other two studies used either Sniffin' Sticks (Körtvélyessy et al., 2015) or the OSIT-J (Kouzuki et al., 2018). The raw OI scores were reported by all studies except one (Lafaille-Magnan et al., 2017), which used a transformed UPSIT error score. In this case, the raw score was calculated from the scatter plot graph. One study (Dhilla Albers et al., 2016) was excluded because a homemade olfactory screening with mixed evaluation was adopted.

Correlation Between the Odor Identification Score and PET Imaging

Meta-analyses were based on the correlation between the OI score and the PET SUVR or DVR. For two studies (Growdon et al., 2015; Vassilaki et al., 2017), the r values were calculated based on the regression coefficients. For correlations of subgroup subjects (CN, MCI, and AD), the r values were obtained via the

authors for one study (Kreisl et al., 2018) and calculated from the scatter plot graph for another study (Bahar-Fuchs et al., 2010). One study (Risacher et al., 2017) reported a non-significant association without available data, in which $z = 0.00$ was assigned accordingly. Our results showed that the OI score was negatively associated with A β PET SUVR or DVR in the mixed group ($r = -0.25$, 95% CI $[-0.42, -0.07]$, $P = 0.008$; **Figure 2**).

Subgroup analysis also showed a negative association in the CN group ($r = -0.15$, 95% CI $[-0.24, -0.05]$, $P = 0.004$). However, the MCI group showed no correlation ($r = -0.2$, 95% CI $[-0.72, 0.46]$, $P = 0.568$). Only one study had an AD group, which also showed no correlation. The combination of MCI and AD together did not change the result (data not shown). The association between the OI score and tau PET imaging was reported by one study (Risacher et al., 2017), showing that the tau level in the mean temporal lobe was negatively associated with the preadjusted UPSIT total score ($r = -0.45$, $P < 0.05$).

Correlation Between the Odor Identification Score and CSF Biomarkers

Meta-analyses were based on the correlation between the OI score and CSF biomarker levels. For two studies, the r values were calculated based on the regression coefficients (Reijs et al., 2017) or from the scatter plot graph (Lafaille-Magnan et al., 2017). One study (Körtvélyessy et al., 2015) reported a non-significant association without available data, in which $z = 0.00$ was assigned accordingly. MCI and AD were analyzed together given the limited data.

Our analysis showed that the OI score was negatively associated with CSF t -tau in the mixed group ($r = -0.17$, 95% CI $[-0.28, -0.05]$, $P = 0.006$; **Figure 3**). The same was true for CSF p -tau ($r = -0.14$, 95% CI $[-0.28, 0.001]$, $P = 0.052$) and A β_{42} ($r = 0.14$, 95% CI $[-0.01, 0.28]$, $P = 0.069$) in the mixed group but only with a marginal association. Subgroup analysis showed no association in the CN or MCI/AD group for CSF A β_{42} or t -tau (data not shown).

Moderator Effects

The present data showed a statistically significant heterogeneous between-study variability for the PET imaging method in the mix ($Q = 15.2$, $P < 0.01$, $\tau^2 = 0.033$, $I^2 = 73.68\%$) and MCI groups ($Q = 10.3$, $P < 0.01$, $\tau^2 = 0.267$, $I^2 = 80.64\%$). *Post hoc* subgroup analyses indicated that the pooled r values in the mixed group remained statistically significant when the moderator variables were adjusted (**Table 3**).

A significant negative correlation ($r = -0.55$, 95% CI $[-0.72, -0.32]$, $P < 0.001$) for the MCI group was observed when these accounted for data from studies that had utilized the 40-item UPSIT, although this only pertained to two studies. **Table 3** provides a summary of the meta-analysis by potential moderator variables of the association between the OI score and PET imaging.

DISCUSSION

This meta-analysis explored the relationships between OI ability and the cerebral measures of amyloid and tau deposition via

TABLE 1 | Characteristics of the included studies.

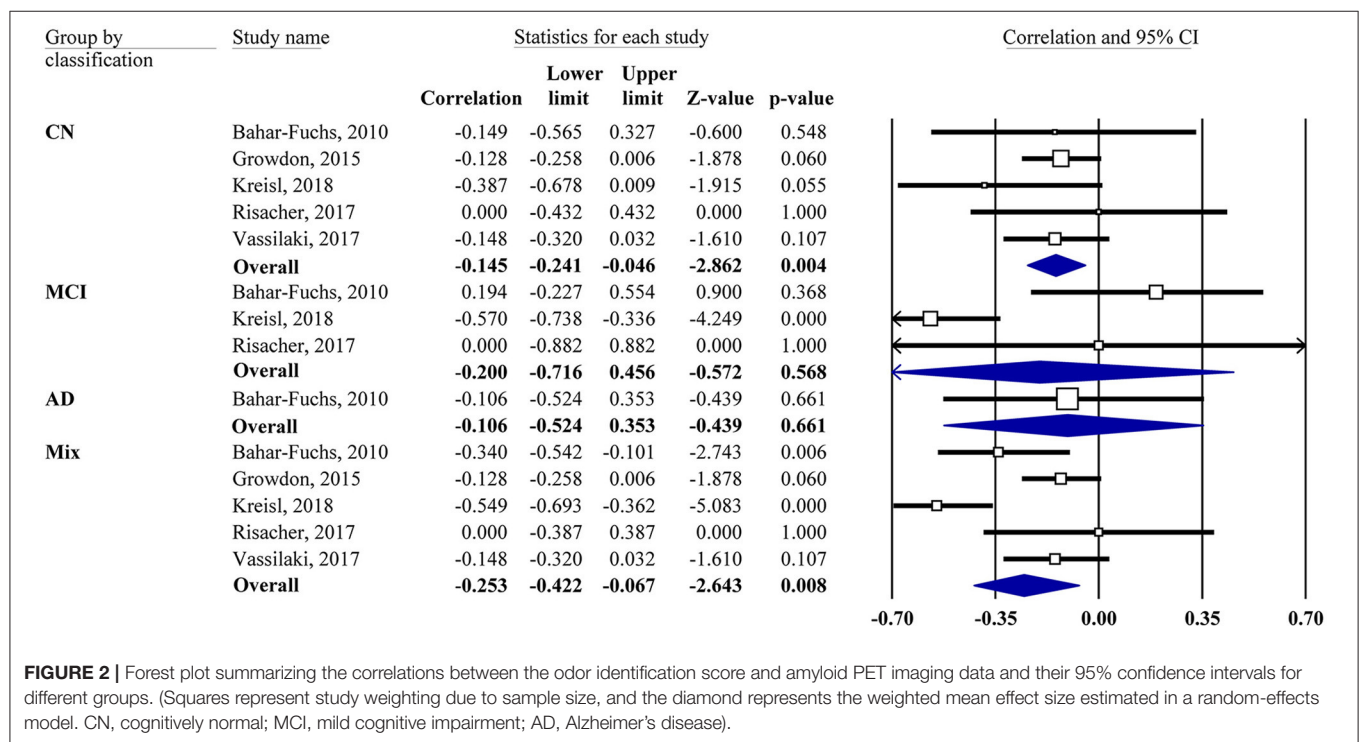
References	Design (follow-up)	Country	N	Cohort	Mean age [year (SD)]	Sex, female (%)	Olfactory test	AD biomarker	Classification	Statistical analysis
Bahar-Fuchs et al. (2010)	XS	Australia	63	Longitudinal PiB PET project at Austin Health	73.6 (8.2)	58.6	UPSIT (6-item)	PET: A β (11 C PiB)	CN, MCI, AD	Pearson correlation
Growdon et al. (2015)	XS	USA	215	Harvard Aging Brain Study	73.9 (5.9)	59.1	UPSIT	PET: A β (11 C PiB)	CN	Multiple linear regression
Kreisl et al. (2018)	LT (1 year)	USA	71	Longitudinal observational study of AD biomarkers	68.5 (7.6)	49.0	UPSIT	PET: A β (11 C PiB)	CN, MCI	Pearson correlation
Risacher et al. (2017)	XS	USA	26	Indiana Alzheimer Disease Center	70.4 (8.8)	63.4	UPSIT	PET: A β (18 F-florbetapir/florbetaben); Tau (18 F-flortaucipir)	CN, SCD, MCI	Pearson correlation
Vassilaki et al. (2017)	XS	USA	119	Mayo Clinic Study of Aging	79.2 (–)	48.5	UPSIT (12-item)	PET: A β (11 C PiB), 18 F-FDG-PET	CN	Multiple linear regression
Körtvélyessy et al. (2015)	XS	Germany	22	Memory Clinic, University of Magdeburg	72.7 (6.9)	66.7	Sniffin (12-item)	CSF: A β_{42} , <i>p</i> -tau, <i>t</i> -tau	AD	Pearson correlation
Kouzuki et al. (2018)	XS	Japan	71	Faculty of Medicine, Tottori University	78.3 (1.1)	43.8	OSIT-J	CSF: A β_{42} , <i>p</i> -tau	CN, MCI, AD	Pearson correlation
Lafaille-Magnan et al. (2017)	XS	Canada	100	The PREVENT-AD cohort	62 (6)	70.0	UPSIT	CSF: A β_{42} , <i>p</i> -tau, <i>t</i> -tau	CN	Multiple linear regression
Reijs et al. (2017)	LT (3 years)	Netherlands	152	The EDAR study	67.4 (9.5)	47.2	UPSIT (12-item)	CSF: A β_{42} , <i>t</i> -tau	CN, MCI, AD, non-AD dementia	Multiple linear regression

XS, cross sectional; LT, longitudinal; UPSIT, University of Pennsylvania Smell Identification Test; OSIT-J, Odor Stick Identification Test for Japanese; PET, positron emission tomography; 11 C PiB, 11 C-Pittsburgh compound B; A β , amyloid β ; CSF, cerebrospinal fluid; A β_{42} , amyloid- β_{42} ; *t*-tau, total tau; *p*-tau, phosphorylated tau; 18 F-FDG, 18 fluorodeoxyglucose; CN, cognitively normal; SCD, subjective cognitive decline; MCI, mild cognitive impairment; AD, Alzheimer's disease.

TABLE 2 | Risk of bias and applicability concern summary: review authors' judgements about each domain for included studies, individually.

Study	Risk of bias				Applicability concerns		
	Patient selection	Index test	Reference standard	Flow and timing	Patient selection	Index test	Reference standard
1. Bahar-Fuchs	😊	😊	😊	😊	😊	😊	😊
2. Growdon	😊	😊	😊	😊	😊	😊	😞
3. Kreisl	😊	😊	😊	😊	😊	😊	😊
4. Risacher	😊	😊	😊	😊	😊	😊	😊
5. Vassilaki	😊	😊	😊	😊	😞	😊	😞
6. Körtvélyessy	?	😊	😊	?	😊	😊	😊
7. Kouzuki	😞	😊	😊	😊	😞	😊	😊
8. Lafaille-Magnan	😞	😊	😊	😊	😞	😞	😊
9. Reijis	😊	😊	😊	😊	😞	😊	😊

😊, low risk; 😞, high risk; ?, unclear risk.



PET imaging or CSF evaluation. Our main finding was that A β (measured by PET) and t -tau (measured by CSF evaluation) depositions were only weakly associated with OI scores across a mixed population (CN, MCI, and AD) of older adults. A weak association was also observed in the CN group between the A β deposition (measured by PET) and OI score. As all the pooled absolute r values were <0.3 , the correlation could be considered negligible. There were no associations between the MCI and AD groups or between CSF A β_{42} and t -tau. In addition, no pooled r value could be computed for the association between the OI score

and tau PET due to the lack of data. These findings suggest that the associations between OI ability and A β and CSF tau burden in older adults are negligible. OI ability is believed to be linked with the pathologic manifestations of AD in postmortem studies (Kovacs et al., 1999; Attems et al., 2005; Attems and Jellinger, 2006; Wilson et al., 2007, 2009; Franks et al., 2015). Among the AD pathologic changes associated with OI, neurofibrillary tangles were particularly noted, especially in olfactory bulb (OB) (Kovacs et al., 1999; Attems et al., 2005; Attems and Jellinger, 2006) and central olfactory regions (entorhinal cortex and CA1/subiculum

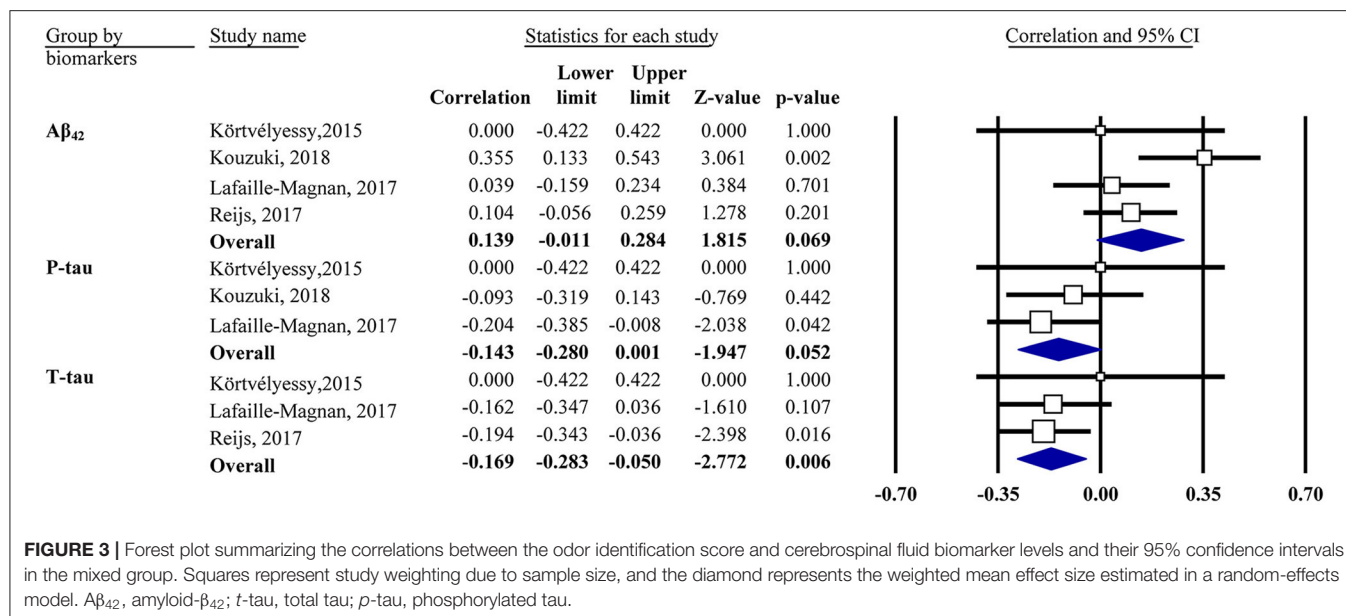


FIGURE 3 | Forest plot summarizing the correlations between the odor identification score and cerebrospinal fluid biomarker levels and their 95% confidence intervals in the mixed group. Squares represent study weighting due to sample size, and the diamond represents the weighted mean effect size estimated in a random-effects model. A β ₄₂, amyloid- β ₄₂; t-tau, total tau; p-tau, phosphorylated tau.

TABLE 3 | Pooled Pearson's *r* values and 95% confidence intervals (CIs) adjusted for moderator variables (for A β PET only).

Moderator variables		MCI		Mix	
		<i>r</i> [95% CI]	<i>f</i> ²	<i>r</i> [95% CI]	<i>f</i> ²
Odor test	UPSIT-L	-0.55 [-0.72, -0.32]***	0	-0.26 [-0.56, 0.1]	85
	UPSIT-S	Bahar-Fuchs et al. (2010)+		-0.23 [-0.4, -0.04]*	40
PET method	PIB	-0.24 [-0.79, 0.53]	90	-0.29 [-0.47, -0.09]**	79
	Non-PIB	Risacher et al. (2017)		Risacher et al. (2017)	
PET measure	SUVr	-0.2 [-0.72, 0.46]	81	-0.35 [-0.57, -0.09]*	79
	DVR	-		Growdon et al. (2015)	
Amyloid analysis	Continuous	-0.2 [-0.72, 0.46]	81	-0.35 [-0.59, -0.05]*	71
	Categorical	-		-0.14 [-0.24, -0.03]*	0
Sample size	>100	-	81	-0.14 [-0.24, -0.03]*	0
	<100	-0.2 [-0.72, 0.46]		-0.35 [-0.59, -0.05]*	71
Method of obtaining <i>r</i>	Reported	Kreisl et al. (2018)	0	-0.45 [-0.63, -0.23]***	54
	Estimated	0.18 [-0.23, 0.53]		-0.13 [-0.23, -0.02]*	0

The results for adjusted covariates equaled those of the odor test.

PET, positron emission tomography; UPSIT, University of Pennsylvania Smell Identification Test, -L = 40 items, -S = 6~12 items; PIB, Pittsburgh Compound B; SUVr, standardized uptake value ratio; DVR, distribution volume ratio; MCI, mild cognitive impairment.

"+" references.

P* < 0.05; *P* < 0.01; ****P* < 0.001.

area of the hippocampus) (Wilson et al., 2007). This was in line with the tau PET imaging study (Risacher et al., 2017) included in our analysis, which indicated a low negative correlation between the tau and OI score in the mean temporal lobe. Of note, this was in response to the idea endorsed by Kametani et al. suggesting that it is tau contributed to the development and progression of AD, not A β (Kametani and Hasegawa, 2018). Nevertheless, the meta-analysis of *in vivo* CSF t-tau, not p-tau, yielded only a very weak association, which was considered negligible. The inconsistency of the two findings might be explained by the following aspects: the histopathological study contained a relatively small sample size with advanced age and a

span of several years between olfactory testing and death. More importantly, *in vitro* neuropathological studies focused mainly on specific olfactory-related regions, while *in vivo* CSF studies could not take the same approach. However, the association with OI for the A β burden on autopsy appeared non-significant, which supported our meta-analysis findings, particularly the results regarding CSF A β , despite a low negative correlation that could be observed in the mixed group with moderator variables adjusted for the A β PET imaging.

The mixed group, in general, showed a negligible correlation between OI ability and the A β and CSF tau burden. However, the MCI and AD groups, both of which are associated with OI

impairment and inclined to be associated with A β or tau burden (Jansen et al., 2015; Roalf et al., 2017; Villemagne et al., 2018; Jung et al., 2019), showed no correlation between the two at all among the different biomarker classifications. The correlation was observed in the MCI group for A β PET when only the studies that applied the 40-item UPSIT were included, which was largely due to one study alone (Kreisl et al., 2018). Although part of the irrelevant finding may be related to the relatively small size of the sample within the included studies, especially for the AD group with A β PET imaging ($n = 20$), we speculate that OI ability is not specific to the underlying AD pathophysiology, especially A β . On the other hand, the CN group is usually characterized by intact OI ability and a lack of A β or tau burden, making the correlation between the two likely. In fact, Kreisl et al. (2018) attributed the correlation between OI ability and PIB SUVR largely to the subjects with high OI scores and low PIB binding in their study. Nevertheless, our results did not show any correlations in the CN group, with a negligible association for A β PET imaging. This result again suggests that OI ability is non-specific for the underlying A β burden.

The weak association between OI ability and the cerebral measures of amyloid and CSF tau levels might be explained by several possibilities. First, like the notion mentioned above, OI impairment may not be specific to AD. It is known that impaired OI is associated with normal aging, and some age-related changes in olfactory function may relate to factors irrelevant to AD pathophysiology (e.g., deterioration of the olfactory epithelium and ossification of the cribriform plate) (Doty et al., 1984; Doty and Kamath, 2014). In addition, many neuropsychiatric disorders, such as Parkinson's disease (Hoyles and Sharma, 2013), dementia with Lewy bodies (Mahlknecht et al., 2015), and schizophrenia (Kamath et al., 2019), are reported to be associated with OI impairment. In addition to AD pathologic alterations, alpha-synucleinopathy of Parkinson's disease and dementia with Lewy bodies in the cortical brain and olfactory-related regions are also observed and are supported by convincing evidence (Wilson et al., 2007; Arnold et al., 2010; Nag et al., 2019).

Second, the limitations of the A β burden itself and its current measures are worth noting. The A β burden is not conclusive in determining the risk of AD or cognitive impairment. The prevalence of incidental A β positivity increases with age, and approximately a quarter of CN elders are amyloid-positive on PET scans or CSF evaluations (Jansen et al., 2015); the so-called asymptomatic cerebral amyloidosis stage may make the correlation between cerebral amyloid and OI impairment fruitless because the latter occurs predominantly in MCI and AD but not CN (Jansen et al., 2015; Jung et al., 2019). It is also worth noting that A β burden reaches a plateau early in the disease process or even in the preclinical phase of the AD (Ingelsson et al., 2004; Serrano-Pozo et al., 2011); hence, it is not the most appropriate to correlate OI with A β in AD, especially in late stage. Furthermore, a more toxic soluble or oligomeric form of A β (Walsh et al., 2002; Shankar et al., 2008), which is considered critical in the AD pathological cascade but has not been measured in the included studies, may potentially correlate with OI ability more directly (Bahar-Fuchs et al., 2010).

Third, the same concept may apply to CSF *t*-tau and *p*-tau, which are often used to stage preclinical AD and are viewed as biomarkers of a "disease state," despite potentially correlating with OI ability (Mattsson et al., 2017; Lian et al., 2019). It was suggested that CSF P-tau levels might vary among AD and occur before measurable cognitive decline, which also makes the correlation difficult (Leuzy et al., 2019; Meyer et al., 2020). However, there are advantages to associating PET tau, viewed as a biomarker of a "disease stage," with dementia status and cognitive decline (Brier et al., 2016; Mattsson et al., 2017). Risacher et al. (2017) stated that tau deposition significantly correlated with OI ability, on the condition that A β was positive. This, to a certain extent, corresponds with the definition of AD under the AT(N) scheme (Jack et al., 2018), which requires that both A β and tau are positive. Therefore, correlating OI ability with PET tau will be promising and plausible, especially when focusing on A β -positive individuals.

Finally, the included PET studies focused mainly on composite gray matter from frontal, parietal, lateral temporal cortex, and other regions of interest (Growdon et al., 2015; Vassilaki et al., 2017; Kreisl et al., 2018) but olfactory structure, while an olfactory region-targeted evaluation approach may strengthen the exploratory association. A number of neuroimaging studies indicate the association between structural and functional degeneration of distinct brain regions and olfactory impairment, mainly to the hippocampus and the primary olfactory cortex (Thomann et al., 2009; Growdon et al., 2015; Vasavada et al., 2015, 2017; Risacher et al., 2017; Vassilaki et al., 2017; Wu et al., 2019). In addition, postmortem studies mentioned above (Kovacs et al., 1999; Attems et al., 2005; Attems and Jellinger, 2006; Wilson et al., 2007, 2009) also state that the association between AD pathologic changes and OI largely reflects in the OB. Thus, it might be wiser to adopt a strategic regional analysis, rather than averaging the biomarker levels for the whole brain. Nevertheless, PET has so far not provided sufficient resolution measuring A β and/or tau deposition in the OB in humans, as stated by Risacher et al. (2017).

Furthermore, the prion-like hypothesis in AD is also worth noting concerning the olfactory impairment. Like the prion detected in olfactory epithelium of sporadic Creutzfeldt-Jakob disease (Tabaton et al., 2004), A β and tau also appeared in olfactory structures in AD and healthy subjects, including olfactory epithelium and OB (Kovacs et al., 1999; Wilson et al., 2007; Arnold et al., 2010; Brozzetti et al., 2020), both are susceptible to protein and enzyme modifications involved in AD pathogenesis (Dibattista et al., 2020). It was hypothesized that pathological modifications lead to the activation of protein accumulation in the OB after environmental insults, and then induces the propagation of the disease within the brain in a prion-like fashion by a templating process (Rey et al., 2018). Thus, OB was considered the entry site for this prion-like spreading in AD. Here, A β was proposed as an initiator for AD pathogenesis, while prion-like propagation of tauopathy dominated the process and might even independent of A β (Walker, 2018). Taken together, we believe these underlying pathologic development starting from olfactory neurons may contribute to the OI impairment, as memory dysfunction in AD and/or MCI was not enough

to explain this deficit (Wilson et al., 2007; Reijs et al., 2017). Hence, the olfactory region-based association, again, between OI ability and A β , tau particularly is important. Recently, a non-invasive nasal brushing technique was used to collect the olfactory neuroepithelium (Brozzetti et al., 2020), from which neurodegeneration-associated proteins were detected, making correlating OI ability with A β and tau levels in peripheral olfactory system *in vivo* possible. This, certainly, may help clarify the relationship between the olfactory function and biomarkers of interest. A comprehensive search, a detailed subgroup analysis, and the appraisal of potential moderators for heterogeneity are the strengths of the study. In addition, active communication with the authors of the included studies and the comprehensive extraction of additional data provided our analysis with more power than the original publications offered.

However, several limitations of our study should also be noted. First, the available data did not allow us to correlate PET tau with OI ability or to identify associations within the AD group. In addition, other olfactory functions (olfactory threshold and discrimination) were not considered in this study. Thus, the inferences in the study cannot be extended to the above situation. Second, the sample sizes in general were modest but relatively small in the AD group and the CSF analysis, which reflects the limited amount of available data in the associated field and limits the power of detecting associations. Third, it was shown that the association was greater if the OI was defined by suggested cutoffs of abnormality, such as anosmia and normosmia (Vassilaki et al., 2017). Unfortunately, no such data could be obtained because only one study took the approach. Fourth, *t*-tau/A β ₄₂ or *p*-tau/A β ₄₂ might correlate with odor identification better than single CSF measures due to their improved ability for defining biomarker positivity, but the data was limited. Two studies reported *p*-tau/A β ₄₂, and the pooled results indicated a weak association ($r = -0.17$, $P = 0.03$). Fifth, it is advisable to take APOE $\epsilon 4$ allele into account when analyzing the associations between OI ability and amyloid- β and tau burden as the latter interacts with APOE $\epsilon 4$ allele. This has not been done as only a few studies adjusted APOE $\epsilon 4$ allele. Finally, the comprehensive data extraction was a double-edged sword, as it may have yielded results that deviate from the original results due to the recalculation and estimation of the data.

Future studies using PET tau imaging with larger sample sizes may help further clarify this issue. Concerning other olfactory functions, a recently published study (Lian et al., 2019) investigated the relationship between the threshold discrimination identification score and CSF A β and tau levels in AD patients with or without olfactory dysfunction (OD), finding that only *t*-tau levels were significantly lower in the AD-OD group, but the significant correlation disappeared after adjusting for age, sex, education, and disease duration. The same was true for the study by Doorduijn et al. (2020), which found no associations between AD biomarker levels and threshold discrimination identification. Another excluded study using odor percept identification performance with a homemade test to correlate with A β PET data also yielded a negative result (Dhillal Albers et al., 2016). These findings appear to be consistent with our meta-analysis results. Additionally, the *p*-tau/*t*-tau ratio has recently been shown to be related to olfaction in peripheral

olfactory systems (Liu et al., 2018); thus, it might be interesting to examine the association between the *p*-tau/*t*-tau ratio and OI ability.

Here, we provide a thorough analysis on the negligible association between OI ability and A β and CSF tau burden, from the limitation of the OI test and A β measures themselves (both are lack of specificity) and the drawbacks of currently averaging the A β levels for the whole brain, to the possible association between the pathologic development (amyloid plaques and tauopathy) and OI impairment based on the prion-like hypothesis in AD. Specifically, we point out that the prion-like spreading A β , especially tau along the olfactory pathway (starting from OB) may contribute to the OI impairment, in parallel of memory dysfunction to some extent. This highlights a strategic regional analysis in the future, and a handful of other ideas, such as treating OI as a categorical variable (e.g., anosmia, normosmia), using *t*-tau/A β ₄₂ or *p*-tau/A β ₄₂, focusing on the APOE $\epsilon 4$ allele carriers, and most importantly measuring by PET tau imaging.

In summary, our meta-analysis suggests that OI impairment correlates marginally with A β PET data but not CSF A β and more weakly correlates with CSF *t*-tau but not *p*-tau. These findings may disappoint those who intend to use OI ability alone for the early detection of AD. Nevertheless, PET tau might be more strongly associated with OI impairment; however, more studies are needed to clarify this association. Importantly, our results should not be regarded as a rationale for denying the value of olfactory testing in AD research. OI test may have limited value predicting amyloid and tau status when used alone, yet it is possible that an enhanced association between the two may be yielded when combined with other biologic markers discussed above (e.g., focusing on APOE $\epsilon 4$ carriers using tau PET imaging with olfactory region-based analysis), and it is still valuable in predicting cognitive decline and progression from MCI to AD dementia. In fact, as a low-cost, non-invasive method of evaluating olfactory function, the assessment of OI ability, combined with global cognitive testing, has the potential to help clinicians identify persons who rarely transition to dementia (Devanand et al., 2019), thus helping practitioners decide whether to apply further diagnostic investigations, such as PET scans, which help reduce the burden and cost of clinical AD trials and as the first diagnostic tau radiotracer for use with PET was approved by the US Food and Drug Administration, further research is possible and warranted.

DATA AVAILABILITY STATEMENT

The original contributions presented in the study are included in the article/supplementary material, further inquiries can be directed to the corresponding author/s.

AUTHOR CONTRIBUTIONS

LT contributed to the study design, data analysis, and interpretation and drafted the manuscript. XL contributed to data analysis and interpretation and critical revision of the manuscript. ZF and MZ contributed to data analysis and revision of the manuscript. XY and HW contributed to the design

of this study, interpretation of data, and critical revision of the manuscript and had primary responsibility for the final content. All authors read and approved the final manuscript. All authors contributed to the article and approved the submitted version.

FUNDING

This work was funded by the National Key R&D Program of China (2018YFC1314200, 2017YFC1311100). The funding

agency had no role in the design of the study, in collection, analysis, or interpretation of the data, in the writing, approval of the manuscript, or decision to submit the manuscript for publication.

ACKNOWLEDGMENTS

We wish to thank the authors of included studies who share the data with us and even give valuable advices to us, especially William Charles Kreisl and Minoru Kouzuki.

REFERENCES

- Alzheimer's Association (2020). Alzheimer's disease facts and figures. *Alzheimer's Dement.* 16, 391–460. doi: 10.1002/alz.12068
- Arnold, S. E., Lee, E. B., Moberg, P. J., Stutzbach, L., Kazi, H., Han, L.-Y., et al. (2010). Olfactory epithelium amyloid-beta and paired helical filament-tau pathology in Alzheimer disease. *Ann. Neurol.* 67, 462–469. doi: 10.1002/ana.21910
- Attems, J., and Jellinger, K. A. (2006). Olfactory tau pathology in Alzheimer disease and mild cognitive impairment. *Clin. Neuropathol.* 25, 265–271.
- Attems, J., Lintner, F., and Jellinger, K. A. (2005). Olfactory involvement in aging and Alzheimer's disease: an autopsy study. *J. Alzheimers Dis.* 7, 149–157; discussion 173–180. doi: 10.3233/JAD-2005-7208
- Bahar-Fuchs, A., Chételat, G., Villemagne, V. L., Moss, S., Pike, K., Masters, C. L., et al. (2010). Olfactory deficits and amyloid- β burden in Alzheimer's disease, mild cognitive impairment, and healthy aging: a PiB PET study. *J. Alzheimers Dis.* 22, 1081–1087. doi: 10.3233/JAD-2010-100696
- Brier, M. R., Gordon, B., Friedrichsen, K., McCarthy, J., Stern, A., Christensen, J., et al. (2016). Tau and A β imaging, CSF measures, and cognition in Alzheimer's disease. *Sci. Transl. Med.* 8:338ra66. doi: 10.1126/scitranslmed.aaf2362
- Brozzetti, L., Sacchetto, L., Cecchini, M. P., Avesani, A., Perra, D., Bongianini, M., et al. (2020). Neurodegeneration-associated proteins in human olfactory neurons collected by nasal brushing. *Front. Neurosci.* 14:145. doi: 10.3389/fnins.2020.00145
- Devanand, D. P., Lee, S., Luchsinger, J. A., Andrews, H., Goldberg, T., Huey, E. D., et al. (2019). Intact global cognitive and olfactory ability predicts lack of transition to dementia. *Alzheimer's Dement.* 15:P1535. doi: 10.1016/j.jalz.2019.08.112
- Devanand, D. P., Lee, S., Manly, J., Andrews, H., Schupf, N., Doty, R. L., et al. (2015). Olfactory deficits predict cognitive decline and Alzheimer dementia in an urban community. *Neurology* 84, 182–189. doi: 10.1212/WNL.0000000000001132
- Dhilla Albers, A., Asafu-Adjei, J., Delaney, M. K., Kelly, K. E., Gomez-Isla, T., Blacker, D., et al. (2016). Episodic memory of odors stratifies Alzheimer biomarkers in normal elderly. *Ann. Neurol.* 80, 846–857. doi: 10.1002/ana.24792
- Dibattista, M., Pifferi, S., Menini, A., and Reisert, J. (2020). Alzheimer's disease: what can we learn from the peripheral olfactory system? *Front. Neurosci.* 14:440. doi: 10.3389/fnins.2020.00440
- Dintica, C. S., Marseglia, A., Rizzuto, D., Wang, R., Seubert, J., Arfanakis, K., et al. (2019). Impaired olfaction is associated with cognitive decline and neurodegeneration in the brain. *Neurology* 92:e700–9. doi: 10.1212/WNL.0000000000006919
- Doorduijn, A. S., de van der Schueren, M. A. E., van de Rest, O., de Leeuw, F. A., Fieldhouse, J. L. P., Kester, M. I., et al. (2020). Olfactory and gustatory functioning and food preferences of patients with Alzheimer's disease and mild cognitive impairment compared to controls: the NUDAD project. *J. Neurol.* 267, 144–152. doi: 10.1007/s00415-019-09561-0
- Doty, R. L., and Kamath, V. (2014). The influences of age on olfaction: a review. *Front. Psychol.* 5:20. doi: 10.3389/fpsyg.2014.00020
- Doty, R. L., Shaman, P., Applebaum, S. L., Giberson, R., Siksorski, L., and Rosenberg, L. (1984). Smell identification ability: changes with age. *Science* 226, 1441–1443. doi: 10.1126/science.6505700
- Franks, K. H., Chuah, M. I., King, A. E., and Vickers, J. C. (2015). Connectivity of pathology: the olfactory system as a model for network-driven mechanisms of alzheimer's disease pathogenesis. *Front. Aging. Neurosci.* 7:234. doi: 10.3389/fnagi.2015.00234
- Growdon, M. E., Schultz, A. P., Dagley, A. S., Amariglio, R. E., Hedden, T., Rentz, D. M., et al. (2015). Odor identification and Alzheimer disease biomarkers in clinically normal elderly. *Neurology* 84, 2153–2160. doi: 10.1212/WNL.0000000000001614
- Hoyle, K., and Sharma, J. C. (2013). Olfactory loss as a supporting feature in the diagnosis of Parkinson's disease: a pragmatic approach. *J. Neurol.* 260, 2951–2958. doi: 10.1007/s00415-013-6848-8
- Ingelsson, M., Fukumoto, H., Newell, K. L., Growdon, J. H., Hedley-Whyte, E. T., Frosch, M. P., et al. (2004). Early A β accumulation and progressive synaptic loss, gliosis, and tangle formation in AD brain. *Neurology* 62, 925–931. doi: 10.1212/01.WNL.0000115115.98960.37
- Jack, C. R., Bennett, D. A., Blennow, K., Carrillo, M. C., Dunn, B., Haeberlein, S. B., et al. (2018). NIA-AA research framework: toward a biological definition of Alzheimer's disease. *Alzheimers Dement.* 14, 535–562. doi: 10.1016/j.jalz.2018.02.018
- Jack, C. R., Wiste, H. J., Therneau, T. M., Weigand, S. D., Knopman, D. S., Mielke, M. M., et al. (2019). Associations of amyloid, tau, and neurodegeneration biomarker profiles with rates of memory decline among individuals without dementia. *JAMA* 321, 2316–2325. doi: 10.1001/jama.2019.7437
- Jansen, W. J., Ossenkoppele, R., Knol, D. L., Tijms, B. M., Scheltens, P., Verhey, F. R. J., et al. (2015). Prevalence of cerebral amyloid pathology in persons without dementia: a meta-analysis. *JAMA* 313, 1924–1938. doi: 10.1001/jama.2015.4668
- Jung, H. J., Shin, I.-S., and Lee, J.-E. (2019). Olfactory function in mild cognitive impairment and Alzheimer's disease: a meta-analysis. *Laryngoscope* 129, 362–369. doi: 10.1002/lary.27399
- Kamath, V., Crawford, J., DuBois, S., Nucifora, F. C. Jr., Nestadt, G., Sawa, A., et al. (2019). Contributions of olfactory and neuropsychological assessment to the diagnosis of first-episode schizophrenia. *Neuropsychology* 33, 203–211. doi: 10.1037/neu0000502
- Kametani, F., and Hasegawa, M. (2018). Reconsideration of amyloid hypothesis and tau hypothesis in alzheimer's disease. *Front. Neurosci.* 12:25. doi: 10.3389/fnins.2018.00025
- Kim, M. J., Moon, S., Oh, B.-C., Jung, D., Choi, K., and Park, Y. J. (2019). Association between diethylhexyl phthalate exposure and thyroid function: a meta-analysis. *Thyroid* 29, 183–192. doi: 10.1089/thy.2018.0051
- Körtvélyessy, P., Gukasjan, A., Sweeney-Reed, C. M., Heinze, H.-J., Thurner, L., and Bittner, D. M. (2015). Progranulin and Amyloid- β levels: relationship to neuropsychology in frontotemporal and alzheimer's disease. *J. Alzheimers Dis.* 46, 375–380. doi: 10.3233/JAD-150069
- Kouzuki, M., Suzuki, T., Nagano, M., Nakamura, S., Katsumata, Y., Takamura, A., et al. (2018). Comparison of olfactory and gustatory disorders in Alzheimer's disease. *Neurol. Sci.* 39, 321–328. doi: 10.1007/s10072-017-3187-z
- Kovacs, T., Cairns, N. J., and Lantos, P. L. (1999). beta-amyloid deposition and neurofibrillary tangle formation in the olfactory bulb in ageing and Alzheimer's disease. *Neuropathol. Appl. Neurobiol.* 25, 481–491. doi: 10.1046/j.1365-2990.1999.00208.x
- Kreisl, W. C., Jin, P., Lee, S., Dayan, E. R., Vallabhajosula, S., Pelton, G., et al. (2018). Odor identification ability predicts PET amyloid status and memory decline in older adults. *J. Alzheimers Dis.* 62, 1759–1766. doi: 10.3233/JAD-170960

- Lafaille-Magnan, M.-E., Poirier, J., Etienne, P., Tremblay-Mercier, J., Frenette, J., Rosa-Neto, P., et al. (2017). Odor identification as a biomarker of preclinical AD in older adults at risk. *Neurology* 89, 327–335. doi: 10.1212/WNL.0000000000004159
- Leuzy, A., Chiotis, K., Lemoine, L., Gillberg, P.-G., Almkvist, O., Rodriguez-Vieitez, E., et al. (2019). Tau PET imaging in neurodegenerative tauopathies—still a challenge. *Mol. Psychiatry* 24, 1112–1134. doi: 10.1038/s41380-018-0342-8
- Lian, T.-H., Zhu, W.-L., Li, S.-W., Liu, Y.-O., Guo, P., Zuo, L.-J., et al. (2019). Clinical, structural, and neuropathological features of olfactory dysfunction in patients with alzheimer's disease. *J. Alzheimer's Dis.* 70, 413–423. doi: 10.3233/JAD-181217
- Liu, Z., Kameshima, N., Nanjo, T., Shiino, A., Kato, T., Shimizu, S., et al. (2018). Development of a high-sensitivity method for the measurement of human nasal A β 42, Tau, and phosphorylated Tau. *J. Alzheimer's Dis.* 62, 737–744. doi: 10.3233/JAD-170962
- Mahlknecht, P., Iranzo, A., Hög, B., Frauscher, B., Müller, C., Santamaria, J., et al. (2015). Olfactory dysfunction predicts early transition to a Lewy body disease in idiopathic RBD. *Neurology* 84, 654–658. doi: 10.1212/WNL.0000000000001265
- Marin, C., Vilas, D., Langdon, C., Alobid, I., López-Chacón, M., Haehner, A., et al. (2018). Olfactory dysfunction in neurodegenerative diseases. *Curr. Allergy Asthma Rep.* 18:42. doi: 10.1007/s11882-018-0796-4
- Mattsson, N., Schöll, M., Strandberg, O., Smith, R., Palmqvist, S., Insel, P. S., et al. (2017). 18F-AV-1451 and CSF T-tau and P-tau as biomarkers in Alzheimer's disease. *EMBO Mol. Med.* 9, 1212–1223. doi: 10.15252/emmm.201707809
- Meyer, P.-F., Binette, A. P., Gonneaud, J., Breiten, J. C. S., and Villeneuve, S. (2020). Characterization of alzheimer disease biomarker discrepancies using cerebrospinal fluid phosphorylated tau and AV1451 positron emission tomography. *JAMA Neurol.* 77, 508–516. doi: 10.1001/jamaneurol.2019.4749
- Moher, D., Shamseer, L., Clarke, M., Ghersi, D., Liberati, A., Petticrew, M., et al. (2015). Preferred reporting items for systematic review and meta-analysis protocols (PRISMA-P) 2015 statement. *Syst. Rev.* 4:1. doi: 10.1186/2046-4053-4-1
- Nag, S., Yu, L., VanderHorst, V. G., Schneider, J. A., Bennett, D. A., Buchman, A. S., et al. (2019). Neocortical lewy bodies are associated with impaired odor identification in community-dwelling elders without clinical PD. *J. Neurol.* 266, 3108–3118. doi: 10.1007/s00415-019-09540-5
- Reijls, B. L. R., Ramakers, I. H. G. B., Elias-Sonnenschein, L., Teunissen, C. E., Koel-Simmelmink, M., Tsolaki, M., et al. (2017). Relation of odor identification with alzheimer's disease markers in cerebrospinal fluid and cognition. *J. Alzheimers Dis.* 60, 1025–1034. doi: 10.3233/JAD-170564
- Rey, N. L., Wesson, D. W., and Brundin, P. (2018). The olfactory bulb as the entry site for prion-like propagation in neurodegenerative diseases. *Neurobiol. Dis.* 109, 226–248. doi: 10.1016/j.nbd.2016.12.013
- Risacher, S. L., Tallman, E. F., West, J. D., Yoder, K. K., Hutchins, G. D., Fletcher, J. W., et al. (2017). Olfactory identification in subjective cognitive decline and mild cognitive impairment: association with tau but not amyloid positron emission tomography. *Alzheimers Dement.* 9, 57–66. doi: 10.1016/j.dadm.2017.09.001
- Roalf, D. R., Moberg, M. J., Turetsky, B. I., Brennan, L., Kabadi, S., Wolk, D. A., et al. (2017). A quantitative meta-analysis of olfactory dysfunction in mild cognitive impairment. *J. Neurol. Neurosurg. Psychiatr.* 88, 226–232. doi: 10.1136/jnnp-2016-314638
- Roberts, R. O., Christianson, T. J. H., Kremers, W. K., Mielke, M. M., Machulda, M. M., Vassilaki, M., et al. (2016). Association between olfactory dysfunction and amnesic mild cognitive impairment and Alzheimer disease dementia. *JAMA Neurol.* 73, 93–101. doi: 10.1001/jamaneurol.2015.2952
- Serrano-Pozo, A., Mielke, M. L., Gómez-Isla, T., Betensky, R. A., Growdon, J. H., Frosch, M. P., et al. (2011). Reactive Glia not only associates with plaques but also parallels tangles in alzheimer's disease. *Am. J. Pathol.* 179, 1373–1384. doi: 10.1016/j.ajpath.2011.05.047
- Shankar, G. M., Li, S., Mehta, T. H., Garcia-Munoz, A., Shepardson, N. E., Smith, I., et al. (2008). Amyloid β -protein dimers isolated directly from alzheimer brains impair synaptic plasticity and memory. *Nat. Med.* 14, 837–842. doi: 10.1038/nm1782
- Sterne, J. A. C., Sutton, A. J., Ioannidis, J. P. A., Terrin, N., Jones, D. R., Lau, J., et al. (2011). Recommendations for examining and interpreting funnel plot asymmetry in meta-analyses of randomised controlled trials. *BMJ* 343:d4002. doi: 10.1136/bmj.d4002
- Tabaton, M., Monaco, S., Cordone, M. P., Colucci, M., Giaccone, G., Tagliavini, F., et al. (2004). Prion deposition in olfactory biopsy of sporadic Creutzfeldt-Jakob disease. *Ann. Neurol.* 55, 294–296. doi: 10.1002/ana.20038
- Thomann, P. A., Dos Santos, V., Toro, P., Schönknecht, P., Essig, M., and Schröder, J. (2009). Reduced olfactory bulb and tract volume in early Alzheimer's disease—a MRI study. *Neurobiol. Aging* 30, 838–841. doi: 10.1016/j.neurobiolaging.2007.08.001
- Tu, L.-H., Wang, H.-L., and Yu, X. (2020). Olfactory dysfunction and common neurocognitive disorder: an update of research progression. *Chinese J. Psychiatr.* 53, 155–158. doi: 10.3760/cma.j.cn113661-20190426-00151
- Vasavada, M. M., Martinez, B., Wang, J., Eslinger, P. J., Gill, D. J., Sun, X., et al. (2017). Central olfactory dysfunction in alzheimer's disease and mild cognitive impairment: a functional MRI study. *J. Alzheimers Dis.* 59, 359–368. doi: 10.3233/JAD-170310
- Vasavada, M. M., Wang, J., Eslinger, P. J., Gill, D. J., Sun, X., Karunanayaka, P., et al. (2015). Olfactory cortex degeneration in Alzheimer's disease and mild cognitive impairment. *J. Alzheimers Dis.* 45, 947–958. doi: 10.3233/JAD-141947
- Vassilaki, M., Christianson, T. J., Mielke, M. M., Geda, Y. E., Kremers, W. K., Machulda, M. M., et al. (2017). Neuroimaging biomarkers and impaired olfaction in cognitively normal individuals. *Ann. Neurol.* 81, 871–882. doi: 10.1002/ana.24960
- Villemagne, V. L., Dor, V., Burnham, S. C., Masters, C. L., and Rowe, C. C. (2018). Imaging tau and amyloid- β proteinopathies in Alzheimer disease and other conditions. *Nat. Rev. Neurol.* 14, 225–236. doi: 10.1038/nrneurol.2018.9
- Waldton, S. (1974). Clinical observations of impaired cranial nerve function in senile dementia. *Acta Psychiatr. Scand.* 50, 539–547. doi: 10.1111/j.1600-0447.1974.tb09714.x
- Walker, L. C. (2018). Prion-like mechanisms in Alzheimer disease. *Handb. Clin. Neurol.* 153, 303–319. doi: 10.1016/B978-0-444-63945-5.00016-7
- Walsh, D. M., Klyubin, I., Fadeeva, J. V., Cullen, W. K., Anwyl, R., Wolfe, M. S., et al. (2002). Naturally secreted oligomers of amyloid β protein potently inhibit hippocampal long-term potentiation in vivo. *Nature* 416, 535–539. doi: 10.1038/416535a
- Whiting, P. F., Rutjes, A. W. S., Westwood, M. E., Mallett, S., Deeks, J. J., Reitsma, J. B., et al. (2011). QUADAS-2: a revised tool for the quality assessment of diagnostic accuracy studies. *Ann. Intern. Med.* 155, 529–536. doi: 10.7326/0003-4819-155-8-201110180-00009
- Wilson, R. S., Arnold, S. E., Schneider, J. A., Boyle, P. A., Buchman, A. S., and Bennett, D. A. (2009). Olfactory impairment in presymptomatic Alzheimer's disease. *Ann. N. Y. Acad. Sci.* 1170, 730–735. doi: 10.1111/j.1749-6632.2009.04013.x
- Wilson, R. S., Arnold, S. E., Schneider, J. A., Tang, Y., and Bennett, D. A. (2007). The relationship between cerebral Alzheimer's disease pathology and odour identification in old age. *J. Neurol. Neurosurg. Psychiatr.* 78, 30–35. doi: 10.1136/jnnp.2006.099721
- Wu, X., Geng, Z., Zhou, S., Bai, T., Wei, L., Ji, G.-J., et al. (2019). Brain structural correlates of odor identification in mild cognitive impairment and alzheimer's disease revealed by magnetic resonance imaging and a chinese olfactory identification test. *Front. Neurosci.* 13:842. doi: 10.3389/fnins.2019.00842
- Yu, J.-T., Li, J.-Q., Suckling, J., Feng, L., Pan, A., Wang, Y.-J., et al. (2019). Frequency and longitudinal clinical outcomes of Alzheimer's AT(N) biomarker profiles: a longitudinal study. *Alzheimers Dement* 15, 1208–1217. doi: 10.1016/j.jalz.2019.05.006

Conflict of Interest: The authors declare that the research was conducted in the absence of any commercial or financial relationships that could be construed as a potential conflict of interest.

Copyright © 2020 Tu, Lv, Fan, Zhang, Wang and Yu. This is an open-access article distributed under the terms of the Creative Commons Attribution License (CC BY). The use, distribution or reproduction in other forums is permitted, provided the original author(s) and the copyright owner(s) are credited and that the original publication in this journal is cited, in accordance with accepted academic practice. No use, distribution or reproduction is permitted which does not comply with these terms.



Progranulin Adsorbs to Polypropylene Tubes and Disrupts Functional Assays: Implications for Research, Biomarker Studies, and Therapeutics

Sushmitha Gururaj[†], Paul J. Sampaogaro[†], Andrea R. Argouarch and Aimee W. Kao^{*}

Memory and Aging Center, Department of Neurology, University of California, San Francisco, San Francisco, CA, United States

OPEN ACCESS

Edited by:

Yu Chen,
Shenzhen Institutes of Advanced
Technology, Chinese Academy
of Sciences (CAS), China

Reviewed by:

Matthias Schmitz,
University Medical Center Göttingen,
Germany
Andrew Bateman,
McGill University Health Centre,
Canada
Sandra Almeida,
University of Massachusetts Medical
School, United States

*Correspondence:

Aimee W. Kao
aimee.kao@ucsf.edu

[†] These authors have contributed
equally to this work

Specialty section:

This article was submitted to
Neurodegeneration,
a section of the journal
Frontiers in Neuroscience

Received: 22 September 2020

Accepted: 16 November 2020

Published: 14 December 2020

Citation:

Gururaj S, Sampaogaro PJ,
Argouarch AR and Kao AW (2020)
Progranulin Adsorbs to Polypropylene
Tubes and Disrupts Functional
Assays: Implications for Research,
Biomarker Studies, and Therapeutics.
Front. Neurosci. 14:602235.
doi: 10.3389/fnins.2020.602235

Progranulin (PGRN) is a tightly regulated, secreted glycoprotein involved in a wide range of biological processes that is of tremendous interest to the scientific community due to its involvement in neoplastic, neurodevelopmental, and neurodegenerative diseases. In particular, progranulin haploinsufficiency leads to frontotemporal dementia. While performing experiments with a HIS-tagged recombinant human (rh) PGRN protein, we observed a measurable depletion of protein from solution due to its adsorption onto polypropylene (PPE) microcentrifuge tubes. In this study, we have quantified the extent of rhPGRN adsorption to PPE tubes while varying experimental conditions, including incubation time and temperature. We found that ~25–35% of rhPGRN becomes adsorbed to the surface of PPE tubes even after a short incubation period. We then directly showed the deleterious impact of PGRN adsorption in functional assays and have recommended alternative labware to minimize these effects. Although the risk of adsorption of some purified proteins and peptides to polymer plastics has been characterized previously, this is the first report of rhPGRN adsorption. Moreover, since PGRN is currently being studied and utilized in both basic science laboratories to perform *in vitro* studies and translational laboratories to survey PGRN as a quantitative dementia biomarker and potential replacement therapy, the reported observations here are broadly impactful and will likely significantly affect the design and interpretation of future experiments centered on progranulin biology.

Keywords: progranulin, adsorption, neurodegeneration, polypropylene, cathepsins

INTRODUCTION

Progranulin (PGRN) is an evolutionarily conserved, cysteine-rich, secreted glycoprotein with a diverse set of functions. The pleiotropic nature of PGRN is evidenced by a growing body of work that details its participation in important biological processes such as vascular protection (Kanazawa et al., 2015), neuronal connectivity and survival (Gass et al., 2012; Ward et al., 2014), wound healing (Zhu et al., 2002), inflammation (Jian et al., 2013; Tanaka et al., 2013; Minami et al., 2014; Xu et al., 2016), and immunity (Matsubara et al., 2012; Jian et al., 2013). In recent years, it has become apparent that cells maintain tight regulation of PGRN levels. Excessive PGRN production is associated with cancers that grow aggressively and metastasize early (He and Bateman, 1999; Yang et al., 2015; Serrero et al., 2016), while PGRN haploinsufficiency and

homozygous loss of function states lead to adult-onset frontotemporal dementia (FTD) (Baker et al., 2006; Cruts et al., 2006) and childhood-onset neuronal ceroid lipofuscinosis (NCL) (Smith et al., 2012), respectively. Intriguingly, PGRN gene (*Pgrn*) delivery has also demonstrated ameliorative effects in animal models of both Alzheimer's (Van Kampen and Kay, 2017) and Parkinson's disease (Van Kampen et al., 2014).

Based on these observations, circulating PGRN has garnered recent attention as a potential quantitative biomarker for neurodegeneration, particularly for FTD. *Pgrn* mutations causing FTD manifest in reduced plasma, serum, and cerebrospinal fluid (CSF) PGRN protein levels compared to non-mutation carriers (Ghidoni et al., 2008; Finch et al., 2009; Sleegers et al., 2009; Nicholson et al., 2014; Meeter et al., 2016; Wilke et al., 2017). Perhaps the strongest argument for the consideration of PGRN levels is that the clinical diagnosis of FTD lies in recent clinical trials testing PGRN replacement therapy, in which successful dose-dependent increases in plasma and CSF PGRN are already being reported (NCT03636204, NCT03987295). However, discrepancies exist within the current literature. For example, reduced serum PGRN do not seem to correlate tightly with reduced PGRN levels in the CSF of both *Pgrn* \pm and *Pgrn* $-/-$ FTD patients, suggesting either differences in peripheral PGRN regulation or potential sources of measurement error in PGRN quantification between these sample types (Wilke et al., 2016).

Our laboratory studies PGRN and its impact on lysosome biology and protein homeostasis (Salazar et al., 2015; Butler et al., 2019a,b,c). In several of our biochemical assays involving human plasma and CSF, we routinely use an \sim 80kDa recombinant HIS-tagged human Progranulin (rhPGRN) protein as a control for the full-length human PGRN protein. While performing these experiments, we observed inconsistencies in our rhPGRN control measurements in enzyme-linked immunosorbent assays (ELISA) and mass spectrometry assays. Troubleshooting these inconsistencies led to the discovery of an important caveat of working with this recombinant protein: PGRN depletes from solution by adsorbing to the polypropylene surface of microcentrifuge tubes. Given the nearly universal presence of polypropylene and other plastic labware in experimental workflows, we performed a detailed characterization of rhPGRN adsorption to polypropylene tubes. This study quantifies the adsorption of PGRN to polypropylene tubes, demonstrates the functional effects of this adsorption, and recommends alternatives to polypropylene to counteract it. Given the significant evidence for PGRN's tight *in vivo* regulatory control and in light of recent diagnostic and therapeutic efforts aimed at modulating PGRN levels in patients (particularly, those with neurodegenerative disease), we present these data in an effort to optimize future work in these areas.

MATERIALS AND METHODS

Materials

Labware—1.5 mL polypropylene microcentrifuge tubes (E&K Scientific Products, No. 695054), 1.5 mL LoBind microcentrifuge tubes (Fisher Scientific Sci, No. E925000090), polypropylene

pipet tips (United States Scientific, No. 1,111–1,700, 1–200 μ L, low binding pipet tips (Sigma-Aldrich, No. CLS4151). Antibodies—anti-progranulin C-terminus (Thermo Fisher #40-3400, 1:1,000).

BSA Coating of Polypropylene Tubes

BSA (Sigma, St. Louis, MO, United States) was dissolved in deionized water at a concentration of 100 mg/mL and sterile filtered. 100 μ L of the BSA solution was incubated in the 1.5 mL polypropylene tubes for 24 h at room temperature. The solution was then aspirated, spun, and all remaining solution was aspirated.

PGRN Adsorption Experiments

Recombinant human PGRN (R&D Systems Inc., No. 2420-PG-050) was prepared to the required concentration in Dulbecco's Phosphate Buffered Solutions (DPBS) (Thermo Fisher Scientific, Waltham, MA, United States). Experiments were performed in 1.5 mL polypropylene tubes, Lobind tubes, or BSA-coated polypropylene tubes. Low binding pipet tips were used in all experiments except in the pipetting loss experiments, where polypropylene tips were used. 30 μ L of 100 nM PGRN solution was made in each tube or in the control tube for the serial transfer and pipetting experiments and 30 μ L of 250, 150, 100, 75, 50, or 25 nM was made in the dilution series experiments. 10' incubations were performed on ice, unless specified as in the temperature and time experiments. To analyze PGRN in solution, either aliquots (5 μ L) or the entire 30 μ L volume were removed as indicated by the figure legends, and mixed with 4X lithium dodecyl sulfate (LDS) (Thermo Fisher Sci, No., NP0007) and 10X reducing agent (Thermo Fisher Sci, No. NP0009). These sample mixtures were boiled and visualized by Western blot. Adsorbed PGRN was analyzed by aspirating all the remaining solution from the tubes, adding 4X Laemmli buffer and 10X reducing agent, and boiling the tubes. Each tube was vortexed before and after boiling, and PGRN was then visualized by Western blot.

In vitro Cleavage Assays

Recombinant human PGRN (R&D Systems Inc., No. 2420-PG-050) was prepared in DPBS (Thermo Fisher Scientific, Waltham, MA, United States). Experiments were performed in 1.5 mL polypropylene tubes and Lobind tubes. Low binding pipet tips were used in all experiments. 400 ng of rhPGRN was incubated with 250 nM of Cathepsin L (R&D Systems, No. 952-CY-010) in the presence of sodium acetate buffer (pH 4.5), 10 μ M of dithiothreitol (DTT), and 10 μ M of ethylenediaminetetraacetic acid (EDTA) for 2.5, 5, 10, and 15 min. These timed incubations were quenched by the addition of 4X LDS (Thermo Fisher Sci No., NP0007) and 10X reducing agent (Thermo Fisher Sci, No. NP0009), and placed on ice. These sample mixtures were then boiled and visualized by Western blot.

Western Blots

Progranulin was visualized by reducing (sodium dodecyl sulfate–polyacrylamide gel electrophoresis) SDS-PAGE using 4–12% Bis-Tris gels (Thermo Fisher sci, No. NP0302BOX). Proteins

were transferred to PVDF membrane (Bio-Rad, No. 1620177) and blocked with 5% milk (Thermo Fisher, No. NC9121673) or Odyssey buffer (Li-cor No. 927-50010) for 2 h at room temperature. Membranes were incubated in primary antibodies overnight at 4°C. Li-cor secondary antibodies were used at 1:5,000 dilution for 1 h at room temperature and blots were imaged using the Odyssey CLx imager.

Analysis of Western Blots

In order to quantify the relative intensity of bands on Western Blots, the captured images from the Odyssey CLx were subject to analysis using ImageJ (Rasband, W.S., ImageJ, United States National Institutes of Health, Bethesda, MD, United States, 1997–2012)¹. For **Figures 1A,B**, % PGRN values were obtained by normalizing to the control band signal. For all of the other figures, % PGRN detected either in solution or adsorbed to the tube for a particular condition was calculated as a fraction of the total signal: $\{[\text{intensity of in solution or adsorbed to tube band}] / (\text{intensity of in solution} + \text{adsorbed to tube bands}) \times 100\}$.

Statistics

All results shown are representative of three independent experiments. All statistics were performed using GraphPad Prism Version 6 (GraphPad Software, La Jolla, CA, United States). For comparisons with control, One-way ANOVA followed by Holm-Sidak's multiple comparisons test was used. For comparisons in all other figures, the difference between protein levels in solution and adsorbed to the tube at a given condition were calculated by paired *t*-tests while differences between the conditions within the in solution and adsorbed groups were calculated by One-way ANOVA followed by Dunnett's multiple comparisons test. In all graphs, error bars indicate the standard deviation of the data. *P* values for the concerned tests are as specified in figure legends.

RESULTS

rhProgranulin Protein Adsorbs to Polypropylene Tubes

It is well established that most proteins and peptides readily bind to experimental surfaces owing to their amphipathic nature (Nakanishi et al., 2001). This very property is exploited beneficially in several bio-techniques, such as the ELISA immuno-assay where the coating of 96-well plastic plates relies on non-specific adsorption, and ion exchange chromatography whose central principle is the binding between charged proteins and resins. However, adsorption can exert undesirable impacts on quantitative protein studies and can lead to inaccurate working concentrations. We observed in our experiments that the incubation of rhPGRN protein in PPE microcentrifuge tubes depleted the protein amounts in solution over time. Therefore, we hypothesized that the rhPGRN was becoming adsorbed to polypropylene tubes.

To quantitatively assess rhPGRN adsorption to polypropylene tubes, 100 nM rhPGRN was incubated in tubes on ice for 10 min,

then serially transferred and incubated for 10 min in a new tube; this procedure was subsequently repeated four more times. Each empty tube was stripped of adsorbed PGRN by boiling with reducing Laemmli buffer and run on SDS-PAGE gels, along with the entirety of the rhPGRN left in tube 6 (**Figure 1A**). Pipetting loss of protein was minimized in these experiments by using low binding pipette tips. Upon comparison with a control sample that underwent no transfers, ~10–25% of PGRN was found to become adsorbed to a tube with each incubation such that after five transfers, only ~15% of the protein remained in solution ($p < 0.0001$) (**Figure 1B**). We also measured this phenomenon via ELISA and found similar results (**Supplementary Figure 1**).

Next, we asked if the concentration of PGRN affects the extent of adsorption; for example, if concentrations lower than 100 nM would be entirely depleted from solution or if higher concentrations might be found in solution still due to oversaturation of the adsorption surface. A concentration series (250–25 nM) was set up in polypropylene tubes for 10-min incubations and the adsorbed and in-solution PGRN were measured (**Figure 1C**). Within the tested concentration range, ~25–35% of protein was consistently found to be adsorbed across all concentrations.

We further examined PGRN loss to tube adsorption as a result of repeated pipetting during routine aspiration and/or dispensing of the solution in experiments. To test this, we prepared 100 nM PGRN solution in polypropylene tubes as previously described but instead of serially transferring the solution into new tubes, we reapplied it to the same tube with a fresh 100 µL polypropylene pipet tip. Samples 1 through 5 were prepared by sequentially increasing the number of times the full volume was aspirated and dispensed with a single tip from one to five, respectively (**Figure 1D**). When compared to a control preparation that was not subjected to pipetting, we found that pipetted samples underwent no measurable adsorption loss. The pipetting and incubation experiments differ primarily in the time of exposure of the sample to the plastic. The exposure time of the pipette tip's binding surface is only a few seconds whereas samples were incubated for 10 min in the tubes. Taken together with the previous results, in experimental practice it appears that polypropylene tubes, but not pipet tips, lead to measurable PGRN adsorption to labware under the conditions tested.

Time and Temperature Impact Adsorption of Recombinant Progranulin to Polypropylene Tubes

Given the aforementioned findings, as well as the fact that experimental conditions such as incubation time and temperature are often important factors in study design, we examined if rhPGRN adsorption to polypropylene tubes is influenced by (1) duration of incubation and (2) temperature. We also briefly looked at frozen storage (**Supplementary Figure 2**). To study incubation time as a factor, adsorbed and in-solution PGRN amounts were measured at the previously tested 10-min incubation timepoint, but also after 1, 4, 8, 16, 24, and 48 h of incubation on ice. Although the majority of PGRN

¹<http://imagej.nih.gov/ij/>

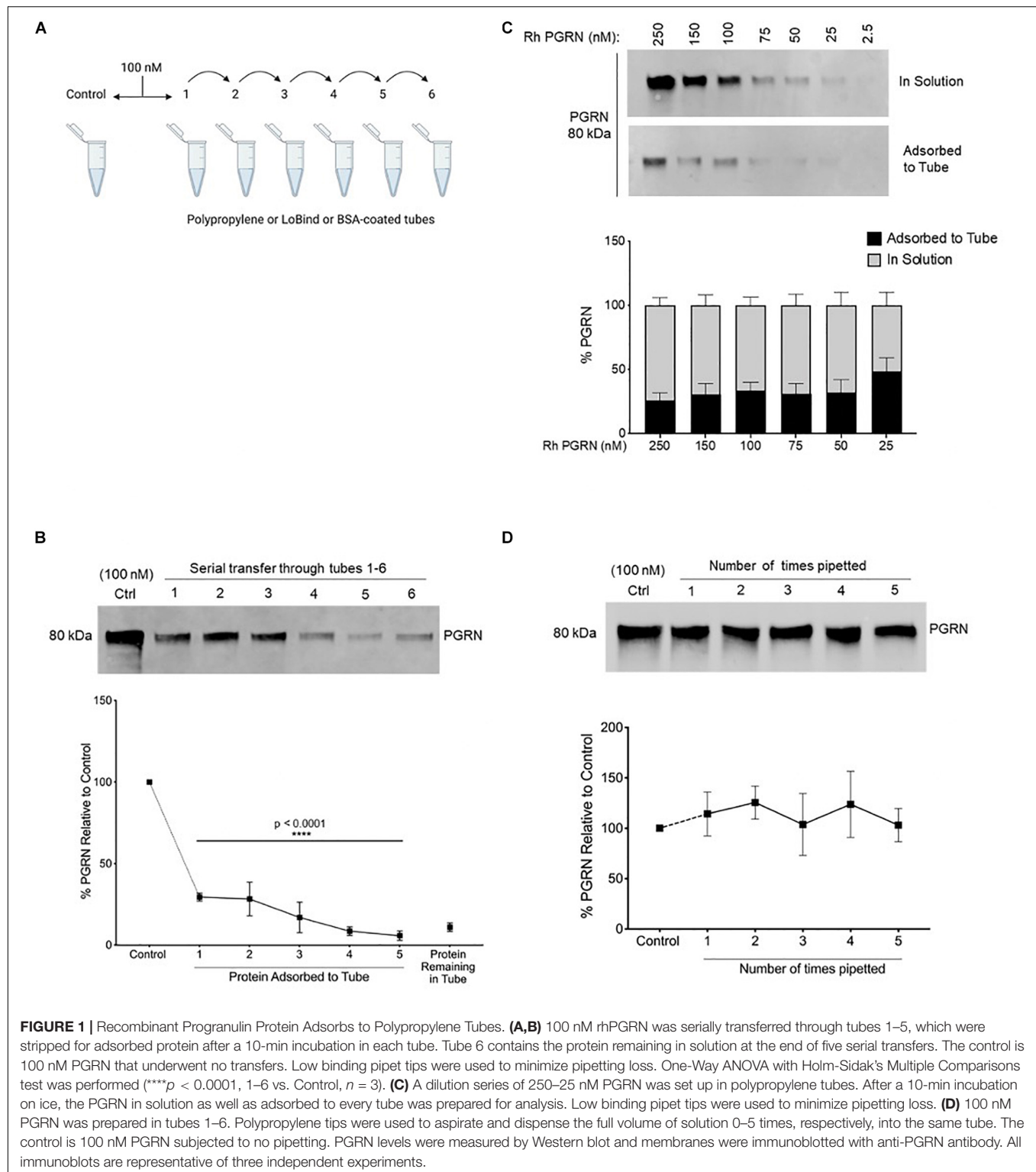


FIGURE 1 | Recombinant Progranulin Protein Adsorbs to Polypropylene Tubes. **(A,B)** 100 nM rhPGRN was serially transferred through tubes 1–5, which were stripped for adsorbed protein after a 10-min incubation in each tube. Tube 6 contains the protein remaining in solution at the end of five serial transfers. The control is 100 nM PGRN that underwent no transfers. Low binding pipet tips were used to minimize pipetting loss. One-Way ANOVA with Holm-Sidak's Multiple Comparisons test was performed ($****p < 0.0001$, 1–6 vs. Control, $n = 3$). **(C)** A dilution series of 250–25 nM PGRN was set up in polypropylene tubes. After a 10-min incubation on ice, the PGRN in solution as well as adsorbed to every tube was prepared for analysis. Low binding pipet tips were used to minimize pipetting loss. **(D)** 100 nM PGRN was prepared in tubes 1–6. Polypropylene tips were used to aspirate and dispense the full volume of solution 0–5 times, respectively, into the same tube. The control is 100 nM PGRN subjected to no pipetting. PGRN levels were measured by Western blot and membranes were immunoblotted with anti-PGRN antibody. All immunoblots are representative of three independent experiments.

adsorption seemed to occur rapidly with ~40% adsorbed at the end of 10 min, we observed a trend toward further protein absorption over time, including a statistically significant increase of ~25–35% additional starting protein found adsorbed to the tube at 24 h ($p = 0.0458$) (Figure 2A). It must be noted that

this 40% adsorption is higher than was reported in previous 10-min incubations (Figures 1B,C). Indeed, we observed inter-experimental variation across our entire study and found the amount of adsorption to have a range as broad as 10–40% between experiments.

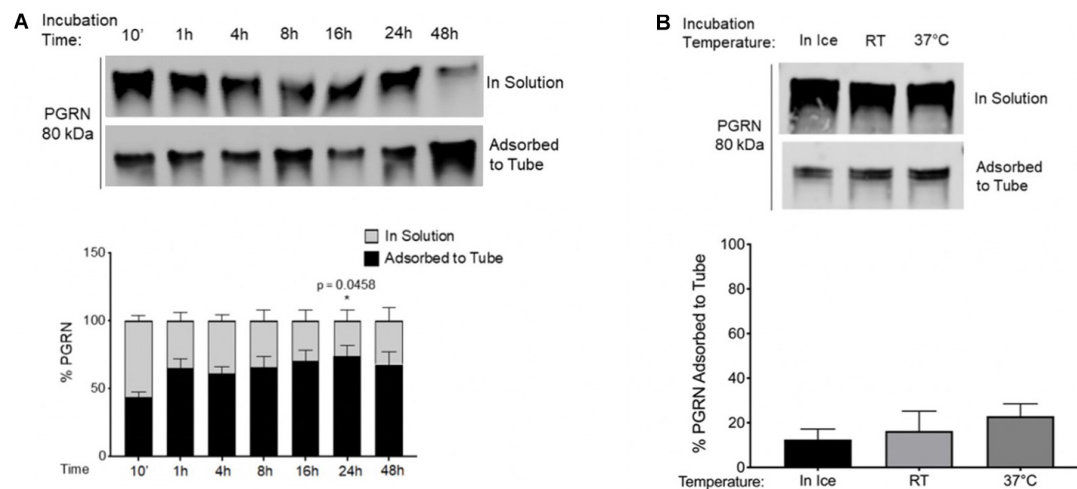


FIGURE 2 | Time and Temperature Impact Adsorption of Recombinant Progranulin to Polypropylene Tubes. **(A)** 100 nM PGRN was incubated for 10', 1, 4, 8, 16, 24, or 48 h in polypropylene tubes on ice. One-Way ANOVA with Dunnett's Multiple Comparisons were performed ($p < 0.05$, 1/4/8/16/24/48 h vs. 10', $n = 3$). **(B)** 100 nM PGRN was incubated in polypropylene tubes for 10' on ice, at room temperature (RT) or at 37°C ($n = 3$). At the end of the incubations, PGRN in solution as well as adsorbed to the tube was prepared for analysis. PGRN levels were measured by Western blot and membranes were immunoblotted with anti-PGRN antibody. All immunoblots are representative of three independent experiments.

PGRN adsorption to PPE may also be temperature dependent. Incubation at room temperature (RT) or at 37°C for 10 min trended toward increasing PGRN adsorption when compared to ice-incubation (**Figure 2B**). These results demonstrate that the considerable amount of basal PGRN adsorption observed under conventionally used experimental guidelines for recombinant proteins is further increased by varying conditions such as duration or temperature of incubations, necessitating additional caution among experimenters when designing protocols with PPE tubes.

PGRN Adsorption Is Reduced in Low Binding and BSA-Coated Tubes

We tested two alternatives to polypropylene tubes: (1) BSA-coated tubes prepared by incubating 100 mg/ml BSA in polypropylene tubes for 24 h at room temperature (**Figure 3**) and (2) commercially available low-binding "LoBind" tubes (**Figure 4**). As in a previous set of experiments, rhPGRN concentrations from 25 to 250 nM were incubated in LoBind or BSA-coated tubes for 10 min on ice. Overall, both LoBind and BSA-coated tubes performed better than polypropylene tubes, with BSA-coated tubes resulting in nearly complete retention of PGRN in solution across the concentration range (**Figures 3A, 4A**). LoBind tubes, on the other hand, resulted in lesser PGRN adsorption loss than polypropylene tubes (~10–15 vs. ~25–35%), but did not completely prevent it.

Additionally, we examined if the two alternative tubes would fare better under conditions that exacerbated rhPGRN adsorption loss in polypropylene tubes, namely longer incubation times and higher incubation temperatures. We found that PGRN adsorption did not increase in a time- or temperature-dependent manner in LoBind (**Figures 3B,C**) or BSA-coated tubes (**Figures 4B,C**). However, a measurable amount of PGRN

adsorption did occur in LoBind tubes at all the measured timepoints, consistent with previous results that it was but a slight improvement to polypropylene tubes. BSA coating, in contrast, prevented adsorption entirely under all tested conditions. Taken together, these results indicate that under the test conditions, BSA-coated tubes appear to be the most reliable at maintaining working concentrations of rhPGRN in solution, followed by LoBind tubes, and polypropylene tubes.

PGRN Adsorption to PPE Tubes Disrupts a Functional Assay

Following the above described characterization, it was critical for us to determine if PGRN adsorption interferes with the results of a functional assay. We routinely study the dynamics of PGRN processing into granulins using *in vitro* protease cleavage assays with rhPGRN and commercially available recombinant human lysosomal proteases. Based on previous work identifying the endo-lysosomal enzyme Cathepsin L (CTSL) as a PGRN protease (Lee et al., 2017), we compared the results from dynamic rhPGRN cleavage assays between polypropylene and Lobind tubes (**Figure 5**). Because BSA is a known CTSL substrate, BSA-coated tubes were not included in this experiment. Here, rhPGRN was incubated with recombinant CTSL at pH 4.5 for 2.5, 5, 10, or 15 min at 37°C. At the end of each timepoint, the full reaction volume was transferred to a new tube and the protein in solution as well as adsorbed to the incubation tube were prepared for western blot analysis as previously described. In this functional assay, the observed PGRN cleavage product (approximately 75 kDa in size) was noticeably absent from solution when the reaction was performed within polypropylene tubes, particularly at the 2.5-min timepoint. Taken together, these results demonstrate that *in vitro* cleavage assay kinetics are also

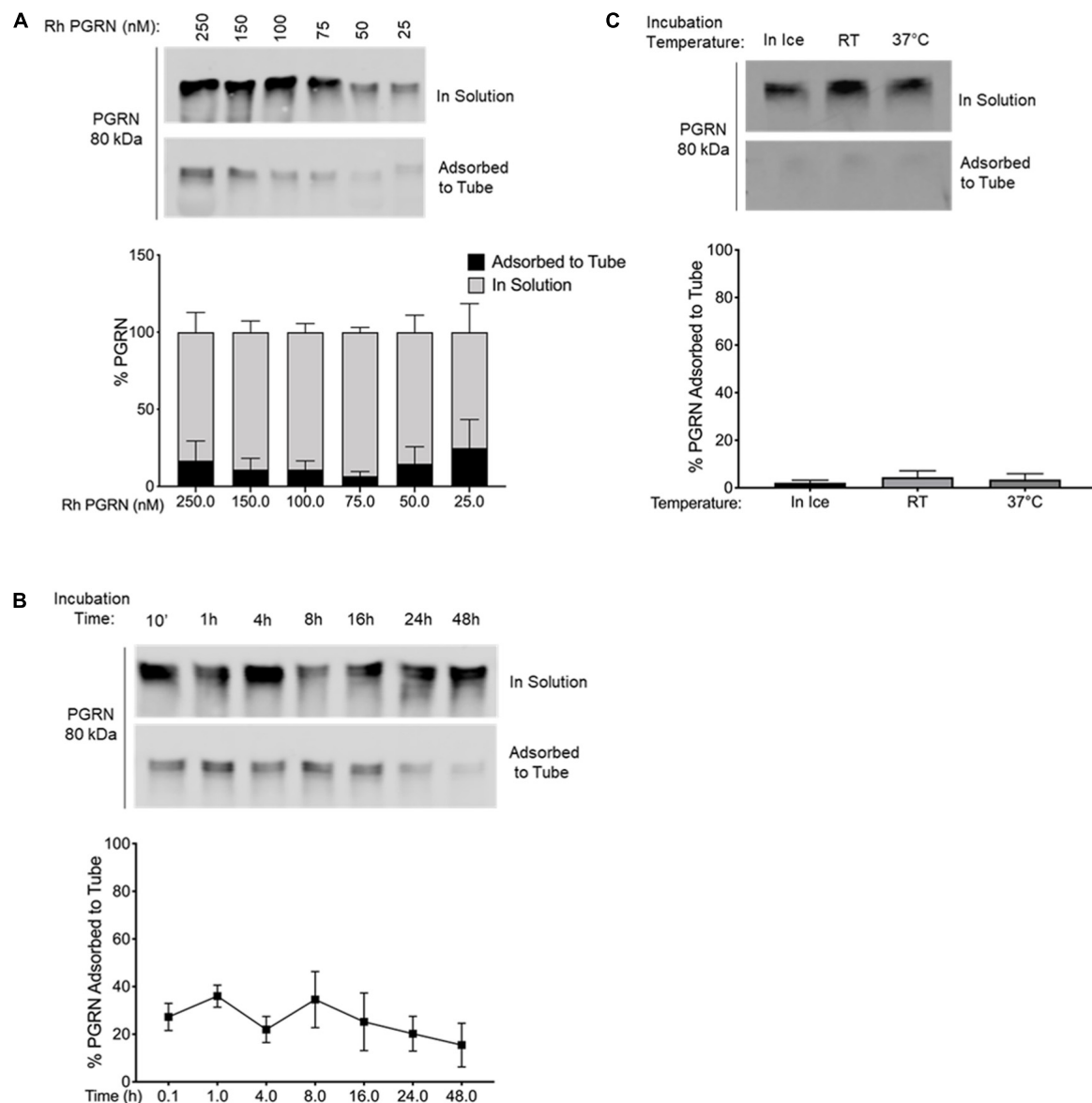


FIGURE 3 | PGRN Adsorption is Prevented in BSA-Coated Tubes. **(A)** A dilution series of 250–25 nM PGRN was set up in BSA-coated polypropylene tubes for 10-min incubations on ice ($n = 3$). **(B)** 100 nM PGRN was incubated for 10', 1, 4, 8, 16, 24, or 48 h in BSA-coated tubes on ice ($n = 3$). **(C)** 100 nM PGRN was incubated in BSA-coated tubes for 10' on ice, at room temperature (RT) or at 37°C ($n = 3$). At the end of the incubations, PGRN in solution as well as adsorbed to the tube was prepared for analysis. PGRN levels were measured by Western blot and membranes were immunoblotted with anti-PGRN antibody. All immunoblots are representative of three independent experiments.

subject to artifactual changes depending on the amount of protein adsorbed to the tube.

DISCUSSION

This study demonstrates that the adsorption of rhPGRN to polypropylene tubes has the potential to create artifacts in working concentrations and hence impact the results of quantitative studies. This adsorption to polypropylene increases proportionally with increased duration of incubation and

temperature. We show that using commercially available LoBind tubes and BSA coated polypropylene tubes can decrease or prevent adsorption, respectively.

Historically, common strategies to combat adsorption include adding detergents and increasing salt concentrations (Smith et al., 1978), coating surfaces with bovine serum albumin (BSA) (Felgner and Wilson, 1976) or polyethylene glycol (PEG) (Kramer et al., 1976), using siliconizing agents (Suelter and DeLuca, 1983), and choosing optimal labware (Goebel-Stengel et al., 2011). More recently, manufacturers have developed novel plastic polymers with lower protein retention properties than

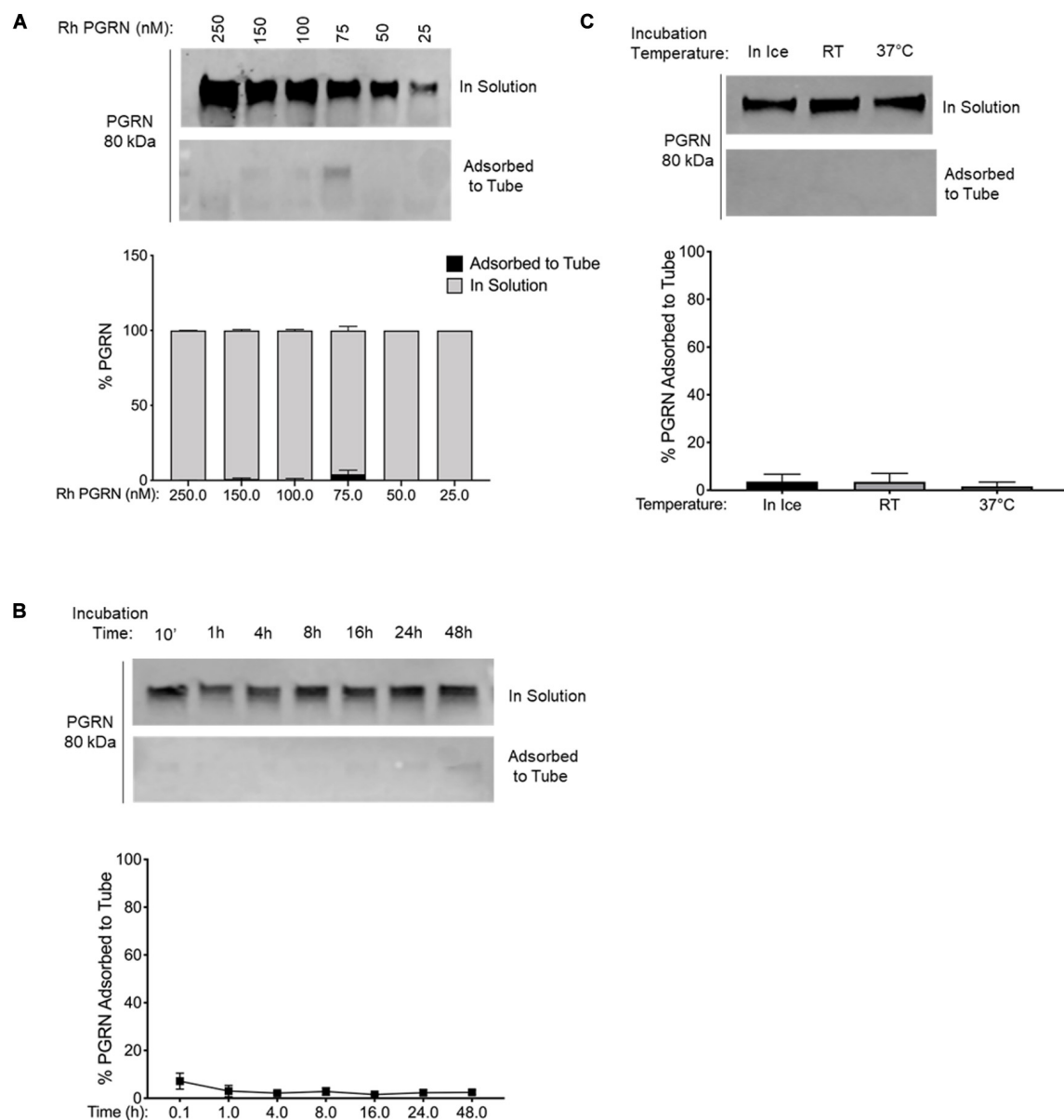


FIGURE 4 | PGRN Adsorption is Reduced in LoBind Tubes. **(A)** A dilution series of 250–25 nM PGRN was set up in LoBind tubes for 10-min incubations on ice ($n = 3$). **(B)** 100 nM PGRN was incubated for 10', 1, 4, 8, 16, 24 or 48 h in LoBind tubes on ice ($n = 3$). **(C)** 100 nM PGRN was incubated in LoBind tubes for 10' on ice, at room temperature (RT) or at 37°C ($n = 3$). At the end of the incubations, PGRN in solution as well as adsorbed to the tube was prepared for analysis. PGRN levels were measured by Western blot and membranes were immunoblotted with anti-PGRN antibody. All immunoblots are representative of three independent experiments.

polypropylene for use in commercially available low binding “LoBind” tubes and pipette tips. Our comparative assessment of BSA-coated and LoBind tubes reveals BSA coating of polypropylene tubes to be an effective and inexpensive step toward preventing PGRN adsorption. The ability of BSA to block PGRN adsorption may be the result of a few factors. First, the polypropylene binding surface may achieve occupancy saturation by BSA and second, BSA may interact directly with the rhPGRN so as to facilitate PGRN protein remaining in solution. Protein adsorption theory suggests that in multi-component solutions,

the former is dominant; a mass transfer phenomenon known as the Vroman Effect dictates that in a collection of proteins capable of electrostatically interacting with polypropylene, the most concentrated protein of the lowest molecular weight would arrive at the surface first, followed by the larger, less abundant ones (Fang et al., 2005). This likely underlies why protein adsorption has been described predominantly in single-component preparations of purified proteins and peptides. However, BSA contamination can be suboptimal and interfere in certain experimental designs, such as the *in vitro* cleavage

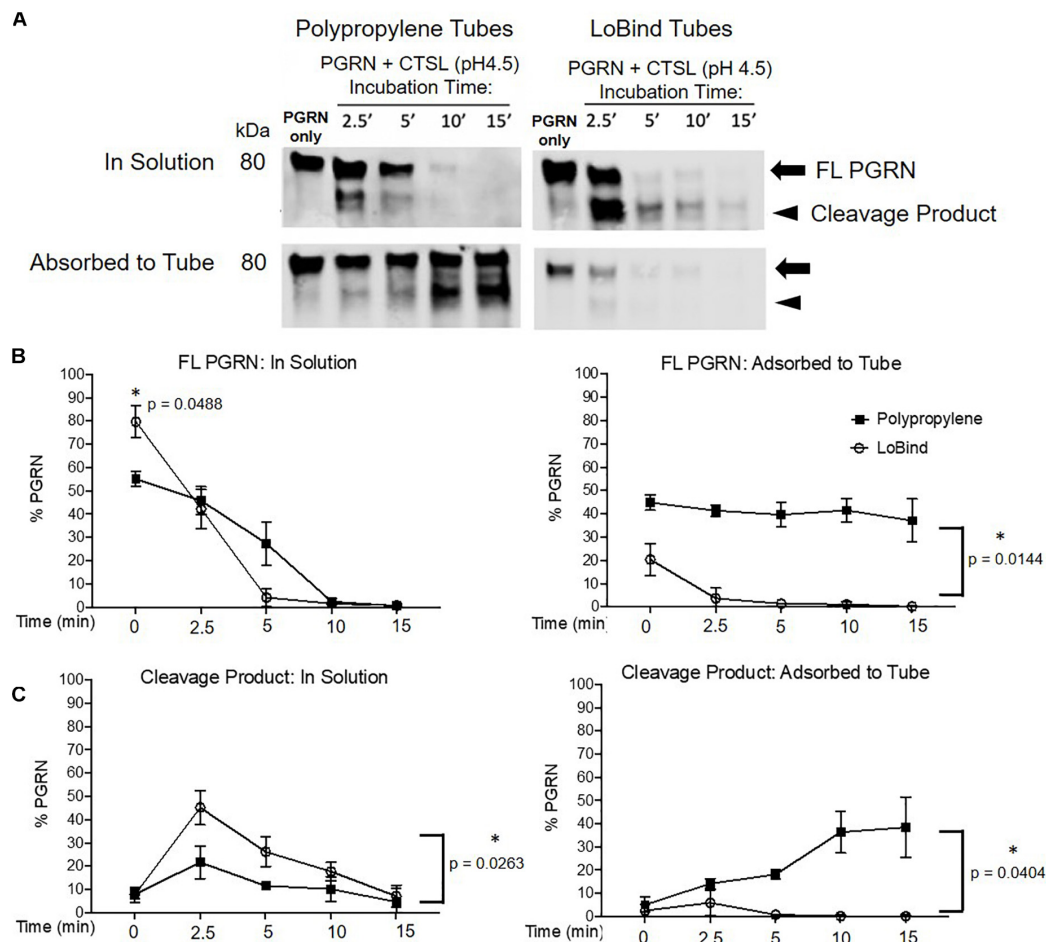


FIGURE 5 | Protease Kinetics of Cathepsin L mediated PGRN Cleavage are Disrupted in Polypropylene Tubes. **(A)** 400 ng PGRN was incubated with 250 nM of Cathepsin L for 2.5, 5, 10 and 15 min in either polypropylene or LoBind tubes. **(B,C)** Quantification of the relative percentage of full-length PGRN and its approximately 75 kDa cleavage product after incubation with Cathepsin L for the aforementioned time points. Paired *t*-tests were performed (**p* < 0.05 in solution vs. adsorbed to tube for every condition, *n* = 3). All immunoblots are representative of three independent experiments.

assays described here. The presence of BSA (a known CTSL substrate) (Völkel et al., 1996) or any other contaminant in the reaction would likely disrupt interactions between the intended binding partners. Of note, our study has not exhausted the available coating alternatives such as glycine, poly-glycine or poly-alanine. Until future studies are performed testing such coating options, we recommend LoBind tubes for studies that preclude introduction of BSA into carefully optimized assay reactions such as ours.

However, the question of whether adsorption exclusively plagues purified protein preparations is worth asking. Complex human body fluids such as blood, plasma, and CSF are the most used sources for the measurement of endogenous PGRN by ELISA immuno-assays. As previously mentioned, inherent to the affordability of currently available plate-based assays is the use of polymer plastic 96-well plates. ELISAs of plasma and serum are likely buffered by albumin, immunoglobulins and other high concentration carrier proteins that effectively coat PPE tubes to prevent lower concentration protein binding to the surface.

Indeed, the major human plasma proteins (albumin, γ -globulin, fibrinogen) are not only significantly more concentrated than PGRN by orders of magnitude, but also smaller by molecular weight, ensuring in theory that they would preferentially bind to the surface as per the Vroman effect (Anderson and Anderson, 2002). Additionally, sandwich ELISA assays such as those presently in the market for human PGRN consist of plates whose wells are coated with the capture antibody at the time of use. In combination, we believe that published reports of endogenous PGRN in human plasma and serum samples may suffer from adsorption-related errors to a negligible degree. However, it is entirely possible that protein adsorption accounts for some fraction of the reduced CSF PGRN levels found in recent studies (Wilke et al., 2016), given the decreased abundance of carrier proteins relative to blood preparations (Hühmer et al., 2006). In support, some instances of protein adsorption from complex biological samples onto tubes have been observed. For example, A β amyloid from mammalian and *C. elegans* extracts undergo adsorption to multi-well plates and Eppendorf tubes

(Murray et al., 2013), and in ventricular CSF, 370 proteins including but not limited to the most abundant proteins were reported as adsorbed to a polycarbonate surface used for microdialysis (Undin et al., 2015). Considering that circulating PGRN is increasingly referenced to as a potential biomarker for FTD and is being tested as a potential replacement therapy in clinical trials, it is imperative that a characterization study similar to ours be done in human plasma, serum, and CSF.

So, what can be done? Until such a comparison study is conducted with endogenous PGRN, it is our recommendation that rigorously consistent experimental practices minimizing adsorption should be used for all *in vitro* PGRN research. Experimental steps and conditions that are routinely part of PGRN studies such as the transfer of samples between tubes, the duration of incubation of samples in tubes, and the incubation temperature, all play an important role in the maintenance of accurate working concentrations in solution. In parallel, we recognize the limitations of our recommendation, as demonstrated by our own limitations with using BSA-coated tubes in *in vitro* assays. Our group is one of many routinely using such assays to understand the proteolytic processing of PGRN into granulins, wherein reaction conditions are established with utmost care to facilitate interactions between rhPGRN and rh proteolytic enzymes. In such instances, we recommend the consistent use of LoBind tubes, which we have adopted in all of our studies.

It must be noted that while our study has characterized adsorption of one particular rhPGRN protein (R&D), several other recombinant PGRN proteins are commercially available. Future studies examining whether polymer binding is a ubiquitous property across all rhPGRN proteins and peptides may shed light on structure, and in turn, function and biology. As a start, certain unique properties of predicted PGRN structures lend toward an interesting hypothesis—the unusually high numbers of disulfide bridges may contribute to an inflexible exterior of hydrophobic residues, a known characteristic of “sticky” proteins. The predicted structure of PGRN may be theorized as sticky throughout given the distribution of disulfide bridges, however, future testing of truncated protein including multi-granulin peptides and individual granulin peptides would help confirm or deny this hypothesis.

In this work, we have observed that ~25–40% of rhPGRN becomes adsorbed to the surface of polypropylene tubes when used for routine experimental use. This phenomenon may lead to unreliable quantification of rhPGRN and may create deleterious

effects with PGRN functional assays. Our study deems it prudent for PGRN researchers, both at the bench and in the clinic, to pay close attention to experimental design, choice of optimal labware, and to prepare PGRN-containing samples in a cautious and consistent manner.

DATA AVAILABILITY STATEMENT

The original contributions presented in the study are included in the article/**Supplementary Material**, further inquiries can be directed to the corresponding author/s.

AUTHOR CONTRIBUTIONS

SG and PS designed all experiments, analyzed all the data, and contributed equally to this work. SG and AK conceived the project. PS performed the PGRN and CTSN *in vitro* experiments and western blots. AA assisted in performing several western blots. SG performed all other experiments. SG, PS, and AK wrote the manuscript. All authors have reviewed and approved this manuscript.

FUNDING

This work was supported by the National Institutes of Health (Grant Nos. R01NS095257, R01AG059052, and P30AG061422) and Paul G. Allen Family Foundation.

ACKNOWLEDGMENTS

We would like to thank Matthew Jacobson and Wilian Coelho for advising us on the experimental design. We thank all members of the Kao lab for helpful discussions. We also thank The Paul G. Allen Family Foundation for research support.

SUPPLEMENTARY MATERIAL

The Supplementary Material for this article can be found online at: <https://www.frontiersin.org/articles/10.3389/fnins.2020.602235/full#supplementary-material>

REFERENCES

- Anderson, N. L., and Anderson, N. G. (2002). The human plasma proteome: history, character, and diagnostic prospects. *Mol. Cell Proteom.* 1, 845–867. doi: 10.1074/mcp.r200007-mcp200
- Baker, M., Mackenzie, I. R., Pickering-Brown, S. M., Gass, J., Rademakers, R., Lindholm, C., et al. (2006). Mutations in progranulin cause tau-negative frontotemporal dementia linked to chromosome 17. *Nature* 442, 916–919. doi: 10.1038/nature05016
- Butler, V. J., Cortopassi, W. A., Argouarch, A. R., Ivry, S. L., Craik, C. S., Jacobson, M. P., et al. (2019a). Progranulin Stimulates the In Vitro Maturation of Pro-Cathepsin D at Acidic pH. *J. Mole. Biol.* 431, 1038–1047. doi: 10.1016/j.jmb.2019.01.027
- Butler, V. J., Cortopassi, W. A., Gururaj, S., Wang, A. L., Pierce, O. M., Jacobson, M. P., et al. (2019b). Multi-Granulin Domain Peptides Bind to Pro-Cathepsin D and Stimulate Its Enzymatic Activity More Effectively Than Progranulin In Vitro. *Biochemistry* 58, 2670–2674. doi: 10.1021/acs.biochem.9b00275
- Butler, V. J., Gao, F., Corrales, C. I., Cortopassi, W. A., Caballero, B., Vohra, M., et al. (2019c). Age- and stress-associated C. elegans granulins impair lysosomal function and induce a compensatory HLH-30/TFEB transcriptional response. *PLoS Genet.* 15:e1008295. doi: 10.1371/journal.pgen.1008295
- Cruts, M., Gijselincx, I., van der Zee, J., Engelborghs, S., Wils, H., Pirici, D., et al. (2006). Null mutations in progranulin cause ubiquitin-positive frontotemporal dementia linked to chromosome 17q21. *Nature* 442, 920–924. doi: 10.1038/nature05017

- Fang, F., Satulovsky, J., and Szeleifer, I. (2005). Kinetics of protein adsorption and desorption on surfaces with grafted polymers. *Biophys. J.* 89, 1516–1533. doi: 10.1529/biophysj.104.055079
- Felgner, P. L., and Wilson, J. E. (1976). Hexokinase binding to polypropylene test tubes. Artificial activity losses from protein binding to disposable plastics. *Anal. Biochem.* 74, 631–635. doi: 10.1016/0003-2697(76)90251-7
- Finch, N., Baker, M., Crook, R., Swanson, K., Kuntz, K., Surtees, R., et al. (2009). Plasma progranulin levels predict progranulin mutation status in frontotemporal dementia patients and asymptomatic family members. *Brain* 132, 583–591. doi: 10.1093/brain/awn352
- Gass, J., Lee, W. C., Cook, C., Finch, N., Stetler, C., Jansen-West, K., et al. (2012). Progranulin regulates neuronal outgrowth independent of sortilin. *Mol. Neurodegener.* 7:33. doi: 10.1186/1750-1326-7-33
- Ghidoni, R., Benussi, L., Glionna, M., Franzoni, M., and Binetti, G. (2008). Low plasma progranulin levels predict progranulin mutations in frontotemporal lobar degeneration. *Neurology* 71, 1235–1239. doi: 10.1212/01.wnl.0000325058.10218.fc
- Goebel-Stengel, M., Stengel, A., Tache, Y., and Reeve, J. R. Jr. (2011). The importance of using the optimal plasticware and glassware in studies involving peptides. *Anal. Biochem.* 414, 38–46. doi: 10.1016/j.ab.2011.02.009
- He, Z., and Bateman, A. (1999). Progranulin Gene Expression Regulates Epithelial Cell Growth and Promotes Tumor Growth in Vivo. *Cancer Res.* 59, 3222–3229.
- Hühmer, A. F., Biringe, R. G., Amato, H., Fonteh, A. N., and Harrington, M. G. (2006). Protein Analysis in Human Cerebrospinal Fluid: Physiological Aspects, Current Progress and Future Challenges. *Dis. Markers* 22, 3–26. doi: 10.1155/2006/158797
- Jian, J., Konopka, J., and Liu, C. (2013). Insights into the role of progranulin in immunity, infection, and inflammation. *J. Leukoc. Biol.* 93, 199–208. doi: 10.1189/jlb.0812429
- Kanazawa, M., Kawamura, K., Takahashi, T., Miura, M., Tanaka, Y., Koyama, M., et al. (2015). Multiple therapeutic effects of progranulin on experimental acute ischaemic stroke. *Brain* 138, 1932–1948. doi: 10.1093/brain/awv079
- Kramer, K. J., Dunn, P. E., Peterson, R. C., Seballos, H. L., Sanburg, L. L., and Law, J. H. (1976). Purification and characterization of the carrier protein for juvenile hormone from the hemolymph of the tobacco hornworm *Manduca sexta* Johannson (Lepidoptera: Sphingidae). *J. Biol. Chem.* 251, 4979–4985.
- Lee, C. W., Stankowski, J. N., Chew, J., Cook, C. N., Lam, Y. W., Almeida, S., et al. (2017). The lysosomal protein cathepsin L is a progranulin protease. *Mol. Neurodegener.* 12:55.
- Matsubara, T., Mita, A., Minami, K., Hosooka, T., Kitazawa, S., Takahashi, K., et al. (2012). PGRN is a key adipokine mediating high fat diet-induced insulin resistance and obesity through IL-6 in adipose tissue. *Cell Metab.* 15, 38–50. doi: 10.1016/j.cmet.2011.12.002
- Meeter, L. H., Patzke, H., Loewen, G., Dopfer, E. G., Pijnenburg, Y. A., van Minkelen, R., et al. (2016). Progranulin Levels in Plasma and Cerebrospinal Fluid in Granulin Mutation Carriers. *Dement. Geriatr. Cogn. Dis. Extra* 6, 330–340. doi: 10.1159/000447738
- Minami, S. S., Min, S. W., Krabbe, G., Wang, C., Zhou, Y., Asgarov, R., et al. (2014). Progranulin protects against amyloid beta deposition and toxicity in Alzheimer's disease mouse models. *Nat. Med.* 20, 1157–1164. doi: 10.1038/nm.3672
- Murray, A. N., Palhano, F. L., Bieschke, J., and Kelly, J. W. (2013). Surface adsorption considerations when working with amyloid fibrils in multiwell plates and Eppendorf tubes. *Prot. Sci.* 22, 1531–1541. doi: 10.1002/pro.2339
- Nakanishi, K., Sakiyama, T., and Imamura, K. (2001). On the adsorption of proteins on solid surfaces, a common but very complicated phenomenon. *J. Biosci. Bioeng.* 91, 233–244. doi: 10.1016/s1389-1723(01)80127-4
- Nicholson, A. M., Finch, N. A., Thomas, C. S., Wojtas, A., Rutherford, N. J., Mielke, M. M., et al. (2014). Progranulin protein levels are differently regulated in plasma and CSF. *Neurology* 82, 1871–1878. doi: 10.1212/wnl.0000000000000445
- Salazar, D. A., Butler, V. J., Argouarch, A. R., Hsu, T. Y., Mason, A., Nakamura, A., et al. (2015). The Progranulin Cleavage Products, Granulins, Exacerbate TDP-43 Toxicity and Increase TDP-43 Levels. *J. Neurosci.* 35, 9315–9328. doi: 10.1523/jneurosci.4808-14.2015
- Serrero, G., Hawkins, D. M., Bejarano, P. A., Ioffe, O., Tkaczuk, K. R., Elliott, R. E., et al. (2016). Determination of GP88 (progranulin) expression in breast tumor biopsies improves the risk predictive value of the Nottingham Prognostic Index. *Diagn. Pathol.* 11:71.
- Sleegers, K., Brouwers, N., Van Damme, P., Engelborghs, S., Gijssels, I., van der Zee, J., et al. (2009). Serum biomarker for progranulin-associated frontotemporal lobar degeneration. *Ann. Neurol.* 65, 603–609. doi: 10.1002/ana.21621
- Smith, J. A., Hurrell, J. G., and Leach, S. J. (1978). Elimination of nonspecific adsorption of serum proteins by Sepharose-bound antigens. *Anal. Biochem.* 87, 299–305. doi: 10.1016/0003-2697(78)90679-6
- Smith, K. R., Damiano, J., Franceschetti, S., Carpenter, S., Canafoglia, L., Morbin, M., et al. (2012). Strikingly different clinicopathological phenotypes determined by progranulin-mutation dosage. *Am. J. Hum. Genet.* 90, 1102–1107. doi: 10.1016/j.ajhg.2012.04.021
- Sueter, C. H., and DeLuca, M. (1983). How to prevent losses of protein by adsorption to glass and plastic. *Anal. Biochem.* 135, 112–119. doi: 10.1016/0003-2697(83)90738-8
- Tanaka, Y., Matsuaki, T., Yamanouchi, K., and Nishihara, M. (2013). Increased lysosomal biogenesis in activated microglia and exacerbated neuronal damage after traumatic brain injury in progranulin-deficient mice. *Neuroscience* 250, 8–19. doi: 10.1016/j.neuroscience.2013.06.049
- Undin, T., Lind, S. B., and Dahlin, A. P. (2015). MS for investigation of time-dependent protein adsorption on surfaces in complex biological samples. *Fut. Sci. OA* 1:FSO32.
- Van Kampen, J. M., and Kay, D. G. (2017). Progranulin gene delivery reduces plaque burden and synaptic atrophy in a mouse model of Alzheimer's disease. *PLoS One* 12:e0182896. doi: 10.1371/journal.pone.0182896
- Van Kampen, J. M., Baranowski, D., and Kay, D. G. (2014). Progranulin gene delivery protects dopaminergic neurons in a mouse model of Parkinson's disease. *PLoS One* 9:e97032. doi: 10.1371/journal.pone.0097032
- Völkel, H., Kurz, U., Linder, J., Klumpp, S., Gnau, V., Jung, G., et al. (1996). Cathepsin L is an intracellular and extracellular protease in *Paramecium tetraurelia*. Purification, cloning, sequencing and specific inhibition by its expressed propeptide. *Eur. J. Biochem.* 238, 198–206. doi: 10.1111/j.1432-1033.1996.0198q.x
- Ward, M. E., Taubes, A., Chen, R., Miller, B. L., Sephton, C. F., Gelfand, J. M., et al. (2014). Early retinal neurodegeneration and impaired Ran-mediated nuclear import of TDP-43 in progranulin-deficient FTLD. *J. Exp. Med.* 211, 1937–1945. doi: 10.1084/jem.20140214
- Wilke, C., Gillardon, F., Deuschle, C., Dubois, E., Hobert, M. A., Müller, et al. (2016). Serum Levels of Progranulin Do Not Reflect Cerebrospinal Fluid Levels in Neurodegenerative Disease. *Curr. Alzheimer Res.* 13, 654–662. doi: 10.2174/1567205013666160314151247
- Wilke, C., Gillardon, F., Deuschle, C., Hobert, M. A., Jansen, I. E., Metzger, F. G., et al. (2017). Cerebrospinal Fluid Progranulin, but Not Serum Progranulin, Is Reduced in GRN-Negative Frontotemporal Dementia. *Neurodegener. Dis.* 17, 83–88. doi: 10.1159/000448896
- Xu, X., Gou, L., Zhou, M., Yang, F., Zhao, Y., Feng, T., et al. (2016). Progranulin protects against endotoxin-induced acute kidney injury by downregulating renal cell death and inflammatory responses in mice. *Int. Immunopharmacol.* 38, 409–419. doi: 10.1016/j.intimp.2016.06.022
- Yang, D., Wang, L. L., Dong, T. T., Shen, Y. H., Guo, X. S., Liu, C. Y., et al. (2015). Progranulin promotes colorectal cancer proliferation and angiogenesis through TNFR2/Akt and ERK signaling pathways. *Am. J. Cancer Res.* 5, 3085–3097.
- Zhu, J., Nathan, C., Jin, W., Sim, D., Ashcroft, G. S., Wahl, S. M., et al. (2002). Conversion of proepithelin to epithelins: roles of SLPI and elastase in host defense and wound repair. *Cell* 111, 867–878. doi: 10.1016/s0092-8674(02)01141-8

Conflict of Interest: The authors declare that the research was conducted in the absence of any commercial or financial relationships that could be construed as a potential conflict of interest.

Copyright © 2020 Gururaj, Sampognaro, Argouarch and Kao. This is an open-access article distributed under the terms of the Creative Commons Attribution License (CC BY). The use, distribution or reproduction in other forums is permitted, provided the original author(s) and the copyright owner(s) are credited and that the original publication in this journal is cited, in accordance with accepted academic practice. No use, distribution or reproduction is permitted which does not comply with these terms.



Network Diffusion Modeling Explains Longitudinal Tau PET Data

Amelie Schäfer^{1*}, Elizabeth C. Mormino² and Ellen Kuhl¹ for the Alzheimer's Disease Neuroimaging Initiative[†]

OPEN ACCESS

Edited by:

Ashish Raj,
University of California, San Francisco,
United States

Reviewed by:

José Luna-Muñoz,
Universidad Nacional Autónoma de
México, Mexico
Brian Andrew Gordon,
Washington University in St. Louis,
United States

*Correspondence:

Amelie Schäfer
amesch@stanford.edu

[†] Data used in preparation of this article were obtained from the Alzheimer's Disease Neuroimaging Initiative (ADNI) database (adni.loni.usc.edu). As such, the investigators within the ADNI contributed to the design and implementation of ADNI and/or provided data but did not participate in analysis or writing of this report. A complete listing of ADNI investigators can be found at: http://adni.loni.usc.edu/wp-content/uploads/how_to_apply/ADNI_Acknowledgement_List.pdf

Specialty section:

This article was submitted to Neurodegeneration, a section of the journal Frontiers in Neuroscience

Received: 28 May 2020

Accepted: 02 December 2020

Published: 23 December 2020

Citation:

Schäfer A, Mormino EC and Kuhl E (2020) Network Diffusion Modeling Explains Longitudinal Tau PET Data. *Front. Neurosci.* 14:566876. doi: 10.3389/fnins.2020.566876

¹ Department of Mechanical Engineering, Stanford University, Stanford, CA, United States, ² Department of Neurology and Neurological Sciences, Stanford School of Medicine, Stanford, CA, United States

Alzheimer's disease is associated with the cerebral accumulation of neurofibrillary tangles of hyperphosphorylated tau protein. The progressive occurrence of tau aggregates in different brain regions is closely related to neurodegeneration and cognitive impairment. However, our current understanding of tau propagation relies almost exclusively on postmortem histopathology, and the precise propagation dynamics of misfolded tau in the living brain remain poorly understood. Here we combine longitudinal positron emission tomography and dynamic network modeling to test the hypothesis that misfolded tau propagates preferably along neuronal connections. We follow 46 subjects for three or four annual positron emission tomography scans and compare their pathological tau profiles against brain network models of intracellular and extracellular spreading. For each subject, we identify a personalized set of model parameters that characterizes the individual progression of pathological tau. Across all subjects, the mean protein production rate was 0.21 ± 0.15 and the intracellular diffusion coefficient was 0.34 ± 0.43 . Our network diffusion model can serve as a tool to detect non-clinical symptoms at an earlier stage and make informed predictions about the timeline of neurodegeneration on an individual personalized basis.

Keywords: tau PET, Neuroimaging, model calibration, Alzheimer's disease, network diffusion model

1. INTRODUCTION

The accumulation of pathological amyloid- β and hyperphosphorylated tau protein is a classical hallmark of Alzheimer's disease that occurs years to decades before a clinical diagnosis is possible (Duyckaerts et al., 2009). The widely accepted amyloid cascade hypothesis is based on the assumption that the abnormal aggregation of amyloid- β is the disease initiator, which then causes a series of pathological events including the production and propagation of misfolded tau protein followed by neurodegeneration, regional atrophy, and ultimately cognitive impairment (Jack and Holtzman, 2013). Even though recent years have brought a better qualitative understanding of the various biomarkers involved in Alzheimer's disease (Jack et al., 2013), little is known about the causal, quantitative, and temporal relationships between those markers. Mathematical models can help establish these relations, but they often lack reliable longitudinal data for model calibration and validation.

Positron emission tomography (PET) is a non-invasive imaging technique that enables the tracking of amyloid and tau distributions in a living brain non-invasively *in vivo* (Johnson et al., 2016; Villemagne et al., 2018). The tau PET tracer [¹⁸F]-AV-1451 binds to paired helical filaments within tau's neurofibrillary tangles (NFT), as proven in postmortem studies when comparing PET

signal to histology (Marquie et al., 2015). Hyperphosphorylated tau plays a central role in disease progression due to its confirmed direct relation to neurodegeneration and cognitive impairment (Bejanin et al., 2017; Xia et al., 2017). This relation was first revealed in postmortem histological analyses showing strong correlations between the location and density of tau neurofibrillary tangles and sites of neurodegeneration (Giannakopoulos et al., 2003). Imaging studies confirmed that the intensity of *in vivo* tau PET signal was strongly correlated to regional tissue atrophy measured in longitudinal magnetic resonance images (MRI) (Gordon et al., 2018; Iaccarino et al., 2018; La Joie et al., 2020).

Today, it has become widely accepted that tau is more closely associated with the neurodegenerative process than amyloid- β (Buckley et al., 2017). The observation of pathological amyloid- β and tau protein is not unique to Alzheimer's disease and is similarly associated with healthy aging (Knopman et al., 2003). However, in Alzheimer's disease patients, the propagation sequence of tau protein differs from the one observed in cognitively unimpaired older adults and seems to follow a consistent, stereotypical and reproducible pattern: In cross-sectional autopsy studies, pathological tau first appeared in the transentorhinal cortex before spreading into neighboring regions in the limbic and temporal cortex. After this, neurofibrillary tangles were found to propagate into a wide range of the association isocortex and finally into the primary sensory cortex (Braak and Braak, 1991; Braak et al., 2006). However, the precise spreading pattern of misfolded tau, from one brain region to another, remains incompletely understood. Evidence from animal models suggests that hyperphosphorylated tau propagates along the brain's anatomical neuronal connections (De Calignon et al., 2012; Liu et al., 2012). This is in line with findings from PET imaging studies, which revealed a striking similarity between patterns of *in vivo* tau PET signal and the brain's connectome (Jones et al., 2017; Pereira et al., 2019). Studies have detected higher PET signal intensity in strongly interconnected regions, indicating increased accumulation of tau in these connectivity hubs (Cope et al., 2018).

Tau PET imaging has only been developed recently and longitudinal studies that follow the spatio-temporal distribution of tau in one and the same subject are still rare. A few longitudinal studies exist, but they are limited to a single follow-up visit (Jack et al., 2018; Harrison et al., 2019). To better understand the spreading of misfolded tau, modeling groups have implemented network diffusion and epidemic spreading models to simulate the propagation of tau through the brain and claim good performance when using functional or structural connectomes as basis for their models (Raj et al., 2012, 2015; Torok et al., 2018; Vogel et al., 2020; Weickenmeier et al., 2019). However, none of these models is validated on longitudinal tau data with multiple points in time. Instead, these studies either base their conclusions on atrophy data by postulating correlations between tau topology and atrophy (Raj et al., 2012, 2015; Torok et al., 2018), or on cross-sectional tau PET images that require additional assumptions regarding the initial conditions and model configuration (Vogel et al., 2020).

Recent studies suggest to model the accumulation and spreading of misfolded protein using partial differential equations on a network model based on the brain connectome (Raj et al., 2012; Iturria-Medina et al., 2014; Henderson et al., 2019). Within this framework, the complex pathogenic cascade of protein production, conversion, aggregation, and clearance is captured in, and simplified to, a Fisher-Kolmogorov model (Fisher, 1937; Kolmogorov et al., 1937; Fornari et al., 2019, 2020). While these models show good qualitative agreement with the pathological stages from histopathology (Braak and Braak, 1991), they have not yet been calibrated and validated with real patient data. A calibrated model of misfolded tau protein would enhance our understanding of disease progression, from a qualitative to a quantitative level. Characterizing the typical time-dependent evolution of disease biomarkers is essential for developing new diagnostic tools to detect non-clinical symptoms at an earlier stage and for evaluating potential new treatments.

Here we use longitudinal tau PET images from 46 subjects to calibrate the parameters of two competing network diffusion models based on either anisotropic intracellular spreading in a connectivity-weighted network or isotropic extracellular spreading in a distance-weighted network. A side-by-side comparison of both models with the longitudinal PET images allows us to test the hypothesis that misfolded tau spreads preferably intracellularly, along neuronal connections. In contrast to previous studies, we do not make artificial assumptions about initial tau seeding or the age at onset. Instead, we directly extract the initial conditions from the first PET scan and use the second, third, and fourth scans for personalized model calibration.

2. MATERIALS AND METHODS

2.1. Image Data Selection

Our study uses longitudinal imaging data from the Alzheimer's Disease Neuroimaging Initiative database (ADNI), a multisite, longitudinal, public database of MRI and PET images for normal cognitive aging, mild cognitive impairment, and early Alzheimer's disease ADNI (2020). We include data from 46 participants who have undergone at least three consecutive annual tau PET scans. Of these, 16 are diagnosed as cognitively normal, 9 with significant memory concern, 19 with mild cognitive impairment, and two with clinically confirmed Alzheimer's disease. A total of 26 are classified as amyloid positive based on previously evaluated β -amyloid PET images (Landau et al., 2013). To decrease bias, we conduct our study blind to diagnosis status. All acquired AV1451-PET scans have previously been preprocessed according to standard ADNI protocols (ADNI, 2020) to be co-registered and averaged, and to have a standardized image and voxel size and a uniform image resolution of 8 mm FWHM. For each PET scan, we obtain a corresponding high resolution T1 weighted magnetic resonance image (MRI) from the database, recorded on average within 3 months prior or post PET acquisition. When a concurrent MRI scan is not available, we use data acquired at the closest visit in time. The average time span between longitudinal tau PET scans was 1.0 year, ranging from 0.6 to 2.8 years.

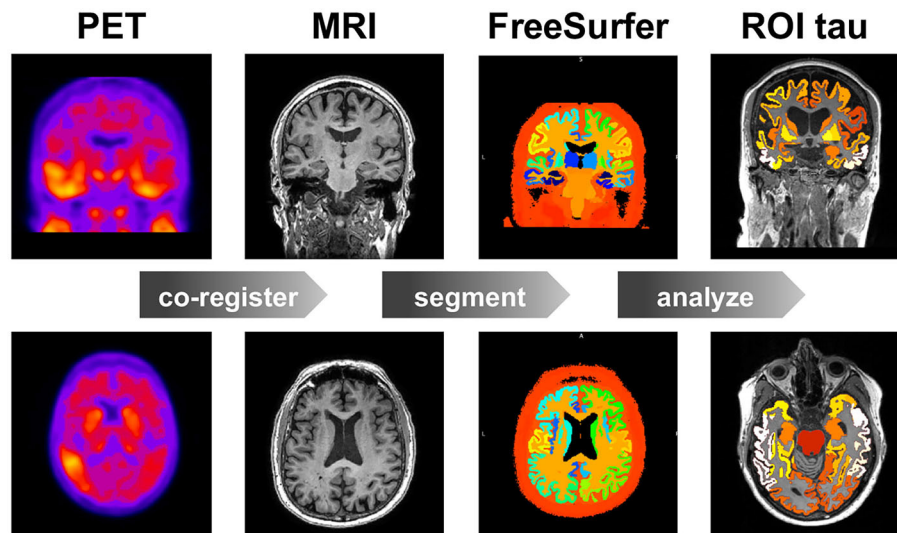


FIGURE 1 | Image data analysis. Workflow for region of interest (ROI) based positron emission tomography (PET) image analysis. For each subject, at each time point, we co-register the PET images to the T1 weighted magnetic resonance images (MRI), which we segment using FreeSurfer to calculate the standardized uptake value ratios (SUVR) for each region of interest (ROI). Our study contains 46 subjects, 3–4 time points, and 83 regions of interest.

2.2. Image Data Analysis

For each subject, we analyze the longitudinal PET data using the method summarized in **Figure 1** (Baker et al., 2017). Briefly, we co-register the PET images to the corresponding MRI scan using SPM (SPM, 2020) with 4th degree spline interpolation and run a full reconstruction of the T1 MRI using FreeSurfer (FreeSurfer, 2020). This segments the brain into 68 cortical and 45 subcortical regions and allows us to extract regional values of tau binding from the PET images. We define an inferior cerebellar gray matter reference region using the SUI template (Diedrichsen, 2006), which we reverse normalize into the subject's native T1 MRI space. To create regional standardized uptake value ratios (SUVR), we normalize all regional uptake values with respect to the tracer uptake value from the reference region. Known off-target binding sites, e.g., the basal ganglia and vascular structures like the choroid plexus and dural venous sinuses, have been shown to contaminate the AV1451 PET signal in subcortical regions and the hippocampus (Lowe et al., 2016; Marquié et al., 2017; Lemoine et al., 2018). We exclude these regions from the analysis and focus our model optimization on the 66 remaining cortical regions.

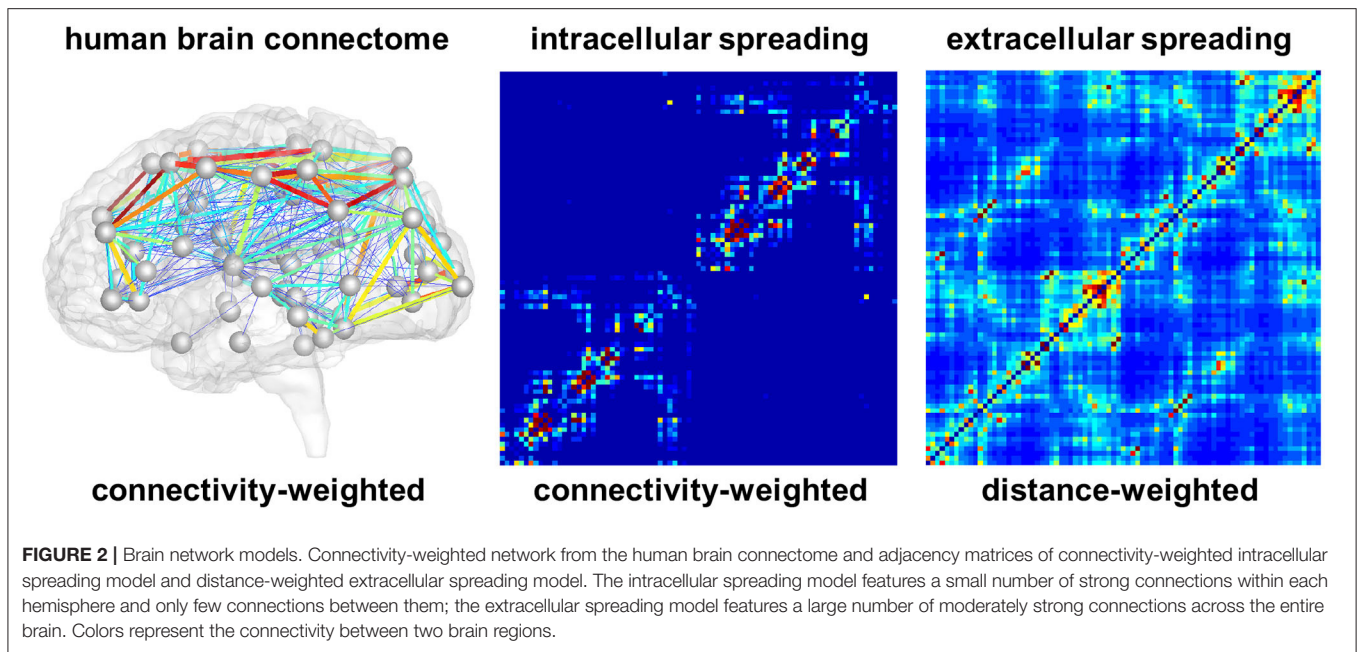
2.3. Brain Network Modeling

We model the spreading of hyperphosphorylated tau in the brain as a diffusion process within a network, which we represent as a weighted undirected graph \mathcal{G} with N nodes and E edges. To test the hypothesis of preferred tau spreading along neuronal connections, we create two competing network models, a connectivity-weighted network for anisotropic intracellular

spreading and a distance-weighted network for isotropic extracellular spreading.

For the connectivity-weighted network, we extract the graph \mathcal{G}^{con} from diffusion tensor MRI data of 418 healthy subjects from the Human Connectome Project (McNab et al., 2013) using the Budapest Reference Connectome v. 3.0 (Szalkai et al., 2017). We map the original graph with $N = 1,015$ nodes onto a graph with $N = 83$ nodes (Fornari et al., 2019). These 83 nodes correspond to the brain regions extracted in the FreeSurfer segmentation of cortex and subcortex, allowing us to directly compare our model degrees of freedom with the regional tau signal. **Figure 2** shows the connectivity-weighted network with strong connections in red and weak connections in blue. In this graph, each edge is weighted by the average number of fibers n_{ij} detected between two nodes i and j divided by the average fiber length l_{ij} along this connection across all 418 brains. This introduces the adjacency matrix of the connectivity-weighted network as $A_{ij}^{\text{con}} = n_{ij}/l_{ij}$. **Figure 2** shows the adjacency matrix of the connectivity-weighted intracellular spreading model with a small number of strong connections within each hemisphere and only few connections between them.

For the distance-weighted network, we construct a graph $\mathcal{G}^{\text{dist}}$ with the same 83 nodes as the first graph \mathcal{G}^{con} . However, for this case, we define an edge between each pair of nodes and weight it by the inverse of the Euclidian distance d_{ij} between the two nodes. This introduces the adjacency matrix of the distance-weighted network as $A_{ij}^{\text{dist}} = 1/d_{ij}$. **Figure 2** shows the adjacency matrix of the distance-weighted extracellular spreading model with a large number of moderately strong connections across the entire brain.



2.4. Network Diffusion Modeling

Motivated by the hypothesis that tau protein misfolds and spreads in a prion-like fashion (Jucker and Walker, 2011; Fornari et al., 2020), we use a Fisher-Kolmogorov model (Fisher, 1937; Kolmogorov et al., 1937) to characterize the accumulation of pathological tau in the brain (Fornari et al., 2019; Thompson et al., 2020). The model is governed by a single non-linear reaction-diffusion equation that predicts the spatio-temporal evolution of the unknown, the concentration of misfolded protein c ,

$$\frac{dc}{dt} = \nabla \cdot (\mathbf{D} \cdot \nabla c) + \alpha c [1 - c], \quad (1)$$

where \mathbf{D} and α denote the diffusion tensor and the local production rate of misfolded protein. The production rate α captures the processes of protein production, clearance, and conversion (Fornari et al., 2019). To model diffusion within a network, we discretize Equation (1) on the undirected graphs \mathcal{G}^{con} and $\mathcal{G}^{\text{dist}}$. We introduce the concentration of misfolded proteins c_i at all $i = 1, \dots, N$ nodes and express the change in the concentration as

$$\frac{dc_i}{dt} = -\kappa \sum_{j=1}^N L_{ij} c_j + \alpha c_i [1 - c_i], \quad (2)$$

where κ characterizes the global diffusion between two regions and α the local production or clearance of misfolded protein. A central element of Equation (2) is the weighted graph Laplacian L_{ij} , a square matrix, which we construct from the adjacency matrix A_{ij} . The sum of all elements across each row of the

adjacency matrix A_{ij} defines the degree matrix D_{ii} ,

$$D_{ii} = \text{diag} \sum_{j=1, j \neq i}^N A_{ij}. \quad (3)$$

The graph Laplacian L_{ij} , the difference of the degree matrix and the adjacency matrix, summarizes the connectivity of the graph,

$$L_{ij} = D_{ij} - A_{ij}. \quad (4)$$

For each subject, we identify a personal diffusion coefficient κ and a personal protein production rate α that best characterize the progression of pathological tau from their individual longitudinal PET scans. Depending on the type of model, we replace the adjacency matrix A_{ij} in Equations (3) and (4) with the connectivity weighted or distance weighted adjacency matrix, A_{ij}^{con} or A_{ij}^{dist} . For comparison, we normalize both matrices such that their entries lie within the $[0, \dots, 1]$ interval. Using these normalized matrices, we identify the intracellular or extracellular diffusion coefficient κ and the production rate α .

2.5. Parameter Identification

The simulation with the network diffusion model provides a region-specific normalized concentration c^{sim} with values between zero, for no misfolded protein, and one, for a maximum misfolded protein concentration, $0 \leq c^{\text{sim}} \leq 1$. To map the recorded PET standardized uptake value ratios into a zero-to-one interval, we fit a two-component Gaussian mixture model to the raw PET data from all subjects, time points, and regions. We assume that many regions and subjects are free from pathological tau and use this distribution to identify a tau positivity threshold of 1.1. We set all values below this threshold to zero and map the remaining values c^{raw} onto the scaled values c^{pet} using

the maximum and minimum non-zero PET signals $c^{\max} = \max\{c^{\text{raw}}\}$ and $c^{\min} = \min\{c^{\text{raw}}\}$ as $c^{\text{pet}} = [c^{\text{raw}} - c^{\min}] / [c^{\max} - c^{\min}]$, such that $0 \leq c^{\text{pet}} \leq 1$. We adopt a least squares optimization to identify the personalized diffusion coefficients κ and production rates α that best reproduce the progression of tau for each subject. Specifically, we optimize the parameter set for the connectivity-weighted and the distance-weighted networks by minimizing the squared error between the simulated concentrations $c_{i,t}^{\text{sim}}$ and the PET recorded concentrations $c_{i,t}^{\text{pet}}$ within one subject for all $i = 1, \dots, n_{\text{roi}}$ regions of interest and all $t = 1, \dots, n_{\text{visit}}$ follow-up visits,

$$\text{err} = \sum_{i=1}^{n_{\text{roi}}} \sum_{t=1}^{n_{\text{visit}}} \beta [c_{i,t}^{\text{sim}}(\kappa, \alpha) - c_{i,t}^{\text{pet}}]^2. \quad (5)$$

Here, β is a scalar factor to improve numerical stability, n_{roi} is the number of cortical regions for which we have high confidence data according to section 2.2.

2.6. Model Performance

For comparison, we perform the optimization on three null models to probe the importance of the different model components. For the first null model, we leave out the term for local protein production, $\alpha = 0$, and optimize solely the diffusion coefficient κ . For the second null model, we leave out the diffusion term, $\kappa = 0$, and optimize solely the protein production rate α . For the third null model, we assume that tau is neither spreading nor produced, $\kappa = 0, \alpha = 0$, which implies that the protein concentration in each region remains constant across all follow-up visits. We identify the subjects with positive production rate, $\alpha > 0$. We assume these are the subjects with pathological tau expression who are more likely to develop or have signs of Alzheimer's disease and focus our further analysis on this subgroup. For the two network models and the three null models, we compare the performance in terms of the global residual error across all subjects, all cortical regions of interest, and all follow-up visits. We plot the observed vs. predicted values and calculate a correlation coefficient to illustrate the quality of the respective fits. We use paired-sample t-tests to determine whether differences in subject-wise prediction error between different models are significant. Furthermore, we use Fisher's R-to-z transform to determine whether differences in correlation coefficients between different models are significant.

2.7. Model Prediction

Our dataset only spans a time period of 2–3 years whereas the accumulation of tau typically spans a period of around 15 years (Bateman et al., 2012). We use the connectivity-weighted intracellular model and distance-weighted extracellular model to predict the tau concentrations across the brains of all 46 subjects for a time window of 15 years. This allows us to explore the long-term performance of the two models, compare their predictions against histopathological findings, and test our hypothesis of intracellular spreading.

3. RESULTS

3.1. Regional Tau PET Concentration

Figure 3 illustrates the regional average standardized uptake value ratios across all subjects and visits on a template brain surface. The temporal lobes show the highest tau PET signal intensity, followed by occipital and frontal lobes. The precentral and postcentral gyrus display the lowest tau signal intensities.

3.2. Longitudinal Tau PET Concentration

Figure 4 illustrates the results of our image analysis for all 46 subjects, shown as blocks of columns, all time points, shown as columns, and 66 cortical regions as well as the hippocampus, shown as rows. The color code indicates the normalized tau standardized uptake value ratios. On the horizontal axis, subjects are ordered according to their overall tau load averaged across all regions and visits, with the most affected subject on the left and the least affected subject on the right. On the vertical axis, regions are ordered with respect to their overall tau load averaged across all subjects and visits with the regions showing the highest involvement at the top and regions with the lowest involvement at the bottom. The inferiortemporal, middletemporal, and fusiform gyrus, the amygdalae, and the hippocampus are the regions that are most consistently affected with high tau signals. They are followed by the inferiorparietal lobule, the precuneus, the entorhinal cortex, and the temporalpole. Interestingly, we see bands of moderately but consistently affected regions involving the orbitofrontal cortex, the frontalpole, and the inferiorfrontal gyrus including the parsorbitalis, parstriangularis, and parsopercularis. For most regions, the right hemisphere seems to be less affected by tau than the left hemisphere. This asymmetry is especially prominent for the temporalpole, the inferiorfrontal gyrus, the middlefrontal gyri, and the posterior cingulate cortex. The precentral, paracentral, and postcentral gyrus are the least affected regions. The hippocampus and amygdalae appear to be affected above average in most subjects, even in subjects with very low tau signal in all other regions of interest.

3.3. Parameter Identification

Figure 5 indicates the ranges of the personalized production rates α and diffusion coefficients κ for the connectivity-weighted intracellular and distance-weighted extracellular diffusion models for 21 subjects. Out of the 46 subjects, 21 exhibited a longitudinal tau signal that was best fit using a positive protein production rate, $\alpha > 0$ and 25 exhibited a signal best fit using a negative production rate, $\alpha < 0$. We postulate that the 21 subjects with a positive production rate are the subjects with pathological tau expression who are more likely to develop Alzheimer's disease and focus on the results of this subgroup. The majority of these 21 subjects, 16 out of 21, were identified with a positive amyloid status. Of the remaining five, two had no amyloid status reported, one reported a positive cerebrospinal fluid amyloid status, and two reported a negative PET and cerebrospinal fluid amyloid status. While the production rates for the connectivity-weighted intracellular and distance-weighted extracellular models with

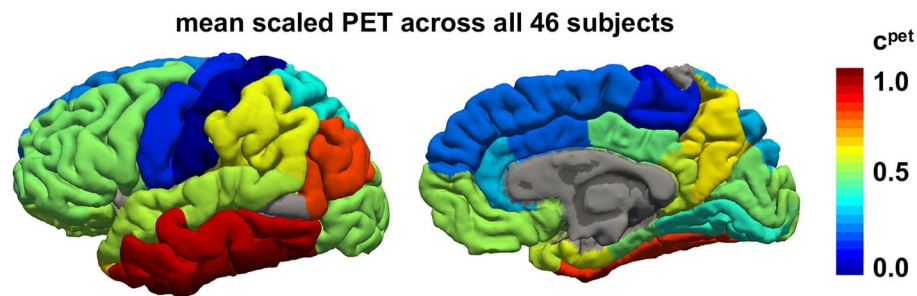


FIGURE 3 | Regional tau PET concentration. Mean tau concentration from PET scans across all 46 subjects with 3–4 annual scans across all brain regions. Red regions consistently exhibit high tau loads in all subjects while blue regions tend to be free of tau in most subjects.

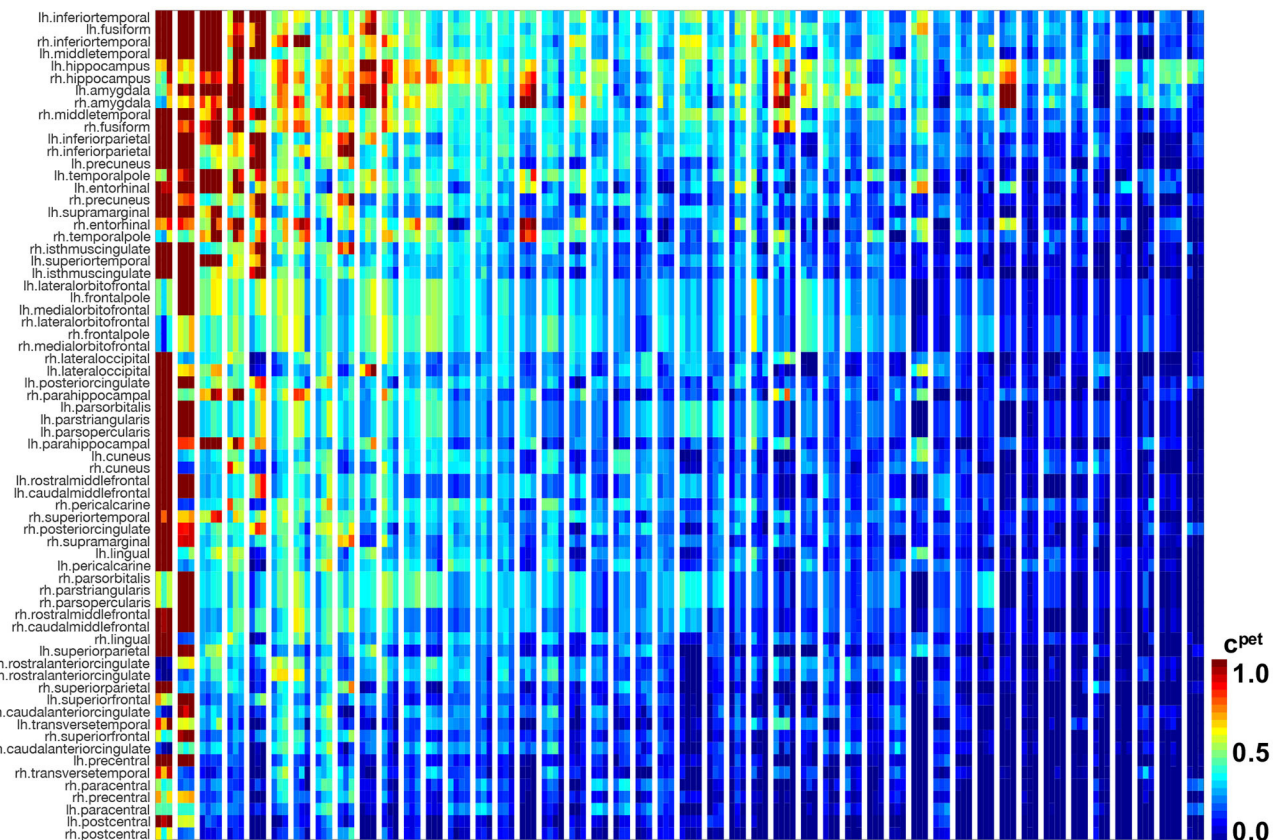


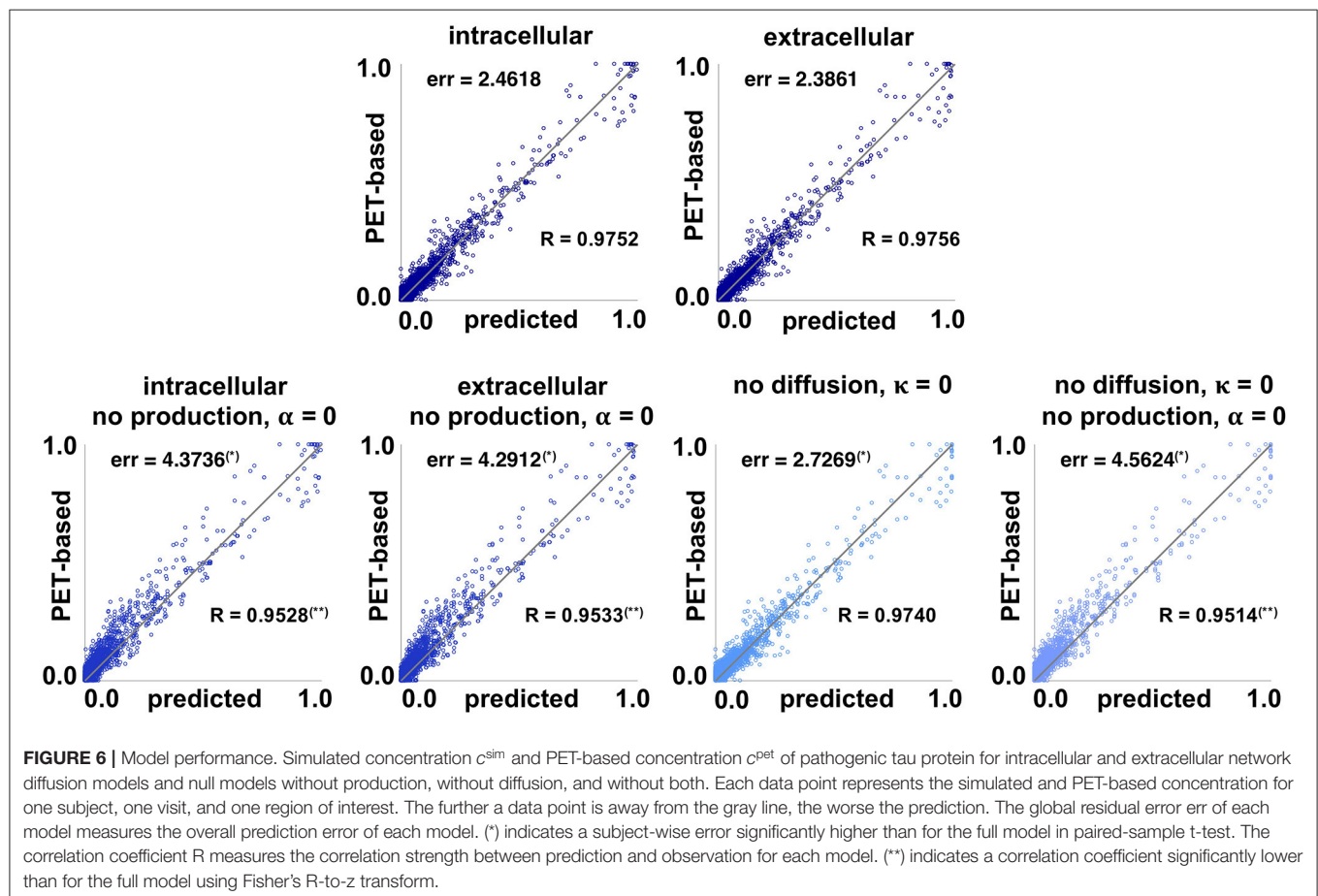
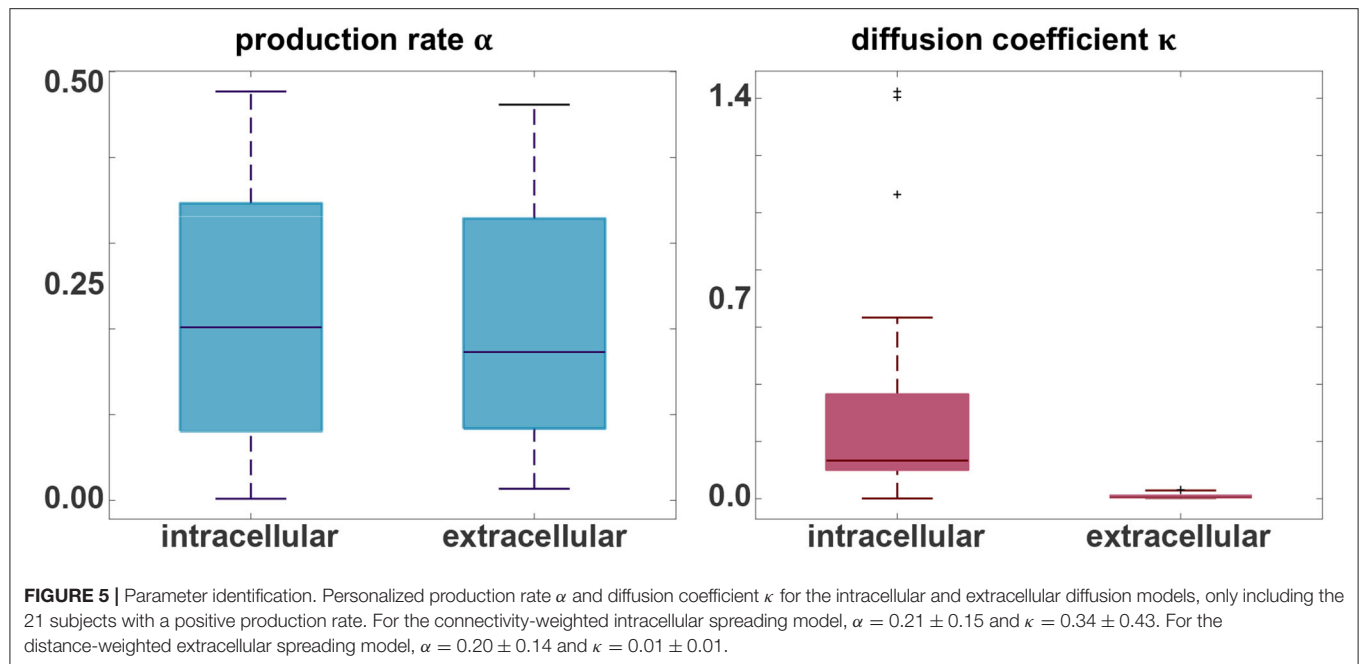
FIGURE 4 | Longitudinal tau PET concentration. Standardized uptake value ratios from PET scans for 46 subjects with 3–4 annual scans in 66 cortical regions and the hippocampus. Regions on the vertical axis are sorted by mean tau load, from top to bottom. Subjects on the horizontal axis are sorted by mean tau load across all regions and visits, from left to right. Each block of columns represents data for one subject. Within each block, each subcolumn represents data from one annual PET scan.

$\alpha = 0.21 \pm 0.15$ and $\alpha = 0.20 \pm 0.14$ are in a similar range, the diffusion coefficient for the connectivity-based model with $\kappa = 0.34 \pm 0.43$ is notably larger than for the distance-weighted model with $\kappa = 0.01 \pm 0.01$. This difference in the diffusion coefficients compensates the difference in magnitude of the entries in the adjacency matrices of the two models, which we can see in **Figure 2**. For the connectivity-weighted intracellular model, the diffusion coefficient κ shows three outliers associated

with subjects that exhibit more and faster spreading than the average subject.

3.4. Model Performance

Figure 6 summarizes the performance of the two network models compared to the four null models described in section 2.6, the intracellular and extracellular spreading models without production, the pure production model



without diffusion, and a model without diffusion and production. Each data point represents the simulated

concentration c^{sim} and PET-based concentration c^{pet} for one subject, one visit, and one region of interest.

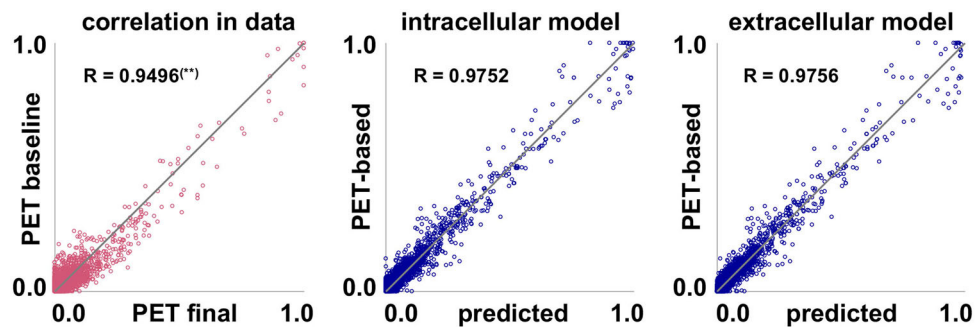


FIGURE 7 | Model performance. Inherent data correlation. Baseline and final PET-based concentrations c^{pet} , and simulated concentration c^{sim} over PET-based concentration c^{pet} of pathogenic tau protein for intracellular and extracellular network diffusion models. Each data point represents the PET-based concentration for one subject, one region of interest, and one visit. (**) Correlation coefficient R is significantly lower than for the two proposed models.

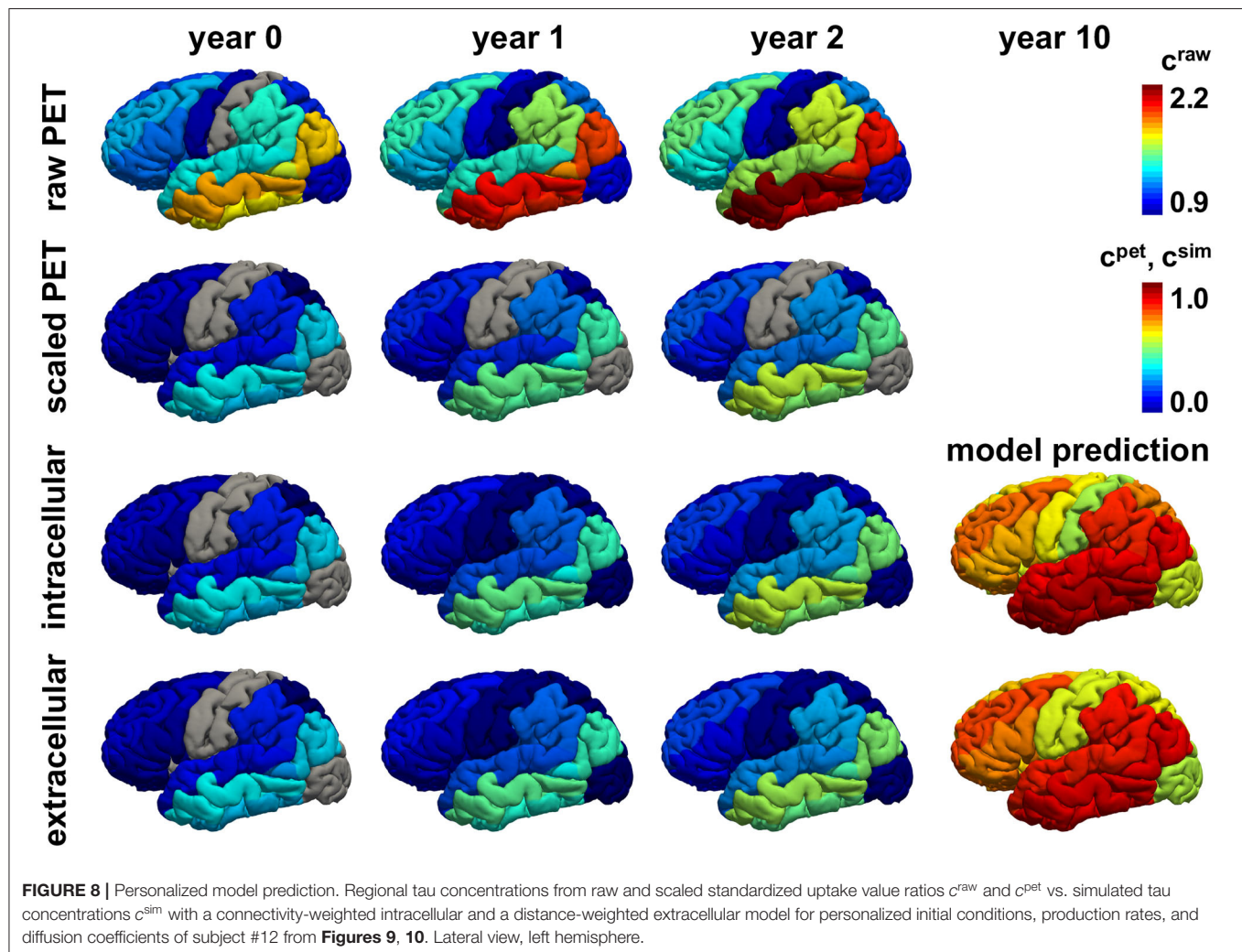
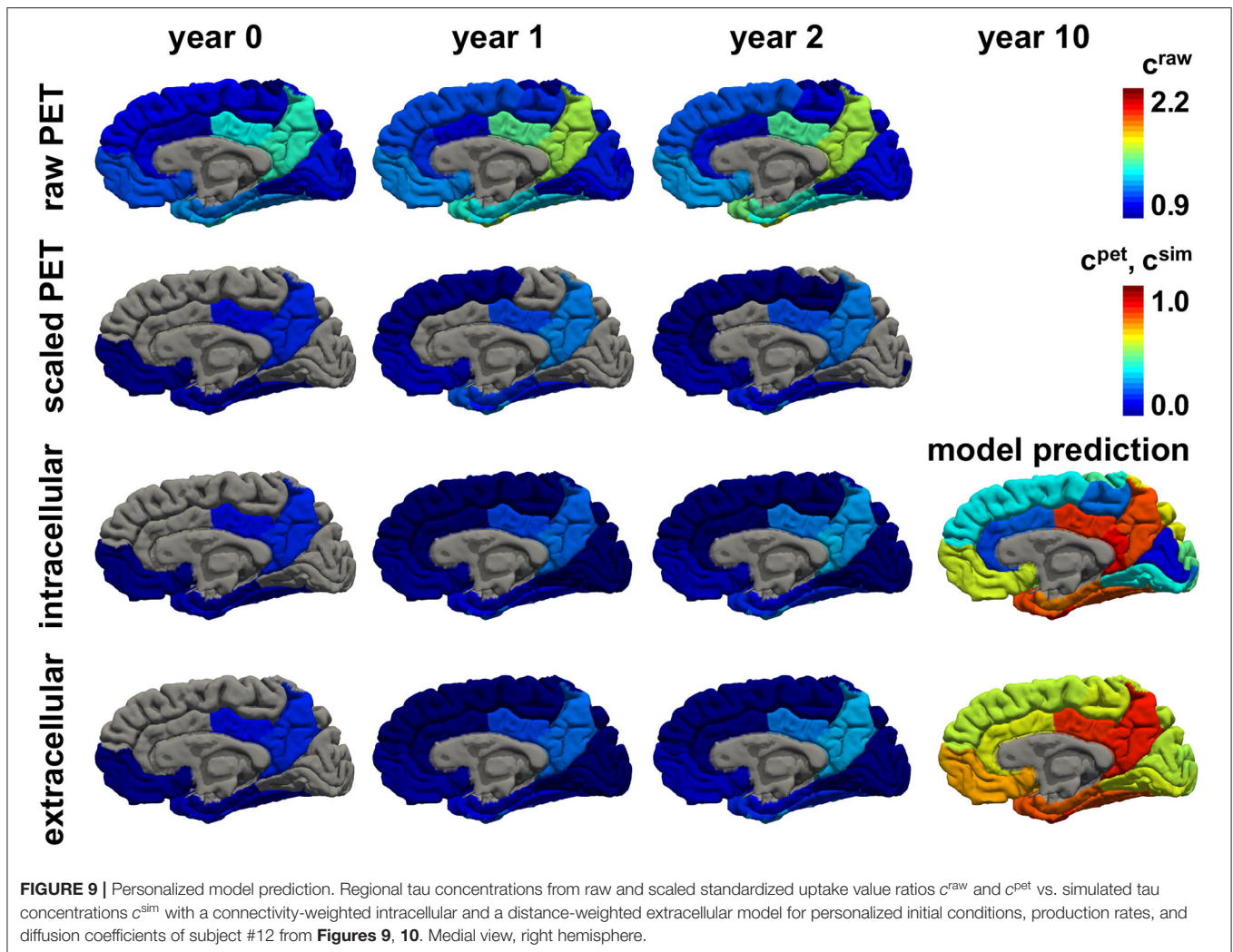


FIGURE 8 | Personalized model prediction. Regional tau concentrations from raw and scaled standardized uptake value ratios c^{raw} and c^{pet} vs. simulated tau concentrations c^{sim} with a connectivity-weighted intracellular and a distance-weighted extracellular model for personalized initial conditions, production rates, and diffusion coefficients of subject #12 from **Figures 9, 10**. Lateral view, left hemisphere.

For an ideal fit, all points would lie on the gray diagonal line.

The lowest residual error, and best correlation between the simulated and PET-based concentration was achieved with the distance-weighted extracellular model with $\text{err} = 2.3861$ and

$R = 0.9756$, followed closely by the connectivity-weighted intracellular model with $\text{err} = 2.4618$ and $R = 0.9752$. A paired-sample t-test showed no significant difference between the subject-wise errors associated with extracellular and intracellular models ($p_{\text{err}} = 0.07$). Fisher's R-to-z transform showed



no significant difference between the correlation coefficients associated with extracellular and intracellular models ($p_R = 0.59$). Eliminating the production term from the diffusion equation, $\alpha = 0$, significantly increased the prediction errors for both the intracellular and extracellular models, to $err = 4.3736$ ($p_{err} = 5.7e-04$) and $err = 4.2912$ ($p_{err} = 6.0e-04$). The correlation coefficients significantly decreased to $R = 0.9528$ ($p_R = 0.0$) and $R = 0.9533$ ($p_R = 0.0$) when eliminating the production term. The prediction error of the null model without diffusion, $\kappa = 0$, with $err = 2.7269$ is significantly higher than with the full models ($p_{err} = 0.002$, $p_{err} = 0.0015$), but significantly lower than with the null models without production ($p_{err} = 0.0012$, $p_{err} = 0.0016$). This is not surprising, when considering how close to zero the diffusion coefficient was for the distance-weighted extracellular model in **Figure 5**. Notably, the correlation coefficient $R = 0.9740$ is not significantly lower for the model without diffusion compared to the full models with diffusion ($p_R = 0.0012$). The final null model, which assumes that all tau concentrations remain constant at the value from the first scan, results in the largest residual error of $err = 4.5624$ with significantly higher subject-wise prediction errors

than all other null models ($p_{err} \leq 0.0051$) and significantly lower correlation strength $R = 0.9514$ ($p_R = 0.0$). On the personalized level, the distance-weighted extracellular model performs better for 13 subjects and the connectivity-weighted intracellular model performs better for the remaining 8. The model performance suggests that the production term α is a critical component of the tau pathology model that significantly affects the quality of model prediction. Additionally, we see that the data imply existing tau propagation from region to region, even though the diffusion term seems to have overall less importance than the production term. Finally, even with the most simplified null model for which the tau PET concentration does not change in time, the data points are, even though slightly scattered, still relatively close to the diagonal line that marks the perfect correlation between simulation and PET data. This emphasizes the limitation of the current approach, which only contains longitudinal data from 2 to 3 years. We will continuously update our model as more time points become available to address this limitation.

Figure 7 illustrates the correlation between baseline and final observed PET data for all subjects and regions of interest. The

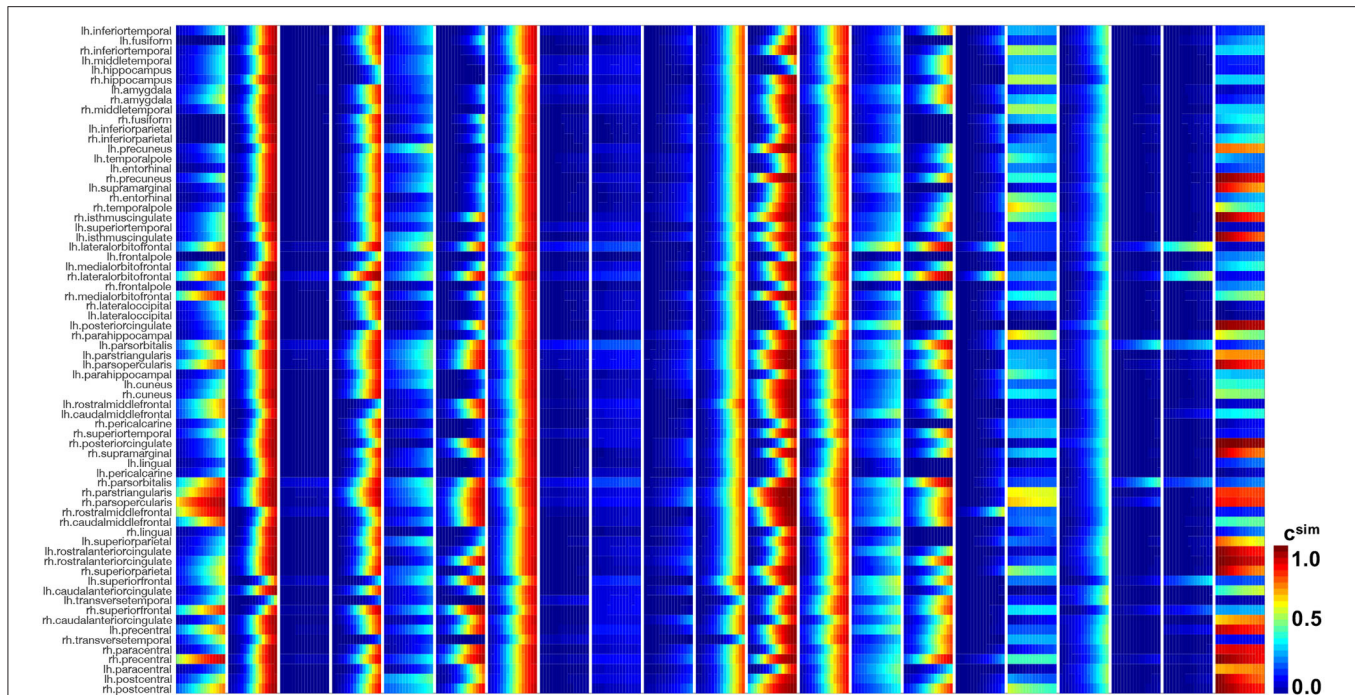


FIGURE 10 | Model prediction of intracellular model. Simulated tau concentrations c^{sim} with connectivity-weighted intracellular model for 21 subjects for 15 years in 66 cortical regions and the hippocampus. Each block of columns represents the simulation for one subject with their personalized initial conditions, production rate α , and diffusion coefficient κ . Within each block, each subcolumn represents simulated concentrations for 1 year.

plot shows that the data inherently exhibits a high correlation, with a correlation coefficient of $R = 0.9496$. This again highlights how small the observed changes in tau load are over the observation period of 2–4 years. Fisher's R-to-z transform however confirms that the correlation significantly increases with our proposed intracellular and extracellular models ($p_R = 0.0$).

3.5. Model Prediction

To investigate the predictive nature of the connectivity-based intracellular and distance-based extracellular models, we simulate the spatio-temporal pathogenic tau distribution for all 21 subjects with positive production rate throughout a period of 15 years using the models from sections 2.3, 2.4 with the personalized initial conditions, production rate α , and diffusion coefficient κ .

Figures 8, 9 show the personalized model predictions for a single subject, with personalized initial conditions, production rates, and diffusion coefficients. The first and second row showcase the PET tau concentrations from the raw and scaled standardized uptake value ratios c^{raw} and c^{pet} for 3 years. The third and fourth row show the simulated tau concentrations c^{sim} from the connectivity-weighted intracellular model with $\alpha = 0.422$ and $\kappa = 0.133$ and the distance-weighted extracellular model with $\alpha = 0.437$ and $\kappa = 0.007$ for the first 3 years and for year 10. Both models first follow the observed PET concentration closely with only marginal differences in the predictions. However, after 10 years, the

predicted tau concentration pattern from the intracellular model is much more heterogeneous than the concentration from the extracellular model. This is especially visible in the medial view of the right hemisphere in Figure 9, where the colors of the intracellular model still range from dark blue to red, whereas in the extracellular model predicts values in the color range from yellow to red.

Figures 10, 11 show the predictions for the connectivity-weighted intracellular model and the distance-weighted extracellular model. Each block of columns represents the simulation for one subject for the 15-year window. For some subjects, the predicted long-term response is similar for both models. However, in most subjects, the predicted pathological pattern differs between the intracellular and extracellular approach. Interestingly, the intracellular model maintains a staggered and sequential involvement of different regions within one subject, the extracellular model predicts a more homogeneous and smoothed spatial distribution of pathological tau protein. In this sense, the intracellular model preserves the inhomogeneous topology of the tau spreading process, in which individual regions of the cortex begin to express high concentrations of pathological tau in a sequential way, with successively more regions affected over time. In contrast, the extracellular model predicts a gradual increase in pathological tau protein, but involves all regions homogeneously at the same time.

even in late disease stages were the primary sensory areas and primary motor field in the precentral and postcentral gyrus. Our data roughly follows this sequence, with the hippocampus and amygdalae affected early on and in many subjects and the postcentral and precentral gyri affected the least across all subjects. The results of our analysis imply less involvement of the entorhinal cortex than expected according to Braak's stages. This discrepancy could originate from technical limitations of our PET image analysis. The entorhinal cortex is a very small structure and the standardized PET image resolution is low due to the multi-site nature of the ADNI database. Thus, uptake value measurements in the entorhinal region could be compromised through bleed in from other regions and tissues.

Unavoidably, all segmentation and co-registration algorithms are associated with a certain error. For FreeSurfer's parcellation and segmentation algorithm, the entorhinal cortex is associated with a relatively low correlation between manual and automated segmentation when compared to other regions (Desikan et al., 2006; McCarthy et al., 2015). Therefore, errors in segmentation, co-registration and the low PET resolution may have caused inaccuracies in our measurements for the entorhinal cortex and led to the resulting low rankings of 15 and 18 in our sequence. However, a longitudinal PET study has recently shown that early tau accumulation can be more widespread and is not necessarily confined just to the entorhinal cortex in all individuals (Jack et al., 2018). The tau PET signal in the hippocampus is known to be often compromised by off-target binding to the nearby choroid plexus (Lemoine et al., 2018). This could explain, why we observe consistently high binding to the hippocampus in our dataset, even in subjects that have a very low tau load in all other regions. Overall, the results from our longitudinal image analysis are reasonable, especially when considering the integral image quality, and are in general agreement with existing literature.

We identified the parameters of two network diffusion models using longitudinal PET data of 46 subjects. We then focused on the 21 subjects with a positive protein production rate. We postulate that those individuals are most likely to follow the typical Alzheimer's disease cascade with prion-like tau pathology. The majority of those subjects had been classified as amyloid positive, which supports our hypothesis, and indicates an abnormal accumulation of amyloid- β prior to the observed accumulation of tau. The distribution of personalized model parameters from the model optimization process exhibits a notable variance considering inter-individual differences in disease progression. In a recent study, which compared the performance of a connectivity-based to a distance-based network model with respect to cross-sectional tau PET data of 312 subjects, the connectivity-based model was clearly superior in reproducing the data (Vogel et al., 2020). However, when directly comparing the two models with respect to our longitudinal tau data, we did not see a clear superiority of the connectivity-weighted model. In fact, both models performed nearly equally well, resulting in good correlations between simulated and observed tau PET distributions over time. This is likely due to the limited time span of our data, covering disease development only within 3–4 years. We found the change in tau burden—especially the propagation from region to region—to be so low that even a model without diffusion term would simulate the data

acceptably well. Solely based on our parameter identification, it is thus not possible to solidly confirm the hypothesis that tau spreads along the brain's connectome. However, when comparing the long-term prediction of the two models, we found that the connectivity-weighted intracellular model predicts more defined and distinct distributions of tau that are in line with the histopathologically observed heterogeneity of tangle spread. As more longitudinal tau PET data become available over the course of the next years, we will revisit our analysis to draw more sophisticated conclusions and confirm or disprove our hypothesis.

While our connectivity-based network diffusion model is able to describe the spatio-temporal evolution in our data well, it is still associated with some residual error. These shortcomings of the model may arise from the fact that there could be other factors influencing the spread of misfolded tau through the brain. For example, it has been suggested that differences in gene expression between regions could cause regionally varying production and clearance rates of healthy or misfolded tau and thereby affect the progression of pathology (Grothe et al., 2018). This regional vulnerability could be included in our model in the future by allowing the production rate α to be a region-specific parameter informed by gene expression.

We have previously proposed and examined a coupled non-linear finite element model for the simulation of Alzheimer's disease related atrophy dependent on local tau pathology (Weickenmeier et al., 2018; Schäfer et al., 2019). The model parameters of our network diffusion model could directly be applied to inform neurodegeneration models. Since more and more studies are confirming a qualitative correlation between tau pathology and regional brain atrophy measurements (Harrison et al., 2019; La Joie et al., 2020), our next step will be to characterize this correlation more quantitatively using our coupled model informed by the here presented longitudinal tau PET data on the one hand and longitudinal atrophy measurements from structural MRI of the same patients on the other hand.

This study comes with several limitations, some of which can naturally be addressed as more data become available: First, the size of our cohort was limited to a small number of subjects with a sufficient number of follow-up tau PET scans. Our data show that there is a lot of inter-subject variability in tau PET data. Including more subjects, will increase statistical power and make it easier to deduce clear trends for disease progression and typical tau pathology. To counteract potential overfitting, in the future, we will use Bayesian hierarchical modeling, a statistical approach allowing for the inference of personalized parameters drawn from a common distribution. This will allow us to account for commonalities between all subjects while simultaneously attesting to inter-subject variability. Second, the maximum number of visits per subject was limited to four. As subjects will return for future scans, we will be able to follow the observations in individual subjects over longer periods of time and evaluate the longitudinal performance of our model. While histopathology shows that truncated tau proteins prevail and the presence of hyperphosphorylated tau decreases as the disease advances, our study does not show a clear trend in this direction, which could be a result of the limited amount of data

and the short time window of observation. We will keep adding future studies of years 5 and 6 to our analysis and hope to see a clearer trend in the future. Third, since ADNI is a multi-center study, the images are acquired on various scanner types with various different resolutions. To balance these differences in image quality, all data used in this work were standardized to the lowest common resolution. This low resolution in PET images intensifies partial volume effects, since multiple tissue types can be contained in one voxel, resulting in contamination of regional intensities through wash-out and bleed-in.

5. CONCLUSION

We proposed a new method to calibrate different network diffusion models using longitudinal tau PET data. We identified personalized model parameters that characterize the individual nature of tau pathology progression in 46 subjects. Specifically, we used the misfolded protein production rate to stratify all subjects into those with a positive production rate, more likely to develop neurodegeneration, and those with a negative production rate. For the subjects with a positive production rate, we found a mean production rate of 0.21 ± 0.15 and a mean intracellular diffusion coefficient of 0.34 ± 0.43 . Our results suggest that the propagation of misfolded tau from region to region is slow in most subjects—barely measurable within a time frame of 3 to 4 years—calling for further investigation once more longitudinal data become available. Our overall findings support the hypothesis that tau pathology propagates across the brain along structural neuronal connections. Ultimately, our method allows us to quantitatively characterize personalized tau pathologies in their spatio-temporal characteristics, which can in turn be used to inform models of other related disease biomarkers, including regional atrophy.

DATA AVAILABILITY STATEMENT

Publicly available datasets were analyzed in this study. This data can be found here: Alzheimer's Disease Neuroimaging Initiative: adni.loni.usc.edu.

AUTHOR CONTRIBUTIONS

AS was responsible for conception and design of the study, data analysis and interpretation, and draft of the manuscript. EM

and EK contributed to and guided study conception and design and provided critical revision of the manuscript for intellectual content. All authors approved the final version of the article to be published.

FUNDING

This work was supported by the Brit and Alex d'Arbeloff Stanford Graduate Fellowship to AS, the National Institutes of Health Grant K01-AG051718 to EM, and a Stanford BioX-IIP Seed Grant and the National Science Foundation Grant CMMI 1727268 to EK.

ACKNOWLEDGMENTS

Data collection and sharing for this project was funded by the Alzheimer's Disease Neuroimaging Initiative (ADNI) (National Institutes of Health Grant U01 AG024904) and DOD ADNI (Department of Defense award number W81XWH-12-2-0012). ADNI is funded by the National Institute on Aging, the National Institute of Biomedical Imaging and Bioengineering, and through generous contributions from the following: AbbVie, Alzheimer's Association; Alzheimer's Drug Discovery Foundation; Araclon Biotech; BioClinica, Inc.; Biogen; Bristol-Myers Squibb Company; CereSpir, Inc.; Cogstate; Eisai Inc.; Elan Pharmaceuticals, Inc.; Eli Lilly and Company; EuroImmun; F. Hoffmann-La Roche Ltd and its affiliated company Genentech, Inc.; Fujirebio; GE Healthcare; IXICO Ltd.; Janssen Alzheimer Immunotherapy Research & Development, LLC.; Johnson & Johnson Pharmaceutical Research & Development LLC.; Lumosity; Lundbeck; Merck & Co., Inc.; Meso Scale Diagnostics, LLC.; NeuroRx Research; Neurotrack Technologies; Novartis Pharmaceuticals Corporation; Pfizer Inc.; Piramal Imaging; Servier; Takeda Pharmaceutical Company; and Transition Therapeutics. The Canadian Institutes of Health Research is providing funds to support ADNI clinical sites in Canada. Private sector contributions are facilitated by the Foundation for the National Institutes of Health (www.fnih.org). The grantee organization is the Northern California Institute for Research and Education, and the study is coordinated by the Alzheimer's Therapeutic Research Institute at the University of Southern California. ADNI data are disseminated by the Laboratory for Neuro Imaging at the University of Southern California.

REFERENCES

- ADNI (2020). *Alzheimer's Disease Neuroimaging Initiative*. Available online at: <http://adni.loni.usc.edu> (accessed July 31, 2020).
- Baker, S. L., Lockhart, S. N., Price, J. C., He, M., Huesman, R. H., Schonhaut, D., et al. (2017). Reference tissue-based kinetic evaluation of 18F-AV-1451 for tau imaging. *J. Nuclear Med.* 58, 332–338. doi: 10.2967/jnumed.116.175273
- Bateman, R. J., Xiong, C., Benzinger, T. L., Fagan, A. M., Goate, A., Fox, N. C., et al. (2012). Clinical and biomarker changes in dominantly inherited Alzheimer's disease. *N. Engl. J. Med.* 367, 795–804. doi: 10.1056/NEJMoa1202753
- Bejanin, A., Schonhaut, D. R., La Joie, R., Kramer, J. H., Baker, S. L., Sosa, N., et al. (2017). Tau pathology and neurodegeneration contribute to cognitive impairment in Alzheimer's disease. *Brain* 140, 3286–3300. doi: 10.1093/brain/awx243
- Braak, H., Alafuzoff, I., Arzberger, T., Kretschmar, H., and Del Tredici, K. (2006). Staging of Alzheimer disease-associated neurofibrillary pathology using paraffin sections and immunocytochemistry. *Acta Neuropathol.* 112, 389–404. doi: 10.1007/s00401-006-0127-z
- Braak, H., and Braak, E. (1991). Neuropathological staging of Alzheimer-related changes. *Acta Neuropathol.* 82, 239–259. doi: 10.1007/BF00308809
- Buckley, R. F., Hanseeuw, B., Schultz, A. P., Vannini, P., Aghjayan, S. L., Properzi, M. J., et al. (2017). Region-specific association of subjective cognitive decline with tauopathy independent of global β -amyloid burden. *JAMA Neurol.* 74, 1455–1463. doi: 10.1001/jamaneurol.2017.2216

- Cho, H., Choi, J. Y., Hwang, M. S., Kim, Y. J., Lee, H. M., Lee, H. S., et al. (2016). *In vivo* cortical spreading pattern of tau and amyloid in the Alzheimer disease spectrum. *Ann. Neurol.* 80, 247–258. doi: 10.1002/ana.24711
- Cope, T. E., Rittman, T., Borchert, R. J., Jones, P. S., Vatansever, D., Allinson, K., et al. (2018). Tau burden and the functional connectome in Alzheimer's disease and progressive supranuclear palsy. *Brain* 141, 550–567. doi: 10.1093/brain/awx347
- De Calignon, A., Polydoro, M., Suárez-Calvet, M., William, C., Adamowicz, D. H., Kopeikina, K. J., et al. (2012). Propagation of tau pathology in a model of early Alzheimer's disease. *Neuron* 73, 685–697. doi: 10.1016/j.neuron.2011.11.033
- Desikan, R. S., Ségonne, F., Fischl, B., Quinn, B. T., Dickerson, B. C., Blacker, D., et al. (2006). An automated labeling system for subdividing the human cerebral cortex on MRI scans into gyral based regions of interest. *Neuroimage* 31, 968–980. doi: 10.1016/j.neuroimage.2006.01.021
- Diedrichsen, J. (2006). A spatially unbiased atlas template of the human cerebellum. *Neuroimage* 33, 127–138. doi: 10.1016/j.neuroimage.2006.05.056
- Duyckaerts, C., Delatour, B., and Potier, M.-C. (2009). Classification and basic pathology of Alzheimer disease. *Acta Neuropathol.* 118, 5–36. doi: 10.1007/s00401-009-0532-1
- Fisher, R. A. (1937). The wave of advance of advantageous genes. *Ann. Eugenics* 7, 355–369. doi: 10.1111/j.1469-1809.1937.tb02153.x
- Fornari, S., Schäfer, A., Jucker, M., Goriely, A., and Kuhl, E. (2019). Prion-like spreading of Alzheimer's disease within the brain's connectome. *J. R. Soc. Interface* 16:20190356. doi: 10.1098/rsif.2019.0356
- Fornari, S., Schäfer, A., Kuhl, E., and Goriely, A. (2020). Spatially-extended nucleation-aggregation-fragmentation models for the dynamics of prion-like neurodegenerative protein-spreading in the brain and its connectome. *J. Theoret. Biol.* 486:110102. doi: 10.1016/j.jtbi.2019.110102
- FreeSurfer (2020). *FreeSurfer Software Suite*. Available online at: <http://surfer.nmr.mgh.harvard.edu> (accessed July 31, 2020).
- Giannakopoulos, P., Herrmann, F., Bussi re, T., Bouras, C., Kovari, E., Perl, D., et al. (2003). Tangle and neuron numbers, but not amyloid load, predict cognitive status in Alzheimer's disease. *Neurology* 60, 1495–1500. doi: 10.1212/01.WNL.0000063311.58879.01
- Gordon, B. A., McCullough, A., Mishra, S., Blazey, T. M., Su, Y., Christensen, J., et al. (2018). Cross-sectional and longitudinal atrophy is preferentially associated with tau rather than amyloid β positron emission tomography pathology. *Alzheimers Dement.* 10, 245–252. doi: 10.1016/j.dadm.2018.02.003
- Grothe, M. J., Sepulcre, J., Gonzalez-Escamilla, G., Jelistratova, I., Sch ll, M., Hansson, O., et al. (2018). Molecular properties underlying regional vulnerability to Alzheimer's disease pathology. *Brain* 141, 2755–2771. doi: 10.1093/brain/awy189
- Harrison, T. M., La Joie, R., Maass, A., Baker, S. L., Swinnerton, K., Fenton, L., et al. (2019). Longitudinal tau accumulation and atrophy in aging and Alzheimer disease. *Ann. Neurol.* 85, 229–240. doi: 10.1002/ana.25406
- Henderson, M. X., Cornblath, E. J., Darwich, A., Zhang, B., Brown, H., Gathagan, R. J., et al. (2019). Spread of α -synuclein pathology through the brain connectome is modulated by selective vulnerability and predicted by network analysis. *Nat. Neurosci.* 22:1248. doi: 10.1038/s41593-019-0457-5
- Iaccarino, L., Tammewar, G., Ayakta, N., Baker, S. L., Bejanin, A., Boxer, A. L., et al. (2018). Local and distant relationships between amyloid, tau and neurodegeneration in Alzheimer's disease. *Neuroimage Clin.* 17, 452–464. doi: 10.1016/j.nicl.2017.09.016
- Iturria-Medina, Y., Sotero, R. C., Toussaint, P. J., Evans, A. C., Alzheimer's Disease Neuroimaging Initiative, et al. (2014). Epidemic spreading model to characterize misfolded proteins propagation in aging and associated neurodegenerative disorders. *PLoS Comput. Biol.* 10:e1003956. doi: 10.1371/journal.pcbi.1003956
- Jack, C. R., and Holtzman, D. M. (2013). Biomarker modeling of Alzheimer's disease. *Neuron* 80, 1347–1358. doi: 10.1016/j.neuron.2013.12.003
- Jack, C. R., Knopman, D. S., Jagust, W. J., Petersen, R. C., Weiner, M. W., Aisen, P. S., et al. (2013). Tracking pathophysiological processes in Alzheimer's disease: an updated hypothetical model of dynamic biomarkers. *Lancet Neurol.* 12, 207–216. doi: 10.1016/S1474-4422(12)70291-0
- Jack, C. R., Wiste, H. J., Schwarz, C. G., Lowe, V. J., Senjem, M. L., Vemuri, P., et al. (2018). Longitudinal tau PET in ageing and Alzheimer's disease. *Brain* 141, 1517–1528. doi: 10.1093/brain/awy059
- Johnson, K. A., Schultz, A., Betensky, R. A., Becker, J. A., Sepulcre, J., Rentz, D., et al. (2016). Tau positron emission tomographic imaging in aging and early Alzheimer disease. *Ann. Neurol.* 79, 110–119. doi: 10.1002/ana.24546
- Jones, D. T., Graff-Radford, J., Lowe, V. J., Wiste, H. J., Gunter, J. L., Senjem, M. L., et al. (2017). Tau, amyloid, and cascading network failure across the Alzheimer's disease spectrum. *Cortex* 97, 143–159. doi: 10.1016/j.cortex.2017.09.018
- Jucker, M., and Walker, L. C. (2011). Pathogenic protein seeding in Alzheimer disease and other neurodegenerative disorders. *Ann. Neurol.* 70, 532–540. doi: 10.1002/ana.22615
- Knopman, D. S., Parisi, J. E., Salviati, A., Floriach-Robert, M., Boeve, B. F., Ivnik, R. J., et al. (2003). Neuropathology of cognitively normal elderly. *J. Neuropathol. Exp. Neurol.* 62, 1087–1095. doi: 10.1093/jnen/62.11.1087
- Kolmogorov, A., Petrovskii, I., and Piskunov, N. (1937). A study of the equation of diffusion with increase in the quantity of matter, and its application to a biological problem. *Byul. Moskovskogo Gos. Univ.* 1, 1–25.
- La Joie, R., Visani, A. V., Baker, S. L., Brown, J. A., Bourakova, V., Cha, J., et al. (2020). Prospective longitudinal atrophy in Alzheimer's disease correlates with the intensity and topography of baseline tau-PET. *Sci. Transl. Med.* 12:aa5732. doi: 10.1126/scitranslmed.aau5732
- Landau, S. M., Lu, M., Joshi, A. D., Pontecorvo, M., Mintun, M. A., Trojanowski, J. Q., et al. (2013). Comparing positron emission tomography imaging and cerebrospinal fluid measurements of β -amyloid. *Ann. Neurol.* 74, 826–836. doi: 10.1002/ana.23908
- Lemoine, L., Leuzy, A., Chiotis, K., Rodriguez-Vieitez, E., and Nordberg, A. (2018). Tau positron emission tomography imaging in tauopathies: the added hurdle of off-target binding. *Alzheimers Dement.* 10, 232–236. doi: 10.1016/j.dadm.2018.01.007
- Liu, L., Drouet, V., Wu, J. W., Witter, M. P., Small, S. A., Clelland, C., and Duff, K. (2012). Trans-synaptic spread of tau pathology *in vivo*. *PLoS ONE* 7:e31302. doi: 10.1371/journal.pone.0031302
- Lowe, V. J., Curran, G., Fang, P., Liesinger, A. M., Josephs, K. A., Parisi, J. E., et al. (2016). An autoradiographic evaluation of AV-1451 Tau PET in dementia. *Acta Neuropathol. Commun.* 4:58. doi: 10.1186/s40478-016-0315-6
- Marqu  , M., Normandin, M. D., Meltzer, A. C., Siao Tick Chong, M., Andrea, N. V., Ant  n-Fern  ndez, A., et al. (2017). Pathological correlations of [F-18]-AV-1451 imaging in non-alzheimer tauopathies. *Ann. Neurol.* 81, 117–128. doi: 10.1002/ana.24844
- Marqu  , M., Normandin, M. D., Vanderburg, C. R., Costantino, I. M., Bien, E. A., Rycyna, L. G., et al. (2015). Validating novel tau positron emission tomography tracer [F-18]-AV-1451 (T807) on postmortem brain tissue. *Ann. Neurol.* 78, 787–800. doi: 10.1002/ana.24517
- McCarthy, C. S., Ramprasad, A., Thompson, C., Botti, J.-A., Coman, I. L., and Kates, W. R. (2015). A comparison of FreeSurfer-generated data with and without manual intervention. *Front. Neurosci.* 9:379. doi: 10.3389/fnins.2015.00379
- McNab, J. A., Edlow, B. L., Witzel, T., Huang, S. Y., Bhat, H., Heberlein, K., et al. (2013). The Human Connectome Project and beyond: initial applications of 300 mT/m gradients. *Neuroimage* 80, 234–245. doi: 10.1016/j.neuroimage.2013.05.074
- Pereira, J. B., Ossenkoppele, R., Palmqvist, S., Strandberg, T. O., Smith, R., Westman, E., et al. (2019). Amyloid and tau accumulate across distinct spatial networks and are differentially associated with brain connectivity. *eLife* 8:e50830. doi: 10.7554/eLife.50830
- Raj, A., Kuceyeski, A., and Weiner, M. (2012). A network diffusion model of disease progression in dementia. *Neuron* 73, 1204–1215. doi: 10.1016/j.neuron.2011.12.040
- Raj, A., LoCastro, E., Kuceyeski, A., Tosun, D., Relkin, N., Weiner, M., et al. (2015). Network diffusion model of progression predicts longitudinal patterns of atrophy and metabolism in Alzheimer's disease. *Cell Rep.* 10, 359–369. doi: 10.1016/j.celrep.2014.12.034
- Sch  fer, A., Weickenmeier, J., and Kuhl, E. (2019). The interplay of biochemical and biomechanical degeneration in Alzheimer's disease. *Comput. Methods Appl. Mech. Eng.* 352, 369–388. doi: 10.1016/j.cma.2019.04.028
- SPM (2020). *Statistical Parametric Mapping*. Available online at: <https://www.fil.ion.ucl.ac.uk/spm> (accessed July 31, 2020).

- Szalkai, B., Kerepesi, C., Varga, B., and Grolmusz, V. (2017). Parameterizable consensus connectomes from the human connectome project: the Budapest reference connectome server v3.0. *Cogn. Neurodyn.* 11, 113–116. doi: 10.1007/s11571-016-9407-z
- Thompson, T. B., Chaggar, P., Kuhl, E., Goriely, A., and Alzheimer's Disease Neuroimaging Initiative. (2020). Protein-protein interactions in neurodegenerative diseases: a conspiracy theory. *PLoS Comput. Biol.* 16:e1008267. doi: 10.1371/journal.pcbi.1008267
- Torok, J., Maia, P. D., Powell, F., Pandya, S., and Raj, A. (2018). A method for inferring regional origins of neurodegeneration. *Brain* 141, 863–876. doi: 10.1093/brain/awx371
- Villemagne, V. L., Doré, V., Burnham, S. C., Masters, C. L., and Rowe, C. C. (2018). Imaging tau and amyloid- β proteinopathies in Alzheimer disease and other conditions. *Nat. Rev. Neurol.* 14, 225–236. doi: 10.1038/nrneurol.2018.9
- Vogel, J. W., Iturria-Medina, Y., Strandberg, O. T., Smith, R., Levitis, E., Evans, A. C., et al. (2020). Spread of pathological tau proteins through communicating neurons in human Alzheimer's disease. *Nat. Commun.* 11:2612. doi: 10.1038/s41467-020-15701-2
- Weickenmeier, J., Jucker, M., Goriely, A., and Kuhl, E. (2019). A physics-based model explains the prion-like features of neurodegeneration in Alzheimer's disease, Parkinson's disease, and amyotrophic lateral sclerosis. *J. Mech. Phys. Solids* 124, 264–281. doi: 10.1016/j.jmps.2018.10.013
- Weickenmeier, J., Kuhl, E., and Goriely, A. (2018). Multiphysics of prionlike diseases: progression and atrophy. *Phys. Rev. Lett.* 121:158101. doi: 10.1103/PhysRevLett.121.158101
- Xia, C., Makaretz, S. J., Caso, C., McGinnis, S., Gomperts, S. N., Sepulcre, J., et al. (2017). Association of *in vivo* [18F] AV-1451 tau PET imaging results with cortical atrophy and symptoms in typical and atypical Alzheimer disease. *JAMA Neurol.* 74, 427–436. doi: 10.1001/jamaneurol.2016.5755

Conflict of Interest: The authors declare that the research was conducted in the absence of any commercial or financial relationships that could be construed as a potential conflict of interest.

Copyright © 2020 Schäfer, Mormino and Kuhl. This is an open-access article distributed under the terms of the Creative Commons Attribution License (CC BY). The use, distribution or reproduction in other forums is permitted, provided the original author(s) and the copyright owner(s) are credited and that the original publication in this journal is cited, in accordance with accepted academic practice. No use, distribution or reproduction is permitted which does not comply with these terms.



The Correlations Between Plasma Fibrinogen With Amyloid-Beta and Tau Levels in Patients With Alzheimer's Disease

Dong-Yu Fan^{1†}, Hao-Lun Sun^{1,2†}, Pu-Yang Sun¹, Jie-Ming Jian¹, Wei-Wei Li¹, Ying-Ying Shen¹, Fan Zeng¹, Yan-Jiang Wang^{1*} and Xian-Le Bu^{1*}

¹ Department of Neurology and Centre for Clinical Neuroscience, Daping Hospital, Third Military Medical University, Chongqing, China, ² Shigatse Branch, Xinqiao Hospital, Third Military Medical University, Shigatse, China

OPEN ACCESS

Edited by:

Yu Chen,
Chinese Academy of Sciences (CAS),
China

Reviewed by:

Scott Edward Counts,
Michigan State University,
United States
Chongzhao Ran,
Harvard Medical School,
United States

*Correspondence:

Yan-Jiang Wang
yanjiang_wang@tmmu.edu.cn
Xian-Le Bu
buxianle@sina.cn

[†] These authors have contributed
equally to this work

Specialty section:

This article was submitted to
Neurodegeneration,
a section of the journal
Frontiers in Neuroscience

Received: 04 November 2020

Accepted: 30 December 2020

Published: 21 January 2021

Citation:

Fan D-Y, Sun H-L, Sun P-Y,
Jian J-M, Li W-W, Shen Y-Y, Zeng F,
Wang Y-J and Bu X-L (2021) The
Correlations Between Plasma
Fibrinogen With Amyloid-Beta
and Tau Levels in Patients With
Alzheimer's Disease.
Front. Neurosci. 14:625844.
doi: 10.3389/fnins.2020.625844

Recent studies show that fibrinogen plays a role in the pathogenesis of Alzheimer's disease (AD), which may be crucial to neurovascular damage and cognitive impairment. However, there are few clinical studies on the relationship between fibrinogen and AD. 59 ¹¹C-PiB-PET diagnosed AD patients and 76 age- and gender-matched cognitively normal controls were included to analyze the correlation between plasma β -amyloid (A β) and tau levels with fibrinogen levels. 35 AD patients and 76 controls with cerebrospinal fluid (CSF) samples were included to further analyze the correlation between CSF A β and tau levels with fibrinogen levels. In AD patients, plasma fibrinogen levels were positively correlated with plasma A β 40 and A β 42 levels, and negatively correlated with CSF A β 42 levels. Besides, fibrinogen levels were positively correlated with CSF total tau (t-tau), and phosphorylated tau-181 (p-tau) levels and positively correlated with the indicators of A β deposition in the brain, such as t-tau/A β 42, p-tau/A β 42 levels. In normal people, fibrinogen levels lack correlation with A β and tau levels in plasma and CSF. This study suggests that plasma fibrinogen levels are positively correlated with A β levels in the plasma and brain in AD patients. Fibrinogen may be involved in the pathogenesis of AD.

Keywords: Alzheimer's disease, fibrinogen, β -amyloid, tau, pathogenesis, biomarkers

INTRODUCTION

Alzheimer's disease (AD) is the most common neurodegenerative disease that causes cognitive and memory impairment (Castellani et al., 2010; Jia et al., 2014). The main pathological hallmarks of AD include extracellular senile plaques containing β -amyloid (A β) and intracellular neurofibrillary tangles formed by phosphorylated tau (Huang and Mucke, 2012; Long and Holtzman, 2019). Recent studies have shown that fibrinogen also plays an important role in the pathogenesis of AD (Cortes-Canteli and Strickland, 2009). Fibrinogen can bind to A β , which intensifies inflammation in the AD brain and accelerates the decline of cognitive function in AD patients (Ahn et al., 2014; Merlini et al., 2019). The A β -fibrinogen interaction may be crucial to the progression of neurovascular damage and cognitive impairment in AD (Xu et al., 2008; Cortes-Canteli et al., 2010). However, there are few clinical studies on the relationship between fibrinogen and A β . This study aims to explore the relationship between fibrinogen and A β levels in AD patients and normal people.

MATERIALS AND METHODS

Study Population

Alzheimer's disease patients were recruited from Chongqing Daping Hospital from December 2018 to May 2020. Age- and gender-matched controls with normal cognition were randomly recruited from the hospital at the same time. Subjects were excluded for the following reasons: (1) a family history of dementia; (2) a concomitant neurologic disorder that could potentially affect the cognitive function or other types of dementia; (3) severe cardiac, pulmonary, hepatic, or renal diseases or any type of tumor; (4) enduring mental illness (e.g., schizophrenia); (5) Diseases that may affect fibrinogen levels (e.g., bleeding disorders, hereditary abnormal fibrinogenemia, etc.); (6) Recently used treatments that affect fibrinogen levels (e.g., blood transfusion); (7) an allergy to the ^{11}C -Pittsburgh compound.

AD Diagnosis and Sampling

The diagnosis of AD was made according to the criteria of the National Institute of Neurological and Communicative Diseases and Stroke/AD and Related Disorders Association following the protocols we used before (Li et al., 2011). Besides, the patients who collected blood all received A β positron emission tomography (PET) examination of Pittsburgh compound B (PiB), and the diagnostic criteria were PiB-PET positive. The demographic data and medical history (such as hypertension, coronary heart disease, and diabetes mellitus) were collected and the cognitive and functional status was assessed based on a neuropsychological battery. Fasting blood was collected between 07:00 and 09:00 to avoid the potential circadian rhythm influence. The blood samples were centrifuged within an hour of collection and EDTA plasma was aliquoted in 0.5 mL polypropylene tubes and stored at -80°C until used. The cerebrospinal fluid (CSF) samples were centrifuged at 2,000g at 4°C for 10 min, and the aliquots were then immediately frozen and stored at -80°C until use. The informed consent was obtained before the acquisition of the blood and CSF samples.

Measurements of Fibrinogen, A β , and Tau Levels

Fibrinogen levels were measured using standard laboratory methods in the Clinical Laboratory, Daping Hospital, Chongqing, China. Fibrinogen—C is the test to measure fibrinogen by the Clusius method and is carried out with the commercial kit HemosIL Fibrinogen assay (Instrumentation Laboratory Company, United States) on ACL-TOP (Instrumentation Laboratory Company, United States). The kit uses an excess of thrombin to convert fibrinogen to fibrin in diluted plasma. Plasma levels of A β 42, A β 40 were measured using the commercially available single-molecule array (SIMOA) Human Neurology 3-Plex A assay kit (Quanterix, United States) on-board of the automated SIMOA HD-1 analyzer (Quanterix, United States). CSF levels of A β 40, A β 42, total tau (t-tau), and phosphorylated tau-181 (p-tau) were measured using the human A β and

tau enzyme-linked immunosorbent assay (ELISA) kits (Innotest, United States). All of the measurements were performed according to the manufacturer's instructions (Wilke et al., 2018).

Statistical Analysis

The differences in demographic characteristics and fibrinogen levels between the groups were assessed with two-tailed independent *t*-tests, Mann–Whitney *U* test, or Chi-square test. Spearman correlation analyses were used to examine the correlations between fibrinogen levels and A β levels. The data are expressed as the mean \pm standard deviation (SD). All hypothesis testing was two-sided, and $p < 0.05$ was defined as statistically significant. The computations were performed with SPSS version 20.0 (SPSS Inc., United States).

RESULTS

Characteristics of the Study Population

The characteristics of the subjects are shown in **Tables 1, 2**. The study consisted of 59 AD patients diagnosed by ^{11}C -PiB PET and 76 age- and gender-matched cognitively normal controls. There were no significant differences in age, sex, education level, or the comorbidity of hypertension, diabetes mellitus, cardiovascular disease, and hyperlipidemia between AD patients and cognitively normal controls. AD patients consisted of a higher proportion of

TABLE 1 | Characteristics of the participants with plasma samples.

Characteristics	Controls (<i>n</i> = 76)	PiB-PET (+)-AD (<i>n</i> = 59)	<i>p</i> -value
Age, mean (SD), y	68.42 (8.52)	66.31 (9.53)	0.180
Female, <i>n</i> (%)	46 (60.5)	33 (57.6)	0.602
Education level, mean (SD), y	9.24 (4.36)	9.61 (4.44)	0.629
MMSE score, mean (SD)	26.28 (3.05)	12.37 (5.06)	<0.001
APOE ϵ 4 carriers, no (%)	8 (10.53)	18 (30.51)	0.004
Diabetes, (%)	11 (14.47)	9 (15.25)	>0.999
Hypertension, (%)	19 (25.00)	15 (25.42)	>0.999
Dyslipidaemia, (%)	21 (27.63)	16 (27.12)	>0.999
Coronary artery disease, (%)	13 (17.11)	11 (18.64)	0.825
Stroke history, (%)	6 (7.89)	3 (5.08)	0.731
Plasma A β 40, mean (SD), pg/mL	284.4 (71.67)	219.2 (107.1)	<0.001
Plasma A β 42, mean (SD), pg/mL	15.42 (4.598)	9.915 (5.126)	<0.001
Plasma t-tau, mean (SD), pg/mL	4.544 (2.536)	5.923 (3.196)	0.006
Plasma t-tau/A β 42, mean (SD), pg/mL	0.3271 (0.2658)	0.8143 (0.8529)	<0.001
Plasma A β 42/A β 40, mean (SD), pg/mL	0.05516 (0.01391)	0.04859 (0.01793)	0.018

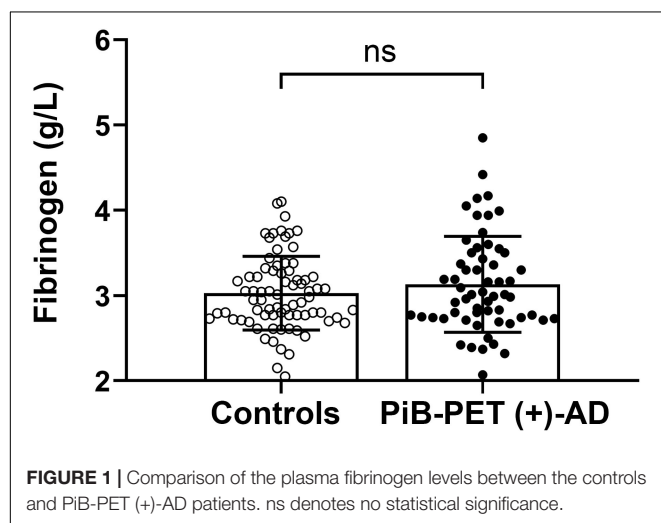
MMSE, mini-mental state examination; APOE ϵ 4, apolipoprotein E ϵ 4 allele; *p*-value, two-tailed independent *t*-tests, Mann–Whitney *U* test or Chi-square test as appropriate.

APOE $\epsilon 4$ carriers ($p = 0.004$) and showed lower MMSE scores ($p < 0.001$). The AD patients had lower levels of both plasma A $\beta 40$ (219.2 ± 107.1 pg/mL vs. 284.4 ± 71.67 pg/mL, $p < 0.001$) and A $\beta 42$ (9.915 ± 5.126 pg/mL vs. 15.42 ± 4.598 pg/mL, $p < 0.001$) than the control group. The AD patients with CSF had lower levels of CSF A $\beta 40$ (9150 ± 3926 pg/mL vs. 12190 ± 4482 pg/mL, $p = 0.001$) and A $\beta 42$ (629.5 ± 286.5 pg/mL vs. 1508 ± 673.2 pg/mL, $p < 0.001$), and higher levels of CSF t-tau (402.3 ± 183.6 pg/mL vs. 184.0 ± 61.38 pg/mL, $p < 0.001$), CSF p-tau (66.09 ± 28.38 pg/mL vs. 42.84 ± 18.18 pg/mL, $p < 0.001$), CSF t-tau/A $\beta 42$ (0.809 ± 0.511 pg/mL vs. 0.146 ± 0.080 pg/mL, $p < 0.001$), and CSF t-tau/A $\beta 42$ (0.1317 ± 0.0844 pg/mL vs. 0.0334 ± 0.0206 pg/mL, $p < 0.001$) than the control group.

Correlation Between Fibrinogen Levels With Plasma A β Levels

There was no significant difference in plasma fibrinogen levels between AD patients and the control group [PiB-PET (+)-AD vs controls: 3.13 ± 0.563 g/L vs. 3.03 ± 0.433 g/L, $p = 0.256$] (Figure 1). There was also no significant difference in fibrinogen levels between APOE $\epsilon 4$ carriers and APOE $\epsilon 4$ non-carriers (Supplementary Figure 1A). Besides, there was no significant correlation between fibrinogen levels and MMSE scores (Supplementary Figure 1B).

Fibrinogen levels in AD patients diagnosed by positive PiB-PET had a significantly positive correlation with plasma A $\beta 42$ levels ($\gamma = 0.263$, $p = 0.045$) and A $\beta 40$ levels ($\gamma = 0.327$, $p = 0.011$). There was no correlation between fibrinogen levels and plasma A $\beta 42$ levels ($\gamma = 0.094$, $p = 0.421$) and A $\beta 40$ levels ($\gamma = 0.111$, $p = 0.340$) in controls. In all subjects, fibrinogen levels had a significantly positive correlation with plasma A $\beta 40$ levels ($\gamma = 0.189$, $p = 0.028$) but not with A $\beta 42$ levels ($\gamma = 0.106$, $p = 0.220$) (Figure 2). There was no correlation between fibrinogen levels in both AD and controls with plasma t-tau levels, A $\beta 42$ /A $\beta 40$ levels, and t-tau/A $\beta 42$ levels (Supplementary Figure 2).



Correlation Between Fibrinogen Levels With CSF A β Levels

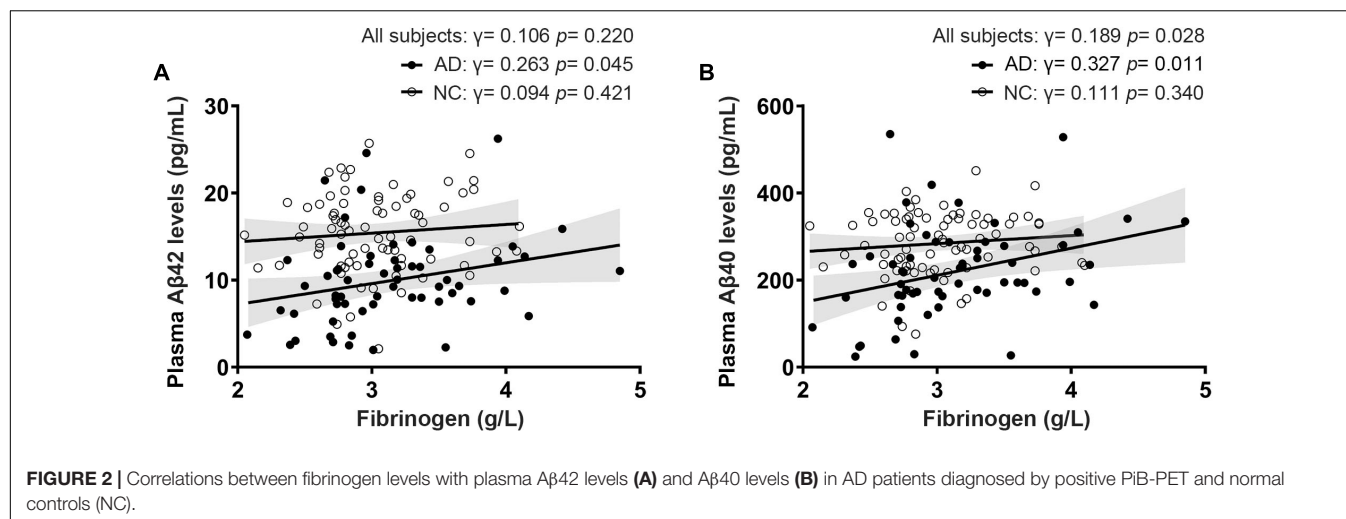
Of all the clinical AD patients, 35 people had CSF collected to further analyze the correlation between fibrinogen levels with CSF A β and tau levels. As shown in Table 2, there were no significant differences in the comorbidity of hypertension, diabetes mellitus, cardiovascular disease, and hyperlipidemia between the two groups. Also, no significant difference was found in the fibrinogen between these two groups (AD vs controls: 2.97 ± 0.510 g/L vs. 3.03 ± 0.433 g/L, $p = 0.541$). Fibrinogen levels in AD patients had significantly positive correlation with CSF A $\beta 42$ levels ($\gamma = -0.339$, $p = 0.049$), but no correlation with CSF A $\beta 40$ levels ($\gamma = -0.204$, $p = 0.271$). There was no correlation between fibrinogen levels in controls with CSF A $\beta 42$ levels ($\gamma = -0.074$, $p = 0.536$) and A $\beta 40$ levels ($\gamma = -0.121$, $p = 0.298$). In all subjects, there was no correlation between fibrinogen levels with CSF A $\beta 42$ levels ($\gamma = -0.053$, $p = 0.591$) and A $\beta 40$ levels ($\gamma = -0.115$, $p = 0.240$) (Figures 3A,B).

Correlation Between Fibrinogen Levels With CSF Tau Levels

To further reveal the relationship between fibrinogen and AD pathological changes, we then detected the t-tau and phosphorylated tau in CSF and analyzed their correlation. Fibrinogen levels in AD patients had significantly positive correlation with CSF t-tau levels ($\gamma = 0.356$, $p = 0.042$) and p-tau levels ($\gamma = 0.426$, $p = 0.012$). There was no correlation between fibrinogen levels in controls with CSF t-tau levels ($\gamma = -0.004$, $p = 0.974$) and p-tau levels ($\gamma = 0.024$, $p = 0.837$). In all subjects, there was no correlation between fibrinogen levels with CSF t-tau levels ($\gamma = 0.086$, $p = 0.373$) and p-tau levels ($\gamma = 0.157$, $p = 0.102$) (Figures 3C,D).

Correlation Between Fibrinogen Levels With CSF Tau/A $\beta 42$ Levels

Compared with a single marker, recent studies have found that the ratio of tau and A $\beta 42$, including t-tau/A $\beta 42$ and p-tau/A $\beta 42$, has a higher correlation with the PiB-PET cortical standard uptake ratio (SUVR), which can better reflect the pathology of A β deposition in the brain (Hansson et al., 2018; Schindler et al., 2018). Based on this, we calculated the correlation between these two ratios and fibrinogen to explore the relationship between fibrinogen and the pathological process in the brain. We found that fibrinogen levels in AD patients had significantly positive correlation with CSF t-tau/A $\beta 42$ levels ($\gamma = 0.524$, $p = 0.002$) and p-tau/A $\beta 42$ levels ($\gamma = 0.427$, $p = 0.013$). There was no correlation between fibrinogen levels in controls with CSF t-tau/A $\beta 42$ levels ($\gamma = 0.081$, $p = 0.494$) and p-tau/A $\beta 42$ levels ($\gamma = 0.074$, $p = 0.538$). In all subjects, fibrinogen levels had a significantly positive correlation with CSF t-tau/A $\beta 42$ levels ($\gamma = 0.206$, $p = 0.034$) but not with p-tau/A $\beta 42$ levels ($\gamma = 0.161$, $p = 0.102$) (Figures 3E,F).



DISCUSSION

This study explored the correlation between fibrinogen levels and Aβ, tau levels in humans for the first time. In AD patients, fibrinogen levels were positively correlated with plasma Aβ40 and Aβ42 levels, and negatively correlated with CSF Aβ42 levels. Besides, fibrinogen levels were positively correlated with CSF

t-tau and p-tau levels and were positively correlated with the indicators of Aβ deposition in the brain, such as t-tau/Aβ42, p-tau/Aβ42 levels. In normal people, fibrinogen levels lack correlation with Aβ and tau levels in plasma and CSF.

Previous studies have shown that the destruction of the blood-brain barrier can cause fibrinogen to enter the brain and accelerate neuronal damage in the pathological process of neurological diseases such as AD (Adams et al., 2004). Therefore, compared with normal people, the pathological development may be aggravated due to a large amount of fibrinogen in the brain of AD patients (Lipinski and Sajdel-Sulkowska, 2006; Cortes-Canteli et al., 2014), and the cognitive function of AD patients decreases as their plasma fibrinogen levels increase (Oijen et al., 2006; Xu et al., 2008). In this study, we found that plasma and CSF Aβ levels in AD patients were significantly correlated with their plasma fibrinogen levels, which further provided clinical evidence that fibrinogen may involve in the development of AD pathological damage.

Platelets are the main place where Aβ is produced in the periphery, so the activation of platelets will increase the production of peripheral Aβ (Chen et al., 1995; Shen et al., 2008). Fibrinogen can induce platelet aggregation and activation, leading to more blood Aβ formation (Bennett, 2001; Chen et al., 2003). The fibrinogen in the brain of AD patients will combine with Aβ deposition to form oligomers with abnormal structures, resulting in a decrease of free fibrinogen levels in the plasma (Ahn et al., 2010). This is also the possible reason why the plasma fibrinogen in AD patients is not significantly increased. These oligomers are difficult to degrade, they can block blood vessels, cause thrombosis and abnormal fibrinolysis, reduce cerebral blood flow perfusion, accelerate neurovascular injury and neuroinflammation, and aggravate the formation of amyloid angiopathy (CAA) (Paul et al., 2007; Cortes-Canteli et al., 2010). The increased binding affinity of Aβ to fibrinogen will aggravate the above process and lead to the occurrence of hereditary cerebral amyloid angiopathy (HCAA) (Cajamarca et al., 2020). In addition to forming complexes with Aβ, fibrinogen in cerebral blood vessels will also form clots with the help of APOE ε4

TABLE 2 | Characteristics of the participants with CSF samples.

Characteristics	Controls (n = 76)	AD (n = 35)	p-value
Age, mean (SD), y	68.42 (8.52)	66.34 (1.47)	0.240
Female, n (%)	46 (60.5)	18 (51.43)	0.412
Education level, mean (SD), y	9.24 (4.36)	9.63 (3.80)	0.652
MMSE score, mean (SD)	26.28 (3.05)	12.03 (4.08)	<0.001
APOE ε4 carriers, No (%)	8 (10.53)	14 (40.00)	0.001
Diabetes, (%)	11 (14.47)	6 (17.14)	0.779
Hypertension, (%)	19 (25.00)	8 (22.86)	0.819
Dyslipidaemia, (%)	21 (27.63)	11 (31.43)	0.822
Coronary artery disease, (%)	13 (17.11)	7 (20.00)	0.792
Stroke history, (%)	6 (7.89)	2 (5.71)	0.726
CSF Aβ40, mean (SD), pg/mL	12190 (4482)	9150 (3926)	0.001
CSF Aβ42, mean (SD), pg/mL	1508 (673.2)	629.5 (286.5)	<0.001
CSF t-tau, mean (SD), pg/mL	184.0 (61.38)	402.3 (183.6)	<0.001
CSF p-tau, mean (SD), pg/mL	42.84 (18.18)	66.09 (28.38)	<0.001
CSF t-tau/Aβ42, mean (SD), pg/mL	0.146 (0.080)	0.8867 (0.672)	<0.001
CSF p-tau/Aβ42, mean (SD), pg/mL	0.0334 (0.0206)	0.1317 (0.0844)	<0.001

MMSE, mini-mental state examination; APOE ε4, apolipoprotein E ε4 allele; p-value, two-tailed independent t-tests, Mann-Whitney U test or Chi-square test as appropriate.

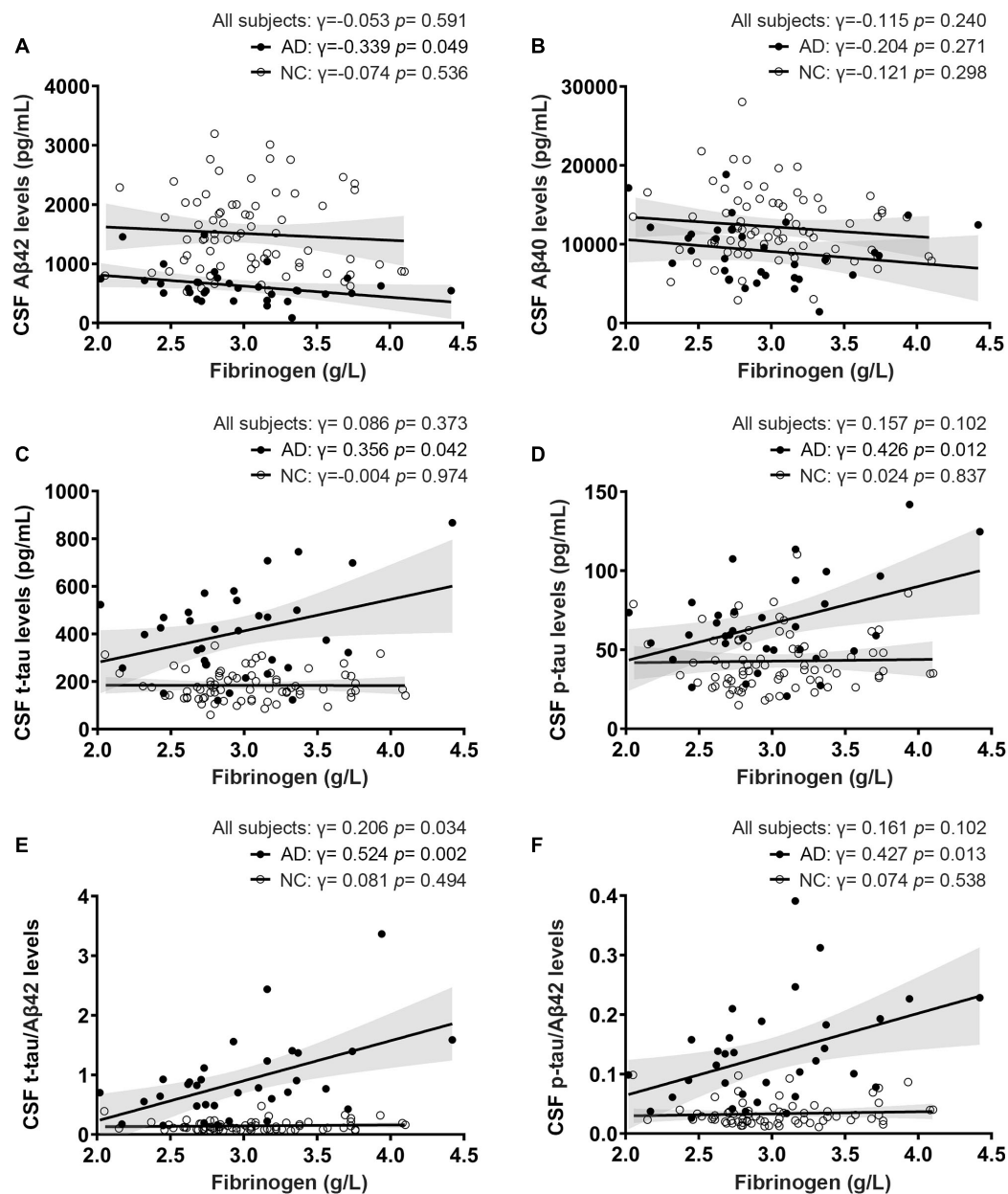


FIGURE 3 | Correlations between fibrinogen levels with CSF A β levels (A,B), tau levels (C,D), and tau/A β 42 levels (E,F) in AD patients and normal controls (NC).

gene and homocysteine, leading to more A β deposition in the cerebral blood vessel wall and CAA formation (Hultman et al., 2013; Chung et al., 2016). Besides, too much fibrinogen in the brain can also lead to insufficient cerebral perfusion, aggravating cerebral hypoxia, and the formation of A β plaques in AD patients (Miners et al., 2018). Animal studies have also observed that removing this part of fibrinogen can alleviate AD-related pathologies in the brain of mice and improve cognitive impairment (Cortes-Canteli et al., 2010). Therefore, there is a positive correlation between plasma A β and fibrinogen levels, and a negative correlation between CSF A β and fibrinogen levels in AD patients, and the more stable A β 42 has a better correlation,

while the integrity of the blood-brain barrier in normal people is not destroyed, which may be the reason for the lack of correlation between them.

According to the A β cascade hypothesis, the increase of A β can further induce the hyperphosphorylation of the microtubule-associated protein tau and accumulation in the cells, forming AD-related pathological changes such as neurofibrillary tangles, and leading to increased levels of t-tau and p-tau in the CSF of AD patients (Huang and Mucke, 2012). This may explain the positive correlation between tau and fibrinogen levels in AD patients. But so far there is no direct evidence that fibrinogen can exacerbate tau phosphorylation.

In addition to the A β pathway, previous studies have also found that fibrinogen can directly affect neuroinflammation by inducing the activation of microglia through CD11b/CD18 integrin receptors and other means (Ryu et al., 2009). Blocking this approach can reduce neuroinflammation, synaptic dysfunction, and cognitive decline in AD mice (Merlini et al., 2019). Fibrinogen may play an important role in the pathogenesis of AD.

This study provides clinical evidence for the relationship between fibrinogen and AD, suggesting that fibrinogen may play a role in the pathogenesis of AD. It is worth noting that this is a cross-sectional observational study, we cannot determine the effect of fibrinogen on the progression of AD. To further clarify the impact, cohort studies need to be continued in the future. In addition, we need to increase the number of CSF samples from AD patients, adopt more accurate detection methods for CSF biomarkers such as SIMOA, and further analyze the correlation between fibrinogen and amyloid-PET SUVR to better verify the effect of fibrinogen on A β deposition in the brain. At the same time, whether drugs to reduce fibrinogen will improve the cognitive function decline of AD patients remains to be further studied.

CONCLUSION

Our research shows that plasma fibrinogen levels are positively correlated with A β levels in the plasma and brain in AD patients, which further shows that fibrinogen can promote A β deposition in the brain and accelerate tau phosphorylation. Fibrinogen may be involved in the pathogenesis of AD.

REFERENCES

- Adams, R., Passino, M., Sachs, B., Nuriel, T., and Akassoglou, K. (2004). Fibrin mechanisms and functions in nervous system pathology. *Mol. Interv.* 4, 163–176. doi: 10.1124/mi.4.3.6
- Ahn, H., Zamołodchikov, D., Cortes-Canteli, M., Norris, E., Glickman, J., and Strickland, S. (2010). Alzheimer's disease peptide beta-amyloid interacts with fibrinogen and induces its oligomerization. *Proc. Natl. Acad. Sci. U.S.A.* 107, 21812–21817. doi: 10.1073/pnas.1010373107
- Ahn, H. J., Glickman, J. F., Poon, K. L., Zamołodchikov, D., Jno-Charles, O. C., Norris, E. H., et al. (2014). A novel A β -fibrinogen interaction inhibitor rescues altered thrombosis and cognitive decline in Alzheimer's disease mice. *J. Exp. Med.* 211, 1049–1062. doi: 10.1084/jem.20131751
- Bennett, J. (2001). Platelet–fibrinogen interactions. *Ann. N. Y. Acad. Sci.* 936, 340–354. doi: 10.1111/j.1749-6632.2001.tb03521.x
- Cajamarca, S., Norris, E., van der Weerd, L., Strickland, S., and Ahn, H. (2020). Cerebral amyloid angiopathy-linked β -amyloid mutations promote cerebral fibrin deposits via increased binding affinity for fibrinogen. *Proc. Natl. Acad. Sci. U.S.A.* 117, 14482–14492. doi: 10.1073/pnas.1921327117
- Castellani, R. J., Rolston, R. K., and Smith, M. A. (2010). Alzheimer disease. *Dis. Mon.* 56, 484–546. doi: 10.1016/j.disamonth.2010.06.001
- Chen, J., Dong, J. F., Sun, C., Bergeron, A., McBride, L., Pillai, M., et al. (2003). Platelet Fc γ RIIA HIS131ARG polymorphism and platelet function: antibodies

DATA AVAILABILITY STATEMENT

The raw data supporting the conclusions of this article will be made available by the authors, without undue reservation.

ETHICS STATEMENT

The studies involving human participants were reviewed and approved by the Institutional Review Board of Daping Hospital. The patients/participants provided their written informed consent to participate in this study.

AUTHOR CONTRIBUTIONS

X-LB, Y-JW, and D-YF designed this study. D-YF, W-WL, J-MJ, and Y-YS performed biomarker testing and clinical the data collection. H-LS, D-YF, P-YS, and FZ analyzed the data. D-YF and H-LS wrote the article. All authors contributed to the article and approved the submitted version.

FUNDING

This study was supported by the Natural Science Foundation Project of Chongqing (No. cstc2020jcyj-msxmX0132).

SUPPLEMENTARY MATERIAL

The Supplementary Material for this article can be found online at: <https://www.frontiersin.org/articles/10.3389/fnins.2020.625844/full#supplementary-material>

- to platelet-bound fibrinogen induce platelet activation. *J. Thromb. Haemost.* 1, 355–362. doi: 10.1046/j.1538-7836.2003.00054.x
- Chen, M., Inestrosa, N., Ross, G., and Fernandez, H. (1995). Platelets are the primary source of amyloid β -Peptide in human blood. *Biochem. Biophys. Res. Commun.* 213, 96–103. doi: 10.1006/bbrc.1995.2103
- Chung, Y. C., Kruyer, A., Yao, Y., Feerman, E., Richards, A., Strickland, S., et al. (2016). Hyperhomocysteinemia exacerbates Alzheimer's disease pathology by way of the β -amyloid fibrinogen interaction. *J. Thromb. Haemost.* 14, 1442–1452. doi: 10.1111/jth.13340
- Cortes-Canteli, M., Mattei, L., Richards, A., Norris, E., and Strickland, S. (2014). Fibrin deposited in the Alzheimer's disease brain promotes neuronal degeneration. *Neurobiol. Aging* 36, 608–617. doi: 10.1016/j.neurobiolaging.2014.10.030
- Cortes-Canteli, M., Paul, J., Norris, E. H., Bronstein, R., Ahn, H. J., Zamołodchikov, D., et al. (2010). Fibrinogen and beta-amyloid association alters thrombosis and fibrinolysis: a possible contributing factor to Alzheimer's disease. *Neuron* 66, 695–709. doi: 10.1016/j.neuron.2010.05.014
- Cortes-Canteli, M., and Strickland, S. (2009). Fibrinogen, a possible key player in Alzheimer's disease. *J. Thromb. Haemost.* 7(Suppl. 1), 146–150. doi: 10.1111/j.1538-7836.2009.03376.x
- Hansson, O., Seibyl, J., Stomrud, E., Zetterberg, H., Trojanowski, J. Q., Bittner, T., et al. (2018). CSF biomarkers of Alzheimer's disease concord with amyloid- β PET and predict clinical progression: a study of fully automated immunoassays in BioFINDER and ADNI cohorts. *Alzheimers Dement.* 14, 1470–1481. doi: 10.1016/j.jalz.2018.01.010

- Huang, Y., and Mucke, L. (2012). Alzheimer mechanisms and therapeutic strategies. *Cell* 148, 1204–1222. doi: 10.1016/j.cell.2012.02.040
- Hultman, K., Strickland, S., and Norris, E. (2013). The APOE $\epsilon 4/\epsilon 4$ genotype potentiates vascular fibrin(ogen) deposition in amyloid-laden vessels in the brains of Alzheimer's disease patients. *J. Cereb. Blood Flow Metab.* 33, 1251–1258. doi: 10.1038/jcbfm.2013.76
- Jia, J., Wang, F., Wei, C., Zhou, A., Jia, X., Li, F., et al. (2014). The prevalence of dementia in urban and rural areas of China. *Alzheimers Dement.* 10, 1–9. doi: 10.1016/j.jalz.2013.01.012
- Li, J., Wang, Y. J., Zhang, M., Xu, Z. Q., Gao, C. Y., Fang, C. Q., et al. (2011). Vascular risk factors promote conversion from mild cognitive impairment to Alzheimer disease. *Neurology* 76, 1485–1491. doi: 10.1212/WNL.0b013e318217e7a4
- Lipinski, B., and Sajdel-Sulkowska, E. (2006). New insight into Alzheimer disease: demonstration of fibrin(ogen)-serum albumin insoluble deposits in brain tissue. *Alzheimer Dis. Assoc. Disord.* 20, 323–326. doi: 10.1097/01.wad.0000213844.21001.a2
- Long, J. M., and Holtzman, D. M. (2019). Alzheimer disease: an update on pathobiology and treatment strategies. *Cell* 179, 312–339. doi: 10.1016/j.cell.2019.09.001
- Merlini, M., Rafalski, V. A., Rios Coronado, P. E., Gill, T. M., Ellisman, M., Muthukumar, G., et al. (2019). Fibrinogen induces microglia-mediated spine elimination and cognitive impairment in an Alzheimer's disease model. *Neuron* 101, 1099–1108. doi: 10.1016/j.neuron.2019.01.014
- Miners, J. S., Schulz, I., and Love, S. (2018). Differing associations between A β accumulation, hypoperfusion, blood-brain barrier dysfunction and loss of PDGFRB pericyte marker in the precuneus and parietal white matter in Alzheimer's disease. *J. Cereb. Blood Flow Metab.* 38, 103–115. doi: 10.1177/0271678X17690761
- Oijen, M., Witteman, J., Hofman, A., Koudstaal, P., and Breteler, M. (2006). Fibrinogen is associated with an increased risk of Alzheimer disease and vascular dementia. *Stroke* 36, 2637–2641. doi: 10.1161/01.STR.0000189721.31432.26
- Paul, J., Strickland, S., and Melchor, J. (2007). Fibrin deposition accelerates neurovascular damage and neuroinflammation in mouse models of Alzheimer's disease. *J. Exp. Med.* 204, 1999–2008. doi: 10.1084/jem.20070304
- Ryu, J. K., Davalos, D., and Akassoglou, K. (2009). Fibrinogen signal transduction in the nervous system. *J. Thromb. Haemost.* 7(Suppl. 1), 151–154. doi: 10.1111/j.1538-7836.2009.03438.x
- Schindler, S. E., Gray, J. D., Gordon, B. A., Xiong, C., Batrla-Utermann, R., Quan, M., et al. (2018). Cerebrospinal fluid biomarkers measured by Elecsys assays compared to amyloid imaging. *Alzheimers Dement.* 14, 1460–1469. doi: 10.1016/j.jalz.2018.01.013
- Shen, M.-Y., Hsiao, G., Fong, T.-H., Chen, H., Chou, D.-S., Lin, C., et al. (2008). Amyloid beta peptide-activated signal pathways in human platelets. *Eur. J. Pharmacol.* 588, 259–266. doi: 10.1016/j.ejphar.2008.04.040
- Wilke, C., Bender, F., Hayer, S. N., Brockmann, K., Schols, L., Kuhle, J., et al. (2018). Serum neurofilament light is increased in multiple system atrophy of cerebellar type and in repeat-expansion spinocerebellar ataxias: a pilot study. *J. Neurol.* 265, 1618–1624. doi: 10.1007/s00415-018-8893-9
- Xu, G., Zhang, H., Zhang, S., Fan, X., and Liu, X. (2008). Plasma fibrinogen is associated with cognitive decline and risk for dementia in patients with mild cognitive impairment. *Int. J. Clin. Pract.* 62, 1070–1075. doi: 10.1111/j.1742-1241.2007.01268.x

Conflict of Interest: The authors declare that the research was conducted in the absence of any commercial or financial relationships that could be construed as a potential conflict of interest.

Copyright © 2021 Fan, Sun, Sun, Jian, Li, Shen, Zeng, Wang and Bu. This is an open-access article distributed under the terms of the Creative Commons Attribution License (CC BY). The use, distribution or reproduction in other forums is permitted, provided the original author(s) and the copyright owner(s) are credited and that the original publication in this journal is cited, in accordance with accepted academic practice. No use, distribution or reproduction is permitted which does not comply with these terms.



Association Study of Alcohol Dehydrogenase and Aldehyde Dehydrogenase Polymorphism With Alzheimer Disease in the Taiwanese Population

Yah-Yuan Wu¹, Yun-Shien Lee^{2,3}, Yu-Li Liu⁴, Wen-Chuin Hsu¹, Wei-Min Ho¹, Yu-Hua Huang¹, Shih-Jen Tsai^{5,6}, Po-Hsiu Kuo^{7,8} and Yi-Chun Chen^{1*}

¹ Department of Neurology, Chang Gung Memorial Hospital, Linkou Medical Center and College of Medicine, Chang Gung University, Taoyuan, Taiwan, ² Department of Biotechnology, Ming Chuan University, Taoyuan, Taiwan, ³ Genomic Medicine Research Core Laboratory, Chang Gung Memorial Hospital, Taoyuan, Taiwan, ⁴ Center for Neuropsychiatric Research, National Health Research Institutes, Zhunan, Taiwan, ⁵ Department of Psychiatry, Taipei Veterans General Hospital, Taipei, Taiwan, ⁶ Division of Psychiatry, National Yang-Ming University, Taipei, Taiwan, ⁷ Department of Public Health, Institute of Epidemiology and Preventive Medicine, National Taiwan University, Taipei, Taiwan, ⁸ Department of Psychiatry, National Taiwan University Hospital, Taipei, Taiwan

OPEN ACCESS

Edited by:

Kin Ying Mok,
University College London,
United Kingdom

Reviewed by:

Xiaopu Zhou,
Hong Kong University of Science
and Technology, Hong Kong
Jinchen Li,
Central South University, China

*Correspondence:

Yi-Chun Chen
ycchen.cgmh@gmail.com;
asd108@adm.cgmh.org.tw

Specialty section:

This article was submitted to
Neurodegeneration,
a section of the journal
Frontiers in Neuroscience

Received: 04 November 2020

Accepted: 05 January 2021

Published: 22 January 2021

Citation:

Wu Y-Y, Lee Y-S, Liu Y-L,
Hsu W-C, Ho W-M, Huang Y-H,
Tsai S-J, Kuo P-H and Chen Y-C
(2021) Association Study of Alcohol
Dehydrogenase and Aldehyde
Dehydrogenase Polymorphism With
Alzheimer Disease in the Taiwanese
Population.
Front. Neurosci. 15:625885.
doi: 10.3389/fnins.2021.625885

Alcohol dehydrogenase (ADH) and aldehyde dehydrogenase (ALDH) are two major alcohol-metabolizing enzymes. Moderate alcohol intake is a protective modified factor in Alzheimer's disease (AD) while heavy alcohol intake and abstinence increased dementia risk. The associations between Alzheimer's disease and alcohol-metabolizing genes are uncertain. This study examined the association of AD with seven *ADH/ALDH* single-nucleotide polymorphisms (SNPs), *ADH1C* rs2241894, *ADH1B* rs1229984, *ALDH1B1* rs2073478, *ALDH2* rs886205, rs4767944, rs4648328, and rs671. We enrolled 157 AD and 168 age- and sex-matched control subjects in pilot study to examine the association of AD with *ADH/ALDH* SNPs. Reconstructed *ALDH2* haplotypes were performed. We measured plasma level of ADH1C and checked the interaction effect of AD-rs2241894 genotype on plasma ADH1C level. In extension study, we further examined 339 AD and 2,504 healthy control from the Taiwan Biobank. In pilot study, we observed that *ADH1C* rs2241894 TT genotype was negatively associated with AD in a recessive genetic model (OR = 0.25, 95% CI 0.09–0.75, $p < 0.0001$) in women. A strong linkage disequilibrium was observed among the four examined SNPs of *ALDH2*. No haplotype was related to AD. The plasma ADH1C level in AD was higher than that in control. After adjusted by age, sex, hypertension, diabetes mellitus, and alcohol, we found a significant interaction effect of AD-rs2241894 genotype on plasma ADH1C level ($p = 0.04$). This interaction effect was attributable to the association between AD and plasma ADH1C level (β estimate = 366, 95% CI 92.7~639.4, $p = 0.009$). The genetic distribution of *ADH1C* rs2241894 showed strong ethnic heterogeneity, in which the T allele was the minor allele accounting for 28.5% in our study and 23.6% in East Asians, while it was a major allele in Americans, Europeans, and the global populations. No association was discovered between AD and the five SNPs: rs2241894, rs1229984,

rs2073478, rs886205, and rs671 in the extension study. In summary, this study revealed a suggestive association between ADH1C rs2241894 and female AD in the pilot study, but failed to confirm this finding in a population database. Further age-matched and large sample size case-control studies are needed before rs2241894 can be interpreted as a protective genetic factor of AD.

Keywords: alcohol dehydrogenase, aldehyde dehydrogenase, Alzheimer's disease, ADH1C level, ADH1C rs2241894

INTRODUCTION

Alzheimer's disease (AD) is the leading cause of dementia, especially in the elderly. The prevalence is 40.2 per 1,000 persons in participants older than 60 years in the community (Fiest et al., 2016). The incidence of the disease doubles every 5 years after 65 years of age (Querfurth and LaFerla, 2010; Hebert et al., 2013). Patients suffer from cognitive decline and eventually progress to loss of daily function or death. Amyloid and tau deposition causes oxidative stress and worsens mitochondrial and synaptic dysfunction (Querfurth and LaFerla, 2010). Non-modifiable risk factors of AD include aging, female sex, and genetic risks, such as carrying the apolipoprotein E (APOE) ε4 allele (Corder et al., 1993), whereas risk factors, such as diabetes mellitus (DM), hypertension (HTN), obesity, smoking, excessive alcohol consumption over 168 g weekly, and educational attainment, are potentially modifiable (Lourida et al., 2019).

Alcohol abuse is a major factor in brain damage (Ridley et al., 2013). According to the Centers for Disease Control and Prevention (CDC) of the United States, heavier drinkers were defined as those consuming more than 28 g of pure alcohol per day in the case of men and 14 g in the case of women (Schoenborn et al., 2013). Fourteen grams of pure alcohol corresponds to a 12-US-fluid-ounce (350 mL) glass of 4.1% beer or a 5-US-fluid-ounce (150 mL) glass of 12% alcohol-by-volume wine. A 23-year follow-up prospective cohort study suggested that alcohol consumption is a risk factor for dementia in both sexes. The effect of alcohol consumption and dementia is considered to be J-shaped, where excessive alcohol intake (>112 g/week) or abstinence increased dementia risk, compared with consuming 9–112 g/week (Sabia et al., 2018). The J-shaped effect was also observed between alcohol and AD. In systemic reviews, drinking patterns are associated with AD and mild cognitive impairment, where abstinence and heavy drinking were associated with an increased risk of AD onset compared with moderate drinking (Rehm et al., 2019).

Alcohol is primarily metabolized by alcohol dehydrogenase (ADH) and aldehyde dehydrogenase (ALDH). The metabolism of alcohol produces acetaldehyde, acetate, and reactive oxygen species. Both high ADH activity and low ALDH activity cause an excess of acetaldehyde and result in oxidative stress (Ohta et al., 2004). ADH families (EC 1.1.1.1) are a group of dehydrogenase enzymes that facilitate the interconversion between alcohols and aldehydes or ketones with the reduction of NAD⁺ to NADH during the biosynthesis of various metabolites. ALDH families (EC 1.2.1.3) are a group of enzymes that catalyze the oxidation of aldehydes (Cederbaum, 2012). ADH and ALDH

variants have been shown to influence alcohol dependence in previous studies (Sun et al., 2019). Lacunar infarction (Suzuki et al., 2004) and neuropsychiatric disease were observed to be associated with the ADH genotype, whereas Parkinson's disease was not (Suzuki et al., 2004; Garcia-Martin et al., 2019; Kim et al., 2020). On the other hand, *ALDH2* polymorphism is related to Parkinson's disease and intracranial hemorrhage (Chen et al., 2019; Huang et al., 2020). The prevalence of the *ADH1B*, *ADH1C*, and *ALDH2* genotypes is higher in Asians (Eng et al., 2007). In the literature review, approximately 30% of people in Asia and 47% of people in Taiwan were found to carry genetic variants of the *ALDH2* A allele by rs671 with reduced enzymatic activity (Chiang et al., 2016). *ALDH1B1*, which shares significant sequence homology with *ALDH2*, is related to drinking habits in Caucasians (Husemoen et al., 2008). The association between *ALDH2* genetic polymorphisms and AD was inconclusive. Some reports suggested that *ALDH2**2 (rs671 variation) is a risk factor for AD in Japanese (Kamino et al., 2000), whereas others reported no association in Japanese and older Korean populations (Kim et al., 2004; Komatsu et al., 2014). *ALDH2* rs886205 affects the methylation of the *ALDH2* premotor region (Pathak et al., 2017). Meta-analysis showed a borderline influence of *ALDH2**2 on AD in a recessive genetic fashion (Hao et al., 2011; Chen et al., 2019), but it was not identified as a true susceptibility AD gene among the 695 gene candidates in the AlzGene database. To date, there have been no studies addressing *ALDH1B1* polymorphisms and AD risks. In ADH1C, the rate of alcohol elimination was proved to be associated with the SNPs across ADH1C and ADH1B (Birley et al., 2009). From GWAS (genome-wide association) of alcohol dependence in African-American, *ADH1C* rs2241894 (p.Thr151 =) is a risk loci mapped to alcohol-metabolizing enzyme genes (Gelernter et al., 2014). No report of the association between AD and ADH1C SNPs so far.

We selected *ADH1C* rs2241894 (*ADH1C*, chr4: 99344976, Synonymous Variant, c.453 A > T, C, p.Thr151 =), *ADH1B* rs1229984 (chr4:99318162, Missense Variant, c.143A > G, p.His48Arg), *ALDH1B1* rs2073478 (chr9:38396068, c.320G > A, p.Arg107His), *ALDH2* rs886205 (G > A, promoter, 5'-untranslated region), *ALDH2* rs4767944 (C > G, T, Intron Variant), *ALDH2* rs4648328 (C > T, intron variant, intron 3), and *ALDH2* rs671 (G > A, missense variant Glu504Lys, exon 12) based on previous evidence of their association with alcohol dependence (Edenberg and Foroud, 2013).

Only a few studies have addressed the associations between AD and alcohol-metabolizing enzymes. Given that the ADH/ALDH pathway is involved in numerous risks of AD, including oxidative stress, HTN, and alcohol consumption, this

study first utilized single-center case-control data for evaluation, and then used Taiwan population genomic data for replication analyses to examine whether these genes are AD-susceptible genes. This study was extended to ALDH-related pathways, which is a novel route to examine the association between AD and the ADH gene.

MATERIALS AND METHODS

Patient and Control Subject Recruitment

This study was designed as a two-step process. First, we enrolled 157 AD patients and 168 age- and sex-matched control subjects in a pilot study. AD diagnosis was made according to the 2011 diagnostic criteria of the National Institute on Aging-Alzheimer's Association workgroups (NIAAA) (McKhann et al., 2011). The control group consisted of sex- and age-matched subjects who visited Chang Gung Memory Hospital (CGMH) for a health exam or treatment for diseases other than neurodegenerative diseases or cerebrovascular diseases.

Second, the number of AD patients was expanded to 339. A total of 2504 healthy participants selected from the Taiwan Biobank were included in the extension study. The Taiwan Biobank is a prospective population-based study that enrolled healthy seniors with extensive baseline phenotypic measurements, genomic data, and stored biological samples. The criteria for selecting the control groups from the Taiwan Biobank were the age range 50–70 years, no history of stroke or dementia, and self-reporting as being of Taiwanese Han Chinese ancestry

(Chen et al., 2016). Details on the Taiwan Biobank can be found on its official website¹.

Selection of SNPs, Genotyping, and Haplotype Construction for Cases and Control

Based on a previously reported association with alcohol dependence (Edenberg and Foroud, 2013), the pilot study analyzed seven SNPs, namely, *ADH1C* rs2241894, *ADH1B* rs1229984, *ALDH1B1* rs2073478, *ALDH2* rs886205, *ALDH2* rs4767944, *ALDH2* rs4648328, and *ALDH2* rs671. Only 5 SNPs were evaluated in extension study because custom Taiwan Biobank chips (Affymetrix, Santa Clara, CA, United States) only contains only 5 ones, namely *ADH1C* rs2241894, *ADH1B* rs1229984, *ALDH1B1* rs2073478, *ALDH2* rs886205. Among these SNPs, *ADH1C* rs2241894 is believed to affect alcohol metabolism. *ADH1B* rs1229984 is a well-studied genetic variant associated with alcohol dependence in Asians. Genomic DNA was extracted from peripheral leukocytes using the Stratagene DNA extraction kit (La Jolla, CA, United States). SNP polymorphisms were genotyped using TaqMan® Assays in the ABI Prism 7900HT Sequence Detection System (catalog #4317596, Applied Biosystems, Foster City, CA, United States) (Schleinitz et al., 2011). Plasma *ADH1C* level was determined using human *ADH1C* ELISA kit (catalog #MBS2889930, MyBioSource, San Diego, CA, United States) and monitored spectrophotometrically at 450 nm on a multifunctional microplate reader (Tecan infinite 200) by following the manufacturer's instructions. Levels of

¹<https://taiwanview.twbiobank.org.tw/index>

TABLE 1 | Background demographic distribution and frequency of the genotype in the pilot study.

	Males (<i>n</i> = 147)			Females (<i>n</i> = 178)		
	AD (<i>n</i> = 73)	Controls (<i>n</i> = 74)	<i>p</i> -Value	AD (<i>n</i> = 84)	Controls (<i>n</i> = 94)	<i>p</i> -Value
Age (years)	69.4 ± 9.0	67.1 ± 5.3	0.06	65.4 ± 5.9	67.0 ± 6.3	0.08
Education (years)	8.4 ± 4.1	9.3 ± 4.7	0.31	7.4 ± 4.5	5.6 ± 4.7	0.01
Hypertension (%)	55.40%	52.51%	0.69	45.2%	44.7%	0.94
Diabetes mellitus (%)	20.30%	21.10%	0.9	36.9%	20.2%	0.01
Alcohol use (%)	17.60%	16.90%	0.92	1.2%	1.1%	0.94
APOE ε4 carrier	<i>n</i> = 73 30.1%	<i>n</i> = 57 12.3%	0.02	<i>n</i> = 84 43.4%	<i>n</i> = 83 21.7%	0.01
<i>ADH1B</i>						
rs1229984 TT/TC/CC	49.4/39.5/11.1	56.2/41.1/2.7	0.14	60.7/35.7/3.6	53.2/42.6/4.3	0.6
<i>ADH1C</i>						
rs2241894 CC/CT/TT	43.8/42.5/13.7	52.1/38.4/9.6	0.55	54.8/44.0/1.2	46.8/43.6/9.6	0.05
<i>ALDH1B1</i>						
rs2073478 GG/GT/TT	47.9/36.6/15.5	52.8/31.9/15.3	0.82	41.0/51.8/7.2	48.4/36.6/15.1	0.07
<i>ALDH2</i>						
rs886205 GG/GA/AA	77.0/21.6/1.4	78.1/20.5/1.4	0.99	82.1/17.9/0.0	74.5/22.3/3.2	0.18
rs4767944 TT/TC/CC	48.6/41.9/9.5	41.1/49.3/9.6	0.63	51.8/41.0/7.2	47.8/38.0/14.1	0.34
rs4648328 CC/CT/TT	67.1/28.8/4.1	57.5/38.4/4.1	0.46	68.7/26.5/4.8	64.9/31.9/3.2	0.66
rs671 GG/GA/AA	46.6/35.6/17.8	46.6/42.5/11.0	0.44	47.6/41.7/10.7	41.5/50.0/8.5	0.53

N, number; AD, Alzheimer disease; ADH, alcohol dehydrogenase; ALDH, aldehyde dehydrogenase. Data are expressed as percentage or mean ± SE. Comparisons between AD cases and controls were analyzed using the χ^2 test or *t*-test where appropriate.

ADH1C were determined from a standard curve. Patterns of linkage disequilibrium (LD) were evaluated using Haploview v4, and haplotypes were reconstructed using PHASE 2.0 (Barrett et al., 2005) based on the LD results. Haplotypes with a frequency <1% were excluded from the association analysis. In participants from the Taiwan Biobank, SNP genotypes were obtained from the data derived from the custom Taiwan Biobank chips and run on the Axiom Genome-Wide Array Plate System (Affymetrix, Santa Clara, CA, United States).

Statistical Analysis and Power Estimation

Pearson's χ^2 -test or *t*-test was used to compare the demographic data and the distributions of genotypes of AD and control. Two-tailed *p*-values were derived from the χ^2 -test or Fisher's exact test. Association analyses were performed stratified by sex. Hardy-Weinberg equilibrium was performed via χ^2 -test for all SNPs at a significance level of 0.05. Multivariable logistic regression was used to analyze the phenotype-genotype associations of AD with ADH and ALDH alleles under dominant, recessive, and additive genetic models. The covariables included age, years of education, HTN, DM, and alcohol use. Since considering Bonferroni correction, the significance level was set to 0.007 in pilot study and 0.01 in extension study. The permutation testing was performed when the *p*-value was under Bonferroni correction in pilot study. Analysis of interaction effect (Chen et al., 2009) was performed to evaluate how carrying APOE ϵ 4 influence the ADH1C rs2241894 to AD susceptibility, because APOE ϵ 4 and ADH1C shared the common pathway of oxidative stress. All the data analyses were performed using SAS software version 9.1.3 (SAS Institute, Cary, NC, United States). Association of the interaction effect between AD and rs2241894 genotypes on the plasma ADH1C level was tested by the general linear models (GLM) with adjustment for age, sex, DM, HTN, and alcohol. We also perform analysis of interaction effect of AD-rs2241894 genotype in ADH1C level.

We evaluated the ability to detect an association between an SNP and AD via a power calculation implemented in QUANTO version 1.0 (Gauderman, 2002). When Minor allele frequency (MAF) > 0.2 under a recessive genetic model at a significance level of 5%, we observed that the power to identify an association was greater than 0.8 when the per-allele genetic effect was greater than 3.5 and 2.0 in the pilot case-control study and in the extension study, respectively.

RESULTS

Demography of the Pilot Case-Control Study

A total of 157 AD patients and 168 controls were included in the pilot study (Table 1). The years of education were higher in the female AD patients than in the controls. The age and sex between the AD patients and the controls were matched in this dataset. The proportion of APOE ϵ 4 carriers was higher in the AD patients than in the controls. The proportion of DM was higher in the female patients with AD than in the controls. There were no differences in age, HTN frequency, and the proportion of alcohol use. As the proportion of alcohol use was remarkably different between sexes, the analyses were stratified by sex.

Genotype Frequency and Association Analysis of the Pilot Case-Control Study

All seven SNPs were in Hardy-Weinberg equilibrium at a significance level of 0.05. The frequencies of each genotype in the AD and control subjects are listed in Table 1. The proportion of ADH1C rs2241894 TT genotype (minor allele T) was significantly lower in the female patients with AD than in the female controls. The association between the SNP genotype and AD is presented in Table 2. In the female group, ADH1C rs2241894 was significantly associated with AD in the recessive genetic model (OR = 0.25, 95% CI 0.09–0.75, *p* < 0.0001). APOE ϵ 4 carriers had no interactive effect between AD and ADH1C

TABLE 2 | Associations of the candidate SNPs with AD in the pilot study.

Gene	SNP	Position	Dominant <i>p</i> -values	Additive <i>p</i> -values, (OR, 95% CI)	Recessive <i>p</i> -values, (OR, 95% CI)
ADH1B: Missense Variant, c.143A > G, p.His48Arg	rs1229984	chr4:99318162	M: 0.496, F: 0.04	M: 0.23, F: 0.07	M: 0.12, F: 0.99
ADH1C: Synonymous Variant, c.453 T > A, C, p.Thr151 =	rs2241894	chr4:99344976	M: 0.487, F: 0.256	M: 0.45, F: 0.04	M: 0.06, <i>F</i> < 0.0001 (0.25, 0.09–0.75)
ALDH1B1: Missense Variant, c.320G > A, p.Arg107His	rs2073478	chr9:38396068	M: 0.66, F: 0.25	M: 0.52, F: 0.83	M: 0.48, F: 0.15
ALDH2: 2KB Upstream Variant, A > G	rs886205	chr12:111766623	M: 0.788, F: 0.193	M: 0.77, F: 0.08	M: 0.84, F: NA
ALDH2: Intron Variant, C > G, T	rs4767944	chr12:111771537	M: 0.205, F: 0.661	M: 0.43, F: 0.39	M: 0.64, F: 0.24
ALDH2: Intron Variant, C > T	rs4648328	chr12:111784984	M: 0.338, F: 0.707	M: 0.45, F: 0.92	M: 0.88, F: 0.53
ALDH2: Missense Variant, c.1510G > A, p.Glu504Lys	rs671	chr12:111803962	M: 0.987, F: 0.388	M: 0.69, F: 0.55	M: 0.41, F: 0.91

M, male, F, female, NA, not applicable, OR, odds ratio, 95% CI = 95% confidence interval. Logistic regression was performed, adjusting for age, education, HTN, DM, and alcohol use.

P-value with Bonferroni correction for significance was 0.007. The permutation testing of 10,000 replicates was performed when the *p*-value was significant under Bonferroni correction.

rs2241894. This study did not find an association between AD and the other six SNPs in the female groups and any candidate SNPs in the male groups (Supplementary Table 1).

Demography of the Extension Study

Among 339 AD patients and 2,504 control subjects in the extension cohort study, there were 123 AD and 1,271 controls in men (Table 3). The AD patients were older than the control subjects. Among men, the mean age was 71.0 (± 10.1) in the AD group and 64.1 (± 2.8) years in the control group ($p < 0.05$). Among women, the mean age was 72.6 (± 8.5) in the AD group and 64.0 (± 3.0) in the control group ($p < 0.05$). The years of education were higher in the AD group than in the control group (AD 8.6 \pm 4.3, control 5.2 \pm 1.2, $p < 0.05$). The proportions of HTN and DM were higher in the AD group than in the control group (HTN AD 50.5%, control 35.4%, $p < 0.05$, DM AD 37.5%, control 8.8%, $p < 0.05$). As the proportion of alcohol

use was remarkably different between sexes, the analyses were stratified by sex.

Genotype Frequency and Association Analysis of the Extension Study

All five SNPs were in the Hardy-Weinberg equilibrium at a significance level of 0.05. The frequencies of each genotype in the AD and control subjects are listed in Table 3. The association between the SNP genotype and AD is presented in Table 4. The *ADH1C* rs2241894 genotype had no association with AD after adjusting for age, years of education, proportion of alcohol use, and comorbidities in both sexes. No association was discovered between AD and the other SNPs (Supplementary Table 2).

Haploview Analysis of *ALDH2* SNPs

In the pilot case-control study, a haplotype block of *ALDH2* was further constructed by rs886205, rs4767944, rs4648328, and rs671

TABLE 3 | Background demographic distribution and frequency of the genotype in the extension study.

	Males (<i>n</i> = 1394)			Females (<i>n</i> = 1449)		
	AD (<i>n</i> = 123)	Controls (<i>n</i> = 1271)	<i>p</i> -Value	AD (<i>n</i> = 216)	Controls (<i>n</i> = 1233)	<i>p</i> -Value
Age (years)	71.0 \pm 10.1	64.1 \pm 2.8	2.3E-66	72.6 \pm 8.5	64.0 \pm 3.0	8.06E-134
Education (years)	8.6 \pm 4.3	5.2 \pm 1.2	1.1E-85	4.9 \pm 4.6	4.6 \pm 1.3	0.06
Hypertension (%)	48.8%	45.6%	0.50	50.5%	35.4%	2.40E-5
Diabetes mellitus (%)	22.0%	14.0%	0.17	37.5%	8.8%	5.80E-31
Alcohol use (%)	14.6%	11.7%	0.35	0.9%	1.1%	0.86
<i>ADH1B</i>						
rs1229984 TT/TC/CC	54.1/35.2/10.7	54.2/39.3/6.6	0.21	48.3/46.40/5.2	54.7/39.3/6.0	0.14
<i>ADH1C</i>						
rs2241894 CC/CT/TT	46.7/46.2/10.7	51.2/42.3/6.6	0.21	57.1/37.2/5.7	55.3/38.1/6.6	0.38
<i>ALDH1B1</i>						
rs2073478 GG/GT/TT	50.8/35.0/14.2	46.1/42.9/11.0	0.21	42.4/48.1/9.5	46.7/42.8/10.5	0.35
<i>ALDH2</i>						
rs886205 GG/GA/AA	77.3/20.3/2.4	77.9/20.8/1.3	0.62	76.5/22.5/0.9	77.5/21.5/1.0	0.90
rs671 GG/GA/AA	50.8/35.2/13.9	50.6/40.8/8.6	0.11	49.1/40.6/10.4	50.6/40.8/8.5	0.67

n, number; AD, Alzheimer disease; ADH, alcohol dehydrogenase; ALDH, aldehyde dehydrogenase. Data are expressed as percentage or mean \pm SE. Comparisons between AD cases and controls were analyzed using the χ^2 test or *t*-test where appropriate.

TABLE 4 | Associations of the candidate SNPs with AD in the extension study.

Gene	SNP	Position	Dominant <i>p</i> -values	Additive <i>p</i> -values	Recessive <i>p</i> -values, (OR, 95% CI)
<i>ADH1B</i> : Missense Variant, c.143A > G, p.His48Arg	rs1229984	chr4:99318162	M: 0.46, F: 0.78	M: 0.41, F: 1.00	M: 0.58, F: 0.59
<i>ADH1C</i> : Synonymous Variant, c.453T > A, C p.Thr151 =	rs2241894	chr4:99344976	M: 0.24, F: 0.39	M: 0.09, F: 0.29	M: 0.08, F: 0.72
<i>ALDH1B1</i> : Missense Variant, c.320G > A, p.Arg107His	rs2073478	chr9:38396068	M: 0.12, F: 0.12	M: 0.34, F: 0.40	M: 0.72, F: 0.77
<i>ALDH2</i> : 2KB Upstream Variant, A > G	rs886205	chr12:111766623	M: 0.48, F: 0.51	M: 0.19, F: 0.46	M: NA, F: 0.60
<i>ALDH2</i> : Missense Variant, c.1510G > A, p.Glu504Lys	rs671	chr12:111803962	M: 0.57, F: 0.65	M: 0.39, F: 0.56	M: 0.29, F: 0.59

M, male, F, female, NA, not applicable, OR, odds ratio, 95% CI = 95% confidence interval, Logistic regression was performed, adjusting for age, education, HTN, DM, and alcohol use. *p*-value with Bonferroni correction for significance was 0.01.

using Haploview (4.2), where there was one block with strong LD (Figure 1). In the haplotype analyses, there was no association between the haplotype and AD susceptibility.

Plasma ADH1C Level

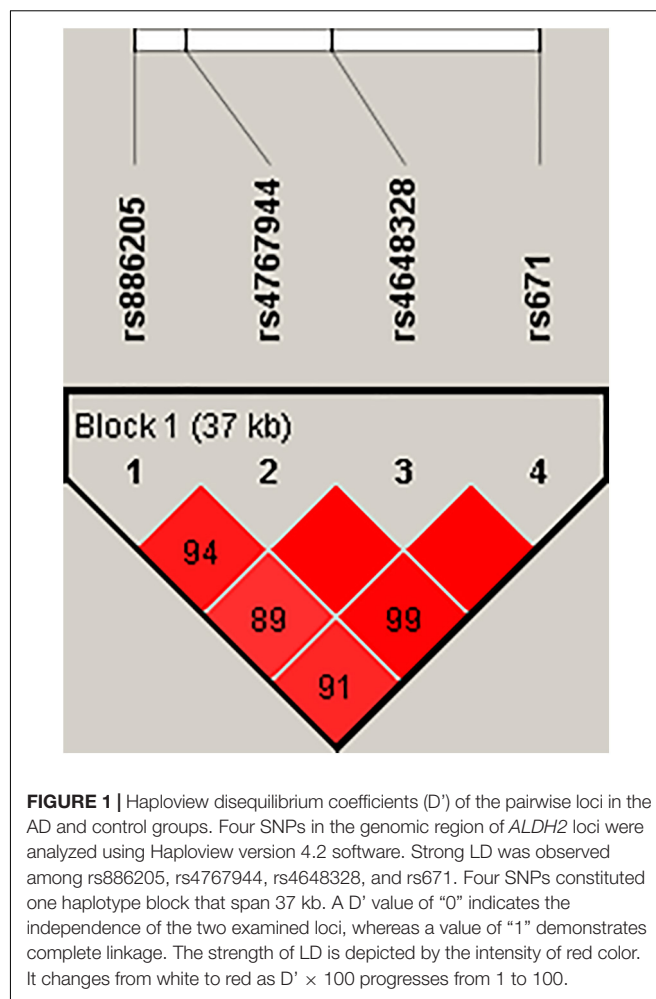
In pilot case-control study, we examined the plasma level of ADH1C. AD had higher ADH1C level in comparison to control group ($n = 78$, $n = 72$, 781 ± 383 , 665 ± 242 , respectively) ($p = 0.03$) (Figure 2A). After adjusted by age, sex, HTN, DM, and alcohol, we found a significant interaction effect of AD-rs2241894 genotype on plasma ADH1C level ($p = 0.04$) (Figure 2B). This interaction effect was attributable to the association between AD and plasma ADH1C level (β estimate = 366, 95% CI 92.7~639.4, $p = 0.009$).

DISCUSSION

Our study demonstrated a suggestive association between AD and *ADH1C* rs2241894 genotypes in a recessive fashion. To the best of our knowledge, this is the first study to propose *ADH1C* rs2241894 genotypes as a protective factor of AD in the Taiwanese female population. Although there was a correlation between AD and *ADH1C* rs2241894 in the pilot study, the result in the extension study was not significant in both sexes, which may indicate the possibility of other confounding factors, such as age and lifestyle. This study did not find associations between AD and *ADH1B* (rs1229984), *ALDH1B1* (rs2073478), and *ALDH2* (rs886205, rs4767944, rs4648328, and rs671), indicating that *ADH1B*, *ALDH1B1*, and *ALDH2* played no role in the relationship between alcohol and AD.

Alcohol elimination was catalyzed by ADH and ALDH (Zakhari, 2006). Class I ADH, consisting of several homo- and heterodimers of alpha, beta, and gamma subunits, exhibits high activity for ethanol oxidation to acetaldehyde, thus playing a major role in ethanol catabolism (Cederbaum, 2012). *ADH1C* encodes the gamma subunit of class I ADH. *ADH1C* cytoplasmic expression was mainly observed in glandular cells of the gastrointestinal tract, including the liver, duodenum, and stomach. *ADH1B* and *ADH1C* have polymorphisms that produce isoenzymes with distinct kinetic properties. Previous studies showed that the genetic variations in ADH genes were related to alcohol consumption (Edenberg and Foroud, 2013); however, this was more evident for the ADH2 gene, whereas the *ADH1C* polymorphism, as in our study, showed a small influence on the risk of alcoholism. In a previous SNP study, *ADH1C* was associated with alcohol elimination rate, whereas rs2241894 was not associated with the *in vivo* kinetic model of alcohol metabolism (Birley et al., 2009).

Alcohol metabolism via ADH produces acetaldehyde and oxygen radicals, which are highly reactive molecules (Zakhari, 2006). Neurons are extremely sensitive to attacks by destructive free radicals. In the brains of AD patients, free radical leads to DNA damage, protein oxidation, lipid peroxidation, and advanced glycosylation, which further aggravates AD pathology including neurofibrillary tangles and senile plaques (Tonnie and Trushina, 2017).



The genetic distribution of *ADH1C* rs2241894 showed strong ethnic heterogeneity, in which the T allele was the minor allele accounting for 28.5% in our study, 23.6% in East Asians, and 40% in South Asians, while it was a major allele in Americans (83.0%), Europeans (76.5%), and the global populations (52.8%) (Huang et al., 2020). *ADH1C* rs2241894 (A > G, synonymous variant Thr151, exon 5) is a synonymous variant. Moreover, we did not find functional SNPs that have LD with rs2241894 on SNPsnap². To the best of our knowledge, there is no report showing an association between AD and rs2241894 or nearby SNPs.

Differences in drinking habit and alcohol metabolism exist between sex. In the United States, epidemiological evidence suggests that nearly 20% of adult males suffer from alcohol abuse or alcoholism-related complications. On the other hand, only approximately 5–6% of adult females are alcoholic or abuse alcohol on a regular basis (Mumenthaler et al., 1999). In Asia, men are prone to alcohol drinking in contrast to women (Millwood et al., 2019), in which we have demonstrated that the rate of alcohol consumption was 0% in women versus 26% in men (Chen et al., 2006, 2009). In addition, the toxic effect of alcohol can be influenced by genes; for example, men carrying

²<https://data.broadinstitute.org/mpg/snpnap/>

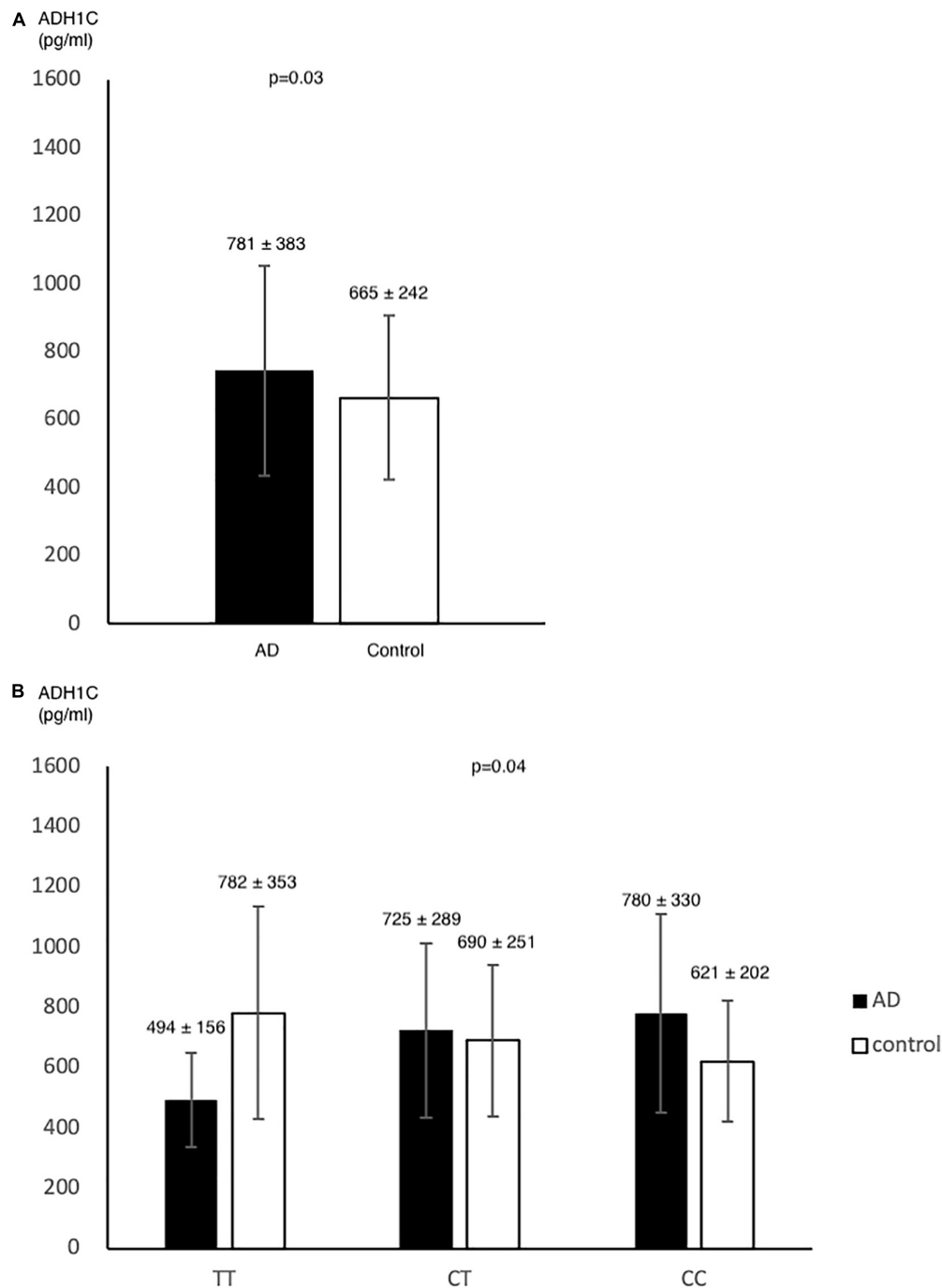


FIGURE 2 | ADH1C level in AD and control. Plasma ADH1C level was higher in AD than in control **(A)**. **(B)** there was a marginal interaction effect between AD and rs2241894 genotype on plasma ADH1C level ($p = 0.04$), in which those carried minor allele T had lower ADH1C level in AD patients but higher ADH1C level in the controls.

APOE $\epsilon 2\epsilon 3$ have a greater tendency to suffer from strokes than those with $\epsilon 3\epsilon 3$ when they have alcohol exposure (Chen et al., 2009). In alcoholic pharmacokinetics, women have increased bioavailability and a faster clearance rate (Mumenthaler et al., 1999). Another example of alcohol-gene interaction is the class III ADH (glutathione-dependent ADH). Women develop higher

blood alcohol levels than men in spite of an equal alcohol intake due to a smaller gastric metabolism in women due to the lesser activity of class III ADH in females (Baraona et al., 2001). Therefore, sex differences in the effects of alcohol metabolism on AD should be tested to illuminate the genetic roles of AD in personalized management (Sultatos et al., 2004).

The association between AD and *ADH1C* rs2241894 was significant in the pilot study but not in the extension study. The conflicting findings may be due to the difference between the two control groups. The controls were older and had more comorbidities in the pilot study than the extension study, but similar to the AD patient group. The subjects from the Taiwan Biobank were younger and healthier, and may have better lifestyles, such as social activities, exercise, and diet. In addition, the number of patients was relatively small compared with the control number in the extension study. The positive result may be caused by a statistical effect.

LIMITATION

This study is the first to discuss the association between *ADH1C* rs2241894 and AD under sex disparities. However, there are some limitations to our study. First, alcohol intake was much lower in Asian females than in males; therefore, the sample size was small, especially for those with alcohol use. Second, the frequencies of alcohol-metabolizing genes differ among ethnicities (Huang et al., 2020). Besides, the sizes of the examined samples are small and have limited power to detect genetic association of minor/modest effect with AD. The discrepancy in the results of pilot and extension study may be caused by age difference between two groups. The result should be interpreted with caution and further studies with age-matched and larger sample size were indicated for further confirmation of the results herein.

CONCLUSION

This study revealed a suggestive association between the genetic variant of *ADH1C* rs2241894 and female AD in Taiwanese population. Carrying the *ADH1C* rs2241894 TT genotype may be a protective factor for elderly female Taiwanese individuals.

DATA AVAILABILITY STATEMENT

The datasets presented in this study can be found in online repositories. The names of the repository/repositories and accession number(s) can be found in the article/**Supplementary Material**.

REFERENCES

- Baraona, E., Abittan, C. S., Dohmen, K., Moretti, M., Pozzato, G., Chayes, Z. W., et al. (2001). Gender differences in pharmacokinetics of alcohol. *Alcohol Clin. Exp. Res.* 25, 502–507.
- Barrett, J. C., Fry, B., Maller, J., and Daly, M. J. (2005). Haploview: analysis and visualization of LD and haplotype maps. *Bioinformatics* 21, 263–265. doi: 10.1093/bioinformatics/bth457
- Birley, A. J., James, M. R., Dickson, P. A., Montgomery, G. W., Heath, A. C., Martin, N. G., et al. (2009). ADH single nucleotide polymorphism associations with alcohol metabolism in vivo. *Hum. Mol. Genet.* 18, 1533–1542. doi: 10.1093/hmg/ddp060
- Cederbaum, A. I. (2012). Alcohol metabolism. *Clin. Liver Dis.* 16, 667–685.
- Chen, C.-H., Yang, J.-H., Chiang, C. W. K., Hsiung, C.-N., Wu, P.-E., Chang, L.-C., et al. (2016). Population structure of Han Chinese in the modern Taiwanese

ETHICS STATEMENT

The studies involving human participants were reviewed and approved by the Institutional Review Board/Ethics Committee (IRB/EC) protocol was approved by the Medical Ethics Committee of Chang Gung Memorial Hospital, and the ethical approval code was IRB 201700444B0C602. The ethical approval for the study was granted by the IRB of the Taiwan Biobank before the study was conducted (approval number: 201506095RINC). The patients/participants provided their written informed consent to participate in this study.

AUTHOR CONTRIBUTIONS

Y-CC: conceptualization, methodology, investigation, resources, data curation, review and editing, project administration, and funding acquisition. Y-YW: methodology, formal analysis, and writing – original draft. Y-SL: resources, bioinformatics, data acquisition, and formal analysis. Y-LL: resources and data acquisition. W-CH, W-MH, and Y-HH: patient enrollment. S-JT: data acquisition and review and editing. P-HK: data acquisition and review and editing. All authors read and approved the final manuscript.

FUNDING

This study was supported by the Ministry of Science and Technology, Executive Yuan, Taiwan (grant numbers MOST108-2314-B-182A-047, 108-2629-B-182A-005, and 109-2629-B-182A-001) and Chang Gung Medical Foundation, Taiwan (grant numbers CMRPG3G0962 and CMRPG3J0932). Open access publication fees was received from above institution.

SUPPLEMENTARY MATERIAL

The Supplementary Material for this article can be found online at: <https://www.frontiersin.org/articles/10.3389/fnins.2021.625885/full#supplementary-material>

- population based on 10,000 participants in the Taiwan biobank project. *Hum. Mol. Genet.* 25, 5321–5331.
- Chen, J., Huang, W., Cheng, C. H., Zhou, L., Jiang, G. B., and Hu, Y. Y. (2019). Association between aldehyde dehydrogenase-2 polymorphisms and risk of Alzheimer's disease and Parkinson's disease: a meta-analysis based on 5,315 individuals. *Front. Neurol.* 10:290. doi: 10.3389/fneur.2019.00290
- Chen, Y. C., Lee-Chen, G. J., Wu, Y. R., Hu, F. J., Wu, H. C., Kuo, H. C., et al. (2009). Analyses of interaction effect between apolipoprotein E polymorphism and alcohol use as well as cholesterol concentrations on spontaneous deep intracerebral hemorrhage in the Taiwan population. *Clin. Chim. Acta* 408, 128–132. doi: 10.1016/j.cca.2009.08.004
- Chen, Y. C., Wu, Y. R., Hsu, W. C., Chen, C. M., Lee, T. H., and Chen, S. T. (2006). Basal Ganglia-thalamic hemorrhage in young adults: a hospital-based study. *Cerebrovasc. Dis.* 22, 33–39. doi: 10.1159/000092335

- Chiang, C. P., Lai, C. L., Lee, S. P., Hsu, W. L., Chi, Y. C., Gao, H. W., et al. (2016). Ethanol-metabolizing activities and isozyme protein contents of alcohol and aldehyde dehydrogenases in human liver: phenotypic traits of the ADH1B*2 and ALDH2*2 variant gene alleles. *Pharmacogenet. Genomics* 26, 184–195. doi: 10.1097/fpc.0000000000000205
- Corder, E. H., Saunders, A. M., Strittmatter, W. J., Schmechel, D. E., Gaskell, P. C., Small, G. W., et al. (1993). Gene dose of apolipoprotein E type 4 allele and the risk of Alzheimer's disease in late onset families. *Science* 261, 921–923. doi: 10.1126/science.8346443
- Edenberg, H. J., and Foroud, T. (2013). Genetics and alcoholism. *Nat. Rev. Gastroenterol. Hepatol.* 10, 487–494.
- Eng, M. Y., Luczak, S. E., and Wall, T. L. (2007). ALDH2, ADH1B, and ADH1C genotypes in Asians: a literature review. *Alcohol Res. Health* 30, 22–27.
- Fiest, K. M., Roberts, J. I., Maxwell, C. J., Hogan, D. B., Smith, E. E., Frolkis, A., et al. (2016). The prevalence and incidence of dementia due to Alzheimer's disease: a systematic review and meta-analysis. *Can. J. Neurol. Sci.* 43(Suppl. 1), S51–S82.
- Garcia-Martin, E., Diez-Fairen, M., Pastor, P., Gomez-Tabales, J., Alonso-Navarro, H., Alvarez, I., et al. (2019). Association between the missense alcohol dehydrogenase rs122984T variant with the risk for Parkinson's disease in women. *J. Neurol.* 266, 346–352. doi: 10.1007/s00415-018-9136-9
- Gauderman, W. J. (2002). Sample size requirements for matched case-control studies of gene-environment interaction. *Stat. Med.* 21, 35–50. doi: 10.1002/sim.973
- Gelernter, J., Kranzler, H. R., Sherva, R., Almasy, L., Koesterer, R., Smith, A. H., et al. (2014). Genome-wide association study of alcohol dependence: significant findings in African- and European-Americans including novel risk loci. *Mol. Psychiatry* 19, 41–49. doi: 10.1038/mp.2013.145
- Hao, P. P., Chen, Y. G., Wang, J. L., Wang, X. L., and Zhang, Y. (2011). Meta-analysis of aldehyde dehydrogenase 2 gene polymorphism and Alzheimer's disease in East Asians. *Can. J. Neurol. Sci.* 38, 500–506. doi: 10.1017/s0317167100011938
- Hebert, L. E., Weuve, J., Scherr, P. A., and Evans, D. A. (2013). Alzheimer disease in the United States (2010–2050) estimated using the 2010 census. *Neurology* 80, 1778–1783. doi: 10.1212/wnl.0b013e31828726f5
- Huang, Y. H., Chang, K. H., Lee, Y. S., Chen, C. M., and Chen, Y. C. (2020). Association of alcohol dehydrogenase and aldehyde dehydrogenase polymorphism with spontaneous deep intracerebral haemorrhage in the Taiwan population. *Sci. Rep.* 10:3641.
- Husemoen, L. L., Fenger, M., Friedrich, N., Tolstrup, J. S., Beenfeldt Fredriksen, S., and Linneberg, A. (2008). The association of ADH and ALDH gene variants with alcohol drinking habits and cardiovascular disease risk factors. *Alcohol Clin. Exp. Res.* 32, 1984–1991.
- Kamino, K., Nagasaka, K., Imagawa, M., Yamamoto, H., Yoneda, H., Ueki, A., et al. (2000). Deficiency in mitochondrial aldehyde dehydrogenase increases the risk for late-onset Alzheimer's disease in the Japanese population. *Biochem. Biophys. Res. Commun.* 273, 192–196. doi: 10.1006/bbrc.2000.2923
- Kim, J. J., Bandres-Ciga, S., Blauwendraat, C., International Parkinson's Disease Genomics Consortium, and Gan-Or, Z. (2020). No genetic evidence for involvement of alcohol dehydrogenase genes in risk for Parkinson's disease. *Neurobiol. Aging* 87, 140 e19–140 e22.
- Kim, J. M., Stewart, R., Shin, I. S., Jung, J. S., and Yoon, J. S. (2004). Assessment of association between mitochondrial aldehyde dehydrogenase polymorphism and Alzheimer's disease in an older Korean population. *Neurobiol. Aging* 25, 295–301. doi: 10.1016/s0197-4580(03)00114-3
- Komatsu, M., Shibata, N., Ohnuma, T., Kuerban, B., Tomson, K., Toda, A., et al. (2014). Polymorphisms in the aldehyde dehydrogenase 2 and dopamine beta hydroxylase genes are not associated with Alzheimer's disease. *J. Neural. Transm. (Vienna)* 121, 427–432. doi: 10.1007/s00702-013-1112-z
- Lourida, I., Hannon, E., Littlejohns, T. J., Langa, K. M., Hypponen, E., Kuzma, E., et al. (2019). Association of lifestyle and genetic risk with incidence of dementia. *JAMA* 322, 430–437. doi: 10.1001/jama.2019.9879
- McKhann, G. M., Knopman, D. S., Chertkow, H., Hyman, B. T., Jack, C. R. Jr., Kawas, C. H., et al. (2011). The diagnosis of dementia due to Alzheimer's disease: recommendations from the National institute on aging-Alzheimer's association workgroups on diagnostic guidelines for Alzheimer's disease. *Alzheimers Dement.* 7, 263–269.
- Millwood, I. Y., Walters, R. G., Mei, X. W., Guo, Y., Yang, L., Bian, Z., et al. (2019). Conventional and genetic evidence on alcohol and vascular disease aetiology: a prospective study of 500 000 men and women in China. *Lancet* 393, 1831–1842. doi: 10.1016/s0140-6736(18)31772-0
- Mumenthaler, M. S., Taylor, J. L., O'Hara, R., and Yesavage, J. A. (1999). Gender differences in moderate drinking effects. *Alcohol Res. Health* 23, 55–64.
- Ohta, S., Ohsawa, I., Kamino, K., Ando, F., and Shimokata, H. (2004). Mitochondrial ALDH2 deficiency as an oxidative stress. *Ann. N. Y. Acad. Sci.* 1011, 36–44. doi: 10.1007/978-3-662-41088-2_4
- Pathak, H., Frieling, H., Bleich, S., Glahn, A., Heberlein, A., Haschemi Nassab, M., et al. (2017). Promoter polymorphism rs886205 genotype interacts With DNA methylation of the ALDH2 regulatory region in alcohol dependence. *Alcohol Alcohol* 52, 269–276.
- Querfurth, H. W., and LaFerla, F. M. (2010). Alzheimer's disease. *N. Engl. J. Med.* 362, 329–344.
- Rehm, J., Hasan, O. S. M., Black, S. E., Shield, K. D., and Schwarzer, M. (2019). Alcohol use and dementia: a systematic scoping review. *Alzheimers Res. Ther.* 11:1. doi: 10.1016/j.alcohol.2019.06.005
- Ridley, N. J., Draper, B., and Withall, A. (2013). Alcohol-related dementia: an update of the evidence. *Alzheimers Res. Ther.* 5:3. doi: 10.1186/alzrt157
- Sabia, S., Fayosse, A., Dumurgier, J., Dugravot, A., Akbaraly, T., Britton, A., et al. (2018). Alcohol consumption and risk of dementia: 23 year follow-up of whitehall II cohort study. *BMJ* 362:k2927. doi: 10.1136/bmj.k2927
- Schleinitz, D., Distefano, J. K., and Kovacs, P. (2011). Targeted SNP genotyping using the TaqMan(R) assay. *Methods Mol. Biol.* 700, 77–87. doi: 10.1007/978-1-61737-954-3_6
- Schoenborn, C. A., Adams, P. F., and Peregoy, J. A. (2013). Health behaviors of adults: United States, 2008–2010. *Vital Health Stat.* 10, 1–184.
- Sultatos, L. G., Pastino, G. M., Rosenfeld, C. A., and Flynn, E. J. (2004). Incorporation of the genetic control of alcohol dehydrogenase into a physiologically based pharmacokinetic model for ethanol in humans. *Toxicol. Sci.* 78, 20–31. doi: 10.1093/toxsci/kfh057
- Sun, Y., Chang, S., Wang, F., Sun, H., Ni, Z., Yue, W., et al. (2019). Genome-wide association study of alcohol dependence in male Han Chinese and cross-ethnic polygenic risk score comparison. *Transl. Psychiatry* 9:249.
- Suzuki, Y., Fujisawa, M., Ando, F., Niino, N., Ohsawa, I., Shimokata, H., et al. (2004). Alcohol dehydrogenase 2 variant is associated with cerebral infarction and lacunae. *Neurology* 63, 1711–1713. doi: 10.1212/01.wnl.0000142971.08275.db
- Tonnies, E., and Trushina, E. (2017). Oxidative stress, synaptic dysfunction, and Alzheimer's disease. *J. Alzheimers Dis.* 57, 1105–1121. doi: 10.3233/jad-161088
- Zakhari, S. (2006). Overview: how is alcohol metabolized by the body? *Alcohol Res. Health* 29, 245–254.

Conflict of Interest: The authors declare that the research was conducted in the absence of any commercial or financial relationships that could be construed as a potential conflict of interest.

Copyright © 2021 Wu, Lee, Liu, Hsu, Ho, Huang, Tsai, Kuo and Chen. This is an open-access article distributed under the terms of the Creative Commons Attribution License (CC BY). The use, distribution or reproduction in other forums is permitted, provided the original author(s) and the copyright owner(s) are credited and that the original publication in this journal is cited, in accordance with accepted academic practice. No use, distribution or reproduction is permitted which does not comply with these terms.



Tau Deletion Prevents Cognitive Impairment and Mitochondrial Dysfunction Age Associated by a Mechanism Dependent on Cyclophilin-D

Claudia Jara^{1,2}, Waldo Cerpa³, Cheril Tapia-Rojas^{2*} and Rodrigo A. Quintanilla^{1*}

¹ Laboratory of Neurodegenerative Diseases, Universidad Autónoma de Chile, Santiago, Chile, ² Laboratory of Neurobiology of Aging, Centro de Biología Celular y Biomedicina (CEBICEM), Universidad San Sebastián, Santiago, Chile, ³ Laboratorio de Función y Patología Neuronal, Departamento de Biología Celular y Molecular, Facultad de Ciencias Biológicas, Pontificia Universidad Católica de Chile, Santiago, Chile

OPEN ACCESS

Edited by:

Kin Ying Mok,
University College London,
United Kingdom

Reviewed by:

Paul Anthony Adlard,
University of Melbourne, Australia
Jose Abisambra,
University of Florida, United States

*Correspondence:

Cheril Tapia-Rojas
cheril.tapia@uss.cl
Rodrigo A. Quintanilla
rodrigo.quintanilla@uautonoma.cl

Specialty section:

This article was submitted to
Neurodegeneration,
a section of the journal
Frontiers in Neuroscience

Received: 23 July 2020

Accepted: 31 December 2020

Published: 10 February 2021

Citation:

Jara C, Cerpa W, Tapia-Rojas C
and Quintanilla RA (2021) Tau Deletion
Prevents Cognitive Impairment
and Mitochondrial Dysfunction Age
Associated by a Mechanism
Dependent on Cyclophilin-D.
Front. Neurosci. 14:586710.
doi: 10.3389/fnins.2020.586710

Aging is an irreversible process and the primary risk factor for the development of neurodegenerative diseases, such as Alzheimer's disease (AD). Mitochondrial impairment is a process that generates oxidative damage and ATP deficit; both factors are important in the memory decline showed during normal aging and AD. Tau is a microtubule-associated protein, with a strong influence on both the morphology and physiology of neurons. In AD, tau protein undergoes post-translational modifications, which could play a relevant role in the onset and progression of this disease. Also, these abnormal forms of tau could be present during the physiological aging that could be related to memory impairment present during this stage. We previously showed that tau ablation improves mitochondrial function and cognitive abilities in young wild-type mice. However, the possible contribution of tau during aging that could predispose to the development of AD is unclear. Here, we show that tau deletion prevents cognitive impairment and improves mitochondrial function during normal aging as indicated by a reduction in oxidative damage and increased ATP production. Notably, we observed a decrease in cyclophilin-D (CypD) levels in aged tau^{-/-} mice, resulting in increased calcium buffering and reduced mitochondrial permeability transition pore (mPTP) opening. The mPTP is a mitochondrial structure, whose opening is dependent on CypD expression, and new evidence suggests that this could play an essential role in the neurodegenerative process showed during AD. In contrast, hippocampal CypD overexpression in aged tau^{-/-} mice impairs mitochondrial function evidenced by an ATP deficit, increased mPTP opening, and memory loss; all effects were observed in the AD pathology. Our results indicate that the absence of tau prevents age-associated cognitive impairment by maintaining mitochondrial function and reducing mPTP opening through a CypD-dependent mechanism. These findings are novel and represent an important advance in the study of how tau contributes to the cognitive and mitochondrial failure present during aging and AD in the brain.

Keywords: tau, Alzheimer's disease, aging, mitochondria, cyclophilin-D, hippocampus, memory

INTRODUCTION

Aging is a biological process associated with progressively accumulating damage in the organism and also is the principal risk factor for several neurodegeneration diseases, including Alzheimer's disease (AD) (Stauch et al., 2014; Xia et al., 2018). Concerning brain function, aging leads to the deterioration of cognitive capacities as a consequence of synaptic alterations (Wyss-Coray, 2016) and loss of neurons in the hippocampus (Swerdlow, 2011; Lopez-Otin et al., 2013). Tau protein regulates the dynamics of microtubules (Tapia-Rojas et al., 2019a). However, post-translational tau modifications dissociate it from the microtubules, leading to the formation of aggregates (Wang et al., 2010; Wyss-Coray, 2016), and inducing alterations in synaptic and cognitive functions (Avila et al., 2013; Zuo et al., 2016). Nevertheless, misfolded tau is detected in the brain of approximately one-third of elderly people without dementia (Elobeid et al., 2016), which may contribute to the neuronal alterations observed in aging. Additionally, these pathological forms of tau play a relevant role in the onset and progression of AD (Xia et al., 2018), but the exact mechanism leading to neural toxicity is unclear. In AD brains, tau is ~three to fourfold more hyperphosphorylated than in normal conditions, forming paired helical filaments (PHF), and intraneuronal neurofibrillary tangles (NFT) (Iqbal et al., 2010).

Mitochondria are organelles required for ATP generation, calcium regulation, and maintenance of redox balance (Sebastian et al., 2017; Perez et al., 2018a). Mitochondrial dysfunction has been proposed as the common denominator connecting aging and the pathogenesis of AD (Du et al., 2012; Jara et al., 2019; Wu et al., 2019). Indeed, mitochondrial and synaptic dysfunction are the early characteristics of AD (Perez et al., 2018a). The loss of mitochondrial function leads to increased production of reactive oxygen species (ROS), decreased ATP formation (Sebastian et al., 2017), and reduced calcium-buffering capacity (Rottenberg and Hoek, 2017). Interestingly, these events could be associated with mitochondrial permeability transition pore (mPTP) opening (Perez and Quintanilla, 2017), which plays a relevant role in aging and AD (Du et al., 2011). Importantly, the formation and opening of the mPTP is enhanced by cyclophilin-D (CypD) expression (Du et al., 2008; Gauba et al., 2017; Hurst et al., 2017; Panel et al., 2018). Also, relevant studies have shown increased CypD levels in AD brain samples and mice models (Du et al., 2008). More importantly, CypD (-/-) mice crossing with APP/PS1 AD mice model that presented neurotoxicity and memory impairment prevented mitochondrial dysfunction, synaptic impairment, and cognitive decline indicating an important contribution to CypD in neurodegenerative changes shown in AD (Du et al., 2011).

Interestingly, a novel association between mitochondrial dysfunction and tau pathology contributing to AD pathology has been shown (Quintanilla et al., 2012, 2014; Perez et al., 2018a). We showed that the expression of pathological forms of tau (phosphorylated and truncated) promote mitochondrial depolarization, mitochondrial fragmentation, and oxidative stress, compromising mitochondrial function (Quintanilla et al., 2009, 2014; Perez et al., 2018b). More importantly, in a recent

study, we showed that tau ablation enhanced cognition and improved mitochondrial function in the hippocampi of young mice compared to wild-type animals (Jara et al., 2018). However, the contribution of tau and mitochondria to the normal aging process is unclear and controversial. Some reports have shown that tau knockdown impairs brain capacity, including motor and cognitive function in the adult brain (Lei et al., 2012; Velazquez et al., 2018). In contrast, Morris et al. (2013) showed that the absence of tau did not affect cognition performance in aged mice. Considering these discrepancies, we investigated the effects of tau absence on behavioral impairment and mitochondrial function during aging, using 18-month-old wild-type (WT) and tau-knockout (tau-/-) mice. We observed that tau-/- mice maintained their cognitive capacities during aging, including hippocampal memory and social behavior. Besides, we observed a reduction in oxidative damage and higher ATP levels in the aged tau-/- animals. Interestingly, we observed reduced levels of CypD and lower sensitivity to calcium overload in hippocampal mitochondria from the aged tau-/- mice, suggesting a reduced activity of mPTP. To corroborate that CypD deficiency is involved in the mitochondrial and cognitive improvement observed in aged tau-/- mice, we overexpressed CypD in the hippocampus of these mice using a lentiviral vector (Li et al., 2012; Parr-Brownlie et al., 2015). Notably, CypD overexpression was sufficient to impair mitochondrial calcium buffer capacity and to reduce ATP production in aged tau-/- mice. Most importantly, the cognitive abilities observed in the aged tau-/- mice were significantly reduced. Thus, genetic reduction of tau preserves mitochondrial bioenergetics and cognitive abilities during aging by a mechanism that involves CypD and possibly the mPTP opening in the hippocampus.

MATERIALS AND METHODS

Animals

Wild-type (WT, C57BL/6J background) and homozygous tau-knockout (tau-/-) mice were obtained from the Jackson Laboratory (B6.129-Maptm1Hnd/J Bar Harbor, ME, Stock N°007251). WT C57BL/6J mice were used as litter control, considering the control suggestions by The Jackson Laboratory and also that tau KO strain have this genetics background. The animals were handled according to the guidelines of the National Institute of Health (NIH, Baltimore, MD). They were maintained at the Bioterio Central of Universidad Autónoma de Chile. All mice were housed at 23°C and on a 12-h light/dark cycle with food and water *ad libitum*. Experimental procedures were approved by the Bioethical and Biosafety Committee of the Universidad Autónoma de Chile. All studies were conducted on wild type (WT) and tau KO (tau-/-) littermates. A total of nine WT and seven tau-/- mice, 18 months old were used in the cognitive tests. For the biochemical studies, we used additional ($n = 3$) WT and tau-/- mice. For mitochondrial analysis, we used a separate cohort with $n = 4$ mice per group. All groups include female and male animals, with differences observed between sex.

Reagents and Antibodies

The primary antibodies used were as follows: Anti- β -tubulin (sc-9104, Santa Cruz Biotechnology, Inc., 1:2,000), anti-Total OXPHOS Human WB Antibody Cocktail (ab110411, Abcam, Inc. 1:2,000), anti-COX IV (11967S, Cell Signaling, 1:1,000), anti- β -actin (sc-47778, Santa Cruz Biotechnology, Inc., 1:1,000), anti-Opal (PA1-16991, Thermo Fisher Scientific, 1:1,000), anti-Cyclophilin D (sc-376061, Santa Cruz Biotechnology, Inc., 1:1,000), anti-ANT (Santa Cruz biotechnology; 1:1,000), anti-Mfn1 (sc-50330, Santa Cruz Biotechnology, Inc. 1:1,000), anti-Mfn2 (sc-50331, Santa Cruz Biotechnology, Inc., 1:1,000), anti-phospho-DRP1 (Ser616) (4494, Cell Signaling, 1:1,000), anti-DRP1 (sc-271583, Santa Cruz Biotechnology, Inc., 1:1,000), anti-nitrotyrosine (141682, US Biological, Life Sciences, 1:500), and anti-4HNE (H6275-02, US Biological, Life Sciences, 1:1,000). The fluorescent dyes used were as follows: MitoTrackerTM Red CM-H2Xros (M7513, Thermo Fisher Scientific), MitoTrackerTM Green FM (M7514, Thermo Fisher Scientific), and VECTASHIELD Mounting Medium with DAPI (H1200, Vector Laboratories, Inc.).

Behavioral Tests

All behavioral tests were monitored using an automatic tracking system (ANY-maze Behavioral tracking software, United Kingdom).

Novel Object Recognition (NOR) Test

NOR tests were performed in a 38 × 38 × 32 cm acrylic box and were performed according to Jara et al. (2018). The animals were habituated in the box for 2 consecutive days, without any object. During testing, each animal was placed in the box containing two identical objects (old objects) for 10 min. Then, the box and objects were cleaned (50% methanol). After 2 h, the animal was exposed to one of the old objects and a new object of different shapes and colors. The recognition index was calculated as the time spent by the mouse exploring the new object divided by the time spent exploring both objects.

Barnes Maze Test

Barnes maze test was performed according to Olesen et al. (2020). The paradigm consists of an elevated circular platform, with 20 equally spaced holes along the perimeter. The animals must learn to escape from the open platform surface to a small chamber located under the platform, guided by visual-spatial cues. For reinforcement, we used aversive white noise. During the acquisition phase, the mouse was placed in a cylindrical black. After 5 s, white noise was switched on, and the mouse explored. The trial ended when the mouse entered the escape chamber or after 3 min of exploration. When the mouse entered the escape chamber, the white noise was turned off. If the mouse did not achieve this criterion, it was guided to the escape chamber. This protocol was repeated thrice on day 1 and twice on day 2. Forty-eight hours after training, the time spent on the mouse until finding the escape chamber was evaluated.

Social Interaction Test

For this task, a previously described protocol was used (Jara et al., 2018). Briefly, the mice were habituated in a three-chamber box (each chamber was 20 × 40 × 22 cm) for 10 min. Subsequently, one object and one unknown mouse were placed inside a cage and were presented to the experimental mouse, one in each lateral chamber. Each mouse was positioned in the central chamber and was allowed to explore the cage for 10 min. In the final part of the test, an unknown mouse replaced the previous object. The experimental mouse was allowed to explore for 10 min.

Object-Based Attention Test

For this task, a previously described protocol was used (Jara et al., 2018). Briefly, the test was performed in a rectangular apparatus, containing two chambers, which included the exploration chamber (40 × 40 × 22 cm) and the test chamber (40 × 20 × 22 cm). First, the animals were exposed to the habituation phase, a session of 10 min exploring both empty chambers. Later, during the acquisition phase, the mice were subjected to a 3-min session exploring five objects (1, 2, 3, 4, and 5) distributed within the chamber. Finally, in the retention phase, immediately after the acquisition phase (<15 s), an old object (used in the acquisition phase) was placed in its original position, and a sixth novel object was placed in the test chamber. The mice explore both objects for 3 min. A recognition index is calculated as $(T6 \times 100)/(T2 + T6)$, where T2 and T6 are the time duration spent by each mouse with objects 2 and 6, respectively.

Total RNA Extraction

Total RNA was isolated from 100 mg of tissue using the TRIzol reagent (Life Technologies, Thermo Fisher Scientific, United States) following the manufacturer's instructions. Residual DNA was removed with RNase free-DNase I, Amplification Grade (Invitrogen, Thermo Fisher Scientific). RNA yield and purity were determined by a TECAN plate reader (Infinite 200 PRO series).

Reverse Transcription for cDNA Synthesis

One microgram of RNA was subjected to reverse transcription using ImProm-II Reverse Transcription System (Promega) by the manufacturer's protocol. For qPCR analysis, the cDNA sample was diluted 10× in nuclease-free water.

Real-Time PCR

The real-time PCR reaction was performed in triplicates in the LightCycler 96 System (Roche Diagnostics GmbH, Roche Applied Science, Mannheim, Germany) using KAPA SYBR FAST qPCR Master Mix (2×) in a final reaction volume of 10 μ l. Amplification conditions consisted of an initial hot start at 95°C for 10 min followed by amplification for 40 cycles (95°C for 15 s, 60°C for 20 s, and 72°C for 20 s). Melting curve analysis was performed immediately after amplification from 55 to 95°C. Values were normalized to 18S expression levels using the Δ CT method.

Gene	Forward primer	Reverse primer
CypD	5'-AGGAGATAGCCCCAGGAGAT-3'	5'-TTGCATACACGGCCTTCTCTT-3'

Western Blot

The hippocampi of WT and tau^{-/-} mice were dissected and immediately processed (Jara et al., 2018). Briefly, the hippocampal tissues were homogenized in RIPA buffer (10 mM Tris-Cl, pH 7.4, EDTA 5 mM, 1% NP-40, 1% sodium deoxycholate, and 1% SDS) supplemented with a protease/phosphatase inhibitors mixture (25 mM NaF, 100 mM Na₃VO₄, and 30 μM Na₄P₂O₇). The protein samples were centrifuged at 14,000 rpm for 15 min at 4°C. The protein concentrations were determined using the BCA Protein Assay Kit (Pierce, Thermo Fisher Scientific, United States). The samples were resolved by SDS-PAGE, followed by immunoblotting on PVDF membranes.

Hippocampal Slices and Staining With Mitochondrial Fluorescent Dyes

Coronal 20-μm-thick slices of unfixed tissue were obtained from the brain of WT and tau^{-/-} mice and stained (Jara et al., 2018; Tapia-Rojas et al., 2019b; Torres et al., 2020). Slices were mounted on slides and incubated with MitoTraker Green FM (mitochondrial mass) plus MitoTraker Red CM-H2Xros (mitochondrial membrane potential), in KRH buffer for 45 min at 37°C. After incubation, the slices were washed three times for 5 min in PBS and mounted with DAPI mounting medium. Images were acquired with a fluorescence microscope (LX 6000X, Leica, Germany).

Measurement of ATP Concentration

ATP concentration was measured in the hippocampal lysates using a luciferin/luciferase bioluminescence assay kit (ATP determination kit #A22066, Molecular Probes, Thermo Fisher Scientific, United States), as previously described (Jara et al., 2018). The amount of ATP in each sample was calculated from standard curves and normalized to the total protein concentration.

Isolation of Hippocampal Mitochondria

Hippocampal mitochondria were isolated as previously described (Jara et al., 2018; Carreras-Sureda et al., 2019). Briefly, four mice per group (WT and tau^{-/-}) were euthanized, and the hippocampi were rapidly removed and suspended in MSH buffer (230 mM mannitol, 70 mM sucrose, 5 mM HEPES, pH 7.4) supplemented with 1 mM EDTA and protease inhibitor cocktail. Homogenates were centrifuged at 600 g for 10 min at 4°C to discard nuclei and cell debris. The supernatant was centrifuged at 8,000 g for 10 min; the mitochondrial pellet was washed twice in MSH without EDTA.

Evaluation of Mitochondrial Calcium Buffering Capacity

Mitochondrial swelling was measured by monitoring absorbance decline at 540 nm in a fresh mitochondrial fraction (Karadayian et al., 2015; Olesen et al., 2020). Intact mitochondria scatter light at 540-nm wavelength. The prolonged mPTP opening provokes the swelling of mitochondria, which reduces the absorbance. Isolated mitochondria were resuspended in MSH buffer containing 5 mM malate, 5 mM glutamate, 1 mM phosphate, and 2 mM MgCl₂. Mitochondrial samples (0.5 mg/ml of total protein) were exposed to different calcium concentrations to generate calcium overload, which induces mitochondrial swelling associated with mPTP opening.

Surgical Procedures

Animals received bilateral intrahippocampal administration of Lenti ORF particles (GFP-tagged)-mouse peptidylprolyl isomerase D (Ppid; cyclophilin D) (Type: Human Tagged ORF Clone Lentiviral Particle; Tag: mGFP; Vector: pLenti-C-mGFP, #RC223397L2V, Origene) by stereotaxic injection (Vargas et al., 2014). A total of $n = 5$ mice were used per group. We used Sham injection in WT and control tau KO mice. Tau^{-/-} mice were anesthetized using isoflurane and placed in a stereotaxic frame (Stoelting, United States). The skull was exposed for several millimeters anterior and posterior to the bregma. Boreholes were made above the left and right hippocampal CA1 (coordinates: 2.46 mm anterior to the bregma, 1.0 mm lateral, 1.5 mm relative to dura mater). One microliter of the lentiviral vector was injected (10⁸ TU/ml). Three weeks after infection, the animals were subjected to cognitive tests and euthanized immediately after for biochemical analysis.

Statistical Analysis

The data are expressed as the mean ± standard error of the mean (S.E.M.). The data was analyzed using the Student's *t*-test with Dunnett's *post-hoc* test or one-way ANOVA followed by Bonferroni's *post-hoc* test. A value of $p < 0.05$ is statistically significant. All statistical analyses were performed using Prism software (GraphPad Software Inc.).

RESULTS

The Absence of Tau Prevents the Impairment of Hippocampus-Dependent Memory During Aging

The hippocampus is susceptible to aging (Bartsch and Wulff, 2015). Neurobiological alterations in the aged hippocampus include oxidative damage and altered communication among neurons (Bettio et al., 2017; Jara et al., 2019). These events result in impaired hippocampal function, affecting learning and memory (Bettio et al., 2017; Jara et al., 2019). Pathological forms of tau have been linked to memory-related disorders, such as AD (Amadoro et al., 2010; Pooler et al., 2013). However,

it is unclear if tau contributes to memory loss during the physiological aging process. To determine the impact of the absence of tau on hippocampal memory impairment during aging, 6- and 18-month-old (mo) WT and tau^{-/-} mice were subjected to behavioral tests, including the Novel Object Recognition (NOR) test, which evaluates recognition memory, and the Barnes maze test, which is a spatial memory task (Broadbent et al., 2004). For the NOR test, mice were subjected to the familiarization phase. During this stage, each animal explored the chamber containing two identical objects, for 10 min (**Figure 1A**). The behaviors of the 18-month-old WT and tau^{-/-} mice during the familiarization phase are shown in the heat maps in **Figure 1B**. We observed that the 18-month WT mice explored the chamber with the two objects for less time than both the aged tau^{-/-} and the 6-month mice of both genotypes (**Figure 1C**). These observations suggested that aged WT mice had reduced explorative abilities, whereas tau^{-/-} mice maintained their capacity. Two hours later, the recognition phase was performed. During this stage, the mice explored the chamber containing a familiar object and a novel object for 5 min (**Figure 1D**). **Figure 1E** presents the heat maps for the performance of the 18-month mice during this phase. The aged tau^{-/-} mice showed preference for the novel object, in contrast to the aged WT mice. Quantitative analysis revealed that during this phase, the 18-month tau^{-/-} animals spent significantly more time exploring the chamber for the novel object compared to the WT mice of the same age (**Figure 1F**). In addition, the behavior of the aged tau^{-/-} mice was similar to that of the 6-month tau^{-/-} mice, suggesting that tau ablation preserves the recognition memory that is normally affected during aging.

Next, we evaluated the impact of tau deletion on spatial learning and memory, another type of hippocampus-dependent memory that is reduced during aging (Rosenbaum et al., 2012). For this purpose, we performed the Barnes maze test (**Figure 1G**). **Figures 1H,I** show the heat maps of 18-month WT and tau^{-/-} mice on training day 1 (**Figure 1H**) and 2 (**Figure 1I**). On each day, we measured the time that the mice spent finding the escape chamber (escape latency). Aged tau^{-/-} mice exhibited reduced escape latency compared to the aged WT mice (**Figure 1J**). These findings suggest that the aged tau^{-/-} mice learn faster than the aged WT mice. However, during the second training day, all experimental groups were located in the escape chamber with a similar latency (**Figure 1K**). Finally, 2 days after training, the trial was performed in the absence of an escape chamber. The behavior of each experimental group is shown in the heat maps and the representative tracks in **Figure 1L**. We evaluated the time spent in the quadrant where the escape chamber was previously located, and interestingly, we observed that the aged tau^{-/-} mice remembered the escape zone, as did the animals belonging to both 6-month groups. In contrast, the 18-month WT mice did not remember the escape chamber location (**Figure 1M**). Therefore, these studies indicate that the absence of tau prevented the loss of spatial memory observed in the aged WT animals. Thus, tau deletion preserves recognition and spatial memory that are normally impaired during aging.

Tau^{-/-} Mice Maintain Their Social Abilities During Aging

During aging, decreased social contact has been reported (Shoji et al., 2016). Sociability and social memory are processed by the prefrontal cortex, hippocampus, hypothalamus, and amygdala (Bicks et al., 2015). In aging, a reduced preference for novel conspecific individuals occurs (Charles and Carstensen, 2010; Smith et al., 2018). To evaluate whether tau deletion modified social abilities during aging, we performed a social interaction test (**Figure 2**; Jara et al., 2018). During the first phase, the mice explored a chamber containing a mouse and an object for 10 min (**Figure 2A**). **Figure 2B** shows heat maps of the 18-month WT and tau^{-/-} mice. We observed that all groups showed a preference for exploring the unknown mouse compared with the unknown object, suggesting a similar ability to socialize (**Figure 2C**). Subsequently, the object was replaced by a new unknown mouse, and the experimental were animals to explore the chamber for another 10 min (**Figure 2D**). The heat maps showed that aged tau^{-/-} mice spent more time with the new mouse compared with the aged WT mice (**Figure 2E**). We found that both 6-month groups preferred exploring the new mouse, in contrast to aged WT mice that spent similar time exploring the known and unknown mice (**Figure 2F**). Interestingly, this analysis also revealed that aged tau^{-/-} mice also preferred exploring the new mouse (**Figure 2F**) indicating that the absence of tau maintains social recognition memory during aging.

Finally, we performed a recognition-based attention test to determine if aging affects the attentive behavior in WT and tau^{-/-} mice, since variations in this behavior could be responsible for the changes detected in memory and social abilities (Chun and Turk-Browne, 2007). For this test, five different objects were placed in the chamber, as indicated in **Figure 2G**. The mice explored the chamber containing the objects for 3 min, and 15 s later, the chamber size was reduced, an old object remained in the chamber (object 2), and a new object was added (object 6). **Figure 2H** showed heat maps of the aged WT and tau^{-/-} mice during the test phase. We found that the aged WT and tau^{-/-} mice spent a similar time exploring the new object (**Figure 2I**). Therefore, our results indicated that 18-month WT and tau^{-/-} mice did not show differences in their attention capacity during aging. Thus, the changes observed between WT and tau^{-/-} mice could be related to memory loss occurring in the aged WT mice that are prevented by the absence of tau.

Tau Absence Prevents Mitochondrial Bioenergetics Failure Observed During Aging

Mitochondrial dysfunction contributes to aging by increasing the production of ROS and promoting deficits in the bioenergetic processes (Chistiakov et al., 2014; Jara et al., 2019). Oxidative damage and aging are strongly connected (Rottenberg and Hoek, 2017). To determine if the absence of tau has a significant effect on the oxidative damage occurring during aging, we dissected the hippocampi of 18-month WT and tau^{-/-} mice, and the samples were analyzed by Western blot.

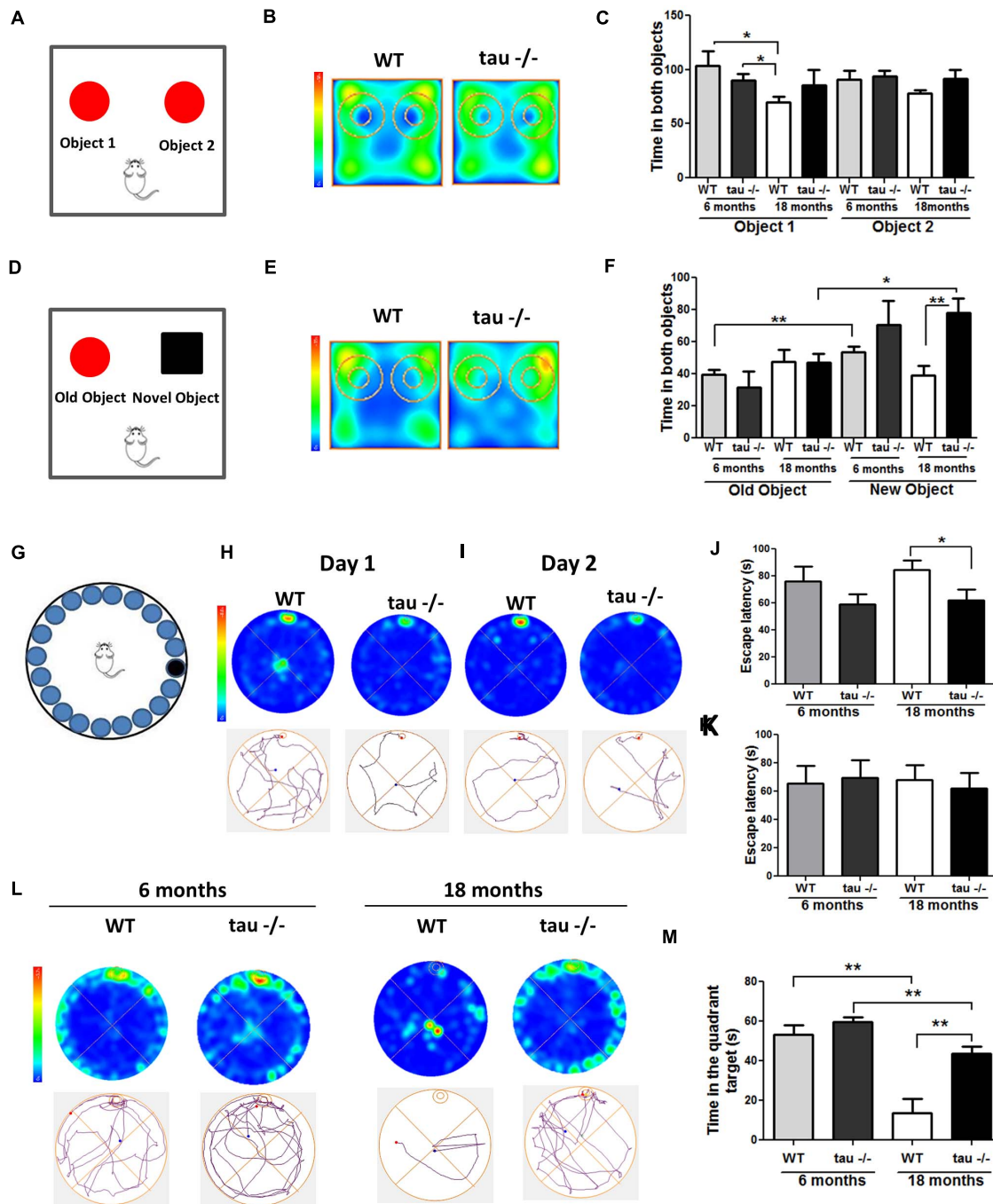


FIGURE 1 | The absence of tau prevents the loss of hippocampal-dependent memory during aging. **(A)** Scheme of the novel object recognition (NOR) test, familiarization phase. **(B)** Heat maps of the aged WT and tau-/- groups in the NOR familiarization phase. **(C)** Graph of exploration time for both objects 1 and 2, during the familiarization phase. **(D)** Scheme of NOR testing phase; 2 h after the familiarization phase, the mice explored a familiar object and a novel object. **(E)** Heat maps of the aged WT and tau-/- groups during the NOR testing phase. **(F)** Graph of exploration time of both old and novel objects, during the testing phase. **(G)** Representation of the Barnes maze. **(H,I)** Heat maps and tracks of aged WT and tau-/- mice in the Barnes maze, during training days 1 and 2. **(J,K)** Escape latency (time each mouse spent to find the escape chamber) on training days 1 and 2. **(L)** Heat maps of aged WT and tau-/- mice and representative tracks until the finding of the escape chamber. **(M)** Graph of the time in the escape chamber quadrant. * $p < 0.05$, ** $p < 0.01$; mean \pm S.E.M.

We evaluated the levels of oxidized proteins using an anti-HNE antibody that recognizes the stably formed HNE-protein adducts (products of lipid peroxidation) (Bettio et al., 2017), and

anti-nitrotyrosine antibody that detects protein modifications involving nitrotyrosine (Jara et al., 2018). Our results showed that the levels of lipid peroxidation products were significantly

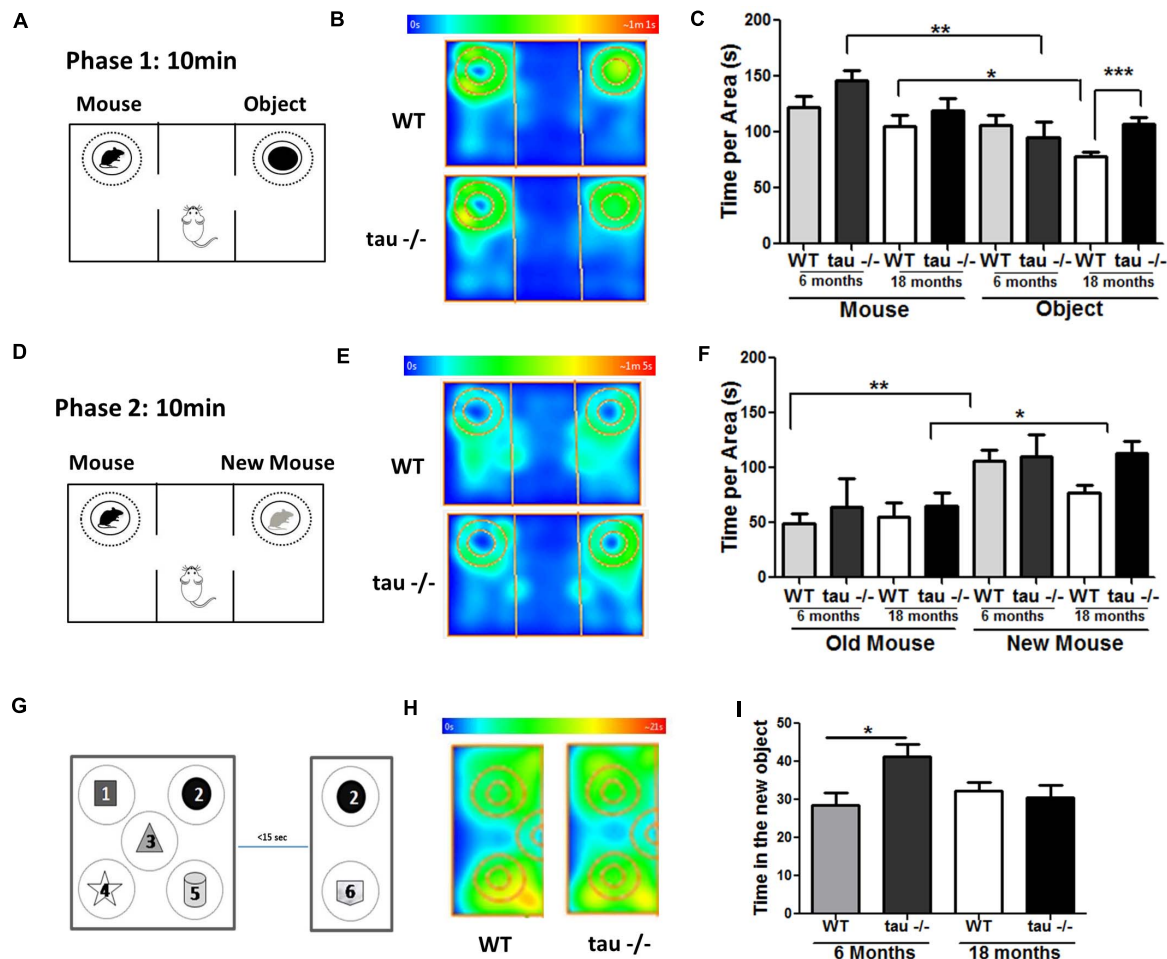


FIGURE 2 | Tau^{-/-} mice maintain their social abilities during aging. **(A)** Scheme of phase 1 of the social interaction test. **(B)** Heat maps of aged WT and tau^{-/-} mice during phase 1 of the social interaction test. **(C)** Graph of the exploration time of both the mouse and the object. **(D)** Scheme of phase 2 of the social interaction test. **(E)** Heat maps of aged WT and tau^{-/-} mice during phase 2 of the social interaction test. **(F)** Graph of the exploration time of both the old and new mice. **(G)** Scheme of the object-based attention test. Mice were exposed to five objects (1–5) for 3 min (exploration phase). After a 15-s interval, the mice were exposed to one old (2) and one novel object (6) for 3 min. **(H)** Heat maps showing data for the aged mice in the test. **(I)** Graph of time spent for the exploration of the new object. * $p < 0.05$, ** $p < 0.01$, *** $p < 0.001$; mean \pm S.E.M.

reduced in the hippocampi of the aged tau^{-/-} mice in comparison to the WT mice of the same age, as indicated by densitometry analysis (Figures 3A,B), whereas nitrotyrosine protein levels showed no significant differences between the two experimental groups (Figures 3A,C). These results show that the absence of tau reduced oxidative damage mediated by peroxidation in the aged tau^{-/-} animals.

On the other hand, mitochondria are dynamic organelles that change their size depending on intracellular and extracellular signals (Sebastian et al., 2017). During aging, mitochondria are prone to gradual deterioration (Chistiakov et al., 2014). For this reason, we measured the mitochondrial mass in the hippocampi of aged WT and tau^{-/-} mice and did not detect any difference between the two groups (Supplementary Figure 1A). Besides, mitochondria undergo continuous cycles of fusion/fission events, influencing their functionality (Sebastian et al., 2017). Therefore, we measured the levels of proteins involved in mitochondrial

dynamics in both aged WT and tau^{-/-} mice (Supplementary Figure 1C). Fusion events are controlled by the dynamin-related GTPases as well as mitofusins (Mfn1 and Mfn2) and optic atrophy 1 (OPA1) proteins, which induce the fusion of outer and inner mitochondrial membranes, respectively (Hood et al., 2018). In contrast, fission is mediated by dynamin-related protein 1 (Drp1), which is recruited to the outer membrane to constrict mitochondria and induce their division, a process that is mainly stimulated by Drp1 phosphorylation at Ser616 (Sebastian et al., 2017). We observed that both fission and fusion protein levels were not significantly different between the experimental groups (Supplementary Figure 1B). Therefore, the absence of tau did not affect the expression of the proteins that regulate mitochondrial dynamics during aging.

Mitochondria are the main producers of ATP in neurons, and during the aging process, they are particularly susceptible to damage (Schon and Manfredi, 2003; Jara et al., 2019).

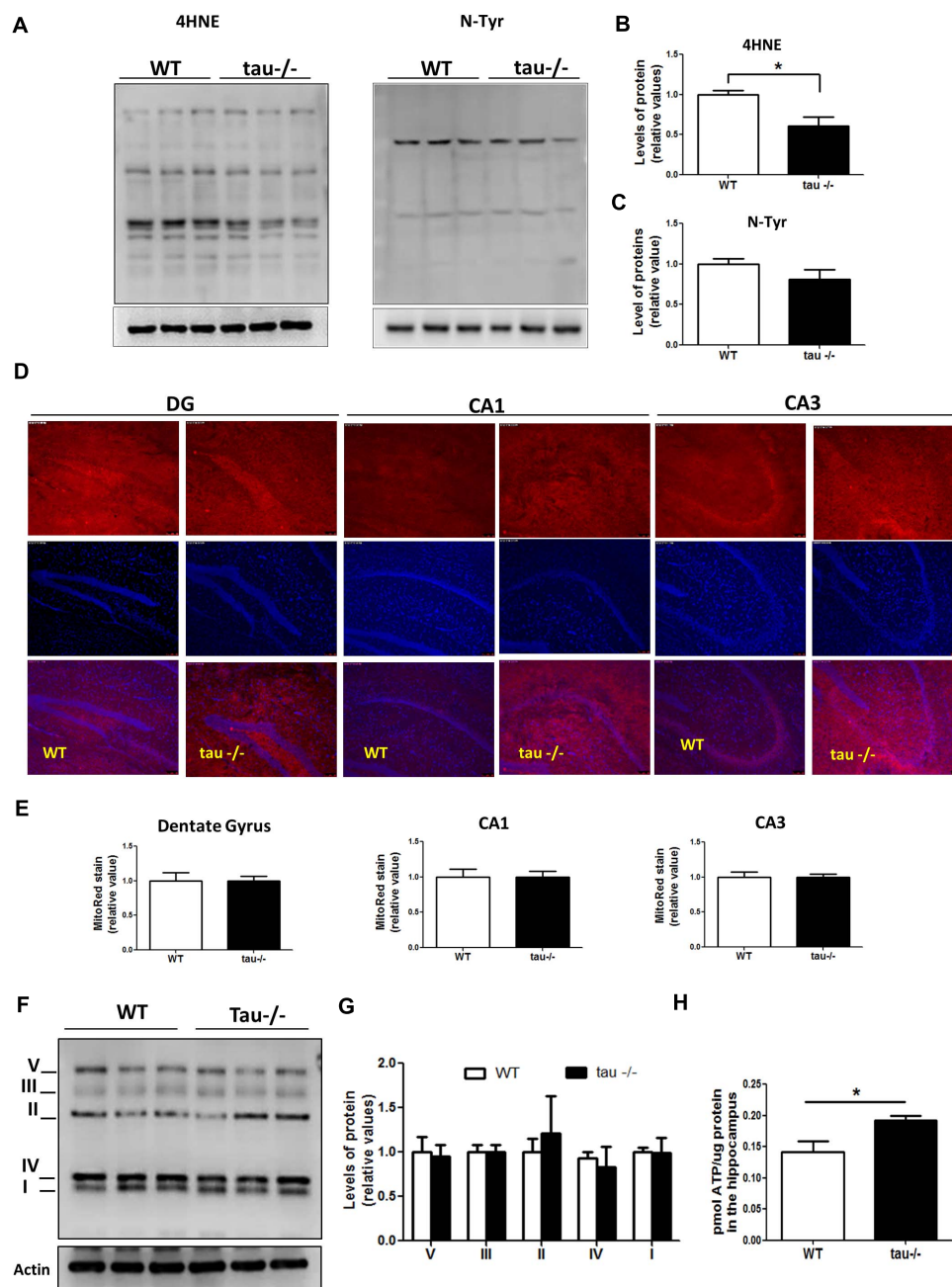


FIGURE 3 | Tau absence prevents mitochondrial bioenergetics impairment observed during aging. **(A)** Western blot of hippocampal lysates from aged WT and $\tau^{-/-}$ mice for the measurement of oxidative damage with antibodies against 4HNE and n-Tyr. **(B,C)** Densitometric analysis of 4HNE **(B)** and n-Tyr **(C)** Western blots. **(D)** Representative images of unfixed hippocampal slices from aged WT and $\tau^{-/-}$ mice, stained with MitoTracker Red CM-H2Xros. **(E)** Quantitative analysis of MitoTracker Red CM-H2Xros fluorescence intensity in the DG, CA1, and CA3 hippocampal regions. **(F)** Western blot and **(G)** densitometric analysis for mitochondrial OXPHOS complexes I–V in whole hippocampal extracts from aged WT and $\tau^{-/-}$ mice. **(H)** ATP concentrations in the hippocampus of aged WT and $\tau^{-/-}$ mice, expressed as pmol of ATP/ μ g of total protein. * $p < 0.05$; mean \pm S.E.M. 4HNE, 4-hydroxynonenal; DG, dentate gyrus; n-Tyr, nitrotyrosine; OXPHOS, oxidative phosphorylation.

To determine whether the absence of tau could be beneficial for mitochondrial bioenergetics during aging, we incubated unfixed hippocampal slices of aged WT and $\tau^{-/-}$ mice with the dye MitoTracker Red CMX2Ros to measure the mitochondrial membrane potential. This dye detects functional

mitochondria, and the fluorescence intensity is proportional to mitochondrial membrane potential (**Figure 3D**; Jara et al., 2018; Tapia-Rojas et al., 2019b). **Figure 3D** showed similar mitochondrial membrane potential levels in all regions of the hippocampus, including the dentate gyrus (DG), CA1, and CA3

of aged WT and tau^{-/-} mice (**Figure 3E**). Also, we evaluated the protein levels of the mitochondrial respiratory complexes involved in oxidative phosphorylation (OXPHOS) using the antibody cocktail OXPHOS that contains a mix of antibodies specific for the five mitochondrial complexes (Jara et al., 2018). We observed that the two groups of mice had similar levels of all mitochondrial complexes (**Figures 3F,G**). Finally, the main mitochondrial function involves the production of ATP, and it is known that during aging, ATP formation is reduced in the hippocampus (Navarro and Boveris, 2010). Interestingly, when we evaluated ATP production, we observed that the 18-month tau^{-/-} mice had significantly higher ATP levels compared to WT mice of the same age (**Figure 3H**). Therefore, our results indicate that the mitochondria in aged tau^{-/-} mice maintain their bioenergetics capacity during aging.

Aged Tau^{-/-} Mice Exhibit Decreased Levels of CypD, Which Reduces mPTP Opening

The levels of CypD are increased in the brain of WT mice during aging (Gauba et al., 2017). This is interesting because CypD is a fundamental protein for the formation of the mPTP (Du et al., 2008, 2011; Jara et al., 2019). To investigate whether tau ablation alters the levels of mPTP components, we performed Western blot analysis using hippocampal lysates from aged WT and tau^{-/-} mice (**Figure 4A**). We observed that the levels of CypD were significantly reduced in the aged tau^{-/-} mice compared with the WT mice of the same age, while the levels of adenine nucleotide translocase (ANT) and ATP synthase proteins, two recognized protein members of mPTP (Perez and Quintanilla, 2017), showed no significant differences between the two groups as observed by densitometry analysis (**Figure 4B**). Interestingly, we also observed decreased mRNA levels of CypD in the 18-month tau^{-/-} mice (**Figure 4C**), suggesting decreased synthesis and expression of CypD.

Importantly, reduced CypD expression prevents mPTP opening in the brain and heart (Du et al., 2011; Hom et al., 2011). Considering that increased calcium concentrations in the mitochondria can induce mPTP opening (Baumgartner et al., 2009), we evaluated the sensitivity to calcium overload (mitochondrial calcium-buffering capacity) in enriched mitochondrial preparations from aged WT and tau^{-/-} hippocampus. Fresh hippocampal mitochondria were exposed to different calcium concentrations (10, 20, 50, 100, and 200 μ M CaCl₂) as indicated in **Figure 4D**. To detect mitochondrial swelling as a consequence of mPTP opening by increasing calcium concentrations, we measured the absorbance changes at 540 nm (Karadayian et al., 2015). **Figure 4E** shows the calcium overload curves of both mouse groups, and interestingly, we observed that the aged tau^{-/-} mice exhibited lower sensitivity to calcium overload compared to the aged WT mice (**Figure 4E**). These observations indicate that tau deletion could reduce premature mitochondrial mPTP opening induced by calcium overload.

Hippocampal CypD Overexpression Reduced Mitochondrial Bioenergetics in the Aged Tau^{-/-} Mice and Induced mPTP Opening

The expression levels of the main proteins involved in mPTP formation are modified during aging (Rottenberg and Hoek, 2017). CypD is increased in the brains of aged WT mice, and this could be responsible for mPTP opening (Gauba et al., 2017). To test the hypothesis that increased expression of CypD in WT mice is involved in mitochondrial dysfunction occurring in aged mice, we overexpressed CypD in aged tau^{-/-} mice (17-month) by lentiviral transduction (**Figure 4F**). Intra-hippocampal viral administration was performed in both cerebral hemispheres. Three weeks after viral infection, the levels of CypD were measured. Similar to **Figure 4B**, we observed that the levels of CypD were significantly reduced in the aged tau^{-/-} mice compared with the WT mice of the same age, while the levels of CypD in the tau^{-/-} group infected with the lentiviral vector are significantly higher (**Figures 4G,H**). Then, we evaluated the mitochondrial sensitivity to calcium overload (**Figure 4I**). We observed that the aged tau^{-/-} mice overexpressing CypD (tau^{-/-} CypD) had increased calcium sensitivity compared to the aged tau^{-/-} mice, which was similar to the aged WT mice (**Figure 4I**). Importantly, these results indicate that CypD overexpression is sufficient to reduce the mitochondrial calcium buffering capacity, similar to WT mice (**Figure 4G**). Finally, we measured the bioenergetics of mitochondria, by the evaluation of ATP production. Most importantly, we observed that the aged tau^{-/-} CypD mice showed reduced ATP production compared with the aged tau^{-/-} mice (**Figure 4J**). Interestingly, the ATP levels produced by the tau^{-/-} CypD mice were similar to the levels observed in aged WT mice, suggesting that tau contributes to bioenergetics defects that occur during aging, by a mechanism that involves CypD. Thus, CypD overexpression in tau^{-/-} mice replicated the mitochondrial defects observed in the aged WT mice and suggested that tau contributes to mitochondrial dysfunction in the hippocampus during the aging process.

Overexpression of CypD Reduced the Improvement in Memory and Social Abilities Exhibited in the Aged Tau^{-/-} Mice

Considering that mitochondrial dysfunction can induce cognitive impairment (Mancuso et al., 2009) and that CypD overexpression in the aged tau^{-/-} mice resulted in a loss of mitochondrial functionality, we sought to evaluate the behavioral performance of the tau^{-/-} CypD mice. First, we evaluated their social capacity using the social interaction task (Jara et al., 2018). **Figure 5A** illustrates the heat maps that represent the behavior of the aged WT, tau^{-/-}, and tau^{-/-} CypD mice during the first stage. The aged tau^{-/-} CypD mice explored for a shorter time than the aged tau^{-/-} control mice, similar to the aged WT mice, showing similar exploration times for both the mouse and the object (**Figure 5B**). In the second stage, when the object was replaced by a new mouse, we observed that only the aged tau^{-/-} mice

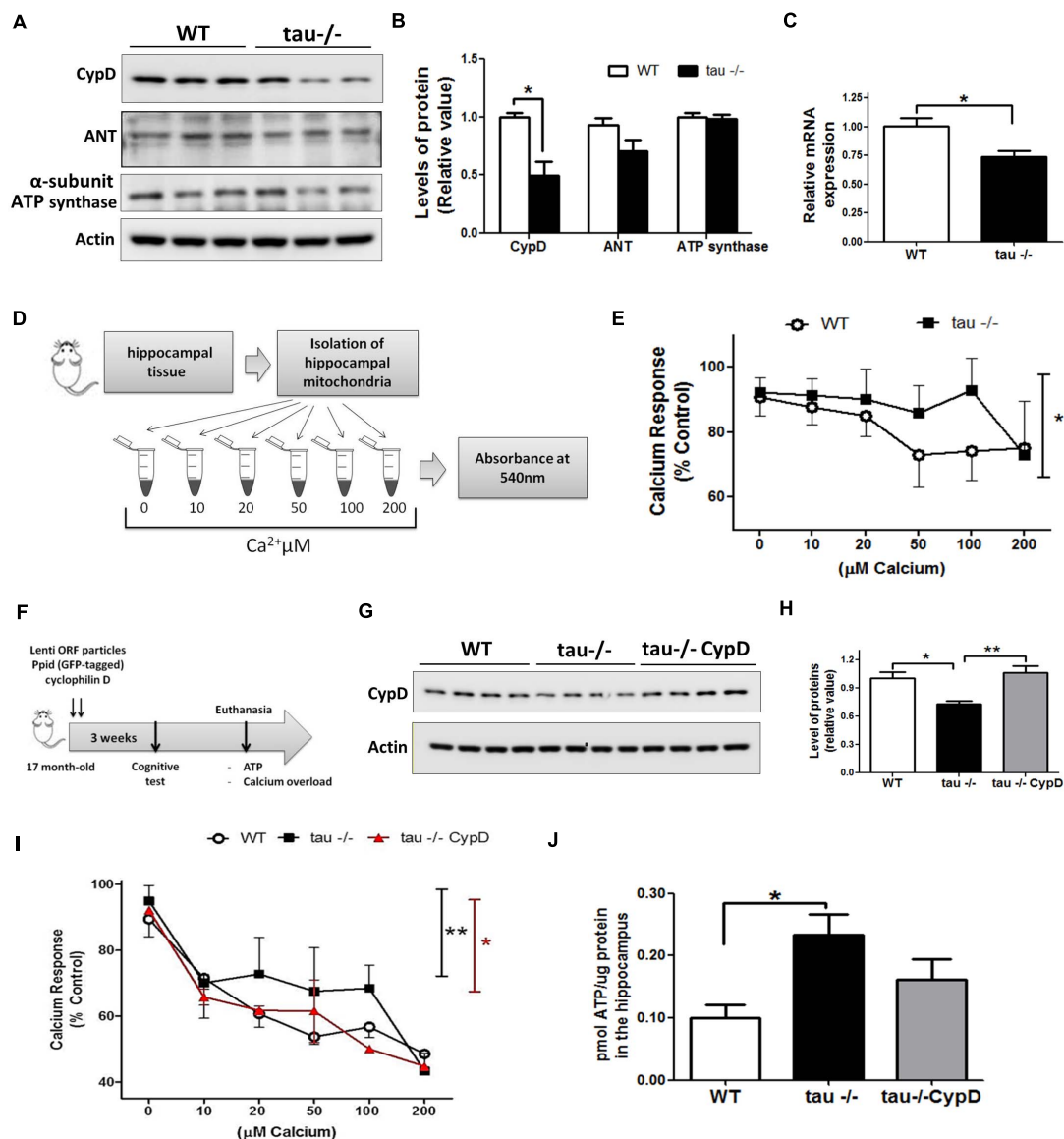


FIGURE 4 | Reduced mitochondrial calcium buffering and improved bioenergetics in the hippocampi of aged tau-/- mice are reverted by overexpression of CypD. **(A)** Western blot of hippocampal lysates and **(B)** densitometric analysis of proteins that form the mPTP, including CypD, ANT, and ATP synthase in aged WT and tau-/- mice. **(C)** Relative mRNA expression of CypD in aged WT and tau-/- mice. **(D)** Representation of mitochondrial membrane swelling after calcium overload to determine mPTP opening in aged WT and tau-/- mice. **(E)** Response of isolated mitochondria after calcium overload. The decreased absorbance indicated mitochondrial swelling. **(F)** Representation of lentiviral vector transduction in tau-/- mice for the overexpression of CypD [Lenti ORF particles (GFP-tagged)-mouse peptidylprolyl isomerase D (Ppid; cyclophilin D) (#RC223397L2V, Origene)]. **(G)** Western blot of hippocampal lysates and **(H)** densitometric analysis of CypD protein in aged WT, tau-/- control, and tau-/- overexpressing CypD mice. **(I)** Graphical representation of the response of isolated mitochondria after calcium overload in aged WT, tau-/- control, and tau-/- CypD mice. **(J)** ATP concentrations measured in whole hippocampal extracts from aged WT, tau-/- and tau-/- CypD mice. ATP concentration is expressed as pmol of ATP/ μ g of total protein extract. * $p < 0.05$, ** $p < 0.01$; mean \pm S.E.M.

spent more time investigating the new mouse (Figure 5C). In contrast, the aged WT and tau-/- CypD mice spent a similar time exploring the new and old mice (Figure 5C). These results indicated that overexpression of CypD in tau-/- mice reduced the social abilities that the aged tau-/- normally maintain during aging. Thus, the impairment of social behavior observed during aging could be related to the changes in CypD expression. Additionally, we subjected the mice to the NOR test. During the

familiarization phase (Figure 5D), all groups of mice spent a similar amount of time exploring the two objects. In contrast, during the recognition phase, as shown in the heat maps, the behaviors of tau-/- mice and tau-/- CypD were different (Figure 5E). The aged tau-/- mice explored the novel object for a significantly longer time, whereas the tau-/- CypD mice spent the same amount of time as the WT mice in investigating the new object (Figure 5F). This indicated that aged tau-/- CypD

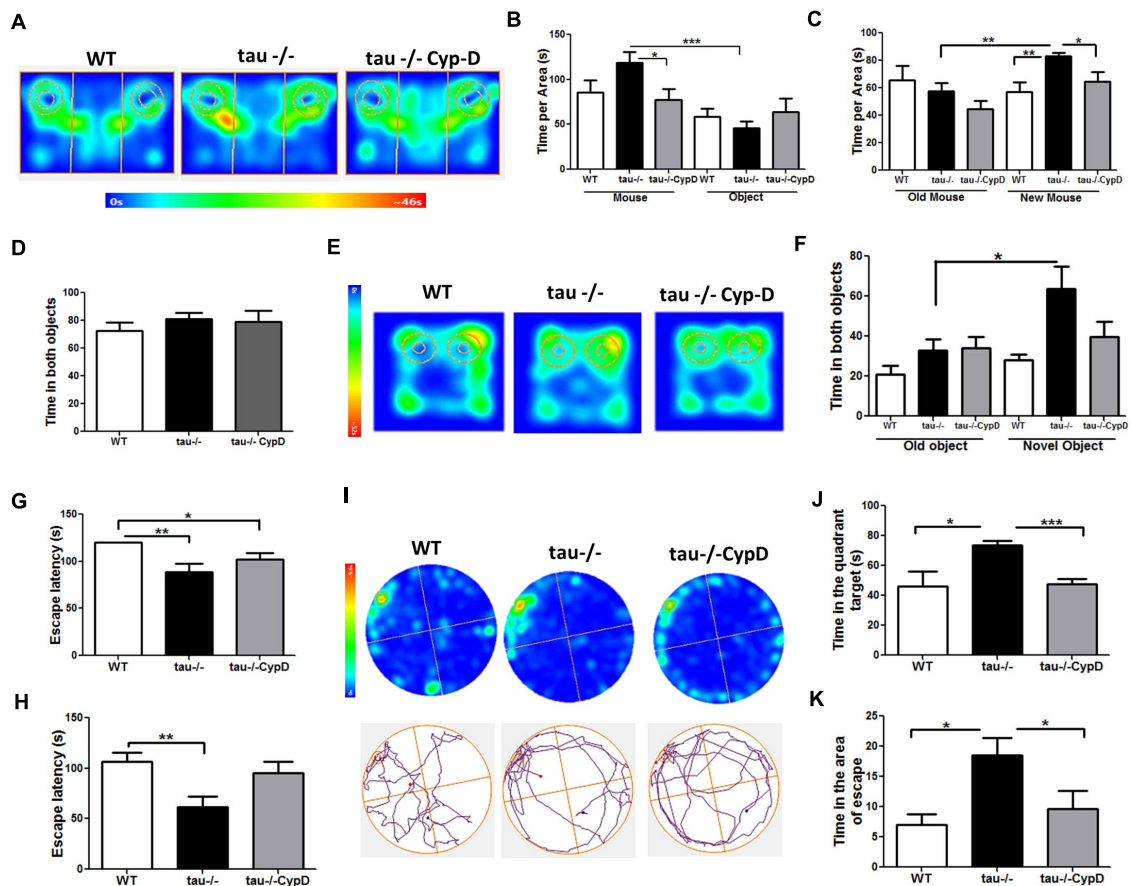


FIGURE 5 | Tau^{-/-} mice overexpressing CypD showed reduced social abilities and hippocampus-dependent memory similar to aged WT mice. **(A)** Heat maps of aged WT, tau^{-/-} control, and tau^{-/-} CypD mice during phase 1 of the social interaction test. **(B)** Graph of the exploration time of both the mouse and object for the aged WT, tau^{-/-} control, and tau^{-/-} CypD mice. **(C)** Graph of the exploration time of both old and new mouse area for the aged WT, tau^{-/-} control, and tau^{-/-} CypD mice. **(D)** Graph of the familiarization phase illustrating the exploration time of both objects 1 and 2 for the aged WT, tau^{-/-} control, and tau^{-/-} CypD mice. **(E)** Heat maps of aged WT, tau^{-/-} control, and tau^{-/-} CypD groups during the NOR testing phase. **(F)** Graph of the exploration time of both the old and novel objects by the aged WT, tau^{-/-} control, and tau^{-/-} CypD mice, during the testing phase. **(G)** and **(H)** for the aged WT, tau^{-/-} control, and tau^{-/-} CypD mice. **(I)** Heat maps and representative tracks of aged WT, tau^{-/-} control, and tau^{-/-} CypD mice while seeking the escape chamber. **(J)** Graph of the time in the quadrant and the area **(K)** that the aged WT, tau^{-/-} control, and tau^{-/-} CypD mice spent to find the escape chamber. * $p < 0.05$, ** $p < 0.01$, *** $p < 0.001$; mean \pm S.E.M.

mice were incapable of recognizing the old object, and therefore, the overexpression of CypD led to the loss of the recognition memory. Finally, we evaluated the effects of CypD overexpression on spatial learning and memory using the Barnes maze test (Figures 5G–I). On each day of training, we measured the escape latency, i.e., the time each mouse spent to find the escape chamber (Figures 5G,H). Our results showed that during the first training day, the aged tau^{-/-} CypD mice and the aged tau^{-/-} mice learned the location of the escape chamber at a similar time. This was in contrast to the aged WT mice that were incapable of finding the escape chamber (Figure 5G). During the second training day, we observed that the aged tau^{-/-} mice exhibited reduced escape latency compared with the aged WT and tau^{-/-} CypD mice (Figure 5H). These results indicated that, although aged tau^{-/-} CypD mice initially learned faster than the aged WT mice, they had a similar behavior at the end of the training. Finally, 2 days after training in the Barnes maze, a new trial was

performed in the absence of the escape chamber (Figures 5J,K). The behaviors of the experimental groups are shown in the heat maps and the representative tracks in Figure 5I. We measured the time that the mice spent in the quadrant of the escape chamber, and interestingly, the aged tau^{-/-} mice remembered the escape zone, in contrast to the WT and tau^{-/-} CypD mice (Figure 5J). More specifically, when we measured the time the mice explored the area around the escape chamber, a similar result was observed; the aged tau^{-/-} mice found the correct location, whereas the tau^{-/-} CypD mice had lost this ability, similar to the WT mice (Figure 5K). Therefore, these results indicated that overexpression of CypD in the absence of tau induced a loss of spatial memory and led to overall impairment of the hippocampal-dependent memory during aging.

Altogether, our results indicated that CypD overexpression in the aged tau^{-/-} mice triggers mitochondrial dysfunction and memory loss similar to the aged WT mice. Thus, these

data strongly suggested that tau contributes to physiological aging by a CypD-dependent mechanism. This is relevant because this is the first study demonstrating that tau negatively affects mitochondrial functionality and cognition during aging and suggests a new target for the treatment of aging-associated alterations.

DISCUSSION

In the present study, we used an aged (18-month) homozygous tau-knockout (tau^{-/-}) to identify the importance of tau in the cognitive and mitochondrial alterations observed during aging. We report that aged WT mice exhibit an impairment of memory and social abilities, accompanied by reduced ATP production and high mitochondrial calcium sensitivity in the hippocampus. We show for the first time that the absence of tau prevents cognitive impairment in aged mice and mitochondrial dysfunction, evidenced by increased ATP production and reduced sensibility to mitochondrial calcium stress. Most importantly, the enhanced mitochondrial calcium-buffering capacity could be related to the reduction in CypD expression, since CypD overexpression in tau^{-/-} mice led to ATP deficiency and premature mitochondrial swelling, probably due to mPTP opening. Thus, our results suggest that tau contributes to the mitochondrial and cognitive impairment in the hippocampus observed during normal aging and eventually to the development of neurodegenerative diseases, such as AD.

Loss of specific cognitive abilities is common during aging and in neurodegenerative diseases, such as AD (Fjell et al., 2014; Jara et al., 2019). The hippocampus is crucial for learning and memory; however, several studies suggest that the function of the hippocampus diminishes with age (Bettio et al., 2017). Likewise, other processes, dependent on the communication with the hippocampus, including social capacity, are affected by aging (Charles and Carstensen, 2010). In this study, we performed a battery of cognitive tests and report that aged tau^{-/-} mice maintain their learning capacity, memorize, and recognize objects and spatial locations, in contrast to aged WT mice that showed a significant reduction in these capacities. Besides, we observed normal sociability in the aged tau^{-/-} mice, while the aged WT mice lost the ability to interact with an unknown new mouse. These results are consistent with a previous report using the same genetic background of tau KO mice by Dawson et al. (2001) (C57BL/6J background; 4- to 5-month-old males) showing that tau deletion prevents memory decline in adult mice exposed to chronic stress (Lopes et al., 2016). While our work provides evidence that tau deletion prevents cognitive impairment during aging, other studies using tauGFP knock-in/knock-out mice (Stock No: 029219 | tauGFP, Jackson Laboratory) or C57BL6/SJL (F1) female mice (Stock No. 100012, Jackson Laboratory) injected with Adeno-associated virus (AAV) construct containing a shRNA to MAPT gene showed that tau ablation in the hippocampus causes learning and memory deficits (Biundo et al., 2018; Velazquez et al., 2018). These contradictory results can probably be explained by the

diverse genetic background, the methodology used to generate the ablation of tau, and the age of the animals used in the study.

Oxidative damage is characteristic of senescence and can affect brain functions (Palomera-Avalos et al., 2017; Jara et al., 2019). Oxidative stress is one of the most studied hypotheses to explain aging and neurodegeneration (Barja, 2014; Jara et al., 2019). Increased oxidative stress in the aging hippocampus is the result of an imbalance between the production of oxidative molecules and the anti-oxidant defense, leading to increased levels of ROS species (Uttara et al., 2009; Huang et al., 2016; Jara et al., 2019). Here, we demonstrate that the loss of tau prevents the oxidative damage associated with the formation of 4-HNE adducts, possibly by reducing ROS formation or increasing anti-oxidant activity. Therefore, these results suggest that the tau protein contributes to oxidative damage during aging, damage that is exacerbated in AD brains.

Mitochondria are the main producers of ROS, a sub-product of the respiratory chain (Chistiakov et al., 2014). Alterations in mitochondrial function lead to increased ROS production (Navarro and Boveris, 2010). In contrast, improvement of mitochondrial function has a beneficial effect (Rottenberg and Hoek, 2017). Supporting this idea, our group has previously reported that reduced oxidative damage in the hippocampus of young tau^{-/-} mice could be the result of improved mitochondrial performance (Jara et al., 2018). Therefore, we evaluated this possibility in aged mice. Interestingly, we detected significantly increased ATP production in the aged tau^{-/-} mice, indicating that mitochondrial bioenergetics are maintained during aging in the absence of tau. This could explain, almost in part, the early mitochondrial dysfunction observed in AD (Wang et al., 2020).

Mitochondrial function is influenced by fusion and fission events (Chistiakov et al., 2014; Wang et al., 2020). We demonstrated that the loss of tau did not induce changes in either fusion or fission proteins. Similarly, differences in the mitochondrial mass could have repercussions for mitochondrial function (Wenz, 2011; Chistiakov et al., 2014). However, we detected similar mitochondrial mass in the aged tau^{-/-} and WT mice, indicating that the improvement of mitochondrial ATP production detected in the absence of tau is independent of mitochondrial dynamics or mass. Another possibility is an inefficient OXPHOS process as a consequence of alterations in the expression and/or activity of OXPHOS complexes (Reinecke et al., 2009; Tatarkova et al., 2011). Our results indicate that mitochondrial membrane potential and OXPHOS proteins did not change in the absence of tau. Therefore, considering that aged tau^{-/-} mice present similar mitochondrial potential levels and expression of the OXPHOS complexes, higher ATP production may result from increased respiratory chain activity ATP synthase dependent. Future studies are needed to explore this possibility.

Mitochondria have additional functions to ATP formation (Perez et al., 2018a; Jara et al., 2019), contributing to cellular homeostasis and cell death (Hurst et al., 2017; Pérez and Quintanilla, 2017). These functions are partially regulated by the mPTP, a channel whose prolonged opening induces deterioration of cellular calcium homeostasis, oxidative stress, and decreased ATP production (Panel et al., 2018). Excessive production of

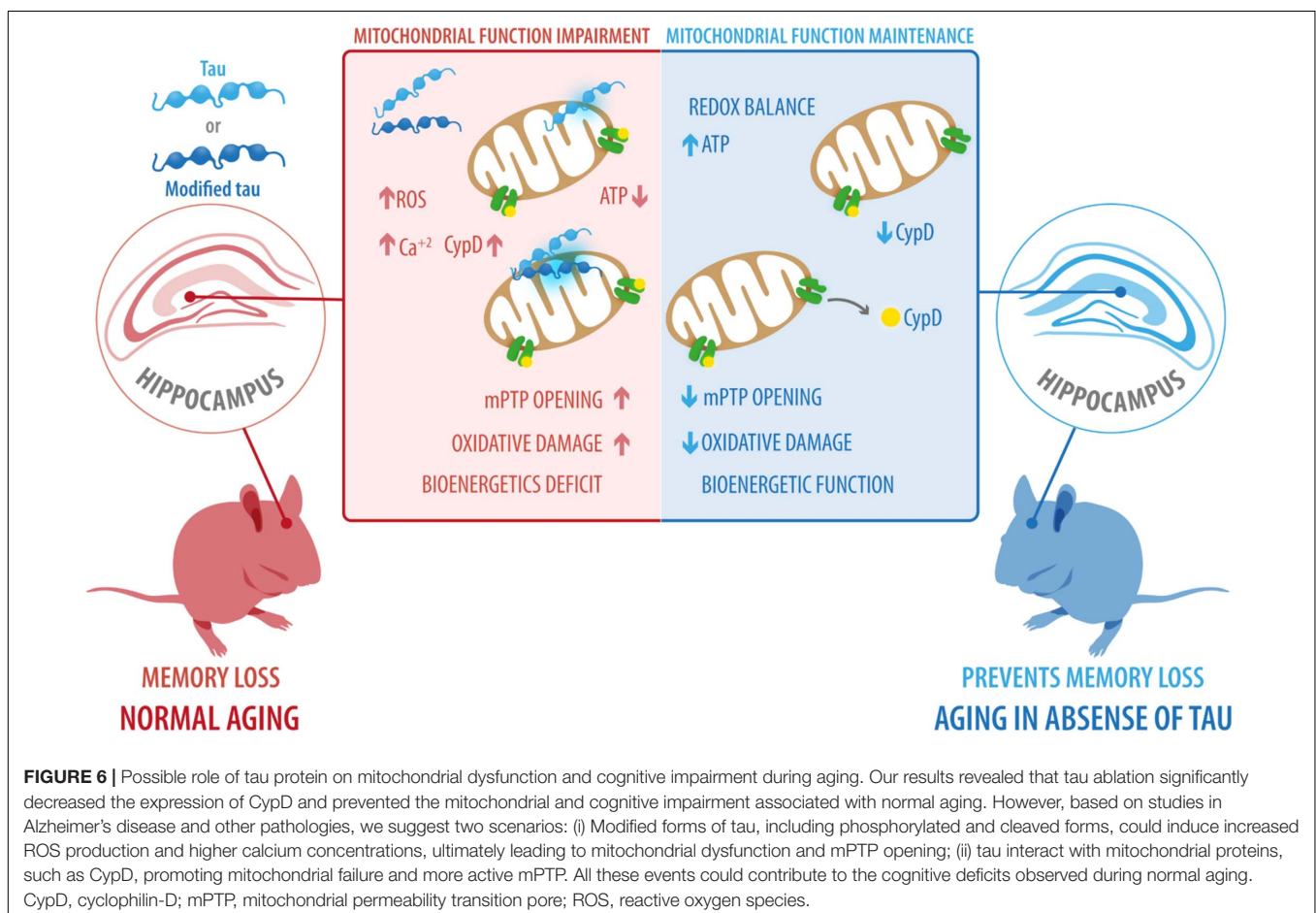
ROS promotes mitochondrial and cellular oxidative damage, and neurodegeneration (Wenz, 2011; Jara et al., 2019). mPTP opening can be triggered by ROS and mitochondrial calcium overload (Hurst et al., 2017) both of which are enhanced in aging and age-related neurodegenerative diseases (Panel et al., 2018). The most known mPTP components are CypD, adenine nucleotide translocase (ANT), and ATP synthase (Rottenberg and Hoek, 2017; Panel et al., 2018), which mediate its function, although currently, its composition and structure, except for CypD, is not completely resolved (Jonas et al., 2015; Panel et al., 2018). We evaluated the components of this multi-protein complex, and interestingly, we observed that aged tau^{-/-} mice had reduced levels of CypD, whereas the levels of the other proteins were similar to the levels seen in the aged WT mice. This is important because CypD is a crucial component for the formation of mPTP (Hom et al., 2011; Gauba et al., 2017; Perez and Quintanilla, 2017). In fact, our results are in concordance with previous studies showing that CypD deficiency increases mitochondrial function and cognitive abilities in transgenic mouse model of AD, indicating a protective effect in mice with neurodegenerative diseases (Du et al., 2011).

Mitochondria act by buffering high calcium concentrations (Hurst et al., 2017). However, when mitochondria are incapable of regulating calcium overload, they undergo swelling and

promote mPTP opening, ultimately resulting in cell death (Perez and Quintanilla, 2017). To evaluate if reduced levels of CypD observed in tau^{-/-} mice decreases the calcium sensibility that leads to mitochondrial swelling, we exposed isolated mitochondria to increasing calcium concentrations (Figure 4). Notably, we observed that the absence of tau reduced calcium sensitivity associated with mPTP opening. This is important because mitochondrial calcium dysregulation leads to prolonged mPTP opening and contributes to neurodegeneration, such as AD (Gauba et al., 2017; Panel et al., 2018). Therefore, we propose a possible role for tau in promoting mitochondrial mPTP-related swelling under physiological conditions, such as aging and neuronal damage that could lead to AD.

To validate that increased CypD levels induced by tau are responsible for mitochondrial and cognitive abnormalities detected in aged WT mice, we overexpressed CypD in aged tau^{-/-} mice using a lentiviral vector.

Three weeks after transduction, we detected reduced mitochondrial bioenergetics in these animals, similar to that observed in aged WT mice. In particular, aged tau^{-/-} mice overexpressing CypD presented reduced levels of ATP, accompanied by increased calcium sensitivity, associated with mPTP opening. These results indicate that the absence of tau contributes to improved mitochondrial function reducing



CypD expression. Considering that mitochondrial function is fundamental for brain function and cognition gave the high energy demand of the synapses (Hara et al., 2014), this could explain the behavioral changes observed in WT mice. We observed negative behavioral changes, suggesting that overexpression of CypD affects recognition and spatial memory, and social abilities in the aged tau^{-/-} mice. It is important to mention that we perform sham surgery in the control group, to reduce the effects of the surgical procedure when we compare these animals with tau^{-/-} mice infected with a lentiviral vector containing CypD-GFP. However, to be sure that the complete effect is related to CypD overexpression and not to the expression of an unrelated gene, such as GFP, a lentiviral vector containing only GFP could be used; nevertheless, we do not have that viral vector at this time. Future studies may revise this question to discard effects related to GFP expression. Also, to confirm the dependence between tau and CypD on mitochondrial and hippocampal function during aging, a knockdown of CypD in aged WT mice will be generated, hoping that this will reduce age-associated cognitive and mitochondrial disturbances.

Our results revealed that tau ablation significantly decreased the expression of CypD and thus prevented the mitochondrial and cognitive impairment associated with normal aging. In light of these findings, additional studies are needed to understand the mechanism by which tau induces increased levels of CypD and mitochondrial dysfunction. However, based on studies on AD or other pathologies, two hypotheses have been proposed: (i) Modified forms of tau could induce increased ROS production and higher calcium concentrations (Panel et al., 2018; Perez et al., 2018a), which could result in mitochondrial dysfunction and ultimately in mPTP opening; (ii) Tau may interact with mitochondrial proteins (Liu et al., 2016), such as CypD (Amadoro et al., 2010) promoting mitochondrial failure and a more active mPTP. All these events could contribute to cognitive deficits observed in normal aging (Figure 6). The hypothesis that tau could interact with CypD are results of previous reports using human AD brain samples in which it was demonstrated that NH₂-derived tau fragment interacts with CypD (Amadoro et al., 2012). This idea is also supported by previous studies of co-immunoprecipitation that indicate that tau interacts with an ample variety of proteins, of which 51% correspond to membrane-bound proteins (Liu et al., 2016). More specifically, within the membrane-associated target, 40.4% correspond to mitochondrial proteins (Liu et al., 2016).

REFERENCES

- Amadoro, G., Corsetti, V., Atlante, A., Florenzano, F., Capsoni, S., Bussani, R., et al. (2012). Interaction between NH₂-tau fragment and Abeta in Alzheimer's disease mitochondria contributes to the synaptic deterioration. *Neurobiol. Aging* 33, 883.e1–883.e25.
- Amadoro, G., Corsetti, V., Stringaro, A., Colone, M., D'aguanno, S., Meli, G., et al. (2010). A NH₂ tau fragment targets neuronal mitochondria at AD synapses: possible implications for neurodegeneration. *J. Alzheimers Dis.* 21, 445–470. doi: 10.3233/jad-2010-100120
- Avila, J., De Barreda, E. G., Pallas-Bazarra, N., and Hernandez, F. (2013). Tau and neuron aging. *Aging Dis.* 4, 23–28.

DATA AVAILABILITY STATEMENT

The raw data supporting the conclusions of this article will be made available by the authors, without undue reservation, to any qualified researcher.

ETHICS STATEMENT

Experimental procedures were approved by the Bioethical and Biosafety Committee of the Universidad Autónoma de Chile and Universidad San Sebastián, Santiago, Chile.

AUTHOR CONTRIBUTIONS

CJ, WC, CT-R, and RQ conceived the study. CJ and CT-R performed all experiments, analyzed the data, and wrote the manuscript. RQ and CT-R edited and prepared the final version of the paper. All authors read and approved the final version.

FUNDING

This work was supported by the FONDECYT: 1170441, 1200178 (to RQ), 1190620 (to WC), 11170546 (to CT-R); CONICYT PAI N°77170091 (to CT-R), and Anillo ACT1411 (to RQ and WC).

SUPPLEMENTARY MATERIAL

The Supplementary Material for this article can be found online at: <https://www.frontiersin.org/articles/10.3389/fnins.2020.586710/full#supplementary-material>

Supplementary Figure 1 | Mitochondrial mass in aged WT and tau^{-/-} mice. **(A)** Representative images of unfixed hippocampal slices from WT and tau^{-/-} mice stained with MitoTracker Green FM. **(B)** Quantitative analysis of MitoGreen staining in the DG, CA1, and CA3 hippocampal regions. **(C)** Western blot of hippocampal lysates and densitometric analysis of proteins involved in mitochondrial fusion, including Mfn1, Mfn2, and OPA1. **(D)** Western blot of hippocampal lysates and densitometric analysis of the proteins involved in mitochondrial fission, including phospho-Drp1, and total Drp1.

- Barja, G. (2014). The mitochondrial free radical theory of aging. *Prog. Mol. Biol. Transl. Sci.* 127, 1–27. doi: 10.1007/978-3-0348-7460-1_1
- Bartsch, T., and Wulff, P. (2015). The hippocampus in aging and disease: from plasticity to vulnerability. *Neuroscience* 309, 1–16. doi: 10.1016/j.neuroscience.2015.07.084
- Baumgartner, H. K., Gerasimenko, J. V., Thorne, C., Ferdek, P., Pozzan, T., Tepikin, A. V., et al. (2009). Calcium elevation in mitochondria is the main Ca²⁺ requirement for mitochondrial permeability transition pore (mPTP) opening. *J. Biol. Chem.* 284, 20796–20803. doi: 10.1074/jbc.M109.025353
- Bettio, L. E. B., Rajendran, L., and Gil-Mohapel, J. (2017). The effects of aging in the hippocampus and cognitive decline. *Neurosci. Biobehav. Rev.* 79, 66–86. doi: 10.1016/j.neubiorev.2017.04.030

- Bicks, L. K., Koike, H., Akbarian, S., and Morishita, H. (2015). Prefrontal cortex and social cognition in mouse and man. *Front. Psychol.* 6:1805. doi: 10.3389/fpsyg.2015.01805
- Biundo, F., Del Prete, D., Zhang, H., Arancio, O., and D'adamio, L. (2018). A role for tau in learning, memory and synaptic plasticity. *Sci. Rep.* 8:3184.
- Broadbent, N. J., Squire, L. R., and Clark, R. E. (2004). Spatial memory, recognition memory, and the hippocampus. *Proc. Natl. Acad. Sci. U.S.A.* 101, 14515–14520. doi: 10.1073/pnas.0406344101
- Carreras-Sureda, A., Jaña, F., Urrea, H., Durand, S., Mortenson, D. E., Sagredo, A., et al. (2019). Non-canonical function of IRE1 α determines mitochondria-associated endoplasmic reticulum composition to control calcium transfer and bioenergetics. *Nat. Cell Biol.* 21, 755–767. doi: 10.1038/s41556-019-0329-y
- Charles, S. T., and Carstensen, L. L. (2010). Social and emotional aging. *Annu. Rev. Psychol.* 61, 383–409.
- Chistiakov, D. A., Sobenin, I. A., Revin, V. V., Orekhov, A. N., and Bobryshev, Y. V. (2014). Mitochondrial aging and age-related dysfunction of mitochondria. *Biomed. Res. Int.* 2014:238463.
- Chun, M. M., and Turk-Browne, N. B. (2007). Interactions between attention and memory. *Curr. Opin. Neurobiol.* 17, 177–184. doi: 10.1016/j.conb.2007.03.005
- Dawson, H. N., Ferreira, A., Eyster, M. V., Ghoshal, N., Binder, L. I., and Vitek, M. P. (2001). Inhibition of neuronal maturation in primary hippocampal neurons from tau deficient mice. *J. Cell Sci.* 114, 1179–1187.
- Du, H., Guo, L., Fang, F., Chen, D., Sosunov, A. A., Mckhann, G. M., et al. (2008). Cyclophilin D deficiency attenuates mitochondrial and neuronal perturbation and ameliorates learning and memory in Alzheimer's disease. *Nat. Med.* 14, 1097–1105. doi: 10.1038/nm.1868
- Du, H., Guo, L., and Yan, S. S. (2012). Synaptic mitochondrial pathology in Alzheimer's disease. *Antioxid Redox Signal* 16, 1467–1475.
- Du, H., Guo, L., Zhang, W., Rydzewska, M., and Yan, S. (2011). Cyclophilin D deficiency improves mitochondrial function and learning/memory in aging Alzheimer disease mouse model. *Neurobiol. Aging* 32, 398–406. doi: 10.1016/j.neurobiolaging.2009.03.003
- Elobeid, A., Libard, S., Leino, M., Popova, S. N., and Alafuzoff, I. (2016). Altered Proteins in the Aging Brain. *J. Neuropathol. Exp. Neurol.* 75, 316–325. doi: 10.1093/jnen/nlw002
- Fjell, A. M., Mcevoy, L., Holland, D., Dale, A. M., Walhovd, K. B., and Alzheimer's Disease Neuroimaging Initiative. (2014). What is normal in normal aging? Effects of aging, amyloid and Alzheimer's disease on the cerebral cortex and the hippocampus. *Prog. Neurobiol.* 117, 20–40. doi: 10.1016/j.pneurobio.2014.02.004
- Gaub, E., Guo, L., and Du, H. (2017). Cyclophilin D promotes brain mitochondrial F1FO ATP synthase dysfunction in aging mice. *J. Alzheimers Dis.* 55, 1351–1362. doi: 10.3233/jad-160822
- Hara, Y., Yuk, F., Puri, R., Janssen, W. G., Rapp, P. R., and Morrison, J. H. (2014). Presynaptic mitochondrial morphology in monkey prefrontal cortex correlates with working memory and is improved with estrogen treatment. *Proc. Natl. Acad. Sci. U.S.A.* 111, 486–491. doi: 10.1073/pnas.1311310110
- Hom, J. R., Quintanilla, R. A., Hoffman, D. L., De Mesy Bentley, K. L., Molkentin, J. D., Sheu, S. S., et al. (2011). The permeability transition pore controls cardiac mitochondrial maturation and myocyte differentiation. *Dev. Cell* 21, 469–478. doi: 10.1016/j.devcel.2011.08.008
- Hood, K. N., Zhao, J., Redell, J. B., Hylin, M. J., Harris, B., Perez, A., et al. (2018). Endoplasmic reticulum stress contributes to the loss of newborn hippocampal neurons after traumatic brain injury. *J. Neurosci.* 38, 2372–2384. doi: 10.1523/jneurosci.1756-17.2018
- Huang, W. J., Zhang, X., and Chen, W. W. (2016). Role of oxidative stress in Alzheimer's disease. *Biomed. Rep.* 4, 519–522.
- Hurst, S., Hoek, J., and Sheu, S. S. (2017). Mitochondrial Ca²⁺ and regulation of the permeability transition pore. *J. Bioenerg. Biomembr.* 49, 27–47. doi: 10.1007/s10863-016-9672-x
- Iqbal, K., Liu, F., Gong, C. X., and Grundke-Iqbal, I. (2010). Tau in Alzheimer disease and related tauopathies. *Curr. Alzheimer Res.* 7, 656–664. doi: 10.2174/156720510793611592
- Jara, C., Aranguiz, A., Cerpa, W., Tapia-Rojas, C., and Quintanilla, R. A. (2018). Genetic ablation of tau improves mitochondrial function and cognitive abilities in the hippocampus. *Redox Biol.* 18, 279–294. doi: 10.1016/j.redox.2018.07.010
- Jara, C., Torres, A. K., Olesen, M. A., and Tapia-Rojas, C. (2019). *Mitochondrial Dysfunction as a Key Event During Aging: From Synaptic Failure to Memory Loss. Book Mitochondrial and Brain Disorders*. London: IntechOpen.
- Jonas, E. A., Porter, G. A. Jr., Beutner, G., Mnatsakanyan, N., and Alavian, K. N. (2015). Cell death disguised: the mitochondrial permeability transition pore as the c-subunit of the F(1)F(O) ATP synthase. *Pharmacol. Res.* 99, 382–392. doi: 10.1016/j.phrs.2015.04.013
- Karadayan, A. G., Bustamante, J., Czerniczyniec, A., Lombardi, P., Cutrera, R. A., and Lores-Arnaiz, S. (2015). Alcohol hangover induces mitochondrial dysfunction and free radical production in mouse cerebellum. *Neuroscience* 304, 47–59. doi: 10.1016/j.neuroscience.2015.07.012
- Lei, P., Ayton, S., Finkelstein, D. I., Spoerri, L., Ciccotosto, G. D., Wright, D. K., et al. (2012). Tau deficiency induces parkinsonism with dementia by impairing APP-mediated iron export. *Nat. Med.* 18, 291–295. doi: 10.1038/nm.2613
- Li, M., Husic, N., Lin, Y., and Snider, B. J. (2012). Production of lentiviral vectors for transducing cells from the central nervous system. *J. Vis. Exp.* 63:e4031. doi: 10.3791/4031
- Liu, C., Song, X., Nisbet, R., and Gotz, J. (2016). Co-immunoprecipitation with Tau isoform-specific antibodies reveals distinct protein interactions and highlights a putative role for 2N Tau in disease. *J. Biol. Chem.* 291, 8173–8188. doi: 10.1074/jbc.m115.641902
- Lopes, S., Teplýtska, L., Vaz-Silva, J., Dioli, C., Trindade, R., Morais, M., et al. (2016). Tau deletion prevents stress-induced dendritic atrophy in prefrontal cortex: role of synaptic mitochondria. *Cereb. Cortex* 27, 2580–2591.
- Lopez-Otin, C., Blasco, M. A., Partridge, L., Serrano, M., and Kroemer, G. (2013). The hallmarks of aging. *Cell* 153, 1194–1217.
- Mancuso, M., Calsolaro, V., Orsucci, D., Carlesi, C., Choub, A., Piazza, S., et al. (2009). Mitochondria, cognitive impairment, and Alzheimer's disease. *Int. J. Alzheimers Dis.* 2009:951548.
- Morris, M., Hamto, P., Adame, A., Devidze, N., Masliah, E., and Mucke, L. (2013). Age-appropriate cognition and subtle dopamine-independent motor deficits in aged tau knockout mice. *Neurobiol. Aging* 34, 1523–1529. doi: 10.1016/j.neurobiolaging.2012.12.003
- Navarro, A., and Boveris, A. (2010). Brain mitochondrial dysfunction in aging, neurodegeneration, and Parkinson's disease. *Front. Aging Neurosci.* 2:34. doi: 10.3389/fnagi.2010.00034
- Olesen, M. A., Torres, A. K., Jara, C., Murphy, M. P., and Tapia-Rojas, C. (2020). Premature synaptic mitochondrial dysfunction in the hippocampus during aging contributes to memory loss. *Redox Biol.* 34:101558. doi: 10.1016/j.redox.2020.101558
- Palomera-Avalos, V., Grinan-Ferre, C., Izquierdo, V., Camins, A., Sanfeliu, C., and Pallas, M. (2017). Metabolic stress induces cognitive disturbances and inflammation in aged mice: protective role of resveratrol. *Rejuvenation Res.* 20, 202–217. doi: 10.1089/rej.2016.1885
- Panel, M., Ghaleh, B., and Morin, D. (2018). Mitochondria and aging: a role for the mitochondrial transition pore? *Aging Cell* 17:e12793. doi: 10.1111/ace1.12793
- Parr-Brownlie, L. C., Bosch-Bouju, C., Schoderboeck, L., Sizemore, R. J., Abraham, W. C., and Hughes, S. M. (2015). Lentiviral vectors as tools to understand central nervous system biology in mammalian model organisms. *Front. Mol. Neurosci.* 8:14. doi: 10.3389/fnmol.2015.00014
- Perez, M. J., Jara, C., and Quintanilla, R. A. (2018a). Contribution of Tau pathology to mitochondrial impairment in neurodegeneration. *Front. Neurosci.* 12:441. doi: 10.3389/fnins.2018.00441
- Pérez, M. J., and Quintanilla, R. A. (2017). Development or disease: duality of the mitochondrial permeability transition pore. *Dev. Biol.* 426, 1–7. doi: 10.1016/j.ydbio.2017.04.018
- Perez, M. J., Vergara-Pulgar, K., Jara, C., Cabezas-Opazo, F., and Quintanilla, R. A. (2018b). Caspase-cleaved Tau impairs mitochondrial dynamics in Alzheimer's disease. *Mol. Neurobiol.* 55, 1004–1018. doi: 10.1007/s12035-017-0385-x
- Perez, M. J., and Quintanilla, R. A. (2017). Development or disease: duality of the mitochondrial permeability transition pore. *Dev. Biol.* 426, 1–7. doi: 10.1016/j.ydbio.2017.04.018
- Pooler, A. M., Polydoro, M., Wegmann, S., Nicholls, S. B., Spires-Jones, T. L., and Hyman, B. T. (2013). Propagation of tau pathology in Alzheimer's disease: identification of novel therapeutic targets. *Alzheimers Res. Ther.* 5:49. doi: 10.1186/alzrt214

- Quintanilla, R. A., Dolan, P. J., Jin, Y. N., and Johnson, G. V. (2012). Truncated tau and Abeta cooperatively impair mitochondria in primary neurons. *Neurobiol. Aging* 33, 619.e25–619.35. doi: 10.1016/j.neuroscience.2020.05.005
- Quintanilla, R. A., Matthews-Roberson, T. A., Dolan, P. J., and Johnson, G. V. (2009). Caspase-cleaved tau expression induces mitochondrial dysfunction in immortalized cortical neurons: implications for the pathogenesis of Alzheimer disease. *J. Biol. Chem.* 284, 18754–18766. doi: 10.1074/jbc.m808908200
- Quintanilla, R. A., Von Bernhardt, R., Godoy, J. A., Inestrosa, N. C., and Johnson, G. V. (2014). Phosphorylated tau potentiates Abeta-induced mitochondrial damage in mature neurons. *Neurobiol. Dis.* 71, 260–269. doi: 10.1016/j.nbd.2014.08.016
- Reinecke, F., Smeitink, J. A., and Van Der Westhuizen, F. H. (2009). OXPHOS gene expression and control in mitochondrial disorders. *Biochim. Biophys. Acta* 1792, 1113–1121. doi: 10.1016/j.bbdis.2009.04.003
- Rosenbaum, R. S., Winocur, G., Binns, M. A., and Moscovitch, M. (2012). Remote spatial memory in aging: all is not lost. *Front. Aging Neurosci.* 4:25. doi: 10.3389/fnagi.2012.00025
- Rottenberg, H., and Hoek, J. B. (2017). The path from mitochondrial ROS to aging runs through the mitochondrial permeability transition pore. *Aging Cell* 16, 943–955. doi: 10.1111/ace1.12650
- Schon, E. A., and Manfredi, G. (2003). Neuronal degeneration and mitochondrial dysfunction. *J. Clin. Invest.* 111, 303–312. doi: 10.1172/jci200317741
- Sebastian, D., Palacin, M., and Zorzano, A. (2017). Mitochondrial dynamics: coupling mitochondrial fitness with healthy aging. *Trends Mol. Med.* 23, 201–215. doi: 10.1016/j.molmed.2017.01.003
- Shoji, H., Takao, K., Hattori, S., and Miyakawa, T. (2016). Age-related changes in behavior in C57BL/6J mice from young adulthood to middle age. *Mol. Brain* 9:11. doi: 10.1016/j.mol.2016.01.003
- Smith, B. M., Yao, X., Chen, K. S., and Kirby, E. D. (2018). A larger social network enhances novel object location memory and reduces hippocampal microgliosis in aged mice. *Front. Aging Neurosci.* 10:142. doi: 10.3389/fnagi.2018.00142
- Stauch, K. L., Purnell, P. R., and Fox, H. S. (2014). Aging synaptic mitochondria exhibit dynamic proteomic changes while maintaining bioenergetic function. *Aging* 6, 320–334. doi: 10.18632/aging.100657
- Swerdlow, R. H. (2011). Brain aging, Alzheimer's disease, and mitochondria. *Biochim. Biophys. Acta* 1812, 1630–1639. doi: 10.1016/j.bba.2011.03.018
- Tapia-Rojas, C., Cabezas-Opazo, F., Deaton, C. A., Vergara, E. H., Johnson, G. V. W., and Quintanilla, R. A. (2019a). It's all about tau. *Prog. Neurobiol.* 175, 54–76. doi: 10.1016/j.pneurobi.2019.03.018
- Tapia-Rojas, C., Torres, A. K., and Quintanilla, R. A. (2019b). Adolescence binge alcohol consumption induces hippocampal mitochondrial impairment that persists during the adulthood. *Neuroscience* 406, 356–368. doi: 10.1016/j.neuroscience.2019.03.018
- Tatarkova, Z., Kuka, S., Racay, P., Lehotsky, J., Dobrota, D., Mistuna, D., et al. (2011). Effects of aging on activities of mitochondrial electron transport chain complexes and oxidative damage in rat heart. *Physiol. Res.* 60, 281–289. doi: 10.33549/physiolres.932019
- Torres, A. K., Tapia-Rojas, C., Cerpa, W., and Quintanilla, R. A. (2020). Stimulation of melanocortin receptor-4 (MC4R) prevents mitochondrial damage induced by binge ethanol protocol in adolescent rat hippocampus. *Neuroscience* 438, 70–85. doi: 10.1016/j.neuroscience.2020.05.005
- Uttara, B., Singh, A. V., Zamboni, P., and Mahajan, R. T. (2009). Oxidative stress and neurodegenerative diseases: a review of upstream and downstream antioxidant therapeutic options. *Curr. Neuropharmacol.* 7, 65–74. doi: 10.2174/157015909787602823
- Vargas, J. Y., Fuenzalida, M., and Inestrosa, N. C. (2014). In vivo activation of Wnt signaling pathway enhances cognitive function of adult mice and reverses cognitive deficits in an Alzheimer's disease model. *J. Neurosci.* 34, 2191–2202. doi: 10.1523/jneurosci.0862-13.2014
- Velazquez, R., Ferreira, E., Tran, A., Turner, E. C., Belfiore, R., Branca, C., et al. (2018). Acute tau knockdown in the hippocampus of adult mice causes learning and memory deficits. *Aging Cell* 17:e12775. doi: 10.1111/ace1.12775
- Wang, W., Zhao, F., Ma, X., Perry, G., and Zhu, X. (2020). Mitochondria dysfunction in the pathogenesis of Alzheimer's disease: recent advances. *Mol. Neurodegener.* 15:30. doi: 10.1007/s12064-020-00068-z
- Wang, Y., Garg, S., Mandelkow, E. M., and Mandelkow, E. (2010). Proteolytic processing of tau. *Biochem. Soc. Trans.* 38, 955–961. doi: 10.1042/bst0380955
- Wenz, T. (2011). Mitochondria and PGC-1alpha in aging and age-associated diseases. *J. Aging Res.* 2011:810619. doi: 10.1155/2011/810619
- Wu, Y., Chen, M., and Jiang, J. (2019). Mitochondrial dysfunction in neurodegenerative diseases and drug targets via apoptotic signaling. *Mitochondrion* 49, 35–45. doi: 10.1016/j.mito.2019.07.003
- Wyss-Coray, T. (2016). Ageing, neurodegeneration and brain rejuvenation. *Nature* 539, 180–186. doi: 10.1038/nature20411
- Xia, X., Jiang, Q., McDermott, J., and Han, J. J. (2018). Aging and Alzheimer's disease: comparison and associations from molecular to system level. *Aging Cell* 17:e12802. doi: 10.1111/ace1.12802
- Zuo, Y. C., Li, H. L., Xiong, N. X., Shen, J. Y., Huang, Y. Z., Fu, P., et al. (2016). Overexpression of Tau rescues Nogo-66-induced neurite outgrowth inhibition in vitro. *Neurosci. Bull.* 32, 577–584. doi: 10.1007/s12264-016-0068-z

Conflict of Interest: The authors declare that the research was conducted in the absence of any commercial or financial relationships that could be construed as a potential conflict of interest.

Copyright © 2021 Jara, Cerpa, Tapia-Rojas and Quintanilla. This is an open-access article distributed under the terms of the Creative Commons Attribution License (CC BY). The use, distribution or reproduction in other forums is permitted, provided the original author(s) and the copyright owner(s) are credited and that the original publication in this journal is cited, in accordance with accepted academic practice. No use, distribution or reproduction is permitted which does not comply with these terms.



Dysregulation of Phosphoinositide 5-Phosphatases and Phosphoinositides in Alzheimer's Disease

Kunie Ando^{1*†}, Christophe Erneux^{2†}, Mégane Homa¹, Sarah Houben¹, Marie-Ange de Fisenne¹, Jean-Pierre Brion¹ and Karelle Leroy¹

¹ Laboratory of Histology, Neuroanatomy and Neuropathology, Faculty of Medicine, Université Libre de Bruxelles Neuroscience Institute, Université Libre de Bruxelles, Brussels, Belgium, ² Institute of Interdisciplinary Research in Human and Molecular Biology (IRIBHM), Campus Erasme, Université Libre de Bruxelles, Brussels, Belgium

Keywords: synaptojanin, microglia, SHIP2, Alzheimer's disease, phosphoinositide phosphatases, phosphoinositides

OPEN ACCESS

Edited by:

Kin Ying Mok,
University College London,
United Kingdom

Reviewed by:

Tamas Balla,
National Institutes of Health (NIH),
United States

*Correspondence:

Kunie Ando
Kunie.Ando@ulb.ac.be

[†]These authors have contributed
equally to this work

Specialty section:

This article was submitted to
Neurodegeneration,
a section of the journal
Frontiers in Neuroscience

Received: 07 October 2020

Accepted: 26 January 2021

Published: 25 February 2021

Citation:

Ando K, Erneux C, Homa M, Houben S, de Fisenne M-A, Brion J-P and Leroy K (2021) Dysregulation of Phosphoinositide 5-Phosphatases and Phosphoinositides in Alzheimer's Disease. *Front. Neurosci.* 15:614855. doi: 10.3389/fnins.2021.614855

INTRODUCTION

Alzheimer's disease (AD) is the most common type of dementia and its prevalence is expected to rise in response to an aging human population. Yet, there is no disease-modifying drug currently available. The neuropathological hallmarks of AD are amyloid plaques composed of amyloid β (A β) peptides derived from successive cleavages of Amyloid Precursor Protein (APP) and neurofibrillary tangles (NFTs) constituted of the microtubule-associated protein tau (Brion, 2006). In AD brains, tau is hyperphosphorylated and aggregated to form paired helical filaments (PHF-tau). The disease pathogenesis precedes the overt clinical symptoms by 10–15 years. Early diagnosis and biomarkers are thus crucial for future clinical trials of AD. However, current standard biomarkers such as amyloid-PET scans are highly expensive and the patients are exposed to a considerable amount of ionizing radiation at each test. Cerebrospinal-fluid analyses for A β and tau are highly invasive due to lumbar punctures (Dolgin, 2018). We need to search for additional biomarkers that are less expensive and less invasive.

Emerging evidence suggests that A β modifies the metabolism of phosphoinositides (PIs) (Berman et al., 2008; Kam et al., 2016). PIs control major signaling pathways and cell processes in eukaryotic cells. Ten enzymes of the inositol and phosphoinositide 5-phosphatases (hereafter, PI 5-phosphatases) have been identified in the human genome i.e., INPP5A, INPP5D (SHIP1), INPPL1 (SHIP2), INPP5G (SYNJ1), INPP5H (SYNJ2), OCRL, INPP5E (Pharbin), INPP5B, INPP5J (PIPP) and INPP5K (SKIP) (Figure 1). Except for INPP5A, PI 5-phosphatases essentially dephosphorylate PI(4,5)P₂ and PI(3,4,5)P₃ at the 5-position of the inositol ring with different degrees of catalytic efficiency and selectivity for each isoenzyme. PI 5-phosphatases are involved in fine-tuning regulation of PI(4,5)P₂ and PI(3,4,5)P₃, key intracellular signaling molecules known to be present in different subcellular compartments of the cells. Recent genetic and epigenetic studies have unequivocally suggested that some of the PI 5-phosphatases are implicated in AD, in addition to several other human diseases (Ramos et al., 2019). In this opinion article, we review recent findings on the PI 5-phosphatases in relation to AD, aging and cognitive functions. Such information could be potentially useful for developing novel biomarkers for AD in the future.











	Names	Structure and implications in AD
PI 5-phosphatases	INPP5A	 <p>DNA methylation is increased in aging neurons (Gasparoni et al., 2018). Correlation between DNA methylation of cg12507869 in blood cells and verbal fluency (Marioni et al., 2018).</p>
	INPP5D (SHIP1)	 <p>rs35349669 of is a LOAD risk locus (Lambert et al., 2013). mRNA is increased in the brain of AD and Tg APP (Castillo et al., 2017). mRNA is increased in the leucocytes of AD patients (Yoshino et al., 2017).</p>
	INPPL1 (SHIP2)	 <p>mRNA is increased in the brain in relation to cognitive decline (Mostafavi et al., 2018). Mediator of Aβ toxicity to tau pathology (Kam et al., 2016) and actin re-organization (Lee et al., 2019).</p>
	INPP5G (SYNJ1)	 <p>Several SNPs associated with age of onset of AD (Miranda et al., 2018). mRNA is increased in AD brains (Zhu et al., 2015; Ando et al., 2020). Insoluble SYNJ1 is enriched in the Sarkosyl insoluble fraction and SYNJ1 is detected in plaque-associated dystrophic neurites, Hirano bodies and some NFTs in AD brains (Ando et al., 2020). SYNJ1 is implicated in Aβ toxicity (Berman et al., 2008), Aβ-induced synaptic morphology change (McIntire et al., 2012), Aβ clearance (Zhu et al., 2013) and autophagosome maturation (Vanhouwaert et al., 2017).</p>
	INPP5H (SYNJ2)	 <p>mRNA is increased in aging neurons (Gasparoni et al., 2018).</p>
	OCRL	 <p>Involved in autophagosome-lysosome fusion (De Leo et al., 2016).</p>
	INPP5E (Pharbin)	 <p>Critical in autophagosome-lysosome fusion in the brain (Hasegawa et al., 2016).</p>
	INPP5B	
	INPP5J (PIPP)	
	INPP5K (SKIP)	
PIs	PI3P	Decreased in AD brain (prefrontal and entorhinal cortex) and in the mouse brain of Tg. PS-APP (Morel et al., 2013).
	PI(3,4,5)P3	Decreased after oligomeric Aβ treatment in cultured neurons via dephosphorylation by SHIP2 (Kam et al., 2016).
	PI(3,4)P2	Increased after oligomeric Aβ treatment in cultured neurons via dephosphorylation of PI(3,4,5)P3 by SHIP2 (Kam et al., 2016).
	PI(4,5)P2	Decreased in AD prefrontal cortex (Morel et al., 2013). Decreased after oligomeric Aβ treatment in neuron via dephosphorylation by SYNJ1 (Berman et al., 2008).

Figure 1

FIGURE 1 | The figure shows the schematic illustrations of the major domains of PI 5-phosphatases and summarizes the implications of PI 5-phosphatases and PIs in AD. Each PI 5-phosphatase contains a highly conserved 5-phosphatase domain shown in green. PI, phosphoinositide; SHIP1, SH2 domain-containing inositol polyphosphate 5-phosphatase-1; SHIP2, SH2 domain-containing inositol polyphosphate 5-phosphatase-2; SYNJ1, Synaptojanin 1; SYNJ2, Synaptojanin 2; OCRL, (Continued)

FIGURE 1 | oculocerebrorenal syndrome of Lowe, PIPP, proline-rich inositol polyphosphate 5-phosphatase; SKIP, skeletal muscle and kidney enriched inositol phosphatase; CAAX, CAAX motif; SH2, Src homology 2; PH, Pleckstrin-homology; PRD, proline-rich domain; NPxY, a conserved tyrosine phosphorylation motif (Asn-Pro-x-Tyr) for binding to a phospho-tyrosine binding (PTB) domain; SAM, sterile alpha motif; SAC1, suppressor of actin 1; RRM, RNA recognition motif; ASH, ASPM-SPD2-Hydin domain; RhoGAP, Rho GTPase-activating protein domain; CB, clathrin binding domain; SRD, serine rich domain; SKICH, SKIP COOH terminal homology domain.

INPP5A and Cognitive Functions

Unlike other PI 5-phosphatase family members, INPP5A recognizes only soluble inositol 1,4,5-trisphosphate [Ins(1,4,5)P₃] and inositol 1,3,4,5-tetrakisphosphate [Ins(1,3,4,5)P₄] as substrates. INPP5A is ubiquitously expressed including in the hippocampus and prefrontal cortex, the brain regions highly affected in AD, and is abundantly detected in cerebellum (Liu et al., 2020). INPP5A negatively controls the mobilization of intracellular calcium by decreasing Ins(1,4,5)P₃ levels (De Smedt et al., 1997). DNA methylation of the *INPP5A* gene is increased in association with aging in neurons (Gasparoni et al., 2018). Meta-analysis of blood-based DNA methylation has shown that the methylation of cg12507869 located in the *INPP5A* gene had a significant negative correlation with phonemic verbal fluency and was associated with logical memory and vocabulary (Marioni et al., 2018). Blood-based DNA methylation of cg12507869 in the *INPP5A* could be thus considered as a potential biomarker for aging and cognitive functions.

SHIP1 and AD

SHIP1 is a hematopoietic-specific PI 5-phosphatase activated downstream of a multitude of receptors for growth factors, cytokines, antigens, immunoglobulin and toll-like receptor agonists. Once activated and correctly localized, SHIP1 generally acts as a negative regulator of signaling processes in hematopoietic cells, for example on the B cell receptor activation signaling pathway (Ramos et al., 2019). SHIP1 is detected in the brain, primarily in microglia reflecting its myeloid origin. Genome-wide association studies (GWAS) have identified the risk variant rs35349669 in *INPP5D*, the gene encoding human SHIP1 for late-onset AD (Lambert et al., 2013). *INPP5D* mRNA is significantly upregulated in human AD brains and in transgenic mouse brains with knock-in mutations of APP^{NL-G-F/NL-G-F} (Castillo et al., 2017). *INPP5D* mRNA expression in peripheral leucocytes is elevated in early AD but is decreased with cognitive decline (Yoshino et al., 2017). Further long-time follow-up of the participants would be necessary to decipher the correlation between the level of *INPP5D* mRNA and cognitive decline. Since SHIP1 converts PI(3,4,5)P₃ to PI(3,4)P₂, the amounts of these PIs in the blood leucocytes may also be altered and needs to be further investigated (as discussed in section PI Metabolism and Autophagic-Endosomal-Lysosomal Abnormalities). Taken together, the level of *INPP5D* mRNA in leucocytes could be an interesting target to develop a blood-based biomarker in the early stages of AD.

SHIP2 and AD

SHIP2, encoded by *INPPL1*, is ubiquitously expressed including in the brain (Muraille et al., 1999). By using PI(3,4,5)P₃ as

substrate, SHIP2 controls PI(3,4)P₂ content, a major SHIP2 product (Ghosh et al., 2018). SHIP2 can also dephosphorylate PI(4,5)P₂, another albeit less potent substrate (Elong Edimo et al., 2016). PI(3,4)P₂ is scarce under normal conditions but increases through signaling following PI 3-kinase activation. This lipid plays critical roles as a second messenger in cell migration, polarity, feedback control of PI(3,4,5)P₃ generation, and basal mTORC1 activity (Ramos et al., 2019). SHIP2 is directly implicated in several human diseases: mutations in *INPPL1* cause opsismodysplasia, a rare autosomal recessive disease characterized by delayed bone maturation (Fradet and Fitzgerald, 2017). SHIP2 is also upregulated in some cancer cells, particularly in aggressive human breast cancer cells (Ghosh et al., 2018). SHIP2 negatively regulates insulin/IGF-I actions and is implicated in type 2 diabetes and metabolic syndrome (Marion et al., 2002). Recent network-based approach has unraveled that SHIP2 is also linked to AD and cognitive decline: upregulation of *INPPL1* transcript in the brain significantly correlates with cognitive decline in human AD patients (Mostafavi et al., 2018). The same study also reported that SHIP2 immunoreactivity was detected in astrocytes and neurons in the *post-mortem* human brain tissues of AD patients and that lentivirus-mediated down regulation of SHIP2 in cultured astrocytes significantly reduced Aβ production (Mostafavi et al., 2018). Other independent studies have reported SHIP2 functions as a mediator of amyloid toxicity via tau hyperphosphorylation (Kam et al., 2016) and actin-cytoskeleton reorganization (Lee et al., 2019). Kam et al. reported that the interaction between Aβ and the FcγRIIb immuno-receptor leads to a translocation of SHIP2 to the plasma membrane to form a protein complex in which SHIP2 dephosphorylates PI(3,4,5)P₃ into PI(3,4)P₂. Increased amounts of PI(3,4)P₂ lead to decreased inhibitory phosphorylation of GSK3β at Ser9 *via* endoplasmic reticulum (ER) stress in cultured neurons (Kam et al., 2016). Consequently, tau phosphorylation by GSK3β is increased by Aβ *via* FcγRIIb-SHIP2 complex (Kam et al., 2016). SHIP2 inhibitors are thus under active scrutiny as a novel therapeutic target for AD. Actually, SHIP2 inhibitors represent new treatments for several diseases: SHIP2 inhibition has been reported to partially rescue memory deficits in transgenic mouse models of diabetes and AD (Soeda et al., 2010; Kam et al., 2016) and to prevent metastasis in breast cancer cells (Ghosh et al., 2018). Since both SHIP1 and SHIP2 play critical roles in antagonizing microglial proliferation and phagocytosis, the use of both SHIP1 and SHIP2 inhibitors has been proposed in AD to enhance basal microglial homeostatic functions for therapeutic purposes (Pedicone et al., 2020). Although SHIP2 could be a potential biomarker and a valuable therapeutic target for AD, it remains largely elusive whether SHIP2 undergoes a significant alteration

in subcellular localization and post-translational modifications during the progression of the disease. SHIP2 has more than 20 putative phosphorylation sites and its phosphatase activity and substrate recognition are, at least partially, regulated by phosphorylation, protein-protein interaction and subcellular localization (Elong Edimo et al., 2011). Given that SHIP2 is translocated to plasma membranes upon A β -Fc γ RIIb interaction (Kam et al., 2016), subcellular localization of SHIP2 should be significantly altered in AD brains. Since Fc γ RIIb activation leads to tyrosine phosphorylation of SHIP2 (Muraille et al., 1999), the post-translational modifications of SHIP2 could be altered in the affected areas of AD brains. It remains to be carefully determined in *post-mortem* brain tissues of AD patients whether there are changes in SHIP2 subcellular localizations, post-translational modifications and the impact of SHIP2 upregulation in AD on PI amounts, particularly PI(3,4,5)P3 and PI(3,4)P2.

SYNJ1 and SYNJ2

SYNJ1 and *SYNJ2* are both highly conserved and their genetic variants are associated with cognitive abilities in a cohort with a mean age of 70 (Lopez et al., 2012). *SYNJ1* is a brain-enriched presynaptic phosphatase involved in synaptic vesicle recycling, clathrin-coated vesicle uncoating at synapse (Cremona et al., 1999) and autophagosomal maturation within presynaptic terminals (Vanhouwaert et al., 2017). *SYNJ1*, whose gene is located in chromosome 21, is linked to endolysosomal abnormalities in Down syndrome (Cossec et al., 2012). Several mutations in *SYNJ1* gene are associated with early-onset Parkinsonism (Tran et al., 2020). Some of the polymorphisms in *SYNJ1* are also linked with age of onset in familial AD, late-onset AD and Down syndrome with AD (Miranda et al., 2018). *SYNJ1* is expressed in neurons and is implicated in A β toxicity (Berman et al., 2008), synaptic toxicity (McIntire et al., 2012) and A β clearance (Zhu et al., 2013). The mRNA level of *SYNJ1* is significantly upregulated in *post-mortem* AD brains in association with *APOE* genotype (Zhu et al., 2015; Ando et al., 2020). *SYNJ1* protein undergoes a significant solubility change and is co-enriched with PHF-tau in the sarkosyl-insoluble fraction (Ando et al., 2020). *SYNJ1* immunoreactivity is detected in actin-positive Hirano bodies, some NFTs and plaque-associated dystrophic neurites in *post-mortem* human AD brains (Ando et al., 2020). Such aberrant alteration of mRNA levels, protein localization, and protein solubility of *SYNJ1* could be applied to establish a valid biomarker for AD. While *SYNJ1* is brain specific, its paralog *SYNJ2* is ubiquitously expressed, but is also abundantly expressed in the synapse. In the temporal cortex from patients with depressive disorder, *SYNJ2* transcript expression is significantly decreased (Aston et al., 2005). Furthermore, differential methylation in the gene of *SYNJ2* has been also reported in association with aging in neuronal cells (Gasparoni et al., 2018).

Potential Involvements of Other PI 5-Phosphatases in AD

The implication of the other members of PI 5-phosphatase family in AD remains largely unknown. Given that AD is associated with autophagic-endosomal-lysosomal dysfunction (Nixon et al., 2008), we speculate that INPP5E and OCRL, highly expressed

in the brain and critical in autophagosome-lysosome fusion (De Leo et al., 2016; Hasegawa et al., 2016), might be involved in dysregulation of autophagy in AD brains.

PI Metabolism and Autophagic-Endosomal-Lysosomal Abnormalities

Consistent with alterations of some PI 5-phosphatases observed in AD brains, there are substantial findings suggesting that PIs undergo dysregulation during the disease progression in AD brains (Stokes and Hawthorne, 1987) and in the AD blood plasma (Mapstone et al., 2014). In the AD prefrontal cortex where both amyloid and tau pathologies are abundant, the amounts of PI 3-phosphate (PI3P) and PI(4,5)P2 are significantly decreased (Morel et al., 2013). Deficiency of PIs in AD brains may be linked to autophagic-endosomal-lysosomal abnormalities observed in neurons of the AD patients even at an early stage (Nixon et al., 2008). Considering that PIs regulate membrane dynamics, we hypothesize that autophagic-endosomal-lysosomal abnormalities could be a potential target for developing AD biomarkers. For instance, endosomal morphology alteration has been observed in iPSC-neurons derived from AD fibroblasts (Israel et al., 2012) and AD blood monocytes (Corlier et al., 2015). Whereas the precise mechanisms underlying endosomal abnormalities remain to be determined, such endosomal alterations in peripheral cells could be considered as a novel potential approach to develop AD biomarkers.

DISCUSSION

Upregulation of some PI 5-phosphatases and PI dysregulations have been evidenced in AD and such alterations could be useful to develop new biomarkers for AD. Careful investigations will be needed to assess if these alterations are AD-specific or also associated with other diseases. Blood-based analyses of some PI 5-phosphatases, PI metabolism, transcriptomic and epigenetic changes have demonstrated alterations in AD and are conceivable strategies toward development of new biomarkers. Further studies will also be needed to evaluate the sensitivity and the specificity of these alterations during the progression of AD compared to currently available other markers such as those of PET and CSF analyses. These studies will be critical for deciphering the most reliable biomarkers and their complementarity for the diagnosis and the prognosis of this devastating disease.

AUTHOR CONTRIBUTIONS

All the coauthors participated in constructing the concept and writing the manuscript. KA, CE, and J-PB contributed conception and design of this article. All authors contributed to manuscript revision, read, and approved the submitted version.

FUNDING

This study was supported by grants from the Belgian Fonds de la Recherche Scientifique Médicale (T.0027.19 to J-PB

and J.0078.18 to CE), the Fund Aline (King Baudouin Foundation) to J-PB, the Foundation for Alzheimer Research (FRA/SAO) to KL, and the Génicot Fund of ULB to J-PB and KL.

REFERENCES

- Ando, K., Ndjim, M., Turbant, S., Fontaine, G., Pregoni, G., Dauphinot, L., et al. (2020). The lipid phosphatase synaptojanin 1 undergoes a significant alteration in expression and solubility and is associated with brain lesions in Alzheimer's disease. *Acta Neuropathol. Commun.* 8:79. doi: 10.1186/s40478-020-00954-1
- Aston, C., Jiang, L., and Sokolov, B. P. (2005). Transcriptional profiling reveals evidence for signaling and oligodendroglial abnormalities in the temporal cortex from patients with major depressive disorder. *Mol. Psychiatry* 10, 309–322. doi: 10.1038/sj.mp.4001565
- Berman, D. E., Dall'armi, C., Voronov, S. V., McIntire, L. B., Zhang, H., Moore, A. Z., et al. (2008). Oligomeric amyloid-beta peptide disrupts phosphatidylinositol-4,5-bisphosphate metabolism. *Nat. Neurosci.* 11, 547–554. doi: 10.1038/nn.2100
- Brion, J. P. (2006). "Cellular changes in Alzheimer's disease," in *Principles and Practice of Geriatric Medicine, 4th Edn*, eds M. S. John Pathy, A. J. Sinclair, and J. E. Morley (Chichester: John Wiley and Sons), 1073–1081. doi: 10.1002/047009057X.ch92
- Castillo, E., Leon, J., Mazzei, G., Abolhassani, N., Haruyama, N., Saito, T., et al. (2017). Comparative profiling of cortical gene expression in Alzheimer's disease patients and mouse models demonstrates a link between amyloidosis and neuroinflammation. *Sci. Rep.* 7:17762. doi: 10.1038/s41598-017-17999-3
- Corlier, F., Rivals, I., Lagarde, J., Hamelin, L., Corne, H., Dauphinot, L., et al. (2015). Modifications of the endosomal compartment in peripheral blood mononuclear cells and fibroblasts from Alzheimer's disease patients. *Transl. Psychiatry* 5:e595. doi: 10.1038/tp.2015.87
- Cossec, J. C., Lavour, J., Berman, D. E., Rivals, I., Hoischen, A., Stora, S., et al. (2012). Trisomy for synaptojanin1 in down syndrome is functionally linked to the enlargement of early endosomes. *Hum. Mol. Genet.* 21, 3156–3172. doi: 10.1093/hmg/dd5142
- Cremona, O., Di Paolo, G., Wenk, M. R., Luthi, A., Kim, W. T., Takei, K., et al. (1999). Essential role of phosphoinositide metabolism in synaptic vesicle recycling. *Cell* 99, 179–188. doi: 10.1016/S0092-8674(00)81649-9
- De Leo, M. G., Staiano, L., Vicinanza, M., Luciani, A., Carissimo, A., Mutarelli, M., et al. (2016). Autophagosome-lysosome fusion triggers a lysosomal response mediated by TLR9 and controlled by OCRL. *Nat. Cell Biol.* 18, 839–850. doi: 10.1038/ncb3386
- De Smedt, F., Missiaen, L., Parys, J. B., Vanweyenberg, V., De Smedt, H., and Erneux, C. (1997). Isoprenylated human brain type I inositol 1,4,5-trisphosphate 5-phosphatase controls Ca²⁺ oscillations induced by ATP in Chinese hamster ovary cells. *J. Biol. Chem.* 272, 17367–17375. doi: 10.1074/jbc.272.28.17367
- Dolgin, E. (2018). Alzheimer's disease is getting easier to spot. *Nature* 559, S10–S12. doi: 10.1038/d41586-018-05721-w
- Elong Edimo, W., Derua, R., Janssens, V., Nakamura, T., Vanderwinden, J. M., Waelkens, E., et al. (2011). Evidence of SHIP2 Ser132 phosphorylation, its nuclear localization and stability. *Biochem. J.* 439, 391–401. doi: 10.1042/BJ20110173
- Elong Edimo, W., Ghosh, S., Derua, R., Janssens, V., Waelkens, E., Vanderwinden, J. M., et al. (2016). SHIP2 controls plasma membrane PI(4,5)P₂ thereby participating in the control of cell migration in 1321 N1 glioblastoma cells. *J. Cell Sci.* 129, 1101–1114. doi: 10.1242/jcs.179663
- Fradet, A., and Fitzgerald, J. (2017). INPPL1 gene mutations in opsismodysplasia. *J. Hum. Genet.* 62, 135–140. doi: 10.1038/jhg.2016.119
- Gasparoni, G., Bultmann, S., Lutsik, P., Kraus, T. F. J., Sordon, S., Vlcek, J., et al. (2018). DNA methylation analysis on purified neurons and glia dissects age and Alzheimer's disease-specific changes in the human cortex. *Epigenetics Chromatin* 11:41. doi: 10.1186/s13072-018-0211-3
- Ghosh, S., Scozzaro, S., Ramos, A. R., Delcambre, S., Chevalier, C., Krejci, P., et al. (2018). Inhibition of SHIP2 activity inhibits cell migration and could prevent metastasis in breast cancer cells. *J. Cell Sci.* 131:jcs216408. doi: 10.1242/jcs.216408
- Hasegawa, J., Iwamoto, R., Otomo, T., Nezu, A., Hamasaki, M., and Yoshimori, T. (2016). Autophagosome-lysosome fusion in neurons requires INPPE, a protein associated with Joubert syndrome. *EMBO J.* 35, 1853–1867. doi: 10.15252/embj.201593148
- Israel, M. A., Yuan, S. H., Bardy, C., Reyna, S. M., Mu, Y., Herrera, C., et al. (2012). Probing sporadic and familial Alzheimer's disease using induced pluripotent stem cells. *Nature* 482, 216–220. doi: 10.1038/nature10821
- Kam, T. I., Park, H., Gwon, Y., Song, S., Kim, S. H., Moon, S. W., et al. (2016). FcγRIIb-SHIP2 axis links Abeta to tau pathology by disrupting phosphoinositide metabolism in Alzheimer's disease model. *eLife* 5:e18691. doi: 10.7554/eLife.18691
- Lambert, J. C., Ibrahim-Verbaas, C. A., Harold, D., Naj, A. C., Sims, R., Bellenguez, C., et al. (2013). Meta-analysis of 74,046 individuals identifies 11 new susceptibility loci for Alzheimer's disease. *Nat. Genet.* 45, 1452–1458. doi: 10.1038/ng.2802
- Lee, H. N., Sim, K. M., Kim, H., Ju, J., Pae, A. N., Park, J. B., et al. (2019). Abeta modulates actin cytoskeleton via SHIP2-mediated phosphoinositide metabolism. *Sci. Rep.* 9:15557. doi: 10.1038/s41598-019-51914-2
- Liu, Q., Huang, S., Yin, P., Yang, S., Zhang, J., Jing, L., et al. (2020). Cerebellum-enriched protein INPP5A contributes to selective neuropathology in mouse model of spinocerebellar ataxias type 17. *Nat. Commun.* 11:1101. doi: 10.1038/s41467-020-14931-8
- Lopez, L. M., Harris, S. E., Luciano, M., Liewald, D., Davies, G., Gow, A. J., et al. (2012). Evolutionary conserved longevity genes and human cognitive abilities in elderly cohorts. *Eur. J. Hum. Genet.* 20, 341–347. doi: 10.1038/ejhg.2011.201
- Mapstone, M., Cheema, A. K., Fiandaca, M. S., Zhong, X., Mhyre, T. R., Macarthur, L. H., et al. (2014). Plasma phospholipids identify antecedent memory impairment in older adults. *Nat. Med.* 20, 415–418. doi: 10.1038/nm.3466
- Marion, E., Kaisaki, P. J., Pouillon, V., Gueydan, C., Levy, J. C., Bodson, A., et al. (2002). The gene INPPL1, encoding the lipid phosphatase SHIP2, is a candidate for type 2 diabetes in rat and man. *Diabetes* 51, 2012–2017. doi: 10.2337/diabetes.51.7.2012
- Marioni, R. E., Mcrae, A. F., Bressler, J., Colicino, E., Hannon, E., Li, S., et al. (2018). Meta-analysis of epigenome-wide association studies of cognitive abilities. *Mol. Psychiatry* 23, 2133–2144. doi: 10.1038/s41380-017-0008-y
- McIntire, L. B., Berman, D. E., Myaeng, J., Staniszevski, A., Arancio, O., Di Paolo, G., et al. (2012). Reduction of synaptojanin 1 ameliorates synaptic and behavioral impairments in a mouse model of Alzheimer's disease. *J. Neurosci.* 32, 15271–15276. doi: 10.1523/JNEUROSCI.2034-12.2012
- Miranda, A. M., Herman, M., Cheng, R., Nahmani, E., Barrett, G., Micevska, E., et al. (2018). Excess synaptojanin 1 contributes to place cell dysfunction and memory deficits in the aging hippocampus in three types of Alzheimer's disease. *Cell Rep.* 23, 2967–2975. doi: 10.1016/j.celrep.2018.05.011
- Morel, E., Lasiecka, Z. M., Chan, R. B., Williamson, R. L., Vetanovets, C., et al. (2013). Phosphatidylinositol-3-phosphate regulates sorting and processing of amyloid precursor protein through the endosomal system. *Nat. Commun.* 4:2250. doi: 10.1038/ncomms3250
- Mostafavi, S., Gaiteri, C., Sullivan, S. E., White, C. C., Tasaki, S., Xu, J., et al. (2018). A molecular network of the aging human brain provides insights into the pathology and cognitive decline of Alzheimer's disease. *Nat. Neurosci.* 21, 811–819. doi: 10.1038/s41593-018-0154-9
- Muraille, E., Pesesse, X., Kuntz, C., and Erneux, C. (1999). Distribution of the src-homology-2-domain-containing inositol 5-phosphatase SHIP-2 in both non-haemopoietic and haemopoietic cells and possible involvement of SHIP-2 in negative signalling of B-cells. *Biochem. J.* 342(Pt 3), 697–705. doi: 10.1042/bj3420697

ACKNOWLEDGMENTS

We apologize that many interesting studies had to be omitted due to the word limitations.

- Nixon, R. A., Yang, D. S., and Lee, J. H. (2008). Neurodegenerative lysosomal disorders: a continuum from development to late age. *Autophagy* 4, 590–599. doi: 10.4161/auto.6259
- Pedicone, C., Fernandes, S., Dungan, O. M., Dormann, S. M., Viernes, D. R., Adhikari, A. A., et al. (2020). Pan-SHIP1/2 inhibitors promote microglia effector functions essential for CNS homeostasis. *J. Cell Sci.* 133:jcs238030. doi: 10.1242/jcs.238030
- Ramos, A. R., Ghosh, S., and Erneux, C. (2019). The impact of phosphoinositide 5-phosphatases on phosphoinositides in cell function and human disease. *J. Lipid Res.* 60, 276–286. doi: 10.1194/jlr.R087908
- Soeda, Y., Tsuneki, H., Muranaka, H., Mori, N., Hosoh, S., Ichihara, Y., et al. (2010). The inositol phosphatase SHIP2 negatively regulates insulin/IGF-I actions implicated in neuroprotection and memory function in mouse brain. *Mol. Endocrinol.* 24, 1965–1977. doi: 10.1210/me.2010-0163
- Stokes, C. E., and Hawthorne, J. N. (1987). Reduced phosphoinositide concentrations in anterior temporal cortex of Alzheimer-diseased brains. *J. Neurochem.* 48, 1018–1021. doi: 10.1111/j.1471-4159.1987.tb05619.x
- Tran, J., Anastacio, H., and Bardy, C. (2020). Genetic predispositions of Parkinson's disease revealed in patient-derived brain cells. *NPJ Parkinsons Dis.* 6:8. doi: 10.1038/s41531-020-0110-8
- Vanhauwaert, R., Kuenen, S., Masius, R., Bademosi, A., Manetsberger, J., Schoovaerts, N., et al. (2017). The SAC1 domain in synaptojanin is required for autophagosome maturation at presynaptic terminals. *EMBO J.* 36, 1392–1411. doi: 10.15252/embj.201695773
- Yoshino, Y., Yamazaki, K., Ozaki, Y., Sao, T., Yoshida, T., Mori, T., et al. (2017). INPP5D mRNA expression and cognitive decline in Japanese Alzheimer's disease subjects. *J. Alzheimers. Dis.* 58, 687–694. doi: 10.3233/JAD-161211
- Zhu, L., Zhong, M., Elder, G. A., Sano, M., Holtzman, D. M., Gandy, S., et al. (2015). Phospholipid dysregulation contributes to ApoE4-associated cognitive deficits in Alzheimer's disease pathogenesis. *Proc. Natl. Acad. Sci. U.S.A.* 112, 11965–11970. doi: 10.1073/pnas.1510011112
- Zhu, L., Zhong, M., Zhao, J., Rhee, H., Caesar, I., Knight, E. M., et al. (2013). Reduction of synaptojanin 1 accelerates Abeta clearance and attenuates cognitive deterioration in an Alzheimer mouse model. *J. Biol. Chem.* 288, 32050–32063. doi: 10.1074/jbc.M113.504365

Conflict of Interest: The authors declare that the research was conducted in the absence of any commercial or financial relationships that could be construed as a potential conflict of interest.

Copyright © 2021 Ando, Erneux, Homa, Houben, de Fisenne, Brion and Leroy. This is an open-access article distributed under the terms of the Creative Commons Attribution License (CC BY). The use, distribution or reproduction in other forums is permitted, provided the original author(s) and the copyright owner(s) are credited and that the original publication in this journal is cited, in accordance with accepted academic practice. No use, distribution or reproduction is permitted which does not comply with these terms.



Quantitative Methods for the Detection of Tau Seeding Activity in Human Biofluids

Aurelien Lathuiliere^{1,2} and Bradley T. Hyman^{1,2*}

¹ Alzheimer Research Unit, Department of Neurology, Massachusetts General Hospital, Charlestown, MA, United States,

² Harvard Medical School, Boston, MA, United States

The ability of tau aggregates to recruit and misfold monomeric tau and propagate across brain regions has been studied extensively and is now recognized as a critical pathological step in Alzheimer's disease (AD) and other tauopathies. Recent evidence suggests that the detection of tau seeds in human samples may be relevant and correlate with clinical data. Here, we review the available methods for the measurement of such tau seeds, their limitations and their potential implementation for the development of the next-generation biomarkers.

OPEN ACCESS

Keywords: tau, seed, biomarker, Alzheimer's disease, cerebrospinal fluid

Edited by:

Kin Ying Mok,
University College London,
United Kingdom

Reviewed by:

Byron Caughey,
Rocky Mountain Laboratories (NIAID),
United States
Zhuohao He,
Chinese Academy of Sciences, China

*Correspondence:

Bradley T. Hyman
bhyman@mgh.harvard.edu

Specialty section:

This article was submitted to
Neurodegeneration,
a section of the journal
Frontiers in Neuroscience

Received: 15 January 2021

Accepted: 25 February 2021

Published: 19 March 2021

Citation:

Lathuiliere A and Hyman BT
(2021) Quantitative Methods
for the Detection of Tau Seeding
Activity in Human Biofluids.
Front. Neurosci. 15:654176.
doi: 10.3389/fnins.2021.654176

INTRODUCTION

The accumulation and deposition of tau protein aggregates in the human brain is a hallmark of Alzheimer's disease (AD) and other tauopathies. The capacity of certain toxic tau species or conformers to propagate from one cell to another and template or "seed" endogenous tau in a prion-like mechanism has been now widely studied and demonstrated in various disease models. *In vitro*, the aggregation of recombinant tau into paired helical filaments is accelerated by the addition of pre-formed seeds, suggesting a seeded nucleation process that results in the elongation of aggregates (Friedhoff et al., 1998; von Bergen et al., 2000). In cellular models, tau aggregates are internalized and induce aggregation of intracellular monomeric tau (Frost et al., 2009; Guo and Lee, 2011; Kfoury et al., 2012). In transgenic mice overexpressing mutant tau, the injection of synthetic tau fibrils or brain lysates from patients with tauopathies induces aggregation of tau and the spread of the pathology to distant brain regions (Clavaguera et al., 2009; Iba et al., 2013). The critical role of tau seeding and spreading in the pathogenesis of AD is further supported by the stereotypical progression of tau pathology across brain regions that has been described by neuropathological studies (Braak and Braak, 1991) and confirmed more recently by molecular imaging studies (Cho et al., 2016; Scholl et al., 2016; Schwarz et al., 2016). Moreover, seed-competent tau is detected in the synaptic compartment in brain regions along the Braak staging before the appearance of the pathology (Holmes et al., 2014; DeVos et al., 2018). This soluble seed-competent species represent a small percentage of total tau that elutes as a high molecular weight (>~300,000) fraction from a size exclusion chromatography column (Takeda et al., 2015, 2016).

Using modern AD biomarkers including tau and amyloid imaging by positron emission tomography (PET), volumetric magnetic resonance imaging (MRI), and cerebrospinal fluid (CSF) measurement of A β and tau (and in the near future plasma levels of A β and tau), one can accurately diagnose AD at a presymptomatic or prodromal stage [reviewed in Cohen et al. (2019), Zetterberg and Bendlin (2020)]. However, there is currently no available biomarker that can predict on a

time scale the clinical fate of an individual with evidence of brain amyloid or tau neuropathology. Recently, we have demonstrated that the tau seeding activity in postmortem AD brain extracts is quantitatively and qualitatively correlated with disease severity and rate of progression (Dujardin et al., 2020). Therefore, the quantification of tau seeds in human biofluids such as CSF could represent a potential prognostic biomarker that may greatly improve individual patient care.

Here, we review the currently available quantitative methods to measure seed-competent tau, their advantages and limitations as well as their potential development for a broader use in a biomarker pipeline.

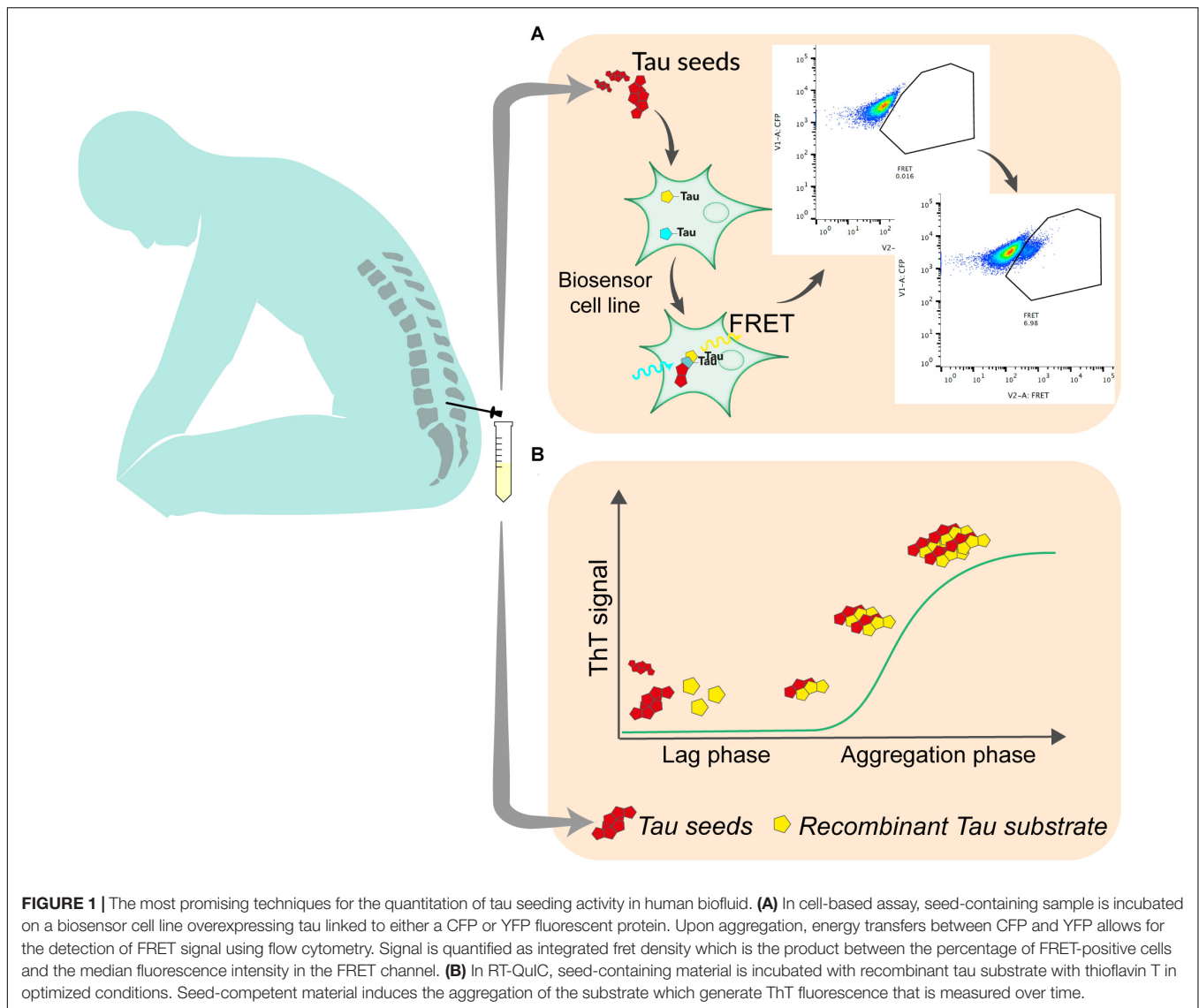
CEREBROSPINAL FLUID BIOCHEMICAL ASSAYS

The measurement of A β 42, total tau (*t*-tau) and phospho-tau (p-tau) in the CSF by immunoassays is a core component of AD clinical criteria (Frisoni et al., 2017; Jack et al., 2018). The typical profile in AD patients is characterized by high level of *t*-tau and p-tau and reduced level of A β 42. The sensitivity and specificity of these measures varies greatly across studies. A recent meta analysis concluded that they may be better used to rule out the diagnosis of AD because of a greater sensitivity than specificity (Ritchie et al., 2017). High CSF *t*-tau is generally considered as a measure of acute injury or ongoing neurodegeneration (Blennow et al., 1995). It is therefore not specific for AD and is found elevated in rapidly progressive dementia such as Creutzfeldt Jakob disease or in acute traumatic brain injury or stroke (Hesse et al., 2000; Ost et al., 2006; Skillback et al., 2014). Elevated CSF p-tau, is found in AD and is therefore useful to discriminate AD from other dementia such as dementia with Lewy bodies or frontotemporal dementia (Hampel et al., 2004). Interestingly, in non-AD tauopathies (or FTLT-tau), even though pathological brain aggregates consist in phosphorylated tau, inconsistent findings are reported in the literature regarding CSF levels of *t*-tau or p-tau. Discrepant studies have reported elevated *t*-tau and p-tau (Casoli et al., 2019), high *t*-tau but normal p-tau (Foiani et al., 2019) normal level of both (Goossens et al., 2018) or even decreased level of both (Wagshal et al., 2015). Those studies rely on ELISA-based quantitation which depend on antibody epitopes. While p-181 epitope is usually used for p-tau detection, the use of other phospho-epitope could potentially help discriminate tauopathies. The CSF biomarkers are useful from a diagnostic perspective in AD. However, their performance in assessing clinical progression of the disease or conversion to dementia is variable in the literature. Some studies found a correlation between elevated *t*-tau and p-tau with faster decline or higher mortality (Samgird et al., 2010; Degerman Gunnarsson et al., 2014). Other longitudinal studies found no correlation or even a relative stability of tau levels during the course of the disease (Andreasen et al., 1999; Sunderland et al., 1999; Vemuri et al., 2009; Williams et al., 2011). A recent study found a correlation between *t*-tau and p-tau levels and faster cognitive decline in ApoE- ϵ 4 carriers

only, which confirmed their limited predictive utility (Wattmo et al., 2020). Recently, the sensitivity of assays to detect p-tau in plasma has been improved. The plasma levels that are typically measured fall in a range between 1 and 10 pg/ml. Several recent studies have demonstrated that elevated plasma p-tau (p-tau181 or p-tau217) levels can discriminate AD from controls or from other neurodegenerative dementias (Janelidze et al., 2020; Palmqvist et al., 2020; Thijssen et al., 2020). Interestingly, plasma p-tau181 seemed to correlate with CSF p-tau181 and tau burden on PET imaging (Janelidze et al., 2020). These promising results need to be confirmed in larger primary care cohorts to validate the feasibility and clinical utility of this new biomarker.

CELL-BASED ASSAYS

The development of reporter cell lines, based on Förster resonance energy transfer (FRET) has been an important step in the understanding of the prion-like propagation of tau (Holmes et al., 2014). This type of biosensor is currently widely used to detect tau seeding activity in brain samples. It relies on the overexpression of the repeat domain (RD) of tau with the pro-aggregating P301L mutation fused to either a cyan fluorescent protein (CFP) or yellow fluorescent protein (YFP). After exposure to exogenous seed-competent tau, fluorescent reporters aggregate, which produce FRET signal that is typically quantified by flow cytometry, 24–72 h after exposure to tau seeds (Furman et al., 2015) (**Figure 1**). The original and most commonly used biosensor cell line is a clonal HEK293T line that was developed by the group of Marc Diamond and that is now commercially available (ATCC CRL-3275). Moreover, a similar reporter system can be used in mouse primary neuronal cells (Holmes et al., 2014). Slightly modified versions of this assay have also been tested by other groups. For instance, different fluorescent protein pairs have been used to increase the dynamic range of the assay (Chen et al., 2019). The addition of liposomes (lipofectamine) to facilitate the transduction of seeds into cells greatly increases the sensitivity of the biosensor assay but bypasses tau uptake mechanisms and therefore does not reflect seeding as it happens in the brain. A recent report suggests that the fusion of tau RD to fluorescent proteins may induce steric hindrance that avoids the elongation of tau aggregates into paired helical filaments (Kaniyappan et al., 2020b). The authors propose that the increase of FRET signal after exposure to seed-competent tau may result from cellular processes different from aggregation. Nevertheless, in a heterogeneous group of AD patients, the use of biosensor cells transduced by lipofection analyzed by live cell imaging and image processing could consistently detect a lag phase followed by an exponential elongation phase and a plateau phase in the aggregation, suggesting that the assay is relevant to seeding in the disease process (Dujardin et al., 2020). The use of such biosensor is therefore an interesting approach to quantify seed-competent tau in human biofluids. While the assay is sensitive enough to quantify seeds in postmortem ventricular CSF (Takeda et al., 2016), lumbar CSF



requires concentration steps that may alter quantitative aspect of measurement (Takeda et al., 2016; Crotti et al., 2019). Thus, some optimization needs to be done to improve the assay sensitivity and tailor it for a clinical use with reasonable volume of CSF. Such optimization may include ways to enhance the aggregation of FRET probes, including using tau constructs that may be more disease-relevant such as fragments covering the whole structure of amyloid core of tau aggregates (Fitzpatrick et al., 2017), or adapting the linker between fluorescent reporters and the tau protein to avoid steric hindrance (Kaniyappan et al., 2020a). In addition, adapting the fluorescent protein pairs to increase the FRET efficiency may also increase the signal produced by reporter cell lines (Bajar et al., 2016). A cell-based assay was able to detect tau seeding in brain from various tauopathies (Sanders et al., 2014). However, whether specific probe construct will be able to discriminate seeds from different pathologies has yet to be demonstrated. Even if some adaptations need to be tested and validated, they appear

realistic and may contribute to push FRET based biosensor to a clinical application. Fluorescence-based assays for routine diagnostics are already used in various clinical fields such as oncology or immunology.

SEED AMPLIFICATION ASSAYS

The capacity of proteopathic seeds from neurodegenerative disorders to self-propagate, recruit and template the aggregation of monomers has been exploited in a wide range of biomarker assays. The demonstration that infectious prions could misfold native prion protein and generate seeds in a cell-free environment opened the way to this type of assay (Kocisko et al., 1994). Various generations of assays using either unaffected brain sample as substrate (Saborio et al., 2001) or *Escherichia coli*-produced recombinant prion protein (Atarashi et al., 2007) have been developed over the years and led to the widely

used technique of Real-Time Quaking-Induced Conversion (RT-QuIC) for the diagnosis of sporadic Creutzfeldt Jakob disease (Atarashi et al., 2011; Orru et al., 2014). This system relies on the incubation in a 96-well plate, of biospecimen, typically CSF, with recombinant prion protein in excess, thioflavin T; in a defined buffer, at a controlled temperature (42°C), with shaking cycles over the course of several days. Thioflavin T fluorescence is measured every 45 min (**Figure 1**). The mean of highest fluorescence values over the course of the analysis is compared to control samples to determine positivity. In the presence of seeding-competent material, the typical trace starts with a lag phase that corresponds to the time needed for aggregating material to reach a concentration that can be detected by thioflavin T. The signal then reaches a plateau that reflects the conversion of all monomer substrate into amyloid (Schmitz et al., 2016). Similar methods have been used to detect seeds in synucleinopathies or tauopathies. The specificity of the seed amplification relies on the design of the substrate protein. Therefore, different RT-QuIC assays have been initially reported to detect specifically 3R, 4R, or 3R/4R seeds in corresponding tauopathies. For the detection of seeds in Pick's disease, which is characterized by 3-repeat tau deposition, a K19 tau fragment from 244 to 372, lacking the second repeat was used (Saijo et al., 2017). The only cysteine was mutated to serine to prevent the formation of disulfide bonds during the reaction. Despite the fact that this fragment does not cover the entire structure of Pick's disease's tau filaments (Falcon et al., 2018), RT-QuIC could detect tau seeds in postmortem CSF with very high sensitivity (Saijo et al., 2017). A modified version of this assay, incorporating a second tau fragment covering the entire cryoEM structure of AD paired helical filaments (residues 306–378) was able to detect seeds in AD brain (Kraus et al., 2019). When an extended 3-repeat cysteine free K12 fragment spanning from 244 to 400 was used, the self-polymerization of the probe was reduced and RT-Quic assay sensitivity and specificity were consequently increased, allowing for the detection of seeds in both 3R (Pick's disease) and 3R/4R [AD, chronic traumatic encephalopathy (CTE)] tauopathies (Metrick et al., 2020). Recently, the same group published an updated assay capable of measuring tau seeds from 4R tauopathies (progressive supranuclear palsy and corticobasal degeneration) with a sensitivity down to 2 femtograms (Saijo et al., 2020). For the first time, the authors described some signal in antemortem lumbar CSF suggesting that RT-QuIC -based assays could, with further optimization, detect, and or quantify seeds in the CSF of AD patients in the future. Interestingly, in both K12 and 4R assays the analysis of ThT amplitude can discriminate the different diseases-specific conformers (AD vs. Pick's or PSP vs. CBD) using the same assay conditions. Combining the two assays may hence be used to infer histopathological diagnosis. One limitation of tau RT-QuIC assays is that they rely on the use of heparin to promote the templating of tau substrate. It was shown that the structure of heparin-induced tau filaments differs from those found in AD or other tauopathies (Zhang et al., 2019). It might be interesting to evaluate substrates that include some post translational

modifications that have been recently associated with seeding (Wesseling et al., 2020).

IN VIVO SEED AMPLIFICATION ASSAYS

It is now well established also that injection of tau seeds into a transgenic animal that over-expresses human tau can lead to tau aggregates after several months (Clavaguera et al., 2009, 2013; Iba et al., 2013; Ahmed et al., 2014). Interestingly, in a mouse model overexpressing equimolar amount of both 3R and 4R tau isoforms the intracerebral injection of pathological tau seeds from different tauopathies (AD, CBD, PSP, and PiD) recruited the corresponding predominant isoform (He et al., 2020). In addition, the seeds from distinct tauopathies recapitulated cell-type specificity of the pathology in the recipient animal. CBD and PSP-derived seeds induced neuronal but also oligodendrocytic and astrocytic pathology as observed in human brain. All together, these results suggest that distinct seeds may carry different conformations that lead to specific isoform recruitment and to transmission to specific cell types. Skachokova et al. (2019) extended these observations to determine if the tau present in lumbar CSF collected from AD patients might also trigger aggregation of endogenous tau, and found that, over a period of about 4 months, CSF injected intrahippocampally into young P301S overexpressing mice did indeed form aggregates, reinforcing the idea that tau seeds detected using *in vitro* assays are biologically relevant in the intact organism as well (; Dujardin et al., 2020). Although not frequently used, animal-based bioassays have been validated for clinical diagnosis (e.g., for the detection of botulinum toxin) and could potentially be used as a platform for the detection of tau seeding activity in human biofluids. However, the accuracy and feasibility of such approach still needs to be demonstrated.

DISCUSSION AND FUTURE DIRECTIONS

The focus of biomarkers to date has been to aid in the diagnosis of neurodegenerative diseases, especially AD. This has been challenging in part because of the widespread recognition that neuropathological lesions can precede symptoms by years if not decades, so that knowing how to interpret positive results in an assay among the “controls” has been problematic. Nonetheless, largely with the aid of elegant studies in genetically defined at risk populations, PET scans for both Amyloid and tau and CSF biomarkers are well established. Yet some limitations remain: none of the tau-based markers are yet useful for non-AD tauopathies, and none of the currently available markers provide insight into the prognosis of an individual patient. Recent studies using brain tissue raise the possibility that there is considerable variability in tau post translational modifications across patients, which also is reflected in seed properties in a tau bioactivity assay (Dujardin et al., 2020; Sepulveda-Falla et al., 2020). If these alterations are also detectable in CSF, such differences may well provide insight into predicting relative rates of progression in living patients as well. Similarly, development of additional

markers of synaptic structure or function, inflammatory status of glia, and blood brain barrier dysfunction may all help in providing critical information for physicians and patients. Finally, biomarkers that provide insight into rates of progression might be valuable in stratifying individuals for enhancing design of clinical trials, and, hopefully in the near future, for decisions about the risk/benefit of therapeutic interventions, as well.

AUTHOR CONTRIBUTIONS

AL reviewed the literature, wrote and edited the manuscript, and made the illustration. BH wrote and edited the manuscript.

Both authors contributed to the article and approved the submitted version.

FUNDING

AL was supported by the Swiss National Science Foundation (P2ELP3_184403), the Alzheimer's Association (AACSF-19-617308), the Professor Dr. Max Cloetta Foundation and Uniscientia Foundation, Vaduz and European Union's Horizon 2020 Research and Innovation Program under the Marie Skłodowska-Curie grant agreement #839098. BH was supported by the Rainwater Trust, the JPB Foundation, NIA R56AG061196 and P30AG062421.

REFERENCES

- Ahmed, Z., Cooper, J., Murray, T. K., Garn, K., McNaughton, E., Clarke, H., et al. (2014). A novel in vivo model of tau propagation with rapid and progressive neurofibrillary tangle pathology: the pattern of spread is determined by connectivity, not proximity. *Acta Neuropathol.* 127, 667–683. doi: 10.1007/s00401-014-1254-6
- Andreasen, N., Minthon, L., Clarberg, A., Davidsson, P., Gottfries, J., Vanmechelen, E., et al. (1999). Sensitivity, specificity, and stability of CSF-tau in AD in a community-based patient sample. *Neurology* 53, 1488–1494. doi: 10.1212/wnl.53.7.1488
- Atarashi, R., Moore, R. A., Sim, V. L., Hughson, A. G., Dorward, D. W., Onwubiko, H. A., et al. (2007). Ultrasensitive detection of scrapie prion protein using seeded conversion of recombinant prion protein. *Nat. Methods* 4, 645–650. doi: 10.1038/nmeth1066
- Atarashi, R., Satoh, K., Sano, K., Fuse, T., Yamaguchi, N., Ishibashi, D., et al. (2011). Ultrasensitive human prion detection in cerebrospinal fluid by real-time quaking-induced conversion. *Nat. Med.* 17, 175–178. doi: 10.1038/nm.2294
- Bajar, B. T., Wang, E. S., Zhang, S., Lin, M. Z., and Chu, J. (2016). A guide to fluorescent protein FRET pairs. *Sensors (Basel)* 16:1488. doi: 10.3390/s16091488
- Blennow, K., Wallin, A., Agren, H., Spenger, C., Siegfried, J., and Vanmechelen, E. (1995). Tau protein in cerebrospinal fluid: a biochemical marker for axonal degeneration in Alzheimer disease? *Mol. Chem. Neuropathol.* 26, 231–245. doi: 10.1007/BF02815140
- Braak, H., and Braak, E. (1991). Neuropathological staging of Alzheimer-related changes. *Acta Neuropathol.* 82, 239–259.
- Casoli, T., Paolini, S., Fabbietti, P., Fattoretti, P., Paciaroni, L., Fabi, K., et al. (2019). Cerebrospinal fluid biomarkers and cognitive status in differential diagnosis of frontotemporal dementia and Alzheimer's disease. *J. Int. Med. Res.* 47, 4968–4980. doi: 10.1177/0300060519860951
- Chen, J. J., Nathaniel, D. L., Raghavan, P., Nelson, M., Tian, R., Tse, E., et al. (2019). Compromised function of the ESCRT pathway promotes endolysosomal escape of tau seeds and propagation of tau aggregation. *J. Biol. Chem.* 294, 18952–18966. doi: 10.1074/jbc.RA119.009432
- Cho, H., Choi, J. Y., Hwang, M. S., Kim, Y. J., Lee, H. M., Lee, H. S., et al. (2016). In vivo cortical spreading pattern of tau and amyloid in the Alzheimer disease spectrum. *Ann. Neurol.* 80, 247–258. doi: 10.1002/ana.24711
- Clavaguera, F., Akatsu, H., Fraser, G., Crowther, R. A., Frank, S., Hench, J., et al. (2013). Brain homogenates from human tauopathies induce tau inclusions in mouse brain. *Proc. Natl. Acad. Sci. U.S.A.* 110, 9535–9540. doi: 10.1073/pnas.1301175110
- Clavaguera, F., Bolmont, T., Crowther, R. A., Abramowski, D., Frank, S., Probst, A., et al. (2009). Transmission and spreading of tauopathy in transgenic mouse brain. *Nat. Cell Biol.* 11, 909–913. doi: 10.1038/ncb1901
- Cohen, A. D., Landau, S. M., Snitz, B. E., Klunk, W. E., Blennow, K., and Zetterberg, H. (2019). Fluid and PET biomarkers for amyloid pathology in Alzheimer's disease. *Mol. Cell. Neurosci.* 97, 3–17. doi: 10.1016/j.mcn.2018.12.004
- Crotti, A., Sait, H. R., McAvoy, K. M., Estrada, K., Ergun, A., Szak, S., et al. (2019). BIN1 favors the spreading of Tau via extracellular vesicles. *Sci. Rep.* 9:9477. doi: 10.1038/s41598-019-45676-0
- Degerman Gunnarsson, M., Lannfelt, L., Ingelsson, M., Basun, H., and Kilander, L. (2014). High tau levels in cerebrospinal fluid predict rapid decline and increased dementia mortality in Alzheimer's disease. *Dement. Geriatr. Cogn. Disord.* 37, 196–206. doi: 10.1159/000355556
- DeVos, S. L., Corjuc, B. T., Oakley, D. H., Nobuhara, C. K., Bannan, R. N., Chase, A., et al. (2018). Synaptic tau seeding precedes tau pathology in human Alzheimer's disease brain. *Front. Neurosci.* 12:267. doi: 10.3389/fnins.2018.00267
- Dujardin, S., Commins, C., Lathuiliere, A., Beerepoot, P., Fernandes, A. R., Kamath, T. V., et al. (2020). Tau molecular diversity contributes to clinical heterogeneity in Alzheimer's disease. *Nat. Med.* 26, 1256–1263. doi: 10.1038/s41591-020-0938-9
- Falcon, B., Zhang, W., Murzin, A. G., Murshudov, G., Garringer, H. J., Vidal, R., et al. (2018). Structures of filaments from Pick's disease reveal a novel tau protein fold. *Nature* 561, 137–140. doi: 10.1038/s41586-018-0454-y
- Fitzpatrick, A. W. P., Falcon, B., He, S., Murzin, A. G., Murshudov, G., Garringer, H. J., et al. (2017). Cryo-EM structures of tau filaments from Alzheimer's disease. *Nature* 547, 185–190. doi: 10.1038/nature23002
- Foiani, M. S., Cicognola, C., Ermann, N., Woollacott, I. O. C., Heller, C., Heslegrave, A. J., et al. (2019). Searching for novel cerebrospinal fluid biomarkers of tau pathology in frontotemporal dementia: an elusive quest. *J. Neurol. Neurosurg. Psychiatry* 90, 740–746. doi: 10.1136/jnnp-2018-319266
- Friedhoff, P., von Bergen, M., Mandelkow, E. M., Davies, P., and Mandelkow, E. (1998). A nucleated assembly mechanism of Alzheimer paired helical filaments. *Proc. Natl. Acad. Sci. U.S.A.* 95, 15712–15717. doi: 10.1073/pnas.95.26.15712
- Frisoni, G. B., Boccardi, M., Barkhof, F., Blennow, K., Cappa, S., Chiotis, K., et al. (2017). Strategic roadmap for an early diagnosis of Alzheimer's disease based on biomarkers. *Lancet Neurol.* 16, 661–676. doi: 10.1016/S1474-4422(17)30159-X
- Frost, B., Jacks, R. L., and Diamond, M. I. (2009). Propagation of tau misfolding from the outside to the inside of a cell. *J. Biol. Chem.* 284, 12845–12852. doi: 10.1074/jbc.M808759200
- Furman, J. L., Holmes, B. B., and Diamond, M. I. (2015). Sensitive detection of proteopathic seeding activity with FRET flow cytometry. *J. Vis. Exp.* 106:e53205. doi: 10.3791/53205
- Goossens, J., Bjerke, M., Van Mossevelde, S., Van den Bossche, T., Goeman, J., De Vil, B., et al. (2018). Diagnostic value of cerebrospinal fluid tau, neurofilament, and progranulin in definite frontotemporal lobar degeneration. *Alzheimers Res. Ther.* 10:31. doi: 10.1186/s13195-018-0364-0
- Guo, J. L., and Lee, V. M. (2011). Seeding of normal Tau by pathological Tau conformers drives pathogenesis of Alzheimer-like tangles. *J. Biol. Chem.* 286, 15317–15331. doi: 10.1074/jbc.M110.209296
- Hampel, H., Buerger, K., Zinkowski, R., Teipel, S. J., Goernitz, A., Andreasen, N., et al. (2004). Measurement of phosphorylated tau epitopes in the differential diagnosis of Alzheimer disease: a comparative cerebrospinal fluid study. *Arch. Gen. Psychiatry* 61, 95–102. doi: 10.1001/archpsyc.61.1.95

- He, Z., McBride, J. D., Xu, H., Changolkar, L., Kim, S. J., Zhang, B., et al. (2020). Transmission of tauopathy strains is independent of their isoform composition. *Nat. Commun.* 11:7. doi: 10.1038/s41467-019-13787-x
- Hesse, C., Rosengren, L., Vanmechelen, E., Vanderstichele, H., Jensen, C., Davidsson, P., et al. (2000). Cerebrospinal fluid markers for Alzheimer's disease evaluated after acute ischemic stroke. *J. Alzheimers Dis.* 2, 199–206. doi: 10.3233/jad-2000-23-402
- Holmes, B. B., Furman, J. L., Mahan, T. E., Yamasaki, T. R., Mirbaha, H., Eades, W. C., et al. (2014). Proteopathic tau seeding predicts tauopathy *in vivo*. *Proc. Natl. Acad. Sci. U.S.A.* 111, E4376–E4385. doi: 10.1073/pnas.1411649111
- Iba, M., Guo, J. L., McBride, J. D., Zhang, B., Trojanowski, J. Q., and Lee, V. M. (2013). Synthetic tau fibrils mediate transmission of neurofibrillary tangles in a transgenic mouse model of Alzheimer's-like tauopathy. *J. Neurosci.* 33, 1024–1037. doi: 10.1523/JNEUROSCI.2642-12.2013
- Jack, C. R. Jr., Bennett, D. A., Blennow, K., Carrillo, M. C., Dunn, B., Haeberlein, S. B., et al. (2018). NIA-AA Research Framework: toward a biological definition of Alzheimer's disease. *Alzheimers Dement.* 14, 535–562. doi: 10.1016/j.jalz.2018.02.018
- Janelidze, S., Mattsson, N., Palmqvist, S., Smith, R., Beach, T. G., Serrano, G. E., et al. (2020). Plasma P-tau181 in Alzheimer's disease: relationship to other biomarkers, differential diagnosis, neuropathology and longitudinal progression to Alzheimer's dementia. *Nat. Med.* 26, 379–386. doi: 10.1038/s41591-020-0755-1
- Kaniyappan, S., Tepper, K., Biernat, J., Chandupatla, R. R., Hübschmann, S., Irsen, S., et al. (2020a). FRET-based Tau seeding assay does not represent prion-like templated assembly of Tau fibers. *bioRxiv [Preprint]* doi: 10.1101/2020.03.25.998831
- Kaniyappan, S., Tepper, K., Biernat, J., Chandupatla, R. R., Hübschmann, S., Irsen, S., et al. (2020b). FRET-based Tau seeding assay does not represent prion-like templated assembly of Tau filaments. *Mol. Neurodegener.* 15:39. doi: 10.1186/s13024-020-00389-1
- Kfoury, N., Holmes, B. B., Jiang, H., Holtzman, D. M., and Diamond, M. I. (2012). Trans-cellular propagation of Tau aggregation by fibrillar species. *J. Biol. Chem.* 287, 19440–19451. doi: 10.1074/jbc.M112.346072
- Kocisko, D. A., Come, J. H., Priola, S. A., Chesebro, B., Raymond, G. J., Lansbury, P. T., et al. (1994). Cell-free formation of protease-resistant prion protein. *Nature* 370, 471–474. doi: 10.1038/370471a0
- Kraus, A., Saijo, E., Metrick, M. A. II, Newell, K., Sigurdson, C. J., Zanusso, G., et al. (2019). Seeding selectivity and ultrasensitive detection of tau aggregate conformers of Alzheimer disease. *Acta Neuropathol.* 137, 585–598. doi: 10.1007/s00401-018-1947-3
- Metrick, M. A. II, Ferreira, N. D. C., Saijo, E., Kraus, A., Newell, K., Zanusso, G., et al. (2020). A single ultrasensitive assay for detection and discrimination of tau aggregates of Alzheimer and Pick diseases. *Acta Neuropathol. Commun.* 8:22. doi: 10.1186/s40478-020-0887-z
- Orru, C. D., Bongianini, M., Tonoli, G., Ferrari, S., Hughson, A. G., Groveman, B. R., et al. (2014). A test for Creutzfeldt-Jakob disease using nasal brushings. *N. Engl. J. Med.* 371, 519–529. doi: 10.1056/NEJMoa1315200
- Ost, M., Nylén, K., Csajbok, L., Ohrfelt, A. O., Tullberg, M., Wikkelso, C., et al. (2006). Initial CSF total tau correlates with 1-year outcome in patients with traumatic brain injury. *Neurology* 67, 1600–1604. doi: 10.1212/01.wnl.0000242732.06714.0f
- Palmqvist, S., Janelidze, S., Quiroz, Y. T., Zetterberg, H., Lopera, F., Stomrud, E., et al. (2020). Discriminative accuracy of plasma phospho-tau217 for Alzheimer disease vs other neurodegenerative disorders. *JAMA* 324, 772–781. doi: 10.1001/jama.2020.12134
- Ritchie, C., Smailagic, N., Noel-Storr, A. H., Ukoumunne, O., Ladds, E. C., and Martin, S. (2017). CSF tau and the CSF tau/ABeta ratio for the diagnosis of Alzheimer's disease dementia and other dementias in people with mild cognitive impairment (MCI). *Cochrane Database Syst. Rev.* 3:CD010803. doi: 10.1002/14651858.CD010803.pub2
- Saborio, G. P., Permanne, B., and Soto, C. (2001). Sensitive detection of pathological prion protein by cyclic amplification of protein misfolding. *Nature* 411, 810–813. doi: 10.1038/35081095
- Saijo, E., Ghetti, B., Zanusso, G., Oblak, A., Furman, J. L., Diamond, M. I., et al. (2017). Ultrasensitive and selective detection of 3-repeat tau seeding activity in Pick disease brain and cerebrospinal fluid. *Acta Neuropathol.* 133, 751–765. doi: 10.1007/s00401-017-1692-z
- Saijo, E., Metrick, M. A. II, Koga, S., Parchi, P., Litvan, I., Spina, S., et al. (2020). 4-Repeat tau seeds and templating subtypes as brain and CSF biomarkers of frontotemporal lobar degeneration. *Acta Neuropathol.* 139, 63–77. doi: 10.1007/s00401-019-02080-2
- Samgard, K., Zetterberg, H., Blennow, K., Hansson, O., Minthon, L., and Londo, E. (2010). Cerebrospinal fluid total tau as a marker of Alzheimer's disease intensity. *Int. J. Geriatr. Psychiatry* 25, 403–410. doi: 10.1002/gps.2353
- Sanders, D. W., Kaufman, S. K., DeVos, S. L., Sharma, A. M., Mirbaha, H., Li, A., et al. (2014). Distinct tau prion strains propagate in cells and mice and define different tauopathies. *Neuron* 82, 1271–1288. doi: 10.1016/j.neuron.2014.04.047
- Schmitz, M., Cramm, M., Llorens, F., Muller-Cramm, D., Collins, S., Atarashi, R., et al. (2016). The real-time quaking-induced conversion assay for detection of human prion disease and study of other protein misfolding diseases. *Nat. Protoc.* 11, 2233–2242. doi: 10.1038/nprot.2016.120
- Scholl, M., Lockhart, S. N., Schonhaut, D. R., O'Neil, J. P., Janabi, M., Ossenkoppele, R., et al. (2016). PET imaging of tau deposition in the aging human brain. *Neuron* 89, 971–982. doi: 10.1016/j.neuron.2016.01.028
- Schwarz, A. J., Yu, P., Miller, B. B., Shcherbinin, S., Dickson, J., Navitsky, M., et al. (2016). Regional profiles of the candidate tau PET ligand 18F-AV-1451 recapitulate key features of Braak histopathological stages. *Brain* 139(Pt 5), 1539–1550. doi: 10.1093/brain/aww023
- Sepulveda-Falla, D., Chavez-Gutierrez, L., Portelius, E., Velez, J. I., Dujardin, S., Barrera-Ocampo, A., et al. (2020). A multifactorial model of pathology for age of onset heterogeneity in familial Alzheimer's disease. *Acta Neuropathol.* 141, 217–233. doi: 10.1007/s00401-020-02249-0
- Skachokova, Z., Martinisi, A., Flach, M., Sprenger, F., Naegelin, Y., Steiner-Monard, V., et al. (2019). Cerebrospinal fluid from Alzheimer's disease patients promotes tau aggregation in transgenic mice. *Acta Neuropathol. Commun.* 7:72. doi: 10.1186/s40478-019-0725-3
- Skillback, T., Rosen, C., Asztely, F., Mattsson, N., Blennow, K., and Zetterberg, H. (2014). Diagnostic performance of cerebrospinal fluid total tau and phosphorylated tau in Creutzfeldt-Jakob disease: results from the Swedish Mortality Registry. *JAMA Neurol.* 71, 476–483. doi: 10.1001/jamaneurol.2013.6455
- Sunderland, T., Wolozin, B., Galasko, D., Levy, J., Dukoff, R., Bahro, M., et al. (1999). Longitudinal stability of CSF tau levels in Alzheimer patients. *Biol. Psychiatry* 46, 750–755. doi: 10.1016/s0006-3223(99)00143-2
- Takeda, S., Commins, C., DeVos, S. L., Nobuhara, C. K., Wegmann, S., Roe, A. D., et al. (2016). Seed-competent high-molecular-weight tau species accumulates in the cerebrospinal fluid of Alzheimer's disease mouse model and human patients. *Ann. Neurol.* 80, 355–367. doi: 10.1002/ana.24716
- Takeda, S., Wegmann, S., Cho, H., DeVos, S. L., Commins, C., Roe, A. D., et al. (2015). Neuronal uptake and propagation of a rare phosphorylated high-molecular-weight tau derived from Alzheimer's disease brain. *Nat. Commun.* 6:8490. doi: 10.1038/ncomms9490
- Thijssen, E. H., La Joie, R., Wolf, A., Strom, A., Wang, P., Iaccarino, L., et al. (2020). Diagnostic value of plasma phosphorylated tau181 in Alzheimer's disease and frontotemporal lobar degeneration. *Nat. Med.* 26, 387–397. doi: 10.1038/s41591-020-0762-2
- Vemuri, P., Wiste, H. J., Weigand, S. D., Shaw, L. M., Trojanowski, J. Q., Weiner, M. W., et al. (2009). MRI and CSF biomarkers in normal, MCI, and AD subjects: diagnostic discrimination and cognitive correlations. *Neurology* 73, 287–293. doi: 10.1212/WNL.0b013e3181af79e5
- von Bergen, M., Friedhoff, P., Biernat, J., Heberle, J., Mandelkow, E. M., and Mandelkow, E. (2000). Assembly of tau protein into Alzheimer paired helical filaments depends on a local sequence motif ((306)VQIVYK(311)) forming beta structure. *Proc. Natl. Acad. Sci. U.S.A.* 97, 5129–5134.
- Wagshal, D., Sankaranarayanan, S., Guss, V., Hall, T., Berisha, F., Lobach, I., et al. (2015). Divergent CSF tau alterations in two common tauopathies: Alzheimer's disease and progressive supranuclear palsy. *J. Neurol. Neurosurg. Psychiatry* 86, 244–250. doi: 10.1136/jnnp-2014-308004

- Wattmo, C., Blennow, K., and Hansson, O. (2020). Cerebro-spinal fluid biomarker levels: phosphorylated tau (T) and total tau (N) as markers for rate of progression in Alzheimer's disease. *BMC Neurol.* 20:10. doi: 10.1186/s12883-019-1591-0
- Wesseling, H., Mair, W., Kumar, M., Schlaffner, C. N., Tang, S., Beerepoot, P., et al. (2020). Tau PTM profiles identify patient heterogeneity and stages of Alzheimer's disease. *Cell* 183, 1699–1713.e13. doi: 10.1016/j.cell.2020.10.029
- Williams, J. H., Wilcock, G. K., Seeburger, J., Dallob, A., Laterza, O., Potter, W., et al. (2011). Non-linear relationships of cerebrospinal fluid biomarker levels with cognitive function: an observational study. *Alzheimers Res. Ther.* 3:5. doi: 10.1186/alzrt64
- Zetterberg, H., and Bendlin, B. B. (2020). Biomarkers for Alzheimer's disease—preparing for a new era of disease-modifying therapies. *Mol. Psychiatry* 26, 296–308. doi: 10.1038/s41380-020-0721-9
- Zhang, W., Falcon, B., Murzin, A. G., Fan, J., Crowther, R. A., Goedert, M., et al. (2019). Heparin-induced tau filaments are polymorphic and differ from those in Alzheimer's and Pick's diseases. *Elife* 8:e43584. doi: 10.7554/eLife.43584
- Conflict of Interest:** The authors declare that the research was conducted in the absence of any commercial or financial relationships that could be construed as a potential conflict of interest.

Copyright © 2021 Lathuiliere and Hyman. This is an open-access article distributed under the terms of the Creative Commons Attribution License (CC BY). The use, distribution or reproduction in other forums is permitted, provided the original author(s) and the copyright owner(s) are credited and that the original publication in this journal is cited, in accordance with accepted academic practice. No use, distribution or reproduction is permitted which does not comply with these terms.



Polygenic Score Models for Alzheimer's Disease: From Research to Clinical Applications

Xiaopu Zhou^{1,2,3}, Yolanda Y. T. Li¹, Amy K. Y. Fu^{1,2,3} and Nancy Y. Ip^{1,2,3*}

¹ Division of Life Science, State Key Laboratory of Molecular Neuroscience and Molecular Neuroscience Center, The Hong Kong University of Science and Technology, Hong Kong, China, ² Hong Kong Center for Neurodegenerative Diseases, Hong Kong Science Park, Hong Kong, China, ³ Guangdong Provincial Key Laboratory of Brain Science, Disease and Drug Development, HKUST Shenzhen Research Institute, Shenzhen–Hong Kong Institute of Brain Science, Shenzhen, China

OPEN ACCESS

Edited by:

Jie Tu,
Chinese Academy of Sciences (CAS),
China

Reviewed by:

Sam Gandy,
Icahn School of Medicine at Mount
Sinai, United States
Chongzhao Ran,
Harvard Medical School,
United States

*Correspondence:

Nancy Y. Ip
boip@ust.hk

Specialty section:

This article was submitted to
Neurodegeneration,
a section of the journal
Frontiers in Neuroscience

Received: 06 January 2021

Accepted: 09 March 2021

Published: 29 March 2021

Citation:

Zhou X, Li YYT, Fu AKY and Ip NY
(2021) Polygenic Score Models
for Alzheimer's Disease: From
Research to Clinical Applications.
Front. Neurosci. 15:650220.
doi: 10.3389/fnins.2021.650220

The high prevalence of Alzheimer's disease (AD) among the elderly population and its lack of effective treatments make this disease a critical threat to human health. Recent epidemiological and genetics studies have revealed the polygenic nature of the disease, which is possibly explainable by a polygenic score model that considers multiple genetic risks. Here, we systemically review the rationale and methods used to construct polygenic score models for studying AD. We also discuss the associations of polygenic risk scores (PRSs) with clinical outcomes, brain imaging findings, and biochemical biomarkers from both the brain and peripheral system. Finally, we discuss the possibility of incorporating polygenic score models into research and clinical practice along with potential challenges.

Keywords: Alzheimer's disease, polygenic score, *APOE*, genetics, polygenic risk score, polygenic hazard score, risk prediction

INTRODUCTION

Alzheimer's disease (AD), an aging-related neurodegenerative disease and the most common form of dementia, is a health threat to societies worldwide. AD has a complex etiology that is influenced by both genetic and environmental factors, which account for its variable risk among individuals. The presence of known coding mutations located in *APP* and *PSEN* genes that exhibit extremely high disease penetrance for early-onset AD can be determined by genetic analysis well before disease onset. Moreover, sporadic late-onset AD (LOAD), which accounts for most AD cases, is suggested to be highly heritable (approximately 60–80%) in the general population (Gatz et al., 2006). Therefore, studying individual genomes might identify individuals at high risk of developing AD, create a time window for intervention, and aid the development of intervention strategies.

However, genome-wide association studies (GWASs) of LOAD have only revealed a few dozen genetic risk loci with mild or moderate disease risk-modifying effects; individually, these cannot adequately explain an individual's risk of having AD at the population level (Lambert et al., 2013; Jansen et al., 2019). The inconsistencies among epidemiological studies regarding the high heritability of LOAD as well as the lack of causal genetic factors that adequately explain disease risk imply that LOAD has a polygenic nature: its risk might be modulated by the aggregate effects of many hidden variants as well as environmental factors. Accordingly, given that polygenic risk

analysis has recently become a key facet in cohort studies of LOAD, herein we systemically review the current approaches to polygenic risk analysis along with their applications in AD.

KEY ELEMENTS OF POLYGENIC SCORE MODELS

Polygenic score models consider the aggregate effects of multiple variants to evaluate genetic contributions to continuous or discrete traits—for instance, gene expression levels or disease status (Chatterjee et al., 2016). Hence, polygenic score models require knowledge about which variants modify the disease in question. Variants are normally selected by screening the summary statistics generated by GWASs with proper filtering of the association *p*-values. Various *p*-value thresholds can be applied (e.g., 0.0001, 0.01, or 0.5) to obtain the pools of variants that exhibit optimal performance for AD classification (Escott-Price et al., 2019b). Meanwhile, several methods have been applied to overcome the redundancy of genetic information (i.e., the effects of the variants on a given disease) due to high linkage disequilibrium among selected variants. For instance, linkage disequilibrium-based pruning, which removes variants in high linkage disequilibrium, or linkage disequilibrium-aware clumping, which simultaneously removes variants in high linkage disequilibrium while retaining variants with the smallest *p*-values, have been applied to select the most informative variants to construct a polygenic score model. In addition to *p*-value-based selection, other statistical learning methods such as lasso regression, which can select the most informative variants for AD classification by removing variants minimally associated with the disease, have been also incorporated into polygenic risk analysis for AD (Romero-Rosales et al., 2020; Zhou et al., 2020).

Once the variants for model construction have been determined, their genotype dosages are summarized into a single value that can represent an individual's status (i.e., their relative risk of having AD). The easiest way to achieve this is to simply sum the number of risk alleles across all selected variants to generate an unweighted polygenic score (Tosto et al., 2017). Meanwhile, two types of weighting measures are commonly introduced into polygenic score models to account for the variable impacts of individual variants on disease risk and generate a more accurate polygenic score model. First, the effect size can be determined from an association test, meta-analysis, or log-transformed odds ratios, thus yielding a weighted polygenic risk score (PRS) model (Tosto et al., 2017). Second, log-transformed hazard ratios generated from association analysis for disease onset age can also be introduced to produce a polygenic hazard score (PHS), which indicates an individual's instantaneous risk of developing a given disease (Tan et al., 2018).

Nevertheless, introducing statistical learning methods into polygenic risk analysis enables simultaneous variant selection and model construction. Such methods, including lasso regression and support vector machines, can directly learn from the raw genotype data and use the same framework to construct

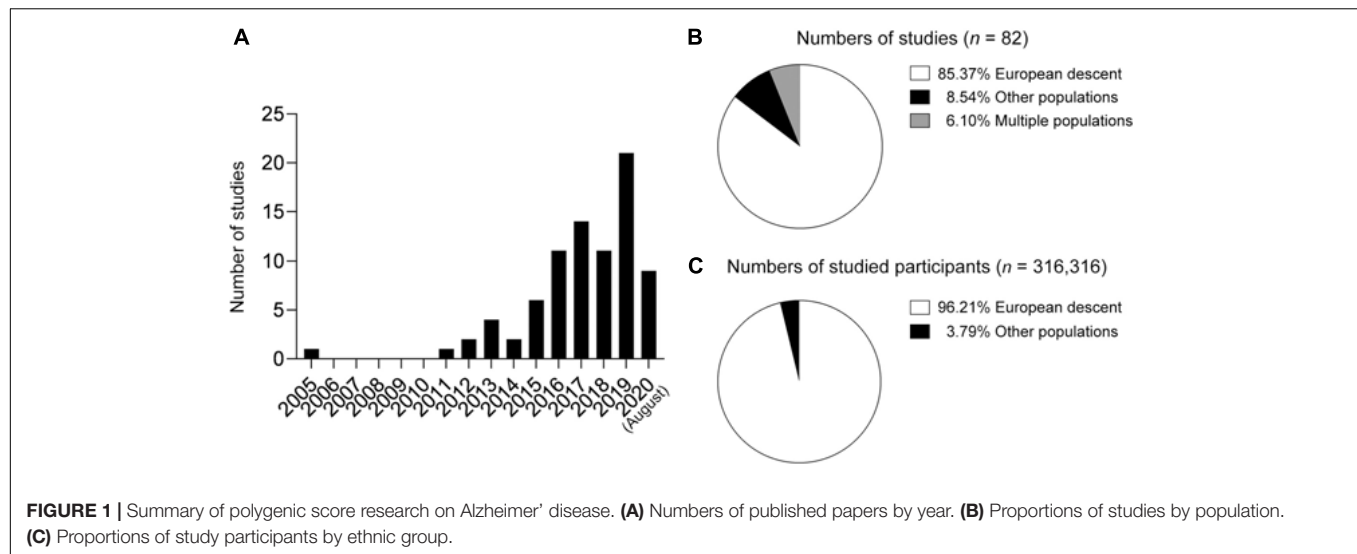
models to predict various outcomes (e.g., phenotypes, cognitive performance, and onset age). Moreover, they may perform better than PRS and PHS models given their ability to better capture both local and global genomic structures.

OVERVIEW OF POLYGENIC SCORE RESEARCH FOR ALZHEIMER'S DISEASE

The number of published research articles associated with AD polygenic score models has dramatically increased over the last 15 years (**Figure 1A**). In 2005, one study reported an AD polygenic score model constructed from nine cholesterol-related single nucleotide polymorphisms (SNPs) including *APOE*- ϵ 4 that exhibited superior performance for classifying AD compared to *APOE*- ϵ 4 alone [area under the receiver operating characteristic curve (AUC) = 0.74 vs. 0.66 for the polygenic score model and *APOE*- ϵ 4, respectively] (Papassotiropoulos et al., 2005). That study was also the first to demonstrate the applicability of polygenic score models to predict AD risk—even before AD GWASs demonstrated the polygenic nature of AD.

Large-scale AD GWASs in populations of European descent bolstered AD polygenic score research in recent years by providing comprehensive information about the effects of individual variants on AD risk at a genome-wide scale. Those studies' summary statistics, which contain the effect sizes of individual variants, can be directly applied as weighting factors to construct a PRS model. In fact, several AD polygenic risk studies were based on the summary statistics generated by the IGAP Consortium published in 2013 (Lambert et al., 2013) and investigated AD polygenic score models in populations of European descent (Marden et al., 2014, 2016; Escott-Price et al., 2015, 2017a,b, 2019a,b; Habes et al., 2016; Harrison et al., 2016; Louwersheimer et al., 2016; Lupton et al., 2016; Mormino et al., 2016; Walter et al., 2016; Darst et al., 2017; Desikan et al., 2017; Foley et al., 2017; Gibson et al., 2017; Hayes et al., 2017, 2020; Marioni et al., 2017; Morgan et al., 2017; Tan et al., 2017, 2019; Xiao et al., 2017; Axelrud et al., 2018, 2019; Cruchaga et al., 2018; Del-Aguila et al., 2018; Ge et al., 2018; Kauppi et al., 2018, 2020; Patel et al., 2018; Stephan et al., 2018; Tasaki et al., 2018; Andrews et al., 2019; Chaudhury et al., 2019; Elman et al., 2019; Guerreiro et al., 2019; Korologou-Linden et al., 2019a,b; Kremen et al., 2019; Lancaster et al., 2019; Leonenko et al., 2019a,b; Logue et al., 2019; Wang et al., 2019; Yu et al., 2019; Ajnakina et al., 2020; Han et al., 2020; Matloff et al., 2020; Reus et al., 2020; Yesavage et al., 2020). Meanwhile, a few other studies focusing on populations of non-European descent also applied the IGAP data to select variants for genotyping analysis (Marden et al., 2014; Tosto et al., 2017; Axelrud et al., 2018, 2019; Li et al., 2020). Notably, the study populations of most AD polygenic risk studies (**Figure 1B**) and studied individuals (**Figure 1C**) were of European descent.

The availability of GWAS results from AD genetics studies has enabled the selection of variants for model construction. Studies using the same IGAP summary statistics can generate models with different numbers of variants (from 6 to 1.1 million sites) by selecting different *p*-value thresholds (Ajnakina et al., 2020;



Han et al., 2020; Reus et al., 2020). Meanwhile, the sample sizes used for polygenic score models also vary among studies: from less than 80 to more than 20,000 participants (Desikan et al., 2017; Chandler et al., 2019). Regarding model construction, PLINK and PRSice are the most widely used tools to select variants and construct polygenic score models. Other statistical analysis methods, such as linear support vector machine (Filipovych et al., 2012), lasso regression (Romero-Rosales et al., 2020; Zhou et al., 2020), multilocus genotype patterns analysis (Barral et al., 2012), and decision tree (Yokoyama et al., 2015; Porter et al., 2018c), have also been adopted to construct polygenic score models for AD.

Of note, polygenic score models have been implemented to investigate the effects of genetic variants on various aspects of AD pathogenesis and progression. Most studies focus on clinical outcomes, specifically the classification of patients with AD (Papassotiropoulos et al., 2005; Sabuncu et al., 2012; Marden et al., 2014; Adams et al., 2015; Escott-Price et al., 2015, 2017b, 2019b; Yokoyama et al., 2015; Lupton et al., 2016; Tosto et al., 2017; Xiao et al., 2017; Cruchaga et al., 2018; Patel et al., 2018; Chaudhury et al., 2019; Leonenko et al., 2019a,b; Zhang et al., 2019; Altmann et al., 2020; Andrews et al., 2020; Zhou et al., 2020). Some other studies investigated the possible associations between AD polygenic score models and the risk of conversion to AD or mild cognitive impairment (MCI) (Filipovych et al., 2012; Rodríguez-Rodríguez et al., 2013; Verhaaren et al., 2013; Carrasquillo et al., 2015; Desikan et al., 2017; Tosto et al., 2017; Kauppi et al., 2018; Chaudhury et al., 2019; Elman et al., 2019; Ajnakina et al., 2020; Altmann et al., 2020; Andrews et al., 2020), cognitive function (Louwersheimer et al., 2016; Del-Aguila et al., 2018; Ge et al., 2018; Kauppi et al., 2018, 2020; Porter et al., 2018a,c,b; Stephan et al., 2018; Tan et al., 2018, 2019; Tasaki et al., 2018; Korologou-Linden et al., 2019a; Han et al., 2020; Zhou et al., 2020), and memory function (Barral et al., 2012; Verhaaren et al., 2013; Marden et al., 2014, 2016; Adams et al., 2015; Carrasquillo et al., 2015; Mormino et al., 2016; Hayes et al., 2017; Marioni et al., 2017; Axelrud et al., 2018; Ge et al., 2018;

Porter et al., 2018a,b,c; Tan et al., 2018, 2019; Altmann et al., 2020). Notably, given that the brain's structure and functions are closely associated with cognitive ability, several studies have also investigated the use of polygenic score models to predict brain status including changes in brain structure (Sabuncu et al., 2012; Habes et al., 2016; Harrison et al., 2016; Nho et al., 2016; Desikan et al., 2017; Foley et al., 2017; Hayes et al., 2017, 2020; Xiao et al., 2017; Ge et al., 2018; Kauppi et al., 2018; Li et al., 2018; Tasaki et al., 2018; Chandler et al., 2019, 2020; Tan et al., 2019; Wang et al., 2019; Altmann et al., 2020; Matloff et al., 2020; Zhou et al., 2020) and function (Xiao et al., 2017; Axelrud et al., 2019; Chandler et al., 2019, 2020). Moreover, some studies investigated biochemical changes indicative of brain status, such as AD pathological hallmarks including amyloid-beta (A β) load and tau tangles (Mormino et al., 2016; Darst et al., 2017; Desikan et al., 2017; Laiterä et al., 2017; Ge et al., 2018; Porter et al., 2018a,b,c; Tan et al., 2018, 2019; Tasaki et al., 2018; Leonenko et al., 2019a; Yu et al., 2019; Altmann et al., 2020), enzyme activity in brain samples (Martiskainen et al., 2015; Laiterä et al., 2017), and levels of proteins (e.g., the "ATN" biomarker panel, which comprises A β , tau, and neurofilament light polypeptide) or metabolites (Papassotiropoulos et al., 2005; Sabuncu et al., 2012; Martiskainen et al., 2015; Louwersheimer et al., 2016; Mormino et al., 2016; Darst et al., 2017; Morgan et al., 2017; Cruchaga et al., 2018; Porter et al., 2018a; Tasaki et al., 2018; Korologou-Linden et al., 2019b; Tan et al., 2019; Altmann et al., 2020; Hayes et al., 2020; Li et al., 2020; Reus et al., 2020; Zhou et al., 2020). Some studies also used polygenic score models to evaluate the extent to which certain diseases or pathways modulate AD risk (Papassotiropoulos et al., 2005; Moskvina et al., 2013; Mukherjee et al., 2015; Walter et al., 2016; Gibson et al., 2017; Hayes et al., 2017; Demichele-Sweet et al., 2018; Creese et al., 2019; Elman et al., 2019; Guerreiro et al., 2019; Kremen et al., 2019; Lancaster et al., 2019; Andrews et al., 2020; Yesavage et al., 2020). Collectively, those studies suggest that genetic factors have crucial roles in modifying AD risk and highlight the potential utility of polygenic score models in AD research and routine clinical

practice. In the following section, we summarize the key findings of each of those aspects.

POLYGENIC SCORE MODELS FOR PREDICTING ALZHEIMER'S DISEASE RISK

The primary goal of a polygenic score model is to classify individuals according to disease risk (AD in this case). Numerous studies conducted in recent decades have established various polygenic score models and report their ability to adequately distinguish patients with AD from cognitively normal individuals. Reported AD prediction accuracy ranges from an AUC of 0.57 (Tosto et al., 2017) to 0.84 (Escott-Price et al., 2017a). Notably, Yokoyama et al. (2015) generated a PRS using a decision tree model and report an AUC of 0.88 for the prediction of AD (vs. 0.69 for *APOE* genotype) in their discovery cohort ($n = 192$). However, this model failed to surpass the accuracy of using *APOE* genotype to predict AD in their replication cohort (AUC = 0.62 vs. 0.63 for the PRS and *APOE* genotype, respectively; $n = 276$). In contrast, several other studies demonstrate that PRS models exhibit superior performance to *APOE* genotype for predicting AD or associated cognitive states as indicated by significant associations between AD and PRSs that do not include *APOE* genotype (Sabuncu et al., 2012; Xiao et al., 2015; Leonenko et al., 2019a,b; Zhang et al., 2019) or PRS results after controlling for *APOE* genotype (Tosto et al., 2017; Escott-Price et al., 2019b). Specifically, in one study recently published by Escott-Price et al. (2019b), the application of a PRS to homozygous *APOE*- $\epsilon 3$ carriers achieved an AUC of 0.831 for the prediction of AD with a comparable AUC of 0.834 after excluding the variants in the *APOE* region in homozygous *APOE*- $\epsilon 3$ carriers. Thus, polygenic effects might account for the non-*APOE*-dependent genetic mechanisms of AD pathogenesis. Meanwhile, a whole-exome sequencing study conducted by Patel et al. (2018) revealed the applicability of polygenic score models using exonic variants to predict AD, yielding an AUC of 0.830 for AD prediction with the inclusion of *APOE* genotype, age, sex, and 19 GWAS-identified SNPs, further implying the polygenic contribution of the exonic regions to the modulation of AD risk.

In addition to disease risk, a few studies investigated the possible contribution of polygenic risk to the modulation of the likelihood of AD conversion, specifically conversion from MCI to AD (Rodríguez-Rodríguez et al., 2013; Tan et al., 2017; Kauppi et al., 2018; Chaudhury et al., 2019) or conversion from cognitive normality to MCI or AD (Carrasquillo et al., 2015; Tan et al., 2017; Logue et al., 2019; Altmann et al., 2020), or the time to develop AD (Verhaaren et al., 2013; Desikan et al., 2017; Tosto et al., 2017; Ajnakina et al., 2020; Andrews et al., 2020). Of note, Tan et al. (2017) studied 1,081 asymptomatic elderly adults and report a PHS model based on 31 SNPs selected from IGAP and ADGC phase 1 data that can accurately predict the risk of conversion from cognitive normality to AD (hazard ratio = 2.36), from MCI to AD (hazard ratio = 1.17), and from cognitive normality or MCI to AD (hazard ratio = 1.31). Furthermore, Kauppi et al. (2018) integrated the PHS with cognitive score and brain atrophy status,

resulting in relatively high accuracy for predicting conversion from MCI to AD (AUC = 0.84).

Notably, Carrasquillo et al. (2015) suggest that only *APOE*-inclusive PRSs are correlated with the likelihood of developing MCI or AD in a longitudinally assessed cohort. Moreover, Rodríguez-Rodríguez et al. (2013) also report that conversion from MCI to AD cannot be successfully predicted by PRSs after controlling for age, sex, and *APOE* genotype. However, the models in both studies included fewer than 10 non-*APOE* variants. Meanwhile, by integrating more variants into the analysis, Altmann et al. (2020) observed significant associations between AD polygenic risk and clinical conversion from non-demented to demented status as well as Clinical Dementia Rating Scale Sum of Boxes (CDR-SB) score after excluding the effect of the *APOE* locus. Therefore, the polygenic risk effects from non-*APOE* loci probably contribute to the likelihood of AD development and progression.

POLYGENIC SCORE MODELS FOR PREDICTING MEMORY AND COGNITIVE FUNCTIONS

Besides disease states, polygenic risk is also correlated with individual memory function (Barral et al., 2012; Verhaaren et al., 2013; Marden et al., 2014, 2016; Adams et al., 2015; Carrasquillo et al., 2015; Mormino et al., 2016; Hayes et al., 2017; Marioni et al., 2017; Axelrud et al., 2018; Ge et al., 2018; Porter et al., 2018a,b,c; Tan et al., 2018, 2019; Altmann et al., 2020). Specifically, a multilocus mapping analysis conducted by Barral et al. (2012) demonstrates an association between episodic memory and specific genetic patterns from GWAS-identified variants; a few other studies also suggest possible associations between polygenic risk and episodic memory function. Specifically, a PRS study conducted by Marden et al. (2014) suggests that AD polygenic risk might modulate both baseline memory and its rate of decline in people of non-Hispanic European descent ($n = 7,172$) or African descent ($n = 1,081$). Again, there is some controversy about the effects of non-*APOE* polygenic risks on memory function. For instance, Carrasquillo et al. (2015) suggests that only *APOE*-inclusive PRSs are correlated with worsening memory function, while Verhaaren et al. (2013) and Porter et al. (2018b) report a significant association between non-*APOE* polygenic risk and memory function. Moreover, Ge et al. (2018) report a significant correlation between high AD polygenic risk and the rate of memory decline after controlling for *APOE*- $\epsilon 4$ genotype. Hence, the polygenic risk effects from non-*APOE* loci likely also influence memory function.

Polygenic scores can also indicate individual cognitive functions. Several studies report associations between polygenic risk and cognitive functions (Louwersheimer et al., 2016; Del-Aguila et al., 2018; Ge et al., 2018; Kauppi et al., 2018, 2020; Porter et al., 2018a,b,c; Stephan et al., 2018; Tan et al., 2018, 2019; Tasaki et al., 2018; Korologou-Linden et al., 2019a; Han et al., 2020; Zhou et al., 2020). For instance, Korologou-Linden et al. (2019a) report an association between PRS and lower total, verbal, and performance intelligence quotients in childhood

and adolescence, and Kauppi et al. (2020) suggest that AD polygenic risk is indicative of individual differences in the rate of cognitive decline in normal aging. Meanwhile, Xiao et al. (2017) and Li et al. (2018) did not identify a significant association between AD polygenic risk and cognitive function in cognitively normal individuals.

POLYGENIC SCORE MODELS FOR PREDICTING BRAIN STATUS

The associations of polygenic scores with memory and cognitive function imply possible alterations of brain structure and functions. Several studies have examined the associations between AD polygenic risk and MRI findings (Sabuncu et al., 2012; Habes et al., 2016; Harrison et al., 2016; Mormino et al., 2016; Nho et al., 2016; Desikan et al., 2017; Foley et al., 2017; Hayes et al., 2017, 2020; Xiao et al., 2017; Ge et al., 2018; Kauppi et al., 2018; Li et al., 2018; Chandler et al., 2019; Tan et al., 2019; Wang et al., 2019; Altmann et al., 2020; Matloff et al., 2020; Zhou et al., 2020), fMRI findings (Xiao et al., 2017; Axelrud et al., 2019; Chandler et al., 2020), and PET imaging findings (Mormino et al., 2016; Darst et al., 2017; Ge et al., 2018; Porter et al., 2018a,b,c; Tan et al., 2018, 2019; Leonenko et al., 2019a; Altmann et al., 2020).

Notably, some studies have examined the associations between AD polygenic risk and the volumetric changes of various brain regions such as the retrosplenial and posterior cingulate cortices (Sabuncu et al., 2012), frontal cortex (Chandler et al., 2019), entorhinal cortex (Harrison et al., 2016; Desikan et al., 2017; Hayes et al., 2020), amygdala (Lupton et al., 2016; Zhou et al., 2020), and hippocampus (Harrison et al., 2016; Lupton et al., 2016; Desikan et al., 2017; Foley et al., 2017; Xiao et al., 2017; Axelrud et al., 2018; Ge et al., 2018; Lancaster et al., 2019; Altmann et al., 2020; Hayes et al., 2020; Matloff et al., 2020; Zhou et al., 2020).

Interestingly, some studies have focused on individuals of varying ages including young adolescents (Li et al., 2018; Chandler et al., 2019) and elderly people (Lupton et al., 2016; Nho et al., 2016; Darst et al., 2017; Desikan et al., 2017; Tan et al., 2019; Hayes et al., 2020). Specifically, Li et al. (2018) and Chandler et al. (2019) report significant associations of AD polygenic risk with gray matter cerebral blood flow and gray matter volume, respectively, in young individuals, indicating a potential long-term effect of polygenic risk on brain function well before AD onset.

In addition to structural changes, AD polygenic risk might be associated with brain A β load (Mormino et al., 2016; Darst et al., 2017; Porter et al., 2018a,c; Tan et al., 2018, 2019; Leonenko et al., 2019a; Altmann et al., 2020) as measured by PET imaging. Moreover, several studies discuss the possible effects of polygenic risk on brain functional changes including hippocampal activation (Xiao et al., 2017; Chandler et al., 2020) and connectivity between specific brain regions (Axelrud et al., 2019), providing additional evidence for the effects of AD polygenic risk on brain function. Meanwhile, A β measured by PET imaging has been introduced to stratify AD patients prior to PRS evaluation (Porter et al., 2018b).

POLYGENIC SCORE MODELS FOR PREDICTING BIOCHEMICAL CHANGES IN THE BRAIN AND PERIPHERAL SYSTEM

Corroborating PET imaging findings, AD polygenic risk is also associated with the levels of several hallmark proteins of AD in postmortem brain tissues. For instance, AD PRSs are reported to be significantly correlated with A β and tau tangle levels (Tasaki et al., 2018), although some studies did not identify such a correlation between AD polygenic risk and A β levels (Laiterä et al., 2017; Yu et al., 2019). Notably, AD polygenic risk might be correlated with the activity of brain γ -secretase (but not β -secretase) (Martiskainen et al., 2015; Laiterä et al., 2017) as well as levels of VGF, IGFBP5, and STX1A in brain tissues as measured by proteomic analysis (Tasaki et al., 2018).

As the ATN biomarkers in cerebrospinal fluid (CSF) are correlated with the brain pathology in AD, several studies also suggest possible correlations between PRSs and CSF biomarkers including A β (Sabuncu et al., 2012; Martiskainen et al., 2015; Darst et al., 2017; Cruchaga et al., 2018; Hayes et al., 2020; Li et al., 2020) and tau or p-tau (Louwersheimer et al., 2016; Darst et al., 2017; Cruchaga et al., 2018; Porter et al., 2018a; Tan et al., 2018; Altmann et al., 2020; Li et al., 2020; Reus et al., 2020). However, Louwersheimer et al. (2016) and Mormino et al. (2016) did not observe a correlation between AD polygenic risk and CSF A β levels. Meanwhile, Reus et al. (2020) examined the associations between polygenic risk and 412 CSF proteins and protein fragments, and found that 48.8% of the candidate proteins were associated with at least one of the 14 constructed scores, implying a possible global alteration of the CSF proteome that is possibly associated with polygenic risk.

Notably, a recent study also implies the involvement of the peripheral immune system in AD pathogenesis (Zhou et al., 2018), while other studies demonstrate associations between AD polygenic risk and plasma proteins (Morgan et al., 2017; Korologou-Linden et al., 2019b; Zhou et al., 2020) or metabolites (Papassotiropoulos et al., 2005; Korologou-Linden et al., 2019b). Specifically, by applying the proximity extension assay to plasma proteomic analysis, we investigated 280 proteins and revealed potential protein candidates (i.e., osteopontin and neurocan core protein) along with a protein network associated with AD polygenic risk—again implying global changes in plasma profiles that might be modulated by polygenic risk (Zhou et al., 2020).

POLYGENIC SCORE MODELS FOR EXAMINING THE INVOLVEMENT OF OTHER DISEASES IN ALZHEIMER'S DISEASE PATHOGENESIS

The complex etiology of AD is reflected by the identification of various modifiable risk factors such as cardiovascular risk factors, hypertension, and immune factors. Polygenic

score models suggest that AD genetic risks are associated with cholesterol levels (Papassotiropoulos et al., 2005), depression (Gibson et al., 2017), schizophrenia (Demichele-Sweet et al., 2018; Creese et al., 2019), frontotemporal lobar degeneration, amyotrophic lateral sclerosis (Adams et al., 2015), insulin sensitivity (Walter et al., 2016), microglial dysfunction (Lancaster et al., 2019), and mitochondrial dysfunction (Andrews et al., 2020). Meanwhile, the polygenic risks for cardiovascular risk factors, frontotemporal lobar degeneration, and amyotrophic lateral sclerosis are implicated in the pathogenesis of MCI (Adams et al., 2015; Elman et al., 2019). Thus, these findings collectively suggest the underlying mechanisms of AD comorbidities and indicate possible pathways for intervention.

APPLICATIONS AND POTENTIAL ISSUES

Given the high prevalence of AD, early risk prediction might facilitate early intervention and greatly mitigate the future growth of the AD patient population. Specifically, polygenic risk factors rooted in individual genomes can be used as biomarkers for the early assessment of relative risk at a population scale. To illustrate the utility of such a strategy, delaying disease onset by 5 years would reduce the predicted AD population among people aged 70 years or above by 41% in the United States. in 2050 (Zissimopoulos et al., 2015). Furthermore, inspiring work by Solomon et al. (2018) further suggests that lifestyle interventions might override the risk effects of *APOE-ε4*, implying a possible means of delaying AD onset once an individual is informed of their relative risk of developing AD. Moreover, a recent study revealed that prior knowledge of genetic risk would also be critical for drug discovery, as drugs targeting proteins encoded in genetic risk loci would be more likely to be successful in phase II and III clinical trials (King et al., 2019). Notably, a polygenic score study of coronary heart disease risk showed that compared to people with lower genetic risk, those with higher genetic risk exhibited a greater decrease in absolute disease risk after receiving statin therapy (Mega et al., 2015). Therefore, conducting population-scale genetic screening for AD might simultaneously support the development of intervention strategies and enable the stratification of individuals according to their risk of AD based on their genetic patterns. More specifically, a hierarchal screening strategy for AD risk evaluation combining genetic, circulatory factors, and brain imaging techniques can be implemented at a populational scale to facilitate disease risk screening and clinical research on personalized interventions in a genotype-aware manner (Figure 2).

Nevertheless, there are potential issues that could hinder the development and implementation of polygenic scoring in routine clinical practice. First, policies protecting patient privacy must be carefully considered, because the results of one person's genetic test might not only indicate their own risks of certain diseases but also those of their close relatives (Clayton et al., 2019). Second, the possible consequences of informing certain individuals about their estimated genetic

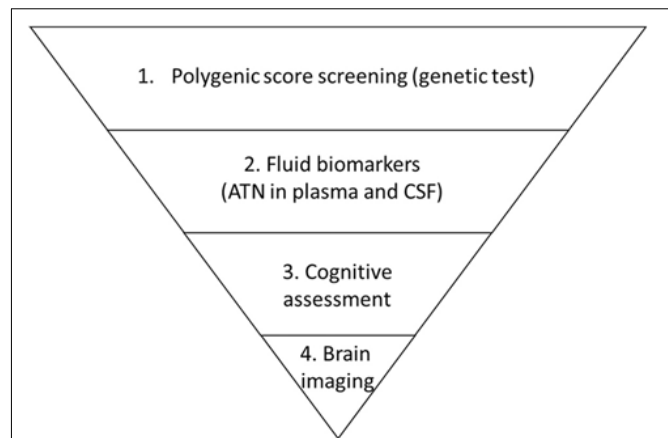


FIGURE 2 | Proposed hierarchal strategy for Alzheimer's disease risk screening. Individuals enrolled in a screening task are first examined according to genetic risk as indicated by polygenic risk analysis. Individuals who have relatively high risk and report symptoms are referred for biomarker examination to evaluate amyloid-beta, tau (and p-tau), and neurofilament light polypeptide levels (i.e., the "ATN" panel) in blood or cerebrospinal fluid (CSF). Those who exhibit altered levels of biomarkers are further referred to clinicians for cognitive assessment followed by brain imaging including magnetic resonance imaging and positron emission tomography.

risks for certain diseases must be carefully considered, as this could have positive and/or negative outcomes. Fortunately, after receiving brain amyloid imaging, cognitively normal people with elevated amyloid loads tend to make more changes to their lifestyle and future plans than those who do not have elevated amyloid loads (Largent et al., 2020). In addition, in one recent study, providing genetic test results illustrating the 3-year risk of developing AD to patients with MCI did not increase the risk of anxiety or depression (Christensen et al., 2020). Meanwhile, different diagnostic criteria across study cohorts might introduce bias into genetics studies and the subsequent construction of polygenic score models, although this can be reduced or eliminated by further incorporating other biomarkers to refine clinical diagnosis (Escott-Price et al., 2017a). Furthermore, the application of polygenic score models can help refine the results of genetic analyses based on control cohorts (i.e., controls in whom the disease of interest has not been investigated in detail) by ruling out individuals at risk of developing diseases (Escott-Price et al., 2019a). Moreover, polygenic score models may be used to define an individual's risk of having a specific neurodegenerative disease, as studies have demonstrated that such models (or the genotyping of specific variants) can predict the risk of Parkinson's disease (Nalls et al., 2016), Huntington's disease (Kremer et al., 1994), amyotrophic lateral sclerosis (Saez-Atienzar et al., 2021), and multiple sclerosis (The International Multiple Sclerosis Genetics Consortium (IMSGC), 2010). In addition, polygenic score models may help estimate the effects of aging on disease risk. Finally, conducting polygenic risk analysis requires the availability of population-specific genetic risk information at the single-variant level. We previously showed that a polygenic score model based on the Chinese population

performs poorly when applied to an AD cohort of European descent (Zhou et al., 2020). The poor performance of that polygenic score model can be explained by the differences in the genomic structures between populations of East-Asian and European descent. Given that there are limited AD GWASs on populations of non-European descent (Zhou et al., 2018; Kunkle et al., 2020), it is critical to comprehensively analyze AD genetic risk in such populations to facilitate the development of polygenic score models and their associated applications in populations worldwide.

AUTHOR CONTRIBUTIONS

XZ, AF, and NI outlined and wrote the review. XZ and YL conducted the literature review and data organization. All authors contributed to the article and approved the submitted version.

REFERENCES

- Adams, H. H. H., De Bruijn, R. F. A. G., Hofman, A., Uitterlinden, A. G., Van Duijn, C. M., Vernooij, M. W., et al. (2015). Genetic risk of neurodegenerative diseases is associated with mild cognitive impairment and conversion to dementia. *Alzheimer's Dement.* 11, 1277–1285. doi: 10.1016/j.jalz.2014.12.008
- Ajnakina, O., Cadar, D., and Steptoe, A. (2020). Interplay between socioeconomic markers and polygenic predisposition on timing of dementia diagnosis. *J. Am. Geriatr. Soc.* 68, 1529–1536. doi: 10.1111/jgs.16406
- Altmann, A., Scelsi, M. A., Shuai, M., de Silva, E., Aksman, L. M., Cash, D. M., et al. (2020). A comprehensive analysis of methods for assessing polygenic burden on Alzheimer's disease pathology and risk beyond APOE. *Brain Commun.* 2:fcz047. doi: 10.1093/braincomms/fcz047
- Andrews, S. J., Fulton-Howard, B., Patterson, C., McFall, G. P., Gross, A., Michaelis, E. K., et al. (2020). Mitonuclear interactions influence Alzheimer's disease risk. *Neurobiol. Aging* 87, 138.e7–138.e14. doi: 10.1016/j.neurobiolaging.2019.09.007
- Andrews, S. J., McFall, G. P., Booth, A., Dixon, R. A., and Anstey, K. J. (2019). Association of Alzheimer's disease genetic risk loci with cognitive performance and decline: a systematic review. *J. Alzheimer's Dis.* 69, 1109–1136. doi: 10.3233/JAD-190342
- Axelrud, L. K., Santoro, M. L., Pine, D. S., Talarico, F., Gadelha, A., Manfro, G. G., et al. (2018). Polygenic risk score for Alzheimer's disease: Implications for memory performance and hippocampal volumes in early life. *Am. J. Psychiatry* 175, 555–563. doi: 10.1176/appi.ajp.2017.17050529
- Axelrud, L. K., Sato, J. R., Santoro, M. L., Talarico, F., Pine, D. S., Rohde, L. A., et al. (2019). Genetic risk for Alzheimer's disease and functional brain connectivity in children and adolescents. *Neurobiol. Aging* 82, 10–17. doi: 10.1016/j.neurobiolaging.2019.06.011
- Barral, S., Bird, T., Goate, A., Farlow, M. R., Diaz-Arrastia, R., Bennett, D. A., et al. (2012). Genotype patterns at PICALM, CR1, BIN1, CLU, and APOE genes are associated with episodic memory. *Neurology* 78, 1464–1471. doi: 10.1212/WNL.0b013e3182553c48
- Carrasquillo, M. M., Crook, J. E., Pedraza, O., Thomas, C. S., Pankratz, V. S., Allen, M., et al. (2015). Late-onset Alzheimer's risk variants in memory decline, incident mild cognitive impairment, and Alzheimer's disease. *Neurobiol. Aging* 36, 60–67. doi: 10.1016/j.neurobiolaging.2014.07.042
- Chandler, H. L., Hodgetts, C. J., Caseras, X., Murphy, K., and Lancaster, T. M. (2020). Polygenic risk for Alzheimer's disease shapes hippocampal scene-selectivity. *Neuropsychopharmacology* 45, 1171–1178. doi: 10.1038/s41386-019-0595-1
- Chandler, H. L., Wise, R. G., Murphy, K., Tansey, K. E., Linden, D. E. J., and Lancaster, T. M. (2019). Polygenic impact of common genetic risk loci for

FUNDING

This work was supported in part by the Research Grants Council of Hong Kong [the Theme-Based Research Scheme (T13-607/12R) and the Collaborative Research Fund (C6027-19GF)], the National Key R&D Program of China (2017YFE0190000 and 2018YFE0203600), the Areas of Excellence Scheme of the University Grants Committee (AoE/M-604/16), the Innovation and Technology Commission (ITCPD/17-9), the Guangdong Provincial Key S&T Program (2018B030336001), and the Shenzhen Knowledge Innovation Program (JCYJ20180507183642005 and JCYJ20170413173717055).

ACKNOWLEDGMENTS

We would like to thank Kin Y. Mok for constructive suggestions on the manuscript.

- Alzheimer's disease on cerebral blood flow in young individuals. *Sci. Rep.* 9:467. doi: 10.1038/s41598-018-36820-3
- Chatterjee, N., Shi, J., and García-Closas, M. (2016). Developing and evaluating polygenic risk prediction models for stratified disease prevention. *Nat. Rev. Genet.* 17, 392–406. doi: 10.1038/nrg.2016.27
- Chaudhury, S., Brookes, K. J., Patel, T., Fallows, A., Guetta-Baranes, T., Turton, J. C., et al. (2019). Alzheimer's disease polygenic risk score as a predictor of conversion from mild-cognitive impairment. *Transl. Psychiatry* 9:154. doi: 10.1038/s41398-019-0485-7
- Christensen, K. D., Karlawish, J., Roberts, J. S., Uhlmann, W. R., Harkins, K., Wood, E. M., et al. (2020). Disclosing genetic risk for Alzheimer's dementia to individuals with mild cognitive impairment. *Alzheimer's Dement. Transl. Res. Clin. Interv.* 6:e12002. doi: 10.1002/trc2.12002
- Clayton, E. W., Evans, B. J., Hazel, J. W., and Rothstein, M. A. (2019). The law of genetic privacy: applications, implications, and limitations. *J. Law Biosci.* 6, 1–36. doi: 10.1093/jlb/lz007
- Creese, B., Vassos, E., Bergh, S., Athanasiu, L., Johar, I., Rongve, A., et al. (2019). Examining the association between genetic liability for schizophrenia and psychotic symptoms in Alzheimer's disease. *Transl. Psychiatry* 9:273. doi: 10.1038/s41398-019-0592-5
- Cruchaga, C., Del-Aguila, J. L., Saef, B., Black, K., Fernandez, M. V., Budde, J., et al. (2018). Polygenic risk score of sporadic late-onset Alzheimer's disease reveals a shared architecture with the familial and early-onset forms. *Alzheimer's Dement.* 14, 205–214. doi: 10.1016/j.jalz.2017.08.013
- Darst, B. F., Kosciak, R. L., Racine, A. M., Oh, J. M., Krause, R. A., Carlsson, C. M., et al. (2017). Pathway-specific polygenic risk scores as predictors of amyloid- β deposition and cognitive function in a sample at increased risk for Alzheimer's disease. *J. Alzheimer's Dis.* 55, 473–484. doi: 10.3233/JAD-160195
- Del-Aguila, J. L., Fernández, M. V., Schindler, S., Ibanez, L., Deming, Y., Ma, S., et al. (2018). Assessment of the genetic architecture of Alzheimer's disease risk in rate of memory decline. *J. Alzheimer's Dis.* 62, 745–756. doi: 10.3233/JAD-170834
- Demichele-Sweet, M. A. A., Weamer, E. A., Klei, L., Vrana, D. T., Hollingshead, D. J., Seltman, H. J., et al. (2018). Genetic risk for schizophrenia and psychosis in Alzheimer disease. *Mol. Psychiatry* 23, 963–972. doi: 10.1038/mp.2017.81
- Desikan, R. S., Fan, C. C., Wang, Y., Schork, A. J., Cabral, H. J., Cupples, L. A., et al. (2017). Genetic assessment of age-associated Alzheimer disease risk: development and validation of a polygenic hazard score. *PLoS Med.* 14:e1002258. doi: 10.1371/journal.pmed.1002258
- Elman, J. A., Panizzon, M. S., Logue, M. W., Gillespie, N. A., Neale, M. C., Reynolds, C. A., et al. (2019). Genetic risk for coronary heart disease alters the influence of Alzheimer's genetic risk on mild cognitive impairment. *Neurobiol. Aging* 84, 237.e5–237.e12. doi: 10.1016/j.neurobiolaging.2019.06.001

- Escott-Price, V., Baker, E., Shoaib, M., Leonenko, G., Myers, A. J., Huentelman, M., et al. (2019a). Genetic analysis suggests high misassignment rates in clinical Alzheimer's cases and controls. *Neurobiol. Aging* 77, 178–182. doi: 10.1016/j.neurobiolaging.2018.12.002
- Escott-Price, V., Myers, A. J., Huentelman, M., and Hardy, J. (2017a). Polygenic risk score analysis of pathologically confirmed Alzheimer disease. *Ann. Neurol.* 82, 311–314. doi: 10.1002/ana.24999
- Escott-Price, V., Myers, A., Huentelman, M., Shoaib, M., and Hardy, J. (2019b). Polygenic risk score analysis of Alzheimer's disease in cases without APOE4 or APOE2 alleles. *J. Prev. Alzheimer's Dis.* 6, 16–19. doi: 10.14283/jpad.2018.46
- Escott-Price, V., Shoaib, M., Pither, R., Williams, J., and Hardy, J. (2017b). Polygenic score prediction captures nearly all common genetic risk for Alzheimer's disease. *Neurobiol. Aging* 49:214.e7. doi: 10.1016/j.neurobiolaging.2016.07.018
- Escott-Price, V., Sims, R., Bannister, C., Harold, D., Vronskaya, M., Majounie, E., et al. (2015). Common polygenic variation enhances risk prediction for Alzheimer's disease. *Brain* 138, 3673–3684. doi: 10.1093/brain/awv268
- Filipovich, R., Gaonkar, B., and Davatzikos, C. (2012). "A composite multivariate polygenic and neuroimaging score for prediction of conversion to Alzheimer's disease," in *Proceedings of the 2012 2nd International Workshop on Pattern Recognition in NeuroImaging, PRNI 2012* (London), 105–108. doi: 10.1109/PRNI.2012.9
- Foley, S. F., Tansey, K. E., Caseras, X., Lancaster, T., Bracht, T., Parker, G., et al. (2017). Multimodal brain imaging reveals structural differences in Alzheimer's disease polygenic risk carriers: a study in healthy young adults. *Biol. Psychiatry* 81, 154–161. doi: 10.1016/j.biopsych.2016.02.033
- Gatz, M., Reynolds, C. A., Fratiglioni, L., Johansson, B., Mortimer, J. A., Berg, S., et al. (2006). Role of genes and environments for explaining Alzheimer disease. *Arch. Gen. Psychiatry* 63, 168–174. doi: 10.1001/archpsyc.63.2.168
- Ge, T., Sabuncu, M. R., Smoller, J. W., Sperling, R. A., and Mormino, E. C. (2018). Dissociable influences of APOE ϵ 4 and polygenic risk of AD dementia on amyloid and cognition. *Neurology* 90, E1605–E1612. doi: 10.1212/WNL.0000000000005415
- Gibson, J., Russ, T. C., Adams, M. J., Clarke, T. K., Howard, D. M., Hall, L. S., et al. (2017). Assessing the presence of shared genetic architecture between Alzheimer's disease and major depressive disorder using genome-wide association data. *Transl. Psychiatry* 7, e1094–e1098. doi: 10.1038/tp.2017.49
- Guerreiro, R., Escott-Price, V., Hernandez, D. G., Kun-Rodrigues, C., Ross, O. A., Orme, T., et al. (2019). Heritability and genetic variance of dementia with Lewy bodies. *Neurobiol. Dis.* 127, 492–501. doi: 10.1016/j.nbd.2019.04.004
- Habes, M., Janowitz, D., Erus, G., Toledo, J. B., Resnick, S. M., Doshi, J., et al. (2016). Advanced brain aging: relationship with epidemiologic and genetic risk factors, and overlap with Alzheimer disease atrophy patterns. *Transl. Psychiatry* 6:e775. doi: 10.1038/tp.2016.39
- Han, S. H., Roberts, J. S., Mutchler, J. E., and Burr, J. A. (2020). Volunteering, polygenic risk for Alzheimer's disease, and cognitive functioning among older adults. *Soc. Sci. Med.* 253:112970. doi: 10.1016/j.socscimed.2020.112970
- Harrison, T. M., Mahmood, Z., Lau, E. P., Karacozoff, A. M., Burggren, A. C., Small, G. W., et al. (2016). An Alzheimer's disease genetic risk score predicts longitudinal thinning of hippocampal complex subregions in healthy older adults. *eNeuro* 3, 795–804. doi: 10.1523/ENEURO.0098-16.2016
- Hayes, J. P., Logue, M. W., Sadeh, N., Spielberg, J. M., Verfaellie, M., Hayes, S. M., et al. (2017). Mild traumatic brain injury is associated with reduced cortical thickness in those at risk for Alzheimer's disease. *Brain* 140, 813–825. doi: 10.1093/brain/aww344
- Hayes, J. P., Moody, J. N., Roca, J. G., and Hayes, S. M. (2020). Body mass index is associated with smaller medial temporal lobe volume in those at risk for Alzheimer's disease. *NeuroImage Clin.* 25:102156. doi: 10.1016/j.nicl.2019.102156
- Jansen, I. E., Savage, J. E., Watanabe, K., Bryois, J., Williams, D. M., Steinberg, S., et al. (2019). Genome-wide meta-analysis identifies new loci and functional pathways influencing Alzheimer's disease risk. *Nat. Genet.* 51, 404–413. doi: 10.1038/s41588-018-0311-9
- Kauppi, K., Fan, C. C., McEvoy, L. K., Holland, D., Tan, C. H., Chen, C. H., et al. (2018). Combining polygenic hazard score with volumetric MRI and cognitive measures improves prediction of progression from mild cognitive impairment to Alzheimer's disease. *Front. Neurosci.* 12:260. doi: 10.3389/fnins.2018.00260
- Kauppi, K., Rönnlund, M., Nordin Adolfsson, A., Pudas, S., and Adolfsson, R. (2020). Effects of polygenic risk for Alzheimer's disease on rate of cognitive decline in normal aging. *Transl. Psychiatry* 10:250. doi: 10.1038/s41398-020-00934-y
- King, E. A., Wade Davis, J., and Degner, J. F. (2019). Are drug targets with genetic support twice as likely to be approved? Revised estimates of the impact of genetic support for drug mechanisms on the probability of drug approval. *PLoS Genet.* 15:e1008489. doi: 10.1371/journal.pgen.1008489
- Korologou-Linden, R., Anderson, E. L., Jones, H. J., Davey Smith, G., Howe, L. D., and Stergiakouli, E. (2019a). Polygenic risk scores for Alzheimer's disease, and academic achievement, cognitive and behavioural measures in children from the general population. *Int. J. Epidemiol.* 48, 1972–1980. doi: 10.1093/ije/dyz080
- Korologou-Linden, R., O'Keeffe, L., Howe, L. D., Davey-Smith, G., Jones, H. J., Anderson, E. L., et al. (2019b). Polygenic risk score for Alzheimer's disease and trajectories of cardiometabolic risk factors in children. *Wellcome Open Res.* 4:125. doi: 10.12688/wellcomeopenres.15359.1
- Kremen, W. S., Panizzon, M. S., Elman, J. A., Granholm, E. L., Andreassen, O. A., Dale, A. M., et al. (2019). Pupillary dilation responses as a midlife indicator of risk for Alzheimer's disease: association with Alzheimer's disease polygenic risk. *Neurobiol. Aging* 83, 114–121. doi: 10.1016/j.neurobiolaging.2019.09.001
- Kremer, B., Goldberg, P., Andrew, S. E., Theilmann, J., Telenius, H., Zeisler, J., et al. (1994). A worldwide study of the Huntington's disease mutation: the sensitivity and specificity of measuring CAG repeats. *N. Engl. J. Med.* 330, 1401–1406. doi: 10.1056/nejm199405193302001
- Kunkle, B. W., Schmidt, M., Klein, H. U., Naj, A. C., Hamilton-Nelson, K. L., Larson, E. B., et al. (2020). Novel Alzheimer disease risk loci and pathways in African American individuals using the African genome resources panel a meta-analysis. *JAMA Neurol.* 78, 102–113. doi: 10.1001/jamaneurol.2020.3536
- Laiterä, T., Paananen, J., Helisalmi, S., Sarajärvi, T., Huovinen, J., Laitinen, M., et al. (2017). Effects of Alzheimer's disease-associated risk loci on amyloid- β accumulation in the brain of idiopathic normal pressure hydrocephalus patients. *J. Alzheimer's Dis.* 55, 995–1003. doi: 10.3233/JAD-160554
- Lambert, J. C., Ibrahim-Verbaas, C. A., Harold, D., Naj, A. C., Sims, R., Bellenguez, C., et al. (2013). Meta-analysis of 74,046 individuals identifies 11 new susceptibility loci for Alzheimer's disease. *Nat. Genet.* 45, 1452–1458. doi: 10.1038/ng.2802
- Lancaster, T. M., Hill, M. J., Sims, R., and Williams, J. (2019). Microglia – mediated immunity partly contributes to the genetic association between Alzheimer's disease and hippocampal volume. *Brain Behav. Immun.* 79, 267–273. doi: 10.1016/j.bbi.2019.02.011
- Largent, E. A., Harkins, K., Van Dyck, C. H., Hachey, S., Sankar, P., and Karlawish, J. (2020). Cognitively unimpaired adults' reactions to disclosure of amyloid PET scan results. *PLoS One* 15:e0229137. doi: 10.1371/journal.pone.0229137
- Leonenko, G., Shoaib, M., Bellou, E., Sims, R., Williams, J., Hardy, J., et al. (2019a). Genetic risk for Alzheimer disease is distinct from genetic risk for amyloid deposition. *Ann. Neurol.* 86, 427–435. doi: 10.1002/ana.25530
- Leonenko, G., Sims, R., Shoaib, M., Frizzati, A., Bossù, P., Spalletta, G., et al. (2019b). Polygenic risk and hazard scores for Alzheimer's disease prediction. *Ann. Clin. Transl. Neurol.* 6, 456–465. doi: 10.1002/acn3.716
- Li, J., Zhang, X., Li, A., Liu, S., Qin, W., Yu, C., et al. (2018). Polygenic risk for Alzheimer's disease influences precuneal volume in two independent general populations. *Neurobiol. Aging* 64, 116–122. doi: 10.1016/j.neurobiolaging.2017.12.022
- Li, W. W., Wang, Z., Fan, D. Y., Shen, Y. Y., Chen, D. W., Li, H. Y., et al. (2020). Association of polygenic risk score with age at onset and cerebrospinal fluid biomarkers of Alzheimer's disease in a Chinese Cohort. *Neurosci. Bull.* 36, 696–704. doi: 10.1007/s12264-020-00469-8
- Logue, M. W., Panizzon, M. S., Elman, J. A., Gillespie, N. A., Hatton, S. N., Gustavson, D. E., et al. (2019). Use of an Alzheimer's disease polygenic risk score to identify mild cognitive impairment in adults in their 50s. *Mol. Psychiatry* 24, 421–430. doi: 10.1038/s41380-018-0030-8
- Louwersheimer, E., Wolfsgruber, S., Espinosa, A., Lacour, A., Heilmann-Heimbach, S., Alegret, M., et al. (2016). Alzheimer's disease risk variants modulate endophenotypes in mild cognitive impairment. *Alzheimer's Dement.* 12, 872–881. doi: 10.1016/j.jalz.2016.01.006
- Lupton, M. K., Strike, L., Hansell, N. K., Wen, W., Mather, K. A., Armstrong, N. J., et al. (2016). The effect of increased genetic risk for Alzheimer's disease on hippocampal and amygdala volume. *Neurobiol. Aging* 40, 68–77. doi: 10.1016/j.neurobiolaging.2015.12.023

- Marden, J. R., Mayeda, E. R., Walter, S., Vivot, A., Tchetgen, E. J. T., Kawachi, I., et al. (2016). Using an Alzheimer disease polygenic risk score to predict memory decline in black and white Americans over 14 years of follow-up. *Alzheimer Dis. Assoc. Disord.* 30, 195–202. doi: 10.1097/WAD.0000000000000137
- Marden, J. R., Walter, S., Tchetgen Tchetgen, E. J., Kawachi, I., and Glymour, M. M. (2014). Validation of a polygenic risk score for dementia in black and white individuals. *Brain Behav.* 4, 687–697. doi: 10.1002/brb3.248
- Marioni, R. E., Campbell, A., Hagenaars, S. P., Nagy, R., Amador, C., Hayward, C., et al. (2017). Genetic stratification to identify risk groups for Alzheimer's disease. *J. Alzheimer's Dis.* 57, 275–283. doi: 10.3233/JAD-161070
- Martiskainen, H., Helisalmi, S., Viswanathan, J., Kurki, M., Hall, A., Herukka, S. K., et al. (2015). Effects of Alzheimer's disease-associated risk loci on cerebrospinal fluid biomarkers and disease progression: a polygenic risk score approach. *J. Alzheimer's Dis.* 43, 565–573. doi: 10.3233/JAD-140777
- Matloff, W. J., Zhao, L., Ning, K., Conti, D. V., and Toga, A. W. (2020). Interaction effect of alcohol consumption and Alzheimer disease polygenic risk score on the brain cortical thickness of cognitively normal subjects. *Alcohol* 85, 1–12. doi: 10.1016/j.alcohol.2019.11.002
- Mega, J. L., Stitzel, N. O., Smith, J. G., Chasman, D. I., Caulfield, M. J., Devlin, J. J., et al. (2015). Genetic risk, coronary heart disease events, and the clinical benefit of statin therapy: an analysis of primary and secondary prevention trials. *Lancet* 385, 2264–2271. doi: 10.1016/S0140-6736(14)61730-X
- Morgan, A. R., Touchard, S., O'Hagan, C., Sims, R., Majounie, E., Escott-Price, V., et al. (2017). The correlation between inflammatory biomarkers and polygenic risk score in Alzheimer's disease. *J. Alzheimer's Dis.* 56, 25–36. doi: 10.3233/JAD-160889
- Mormino, E. C., Sperling, R. A., Holmes, A. J., Buckner, R. L., De Jager, P. L., Smoller, J. W., et al. (2016). Polygenic risk of Alzheimer disease is associated with early- and late-life processes. *Neurology* 87, 481–488. doi: 10.1212/WNL.0000000000002922
- Moskvina, V., Harold, D., Russo, G. C., Vedernikov, A., Sharma, M., Saad, M., et al. (2013). Analysis of genome-wide association studies of Alzheimer disease and of Parkinson disease to determine if these 2 diseases share a common genetic risk. *JAMA Neurol.* 70, 1268–1276. doi: 10.1001/jamaneurol.2013.448
- Mukherjee, S., Walter, S., Kauwe, J. S. K., Saykin, A. J., Bennett, D. A., Larson, E. B., et al. (2015). Genetically predicted body mass index and Alzheimer's disease-related phenotypes in three large samples: Mendelian randomization analyses. *Alzheimer's Dement.* 11, 1439–1451. doi: 10.1016/j.jalz.2015.05.015
- Nalls, M. A., Keller, M. F., Hernandez, D. G., Chen, L., Stone, D. J., and Singleton, A. B. (2016). Baseline genetic associations in the Parkinson's progression markers initiative (PPMI). *Mov. Disord.* 31, 79–85. doi: 10.1002/mds.26374
- Nho, K., Saykin, A. J., and Nelson, P. T. (2016). Hippocampal sclerosis of aging, a common Alzheimer's disease "Mimic": risk genotypes are associated with brain atrophy outside the temporal lobe. *J. Alzheimer's Dis.* 52, 373–383. doi: 10.3233/JAD-160077
- Papassotiropoulos, A., Wollmer, M. A., Tsolaki, M., Brunner, F., Molyva, D., Lütjohann, D., et al. (2005). A cluster of cholesterol-related genes confers susceptibility for Alzheimer's disease. *J. Clin. Psychiatry* 66, 940–947. doi: 10.4088/jcp.v66n0720
- Patel, T., Brookes, K. J., Turton, J., Chaudhury, S., Guetta-Baranes, T., Guerreiro, R., et al. (2018). Whole-exome sequencing of the BDR cohort: evidence to support the role of the PILRA gene in Alzheimer's disease. *Neuropathol. Appl. Neurobiol.* 44, 506–521. doi: 10.1111/nan.12452
- Porter, T., Burnham, S. C., Milicic, L., Savage, G., Maruff, P., Lim, Y. Y., et al. (2018a). Utility of an Alzheimer's disease risk-weighted polygenic risk score for predicting rates of cognitive decline in preclinical Alzheimer's disease: a prospective longitudinal study. *J. Alzheimer's Dis.* 66, 1193–1211. doi: 10.3233/JAD-180713
- Porter, T., Burnham, S. C., Savage, G., Lim, Y. Y., Maruff, P., Milicic, L., et al. (2018b). A polygenic risk score derived from episodic memory weighted genetic variants is associated with cognitive decline in preclinical Alzheimer's disease. *Front. Aging Neurosci.* 10:423. doi: 10.3389/fnagi.2018.00423
- Porter, T., Villemagne, V. L., Savage, G., Milicic, L., Ying Lim, Y., Maruff, P., et al. (2018c). Cognitive gene risk profile for the prediction of cognitive decline in presymptomatic Alzheimer's disease. *Pers. Med. Psychiatry* 7–8, 14–20. doi: 10.1016/j.pmpip.2018.03.001
- Reus, L. M., Stringer, S., Posthuma, D., Teunissen, C. E., Scheltens, P., Pijenburg, Y. A. L., et al. (2020). Degree of genetic liability for Alzheimer's disease associated with specific proteomic profiles in cerebrospinal fluid. *Neurobiol. Aging* 93, 144.e1–144.e15. doi: 10.1016/j.neurobiolaging.2020.03.012
- Rodriguez-Rodriguez, E., Sánchez-Juan, P., Vázquez-Higuera, J. L., Mateo, I., Pozueta, A., Berciano, J., et al. (2013). Genetic risk score predicting accelerated progression from mild cognitive impairment to Alzheimer's disease. *J. Neural Transm.* 120, 807–812. doi: 10.1007/s00702-012-0920-x
- Romero-Rosales, B. L., Tamez-Pena, J. G., Nicolini, H., Moreno-Treviño, M. G., and Treviño, V. (2020). Improving predictive models for Alzheimer's disease using GWAS data by incorporating misclassified samples modeling. *PLoS One* 15:e0232103. doi: 10.1371/journal.pone.0232103
- Sabuncu, M. R., Buckner, R. L., Smoller, J. W., Lee, P. H., Fischl, B., and Sperling, R. A. (2012). The association between a polygenic Alzheimer score and cortical thickness in clinically normal subjects. *Cereb. Cortex* 22, 2653–2661. doi: 10.1093/cercor/bhr348
- Saez-Atienzar, S., Bandres-Ciga, S., Langston, R. G., Kim, J. J., Choi, S. W., Reynolds, R. H., et al. (2021). Genetic analysis of amyotrophic lateral sclerosis identifies contributing pathways and cell types. *Sci. Adv.* 7:eabd9036. doi: 10.1126/sciadv.abd9036
- Solomon, A., Turunen, H., Ngandu, T., Peltonen, M., Levälähti, E., Helisalmi, S., et al. (2018). Effect of the apolipoprotein e genotype on cognitive change during a multidomain lifestyle intervention a subgroup analysis of a randomized clinical trial. *JAMA Neurol.* 75, 462–470. doi: 10.1001/jamaneurol.2017.4365
- Stephan, Y., Sutun, A. R., Luchetti, M., Caille, P., and Terracciano, A. (2018). Polygenic score for Alzheimer disease and cognition: the mediating role of personality. *J. Psychiatr. Res.* 107, 110–113. doi: 10.1016/j.jpsychires.2018.10.015
- Tan, C. H., Bonham, L. W., Fan, C. C., Mormino, E. C., Sugrue, L. P., Broce, I. J., et al. (2019). Polygenic hazard score, amyloid deposition and Alzheimer's neurodegeneration. *Brain* 142, 460–470. doi: 10.1093/brain/awy327
- Tan, C. H., Fan, C. C., Mormino, E. C., Sugrue, L. P., Broce, I. J., Hess, C. P., et al. (2018). Polygenic hazard score: an enrichment marker for Alzheimer's associated amyloid and tau deposition. *Acta Neuropathol.* 135, 85–93. doi: 10.1007/s00401-017-1789-4
- Tan, C. H., Hyman, B. T., Tan, J. X., Hess, C. P., Dillon, W. P., Schellenberg, G. D., et al. (2017). Polygenic hazard scores in preclinical Alzheimer disease. *Ann. Neurol.* 82, 484–488. doi: 10.1002/ana.25029
- Tasaki, S., Gaiteri, C., Mostafavi, S., De Jager, P. L., and Bennett, D. A. (2018). The molecular and neuropathological consequences of genetic risk for Alzheimer's dementia. *Front. Neurosci.* 12:699. doi: 10.3389/fnins.2018.00699
- The International Multiple Sclerosis Genetics Consortium (IMSGC) (2010). Evidence for polygenic susceptibility to multiple sclerosis-the shape of things to come. *Am. J. Hum. Genet.* 86, 621–625. doi: 10.1016/j.ajhg.2010.02.027
- Tosto, G., Bird, T. D., Tsuang, D., Bennett, D. A., Boeve, B. F., Cruchaga, C., et al. (2017). Polygenic risk scores in familial Alzheimer disease. *Neurology* 88, 1180–1186. doi: 10.1212/WNL.0000000000003734
- Verhaaren, B. F. J., Vernooij, M. W., Koudstaal, P. J., Uitterlinden, A. G., Van Duijn, C. M., Hofman, A., et al. (2013). Alzheimer's disease genes and cognition in the nondemented general population. *Biol. Psychiatry* 73, 429–434. doi: 10.1016/j.biopsych.2012.04.009
- Walter, S., Marden, J. R., Kubzansky, L. D., Mayeda, E. R., Crane, P. K., Chang, S. C., et al. (2016). Diabetic phenotypes and late-life dementia risk: a mechanism-specific mendelian randomization study. *Alzheimer Dis. Assoc. Disord.* 30, 15–20. doi: 10.1097/WAD.0000000000000128
- Wang, T., Han, Z., Yang, Y., Tian, R., Zhou, W., Ren, P., et al. (2019). Polygenic risk score for Alzheimer's disease is associated with Ch4 volume in normal subjects. *Front. Genet.* 10:519. doi: 10.3389/fgene.2019.00519
- Xiao, E., Chen, Q., Goldman, A. L., Tan, H. Y., Healy, K., Zoltick, B., et al. (2017). Late-onset Alzheimer's disease polygenic risk profile score predicts hippocampal function. *Biol. Psychiatry Cogn. Neurosci. Neuroimaging* 2, 673–679. doi: 10.1016/j.bpsc.2017.08.004
- Xiao, Q., Liu, Z. J., Tao, S., Sun, Y. M., Jiang, D., Li, H. L., et al. (2015). Risk prediction for sporadic Alzheimer's disease using genetic risk score in the Han Chinese population. *Oncotarget* 6, 36955–36964. doi: 10.18632/oncotarget.6271
- Yesavage, J. A., Noda, A., Heath, A., McNERney, M. W., Domingue, B. W., Hernandez, Y., et al. (2020). Sleep-wake disorders in Alzheimer's disease: further genetic analyses in relation to objective sleep measures. *Int. Psychogeriatr.* 32, 807–813. doi: 10.1017/S1041610219001777

- Yokoyama, J. S., Bonham, L. W., Sears, R. L., Klein, E., Karydas, A., Kramer, J. H., et al. (2015). Decision tree analysis of genetic risk for clinically heterogeneous Alzheimer's disease. *BMC Neurol.* 15:47. doi: 10.1186/s12883-015-0304-6
- Yu, L., Petyuk, V. A., Tasaki, S., Boyle, P. A., Gaiteri, C., Schneider, J. A., et al. (2019). Association of cortical β -amyloid protein in the absence of insoluble deposits with Alzheimer disease. *JAMA Neurol.* 76, 818–826. doi: 10.1001/jamaneurol.2019.0834
- Zhang, C., Hu, R., Zhang, G., Zhe, Y., Hu, B., He, J., et al. (2019). A weighted genetic risk score based on four APOE-independent Alzheimer's disease risk loci may supplement APOE E4 for better disease prediction. *J. Mol. Neurosci.* 69, 433–443. doi: 10.1007/s12031-019-01372-2
- Zhou, X., Chen, Y., Ip, F. C. F., Lai, N. C. H., Li, Y. Y. T., Jiang, Y., et al. (2020). Genetic and polygenic risk score analysis for Alzheimer's disease in the Chinese population. *Alzheimer's Dement.* 12:e12074. doi: 10.1002/dad2.12074
- Zhou, X., Chen, Y., Mok, K. Y., Zhao, Q., Chen, K., Chen, Y., et al. (2018). Identification of genetic risk factors in the Chinese population implicates a role of immune system in Alzheimer's disease pathogenesis. *Proc. Natl. Acad. Sci. U.S.A.* 115, 1697–1706. doi: 10.1073/pnas.1715554115
- Zissimopoulos, J., Crimmins, E., and St. Clair, P. (2015). The value of delaying Alzheimer's disease onset. *Forum Health Econ. Policy* 18, 25–39. doi: 10.1515/fhep-2014-0013

Conflict of Interest: The authors declare that the research was conducted in the absence of any commercial or financial relationships that could be construed as a potential conflict of interest.

The handling editor declared a past collaboration with one of the authors NI.

Copyright © 2021 Zhou, Li, Fu and Ip. This is an open-access article distributed under the terms of the Creative Commons Attribution License (CC BY). The use, distribution or reproduction in other forums is permitted, provided the original author(s) and the copyright owner(s) are credited and that the original publication in this journal is cited, in accordance with accepted academic practice. No use, distribution or reproduction is permitted which does not comply with these terms.



OPEN ACCESS

Edited by:

Yu Chen,
Shenzhen Institutes of Advanced
Technology, Chinese Academy
of Sciences (CAS), China

Reviewed by:

Alessandro Martorana,
University of Rome Tor Vergata, Italy
Yu-Hui Liu,
Third Military Medical University,
China
Xiaopu Zhou,
Hong Kong University of Science
and Technology, Hong Kong

*Correspondence:

Lucilla Parnetti
lucilla.parnetti@unipg.it
Giuseppe Di Fede
giuseppe.difede@istituto-besta.it

[†] These authors have contributed
equally to this work and share first
authorship

[‡] These authors have contributed
equally to this work and share last
authorship

Specialty section:

This article was submitted to
Neurodegeneration,
a section of the journal
Frontiers in Neuroscience

Received: 30 December 2020

Accepted: 08 March 2021

Published: 31 March 2021

Citation:

Bellomo G, Indaco A,
Chiasserini D, Maderna E,
Paolini Paoletti F, Gaetani L,
Paciotti S, Petricciuolo M, Tagliavini F,
Giaccone G, Parnetti L and Di Fede G
(2021) Machine Learning Driven
Profiling of Cerebrospinal Fluid Core
Biomarkers in Alzheimer's Disease
and Other Neurological Disorders.
Front. Neurosci. 15:647783.
doi: 10.3389/fnins.2021.647783

Machine Learning Driven Profiling of Cerebrospinal Fluid Core Biomarkers in Alzheimer's Disease and Other Neurological Disorders

Giovanni Bellomo^{1†}, Antonio Indaco^{2†}, Davide Chiasserini^{3†}, Emanuela Maderna², Federico Paolini Paoletti⁴, Lorenzo Gaetani⁴, Silvia Paciotti¹, Maya Petricciuolo¹, Fabrizio Tagliavini², Giorgio Giaccone², Lucilla Parnetti^{1,4} and Giuseppe Di Fede^{2**}**

¹ Laboratory of Clinical Neurochemistry, Section of Neurology, Department of Medicine and Surgery, University of Perugia, Perugia, Italy, ² Neurology 5/Neuropathology Unit, Fondazione IRCCS Istituto Neurologico C. Besta, Milan, Italy, ³ Section of Biochemistry, Department of Medicine and Surgery, University of Perugia, Perugia, Italy, ⁴ Section of Neurology, Department of Medicine and Surgery, University of Perugia, Perugia, Italy

Amyloid-beta (A β) 42/40 ratio, tau phosphorylated at threonine-181 (p-tau), and total-tau (t-tau) are considered core biomarkers for the diagnosis of Alzheimer's disease (AD). The use of fully automated biomarker assays has been shown to reduce the intra- and inter-laboratory variability, which is a critical factor when defining cut-off values. The calculation of cut-off values is often influenced by the composition of AD and control groups. Indeed, the clinically defined AD group may include patients affected by other forms of dementia, while the control group is often very heterogeneous due to the inclusion of subjects diagnosed with other neurological diseases (OND). In this context, unsupervised machine learning approaches may overcome these issues providing unbiased cut-off values and data-driven patient stratification according to the sole distribution of biomarkers. In this work, we took advantage of the reproducibility of automated determination of the CSF core AD biomarkers to compare two large cohorts of patients diagnosed with different neurological disorders and enrolled in two centers with established expertise in AD biomarkers. We applied an unsupervised Gaussian mixture model clustering algorithm and found that our large series of patients could be classified in six clusters according to their CSF biomarker profile, some presenting a typical AD-like profile and some a non-AD profile. By considering the frequencies of clinically defined OND and AD subjects in clusters, we subsequently computed cluster-based cut-off values for A β 42/A β 40, p-tau, and t-tau. This approach promises to be useful for large-scale biomarker studies aimed at providing efficient biochemical phenotyping of neurological diseases.

Keywords: Alzheimer's disease, biomarkers, dementia, cerebrospinal fluid, amyloid-beta, tau, machine learning, clustering analysis

INTRODUCTION

Alzheimer's disease (AD) is the most common neurodegenerative disorder evolving to dementia (Goedert and Spillantini, 2006). Increasing knowledge of the molecular mechanisms underlying the pathogenesis of AD has progressively improved the protocols employed for its diagnosis in clinical practice (Jack et al., 2018). However, AD is also recognized as a heterogeneous disorder that may occur under several distinct phenotypes which can mimic other forms of dementias and other neurodegenerative conditions (Di Fede et al., 2018). Such phenotypic heterogeneity sometimes makes the differential diagnosis between AD and other similar neurological diseases problematic (Sawyer et al., 2017; de Souza et al., 2019; Villain and Dubois, 2019). Cerebrospinal fluid (CSF) core biomarkers for AD – i.e., amyloid-beta (A β) 42/40 ratio, tau phosphorylated at threonine-181 (p-tau), and total-tau (t-tau) – are largely used in clinical settings, research, and drug trials (Paterson et al., 2018; Gaetani et al., 2020). However, their clinical utility to differentiate AD from non-AD neurodegenerative dementias, such as dementia with Lewy bodies (DLB) or frontotemporal dementia (FTD), is less established (Bartlett et al., 2012; Molinuevo et al., 2014). For a long time, manual enzyme-linked immunosorbent assay (ELISA) has been widely employed as the reference method for the analysis of the CSF AD biomarkers. However, its broad-scale use is critically hampered by the assay variability, which influences the measurement of the analytes and the interpretation of the outcome data, especially in the routine clinical context (Mattsson et al., 2012; Le Bastard et al., 2015). Due to these concerns, ELISA was recently replaced in worldwide laboratories by fully automated assays – such as chemiluminescence enzyme immunoassay (CLEIA) – which offer grounds to cut sample manipulation steps and to reduce the intra- and inter-laboratory variability for CSF biomarker measurement (Kollhoff et al., 2018). Nevertheless, there is still a need for harmonization of CSF biomarker assays across centers involved in AD diagnostics (Mattsson-Carlgrén et al., 2020). For instance, the lack of established universal biomarker cut-offs makes the calculation of internal reference values mandatory for each laboratory both for clinical and research purposes. This calculation is often critically influenced by the choice and composition of AD and control groups; the clinically defined AD group may include patients affected by other forms of dementia (e.g., FTD and DLB) due to misdiagnosis, while the control group is often very heterogeneous due to the inclusion of subjects diagnosed with other neurological diseases (OND) who underwent lumbar puncture (LP) for diagnostic purposes. On the one hand, OND may better represent the real cases afferent to neurology clinics compared to healthy subjects. However, the heterogeneity of the inclusion criteria adopted in each center for the definition of OND controls represents a source of variability for the calculation of biomarkers cut-off values. In addition, the absence of standardized methodological and statistical approaches represents one of the most critical issues to study the distribution of CSF core AD biomarkers in different subgroups of patients and to validate in larger cohorts the cut-off values able to discriminate between AD and other

AD-mimicking disorders (Simrén et al., 2020). In this context, unsupervised machine learning approaches may overcome both misdiagnosis and the lack of standardization of inclusion criteria providing unbiased cut-off values and data-driven patient stratification according to the sole distribution of biomarkers. In this work, we took advantage of the reproducibility of automated determination of the CSF core AD biomarkers to compare two large cohorts of patients diagnosed with different neurological disorders and enrolled in two centers with established expertise in AD biomarkers. We applied an unsupervised Gaussian mixture model (GMM) clustering algorithm and found that our large series of patients could be classified in six clusters according to their CSF biomarker profile, some presenting a typical AD-like profile and some a typical non-AD profile. By considering the frequencies of clinically defined OND and AD subjects in clusters, we subsequently computed cluster-based cut-off values for A β 42/A β 40, p-tau, and t-tau.

MATERIALS AND METHODS

Patients

A total of 616 prospectively collected CSF samples from patients referring to the Neurology Clinic, University of Perugia (cohort 1), and from the Carlo Besta Neurological Institute, Milan (cohort 2), were used in this study. All patients underwent a standardized assessment including medical history, physical and neurological examination, laboratory tests, neuropsychological evaluation, and brain imaging (computed tomography or magnetic resonance imaging, MRI). 18Fluoro-2-deoxyglucose positron emission tomography (FDG-PET), dopamine transporter single photon emission computed tomography (DaT-Scan), and electroencephalogram were also performed in selected cases, according to clinical suspicion. According to the purposes of our investigation, clinical diagnoses were made by consensus in a multidisciplinary meeting of neurologists with a deep expertise in the field of neurodegenerative diseases, without knowledge of CSF results. Therefore, we did not consider the most updated criteria for AD diagnosis, based on A/T/(N) classification (Jack et al., 2018), but rather we defined patients as affected by AD or other neurological disorders only according to the available clinical criteria, as follows. Patients with neurodegenerative disorders included 257 patients with probable AD (Dubois et al., 2007) both at dementia and prodromal (MCI) stages, 50 frontotemporal dementia (FTD) patients (Faber, 1999), 56 patients with Parkinson's disease (PD) (Postuma et al., 2015), 7 PD with dementia (PDD) patients (Emre et al., 2007), 21 patients with dementia with Lewy bodies (DLB) (McKeith et al., 2017), 58 patients with atypical parkinsonism or parkinsonism of different etiology (Gilman et al., 2008; Armstrong et al., 2013; Höglinger et al., 2017; Rektor et al., 2018), 1 patients with amyotrophic lateral sclerosis (ALS) (Traynor et al., 2000), 8 patients with Creutzfeldt-Jakob disease (CJD) (Manix et al., 2015), 27 patients with normal pressure hydrocephalus (NPH) (Relkin et al., 2005), and 2 patients with genetically confirmed degenerative spinocerebellar ataxia (SCA). Patients were classified as having subjective cognitive decline (SCD) if they complained cognitive

deficits but neuropsychological evaluation was normal or showed subtle deficits not fulfilling criteria for mild cognitive impairment (MCI) (8 patients). Patients with stable MCI (sMCI) showed unchanged neuropsychological results after 1-year follow-up (20 patients). Other diagnostic groups included vascular dementia (5 patients) (Román et al., 1993), cerebral amyloid angiopathy (CAA) (Smith and Greenberg, 2003) (3 patients), autoimmune encephalitis (8 patients) (Graus et al., 2016), encephalopathies of different etiology (2 patients), relapsing-remitting multiple sclerosis (MS) (Thompson et al., 2018) (6 patients), and cognitively impaired late-onset epilepsy (1 patient) (Scheffer et al., 2017). Patients categorized as having cerebrovascular diseases (CVD) showed significant brain small vessel disease at MRI (i.e., white matter changes, microbleeds, and lacunar infarcts) without fulfilling diagnostic criteria for VaD and CAA (3 patients). Dementia of unknown origin (uDEM) was defined for those subjects in which brain imaging including both MRI and nuclear imaging excluded vascular and neurodegenerative origins (3 patients). Cognitively unimpaired patients referring to our centers for psychiatric disorders or neurological conditions like headaches, seizures, mononeuropathies, and polyneuropathies, in which brain imaging did not reveal gross abnormalities nor underlying neurodegenerative diseases, were classified as control subjects with other neurological diseases (OND) (71 patients).

Samples Collection and Analysis

Lumbar puncture was performed according to international guidelines (Teunissen et al., 2009); 10–12 mL of CSF was collected in sterile polypropylene tubes (Sarstedt® tubes, code: 62.610.210) and centrifuged for 10 min (2000 × g), at room temperature. Aliquots of 0.5 mL were frozen at –80°C in polypropylene tubes (Sarstedt® tubes, code: 72.730.007). CSF samples were analyzed on the fully automated chemiluminescent platform Lumipulse G600-II (Fujirebio Inc) for β -amyloid 1–42 (A β 42), β -amyloid 1–40 (A β 40), t-tau and p-tau (Thr181) levels. For cohort 1, all the CSF samples were analyzed directly in their 0.5 mL storage tubes, while for cohort 2 samples were analyzed by transferring them in Hitachi® polystyrene sample caps (code: 80351). Throughout this work, A β 42/A β 40 ratio was used since it represents a more robust marker of amyloidosis with respect to the sole A β 42 (Biscetti et al., 2019). Moreover, the use of A β 42/A β 40 can also partially compensate the above-mentioned methodological difference between the two centers, since the A β absorption due to tube transfer (Toombs et al., 2014) is thought to act similarly for the 1–40 and 1–42 A β isoforms (Lewczuk et al., 2006).

Cohorts Merging

A preliminary experiment was carried out to assess the inter-center variability of the CSF biomarkers and the possibility to merge the two cohorts. A total of 40 CSF samples (20 from each center) were measured with Lumipulse-G automated platforms in the two laboratories by using kits originating from the same batches. The composition of this validation cohort is reported in **Supplementary Table 1**. The concordance between the measurements was assessed by correlation analysis.

Statistical Methods

The data analysis was performed by using R software v 3.6 (R Core Team, 2013).

Correlation Analysis

Because of the known non-optimal normality of biomarker data (Bellomo et al., 2020a), Passing Bablok regressions (Passing and Bablok, 1983) were preferred to parametric least squares regressions. Confidence intervals (CI) for the fitted parameters were calculated with the bootstrap method (Carpenter and Bithell, 2000). Principal component analysis (PCA) was then applied to the whole dataset to graphically show the absence of a significant separation among samples belonging to different cohorts. The R-package *mcr* was used for these calculations [*mcr* package | R Documentation (2021)].

Cluster Analysis

The GMM algorithm (Figueiredo and Jain, 2002) of the machine learning Python package Scikit-learn v 0.23.2 (Pedregosa et al., 2011) was used for the cluster analysis. Biomarker values were all z-scored prior to the analysis. The optimal number of clusters was chosen minimizing the Bayesian information criterion (BIC) function (Schwarz, 1978). After the clustering, all the samples biomarker values were back-transformed into the original dimensions. Median biomarker values together with the 95% data range were calculated for each cluster. The prevalences of diagnostic categories in each cluster were represented in percentages in a heatmap. Both diagnostic groups and clusters were grouped according to a hierarchical clustering (Rokach and Maimon, 2005; Gu, 2021). Euclidean distance and average linkage were used as parameters for clustering.

Calculation of Cut-Off Values

Cut-off values were calculated for OND vs. AD and among clusters by maximizing Youden's index with the p-ROC package in R v3.6 (Robin et al., 2011). Cut-off CI were calculated by using 2000 bootstrap replicates.

Calculation of Cut-Off Values on Age- and Gender-Matched Subsets

Age histogram matching was performed by random exclusion of subjects within bins of 5 years width. Exclusion of samples according to gender was subsequently conducted until *p*-values > 0.25 were obtained by logistic regression (Dobson and Barnett, 2018; glm function | R Documentation, 2021) both for age and gender. Recalculation of cut-off values for the age- and gender-matched subsets was performed as described in section "Calculation of Cut-Off Values."

RESULTS

Patients Demographical Data

A total of 616 patients whose CSF samples were tested for AD biomarker by Lumipulse-G, were included in the study regardless of age and clinical diagnoses. Among them, 257 were clinically diagnosed as AD and 71 cognitively unimpaired subjects affected

by minor neurological non-neurodegenerative disorders were classified as OND. The whole cohort originated by merging two sub-cohorts: 303 subjects referred to the biobank of the Neurology clinic of the University of Perugia (cohort 1), while 313 referred to the biobank of the Carlo Besta Neurological Institute of Milan (cohort 2). The demographical details of the subjects included are reported in **Supplementary Table 3**.

Merging of the Two Cohorts

Assessment of CSF AD biomarkers with Lumipulse-G CLEIA technology showed very low inter-center variability in external quality control programs (Leitão et al., 2019; Paciotti et al., 2019). However, we performed a small scale inter-center variability study, measuring a total of 40 samples across the two centers involved, to assess the possibility to merge the cohorts from Perugia (cohort 1, 303 subjects) and Milan (cohort 2, 313 subjects). Patients' diagnoses, mean biomarker values and inter-assay/inter-laboratory coefficients of variations (CV) are reported for all of these samples in **Supplementary Table 1**. As expected,

the mean inter-assay CV of A β 42/A β 40 (7%) was lower compared to the ones of A β 42 (12%) and A β 40 (9%). Mean inter-assay CV of p-tau (4%) and t-tau (9%) were also relatively low. Correlation and Passing-Bablok linear regression analyses showed a good agreement between the measurements performed in the two centers (**Figures 1A–C**). A Pearson's correlation coefficient above 0.9 was found for each of the tested biomarkers and all the measured slopes were equal to 1 within their 95% CI. Intercepts for A β 42/A β 40 and p-tau were null within their 95% CI, whereas a non-null negative intercept was obtained for t-tau, although being small compared to usual nominal t-tau values. The results of Passing-Bablok linear regression analysis for A β 42 and A β 40 are shown in **Supplementary Table 2**. As expected (Lewczuk et al., 2006), we found a greater deviance from identity between the measurements of these two peptides performed in the two laboratories with respect to their ratio. We subsequently analyzed all the 616 samples included in the study by means of PCA. Projection of the data into the principal components space (**Figure 1D**)

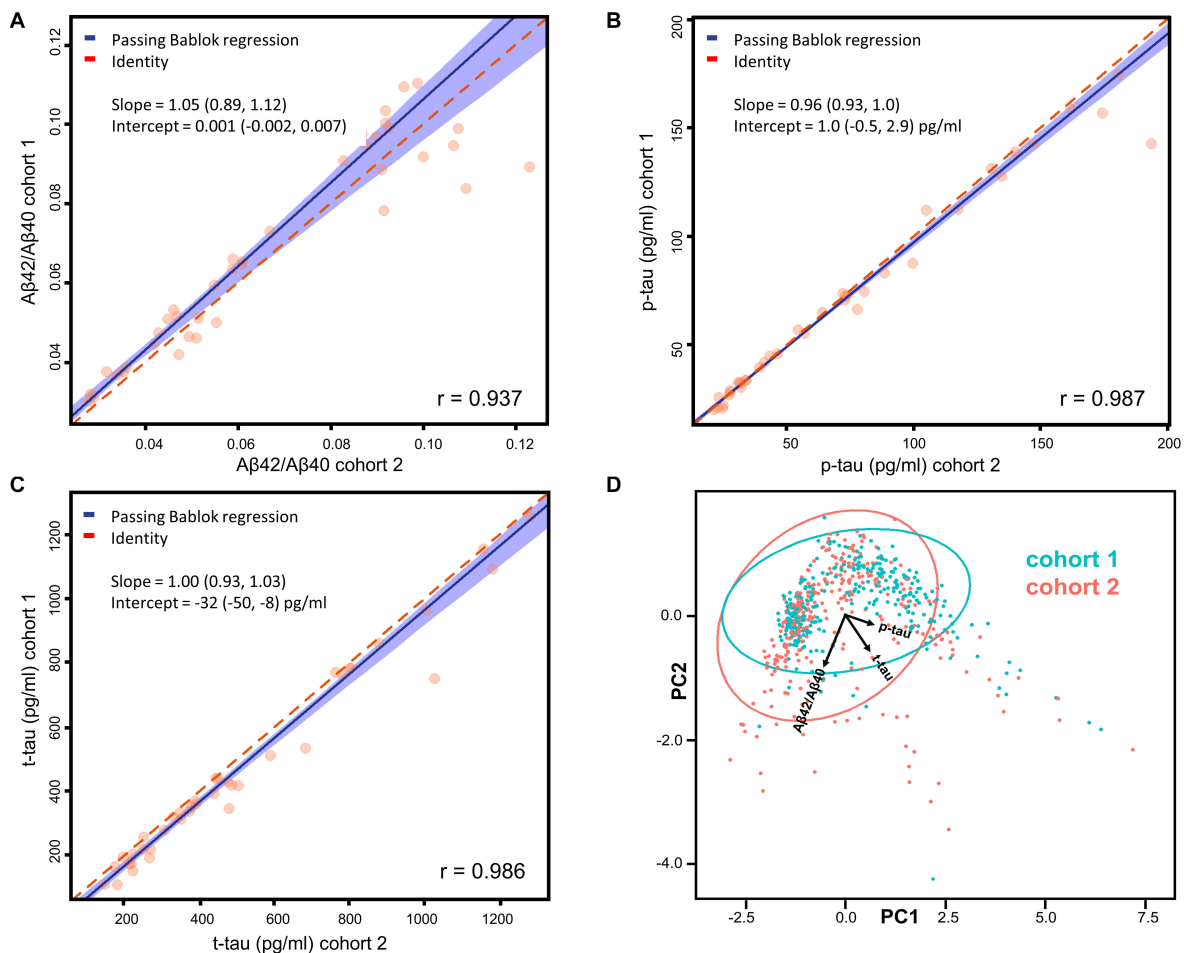


FIGURE 1 | (A–C) Passing-Bablok regression analyses of A β 42/A β 40, p-tau, and t-tau measured on 40 samples (20 from each cohort) in the two centers. Correlations have been calculated in terms of Pearson's correlation coefficients (r). Fitted slopes and intercepts with their 95% CI are also shown. **(D)** Plot (PC1 vs. PC2) relative to the PCA performed on the whole dataset with samples belonging to different cohorts highlighted in different colors. The ellipses relative to the 95% data range of each cohort are also shown together with the projections of A β 42/A β 40, p-tau and t-tau in the PC1-PC2 space.

showed that the measurement from the two centers did not show any significant grouping related to the site of analysis, as shown by the ellipses representative of the 95% data range of the two cohorts.

Both the regression and the PCA analysis showed that the inter-center variability was negligible for A β 42/A β 40, p-tau and t-tau. Cut-off values for A β 42, A β 42/A β 40, p-tau and t-tau for cohort 1, cohort 2 and for the two cohorts merged are also reported in the **Supplementary Table 4**. The calculated cut-off values did not significantly differ within their 95% CI between cohort 1 and 2. Thus, we proceeded to merge the two cohorts for subsequent analyses, without applying any correction factor for A β 42/A β 40, p-tau and t-tau.

Clustering

For the unsupervised cluster analysis, we included all the subjects who consecutively underwent LP in the two centers and whose CSF was assayed for A β 42/A β 40, p-tau and t-tau with Lumipulse-G ($N = 616$). Considering the results of the PCA plotted in **Figure 1D**, we decided to apply GMM as clustering algorithm (Pedregosa et al., 2011). Other clustering algorithms such as K-means are known for not providing good fittings for anisotropic data. In order to standardize the dimensions of the three biomarkers considered, biomarker values were substituted with the corresponding Z-scores before the analysis and then back-transformed for plotting and data interpretation. The optimal number of clusters was decided according to BIC (Schwarz, 1978). A plot relative to the BIC

function is shown in **Supplementary Figure 1**. Accordingly, the optimal number of clusters turned out to be 6. The results of the unsupervised clustering analysis are shown in **Figure 2A**, GMM centroids and covariance matrices are reported in **Supplementary Table 5**. As it can be seen by comparing the 3D scatter plots in **Figures 2A,B**, most AD and OND samples were assigned to different clusters. In particular, most OND were included in cluster 1 while most AD subjects (95%) were comprised in clusters 3, 4, 5, and 6. Considering the biomarker 95% data ranges of each cluster (**Figure 2C**), clusters 3–6 corresponded to low A β 42/A β 40 values and high values of p-tau and t-tau, which, according to the A/T/(N) criteria (Jack et al., 2018), correspond to the presence of amyloidosis, tauopathy and tau-related neurodegeneration, respectively. These four clusters mainly differed in p-tau and t-tau values (**Figure 2C**). Among AD patients, for all the AD clusters, the prevalences of demented subjects ($N = 253$) did not significantly differ from the prevalences of subjects in the MCI phase ($N = 53$) by applying Fisher's exact test for count data. Cluster 1 was instead characterized by higher values of A β 42/A β 40 and small values of p-tau and t-tau. Biomarker values in cluster 2 were instead highly variable with respect to the other clusters (wide 95% data ranges for all the three biomarkers). This cluster was characterized by smaller A β 42/A β 40 median values with respect to clusters 3–6 and higher p-tau and t-tau median values compared to cluster 1.

The percentages of AD patients, OND and other sufficiently represented ($N > 6$) clinical conditions in each cluster are

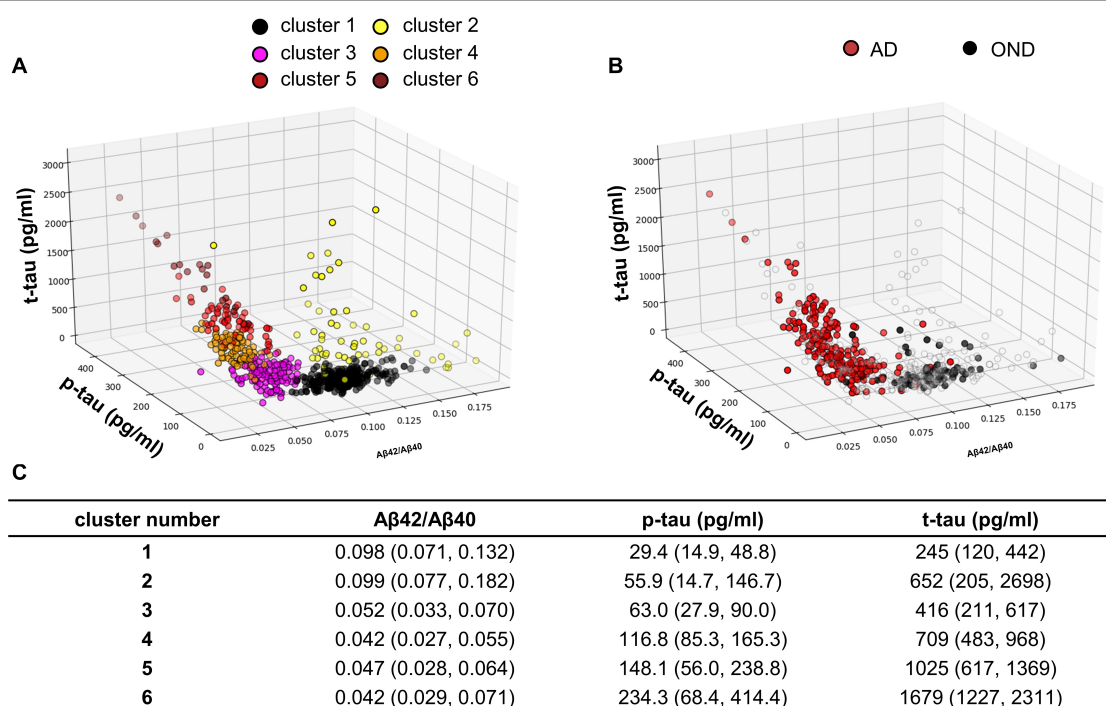


FIGURE 2 | (A) Samples distribution in the core AD biomarkers space. The colors indicate the cluster to which the sample is belonging, after GMM analysis.

(B) Samples belonging to AD patients and OND are highlighted in red and black, respectively. **(C)** Median biomarker values with the 95% data range of each cluster represented in brackets.

reported in **Figure 3**. Interestingly, not only AD but also PDD, DLB, and CBD had a relevant presence (>20%) in clusters 3–6. Conversely, MS, PSP, sMCI, and synucleinopathies without dementia (PD and MSA) majorly colocalize with OND in cluster 1. The composition of cluster 2 was instead highly variable, consisting in the totality of CJD subjects and relevant percentages ($\geq 20\%$) of NPH, ENC, FTD, and VAD. Considering the distribution of clinically defined OND and AD subjects in the clusters together with the clusters data ranges with respect to the calculated biomarkers cut-off values, we decided to indicate cluster 1 as the “control” cluster and clusters 3–6 as “AD-clusters”. Grouping of the clusters and of the clinical diagnoses showed that cluster 1, the control cluster, was the most distant from the others, followed by cluster 2 which was included in a separated branch with respect to cluster 3–6. The clinical diagnosis showed also a peculiar grouping, with AD, PDD, and DLB in the same branch of the dendrogram, while the other conditions (mostly included in clusters 1 and 2) in a second large branch. CJD clustered separately from all the other conditions being characterized by high A β 42/A β 40 ratios and high t-tau values.

According to the prevalence of AD and OND in clusters 1–6, we calculated cut-off values for each biomarker considering AD vs. OND clinical diagnoses, control cluster vs. AD clusters and cluster 2 vs. AD clusters. The results are shown in **Table 1**.

We noticed that the cut-offs of the comparison control cluster vs. AD clusters were relatively similar to what obtained using the clinical diagnosis grouping (OND vs. AD), being mostly comprised within the 95% CI. Cut-off values for control cluster vs. AD clusters remained unchanged also by considering an age- and gender-matched subsets of the population (**Supplementary Figure 2**).

TABLE 1 | Cut-off values for the three core AD biomarkers with their 95% CI were calculated by maximizing the Youden's index for AD vs. OND, between samples belonging to the AD clusters (cluster 3, 4, 5, and 6) and “control” cluster (cluster 1) and between samples belonging to the AD clusters and cluster 2.

	A β 42/A β 40	p-tau (pg/ml)	t-tau (pg/ml)
OND vs. AD	0.073 (0.063, 0.079)	53.5 (47.2, 57.5)	371 (332, 393)
Control cluster vs. AD clusters	0.072 (0.070, 0.074)	50.0 (46.2, 52.3)	392 (359, 396)
Cluster 2 vs. AD clusters	0.073 (0.072, 0.078)	71.6 (50.6, 82.8)	1403 (485, 1999)

On the other hand, the cluster 2 vs. AD clusters comparison showed significant differences in the absolute values of cut-offs for t-tau and p-tau, while the A β 42/A β 40 ratio did not change significantly.

DISCUSSION

In the last decade, CSF A β 42/A β 40 ratio, p-tau and t-tau emerged as reliable markers of brain amyloidosis, tauopathy and tau-related neurodegeneration. The introduction of these markers into clinical practice has substantially helped the neurologist to change the definition of AD from a syndromal to a molecular construct (Jack et al., 2018). In particular, considering the well-established A/T/(N) system (Jack et al., 2018), AD is now defined by the presence of both brain amyloidosis (A+) and tauopathy (T+), with neurodegeneration (N+) being a non-necessary condition. The recent advent of automated platforms for core AD biomarker assessment in CSF, has been of substantial help in limiting both intra and inter-assay variability with

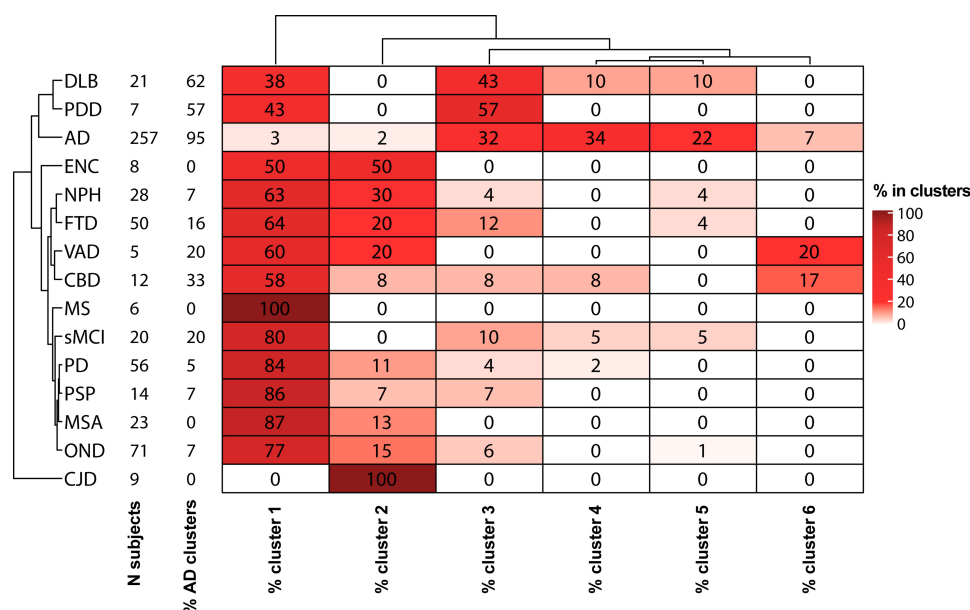


FIGURE 3 | Heatmap descriptive of the GMM cluster analysis results. For each diagnostic category with a sample size (N subjects) ≥ 5 , the percentages of samples in each cluster are shown. Hierarchical clustering was used for ordering diagnostic groups and clusters.

respect to manual ELISA (Le Bastard et al., 2015). In this work, we used the reproducibility of automated CSF core AD biomarker determination to compare two large cohorts of patients diagnosed with various neurological disorders and enrolled in two centers with proven expertise in AD biomarkers. After a small round-robin validation step on 40 CSF samples, we were able to confirm the good reproducibility of the determinations between the two centers using the automated procedure. In order to overcome the diagnostic heterogeneity of both AD and control groups, we applied unsupervised GMMs to cluster the patients ($n = 616$) according to their CSF biomarker profile and investigate the degree of overlap between the clinical diagnosis and the data-driven classification of the subjects. The data spontaneously grouped in six clusters, 4 of these (clusters 3–6) contained the 95% of clinically defined AD patients (**Figure 3**), characterized by low A β 42/A β 40 values and high values of p-tau and t-tau (**Figure 2C**). Interestingly, high percentages (>50%) of synucleinopathies with dementia (DLB and PDD) and CBD (33%) fell in these clusters. This fact is not surprising, since the presence of brain amyloidosis and tauopathy is a feature of both DLB and PDD (Irwin et al., 2013; Irwin and Hurtig, 2018; Bellomo et al., 2020b). Cluster 1 instead contained the majority of OND subjects (77%), and PD (84%), MSA (87%), PSP (86%), and MS (100%) patients, suggesting that AD pathology is not frequent in these conditions. This result, together with the high concordance between cut-off values for the OND vs. AD and control cluster vs. AD clusters comparisons, suggest that these conditions may be treated as controls with respect to core AD biomarkers. The inclusion of NPH in control groups should be instead avoided since neurodegeneration and dilution effects may significantly alter the concentration of t-tau and A β peptides (Graff-Radford, 2014), in a way that is not fully compensated by computing their ratio. By considering the clusters with highest and lowest frequencies of AD and OND subjects, we were able to compute cluster-defined cut-off values. In our work, the cut-off values calculated by the clustering method were concordant to the ones calculated by relying on clinical diagnoses for AD vs. OND, but this approach may be of more substantial help while facing low numbers of well clinically characterized OND and/or AD subjects. The cut-off values calculated for AD clusters vs. control cluster were substantially unchanged considering age- and gender-matched subsets of the clusters (**Supplementary Figure 2**), thus reinforcing the reliability of the approach used. Because of these advantages, unsupervised and partially supervised machine-learning algorithms (like the one we applied) have recently started to be applied in neurodegenerative diseases diagnostics (Skillbäck et al., 2015; Racine et al., 2016; Toschi et al., 2019). Moreover, these approaches represent a best choice while dealing with a large number of biomarkers or candidate biomarkers (Solorio-Fernández et al., 2020), e.g., in omics studies (Lopez et al., 2018). The inclusion of a wide panel of CSF markers, possibly linked to different biological pathways, may help in differentiating synucleinopathies with dementia and FTD from AD and synucleinopathies without dementia and PSP from controls. As a limitation of our study, we must report the small sample size of some diagnostic categories (e.g., MS, VAD and PDD). Thus, the frequencies of these categories in clusters may

potentially be biased. Another limitation is the lack of amyloid PET, which is of substantial help in identifying brain amyloidosis and well correlates with brain amyloidosis markers such as CSF A β 42 and A β 42/A β 40 (Alcolea et al., 2019; Leitão et al., 2019). However, this partially supervised approach is insensitive to the presence of hidden interfering pathologies in control subjects and to the presence of few AD misdiagnosis, which may occur when the diagnosis is made prevalently by the examination of clinical features. Since the definition of AD and control clusters depended only on the prevalences of clinically defined AD and OND subjects within each cluster, we expect that this approach may provide reliable results as long as the diagnosis/exclusion of AD is correct in the majority of the cases. As an example, considering the biomarker distributions presented in this study, to misclassify the control cluster it would have required at least 28 out of 71 OND subjects (40%) misdiagnosed for AD.

Overall, our findings suggest that automated assays are amenable for large-scale biomarker studies across centers. Furthermore, the use of unsupervised (or partially supervised) machine learning approaches may help the biochemical phenotyping of neurological disorders, being also a robust option for the definition of cut-off values. The implementation of such approaches in biomarker research could substantially improve the development of adequate diagnostic protocols and increase the quality of diagnostic tools for complex and heterogeneous disorders presenting with overlapping clinical syndromes, like dementias.

DATA AVAILABILITY STATEMENT

Raw data were generated at University of Perugia and Carlo Besta Neurological Institute. Derived data supporting the findings of this study are available from the corresponding authors (LP and GDF) on request.

ETHICS STATEMENT

The studies involving human participants were reviewed and approved by the Ethics Committee from Fondazione IRCCS Istituto Neurologico Carlo Besta, Milan, and University of Perugia. The patients/participants provided their written informed consent to participate in this study.

AUTHOR CONTRIBUTIONS

GB analyzed the data and wrote the first draft. AI analyzed the CSF samples at Carlo Besta Neurological Institute and revised the manuscript. DC conceptualized the data analysis and contributed to writing the first draft of the manuscript. EM contributed in analyzing the CSF samples at Carlo Besta Neurological Institute. FPP contributed to the sample collection and assisted with data management of samples. LG contributed to the sample selection and collection. SP and MP analyzed the samples at the University of Perugia and revised the manuscript. FT and GG contributed in the conceptualization of the study

and revised the manuscript. GDF and LP designed the study and revised the final version of the manuscript. All the authors read and approved the final version of the manuscript.

FUNDING

This work was supported by the Current Research Program from Italian Ministry of Health (RC 2018–20) to GG and GDF,

REFERENCES

- Alcolea, D., Pegueroles, J., Muñoz, L., Camacho, V., López-Mora, D., Fernández-León, A., et al. (2019). Agreement of amyloid PET and CSF biomarkers for Alzheimer's disease on Lumipulse. *Ann. Clin. Transl. Neurol.* 6, 1815–1824. doi: 10.1002/acn3.50873
- Armstrong, M. J., Litvan, I., Lang, A. E., Bak, T. H., Bhatia, K. P., Borroni, B., et al. (2013). Criteria for the diagnosis of corticobasal degeneration. *Neurology* 80, 496–503. doi: 10.1212/WNL.0b013e31827f0fd1
- Bartlett, J. W., Frost, C., Mattsson, N., Skillbäck, T., Blennow, K., Zetterberg, H., et al. (2012). Determining cut-points for Alzheimer's disease biomarkers: statistical issues, methods and challenges. *Biomark. Med.* 6, 391–400. doi: 10.2217/bmm.12.49
- Bellomo, G., Cataldi, S., Paciotti, S., Paolini Paoletti, F., Chiasserini, D., and Parnetti, L. (2020a). Measurement of CSF core Alzheimer disease biomarkers for routine clinical diagnosis: do fresh vs frozen samples differ? *Alzheimers Res. Ther.* 12:121. doi: 10.1186/s13195-020-00689-0
- Bellomo, G., Paolini Paoletti, F., Chipi, E., Petricciolo, M., Simoni, S., Tambasco, N., et al. (2020b). A/T/(N) Profile in Cerebrospinal Fluid of Parkinson's Disease with/without Cognitive Impairment and Dementia with Lewy Bodies. *Diagnostics* 10:1015. doi: 10.3390/diagnostics10121015
- Biscetti, L., Salvadori, N., Farotti, L., Cataldi, S., Eusebi, P., Paciotti, S., et al. (2019). The added value of Aβ42/Aβ40 in the CSF signature for routine diagnostics of Alzheimer's disease. *Clin. Chim. Acta* 494, 71–73. doi: 10.1016/j.cca.2019.03.001
- Carpenter, J., and Bithell, J. (2000). Bootstrap confidence intervals: when, which, what? A practical guide for medical statisticians. *Statist. Med.* 19, 1141–1164. doi: 10.1002/(SICI)1097-0258(20000515)19:9<1141::AID-SIM479>3.0.CO;2-F
- de Souza, L. C., Mariano, L. I., de Moraes, R. F., and Caramelli, P. (2019). Behavioral variant of frontotemporal dementia or frontal variant of Alzheimer's disease? A case study. *Dement. Neuropsychol.* 13, 356–360. doi: 10.1590/1980-57642018dn13-030015
- Di Fede, G., Catania, M., Maderna, E., Ghidoni, R., Benussi, L., Tonoli, E., et al. (2018). Molecular subtypes of Alzheimer's disease. *Sci. Rep.* 8:3269. doi: 10.1038/s41598-018-21641-1
- Dobson, A. J., and Barnett, A. G. (2018). *An Introduction to Generalized Linear Models*. Florida, FL: CRC Press.
- Dubois, B., Feldman, H. H., Jacova, C., Dekosky, S. T., Barberger-Gateau, P., Cummings, J., et al. (2007). Research criteria for the diagnosis of Alzheimer's disease: revising the NINCDS-ADRDA criteria. *Lancet Neurol.* 6, 734–746. doi: 10.1016/S1474-4422(07)70178-3
- Emre, M., Aarsland, D., Brown, R., Burn, D. J., Duyckaerts, C., Mizuno, Y., et al. (2007). Clinical diagnostic criteria for dementia associated with Parkinson's disease. *Mov. Disord.* 22, 1689–1707. doi: 10.1002/mds.21507
- Faber, R. (1999). Frontotemporal lobar degeneration: a consensus on clinical diagnostic criteria. *Neurology* 53:1159. doi: 10.1212/wnl.53.5.1158-b
- Figueiredo, M. A. T., and Jain, A. K. (2002). Unsupervised learning of finite mixture models. *IEEE Transact. Pattern Anal. Machine Intellig.* 24, 381–396. doi: 10.1109/34.990138
- Gaetani, L., Paoletti, F. P., Bellomo, G., Mancini, A., Simoni, S., Di Filippo, M., et al. (2020). CSF and Blood Biomarkers in Neuroinflammatory and Neurodegenerative Diseases: Implications for Treatment. *Trends Pharmacol. Sci.* 41, 1023–1037. doi: 10.1016/j.tips.2020.09.011
- Gilman, S., Wenning, G. K., Low, P. A., Brooks, D. J., Mathias, C. J., Trojanowski, J. Q., et al. (2008). Second consensus statement on the diagnosis of multiple system atrophy. *Neurology* 71, 670–676. doi: 10.1212/01.wnl.0000324625.00404.15
- glm function | R Documentation (2021). *Fitting Generalized Linear Models*. Available online at: <https://www.rdocumentation.org/packages/stats/versions/3.6.2/topics/glm> (accessed March 3, 2021)
- Goedert, M., and Spillantini, M. G. (2006). A century of Alzheimer's disease. *Science* 314, 777–781. doi: 10.1126/science.1132814
- Graff-Radford, N. R. (2014). Alzheimer CSF biomarkers may be misleading in normal-pressure hydrocephalus. *Neurology* 83, 1573–1575. doi: 10.1212/WNL.0000000000000916
- Graus, F., Titulaer, M. J., Balu, R., Benseler, S., Bien, C. G., Cellucci, T., et al. (2016). A clinical approach to diagnosis of autoimmune encephalitis. *Lancet Neurol.* 15, 391–404. doi: 10.1016/S1474-4422(15)00401-9
- Gu, Z. (2021). *ComplexHeatmap: Make Complex Heatmaps. Bioconductor version: Release (3.12)*. doi: 10.18129/B9.bioc.ComplexHeatmap
- Höglinger, G. U., Respondek, G., Stamelou, M., Kurz, C., Josephs, K. A., Lang, A. E., et al. (2017). Clinical diagnosis of progressive supranuclear palsy: The movement disorder society criteria. *Mov. Disord.* 32, 853–864. doi: 10.1002/mds.26987
- Irwin, D. J., and Hurtig, H. I. (2018). The Contribution of Tau, Amyloid-Beta and Alpha-Synuclein Pathology to Dementia in Lewy Body Disorders. *J. Alzheimers Dis. Parkinsonism* 8:1000444. doi: 10.4172/2161-0460.1000444
- Irwin, D. J., Lee, V. M.-Y., and Trojanowski, J. Q. (2013). Parkinson's disease dementia: convergence of α-synuclein, tau and amyloid-β pathologies. *Nat. Rev. Neurosci.* 14, 626–636. doi: 10.1038/nrn3549
- Jack, C. R., Bennett, D. A., Blennow, K., Carrillo, M. C., Dunn, B., Haeberlein, S. B., et al. (2018). NIA-AA Research Framework: Toward a biological definition of Alzheimer's disease. *Alzheimers Dement.* 14, 535–562. doi: 10.1016/j.jalz.2018.02.018
- Kollhoff, A. L., Howell, J. C., and Hu, W. T. (2018). Automation vs. Experience: Measuring Alzheimer's Beta-Amyloid 1-42 Peptide in the CSF. *Front. Aging Neurosci.* 10:253. doi: 10.3389/fnagi.2018.00253
- Le Bastard, N., De Deyn, P. P., and Engelborghs, S. (2015). Importance and impact of preanalytical variables on Alzheimer disease biomarker concentrations in cerebrospinal fluid. *Clin. Chem.* 61, 734–743. doi: 10.1373/clinchem.2014.236679
- Leitão, M. J., Silva-Spínola, A., Santana, I., Olmedo, V., Nadal, A., Le Bastard, N., et al. (2019). Clinical validation of the Lumipulse G cerebrospinal fluid assays for routine diagnosis of Alzheimer's disease. *Alzheimers Res. Ther.* 11:91. doi: 10.1186/s13195-019-0550-8
- Lewczuk, P., Beck, G., Esselmann, H., Bruckmoser, R., Zimmermann, R., Fiszer, M., et al. (2006). Effect of Sample Collection Tubes on Cerebrospinal Fluid Concentrations of Tau Proteins and Amyloid β Peptides. *Clin. Chem.* 52, 332–334. doi: 10.1373/clinchem.2005.058776
- Lopez, C., Tucker, S., Salameh, T., and Tucker, C. (2018). An unsupervised machine learning method for discovering patient clusters based on genetic signatures. *J. Biomed. Informat.* 85, 30–39. doi: 10.1016/j.jbi.2018.07.004
- Manix, M., Kalakoti, P., Henry, M., Thakur, J., Menger, R., Guthikonda, B., et al. (2015). Creutzfeldt-Jakob disease: updated diagnostic criteria, treatment algorithm, and the utility of brain biopsy. *Neurosurg. Focus* 39:E2. doi: 10.3171/2015.8.FOCUS15328
- Mattsson, N., Zegers, I., Andreasson, U., Bjerke, M., Blankenstein, M. A., Bowser, R., et al. (2012). Reference measurement procedures for Alzheimer's disease cerebrospinal fluid biomarkers: definitions and approaches with focus on amyloid β42. *Biomark. Med.* 6, 409–417. doi: 10.2217/bmm.12.39

SUPPLEMENTARY MATERIAL

The Supplementary Material for this article can be found online at: <https://www.frontiersin.org/articles/10.3389/fnins.2021.647783/full#supplementary-material>

- Mattsson-Carlsson, N., Palmqvist, S., Blennow, K., and Hansson, O. (2020). Increasing the reproducibility of fluid biomarker studies in neurodegenerative studies. *Nat. Commun.* 11:6252. doi: 10.1038/s41467-020-19957-6
- McKeith, I. G., Boeve, B. F., Dickson, D. W., Halliday, G., Taylor, J.-P., Weintraub, D., et al. (2017). Diagnosis and management of dementia with Lewy bodies: Fourth consensus report of the DLB Consortium. *Neurology* 89, 88–100. doi: 10.1212/WNL.0000000000004058
- mcr package | R Documentation (2021). *Method Comparison Regression v1.2.1*. Available online at: <https://www.rdocumentation.org/packages/mcr/versions/1.2.1> (accessed March 3, 2021)
- Molinie, J. L., Blennow, K., Dubois, B., Engelborghs, S., Lewczuk, P., Perret-Liaudet, A., et al. (2014). The clinical use of cerebrospinal fluid biomarker testing for Alzheimer's disease diagnosis: A consensus paper from the Alzheimer's Biomarkers Standardization Initiative. *Alzheimer's Dement.* 10, 808–817. doi: 10.1016/j.jalz.2014.03.003
- Paciotti, S., Sepe, F. N., Eusebi, P., Farotti, L., Cataldi, S., Gatticchi, L., et al. (2019). Diagnostic performance of a fully automated chemiluminescent enzyme immunoassay for Alzheimer's disease diagnosis. *Clin. Chim. Acta* 494, 74–78. doi: 10.1016/j.cca.2019.03.1612
- Passing, H., and Bablok. (1983). A new biometrical procedure for testing the equality of measurements from two different analytical methods. Application of linear regression procedures for method comparison studies in clinical chemistry, Part I. *J. Clin. Chem. Clin. Biochem.* 21, 709–720. doi: 10.1515/cclm.1983.21.11.709
- Paterson, R. W., Slattery, C. F., Poole, T., Nicholas, J. M., Magdalinos, N. K., Toombs, J., et al. (2018). Cerebrospinal fluid in the differential diagnosis of Alzheimer's disease: clinical utility of an extended panel of biomarkers in a specialist cognitive clinic. *Alzheimer's Res. Ther.* 10:32. doi: 10.1186/s13195-018-0361-3
- Pedregosa, F., Varoquaux, G., Gramfort, A., Michel, V., Thirion, B., Grisel, O., et al. (2011). Scikit-learn: Machine Learning in Python. *J. Machine Learning Res.* 12, 2825–2830.
- Postuma, R. B., Berg, D., Stern, M., Poewe, W., Olanow, C. W., Oertel, W., et al. (2015). MDS clinical diagnostic criteria for Parkinson's disease. *Mov. Disord.* 30, 1591–1601. doi: 10.1002/mds.26424
- R Core Team (2013). *R: A language and environment for statistical computing*. Vienna: R Core Team.
- Racine, A. M., Kosik, R. L., Berman, S. E., Nicholas, C. R., Clark, L. R., Okonkwo, O. C., et al. (2016). Biomarker clusters are differentially associated with longitudinal cognitive decline in late midlife. *Brain* 139, 2261–2274. doi: 10.1093/brain/aww142
- Rektor, I., Bohnen, N. I., Korczyn, A. D., Gryb, V., Kumar, H., Kramberger, M. G., et al. (2018). An updated diagnostic approach to subtype definition of vascular parkinsonism - Recommendations from an expert working group. *Parkinson. Relat. Disord.* 49, 9–16. doi: 10.1016/j.parkreldis.2017.12.030
- Relkin, N., Marmarou, A., Klinge, P., Bergsneider, M., and Black, P. M. (2005). Diagnosing idiopathic normal-pressure hydrocephalus. *Neurosurgery* 57, S4–S16. doi: 10.1227/01.neu.0000168185.29659.c5
- Robin, X., Turck, N., Hainard, A., Tiberti, N., Lisacek, F., Sanchez, J.-C., et al. (2011). pROC: an open-source package for R and S+ to analyze and compare ROC curves. *BMC Bioinformatics* 12:77. doi: 10.1186/1471-2105-12-77
- Rokach, L., and Maimon, O. (2005). "Clustering Methods," in *Data Mining and Knowledge Discovery Handbook*, eds O. Maimon and L. Rokach (Boston, MA: Springer), 321–352. doi: 10.1007/0-387-25465-X_15
- Román, G. C., Tatamichi, T. K., Erkinjuntti, T., Cummings, J. L., Masdeu, J. C., García, J. H., et al. (1993). Vascular dementia: diagnostic criteria for research studies. Report of the NINDS-AIREN International Workshop. *Neurology* 43, 250–260. doi: 10.1212/wnl.43.2.250
- Sawyer, R. P., Rodriguez-Porcel, F., Hagen, M., Shatz, R., and Espay, A. J. (2017). Diagnosing the frontal variant of Alzheimer's disease: a clinician's yellow brick road. *J. Clin. Mov. Disord.* 4:2. doi: 10.1186/s40734-017-0052-4
- Scheffer, I. E., Berkovic, S., Capovilla, G., Connolly, M. B., French, J., Guilhoto, L., et al. (2017). ILAE classification of the epilepsies: Position paper of the ILAE Commission for Classification and Terminology. *Epilepsia* 58, 512–521. doi: 10.1111/epi.13709
- Schwarz, G. (1978). Estimating the Dimension of a Model. *Ann. Statist.* 6, 461–464. doi: 10.1214/aos/1176344136
- Simrén, J., Ashton, N. J., Blennow, K., and Zetterberg, H. (2020). An update on fluid biomarkers for neurodegenerative diseases: recent success and challenges ahead. *Curr. Opin. Neurobiol.* 61, 29–39. doi: 10.1016/j.conb.2019.11.019
- Skillbäck, T., Farahmand, B. Y., Rosén, C., Mattsson, N., Nägga, K., Kilander, L., et al. (2015). Cerebrospinal fluid tau and amyloid- β 42 in patients with dementia. *Brain* 138, 2716–2731. doi: 10.1093/brain/awv181
- Smith, E. E., and Greenberg, S. M. (2003). Clinical diagnosis of cerebral amyloid angiopathy: validation of the Boston criteria. *Curr. Atheroscler. Rep.* 5, 260–266. doi: 10.1007/s11883-003-0048-4
- Solorio-Fernández, S., Carrasco-Ochoa, J. A., Martínez-Trinidad, J., and Fco. (2020). A review of unsupervised feature selection methods. *Artif. Intell. Rev.* 53, 907–948. doi: 10.1007/s10462-019-09682-y
- Teunissen, C. E., Petzold, A., Bennett, J. L., Berven, F. S., Brundin, L., Comabella, M., et al. (2009). A consensus protocol for the standardization of cerebrospinal fluid collection and biobanking. *Neurology* 73, 1914–1922. doi: 10.1212/WNL.0b013e3181c47cc2
- Thompson, A. J., Banwell, B. L., Barkhof, F., Carroll, W. M., Coetzee, T., Comi, G., et al. (2018). Diagnosis of multiple sclerosis: 2017 revisions of the McDonald criteria. *Lancet Neurol.* 17, 162–173. doi: 10.1016/S1474-4422(17)30470-2
- Toombs, J., Paterson, R. W., Schott, J. M., and Zetterberg, H. (2014). Amyloid-beta 42 adsorption following serial tube transfer. *Alzheimer's Res. Ther.* 6:5. doi: 10.1186/alzrt236
- Toschi, N., Lista, S., Baldacci, F., Cavedo, E., Zetterberg, H., Blennow, K., et al. (2019). Biomarker-guided clustering of Alzheimer's disease clinical syndromes. *Neurobiol. Aging* 83, 42–53. doi: 10.1016/j.neurobiolaging.2019.08.032
- Traynor, B. J., Codd, M. B., Corr, B., Forde, C., Frost, E., and Hardiman, O. M. (2000). Clinical features of amyotrophic lateral sclerosis according to the El Escorial and Airlie House diagnostic criteria: A population-based study. *Arch. Neurol.* 57, 1171–1176. doi: 10.1001/archneur.57.8.1171
- Villain, N., and Dubois, B. (2019). Alzheimer's Disease Including Focal Presentations. *Semin. Neurol.* 39, 213–226. doi: 10.1055/s-0039-1681041

Conflict of Interest: The authors declare that the research was conducted in the absence of any commercial or financial relationships that could be construed as a potential conflict of interest.

Copyright © 2021 Bellomo, Indaco, Chiasserini, Maderna, Paolini Paoletti, Gaetani, Paciotti, Petricciolo, Tagliavini, Giaccone, Parnetti and Di Fede. This is an open-access article distributed under the terms of the Creative Commons Attribution License (CC BY). The use, distribution or reproduction in other forums is permitted, provided the original author(s) and the copyright owner(s) are credited and that the original publication in this journal is cited, in accordance with accepted academic practice. No use, distribution or reproduction is permitted which does not comply with these terms.



Changes of Regional Neural Activity Homogeneity in Preclinical Alzheimer's Disease: Compensation and Dysfunction

Zhen Zhang^{1†}, Liang Cui^{1†}, Yanlu Huang¹, Yu Chen², Yuehua Li^{3*} and Qihao Guo^{1*}

¹ Department of Gerontology, Shanghai Jiao Tong University Affiliated Sixth People's Hospital, Shanghai, China, ² The Brain Cognition and Brain Disease Institute, Shenzhen Institute of Advanced Technology, Chinese Academy of Sciences, Shenzhen–Hong Kong Institute of Brain Science–Shenzhen Fundamental Research Institutions, Shenzhen, China, ³ Department of Radiology, Shanghai Jiao Tong University Affiliated Sixth People's Hospital, Shanghai, China

OPEN ACCESS

Edited by:

Sadayuki Hashioka,
Shimane University, Japan

Reviewed by:

Maria Aparecida Bicalho,
Federal University of Minas Gerais,
Brazil
Bin Zhang,
Guangzhou Medical University, China

*Correspondence:

Yuehua Li
liyuehua312@163.com
Qihao Guo
qhguo@sjtu.edu.cn

[†] These authors have contributed
equally to this work and share first
authorship

Specialty section:

This article was submitted to
Neurodegeneration,
a section of the journal
Frontiers in Neuroscience

Received: 26 December 2020

Accepted: 26 May 2021

Published: 17 June 2021

Citation:

Zhang Z, Cui L, Huang Y, Chen Y,
Li Y and Guo Q (2021) Changes
of Regional Neural Activity
Homogeneity in Preclinical
Alzheimer's Disease: Compensation
and Dysfunction.
Front. Neurosci. 15:646414.
doi: 10.3389/fnins.2021.646414

Introduction: Subjective cognitive decline (SCD) is the preclinical stage of Alzheimer's disease and may develop into amnesic mild cognitive impairment (aMCI). Finding suitable biomarkers is the key to accurately identifying SCD. Previous resting-state functional magnetic resonance imaging (rs-fMRI) studies on SCD patients showed functional connectivity disorders. Our goal was to explore whether local neurological homogeneity changes in SCD patients, the relationship between these changes and cognitive function, and similarities of neurological homogeneity changes between SCD and aMCI patients.

Materials and Methods: 37 cases of the healthy control (HC) group, 39 cases of the SCD group, and 28 cases of the aMCI group were included. Participants underwent rs-fMRI examination and a set of neuropsychological test batteries. Regional homogeneity (ReHo) was calculated and compared between groups. ReHo values were extracted from meaningful regions in the SCD group, and the correlation between ReHo values with the performance of neuropsychological tests was analyzed.

Results: Our results showed significant changes in the ReHo among groups. In the SCD group compared with the HC group, part of the parietal lobe, frontal lobe, and occipital lobe showed decreased ReHo, and the temporal lobe, part of the parietal lobe and the frontal lobe showed increased ReHo. The increased area of ReHo was negatively correlated with the decreased area, and was related to decrease on multiple neuropsychological tests performance. Simultaneously, the changed areas of ReHo in SCD patients are similar to aMCI patients, while aMCI group's neuropsychological test performance was significantly lower than that of the SCD group.

Conclusion: There are significant changes in local neurological homogeneity in SCD patients, and related to the decline of cognitive function. The increase of neurological homogeneity in the temporal lobe and adjacent area is negatively correlated with cognitive function, reflecting compensation for local neural damage. These changes in

local neurological homogeneity in SCD patients are similar to aMCI patients, suggesting similar neuropathy in these two stages. However, the aMCI group's cognitive function was significantly worse than that of the SCD group, suggesting that this compensation is limited. In summary, regional neural activity homogeneity may be a potential biomarker for identifying SCD and measuring the disease severity.

Keywords: subjective cognitive decline, mild cognitive impairment, regional homogeneity, resting-state functional MRI, cognitive function

INTRODUCTION

Alzheimer's disease (AD) is the most common cause of dementia in the elderly. The pathophysiological changes leading to AD have begun years or even decades before AD symptoms appear (Sperling et al., 2011). According to the recommendations from US National Institute on Aging-Alzheimer's Association (NIA-AA), the progress from normal to AD can be divided into three stages: (1) the preclinical stage, (2) the mild cognitive impairment (MCI) stage, and (3) dementia stage (Jack et al., 2011). In these stages, neuronal damage and cognitive decline progress continuously and irreversibly. Therefore, it is essential to identify potential patients with AD as early as possible.

Subjective cognitive decline (SCD) is considered the last stage of the preclinical stage of AD. SCD refers to individuals subjectively perceive the decline of their memory or other cognitive abilities compared with their previous cognitive ability (Jessen et al., 2014). The decline is gradually developed and not caused by any acute events, while there is no objective cognitive impairment. Performing neuropsychological testing on people with SCD will find that they do not meet the MCI diagnostic criteria. At this stage, individuals suffer only mild neuropathological damage and still have a considerable cognitive reserve; therefore, SCD is considered a critical window for intervention to prevent individuals from progressing to AD (Jessen et al., 2014; Rabin et al., 2017).

If the neuropathological changes continue to deteriorate, individuals with SCD may progress to MCI. MCI is an early but objective state of cognitive impairment (Petersen, 2004; Albert et al., 2011), in which the amnesic mild cognitive impairment (aMCI) subtype is closely related to AD. The aMCI patients' general cognitive function is impaired, with memory function as the primary manifestation. Although still retain roughly intact functional activities, patients with aMCI have a high conversion rate to AD (Mitchell and Shiri-Feshki, 2009).

To accurately identify potential AD patients, it is necessary to select appropriate biomarkers, which is particularly important for SCD patients because they have no obvious

abnormal neuropsychological test performance at this stage. At present, the core biomarkers in AD are mainly divided into cerebrospinal fluid and imaging biomarkers (Scheltens et al., 2016). cerebrospinal fluid biomarkers mainly including A β 42, total tau, and phosphorylated tau, while imaging biomarkers mainly including A β 42 and tau PET CT. The biomarkers in cerebrospinal fluid have good sensitivity (Shaw et al., 2009; Visser et al., 2009) but can only be detected by invasive examination, making it difficult for these biomarkers to be widely used. Therefore, we need more non-invasive markers. Resting-state functional magnetic resonance imaging (rs-fMRI) is a method to explore the functional activity of the brain; much progress has been made in the use of rs-fMRI in the fields of MCI and AD, proving that there are significant brain function changes in these stages (Pan et al., 2017; Bi et al., 2020a,b; Moguilner et al., 2020). In the field of SCD, rs-fMRI has also been used, mainly focused on brain network connectivity changes. A previous study (Dillen et al., 2017) has shown that the functional connectivity among nodes in the default mode network of SCD patients is weakened; the connectivity between the default mode network and hippocampus is also affected. These changes in connectivity are related to the decline of memory ability. Another study (Viviano et al., 2019) found that the posterior memory network's connectivity in patients with SCD also decreased, but no significant changes were found in simultaneous diffusion-weighted image analysis. A study of SCD using machine learning (Yan et al., 2019) confirmed changes in the default network connectivity and found changes in the subcortical structure network. Based on these studies on large-scale network connectivity, a recent study (Wang et al., 2019) went one step further and found primary medium-scale network damage in SCD patients. Some studies found the correlation between rs-fMRI and classical pathological biomarkers in the preclinical stage of AD, which suggest that fMRI can be considered a potential imaging biomarker. A study using amyloid-PET, FDG-PET, and fMRI found left frontal cortex connectivity underlies cognitive reserve in prodromal Alzheimer disease, suggested that functional changes in the prodromal stage of AD are consistent with the pathological changes (Franzmeier et al., 2017). Another study on MCI found a correlation between local functional activity and the A β /p Tau ratio of cerebrospinal fluid, which may be a sensitive indicator of AD pathology (Ren et al., 2016). Using machine learning to analyze the fMRI and cerebrospinal fluid biomarkers of SCD individuals in the ADNI database, researchers found that

Abbreviations: SCD, subjective cognitive decline; aMCI, amnesic mild cognitive impairment; Rs-fMRI, resting-state functional magnetic resonance imaging; ReHo, regional homogeneity; AD, Alzheimer's disease; MMSE, Mini-Mental State Examination; ACE-III, Addenbrooke's Cognitive Examination; MoCA-B, Montreal Cognitive Assessment-Basic; AVLT, Auditory Verbal Learning Test; BVMPT, Brief Visuospatial Memory Test; AFT, Animal Verbal Fluency Test; BNT, Boston Naming Test; ST, Silhouettes Test; STT, Shape Trail Test; JLO, Judgment of Line Orientation; DST, Digit Span Test; MNI, Montreal Neurological Institute; ROI, Region of interest; DRR, decreased ReHo region; IRR, increased ReHo region; AAL, anatomical automatic labeling atlas.

SCD individuals showed higher nodal topological properties associated with A β levels and memory function, suggested the compensatory mechanism of the functional connectivity (Chen et al., 2020). A subsequent RS-fMRI study based on the DELCODE cohort suggested that local brain function changes in patients with SCD were associated with A β load (Li et al., 2021).

Previous studies have revealed changes in the strength of connectivity in SCD patients but did not explain why these changes occur. To explore the possible mechanisms behind connectivity changes, we first need to find a suitable local brain function indicator. Regional homogeneity (ReHo) (Zang et al., 2004) is a stable indicator to detect regional synchronization and can be used to evaluate the regional neural activity homogeneity. Using Kendall's coefficient concordance, ReHo can evaluate the time series similarity between local voxels and adjacent voxels. The abnormality of ReHo, including decrease or increase, may reflect the disorder and compensation of local brain function and may explain the internal cause of whole-brain network disorder (Zuo et al., 2013; Xiong et al., 2020). With these characteristics, ReHo is a very suitable indicator to study the local brain function changes in patients with SCD. In addition, A regional functional synchronization study found that ReHo might have distinctive association patterns with A β retention in elders with normal cognitive (Kang et al., 2017). By measuring ReHo and biomarkers, researchers found the ReHo in different regions of aMCI patients is related to cognitive function and cerebrospinal fluid A β 42 level (Luo et al., 2018). These studies suggested that in the preclinical stage of AD, regional neural activity homogeneity may be related to pathological changes to some extent.

The aim of this study was to reveal the regional neural activity homogeneity changes in patients with SCD and the significance of these changes. We used rs-fMRI ReHo to compare the differences between SCD patients and normal subjects. In order to verify whether SCD is a preclinical stage of AD, we also included patients with aMCI for the same analysis to find out whether there is a similarity between the SCD and aMCI groups. In order to clarify the relationship between regional neural activity homogeneity and cognitive function, we used a variety of neuropsychological tests to analyze the correlation with ReHo.

Based on the current existing facts: (1) SCD is a preclinical state of neurodegenerative disease; there are local neuropathological changes at this stage, and (2) the neuropsychological manifestations of SCD patients are still roughly within the normal range. We make the following hypothesis: (1) there are corresponding changes in regional brain function in patients with SCD, and the scope of this change is large enough to affect large-scale brain functional connectivity; (2) generally normal cognitive function in SCD patients may be due to a certain degree of functional compensation; (3) as the precursor stage of aMCI, the changes of regional brain function in SCD may be similar to aMCI to some extent; (4) in patients with SCD, there may be a correlation between their cognitive ability and these regional brain function changes, which will lead to a gradual decline in their cognitive function if the changes continue to progress.

MATERIALS AND METHODS

Participants

Participants were recruited from the community through advertising between August 2018 to November 2019. The recruitment was carried out in the neuropsychological testing room of the Department of Geriatrics, Shanghai Jiao Tong University Affiliated Sixth People's Hospital, Shanghai, China. A total of 104 participants were included.

The Healthy Control Group (HC Group)

HCs were additionally required to have no significant impairment in cognitive function, no memory complaints or memory loss observed, MMSE score \geq the cutoff (Katzman et al., 1988), a CDR score of 0 (Morris, 1993), and a Hamilton Depression Rating Scale score of 12 or less in the past 2 weeks (Worboys, 2013). MRI manifestations: no key parts such as thalamus and hippocampal infarction; no white matter damage (Fazekas Scale \geq 3) (Fazekas et al., 1987).

Thirty-seven healthy participants were classified as the HC group [15 men; age: mean = 63.86 years, standard deviation (SD) = 8.25 years; the number of years of full-time education: mean = 12.11 years, SD = 3.42 years; Mini-Mental State Examination (MMSE): mean = 28.57, SD = 1.21].

The Subjective Cognitive Decline Group (SCD Group)

The diagnosis criteria of SCD was based on features referred to SCD plus (preclinical AD) (Jessen et al., 2014): (a) subjective decline in memory, rather than other domains of cognition; (b) onset of SCD with the last five years; (c) concerns (worries) associated with SCD; (d) feeling of worse performance than others of the same age group; (e) normal performance on Neuropsychological scale and did not reach the criteria for MCI or dementia. We used the SCD-initiative (SCD-I) framework to include individuals with SCD (Jessen et al., 2018; Miebach et al., 2019), who have the following performance: Reported subjective cognitive decline (worse than peers) and worried about it; the first occurrence of subjective cognitive decline was less than 5 years before the interview; after adjusting for age, sex and education, compared with HCs, the score difference of each test in the neuropsychological battery was less than 1.5 standard deviations.

Thirty-nine patients diagnosed with SCD were included (14 men; age: mean = 64.56 years, SD = 7.34 years; number of years of full-time education: mean = 11.69 years, SD = 3.30 years; MMSE: mean = 27.90, SD = 1.94).

The Amnesic Mild Cognitive Impairment (aMCI Group)

The inclusion criteria for aMCI was referred from the criteria proposed by Jak/Bondi (Bondi et al., 2014): (1) Cognitive concern or complaints by the subject, informant, nurse, or physician during the last year; (2) Mini-Mental State Examination (MMSE) above cut-off ($> 24/30$); (3) objective memory impairment assessment by long-delay free recall and recognition of Auditory Verbal Learning Test (AVLT) in at

least 1.0 standard deviation (SD) below the norm for age and education; (4) Maintained activities of daily living or slight impairment in instrumental activities of daily living, in other words, no more than one item from the Activities of Daily Living Scale (ADL)-Chinese version suffered obvious changes; (5) Absence of dementia, according to the NIA-AA criteria.

Twenty-eight patients diagnosed with aMCI were included (13 men; age: mean = 65.71 years, SD = 6.90 years; number of years of full-time education: mean = 12.19 years, SD = 3.16 years; MMSE: mean = 27.07, SD = 1.72).

The Exclusion Criteria

The exclusion criteria were: (a) patients diagnosed or with a history of head injury, head surgery, mental diseases, brain tumors, acute cerebral hemorrhage, cerebral ischemia, non-degenerative brain injury; (b) patients with severe visual or hearing impairment; and (c) patients who could not undergo MRI. To exclude other possible causes for the amnesic impairment, each subject had a uniform structured evaluation performed by a neurologist, which included a medical history inquiry and neurological examination. Blood tests included complete blood count, thyroid function tests, serum vitamin B12, and Venereal Disease Research Laboratories test.

Neuropsychological Assessments

All participants underwent extensive neuropsychological tests, included: MMSE (total score: 30) (Folstein et al., 1975), Addenbrooke's Cognitive Examination (ACE-III) (total score: 100) (Mioshi et al., 2006), Montreal Cognitive Assessment-Basic (MoCA-B) (total score: 30) (Huang et al., 2018b), Auditory Verbal Learning Test (AVLT) (score: 12 per round, immediate recall score equals the sum of the first, second and third recall scores, recognition score: 24) (Zhao et al., 2015), Brief Visuospatial Memory Test (BVMt) (score: 12 per round, immediate recall score equals the sum of the first, second and third recall scores) (Pliskin et al., 2020), Animal Verbal Fluency Test (AFT) (Zhao et al., 2013a), Boston Naming Test (BNT) (total score: 30) (Mack et al., 1992), Silhouettes Test (ST) (total score: 15) (Huang et al., 2018a), Shape Trail Test (STT) (Zhao et al., 2013b), Stroop Test (total score: 24) (Chen et al., 2019), Judgment of Line Orientation (JLO) (total score: 30) (Qualls et al., 2000), and Digit Span Test (DST) (sequence score: 12; reverse score: 10) (Johansson and Berg, 1989).

Functional Magnetic Resonance Imaging Image Acquisition

Resting-state fMRI was performed with a 3.0-Tesla scanner (SIEMENS MAGNETOM Prisma 3.0T, Siemens, Erlangen, Germany). parameters were: echo-planar imaging (EPI) sequence, transverse plane, repetition time = 800 ms, echo time = 37 ms, flip angle = 52°, matrix size = 104 × 104, field of view = 208 mm × 208 mm, slice number = 72 slices, slice thickness = 2 mm, and voxel size = 2 mm × 2 mm × 2 mm. The scan obtained 488 slices and took a total of 404 s. During

the entirety of the scan, the participants were asked to lie in the scanner, close their eyes but not fall asleep, try to keep their heads still, and not to think systematically.

TABLE 1 | Demographic data and neuropsychological tests between groups.

	HC (n = 37)	SCD (n = 39)	aMCI (n = 28)	Test statistic
Age (year) ^a	63.86 ± 8.25	64.56 ± 7.337	65.71 ± 6.895	0.478
Sex ^b	Male = 15	Male = 14	Male = 13	0.751
Edu years (year) ^a	12.108 ± 3.422	11.692 ± 3.300	12.185 ± 3.1627	0.227
Hypertension ^b	24.3%	28.2%	32.1%	0.488
Hyper-cholesterolemia ^b	8.1%	12.8%	10.7%	0.447
Diabetes ^b	13.5%	10.2%	14.3%	0.296
General cognitive function				
MMSE ^c	29 (28,30)	28 (27,29)	27 (26,28)*	12.069
ACE-III ^c	87 (82.5,90.5)	82 (77,86)*	75 (73,81)**†	26.792
MoCA-B ^c	27 (26,28)	26 (23,28)	23 (22,25)**†	25.177
Memory function				
AVLT immediate recall ^c	18 (15.5,20.5)	19 (15,21)	12 (11,14)**†	37.136
AVLT 4th recall ^c	6 (5,8)	6 (5,8)	3 (2,2.75)**†	47.123
AVLT 5th recall ^c	6 (4.5,7.5)	6 (5,7)	2 (1,3)**†	49.797
AVLT 6th recall ^c	6 (5,7.5)	5 (4,7)	2 (2,3)**†	44.665
AVLT recognition ^c	22 (21,23)	22 (21,24)	18 (16,18.75)**†	55.987
BVMT immediate recall ^c	22 (16.5,26)	21 (17,25)	18 (14.25,20.75)*	6.586
BVMT 4th recall ^c	10 (7.5,11.5)	10 (8,11)	8 (5.25,10)	6.074
BVMT 5th recall ^c	10 (8,11.5)	10 (8,11)	8 (5.25,10)	6.269
BVMT 6th recall ^c	5 (5,6)	5 (5,6)	4 (4,4)**†	23.940
BVMT recognition ^c	12 (12,12)	12 (12,12)	12 (10,12)**†	20.005
Language function				
AFT ^c	19 (18.5,21.0)	17 (15,20)*	16 (14,17.75)**	16.042
BNT ^c	26 (24,27)	24 (22,27)	23 (21.25,26)*	6.542
Executive function				
STT-A total time (sec) ^c	40 (34,51)	44 (36,55)	52.5 (39.25,61.25)*	8.225
STT-B total time (sec) ^c	113 (89,137)	116 (95,136)	127.5 (109.25,171.00)	
Stroop test A ^c	24 (24,24)	24 (24,24)	24 (24,24)	1.829
Stroop test B ^c	24 (23,24)	24 (23,24)	23 (20,24)	11.985
Spatial Function				
ST ^a	10.5 ± 2.61	9.7 ± 2.46	10.0 ± 2.16	1.206
JLO ^a	21.2 ± 5.04	20.7 ± 4.82	21.4 ± 4.32	0.186
Attention function				
DST sequence ^c	8 (7.5,8.5)	8 (6,8)	7 (5,8)*	8.837
DST reverse ^c	5 (4,6)	5 (4,5)	4.5 (4,5)	3.137

^aANOVA test, ^bChi-square test; ^cKruskal-Wallis H-test; *compared with HC group, $p < 0.05$; **compared with HC group, $p < 0.001$; †compared with SCD group, $p < 0.05$; ‡compared with SCD group, $p < 0.001$. MMSE, Mini-Mental State Examination. ACE-III, Addenbrooke's Cognitive Examination. MoCA-B, Montreal Cognitive Assessment-Basic. AVLT, Auditory Verbal Learning Test. BVMT, Brief Visuospatial Memory Test. AFT, Animal Verbal Fluency Test. BNT, Boston Naming Test. STT, Shape Trail Test. ST, Silhouettes Test. JLO, Judgment of Line Orientation. DST, Digit Span Test.

Imaging Data Processing

The data were processed using Statistical Parametric Mapping 12 (SPM12)¹ and RESTplus² toolkits (Jia et al., 2019). In order to stabilize the magnetic field of the MRI scanner and allow the participant to adapt to the noise, the first 20 time points were removed. Next, the following preprocessing steps were carried out: slice timing to correct differences in image acquisition time between slices, realignment for the correction of head motion (excessive head movement: ≥ 3 mm or 3°), spatially normalized to the Montreal Neurological Institute (MNI) space and resampled to 3 mm isotropic voxels, remove linear and quadratic trends of the time-series signals, regress out the white matter, cerebrospinal fluid, global mean signal, and Friston-24 motion parameters, and band-pass (0.01–0.08 Hz) filter.

The ReHo was obtained by calculating the Kendall coordination coefficient of the time process for each of the 27 nearest neighboring voxels and then standardized by dividing each voxel's value by the global average. Finally, the standardized mean ReHo graphs were spatially smoothed using a Gaussian kernel (FWHM = 6 mm).

Statistical Analysis

SPSS (IBM SPSS Statistics, Version 26.0. IBM Corp, Armonk, NY, United States) software was used to analyze demographic data and neuropsychological test scores. Data were tested for normality using a Shapiro-Wilk normality test. Normally distributed data were presented as means \pm SD. The non-normally distributed data were expressed as the median (quartile range). Pearson Chi-Square test was used to test the differences for sex, hypertension, hypercholesterolemia, and diabetes. The analysis of variance (ANOVA) was used to analyze the age, education years, and neuropsychological test scores conformed to normality among the three groups. For neuropsychological test scores that do not conform to the normal distribution, a non-parametric test (Kruskal-Wallis H-test) was performed among the three groups. In *post-hoc* analysis, Bonferroni's correction was applied when multiple comparisons were performed. To

analyze the correlation between neuropsychological tests and ReHo values, we conducted Spearman rank correlation analysis.

SPM12 was used to establish a statistical model to analyze the differences in ReHo. ANOVA analysis was carried out among the three groups to determine the areas where there were differences. The independent-sample *t*-test was then carried out for comparing ReHo between the SCD group with the HC group and the aMCI group with the HC group. False Discovery Rate (FDR) correction for multiple comparisons was performed ($p < 0.001$, $k > 10$ voxels) using RESTplus toolkits. To separately show the differences between the SCD group compared with the HC group and the aMCI group compared with the HC group, we performed whole-brain two-sample *t*-tests. In order to display the results of two *t*-tests together without increasing the false-positive rate, the FDR correction threshold was adjusted to 0.0005.

Compared with the HC group, the significant clusters that survived after the multiple comparison correction were defined as regions of interest (ROIs). If only one cluster survived, it was considered the significant cluster and chosen as ROI. If multiple clusters survived, the cluster with the highest peak *t*-value and the largest volume was considered the most significant and was defined as the ROI. The ReHo values of ROIs were extracted and used for Spearman rank correlation analysis.

The imaging results were visualized using BrainNet Viewer³ (Xia et al., 2013) and RESTplus.

RESULTS

Demographic Data and Neuropsychological Performances

Comparison of Demographic Data Between Groups

There were no statistical differences in age, sex, and education years among the three groups. There were no statistical differences in hypertension (24.3% in HC group, 28.2% in SCD group, 32.1% in aMCI group), hypercholesterolemia (8.1% in HC group, 12.8% in SCD group, 10.7% in aMCI group), and diabetes

¹<http://www.fil.ion.ucl.ac.uk/spm/software/spm12/>

²<http://restfmri.net/forum/restplus>

³<http://www.nitrc.org/projects/bnv/>

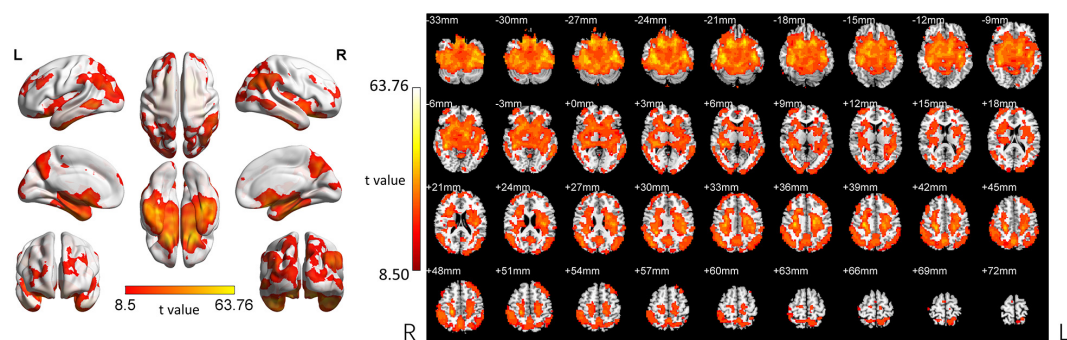


FIGURE 1 | ANOVA revealed differences among the three groups. ReHo was significantly different among the three groups (Two-tailed ANOVA-test; FDR $p < 0.001$, $k > 10$ voxels). ANOVA, one way analysis of variance. The color bars indicate *t*-values, blue color represents negative values and red color represents positive values. L, Left; R, Right.

(13.5% in HC group, 10.2% in SCD group, 14.3% in aMCI group) among the three groups.

Comparison of Neuropsychological Performance Between Groups

Multi-group comparisons found differences in MMSE, ACE-III, MoCA-B, AVLT immediate recall, AVLT 4th recall, AVLT 5th recall, AVLT 6th recall, AVLT recognition, BVMT immediate recall, BVMT 6th recall, BVMT recognition, AFT, BNT, STT-A total time, and DST sequence (Table 1). There were no significant difference between the three groups in BVMT-4th recall, BVMT-5th recall, ST, STT-B total time, JLO (Table 1). *Post-hoc* analysis with Bonferroni's correction was conducted to confirm differences occurred between groups.

Comparison between the SCD group and the HC group

In the following neuropsychological tests, there were significant differences between the SCD group and the HC group: ACE-III [82 (77, 86) vs. 87 (82.5, 90.5), $p = 0.002$], VFT [17 (15, 20) vs. 19 (18.5, 21.0), $p = 0.002$] (Table 1).

Comparison between the aMCI group and the HC group

In the following neuropsychological tests, there were significant differences between the aMCI group and the HC group: MMSE [27 (26, 28) vs. 29 (28, 30), $p = 0.002$], ACE-III [75 (73, 81) vs. 87 (82.5, 90.5), $p = 0.000$], MoCA-B [23 (22, 25) vs. 27 (26, 28), $p = 0.000$], AVLT immediate recall [12 (11, 14) vs. 18 (15.5, 20.5), $p = 0.000$], AVLT 4th recall [3 (2, 2.75) vs. 6 (5, 8), $p = 0.000$], AVLT 5th recall [2 (1, 3) vs. 6 (4.5, 7.5), $p = 0.000$], AVLT 6th recall [2 (2, 3) vs. 6 (5.0, 7.5), $p = 0.000$], AVLT recognition [18 (16, 18.75) vs. 22 (21, 23), $p = 0.000$], BVMT immediate recall [18 (14.25, 20.75) vs. 22 (16.5, 26), $p = 0.036$], BVMT-6th recall [4 (4, 4) vs. 5 (5, 6), $p = 0.000$], BVMT-recognition [12 (10, 12) vs. 12 (12, 12), $p = 0.000$], VFT [16 (14, 17.75) vs. 19 (18.5, 21.0), $p = 0.000$], BNT [23 (21.25, 26) vs. 26 (24, 27), $p = 0.033$], DST-sequence [7 (5, 8) vs. 8 (7.5, 8.5), $p = 0.015$] (Table 1).

Comparison between the aMCI group and the SCD group

In the following neuropsychological tests, there were significant differences between the aMCI group and the SCD group: ACE-III [75 (73, 81) vs. 82 (77, 86), $p = 0.021$], MoCA-B [23 (22, 25) vs. 27 (26, 28), $p = 0.007$], AVLT immediate recall [12 (11, 14) vs. 19 (15, 21), $p = 0.000$], AVLT 4th recall [3 (2, 2.75) vs. 6 (5, 8), $p = 0.000$], AVLT 5th recall [2 (1, 3) vs. 6 (5, 7), $p = 0.000$], AVLT 6th recall [2 (2, 3) vs. 6 (4, 7), $p = 0.000$], AVLT recognition [18 (16, 18.75) vs. 22 (21, 24), $p = 0.000$], BVMT-6th recall [4 (4, 4) vs. 5 (5, 6), $p = 0.000$], BVMT-recognition [12 (10, 12) vs. 12 (12, 12), $p = 0.001$], STT-A total time [52.5 (39.25, 61.25) vs. 40 (34, 51), $p = 0.012$] (Table 1).

rs-fMRI ReHo

ANOVA Analysis

ReHo was significantly different between the three groups. The ANOVA showed that the differential brain regions were located in Temporal_Inf_L/R, Fusiform_L/R, Temporal_Sup_L/R, Insula_L/R, ParaHippocampal_L/R, Temporal_Pole_Sup_L/R, Hippocampus_L/R, Frontal_Inf_Orb_L/R, Temporal_Mid_L/R,

TABLE 2 | ANOVA revealed differences among three groups.

CLUSTER (AAL)	Volume (voxels)	CLUSTER (AAL)	Volume (voxels)
Cluster 1	Total: 22,347	Cluster 2	Total: 6,158
Peak (MNI): 39 -18 -24	Peak t: 63.7643	Peak (MNI): 3 -66 45	Peak t: 41.1763
Temporal_Inf_L	584	Precuneus_L	499
Temporal_Inf_R	495	Occipital_Mid_L	448
Fusiform_R	458	Precuneus_R	448
Fusiform_L	438	Angular_R	408
Temporal_Sup_L	392	Occipital_Mid_R	328
Insula_R	358	Temporal_Mid_R	315
Insula_L	340	Parietal_Inf_R	311
ParaHippocampal_R	325	Temporal_Mid_L	311
Cerebellum_4_5_L	315	Parietal_Inf_L	271
Cerebellum_6_R	299	SupraMarginal_R	244
ParaHippocampal_L	283	Parietal_Sup_L	235
Temporal_Pole_Sup_L	274	Angular_L	233
Hippocampus_R	268	Parietal_Sup_R	216
Hippocampus_L	267	Occipital_Sup_R	191
Frontal_Inf_Orb_L	251	Cuneus_R	168
Cerebellum_6_L	244	Cuneus_L	155
Frontal_Inf_Orb_R	242	Occipital_Sup_L	153
Temporal_Mid_L	228	Postcentral_R	110
Putamen_L	227		
Temporal_Sup_R	215		
Putamen_R	214		
Cerebellum_4_5_R	196		
Caudate_R	185		
Caudate_L	184		
Temporal_Pole_Sup_R	179		
Postcentral_L	172		
Rolandic_Oper_L	160		
Precentral_L	158		
Frontal_Sup_Orb_R	127		
Rectus_R	117		
Temporal_Pole_Mid_R	112		
Frontal_Sup_Orb_L	100		

ANOVA, one way analysis of variance. AAL, anatomical automatic labeling atlas. MNI, Montreal Neurological Institute space. Only clusters of more than 100 voxels were reported.

Putamen_L/R, Caudate_L/R, Postcentral_L/R, Rolandic_Oper_L, Precentral_L, Frontal_Sup_Orb_L/R, Rectus_R, Temporal_Pole_Mid_R, Precuneus_L/R, Occipital_Mid_L/R, Angular_L/R, Parietal_Inf_L/R, SupraMarginal_R, Parietal_Sup_L/R, Occipital_Sup_L/R, and Cuneus_L/R (Two-tailed ANOVA-test; FDR $p < 0.001$, $k > 10$ voxels) (Figure 1 and Table 2).

The SCD Group Compared With the HC Group

In the following areas, the ReHo of the SCD group decreased compared to the HC group: Occipital_Mid_L/R, Precuneus_R, Angular_L/R, Parietal_Inf_L/R, Temporal_Mid_L/R, Parietal_Sup_L/R, SupraMarginal_R, Occipital_Sup_L/R, Cuneus_L, Frontal_Mid_L/R, Frontal_Sup_L/R, and Frontal_Sup_Medial_L (Two-tailed, FDR $p < 0.001$, $k > 10$ voxels) (Figure 2 and Table 3). In the following areas, the ReHo of the SCD

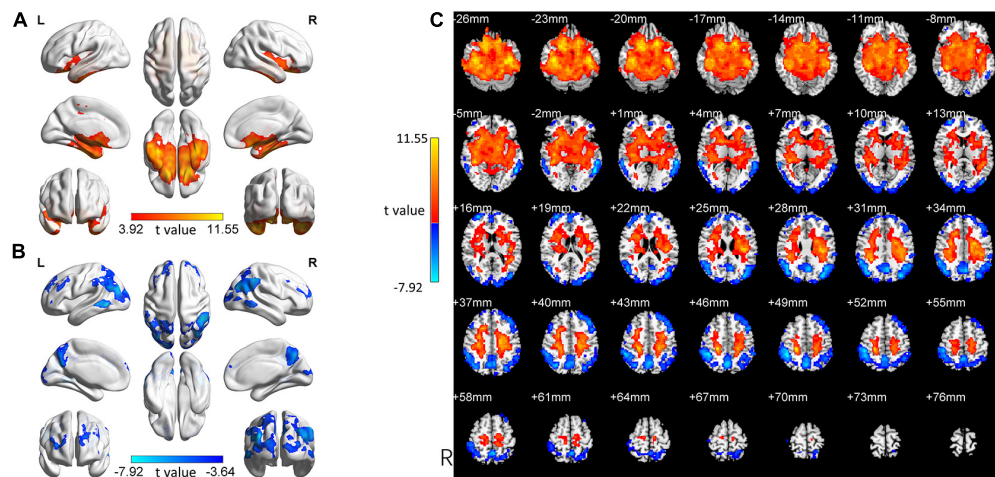


FIGURE 2 | Changed ReHo in the SCD group compared with the HC group. **(A)** The brain regions with increased ReHo in the SCD group compared with the HC group. **(B)** The brain regions with decreased ReHo in the SCD group compared with the HC group. **(C)** Brain regions with increased and decreased ReHo in the SCD group compared with the HC group. Two-tailed t -test; FDR < 0.0005 , $k > 10$ voxels. The color bars indicate t -values, blue color represents negative values and red color represents positive values. L, Left; R, Right.

group increased compared to the HC group: Temporal_Inf_L/R, Fusiform_L/R, Temporal_Sup_L/R, Insula_L/R, ParaHippocampal_L/R, Hippocampus_L/R, Frontal_Inf_Orb_L/R, Temporal_Pole_Sup_L/R, Putamen_L/R, Temporal_Mid_L, Caudate_L/R, Postcentral_L, Rolandic_Oper_L, Precentral_L, Frontal_Sup_Orb_R, Rectus_R, and Temporal_Pole_Mid_R (Two-tailed, FDR $p < 0.0005$, $k > 10$ voxels) (Figure 2 and Table 4).

The aMCI Group Compared With the HC Group

Comparing the aMCI group with the HC, the brain area with ReHo changes was very similar to the SCD group (Tables 3, 4).

In the following areas, the ReHo of the aMCI group decreased compared to the HC group: Frontal_Mid_L/R, Frontal_Sup_L/R, Precuneus_L, Angular_L/R, Precuneus_R, Parietal_Inf_L/R, Temporal_Mid_L/R, Occipital_Mid_L, SupraMarginal_R, Occipital_Mid_R, Parietal_Sup_L/R, Occipital_Sup_L/R, and Cuneus_R (Two-tailed, FDR $p < 0.001$, $k > 10$ voxels) (Figure 3 and Table 3). Bonferroni's correction was used for *Post-hoc* analyses. In the following areas, the ReHo of the aMCI group increased compared to the HC group: Temporal_Inf_L/R, Fusiform_L/R, Temporal_Sup_L/R, Insula_L/R, ParaHippocampal_L/R, Temporal_Pole_Sup_L/R, Hippocampus_L/R, Frontal_Inf_Orb_L/R, Putamen_L/R, Temporal_Mid_L, Caudate_L/R, Postcentral_L, Frontal_Sup_Orb_L/R, Precentral_L, Rectus_R, Rolandic_Oper_L, and Temporal_Pole_Mid_R (Two-tailed, FDR $p < 0.0005$, $k > 10$ voxels) (Figure 3 and Table 4).

Similarity Between the aMCI Group and the SCD Group

Our study focused on comparing the SCD group and the aMCI group with the HC group to explore the change patterns of these two groups (SCD and aMCI group). We visually observed the

change patterns in the SCD group and the aMCI group and found these two groups were very similar (Figures 2, 3).

Correlation Analysis

Define ROI

In the SCD group, the significant cluster with increased ReHo (Table 3, SCD group $>$ HC group, cluster 1, peak coordinate: -42 -18 -24) was defined as increased ReHo ROI (IRR). The most significant cluster with decreased ReHo (Table 4, SCD group $<$ HC group, cluster 1, Peak coordinate: 45 -45 48) was defined as decreased ReHo ROI (DRR). The ReHo values of these two ROIs were extracted and analyzed with spearman rank correlation.

Correlation Between ReHo With Neuropsychological Performances

The ReHo value of DRR and IRR was significantly negatively correlated ($r = -0.517$, $p = 0.001$) (Spearman rank correlation, two-tailed) (Figure 4). The ReHo value of DRR was significantly positively correlated with AFT ($r = 0.352$, $p = 0.028$) (Spearman rank correlation, two-tailed) (Figure 4). The ReHo value of IRR was significantly negatively correlated with ACE-III ($r = -0.456$, $p = 0.004$), MoCA-B ($r = -0.351$, $p = 0.028$), BVMT immediate recall ($r = -0.352$, $p = 0.044$), BVMT 4th recall ($r = -0.337$, $p = 0.036$), BVMT 5th recall ($r = -0.370$, $p = 0.021$), BVMT recognition ($r = -0.433$, $p = 0.006$), AFT corrections ($r = -0.397$, $p = 0.012$), ST ($r = -0.433$, $p = 0.006$), JLO ($r = -0.353$, $p = 0.027$), DST sequence ($r = -0.416$, $p = 0.008$) (Spearman rank correlation, two-tailed) (Figure 4).

DISCUSSION

Prior studies have noted the importance of SCD. Although it is generally believed that neuropathological changes have occurred

TABLE 3 | Brain regions with decreased ReHo in the SCD group and the aMCI group compared to the HC group.

SCD group < HC group		aMCI group < HC group	
Cluster (AAL)	Volume (voxels)	Cluster (AAL)	Volume (voxels)
Cluster 1	Total: 5122	Cluster 1	Total: 889
Peak (MNI): 45 -45 48	Peak t: -7.9188	Peak (MNI): 48 24 36	Peak t: -7.4097
Precuneus_L	446	Frontal_Mid_R	423
Occipital_Mid_L	412	Frontal_Sup_R	219
Precuneus_R	382	Cluster 2	total: 4706
Angular_R	348	Peak: 3 -63 45	Peak t: -9.9902
Parietal_Inf_L	328	Precuneus_L	429
Parietal_Inf_R	306	Angular_R	408
Temporal_Mid_R	270	Precuneus_R	393
Temporal_Mid_L	267	Parietal_Inf_R	282
Occipital_Mid_R	261	Temporal_Mid_L	277
Parietal_Sup_L	244	Occipital_Mid_L	257
Angular_L	223	SupraMarginal_R	250
SupraMarginal_R	178	Angular_L	224
Parietal_Sup_R	154	Temporal_Mid_R	211
Occipital_Sup_R	135	Occipital_Mid_R	187
Cuneus_L	124	Parietal_Inf_L	174
Occipital_Sup_L	110	Parietal_Sup_R	148
Cluster 2	total: 503	Parietal_Sup_L	142
Peak: 33 57 15	Peak t: -7.0202	Occipital_Sup_L	133
Frontal_Mid_R	321	Occipital_Sup_R	125
Frontal_Sup_R	106	Cuneus_R	121
Cluster 3	total: 1021	Cluster 3	total: 527
Peak: -42 30 39	Peak t: -6.6576	Peak (MNI): -42 33 36	Peak t: -6.5666
Frontal_Mid_L	352	Frontal_Mid_L	273
Frontal_Sup_L	172	Frontal_Sup_L	101
Frontal_Sup_Medial_L	144		

AAL, anatomical automatic labeling atlas. MNI, Montreal Neurological Institute space. Only clusters of more than 100 voxels were reported.

at this stage, it is still difficult to detect such changes non-invasively. The first question in this study sought to determine is whether it is possible to find changes in neural activity homogeneity in the brains of SCD patients and the characteristics of these changes in different brain regions. If these changes did exist, the second question this study aimed to address was whether they were associated with cognitive decline. The third question we wanted to discuss was the similarity and significance of these changes in patients with SCD and aMCI. Regarding the first question, we found that in SCD patients, there were increased and decreased ReHo in several brain regions, suggesting that these regions had changed neurological activity homogeneity. Besides, there was a correlation between the increased and decreased areas of ReHo. On the second question, we found correlation between changed ReHo and neuropsychological performance, suggesting that the homogeneity of neural activity may be related to cognitive ability. At last, it was worth noting that the areas with changed ReHo in the SCD group were quite similar to the aMCI patients. These results suggest that regional neural activity homogeneity may be a potential biomarker for identifying SCD and measuring the disease severity.

TABLE 4 | Brain regions with increased ReHo in the SCD group and the aMCI group compared to the HC group.

SCD group > HC group		aMCI group > HC group	
Cluster (AAL)	Volume (voxels)	Cluster (AAL)	Volume (voxels)
Cluster 1	Total: 21,873	Cluster 1	Total: 22,001
Peak (MNI): -42 -18 -24	Peak t: 11.5543	Peak (MNI): 36 -33 -24	Peak t: 11.7286
Temporal_Inf_L	558	Temporal_Inf_L	590
Fusiform_R	452	Temporal_Inf_R	486
Temporal_Inf_R	438	Fusiform_R	442
Fusiform_L	432	Fusiform_L	413
Temporal_Sup_L	379	Temporal_Sup_L	359
Insula_R	344	Insula_R	319
Insula_L	318	ParaHippocampal_R	310
Cerebelum_4_5_L	311	Cerebelum_4_5_L	298
ParaHippocampal_R	308	Cerebelum_6_R	281
Cerebelum_6_R	292	ParaHippocampal_L	281
ParaHippocampal_L	280	Temporal_Pole_Sup_L	273
Hippocampus_L	266	Insula_L	272
Hippocampus_R	256	Hippocampus_L	268
Frontal_Inf_Orb_R	252	Hippocampus_R	263
Temporal_Pole_Sup_L	251	Cerebelum_6_L	227
Frontal_Inf_Orb_L	240	Frontal_Inf_Orb_L	226
Cerebelum_4_5_R	229	Frontal_Inf_Orb_R	225
Cerebelum_6_L	223	Putamen_L	217
Putamen_R	221	Temporal_Mid_L	214
Putamen_L	221	Putamen_R	201
Temporal_Mid_L	214	Temporal_Sup_R	200
Caudate_L	208	Caudate_R	189
Caudate_R	191	Cerebelum_4_5_R	184
Temporal_Sup_R	188	Caudate_L	173
Postcentral_L	159	Temporal_Pole_Sup_R	162
Temporal_Pole_Sup_R	158	Postcentral_L	126
Rolandic_Oper_L	158	Frontal_Sup_Orb_R	126
Precentral_L	152	Precentral_L	125
Frontal_Sup_Orb_R	122	Rectus_R	120
Rectus_R	109	Rolandic_Oper_L	120
Vermis_4_5	102	Cerebelum_8_L	119
Temporal_Pole_Mid_R	100	Cerebelum_9_R	117
		Frontal_Sup_Orb_L	104
		Temporal_Pole_Mid_R	101

AAL, anatomical automatic labeling atlas. MNI, Montreal Neurological Institute space. Only clusters of more than 100 voxels were reported.

In the ANOVA analysis of rs-fMRI, ReHo changes in a wide range of brain areas were shown among the three groups. Further comparisons between groups showed that compared with the HC group, both the SCD group and aMCI group showed similar and regular changes in brain areas. In the SCD group, the ReHo decreased in part of the parietal lobe, frontal lobe, occipital lobe, and temporal lobe. The correlation analysis showed that the ReHo of DRR was positively correlated with AFT scores, suggesting that the decrease of neural activity homogeneity in these areas may be related to the impairment of language fluency. Most of these involved areas have been confirmed to be related to cognitive function in previous studies. The parietal lobe

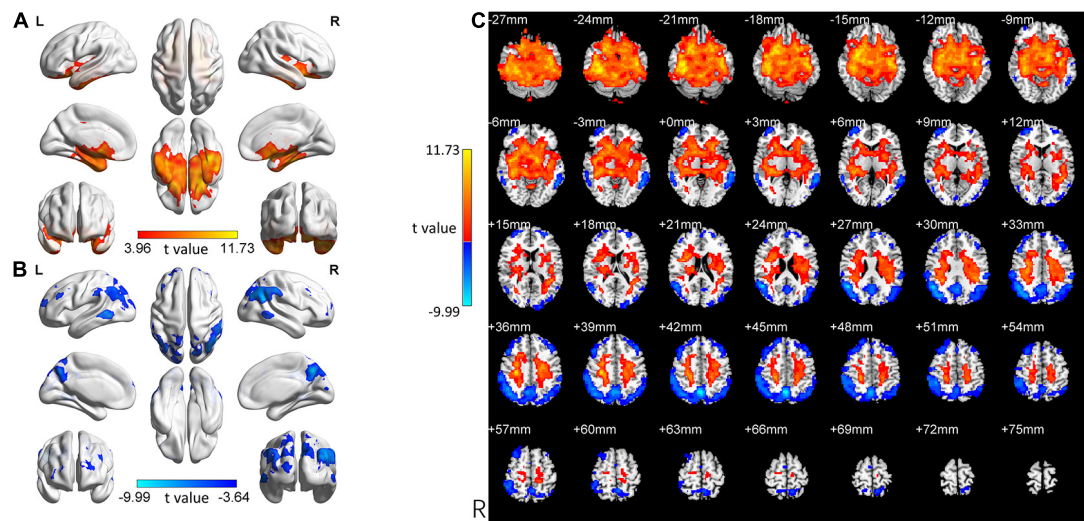


FIGURE 3 | Changed ReHo in the aMCI group compared with the HC group. **(A)** The brain regions with increased ReHo in the aMCI group compared with the HC group. **(B)** The brain regions with decreased ReHo in the aMCI group compared with the HC group. **(C)** Brain regions with increased and decreased ReHo in the aMCI group compared with the HC group. Two-tailed *t*-test; FDR < 0.0005, *k* > 10 voxels. The color bars indicate *t*-values, blue color represents negative values and red color represents positive values. L, Left; R, Right.

is a critical node for integrating cognitive activities; although recruitment is distributed in multiple brain regions in every cognitive activity, the parietal lobe is a converging area. A study (Bzdok et al., 2016) found that the function of rostral-ventral and caudo-ventral regions in the parietal lobe was significantly associated with social-cognitive and language processing. In the frontal lobe and cognition related field, a study on MCI (Garcia-Alvarez et al., 2019) found that damage to the cortex and functional circuits of the frontal lobe is associated with a decline in working memory and executive function, as well as with the loss of daily function. A study using near-infrared spectroscopy (Chaudhary et al., 2011) revealed that the oxy-hemoglobin increased during the verbal fluency task while the deoxy-hemoglobin decreased in the frontal cortex. Although the occipital lobe is mainly involved in visual function, recent studies have suggested that the occipital lobe is also associated with cognitive decline in MCI and AD patients. A multimodal imaging study in healthy group, MCI group, and AD group showed that the number of connections between brain regions gradually decreased, especially in the occipital-parietal lobe (Li et al., 2018). Another study focused on cholinergic impairment in MCI patients found that Acetylcholinesterase activity was mainly reduced in the lateral temporal cortex and the occipital lobe (Richter et al., 2019). These studies suggest that the occipital lobe and cognitive impairment relationship are probably closely related to the parietal and temporal lobes. Our results matched those observed in earlier studies. It is worth noting that the ReHo value of DRR seems to be only correlated with verbal fluency, and no obvious correlation with other cognitive domains has been found. This suggests that the decrease of neural homogeneity in these areas may not independently reflect the degree of cognitive impairment. In previous studies on SCD, it has been found that these areas, such as the parietal and frontal lobes, play a role in the

cognitive decline of SCD mainly through abnormal connections with other parts of the brain or networks (Viviano et al., 2019; Wang et al., 2019).

It is somewhat surprising that our study found a much larger area with significantly increased ReHo in the SCD group. These areas are centered on the temporal lobe and extend to the adjacent part of the occipital lobe, parietal lobe, and subcortical structures. The temporal lobe's structural changes, especially in the medial temporal lobe and the hippocampus, have been identified as typical MRI markers of AD (Scheltens et al., 2016; Lane et al., 2018). In a study using FDG-PET (Pagani et al., 2017), researchers established a cohort of MCI due to AD through longitudinal follow-up. They found that in MCI patients who eventually converted to AD, FDG uptake was lower in temporal and parietal cortices; in MCI patients who did not convert to AD, the FDG intake in these areas did not change. This study further confirmed that the temporal lobe and parietal lobe play an essential role in predicting MCI patients' development to AD. Some PET studies using tracers for tau protein found uptake in orbitofrontal, parietal, hippocampal, and temporal cortices in humans with AD (Fodero-Tavoletti et al., 2011; Villemagne et al., 2014). An amyloid PET study found a high binding affinity for A β in the frontal, temporal, and posterior cingulate cortices in AD patients (Maya et al., 2016). These PET studies using special tracers provide pathological evidence for multiple brain areas dominated by the temporal lobes. In addition, some studies (Hilal et al., 2015; Koshiyama et al., 2018) have revealed the role of specific subcortical nuclei in cognitive and social function, and these observations were similar to our results.

Due to the resolution and sensitivity characteristics, no consistent conclusion of studies using PET in the preclinical stage of AD has been reached so far. Structural damage often occurs at a later stage; therefore, it is also difficult to locate specific

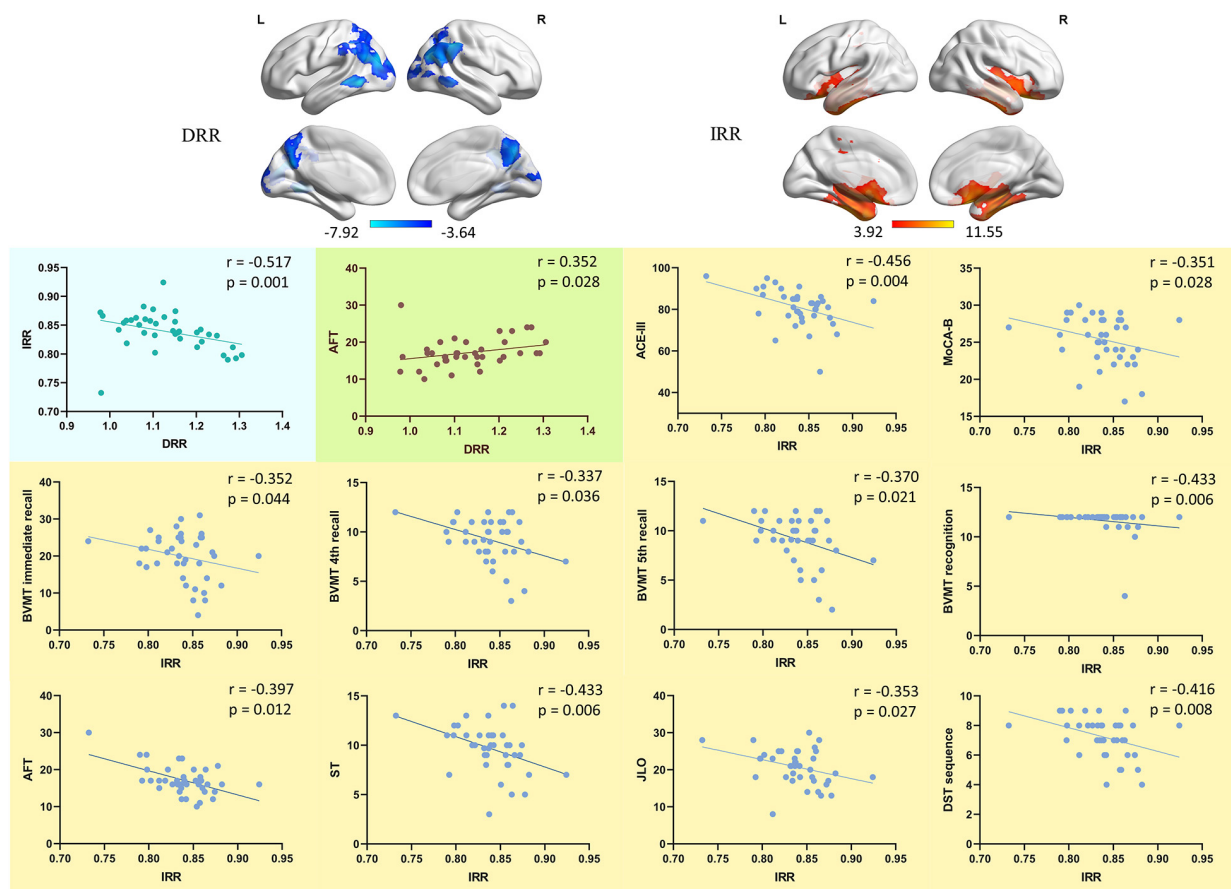


FIGURE 4 | The correlation of DRR/IRR and neuropsychological performance. The correlation between the ReHo value of DRR/IRR and the neuropsychological tests performance. DRR, decreased ReHo region. IRR, increased ReHo region. ACE-III, Addenbrooke's Cognitive Examination. MoCA-B, Montreal Cognitive Assessment-Basic. BVMT, Brief Visuospatial Memory Test. AFT, Animal Verbal Fluency Test. ST, Silhouettes Test. JLO, Judgment of Line Orientation. DST, Digit Span Test.

damaged brain regions of SCD patients through structural MRI. Rs-fMRI has a high spatial resolution and sensitivity to changes in neural activity and function. Moreover, it does not need to perform tasks to stimulate neural activities, which makes rs-fMRI has good stability and repeatability. We had predicted that compensatory phenomena in the brain of patients with SCD could be detected by rs-fMRI, but the scope of compensation found in the study is beyond our expectations. We cautiously speculate that this compensation may be one reason why SCD patients can retain roughly normal cognitive abilities. The results of the subsequent correlation analysis confirmed this speculation to a certain extent. We analyzed the correlation between the ReHo value of IRR (the ROI representing the increased ReHo area) and neuropsychological test performance, found that the ReHo of IRR was negatively correlated with multiple neuropsychological tests performance. These neuropsychological tests include ACE-III and MoCA-B reflecting general cognitive function; BMVT reflecting memory function; AFT and ST reflecting language function; JLO reflecting spatial function; and DST reflecting attention function. These different cognitive domains' performance decreased with the increase of the ReHo

value of IRR, indirectly indicating that the increase in local neural activity homogeneity in these areas reflects brain damage aggravation. ReHo has shown the relation with brain function compensation in different studies (Chen et al., 2016; Guo et al., 2016), suggesting that we should pay attention to the role of ReHo in the research of relatively mild diseases that may have functional compensation.

Compared with the HC group, the distribution of brain regions with changed ReHo in the SCD and aMCI groups was similar. We think there might be multiple possible reasons. The first reason is that SCD is the latest stage of preclinical AD, and its outcome is likely to be aMCI. The two stages are closely linked in the course of the disease, so there is likely to be a significant similarity in neurological damage manifestations. The second reason is that the primary method used to distinguish these two stages is neuropsychological testing. Commonly used neuropsychological tests may not have sufficient sensitivity and specificity in the early stage of the disease; therefore, there may be some overlap in the diagnosis of these two stages to a certain extent (Jessen et al., 2020). The third reason is that our research participants were recruited through advertising and

volunteered for a full set of complex and lengthy tests. These participants who actively participated in the study may have more concerns about memory complaints, which may cause the participants in the SCD group to be more severe than the cohort obtained by community screening. This reason may aggravate the problem of diagnosis overlap caused by the second reason. Therefore, the results of our research need to be interpreted and promoted cautiously. Our study found that although certain brain areas of MCI patients also showed improved local neurological uniformity similar to those of SCD patients, their neuropsychological test performance was significantly lower than that of SCD patients. This suggests that this kind of compensation is limited, and there is a ceiling effect. When the disease reaches a certain level, this compensation will not be able to maintain the patient's relatively normal cognitive function.

CONCLUSION

We used rs-fMRI to study the regional neural activity homogeneity of SCD patients' brains and found significant changes. Part of the parietal, frontal, and occipital lobes showed decreased neural homogeneity and positively correlated with some cognitive domains' decline. The temporal lobe, part of the parietal lobe and frontal lobe, showed an increase in neural homogeneity. The ReHo value of the area with increased neural homogeneity is negatively correlated with multiple neuropsychological tests' performance, suggesting that the increased regional neural activity homogeneity in SCD patients may be a compensatory manifestation of neural damage. Simultaneously, the neurological homogeneity of SCD patients is similar to that of aMCI patients, which confirms that patients in these two stages have similar neuropathy. However, the aMCI group's cognitive function was significantly worse than that of the SCD group, suggesting that this compensation is limited. In summary, regional neural activity homogeneity may be a potential biomarker for identifying SCD and measuring the disease severity.

LIMITATION

However, there are some limitations in this study, which can restrict the generalizability of our results. First, the sample size was not large enough, and AD patients were not included in

the study. Second, although a complete set of neuropsychological tests was used, there might be some overlap between SCD and aMCI groups. Third, we did not perform the examination of pathological biomarkers. Considering the limitations mentioned above, the results of this study should be interpreted with caution. In follow-up research, We should expand the sample size, explore a more sensitive neuropsychological test diagnostic approach, and examine pathological biomarkers.

DATA AVAILABILITY STATEMENT

The raw data supporting the conclusions of this article will be made available by the authors, without undue reservation.

ETHICS STATEMENT

The studies involving human participants were reviewed and approved by the Ethics Committee of Shanghai Jiao Tong University Affiliated Sixth People's Hospital. The patients/participants provided their written informed consent to participate in this study.

AUTHOR CONTRIBUTIONS

ZZ: data analysis, data curation, revision. LC: methodology, data analysis, investigation, data curation, writing—original draft, visualization. YH: investigation, writing—review, editing. YC: review, commentary. YL: resources, project administration. QG: resources, supervision, project administration, funding acquisition, review, and revision. All authors contributed to manuscript revision, read, and approved the submitted version.

FUNDING

This work was supported by the National Key R&D Program of China (2016YFC1306305) and National Key R&D Program of China (2018YFE0203600).

ACKNOWLEDGMENTS

We want to thank all the authors that participated in this study.

REFERENCES

- Albert, M. S., DeKosky, S. T., Dickson, D., Dubois, B., Feldman, H. H., Fox, N. C., et al. (2011). The diagnosis of mild cognitive impairment due to Alzheimer's disease: recommendations from the National Institute on Aging-Alzheimer's Association workgroups on diagnostic guidelines for Alzheimer's disease. *Alzheimers Dement.* 7, 270–279. doi: 10.1016/j.jalz.2011.03.008
- Bi, X. A., Hu, X., Wu, H., and Wang, Y. (2020a). Multimodal data analysis of Alzheimer's Disease based on clustering evolutionary random forest. *IEEE J. Biomed. Health Inform.* 24, 2973–2983. doi: 10.1109/JBHI.2020.2973324
- Bi, X. A., Liu, Y., Xie, Y., Hu, X., and Jiang, Q. (2020b). Morbigenous brain region and gene detection with a genetically evolved random neural network cluster approach in late mild cognitive impairment. *Bioinformatics* 36, 2561–2568. doi: 10.1093/bioinformatics/btz967
- Bondy, M. W., Edmonds, E. C., Jak, A. J., Clark, L. R., Delano-Wood, L., McDonald, C. R., et al. (2014). Neuropsychological criteria for mild cognitive impairment improves diagnostic precision, biomarker associations, and progression rates. *J. Alzheimers Dis.* 42, 275–289. doi: 10.3233/JAD-140276
- Bzdok, D., Hartwigsen, G., Reid, A., Laird, A. R., Fox, P. T., and Eickhoff, S. B. (2016). Left inferior parietal lobe engagement in social cognition and language. *Neurosci. Biobehav. Rev.* 68, 319–334. doi: 10.1016/j.neubiorev.2016.02.024

- Chaudhary, U., Hall, M., DeCerce, J., Rey, G., and Godavarty, A. (2011). Frontal activation and connectivity using near-infrared spectroscopy: verbal fluency language study. *Brain Res. Bull.* 84, 197–205. doi: 10.1016/j.brainresbull.2011.01.002
- Chen, H., Sheng, X., Luo, C., Qin, R., Ye, Q., Zhao, H., et al. (2020). The compensatory phenomenon of the functional connectome related to pathological biomarkers in individuals with subjective cognitive decline. *Transl. Neurodegener.* 9:21. doi: 10.1186/s40035-020-00201-6
- Chen, J., Fan, C., Li, J., Han, Q., Lin, J., Yang, T., et al. (2016). Increased intraregional synchronized neural activity in adult brain after prolonged adaptation to high-altitude hypoxia: a resting-state fMRI study. *High Alt. Med. Biol.* 17, 16–24. doi: 10.1089/ham.2015.0104
- Chen, K., Huang, L., Lin, B., Zhou, Y., Zhao, Q., and Guo, Q. (2019). The number of items on each stroop test card is unrelated to its sensitivity. *Neuropsychobiology* 77, 38–44. doi: 10.1159/000493553
- Dillen, K. N. H., Jacobs, H. I. L., Kukolja, J., Richter, N., von Reutern, B., Onur, O. A., et al. (2017). Functional disintegration of the default mode network in prodromal Alzheimer's disease. *J. Alzheimers Dis.* 59, 169–187. doi: 10.3233/JAD-161120
- Fazekas, F., Chawluk, J. B., Alavi, A., Hurtig, H. I., and Zimmerman, R. A. (1987). MR signal abnormalities at 1.5 T in Alzheimer's dementia and normal aging. *AJR Am. J. Roentgenol.* 149, 351–356. doi: 10.2214/ajr.149.2.351
- Fodero-Tavoletti, M. T., Okamura, N., Furumoto, S., Mulligan, R. S., Connor, A. R., McLean, C. A., et al. (2011). 18F-THK523: a novel in vivo tau imaging ligand for Alzheimer's disease. *Brain* 134(Pt 4), 1089–1100. doi: 10.1093/brain/awr038
- Folstein, M. F., Folstein, S. E., and McHugh, P. R. (1975). Mini-mental state". A practical method for grading the cognitive state of patients for the clinician. *J. Psychiatr. Res.* 12, 189–198. doi: 10.1016/0022-3956(75)90026-6
- Franzmeier, N., Duering, M., Weiner, M., Dichgans, M., Ewers, M., and Alzheimer's Disease Neuroimaging Initiative (2017). Left frontal cortex connectivity underlies cognitive reserve in prodromal Alzheimer disease. *Neurology* 88, 1054–1061. doi: 10.1212/WNL.0000000000003711
- Garcia-Alvarez, L., Gomar, J. J., Sousa, A., Garcia-Portilla, M. P., and Goldberg, T. E. (2019). Breadth and depth of working memory and executive function compromises in mild cognitive impairment and their relationships to frontal lobe morphometry and functional competence. *Alzheimers Dement. (Amst.)* 11, 170–179. doi: 10.1016/j.dadm.2018.12.010
- Guo, Z., Huang, X., Wang, M., Jones, J. A., Dai, Z., Li, W., et al. (2016). Regional homogeneity of intrinsic brain activity correlates with auditory-motor processing of vocal pitch errors. *Neuroimage* 142, 565–575. doi: 10.1016/j.neuroimage.2016.08.005
- Hilal, S., Amin, S. M., Venketasubramanian, N., Niessen, W. J., Vrooman, H., Wong, T. Y., et al. (2015). Subcortical atrophy in cognitive impairment and dementia. *J. Alzheimers Dis.* 48, 813–823. doi: 10.3233/JAD-150473
- Huang, L., Chen, K. L., Lin, B. Y., Tang, L., Zhao, Q. H., Li, F., et al. (2018a). An abbreviated version of silhouettes test: a brief validated mild cognitive impairment screening tool. *Int. Psychogeriatr.* 19, 1–8. doi: 10.1017/S1041610218001230
- Huang, L., Chen, K. L., Lin, B. Y., Tang, L., Zhao, Q. H., Lv, Y. R., et al. (2018b). Chinese version of montreal cognitive assessment basic for discrimination among different severities of Alzheimer's disease. *Neuropsychiatr. Dis. Treat.* 14, 2133–2140. doi: 10.2147/NDT.S174293
- Jack, C. R. Jr., Albert, M. S., Knopman, D. S., McKhann, G. M., Sperling, R. A., Carrillo, M. C., et al. (2011). Introduction to the recommendations from the National Institute on Aging-Alzheimer's Association workgroups on diagnostic guidelines for Alzheimer's disease. *Alzheimers Dement.* 7, 257–262. doi: 10.1016/j.jalz.2011.03.004
- Jessen, F., Amariglio, R. E., Buckley, R. F., van der Flier, W. M., Han, Y., Molinuevo, J. L., et al. (2020). The characterisation of subjective cognitive decline. *Lancet Neurol.* 19, 271–278. doi: 10.1016/S1474-4422(19)30368-0
- Jessen, F., Amariglio, R. E., van Bostel, M., Breteler, M., Ceccaldi, M., Chetelat, G., et al. (2014). A conceptual framework for research on subjective cognitive decline in preclinical Alzheimer's disease. *Alzheimers Dement.* 10, 844–852. doi: 10.1016/j.jalz.2014.01.001
- Jessen, F., Spottke, A., Boecker, H., Brosseron, F., Buerger, K., Catak, C., et al. (2018). Design and first baseline data of the DZNE multicenter observational study on predementia Alzheimer's disease (DELCODE). *Alzheimers Res. Ther.* 10:15. doi: 10.1186/s13195-017-0314-2
- Jia, X.-Z., Wang, J., Sun, H.-Y., Zhang, H., Liao, W., Wang, Z., et al. (2019). RESTplus: an improved toolkit for resting-state functional magnetic resonance imaging data processing. *Sci. Bull.* 64, 953–954. doi: 10.1016/j.scib.2019.05.008
- Johansson, B., and Berg, S. (1989). The robustness of the terminal decline phenomenon: longitudinal data from the digit-span memory test. *J. Gerontol.* 44, 184–186. doi: 10.1093/geronj/44.6.p184
- Kang, D. W., Choi, W. H., Jung, W. S., Um, Y. H., Lee, C. U., and Lim, H. K. (2017). Impact of amyloid burden on regional functional synchronization in the cognitively normal older adults. *Sci. Rep.* 7:14690. doi: 10.1038/s41598-017-15001-8
- Katzman, R., Zhang, M. Y., Ouang Ya, Q., Wang, Z. Y., Liu, W. T., Yu, E., et al. (1988). A Chinese version of the mini-mental state examination; impact of illiteracy in a Shanghai dementia survey. *J. Clin. Epidemiol.* 41, 971–978. doi: 10.1016/0895-4356(88)90034-0
- Koshiyama, D., Fukunaga, M., Okada, N., Yamashita, F., Yamamori, H., Yasuda, Y., et al. (2018). Role of subcortical structures on cognitive and social function in schizophrenia. *Sci. Rep.* 8:1183. doi: 10.1038/s41598-017-18950-2
- Lane, C. A., Hardy, J., and Schott, J. M. (2018). Alzheimer's disease. *Eur. J. Neurol.* 25, 59–70. doi: 10.1111/ene.13439
- Li, Q., Wu, X., Xie, F., Chen, K., Yao, L., Zhang, J., et al. (2018). Aberrant connectivity in mild cognitive impairment and Alzheimer disease revealed by multimodal neuroimaging data. *Neurodegener. Dis.* 18, 5–18. doi: 10.1159/000484248
- Li, S., Daamen, M., Scheef, L., Gaertner, F. C., Buchert, R., Buchmann, M., et al. (2021). Abnormal regional and global connectivity measures in subjective cognitive decline depending on cerebral amyloid status. *J. Alzheimers Dis.* 79, 493–509. doi: 10.3233/JAD-200472
- Luo, X., Jiaerken, Y., Huang, P., Xu, X. J., Qiu, T., Jia, Y., et al. (2018). Alteration of regional homogeneity and white matter hyperintensities in amnesic mild cognitive impairment subtypes are related to cognition and CSF biomarkers. *Brain Imaging Behav.* 12, 188–200. doi: 10.1007/s11682-017-9680-4
- Mack, W. J., Freed, D. M., Williams, B. W., and Henderson, V. W. (1992). Boston naming test: shortened versions for use in Alzheimer's disease. *J. Gerontol.* 47, 154–158. doi: 10.1093/geronj/47.3.p154
- Maya, Y., Okumura, Y., Kobayashi, R., Onishi, T., Shoyama, Y., Barret, O., et al. (2016). Preclinical properties and human in vivo assessment of 123I-ABC577 as a novel SPECT agent for imaging amyloid-beta. *Brain* 139(Pt 1), 193–203. doi: 10.1093/brain/awv305
- Miebach, L., Wolfsgruber, S., Polcher, A., Peters, O., Menne, F., Luther, K., et al. (2019). Which features of subjective cognitive decline are related to amyloid pathology? Findings from the DELCODE study. *Alzheimers Res. Ther.* 11:66. doi: 10.1186/s13195-019-0515-y
- Mioshi, E., Dawson, K., Mitchell, J., Arnold, R., and Hodges, J. R. (2006). The Addenbrooke's cognitive examination revised (ACE-R): a brief cognitive test battery for dementia screening. *Int. J. Geriatr. Psychiatry* 21, 1078–1085. doi: 10.1002/gps.1610
- Mitchell, A. J., and Shiri-Feshki, M. (2009). Rate of progression of mild cognitive impairment to dementia—meta-analysis of 41 robust inception cohort studies. *Acta Psychiatr. Scand.* 119, 252–265. doi: 10.1111/j.1600-0447.2008.01326.x
- Moguliner, S., Garcia, A. M., Perl, Y. S., Tagliazucchi, E., Piguert, O., Kumfor, F., et al. (2020). Dynamic brain fluctuations outperform connectivity measures and mirror pathophysiological profiles across dementia subtypes: a multicenter study. *Neuroimage* 225:117522. doi: 10.1016/j.neuroimage.2020.117522
- Morris, J. C. (1993). The clinical dementia rating (CDR): current version and scoring rules. *Neurology* 43, 2412–2414. doi: 10.1212/wnl.43.11.2412-a
- Pagani, M., Nobili, F., Morbelli, S., Arnaldi, D., Giuliani, A., Oberg, J., et al. (2017). Early identification of MCI converting to AD: a FDG PET study. *Eur. J. Nucl. Med. Mol. Imaging* 44, 2042–2052. doi: 10.1007/s00259-017-3761-x
- Pan, P., Zhu, L., Yu, T., Shi, H., Zhang, B., Qin, R., et al. (2017). Aberrant spontaneous low-frequency brain activity in amnesic mild cognitive impairment: a meta-analysis of resting-state fMRI studies. *Ageing Res. Rev.* 35, 12–21. doi: 10.1016/j.arr.2016.12.001
- Petersen, R. C. (2004). Mild cognitive impairment as a diagnostic entity. *J. Intern. Med.* 256, 183–194. doi: 10.1111/j.1365-2796.2004.01388.x
- Pliskin, J. I., DeDios Stern, S., Resch, Z. J., Saladino, K. F., Ovsiew, G. P., Carter, D. A., et al. (2020). Comparing the psychometric properties of eight embedded performance validity tests in the re auditory verbal learning test, wechsler memory scale logical memory, and brief visuospatial memory test-revised

- recognition trials for detecting invalid neuropsychological test performance. *Assessment* 1073191120929093. doi: 10.1177/1073191120929093 [Epub ahead of print].
- Qualls, C. E., Bliwise, N. G., and Stringer, A. Y. (2000). Short forms of the benton judgment of line orientation test: development and psychometric properties. *Arch. Clin. Neuropsychol.* 15, 159–163. doi: 10.1016/s0887-6177(98)00043-2
- Rabin, L. A., Smart, C. M., and Amariglio, R. E. (2017). Subjective cognitive decline in preclinical Alzheimer's disease. *Annu. Rev. Clin. Psychol.* 13, 369–396. doi: 10.1146/annurev-clinpsy-032816-045136
- Ren, P., Lo, R. Y., Chapman, B. P., Mapstone, M., Porsteinsson, A., Lin, F., et al. (2016). Longitudinal alteration of intrinsic brain activity in the striatum in mild cognitive impairment. *J. Alzheimers Dis.* 54, 69–78. doi: 10.3233/JAD-160368
- Richter, N., Nellessen, N., Dronse, J., Dillen, K., Jacobs, H. I. L., Langen, K. J., et al. (2019). Spatial distributions of cholinergic impairment and neuronal hypometabolism differ in MCI due to AD. *Neuroimage Clin.* 24:101978. doi: 10.1016/j.nicl.2019.101978
- Scheltens, P., Blennow, K., Breteler, M. M. B., de Strooper, B., Frisoni, G. B., Salloway, S., et al. (2016). Alzheimer's disease. *Lancet* 388, 505–517. doi: 10.1016/s0140-6736(15)01124-1
- Shaw, L. M., Vanderstichele, H., Knapik-Czajka, M., Clark, C. M., Aisen, P. S., Petersen, R. C., et al. (2009). Cerebrospinal fluid biomarker signature in Alzheimer's disease neuroimaging initiative subjects. *Ann. Neurol.* 65, 403–413. doi: 10.1002/ana.21610
- Sperling, R. A., Aisen, P. S., Beckett, L. A., Bennett, D. A., Craft, S., Fagan, A. M., et al. (2011). Toward defining the preclinical stages of Alzheimer's disease: recommendations from the National Institute on Aging-Alzheimer's Association workgroups on diagnostic guidelines for Alzheimer's disease. *Alzheimers Dement.* 7, 280–292. doi: 10.1016/j.jalz.2011.03.003
- Villemagne, V. L., Furumoto, S., Fodero-Tavoletti, M. T., Mulligan, R. S., Hodges, J., Harada, R., et al. (2014). In vivo evaluation of a novel tau imaging tracer for Alzheimer's disease. *Eur. J. Nucl. Med. Mol. Imaging* 41, 816–826. doi: 10.1007/s00259-013-2681-7
- Visser, P. J., Verhey, F., Knol, D. L., Scheltens, P., Wahlund, L. O., Freund-Levi, Y., et al. (2009). Prevalence and prognostic value of CSF markers of Alzheimer's disease pathology in patients with subjective cognitive impairment or mild cognitive impairment in the DESCRIPA study: a prospective cohort study. *Lancet Neurol.* 8, 619–627. doi: 10.1016/S1474-4422(09)70139-5
- Viviano, R. P., Hayes, J. M., Pruitt, P. J., Fernandez, Z. J., van Rooden, S., van der Grond, J., et al. (2019). Aberrant memory system connectivity and working memory performance in subjective cognitive decline. *Neuroimage* 185, 556–564. doi: 10.1016/j.neuroimage.2018.10.015
- Wang, Z., Qiao, K., Chen, G., Sui, D., Dong, H. M., Wang, Y. S., et al. (2019). Functional connectivity changes across the spectrum of subjective cognitive decline, amnesic mild cognitive impairment and Alzheimer's disease. *Front. Neuroinform.* 13:26. doi: 10.3389/fninf.2019.00026
- Worboys, M. (2013). The Hamilton Rating Scale for Depression: The making of a “gold standard” and the unmaking of a chronic illness, 1960–1980. *Chronic Illn.* 9, 202–219. doi: 10.1177/1742395312467658
- Xia, M., Wang, J., and He, Y. (2013). BrainNet viewer: a network visualization tool for human brain connectomics. *PLoS One* 8:e68910. doi: 10.1371/journal.pone.0068910
- Xiong, Y., Chen, X., Zhao, X., Fan, Y., Zhang, Q., and Zhu, W. (2020). Altered regional homogeneity and functional brain networks in Type 2 diabetes with and without mild cognitive impairment. *Sci. Rep.* 10:21254. doi: 10.1038/s41598-020-76495-3
- Yan, T., Wang, Y., Weng, Z., Du, W., Liu, T., Chen, D., et al. (2019). Early-stage identification and pathological development of Alzheimer's disease using multimodal MRI. *J. Alzheimers Dis.* 68, 1013–1027. doi: 10.3233/JAD-181049
- Zang, Y., Jiang, T., Lu, Y., He, Y., and Tian, L. (2004). Regional homogeneity approach to fMRI data analysis. *Neuroimage* 22, 394–400. doi: 10.1016/j.neuroimage.2003.12.030
- Zhao, Q., Guo, Q., and Hong, Z. (2013a). Clustering and switching during a semantic verbal fluency test contribute to differential diagnosis of cognitive impairment. *Neurosci. Bull.* 29, 75–82. doi: 10.1007/s12264-013-1301-7
- Zhao, Q., Guo, Q., Li, F., Zhou, Y., Wang, B., and Hong, Z. (2013b). The shape trail test: application of a new variant of the trail making test. *PLoS One* 8:e57333. doi: 10.1371/journal.pone.0057333
- Zhao, Q., Guo, Q., Liang, X., Chen, M., Zhou, Y., Ding, D., et al. (2015). Auditory verbal learning test is superior to rey-osterrieth complex figure memory for predicting mild cognitive impairment to Alzheimer's disease. *Curr. Alzheimer Res.* 12, 520–526. doi: 10.2174/1567205012666150530202729
- Zuo, X. N., Xu, T., Jiang, L., Yang, Z., Cao, X. Y., He, Y., et al. (2013). Toward reliable characterization of functional homogeneity in the human brain: preprocessing, scan duration, imaging resolution and computational space. *Neuroimage* 65, 374–386. doi: 10.1016/j.neuroimage.2012.10.017

Conflict of Interest: The authors declare that the research was conducted in the absence of any commercial or financial relationships that could be construed as a potential conflict of interest.

Copyright © 2021 Zhang, Cui, Huang, Chen, Li and Guo. This is an open-access article distributed under the terms of the Creative Commons Attribution License (CC BY). The use, distribution or reproduction in other forums is permitted, provided the original author(s) and the copyright owner(s) are credited and that the original publication in this journal is cited, in accordance with accepted academic practice. No use, distribution or reproduction is permitted which does not comply with these terms.



Parametric Estimation of Reference Signal Intensity for Semi-Quantification of Tau Deposition: A Flortaucipir and [¹⁸F]-APN-1607 Study

OPEN ACCESS

Edited by:

Kin Ying Mok,
University College London,
United Kingdom

Reviewed by:

Xiaoli Lan,
Huazhong University of Science
and Technology, China
Michael Navitsky,
Avid Radiopharmaceuticals, Inc.,
United States

*Correspondence:

Chuantao Zuo
zuochuantao@fudan.edu.cn
Jiehui Jiang
jiangjiehui@shu.edu.cn

[†] These authors have contributed
equally to this work

Specialty section:

This article was submitted to
Neurodegeneration,
a section of the journal
Frontiers in Neuroscience

Received: 24 August 2020

Accepted: 25 May 2021

Published: 21 June 2021

Citation:

Zhang H, Wang M, Lu J, Bao W,
Li L, Jiang J, Zuo C and
Alzheimer's Disease
Neuroimaging Initiative (2021)
Parametric Estimation of Reference
Signal Intensity
for Semi-Quantification of Tau
Deposition: A Flortaucipir
and [¹⁸F]-APN-1607 Study.
Front. Neurosci. 15:598234.
doi: 10.3389/fnins.2021.598234

Huiwei Zhang^{1†}, Min Wang^{2†}, Jiaying Lu¹, Weiqi Bao¹, Ling Li¹,
Jiehui Jiang^{2*}, Chuantao Zuo^{1*} and Alzheimer's Disease Neuroimaging Initiative

¹ PET Center, Huashan Hospital, Fudan University, Shanghai, China, ² Shanghai Institute for Advanced Communication
and Data Science, Shanghai University, Shanghai, China

Background: Tau positron emission tomography (PET) imaging can reveal the pathophysiology and neurodegeneration that occurs in Alzheimer's disease (AD) *in vivo*. The standardized uptake value ratio (SUVR) is widely used for semi-quantification of tau deposition but is susceptible to disturbance from the reference region and the partial volume effect (PVE). To overcome this problem, we applied the parametric estimation of reference signal intensity (PERSI) method—which was previously evaluated for flortaucipir imaging—to two tau tracers, flortaucipir and [¹⁸F]-APN-1607.

Methods: Two cohorts underwent tau PET scanning. Flortaucipir PET imaging data for cohort I (65 healthy controls [HCs], 60 patients with mild cognitive impairment [MCI], and 12 AD patients) were from the AD Neuroimaging Initiative database. [¹⁸F]-APN-1607 ([¹⁸F]-PM-PBB3) PET imaging data were for Cohort II, which included 21 patients with a clinical diagnosis of amyloid PET-positive AD and 15 HCs recruited at Huashan Hospital. We used white matter (WM) postprocessed by PERSI (PERSI-WM) as the reference region and compared this with the traditional semi-quantification method that uses the whole cerebellum as the reference. SUVRs were calculated for regions of interest including the frontal, parietal, temporal, and occipital lobes; anterior and posterior cingulate; precuneus; and Braak I/II (entorhinal cortex and hippocampus). Receiver operating characteristic (ROC) curve analysis and effect sizes were used to compare the two methods in terms of ability to discriminate between different clinical groups.

Results: In both cohorts, regional SUVR determined using the PERSI-WM method was superior to using the cerebellum as reference region for measuring tau retention in AD patients (e.g., SUVR of the temporal lobe: flortaucipir, 1.08 ± 0.17 and [¹⁸F]-APN-1607, 1.57 ± 0.34); and estimates of the effect size and areas under the ROC curve (AUC) indicated that it also increased between-group differences (e.g., AUC of the temporal lobe for HC vs AD: flortaucipir, 0.893 and [¹⁸F]-APN-1607: 0.949).

Conclusion: The PERSI-WM method significantly improves diagnostic discrimination compared to conventional approach of using the cerebellum as a reference region and can mitigate the PVE; it can thus enhance the efficacy of semi-quantification of multiple tau tracers in PET scanning, making it suitable for large-scale clinical application.

Keywords: APN-1607, flortaucipir, tau, neurodegeneration, Alzheimer's disease

INTRODUCTION

Tau protein is a microtubule-associated protein that is abundantly expressed in the central nervous system (Goedert et al., 1991). Abnormal tau hyperphosphorylation in neurons causes the protein to self-aggregate and form paired helical filaments (PHFs) that contribute to the pathogenesis of neurodegenerative diseases. In Alzheimer's disease (AD), the deposition of amyloid β (A β) is the initial pathologic event leading to the formation of senile plaques (SPs) followed by neurofibrillary tangles (NFTs), leading to neuronal loss and cognitive decline (Braak and Braak, 1991). Diseases involving tau protein misfolding or hyperphosphorylation and accumulation are known as tauopathies; these include AD, frontotemporal dementia with parkinsonism linked to chromosome 17 (FTDP-17), Pick's disease, progressive supranuclear palsy (PSP), corticobasal degeneration (CBD), and chronic traumatic encephalopathy (Villemagne et al., 2015; Okamura et al., 2018). According to the 2018 National Institute on Aging and Alzheimer's Association guidelines for AD, SPs and NFTs can be detected *in vivo* by positron emission tomography (PET) imaging with A β and tau tracers to differentiate dementia from other neurodegenerative diseases. In addition to A β deposition, tau retention is a major factor contributing to AD pathogenesis.

The first generation of radiolabeled tau tracers for PET were developed based on different binding targets of tau PHFs such as quinoline derivatives (e.g., [^{18}F]THK523, [^{18}F]THK5105, [^{18}F]THK5117, and [^{18}F]THK5351), PBB3-based tracers (e.g., [^{11}C]PBB3), and benzimidazole pyrimidine derivatives (e.g., flortaucipir/[^{18}F]-AV-1451/[^{18}F]-T807 and [^{18}F]T808). The second generation of tracers show improved binding selectivity and pharmacokinetics and include [^{18}F]AM-PBB3 and [^{18}F]-APN-1607/[^{18}F]PM-PBB3 (Leuzy et al., 2019); and [^{18}F]RO-948, [^{18}F]GTP1, and [^{18}F]MK-6240 (Okamura et al., 2018). In AD clinical trial, these tracers have demonstrated high binding affinity for tau PHFs and tau selectivity (Scholl et al., 2016; Shimada et al., 2017; Sone et al., 2017; Lu et al., 2020). Additionally, the amount of tracer that was retained and the brain regions in which it was detected in AD was significantly correlated with the clinical severity of dementia (Devous et al., 2018; Villemagne et al., 2018). This is one of the advantages of tau PET over A β PET, as amyloid burden shows little association with dementia severity (Rabinovici and Jagust, 2009). Reliable and reproducible methods for tau quantification in PET images are critical for diagnosis.

Semi-quantitative methods are non-invasive and widely used to eliminate the effects of arterial blood sampling in clinical studies, and have been applied to tau PET in AD (Shcherbinin et al., 2016). Conventionally, in PET images of

target-specific biomarker retention, AD biomarkers are measured by standardized uptake value ratio (SUVR) in regions of interest (ROIs), which is the ratio of average activity concentration in the target ROI relative to that in the reference region. In the calculation of SUVR, inter-subject variation should be minimized. Global mean normalization or normalization to an anatomic reference region can be done easily in clinical practice as it does not require complex mathematical modeling. Proper normalization reference region can enhance cross-sectional accuracy and longitudinal coherence in PET studies (Zhang et al., 2017). Optimal reference regions vary for different PET tracers, and include the cerebellum, pons, and sensorimotor cortex.

The cerebellum was shown to be devoid of NFT deposition (Marquie et al., 2015); therefore, the whole cerebellum or cerebellar gray matter (GM) is commonly used as reference region for tau PET in AD. In several studies, tau PET images were resampled by normalizing the subject-specific magnetic resonance imaging (MRI) template to the T1 MRI template for spatial normalization of ROIs, with the cerebellar GM as the reference (Shcherbinin et al., 2016; Kang et al., 2017; Kitamura et al., 2018; Wong et al., 2018; Lohith et al., 2019; Lu et al., 2020; Mueller et al., 2020). However, cerebellar GM or the whole cerebellum has the disadvantages of small size, low signal detection sensitivity, and susceptibility to noise and truncation. In particular, in longitudinal studies, the partial volume effect (PVE) can cause a spillover or cross-contamination of counts between adjacent structures due to limited spatial resolution (Meechai et al., 2015). Therefore, a reliable technique for tau PET image analysis is needed that minimizes the influence of these factors.

A subject-specific, data-driven technique known as parametric estimation of reference signal intensity (PERSI) was recently proposed for the analysis of flortaucipir PET images (Southekal et al., 2018). This method reduces inter-subject variability while enhancing discrimination between cohorts by using white matter (WM) as the reference region for count normalization based on signal intensity histograms, as tau binding by WM is considered negligible. PERSI can mitigate the PVE by distinguishing voxels associated with non-specific binding, which have lower signal intensity, from those that reflect contamination.

To determine whether the PERSI method is applicable to different tau tracers, in this study we applied the method to the analysis of data from tau PET imaging with flortaucipir and [^{18}F]-APN-1607. We first retested the PERSI method in a cohort that underwent PET imaging with flortaucipir as the tau tracer (Cohort I, including healthy controls [HCs] and patients with mild cognitive impairment [MCI] and AD), which has been previously reported. As PERSI has

not been validated for second-generation tau tracers, we then applied the method to a second cohort that underwent PET imaging with [^{18}F]-APN-1607 (Cohort II, including HCs and AD patients). We evaluated the count normalization performance of PERSI using WM as a reference region in the PET images.

MATERIALS AND METHODS

Subjects

We retrospectively analyzed data from two cohorts who underwent tau PET scans. Flortaucipir PET scans and corresponding structural MRI scans for Cohort I was obtained from the AD Neuroimaging Initiative (ADNI) database¹ and its extensions. This cohort consisted of 65 HCs along with 60 MCI and 12 AD patients. The primary goal of the ADNI was to test whether serial MRI and PET imaging findings, biological markers, and data from clinical and neuropsychologic assessments can be combined to predict and measure the progression of MCI and AD. In Cohort II, 21 AD patients clinically diagnosed as amyloid PET-positive (based on visual evaluation by three nuclear medicine specialists with 8 years of clinical experience on average) and 15 HCs underwent [^{18}F]-APN-1607 PET scanning. Clinically probable AD was determined based on current diagnostic criteria (McKhann et al., 2011). Experienced neurologists from the cognitive impairment clinic administered the Mini-Mental State Examination (MMSE) to all subjects. The demographic and clinical characteristics of the participants are summarized in **Table 1**.

The inclusion and exclusion criteria for the diagnostic categories of ADNI were as follows: (1) age between 55–85 years; (2) participants underwent flortaucipir PET and structural MRI scanning; (3) participants underwent a battery of neuropsychologic and cognitive examinations including the Montreal Cognitive Assessment (MoCA), Clinical Dementia Rating–Sum of Boxes (CDR-SB), and MMSE; (4) HCs had MMSE scores between 24–30 (inclusive), were non-depressed, non-MCI, and non-demented; and (5) severe AD patients with MMSE < 10 or MoCA < 10 were excluded. The detailed diagnosis-specific

inclusion and exclusion criteria for the HC, MCI, and AD groups can be found in the ADNI dataset².

All procedures in this study were in accordance with the ethical standards of the institutional research committee and with the Helsinki Declaration of 1975 and its later amendments. This study was approved by the institutional review boards of ADNI and the Institutional Review Board of Huashan Hospital (HIRB), Fudan University, China (no. 2018-363). Written, informed consent was obtained from each subject.

PET Imaging and Data Preprocessing

Flortaucipir PET images for Cohort I were obtained 75–105 min after administration of 370 MBq (10.0 mCi) \pm 10% flortaucipir. Detailed information on data acquisition is provided in the study protocol in the ADNI database.

Subjects in Cohort II were scanned with a Siemens Biograph 64 PET/computed tomography (CT) system (Siemens, Erlangen, Germany) in three-dimensional (3D) mode at Huashan Hospital. A low-dose CT transmission scan was performed before PET scanning for attenuation correction. Static emission scans were acquired 90–110 min after intravenous injection of 370 MBq [^{18}F]-APN-1607. Image reconstruction was performed with the ordered subset expectation maximization 3D method with six iterations and 21 subsets, Gaussian filtering, and a full width at half-maximum (FWHM) of 3.5 mm. The subjects also underwent anatomic MRI in a 3.0-T horizontal magnet (Discovery MR750; GE Medical Systems, Boston, MA, United States) at Huashan Hospital (Lu et al., 2020).

Positron emission tomography image preprocessing was performed using the Statistical Parametric Mapping 12 (SPM 12; Wellcome Department of Cognitive Neurology, University College London, London, UK) package in Matlab (MathWorks, Sherborn, MA, United States). The unified segmentation and normalization algorithms of SPM12 were used to spatially normalize the T1-weighted MR images acquired at screening to the Montreal Neurological Institute (MNI) brain template while simultaneously generating probabilistic segmentations for GM, WM, and cerebrospinal fluid. The PET images were also spatially normalized to MNI space using deformation field images generated from the MRI segment.

¹adni.loni.usc.edu

²<http://adni.loni.usc.edu/methods/documents/>

TABLE 1 | Clinical and demographic characteristics of the study subjects.

Group		Sex, M/F	Age, years	Education, years	MMSE	MoCA	CDR-SB
Flortaucipir (ADNI database)	HC (65)	24/41	74.1 ± 3.89	16.6 ± 2.32	29.2 ± 0.98	26.4 ± 2.47	0.046 ± 0.14
	MCI (60)	21/39	75.0 ± 5.96	16.3 ± 2.68	28.3 ± 1.74*	24.8 ± 2.76	1.18 ± 0.75*
	AD (12)	6/6	77.5 ± 9.71	16.4 ± 2.57	22.7 ± 2.42*	18.1 ± 4.36	5 ± 2*
[¹⁸ F]-APN-1607	HC (15)	10/5	60.8 ± 4.3	9.47 ± 3.3	27.6 ± 1.3	/	0
	AD (21)	11/10	60.3 ± 10.6	11.3 ± 5.15*	16.7 ± 7.6*	/	8.62 ± 3.8*

Data are presented as mean \pm standard deviation.

* $P < 0.05$ (two-sample *t*-test).

AD, Alzheimer's disease; ADNI, Alzheimer's Disease Neuroimaging Initiative; CDR-SB, Clinical Dementia Rating – Sum of Boxes; HC, healthy control subjects; MCI, patients with mild cognitive impairment; MoCA, Montreal Cognitive Assessment; MMSE, Mini-Mental State Examination.

PET Quantification Analysis

We evaluated the performance of the PERSI method for [^{18}F]-APN-1607 PET imaging quantification. The threshold of the WM probabilistic segmentation from individual T1-weighted MR images was set as 0.9 to generate a binary WM image. PET images spatially normalized to MNI space were masked with the individual WM image. The voxels within this WM region were plotted as a histogram and then fitted to a bimodal Gaussian distribution using a non-linear trust region reflective algorithm. For higher intensity peaks, the PERSI method identifies voxels with contamination based on counts from adjacent cortical tissues with confirmed flortaucipir uptake; lower intensity peaks reflect a stable reference signal intensity. We removed voxels in higher intensity peaks and retained those in lower intensity peaks (i.e., the FWHM of the lower peak location) as the individual reference region. Thus, PET images for each subject used this subject-specific WM region as the reference for count normalization and smoothing with a Gaussian filter of 8 mm FWHM (Southekal et al., 2018).

For comparison, we calculated the SUVR of different groups using additional reference regions: (1) the traditional reference region consisting of the whole cerebellum, and (2) WM based on PERSI. The whole brain was parcellated into the following regions for SUVR calculations: frontal, parietal, temporal, and occipital lobes; anterior and posterior cingulate; precuneus; and Braak I/II (entorhinal cortex and hippocampus) (Scholl et al., 2016), which are regions known to be associated with progressive neurodegeneration in AD. The whole cerebellum and all ROIs were manually delineated on the Automated Anatomical Labeling template (Tzourio-Mazoyer et al., 2002).

Statistical Analysis

Demographic characteristics were compared between AD and HC groups using the two-sample *t*-test or chi-squared test. Effect sizes for the ability of SUVR to discriminate between dementia patients and HC subjects were evaluated with Cohen's *d* ($d = [\text{mean}_1 - \text{mean}_2] / \sqrt{(\text{std}_1^2 + \text{std}_2^2)/2}$). We also carried out receiver operating characteristic (ROC) curve analyses for each regional SUVR to assess the capacity for discrimination between diagnostic groups based on the area under the ROC curve (AUC) value. All statistical analyses were performed using SPSS v22.0 software (SPSS Inc., Chicago, IL, United States). *P*-values < 0.05 were considered significant.

RESULTS

Application of the PERSI Method to Flortaucipir PET Images

To compare quantitative efficacy using PERSI-WM vs the whole cerebellum as the reference region, we examined flortaucipir SUVRs within each group of predefined ROIs. SUVRs derived from PERSI-WM revealed significantly higher tau retention in the frontal, parietal, temporal, and occipital lobes, posterior cingulate, precuneus, and Braak I/II in AD and MCI patients compared to HCs (Figure 1). Braak I/II had the highest tau

retention (1.51 ± 0.23). Interestingly, in the anterior cingulate, SUVRs derived from the cerebellum showed comparable tau retention in MCI and AD patients, whereas SUVRs derived from PERSI-WM showed higher tau retention in the AD group than in the MCI group, suggesting that this method is superior to using the cerebellum as a reference region.

We next carried out ROC curve analysis and calculated effect sizes to evaluate the diagnostic utility of PERSI-WM compared to the cerebellum (Table 2). PERSI-WM yielded larger effect sizes and AUCs in all ROIs than the cerebellum; the AUCs were 0.517–0.951 between the HC and AD groups and 0.472–0.874 between the HC and MCI groups in all ROIs. PERSI-WM had the largest effect size (Cohen's *d*) compared to HCs (AD, 1.37; MCI, 0.282) in the temporal lobe and the largest AUC compared to HCs (AD, 0.951; MCI 0.874) in Braak I/II. Estimates of the effect size and AUCs indicated that PERSI-WM increased between-group differences compared to the whole cerebellum (Table 2).

Validation of the PERSI Method With [^{18}F]-APN-1607 PET Images

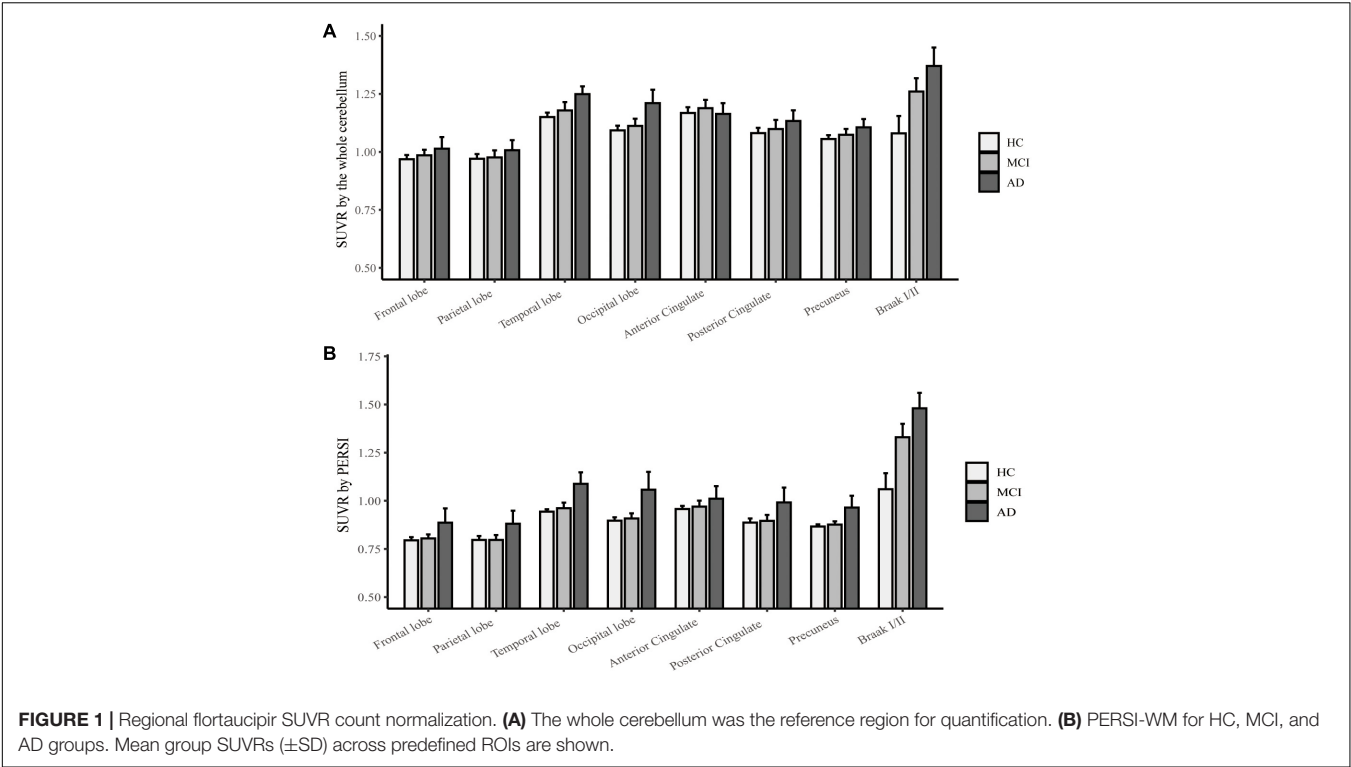
Typical signal intensity histograms of the WM used to derive the PERSI reference region for representative participants (HC and AD patient) are shown in Figure 2. In HCs, only a single major peak was observed whereas in AD patients, voxels that had spilled into the WM were captured by a higher peak.

To compare the quantitative efficacy between PERSI-WM and cerebellum as reference regions, we examined [^{18}F]-APN-1607 SUVRs within each group of predefined ROIs. SUVRs derived from PERSI-WM showed significantly higher tau retention in the frontal, parietal, temporal, and occipital lobes; anterior and posterior cingulate; precuneus and Braak I/II in the AD group than in the HC group (Figure 3), with the highest tau retention in precuneus (1.73 ± 0.53).

We next carried out ROC curve analysis and calculated effect sizes to evaluate the diagnostic utility of PERSI-WM compared to the cerebellum. PERSI-WM had larger effect sizes and AUCs in ROIs compared to the cerebellum (Table 3). PERSI-WM had the largest effect size (Cohen's *d*) compared to HCs in the precuneus (AD: 3.64) and in the temporal lobe (AD: 2.53). The AUC between the HC and AD groups was 0.933–0.975 in all ROIs. Estimates of the effect size and AUCs indicated that the PERSI-WM method increased between-group differences compared to the whole cerebellum (Table 3).

DISCUSSION

In tauopathies, tau PHFs can be non-invasively detected *in vivo* by PET imaging with different tau tracers such as benzimidazole pyrimidine derivatives (flortaucipir) and PBB3-based tracers ([^{18}F]-APN-1607). In this study, we evaluated the utility and reliability of the PERSI method for analyzing data from PET imaging using 2 different tau tracers—i.e., flortaucipir and [^{18}F]-APN-1607. We found that PERSI-WM had larger effect sizes and AUC values between diagnostic groups based on tau retention in specific ROIs. These results demonstrate that



PERSI-WM has better diagnostic performance for dementia than the traditional method of using the cerebellum as the reference region.

TABLE 2 | Mean standardized uptake value ratio of cortical regions by diagnostic group (Cohort I).

Cortical region	Reference area†	AUC		Effect size‡	
		HC-MCI	HC-AD	HC-MCI	HC-AD
Frontal lobe	Cerebellum	0.561	0.517	0.198	0.33
	PERSI-WM	0.535	0.561	0.178	0.70
Parietal lobe	Cerebellum	0.513	0.521	0.056	0.27
	PERSI-WM	0.508	0.60	0.01	0.64
Temporal lobe	Cerebellum	0.581	0.753	0.252	0.82
	PERSI-WM	0.523	0.893	0.282	1.37
Occipital lobe	Cerebellum	0.546	0.697	0.183	0.74
	PERSI-WM	0.595	0.801	0.161	1.01
Anterior cingulate	Cerebellum	0.572	0.642	0.22	0.51
	PERSI-WM	0.598	0.615	0.28	0.449
Posterior cingulate	Cerebellum	0.503	0.533	0.137	0.35
	PERSI-WM	0.521	0.633	0.211	0.72
Precuneus	Cerebellum	0.554	0.597	0.209	0.44
	PERSI-WM	0.472	0.681	0.229	0.928
Braak I/II	Cerebellum	0.762	0.856	0.476	0.672
	PERSI-WM	0.874	0.951	0.521	0.923

†Cerebellum, the whole cerebellum served as a reference region for quantification; PERSI-WM, parametric estimation of reference signal intensity with white matter as the reference region.
‡Presented as standardized Cohen's d; values in bold type represent superior diagnostic ability.
AD, Alzheimer's disease; AUC, area under the receiver operating characteristic curve; HC, healthy control subjects; MCI, patients with mild cognitive impairment; SUVR, standardized uptake value ratio.

We used the PERSI-WM method for count normalization in flortaucipir and [¹⁸F]-APN-1607 imaging. The results obtained for the two tau tracers were consistent; in both cases, the ability to distinguish between diagnostic groups was greater with SUVRs based on WM than with those based on the cerebellum. Additionally, in the anterior cingulate, SUVRs derived from the cerebellum showed high tau retention in MCI and AD patients whereas those derived from PERSI-WM showed higher tau retention in AD patients than in MCI patients. This suggests that in clinical practice, suboptimal count normalization can result in misdiagnosis or inaccurate assessment of disease severity. PERSI has been shown to improve diagnostic accuracy (Southeast et al., 2018). Our results provide evidence that the PERSI-WM method is superior to the conventional method of using the cerebellum as a reference region for the diagnosis of dementia, and suggest that the former is more useful for tau and Aβ PET imaging.

In this study, tau retention was detected in brain regions that are susceptible to neurodegeneration in AD including the frontal, parietal, temporal, and occipital lobes; anterior and posterior cingulate; precuneus; and Braak I/II (entorhinal cortex and hippocampus). Several tau tracers show elevated signals in the temporal region and more broadly throughout the cortex in AD patients than in HCs (Wong et al., 2018; Lohith et al., 2019; Lu et al., 2020; Mueller et al., 2020). Tau retention was detected in Braak I/II in the early stages of AD and MCI (Maass et al., 2017), which is supported by our results. We observed relatively high tau retention in the temporal and occipital lobes in Cohort I (flortaucipir cohort) and in the precuneus and posterior cingulate in Cohort II ([¹⁸F]-APN-1607); the latter is relatively consistent with a previous report on [¹⁸F]-APN-1607 tau retention based on effect sizes in the same brain regions, which also found

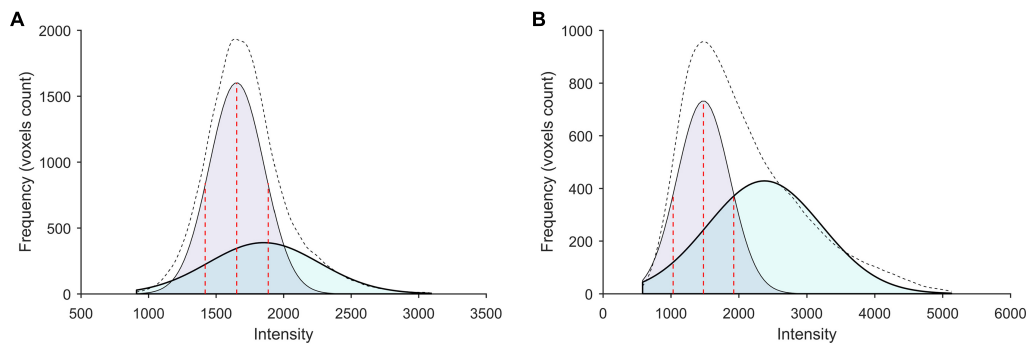


FIGURE 2 | Subject-specific WM histograms for two typical subjects evaluated by [^{18}F]-APN-1607 PET. **(A)** A 56-year-old HC (male). **(B)** A 56-year-old AD patient (female). Purple and cyan areas represent lower- and higher-intensity signals, respectively; the black dotted line shows the sum of two peaks (bimodal Gaussian distribution). For AD patients, voxels that spilled into the WM were captured by the higher peak.

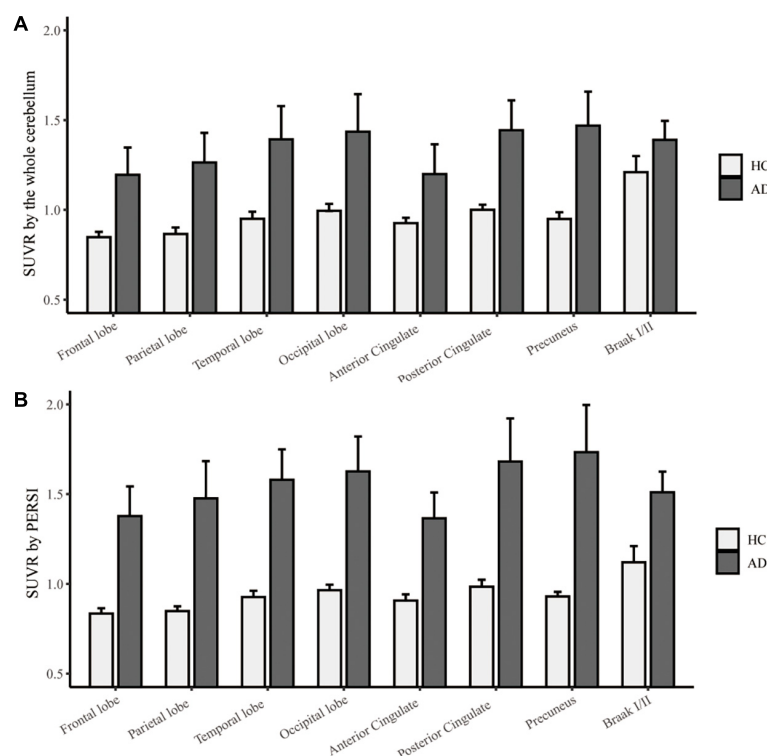


FIGURE 3 | Regional [^{18}F]-APN-1607 SUVR count normalization. **(A)** The whole cerebellum was the reference region for quantification. **(B)** PERSI-WM for HC and AD groups. Mean group SUVRs (\pm SD) across predefined ROIs are shown.

that PERSI-WM had better diagnostic performance than the cerebellar cortex (Lu et al., 2020).

We used the same PERSI method to calculate SUVRs for two tracers in two different cohorts. PERSI-WM could effectively distinguish AD patients from HCs in Cohort II. Based on MMSE and CDR-SB scores, cognitive decline was more severe in AD patients of Cohort II than in those of Cohort I; this suggests that the former had higher tau retention, which could result in a larger effect size and AUC, although further investigation in a larger population is required to confirm this possibility.

In both Cohort I and II, SUVR in HC were <1.0 in some brain regions such as the frontal and parietal lobes, especially with the PERSI method. SUVR of cortex <1.0 have been obtained for other tau tracers using cerebellum GM as a reference region, including [^{18}F]-AV-1451 (Shcherbinin et al., 2016), [^{18}F]-PI-2620 (Mueller et al., 2020), [^{18}F]-MK-6240 (Lohith et al., 2019), and [^{18}F]-RO-948 (Wong et al., 2018). Shcherbinin et al. (2016) reported a [^{18}F]-AV-1451 study with four young cognitively normal (YCN) subjects, five old cognitively normal (OCN) subjects, five MCI and four AD. Although mean SUVR from 80

TABLE 3 | Mean standardized uptake value ratio of cortical regions by diagnostic group (Cohort II).

Cortical region	Reference [†]	AUC	Effect size [‡]
Frontal lobe	Cerebellum	0.914	1.52
	PERSI-WM	0.975	2.38
Parietal lobe	Cerebellum	0.930	1.55
	PERSI-WM	0.956	2.97
Temporal lobe	Cerebellum	0.937	1.61
	PERSI-WM	0.949	2.53
Occipital lobe	Cerebellum	0.922	1.54
	PERSI-WM	0.971	2.66
Anterior cingulate	Cerebellum	0.803	1.15
	PERSI-WM	0.949	1.79
Posterior cingulate	Cerebellum	0.921	1.83
	PERSI-WM	0.933	2.48
Precuneus	Cerebellum	0.943	1.93
	PERSI-WM	0.968	3.64
Braak I/II	Cerebellum	0.823	0.64
	PERSI-WM	0.937	1.33

[†] Cerebellum, the whole cerebellum served as a reference region for quantification; PERSI-WM, parametric estimation of reference signal intensity with white matter as the reference region.

[‡] Presented as standardized Cohen's *d*.

AUC, area under the receiver operating characteristic curve.

to 100 min after injection of all 4 groups were above 1.0 in five target ROIs including the frontal, lateral parietal, occipital, mesial temporal and lateral temporal lobe. However in the time courses of regional SUVR for subjects in each diagnostic category figure, some YCN and/or OCN subjects showed SUVRs <1.0 in the above six target ROIs. Mueller et al. (2020) reported a [¹⁸F]-PI-2620 study with 10 HC and 12 AD. In the Supplementary Table 1 of Muller's study, HC showed mean SUVR <1.0 in posterior cingulate from 60 to 90 min after injection. Interestingly, SUVR in subcortical WM was <1.0 (0.90 ± 0.10) at same time. This suggested that PERSI based on WM may have less binding than cerebellum. Lohith et al. (2019) reported a [¹⁸F]-MK-6240 study with four HC and six MCI or AD. In the regional (representative cortical and subcortical) SUVR-time course with cerebellar cortex as reference figure, 2 HC showed SUVR <1.0 in temporal cortex and hippocampus from 60 to 90 min after injection. Wong et al. (2018) reported a [¹⁸F]-RO-948 study with six HC and four AD. Supplementary Table 4 of Wong's study showed SUVR of HC <1 in hippocampus, parahippocampus and insula. Therefore, SUVR of some cortex region <1 maybe reflect non-specific binding of the tracer to neuro-pigments, which has been observed in *in vitro* autoradiography studies. SUVRs <1 can mostly be attributed to off-target binding in WM (Lohith et al., 2019). The WM is a key aspect of the PERSI method that can yield lower SUVRs compared to the cerebellum.

This study had several shortcomings. (1) The size of the [¹⁸F]-APN-1607 cohort was relatively small, and only HCs and AD patients were included. The PERSI method is a data-driven approach for reducing spatial variability; therefore, additional [¹⁸F]-APN-1607 data are needed to fully verify the applicability of the PERSI method for the diagnosis of dementia, including from different disease stages such as MCI. (2) In a [¹⁸F]-APN-1607

PET study, AD patients showed higher binding than HCs in regions outside the cerebral cortex such as the caudate and putamen (Lu et al., 2020); and in a flortaucipir study, the putamen showed higher binding in AD patients than in HCs. We focused only on ROIs in the cerebral cortex in the present study, but future investigations should include more ROIs in other brain regions. (3) For longitudinal studies, the PERSI method can mitigate the influence of the PVE. AD is a chronic neurodegenerative disease with long course, with AD patients followed up multiple times over a long period. As both cortical atrophy and tracer uptake kinetics can change over time, the WM as a reference region can be variably affected at different time points. PERSI can alleviate the PVE by detecting the optimal reference signal based on voxel intensity, such that the results are less affected by differences in uptake pattern or image processing errors at different time points (Landau et al., 2015; Southekal et al., 2018). There were no longitudinal data for the two tau tracers examined in this study, although these could enhance the applicability of the PERSI method. (4) In the present study, the flortaucipir data were obtained from the ADNI database; as such, our analyses were retrospective. A prospective study with flortaucipir PET is needed to validate our results. (5) Although we tested the PERSI method with different tracers in two cohorts, the study population included only AD patients with amyloid deposition, with no amyloid-negative dementia patients. For more definitive conclusions, amyloid status and findings from anatomic MRI or glucose metabolism PET imaging should be considered. (6) Because of the small size of Cohort II ([¹⁸F]-APN-1607 PET), we did not examine voxel-wise correlations between cognitive impairment (e.g., MMSE score) and [¹⁸F]-APN-1607 binding in the cerebral cortex of AD patients, although this is important to confirm the broader clinical utility of the PERSI method.

CONCLUSION

The PERSI-WM method is superior to the conventional method of using the cerebellum as a reference region for semi-quantification of tau deposition and detection of multiple tau tracers in PET imaging; it can also mitigate the influence of the PVE. Thus, the PERSI method can be promising for the accurate diagnosis of dementia based on PET imaging.

ALZHEIMER'S DISEASE NEUROIMAGING INITIATIVE

Alzheimer's Association; Alzheimer's Drug Discovery Foundation; Araclon Biotech; BioClinica, Inc.; Biogen; Bristol-Myers Squibb Company; CereSpir, Inc.; Eisai, Inc.; Elan Pharmaceuticals, Inc.; Eli Lilly and Company; EuroImmun; F. Hoffmann-La Roche Ltd. and its affiliated company Genentech, Inc.; Fujirebio; GE Healthcare; IXICO, Ltd.; Janssen Alzheimer Immunotherapy Research & Development, LLC; Johnson & Johnson Pharmaceutical Research & Development LLC; Lumosity; Lundbeck; Merck & Co., Inc.; Meso Scale Diagnostics, LLC.; NeuroRx Research; Neurotrack Technologies; Novartis

Pharmaceuticals Corporation; Pfizer, Inc.; Piramal Imaging; Servier; Takeda Pharmaceutical Company; and Transition Therapeutics. The Canadian Institutes of Health Research is providing funds to support ADNI clinical sites in Canada. Private sector contributions are facilitated by the Foundation for the National Institutes of Health (<https://www.fnih.org>). The grantee organization was the Northern California Institute for Research and Education, and the study was coordinated by the Alzheimer's Disease Cooperative Study at the University of California, San Diego. ADNI data are disseminated by the Laboratory for Neuroimaging at the University of Southern California.

DATA AVAILABILITY STATEMENT

The raw data supporting the conclusions of this article will be made available by the authors, without undue reservation.

ETHICS STATEMENT

The studies involving human participants were reviewed and approved by the Institutional Review Board of Huashan Hospital (HIRB), Fudan University. The patients/participants provided their written informed consent to participate in this study.

AUTHOR CONTRIBUTIONS

HZ and MW conceived and designed the experiments, analyzed and interpreted the data, and wrote the manuscript. JL, WB, and

LL performed the experiments and wrote the manuscript. CZ and JJ analyzed and interpreted the data and wrote the manuscript. All authors read and approved the final version of the article for publication.

FUNDING

This study was supported by grants from the National Natural Science Foundation of China (nos. 61603236, 81671239, 81401135, 81771483, 81361120393, and 81901367) and Shanghai Municipal Science and Technology Major Project (no. 2017SHZDZX01). APRINOIA Therapeutics (Suzhou, China) provided the tosylate precursor used for the radiosynthesis of [^{18}F]-APN-1607. Data collection and sharing for this project was funded by the Alzheimer's Disease Neuroimaging Initiative (ADNI) (National Institutes of Health grant no. U01 AG024904) and Department of Defense (DOD) ADNI (DOD award no. W81XWH-12-2-0012). ADNI was funded by the National Institute of Aging and the National Institute of Biomedical Imaging and Bioengineering. The Canadian Institutes of Health Research is providing funds to support ADNI clinical sites in Canada. Private sector contributions are facilitated by the Foundation for the National Institutes of Health (<https://www.fnih.org>). The grantee organization was the Northern California Institute for Research and Education, and the study was coordinated by the Alzheimer's Disease Cooperative Study at the University of California, San Diego. ADNI data are disseminated by the Laboratory for Neuroimaging at the University of Southern California.

REFERENCES

- Braak, H., and Braak, E. (1991). Neuropathological staging of Alzheimer-related changes. *Acta Neuropathol.* 82, 239–259. doi: 10.1007/BF00308809
- Devous, M. D. Sr., Joshi, A. D., Navitsky, M., Southekal, S., Pontecorvo, M. J., Shen, H., et al. (2018). Test-Retest reproducibility for the tau PET imaging agent flortaucipir F 18. *J. Nucl. Med.* 59, 937–943. doi: 10.2967/jnumed.117.200691
- Goedert, M., Crowther, R. A., and Garner, C. C. (1991). Molecular characterization of microtubule-associated proteins tau and MAP2. *Trends Neurosci.* 14, 193–199. doi: 10.1016/0166-2236(91)90105-4
- Kang, J. M., Lee, S. Y., Seo, S., Jeong, H. J., Woo, S. H., Lee, H., et al. (2017). Tau positron emission tomography using [(18)F]THK5351 and cerebral glucose hypometabolism in Alzheimer's disease. *Neurobiol. Aging* 59, 210–219. doi: 10.1016/j.neurobiolaging.2017.08.008
- Kitamura, S., Shimada, H., Niwa, F., Endo, H., Shinotoh, H., Takahata, K., et al. (2018). Tau-induced focal neurotoxicity and network disruption related to apathy in Alzheimer's disease. *J. Neurol. Neurosurg. Psychiatry* 89, 1208–1214. doi: 10.1136/jnnp-2018-317970
- Landau, S. M., Fero, A., Baker, S. L., Koeppe, R., Mintun, M., Chen, K., et al. (2015). Measurement of longitudinal beta-amyloid change with 18F-florbetapir PET and standardized uptake value ratios. *J. Nucl. Med.* 56, 567–574. doi: 10.2967/jnumed.114.148981
- Leuzy, A., Chiotis, K., Lemoine, L., Gillberg, P. G., Almkvist, O., Rodriguez-Vieitez, E., et al. (2019). Tau PET imaging in neurodegenerative tauopathies—still a challenge. *Mol. Psychiatry* 24, 1112–1134. doi: 10.1038/s41380-018-0342-8
- Lohith, T. G., Bennacef, I., Vandenberghe, R., Vandenbulcke, M., Salinas, C. A., Declercq, R., et al. (2019). Brain imaging of Alzheimer dementia patients and elderly controls with (18)F-MK-6240, a PET tracer targeting neurofibrillary tangles. *J. Nucl. Med.* 60, 107–114. doi: 10.2967/jnumed.118.208215
- Lu, J., Bao, W., Li, M., Li, L., Zhang, Z., Alberts, I., et al. (2020). Associations of [(18)F]-APN-1607 Tau PET binding in the brain of Alzheimer's disease patients with cognition and glucose metabolism. *Front. Neurosci.* 14:604. doi: 10.3389/fnins.2020.00604
- Maass, A., Landau, S., Baker, S. L., Horng, A., Lockhart, S. N., La Joie, R., et al. (2017). Comparison of multiple tau-PET measures as biomarkers in aging and Alzheimer's disease. *Neuroimage* 157, 448–463. doi: 10.1016/j.neuroimage.2017.05.058
- Marquie, M., Normandin, M. D., Vandenburg, C. R., Costantino, I. M., Bien, E. A., Rycyna, L. G., et al. (2015). Validating novel tau positron emission tomography tracer [F-18]-AV-1451 (T807) on postmortem brain tissue. *Ann. Neurol.* 78, 787–800. doi: 10.1002/ana.24517
- McKhann, G. M., Knopman, D. S., Chertkow, H., Hyman, B. T., Jack, C. R. Jr., Kawas, C. H., et al. (2011). The diagnosis of dementia due to Alzheimer's disease: recommendations from the National Institute on Aging-Alzheimer's Association workgroups on diagnostic guidelines for Alzheimer's disease. *Alzheimers Dement.* 7, 263–269. doi: 10.1016/j.jalz.2011.03.005
- Meechai, T., Tepmongkol, S., and Pluempitwiriyawej, C. (2015). Partial-volume effect correction in positron emission tomography brain scan image using super-resolution image reconstruction. *Br. J. Radiol.* 88:20140119. doi: 10.1259/bjr.20140119
- Mueller, A., Bullich, S., Barret, O., Madonia, J., Berndt, M., Papin, C., et al. (2020). Tau PET imaging with (18)F-PI-2620 in patients with Alzheimer disease and healthy controls: a first-in-humans study. *J. Nucl. Med.* 61, 911–919. doi: 10.2967/jnumed.119.236224
- Okamura, N., Harada, R., Ishiki, A., Kikuchi, A., Nakamura, T., and Kudo, Y. (2018). The development and validation of tau PET tracers: current status and future directions. *Clin. Transl. Imaging* 6, 305–316. doi: 10.1007/s40336-018-0290-y

- Rabinovici, G. D., and Jagust, W. J. (2009). Amyloid imaging in aging and dementia: testing the amyloid hypothesis in vivo. *Behav. Neurol.* 21, 117–128. doi: 10.3233/BEN-2009-0232
- Scholl, M., Lockhart, S. N., Schonhaut, D. R., O'neil, J. P., Janabi, M., Ossenkoppele, R., et al. (2016). PET imaging of tau deposition in the aging human brain. *Neuron* 89, 971–982. doi: 10.1016/j.neuron.2016.01.028
- Shcherbinin, S., Schwarz, A. J., Joshi, A., Navitsky, M., Flitter, M., Shankle, W. R., et al. (2016). Kinetics of the Tau PET tracer 18F-AV-1451 (T807) in subjects with normal cognitive function, mild cognitive impairment, and Alzheimer disease. *J. Nucl. Med.* 57, 1535–1542. doi: 10.2967/jnumed.115.170027
- Shimada, H., Kitamura, S., Shinotoh, H., Endo, H., Niwa, F., Hirano, S., et al. (2017). Association between Aβeta and tau accumulations and their influence on clinical features in aging and Alzheimer's disease spectrum brains: a [(11)C]PBB3-PET study. *Alzheimers Dement. (Amst.)* 6, 11–20. doi: 10.1016/j.dadm.2016.12.009
- Sone, D., Imabayashi, E., Maikusa, N., Okamura, N., Furumoto, S., Kudo, Y., et al. (2017). Regional tau deposition and subregion atrophy of medial temporal structures in early Alzheimer's disease: a combined positron emission tomography/magnetic resonance imaging study. *Alzheimers Dement. (Amst.)* 9, 35–40. doi: 10.1016/j.dadm.2017.07.001
- Southekal, S., Devous, M. D. Sr., Kennedy, I., Navitsky, M., Lu, M., Joshi, A. D., et al. (2018). Flortaucipir F 18 quantitation using parametric estimation of reference signal intensity. *J. Nucl. Med.* 59, 944–951. doi: 10.2967/jnumed.117.200006
- Tzourio-Mazoyer, N., Landeau, B., Papathanassiou, D., Crivello, F., Etard, O., Delcroix, N., et al. (2002). Automated anatomical labeling of activations in SPM using a macroscopic anatomical parcellation of the MNI MRI single-subject brain. *Neuroimage* 15, 273–289. doi: 10.1006/nimg.2001.0978
- Villemagne, V. L., Dore, V., Burnham, S. C., Masters, C. L., and Rowe, C. C. (2018). Imaging tau and amyloid-beta proteinopathies in Alzheimer disease and other conditions. *Nat. Rev. Neurol.* 14, 225–236. doi: 10.1038/nrneurol.2018.9
- Villemagne, V. L., Fodero-Tavoletti, M. T., Masters, C. L., and Rowe, C. C. (2015). Tau imaging: early progress and future directions. *Lancet Neurol.* 14, 114–124. doi: 10.1016/S1474-4422(14)70252-2
- Wong, D. F., Comley, R. A., Kuwabara, H., Rosenberg, P. B., Resnick, S. M., Ostrowitzki, S., et al. (2018). Characterization of 3 novel tau radiopharmaceuticals, (11)C-RO-963, (11)C-RO-643, and (18)F-RO-948, in healthy controls and in Alzheimer subjects. *J. Nucl. Med.* 59, 1869–1876. doi: 10.2967/jnumed.118.209916
- Zhang, H., Wu, P., Ziegler, S. I., Guan, Y., Wang, Y., Ge, J., et al. (2017). Data-driven identification of intensity normalization region based on longitudinal coherency of (18)F-FDG metabolism in the healthy brain. *Neuroimage* 146, 589–599. doi: 10.1016/j.neuroimage.2016.09.031

Conflict of Interest: The authors declare that the research was conducted in the absence of any commercial or financial relationships that could be construed as a potential conflict of interest.

Copyright © 2021 Zhang, Wang, Lu, Bao, Li, Jiang, Zuo and Alzheimer's Disease Neuroimaging Initiative. This is an open-access article distributed under the terms of the Creative Commons Attribution License (CC BY). The use, distribution or reproduction in other forums is permitted, provided the original author(s) and the copyright owner(s) are credited and that the original publication in this journal is cited, in accordance with accepted academic practice. No use, distribution or reproduction is permitted which does not comply with these terms.



Identification of Electroencephalogram Signals in Alzheimer's Disease by Multifractal and Multiscale Entropy Analysis

Momo Ando¹, Sou Nobukawa^{1,2*}, Mitsuru Kikuchi^{3,4} and Tetsuya Takahashi^{4,5,6}

¹ Graduate School of Information and Computer Science, Chiba Institute of Technology, Narashino, Japan, ² Department of Computer Science, Chiba Institute of Technology, Narashino, Japan, ³ Department of Psychiatry and Behavioral Science, Kanazawa University, Ishikawa, Japan, ⁴ Research Center for Child Mental Development, Kanazawa University, Ishikawa, Japan, ⁵ Department of Neuropsychiatry, University of Fukui, Fukui, Japan, ⁶ Uozu Shinkei Sanatorium, Uozu, Japan

OPEN ACCESS

Edited by:

Yu Chen,
Shenzhen Institutes of Advanced
Technology, Chinese Academy of
Sciences (CAS), China

Reviewed by:

Men-Tzung Lo,
National Central University, Taiwan
Andras Eke,
Semmelweis University, Hungary
Renato Anghinah,
University of São Paulo, Brazil

*Correspondence:

Sou Nobukawa
nobukawa@cs.it-chiba.ac.jp

Specialty section:

This article was submitted to
Neurodegeneration,
a section of the journal
Frontiers in Neuroscience

Received: 14 February 2021

Accepted: 01 June 2021

Published: 28 June 2021

Citation:

Ando M, Nobukawa S, Kikuchi M and
Takahashi T (2021) Identification of
Electroencephalogram Signals in
Alzheimer's Disease by Multifractal
and Multiscale Entropy Analysis.
Front. Neurosci. 15:667614.
doi: 10.3389/fnins.2021.667614

Alzheimer's disease (AD) is the most common form of dementia and is a progressive neurodegenerative disease that primarily develops in old age. In recent years, it has been reported that early diagnosis of AD and early intervention significantly delays disease progression. Hence, early diagnosis and intervention are emphasized. As a diagnostic index for AD patients, evaluating the complexity of the dependence of the electroencephalography (EEG) signal on the temporal scale of Alzheimer's disease (AD) patients is effective. Multiscale entropy analysis and multifractal analysis have been performed individually, and their usefulness as diagnostic indicators has been confirmed, but the complementary relationship between these analyses, which may enhance diagnostic accuracy, has not been investigated. We hypothesize that combining multiscale entropy and fractal analyses may add another dimension to understanding the alteration of EEG dynamics in AD. In this study, we performed both multiscale entropy and multifractal analyses on EEGs from AD patients and healthy subjects. We found that the classification accuracy was improved using both techniques. These findings suggest that the use of multiscale entropy analysis and multifractal analysis may lead to the development of AD diagnostic tools.

Keywords: EEG signal, Alzheimer's disease, multifractal, multiscale entropy, early diagnosis

1. INTRODUCTION

Alzheimer's disease (AD) is the most common form of dementia and is a progressive neurodegenerative disease that primarily develops in old age (Liu et al., 2014). The World Health Organization estimates that the global prevalence of AD will increase to 0.6% in 2030 and 1.2% by 2046 (Brookmeyer et al., 2007). Although there is no effective treatment for AD, in recent years, it has been reported that early diagnosis of AD and early intervention significantly delay the progression of the disease. Hence, it would be ideal to diagnose AD early in its clinical course (Liu et al., 2014).

In AD, there are three significant anatomical changes: progressive neuronal death, neurofibrillary tangles, and senile plaques in extensive brain areas (Sims et al., 2017; Yamaguchi-Kabata et al., 2018). Positron emission tomography (PET) and magnetic resonance imaging (MRI)

are often used to diagnose AD and detect neurotransmitter activity disorders, amyloid beta plaque deposition, and brain atrophy (Ewers et al., 2011; McKhann et al., 2011; Sperling et al., 2011). As methods focused on functional neural activity, studies based on the temporal behavior of neural activity were conducted using electroencephalography (EEG), magnetoencephalography (MEG), and functional magnetic resonance imaging (fMRI) (Greicius et al., 2004; Jeong, 2004; Stam, 2005; Dickerson and Sperling, 2008; Takahashi, 2013; Yang and Tsai, 2013; Wang et al., 2017; Nobukawa et al., 2020).

Among all these evaluations, EEG is cost-effective, widely available, and non-invasive, making it ideal for clinical applications (Vecchio et al., 2013; Kulkarni and Bairagi, 2018). AD's pathological progression alters EEG behavior, such as slow waves, low synchronization of neural activity among brain regions, and low temporal complexity. Complexity analysis is a good approach to detect cortical disconnection in AD because this state impairs mutual neural interaction among widespread brain regions. Studies assessing EEG signals' complexity in patients with AD focused on deterministic chaos and fractal dimensions, such as the correlation dimension and Lyapunov exponent (Kantz and Schreiber, 2004). These studies reported a reduction in the complexity of neural activity in AD patients (Woyshville and Calabrese, 1994; Besthorn et al., 1995; Jelles et al., 1999; Jeong, 2004; Smits et al., 2016; Al-Nuaimi et al., 2017). Moreover, EEG dynamics at each temporal scale and frequency band, such as theta, beta, and gamma bands, are associated with different memory function components, cognitive and perceptual function (Klimesch et al., 2007). Hence, as a diagnostic index for AD patients with various brain function defects, the evaluation of the complexity with temporal scale dependence in EEG signal is effective (Mizuno et al., 2010; Nobukawa et al., 2019, 2020).

Multiscale entropy (MSE) analysis and multifractal (MF) analysis are known as typical temporal scale complexity dependency analyses (Takahashi, 2013; Yang and Tsai, 2013). In addition to EEG's temporal dependency in AD, MSE analysis also showed lower complexity on a small temporal scale in the frontal region in AD; in comparison, higher complexity was observed across this brain region in AD on a larger temporal scale (Mizuno et al., 2010; Ni et al., 2016). Zorick et al. reported that a statistical model based on MF analysis could detect clinical stages of severity and degree of progress from cognitive impairment to AD (Zorick et al., 2020). As described above, MSE and MF analyses have a high ability to detect the complexity in EEG signals of AD. As such, these indices might become biomarkers for AD to evaluate the alteration of EEG complexity (Mizuno et al., 2010; Ni et al., 2016; Nobukawa et al., 2020).

Recent studies have focused on the enhancement of classification accuracy combining several feature values, including complexity indexes in EEG of AD patients (Wang et al., 2015; Gómez et al., 2017; Ieracitano et al., 2020; Nobukawa et al., 2020). Particularly, Wang et al. (2015) and Gómez et al. (2017) showed that combinations of spectrum and bispectrum entropy measures enhance the accuracy of EEG signals classification in AD. Therefore, these combinations of complexity measures are a new avenue for the diagnosis of AD EEG signals. Furthermore, Cukic et al. showed that multiscale

TABLE 1 | Physical characteristics of healthy control (HC) and subjects with Alzheimer's disease (AD).

	HC participants	AD participants	p-values
Male/female	7/11	5/11	0.72
Age(year)	59.3 (5.3, 55–66)	57.5 (4.7, 43–64)	0.31
MMSE score	NA	15.5 (4.7, 10–26)	NA

analysis (MSE) and fractal dimension provide complementary information on brain activity in healthy subjects (Cukic et al., 2018). This complementary relationship may enhance the accuracy of AD identification. In this context, we hypothesize that the combination of MSE and fractal analysis may contribute to a better understanding of EEG dynamics' alteration in AD. In this study, we performed MSE analysis and multifractal analysis on the EEGs of patients with AD and healthy controls (HC).

2. MATERIALS AND METHODS

2.1. Subject

The subjects of this study were 16 patients with AD and 18 sex-matched and aged-matched healthy old individuals (see **Table 1**) (Mizuno et al., 2010; Nobukawa et al., 2019, 2020). The sample size of AD and HC groups was determined based on previous works on complexity analysis (Abásolo et al., 2008; Mizuno et al., 2010; Nobukawa et al., 2019, 2020). For this study, we defined healthy old individuals as nonsmokers and not on medication. Subjects with medical or neurological conditions, including epilepsy or head trauma in the past, and subjects with a history of alcohol or drug dependence were excluded. We recruited patients with AD or probable AD who met the NINCDS-ADRDA criteria and in a state before the onset of primary dementia based on DSM-IV criteria. Recruited patients with AD were not receiving medications that act on the central nervous system.

Each patient was evaluated using the Function Assessment Stage (FAST) and Mini-Mental State Examination (MMSE). Three patients had mild dementia (FAST 3); seven moderate dementia (FAST 4); and six severe dementia (FAST 5). The MMSE score ranged from 10 to 26, with an average of 15.56. **Table 1** shows subjects' characteristics. All subjects provided informed consent prior to the start of the study. The research protocol was approved by the Ethics Committee of Kanazawa University. All procedures in this study were conducted in accordance with the Declaration of Helsinki.

2.2. EEG Recordings

As reported in previous studies, methods have been established to record and preprocess EEG data (Mizuno et al., 2010). When recording the EEG, the participants were seated in an electrically shielded and soundproof recording room, and the room lighting was controlled. For the EEG measurement, 16 electrodes (Fp1, Fp2, F3, F4, C3, C4, P3, P4, O1, O2, F7, F8, Fz, Pz, T5, and T6) were used in the electrode arrangement called the International 10–20 System. EEG activity was measured using the binaural connection as a reference.

EEG-4518 manufactured by Nihon Kohden Co., Ltd. Tokyo, Japan, was used for measurement. Eye movements were tracked using bipolar electrocardiography (EOG). The EEG signal was recorded using a sampling frequency of 200 Hz and bandpass filtered at 2.0–60 Hz. As pre-processing steps were not conducted (i.e., filtering except for bandpass, artifacts removal, or data reconstruction), because such processing may destroy the data's intrinsic dynamics, we visually selected epochs without artifacts. The electrode/skin conductance impedance was carefully controlled at each electrode to $< 5k\Omega$. Each subject's EEG signal was measured for 10–15 min in a resting state with eyes closed. A video surveillance system was used to visually inspect the subjects' alertness and to confirm that only epochs with closed eyes and a wakefulness state (not light sleep) were measured. Visual inspection of EEG and EOG records identified EEG time series segments recorded in a wakefulness state with closed eyes. Subjects were considered fully awake when predominant alpha activity appeared in the posterior region in response to the fast eye movements of the EOG channel (Wada et al., 1996). MSE analysis and MF analysis were conducted against a continuous 50-s (10000 data points) epoch.

2.3. Multifractal Analysis

In MF analysis, wavelet leaders derived from the coefficients of the discrete wavelet transform are widely used (Jaffard et al., 2006; Wendt and Abry, 2007). The discrete wavelet coefficient of the discrete signal $X(t)$ is given by

$$d_X(j, k) = \int_{\mathbb{R}} X(t) 2^j \psi_0(2^{-j}t - k) dt \quad (j = 1, 2, \dots, k = 1, 2, \dots), \quad (1)$$

where ψ_0 is a compact-supported mother wavelet function. One-dimensional wavelet leaders were expressed by

$$L_X(j, k) = \sup_{\lambda' \subset 3\lambda_{j,k}} |d_X(j, k)|. \quad (2)$$

Here, $\lambda = \lambda_{j,k} = [k2^j, (k+1)2^j]$ represents the time interval of scale 2^j , and $3\lambda_{j,k-1} = \cup \lambda_{j,k} \cup \lambda_{j,k+1}$ represents the adjacent time (Wendt and Abry, 2007). The singular value spectrum $D(h)$, which is the distribution of the fractal dimension represented by the Hölder exponent h , is represented by wavelet leaders (Jaffard et al., 2006; Wendt and Abry, 2007):

$$D(h) = \inf_{q \neq 0} (1 + qh - \zeta_L(q)). \quad (3)$$

Here, q indicates the moment for scaling index $\zeta_L(q)$. The scaling index $\zeta_L(q)$ and the structural function $S_L(q, j)$ are represented by Equations (4, 5), respectively:

$$\zeta_L(q) = \liminf_{j \rightarrow 0} \left(\frac{\log_2 S_L(q, j)}{j} \right), \quad (4)$$

$$S_L(q, j) = \frac{1}{n_j} \sum_{k=1}^{n_j} |L_X(j, k)|^q. \quad (5)$$

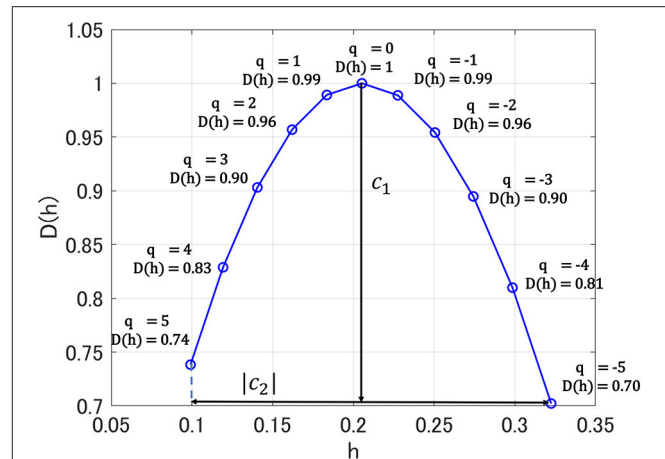


FIGURE 1 | Singular value spectra $D(h)$ in multi-fractal analysis for one healthy control (HC) subject. Here, h exhibits Hölder exponent. c_1 shows h -value where $D(h) = 1.0$ ($q = 0$); absolute value of c_2 corresponds to the range of $D(h)$ distribution between $q = -5$ and 5 .

Here, n_j indicates the number of samples of X when the scale is 2^j . As Hölder exponent h approaches 1.0, the shape of the time series becomes more differentiable. In contrast, as Hölder exponent h approaches zero, the shape of the time series becomes nearly discontinuous. If the scaling index $\zeta_L(q)$ is a linear function and $D(h)$ converges to a particular h , then the signal is monofractal. On the other hand, in the scaling index, where $\zeta_L(q)$ deviates from linearity and $D(h)$ is distributed over a wide range of h , the signal is multifractal. In this study, to capture the profile of $D(h)$, we used the primary cumulant c_1 of $D(h)$, which corresponds to a dominant component of $D(h)$ as smoothness index estimated in the entire time-series. Moreover, we used the secondary cumulant c_2 , which corresponds to the magnitude of fluctuation intermittently appearing as the index for multifractality. **Figure 1** shows the results of multi-fractal analysis of one HC subject. c_1 shows h -value where $D(h) = 1.0$ ($q = 0$), which corresponds to the degree of differentiability in the dominant component of the entire time-series, i.e., smoothness. The absolute value of c_2 corresponds to the range of $D(h)$ distribution between $q = -5$ and 5 . In the monofractal time-series, $D(h)$ converges at a particular h (in the time-series with no multifractality, $D(h)$ converges at h -value with $q = 2$), while in the multifractal time-series, the range of $D(h)$ becomes wider (Ihlen, 2012; Mukli et al., 2015). Therefore, the degree of variation of $D(h)$ corresponding to c_2 reflects the multifractality. In this study, multifractal analysis was performed using the wavelet toolbox of MATLAB (<https://jp.mathworks.com/products/wavelet.html>).

2.4. Multiscale Entropy Analysis

To perform the multiscale entropy (MSE) analysis, we used the dependence of the EEG time series complexity on the temporal scale (Costa et al., 2002). The sample entropy for the time-series

of random Z-scored variable $\{x_1, x_2, \dots, x_N\}$ is defined as

$$h(r, m) = -\log \frac{C_{m+1}(r)}{C_m(r)}. \quad (6)$$

$C_m(r)$ is the probability of $|\mathbf{x}_i^m - \mathbf{x}_j^m| < r (i \neq j, i, j = 1, 2, \dots)$. \mathbf{x}_i^m indicates an m -dimensional vector $\mathbf{x}_i^m = \{x_i, x_{i+1}, \dots, x_{i+m-1}\}$. $\{x_i, x_{i+1}, \dots, x_N\}$ is obtained course-grained process:

$$x_j = \frac{1}{\tau} \sum_{i=(j-1)\tau+1}^{j\tau} y_i (1 \leq j \leq \frac{N}{\tau}). \quad (7)$$

where, $\{y_1, y_2, \dots, y_N\}$ is observed signals. $\tau (\tau = 1, 2, \dots)$ is the temporal scale. In this study, we set $m = 2$ and $r = 0.2$ (Costa et al., 2002). In this study, MSE analysis was performed using the Physio Toolkit, a toolbox of MATLAB (<http://physionet.incor.usp.br/physiotools/sampen/>).

2.5. Statistical Analysis

For c_1 and c_2 , repeated measures analysis of variance (ANOVA) with the groups (HC vs. AD) as the between-subject factor and the electrodes (16 electrodes from Fp1 to T6) as the within-subject factors was performed to test for group differences. The result of ANOVA is represented by F -value based on a comparison of variances within/between groups. The Greenhouse-Geisser adjustment was applied in degrees of freedom. The α bilateral level of 0.05 was used, considered a statistically significant criterion to avoid type I errors. *Post-hoc t*-tests were used to assess the significant main effects of group and per-electrode interactions. Benjamini–Hochberg false discovery rate (FDR) correction was applied to the t -score for multiple comparisons in c_1 and c_2 ($q < 0.05$) (16 p -values: 16 electrodes).

For sample entropy, repeated measures ANOVA with groups (HC vs. AD) as the between-subject factor and electrode (16 electrodes from Fp1 to T6) and temporal scale (30 temporal scales) as within-subject factors, was performed to test for group differences. The Greenhouse-Geisser adjustment and α bilateral level of 0.05 were applied. The result of ANOVA is represented by F -value based on a comparison of variances within/between groups. *Post-hoc t*-tests were used to assess the significant main effects of the group and per-electrode and per-temporal-scale interactions. The FDR correction was applied to the t -score for multiple comparisons ($q < 0.05$) (480 p -values: 16 electrode \times 30 scales).

Receiver operating characteristic (ROC) curves were used to evaluate the ability to identify AD. To identify AD, a logistic regression model based on the sample entropy, c_1 and c_2 , was used. Here, the logistic regression model outputs the identification probability of AD for each subject. Subsequently, the true positive rate/false positive rate at each threshold of identification probability from 0 to 1.0 in both groups are measured. Principal component analysis is used as a preprocess for dimensionality reduction. Logistic regression was applied to the 1st–3rd principal components of each evaluation index. The identification accuracy was evaluated by measuring the area under the ROC curve (AUC), which is an index of identification accuracy. Subsequently, according to AUC values,

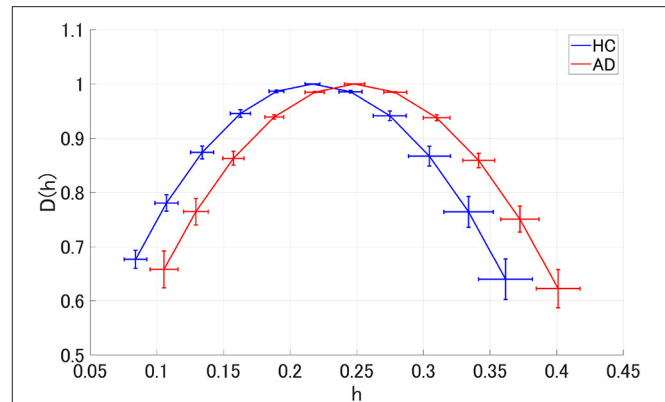


FIGURE 2 | Singular value spectra of Alzheimer's disease (AD) group and HC group. The mean and standard deviation among each group of $D(h)$ and h . Since the distribution is wide, it is considered that it reflects the multi-fractal property of both groups' EEG signal.

TABLE 2 | AD vs. HC repeated measure ANOVA analysis results [F -value (p value)] in multifractal (MF) analysis results, F and p value with $p < 0.05$ are represented by bold characters.

	Group	Group \times nodes
c_1	$F = 9.088$ ($p = 0.005$)	$F = 1.460$ ($p = 0.204$)
c_2	$F = 0.654$ ($p = 0.425$)	$F = 1.981$ ($p = 0.072$)

the classification accuracy is graded in logistic regression models based on the sample entropy, c_1 and c_2 . Here, $AUC = 1.0$ corresponds to complete identification, and $AUC = 0.5$ corresponds to random identification.

3. RESULTS

3.1. Multifractal Analysis

We performed MF analysis on both HC and AD groups. **Figure 2** shows the mean and standard deviation for each group of $D(h)$ and h . Since the distribution is wide, it reflects the multi-fractal property (Sikdar et al., 2018) of both groups' EEG signal. **Table 2** shows the repeated measures ANOVA results of 1st (c_1) and 2nd (c_2) cumulants of singular spectrum. The significant main effect in c_1 was confirmed. The mean values of c_1 and c_2 in the AD and HC groups and the result of the *post-hoc t*-test between AD and HC are shown in **Figure 3**. The significantly higher c_1 values in the AD group ($q < 0.050$ corresponding to $p < 0.012$) was confirmed at F3, Fz, F4, C3, C4, P3, Pz, and P4.

3.2. Multi Scale Entropy Analysis

We performed an MSE analysis in the HC and AD groups. **Table 3** shows the repeated measures ANOVA results of MSE analysis. Significant group \times scale interactions without the main effect of sample entropy were confirmed. As *post hoc t*-test, the mean values of sample entropy in HC and AD groups and the t -value between HC and AD are shown in **Figure 4**. The results demonstrated a significantly lower sample entropy

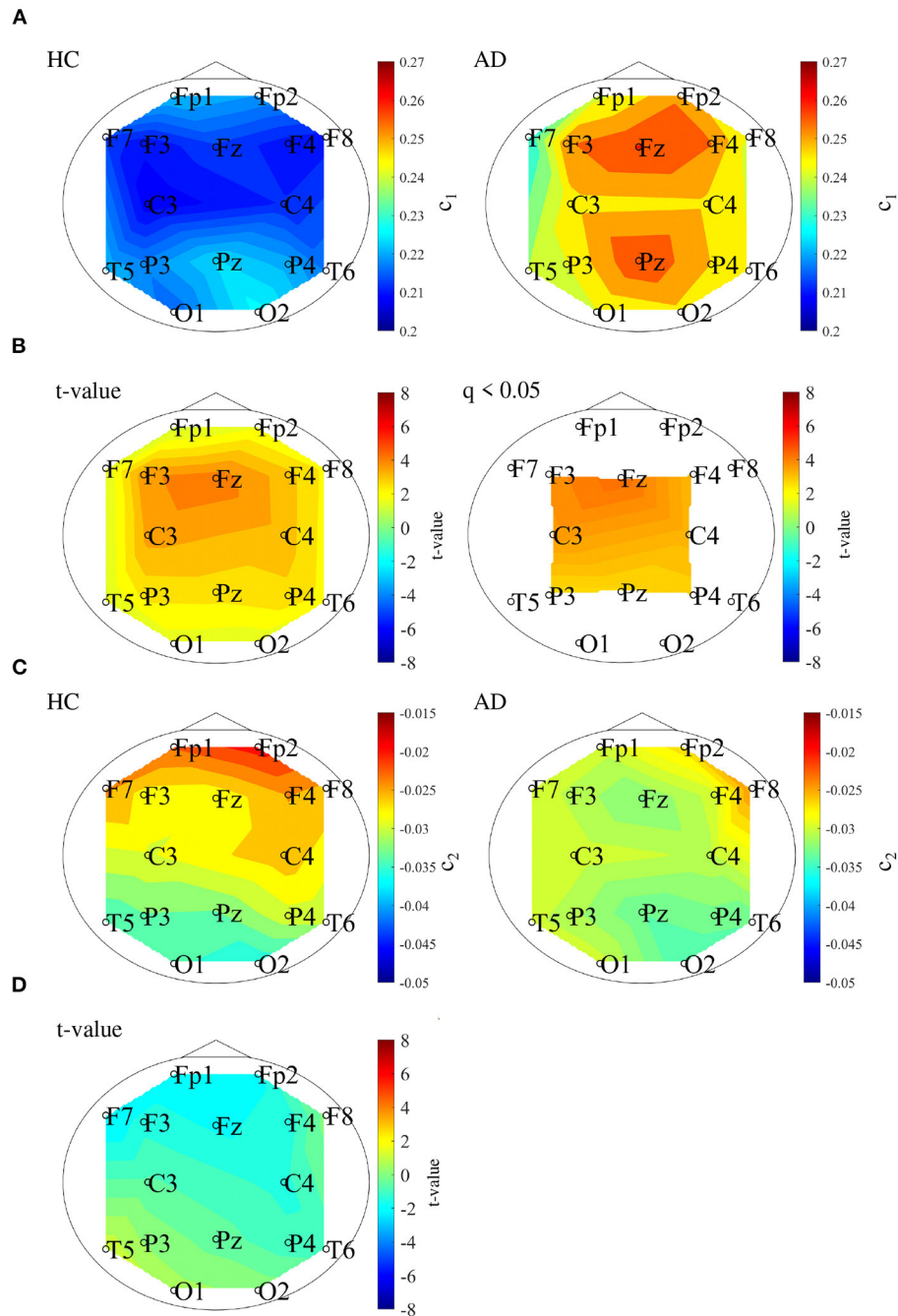


FIGURE 3 | (A) 1st cumulant of singular value spectrum c_1 . Mean value of c_1 in the HC (left) and AD (right) groups. **(B)** t -values between the AD and HC groups. The warm (cold) color represents higher (smaller) c_1 values of AD than those for HC. The left and right correspond to the t -value and t -value satisfying the false discovery rate (FDR) correction criteria $q < 0.050$ corresponding to ($p < 0.012$). c_1 of the AD group had significantly higher values at F3, Fz, F4, C3, C4, P3, Pz, and P4. **(C)** 2nd cumulant of singular value spectrum c_2 . Mean value of c_2 in the HC (left) and AD (right) groups. **(D)** t -value between the AD and HC groups warm (cold) color represents higher (smaller) c_2 values of AD than those for HC. There are no-significant high/low t -values satisfying FDR correction criteria $q < 0.05$ (corresponding to $p < 0.003$).

of AD ($q < 0.050$ corresponding to $p < 0.002$) in the temporal scale region 1 to 5 (0.005 to 0.025 s). The result of MSE analysis was reported in our previous studies (Mizuno et al., 2010; Nobukawa et al., 2020). Particularly, in the study by

Mizuno et al. (2010), multiscale entropy analysis against AD EEG signals was reported, while our recent study (Nobukawa et al., 2020) showed the relationship between functional connectivity characterized by phase synchronization and multiscale entropy in AD EEG signals.

3.3. ROC Curve

To evaluate the classification ability in c_1 and c_2 , we evaluated ROC curves. **Figure 5** shows the result of ROC in the case with 1st–3rd principal components in each evaluated index. In the sample entropy case, the values are averaged in 1 to 5 temporal scale. AUC in the c_1 case exhibits the highest classification ability (AUC = 0.85 in the case c_1 ; AUC = 0.78, in the case of c_2 ; AUC = 0.82 in the case sample entropy). Furthermore,

TABLE 3 | AD vs. HC repeated measure ANOVA results [F -value (p -value)] in multi scale entropy (MSE) analysis results, F and p value with $p < 0.05$ are represented by bold characters.

Group	Group \times node	Group \times scale	Group \times node \times scale
$F = 1.233$ ($p = 0.275$)	$F = 1.860$ ($p = 0.129$)	$F = 11.457$ ($p = 0.003$)	$F = 0.979$ ($p = 0.451$)

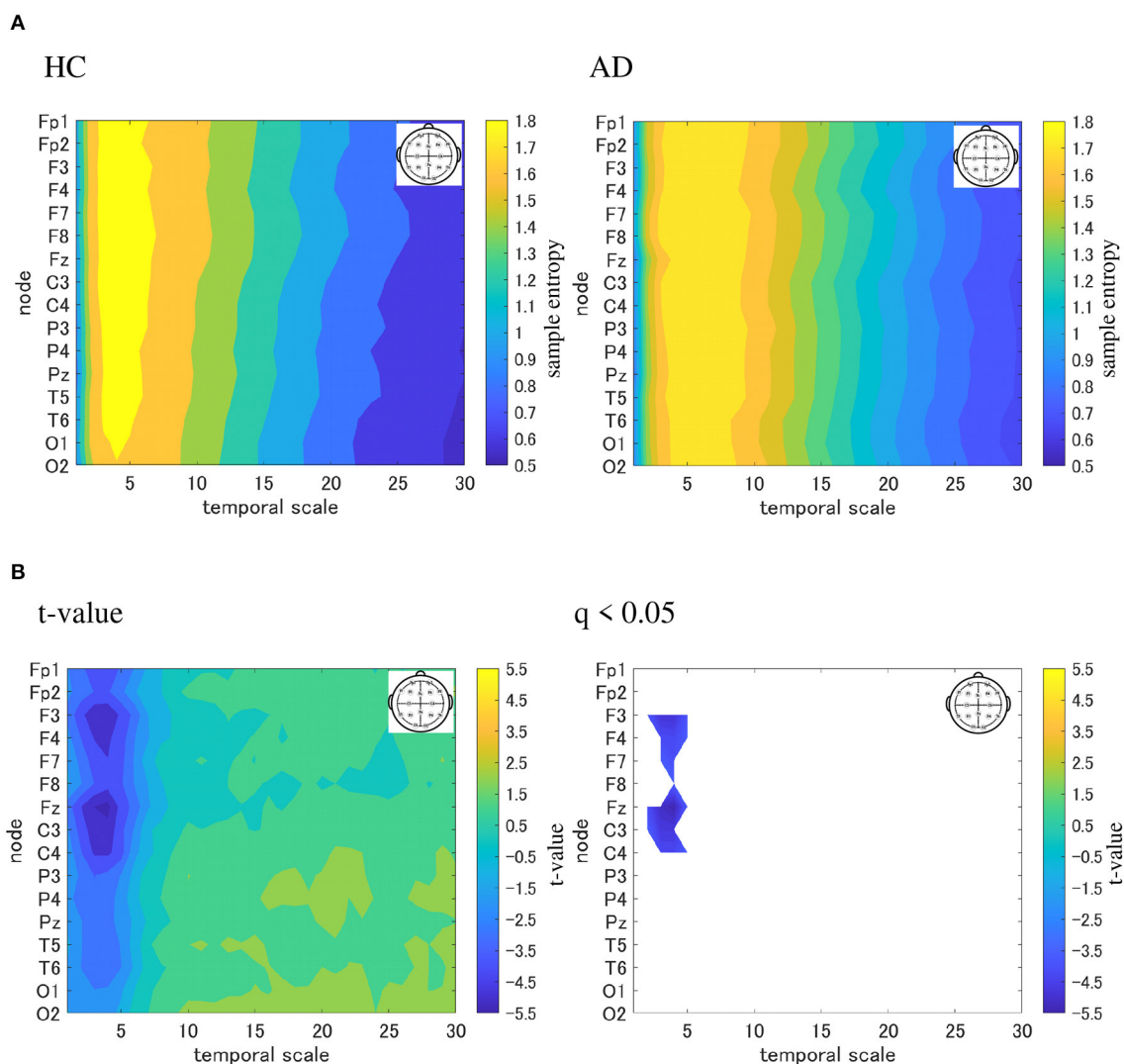


FIGURE 4 | Multi-scale entropy analysis in HC and AD group. The horizontal axis represents the temporal-scale factor, τ . **(A)** Mean values of sample entropy from 1 (0.005 s) to 30 (0.15 s) scale factors in HC (left part) and AD (right part). **(B)** t -value between the AD and HC groups (left part). The warm (cold) color represents a higher (smaller) sample entropy value for AD than that for HC. The t -value satisfying the FDR correction criteria $q < 0.050$ corresponding to ($p < 0.002$). Significantly smaller sample entropy of AD low temporal scale regions 1 to 5 (0.005 to 0.025 s).

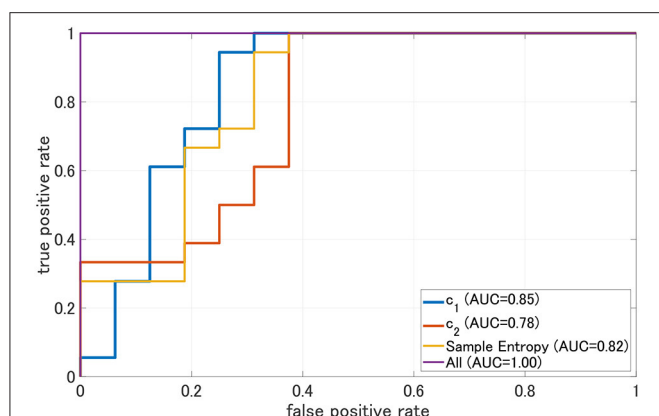


FIGURE 5 | Receiver operating characteristic curve (ROC) for c_1 , c_2 , and sample entropy. The area under the ROC curve (AUC) is shown in the legend. As classifier, logistic regression is used. In this case, c_1 , c_2 , and sample entropy, each 1st–3rd principal component was used separately. In the case represented by “ALL”, all 1st–3rd principal components component of c_1 , c_2 , sample entropy were used. We evaluated ROC in the case using all these values; the results show the enhancement of classification ability (AUC = 1.00).

we evaluated ROC using all these values; the results showed an enhancement of classification ability (AUC = 1.00). To investigate why the combination of c_1 , c_2 , and sample entropy enhances classification ability, we evaluated their relationship by correlation analysis. **Figure 6** shows a scatterplot among the 1st component of c_1 , c_2 and sample entropy used for ROC evaluation in **Figure 5**. The correlation coefficients R are shown in **Table 4**. The results show a high negative and positive correlation between c_1 and sample entropy, a positive correlation between c_2 and sample entropy, and a relatively low negative correlation between c_1 and c_2 . This relatively low correlation between c_1 and c_2 suggests that c_2 includes complementary information regarding multifractality in the classification. Moreover, to investigate the correlation between c_1 and c_2 , not the principal components, the correlation coefficient R between c_1 and c_2 in HC and AD groups is demonstrated in **Figure 7**. The results show the spatial dependency of correlation coefficient R , which might contribute to the enhancement of classification accuracy shown in **Figure 7**.

To demonstrate that the decision region for AD is determined by c_1 , c_2 , and sample entropy, decision regions for AD with decision probability > 0.9 by logistic regression model were depicted on the plane between the 1st principal component of c_1 and the 1st principal component of c_2 and the plane between the 1st principal component of c_1 and the 1st principal component of the sample entropy (see **Figure 8**). Here, all other components except the plane axis were set to average among subjects in both the HC and AD groups. As a result, we confirmed that the decision region exhibits dependent on all of them.

4. DISCUSSIONS

This study evaluated AD identification accuracy by focusing on the complementary relationship between two complexity analyses. The MF and MSE of EEG signals in HC and AD

were evaluated, and classification accuracies quantified by the AUC of logistic regression models were compared. The results of c_1 as the index for the smoothness of the EEG time series by MF analysis showed that c_1 of AD significantly increased. However, the results of c_2 , as the index for the EEG time series' multifractal nature by MF analysis, show that no significant AD alteration was observed. MSE analysis showed a significant region-specific reduction of small-temporal-scale sample entropy of AD (corresponding to the complexity of faster temporal EEG behaviors). In the comparison of classification accuracy between c_1 , c_2 , and small-temporal-scale sample entropy, c_1 exhibits the highest classification accuracy. Moreover, the classification accuracy with c_1 was enhanced by considering the complementary relationship of c_2 and sample entropy.

We must discuss the reason why c_1 as the degree of smoothness increase in AD. In the alteration of EEG/MEG signals in AD, a reduction in temporal complexity has been widely observed (Woyshville and Calabrese, 1994; Besthorn et al., 1995; Jelles et al., 1999; Jeong, 2004; Wickramasinghe and Geisler, 2008; Smits et al., 2016; Kulkarni, 2018; Smailovic et al., 2019). Correspondingly, our results of sample entropy at a small temporal scale also exhibited a reduction in complexity. Considering the negative correlation between c_1 and the small-temporal-scale sample entropy (see **Table 4**), the increase in c_1 , that is, the enhancement of EEG signal smoothness in AD, was caused by the decrease in small-temporal-scale complexity. Therefore, the enhancement of c_1 reflects the loss of temporal complexity of neural activity in AD. This finding agrees with previous studies on MF analysis in AD (Jaffard et al., 2006; Wendt and Abry, 2007).

Furthermore, we must consider why small temporal scale complexity decreases in AD. Dysfunction of the gamma-aminobutyric acid (GABA) signaling system caused by deposition of amyloid β and tau protein have been reported. These changes lead to the reduced oscillation of the gamma band activity produced by GABA signaling (Nava-Mesa et al., 2014; Govindpani et al., 2017; Calvo-Flores Guzmán et al., 2018). Consequently, dysfunction of the mutual interaction of gamma band activity can reduce the complexity more on the faster than on the slower temporal scales (Ahmadlou et al., 2011; Nobukawa et al., 2019).

Next, it is necessary to consider why the classification accuracy was highest when c_1 , c_2 , and sample entropy were used. According to Cukic *et al.*, sample entropy and fractal dimension by mono-fractal analysis show a complementary relationship among temporal scales (Cukic et al., 2018), and this relationship can enhance the ability to detect an alteration of complexity. Our results (see **Figure 8**) also showed that a decision region for AD with decision probability > 0.9 by logistic regression model exhibits a dependency on c_1 , c_2 , and sample entropy. Therefore, the combination of c_1 corresponding to the fractal dimension and sample entropy might enhance the accuracy of AD detection. In addition to these findings, a recent MF analysis in AD showed that the multifractal degree reflects disease-specific alterations of complexity (Zorick et al., 2020). Although the classification ability in case of separate use of multifractals measured by c_2

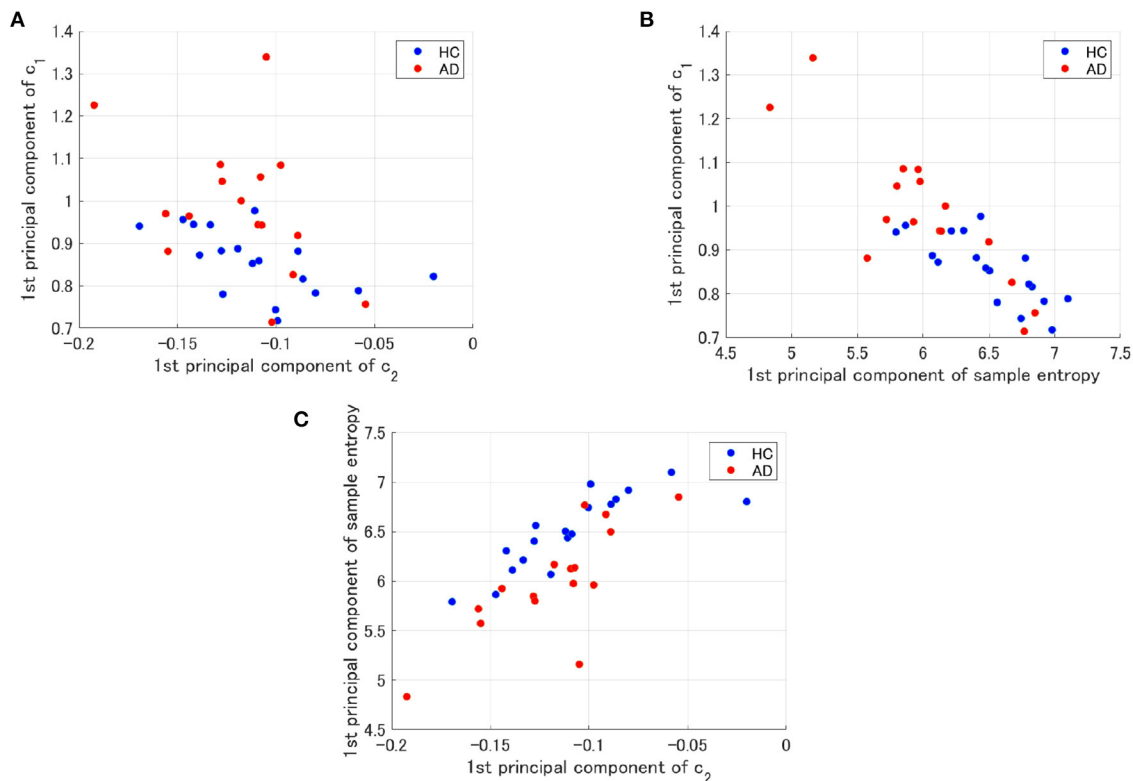


FIGURE 6 | Scatter plots for 1st principal component of c_1 , c_2 and sample entropy used to evaluate of ROC in **Figure 5**. **(A)** Scatter plots between c_1 and c_2 . The result showed a relatively low negative correlation [$R = -0.56(\text{HC}), R = -0.42(\text{AD})$]. **(B)** Scatter plots between c_1 and the sample entropy. The results showed a high negative correlation [$R = -0.77(\text{HC}), R = -0.85(\text{AD})$]. **(C)** Scatter plots of the between sample entropy and c_2 . The result showed a positive correlation [$R = 0.82(\text{HC}), R = 0.78(\text{AD})$].

TABLE 4 | Correlation coefficient values (R) for each combination of c_1 , c_2 , and sample entropy in HC and AD.

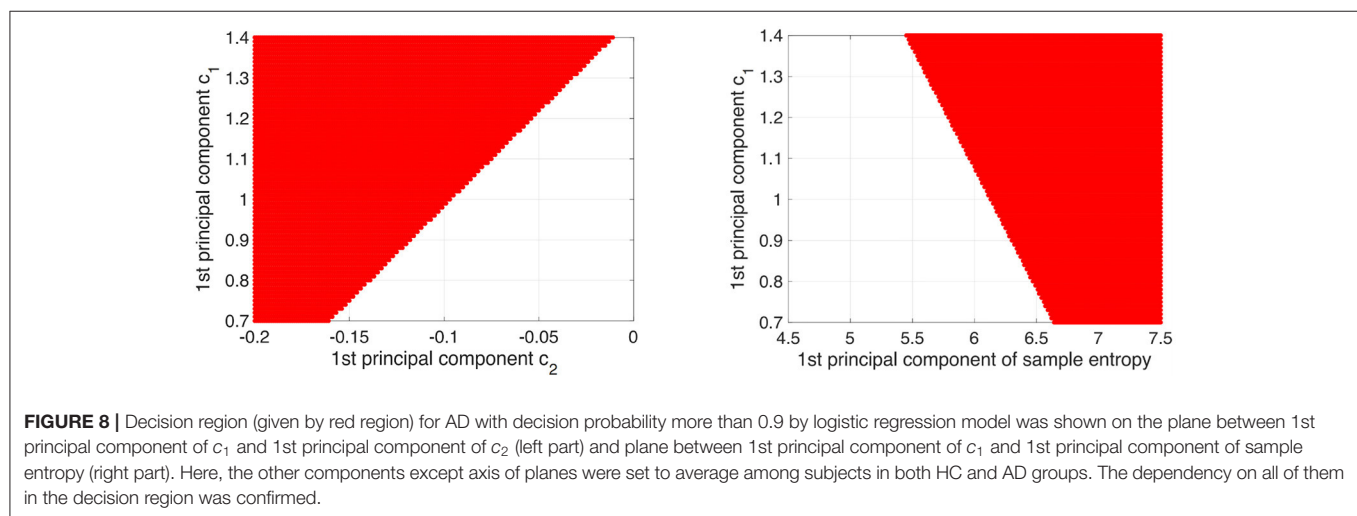
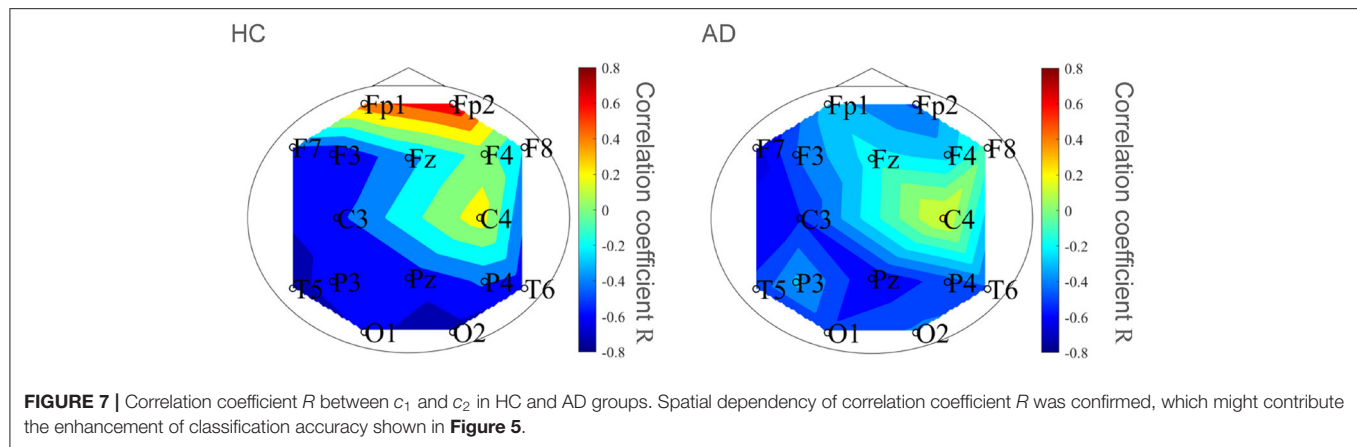
c_1 vs. c_2	c_1 vs. Sample entropy	Sample entropy vs. c_2	
Correlation coefficient(HC)	$R = -0.56$	$R = -0.77$	$R = 0.82$
Correlation coefficient(AD)	$R = -0.42$	$R = -0.85$	$R = 0.78$

is relatively low, the combination with c_2 may contribute to the improvement of classification accuracy.

To investigate whether the high heterogeneity of severity in patients with AD affects classification, we investigated distributions of c_1 , c_2 , and mean sample entropy in a scale from 1 to 5 according to severity as classified by FAST (3 (mild dementia), 4 (moderate dementia), and 5 (severe dementia), through repeated measures ANOVA with severity as a between-subject factor and electrode as a within-subjects factor. The results showed that severity did not have any significant main effect or interaction in c_1 ($F = 0.412$, $p = 0.671$), c_2 ($F = 0.706$, $p = 0.512$), and sample entropy ($F = 0.532$, $p = 0.6$); while a significant interaction between severity and electrodes in c_1 ($F = 2.103$, $p = 0.036$) appeared. Therefore, although in larger AD groups a severity-dependent effect may appear, the bias of

high heterogeneity of severity is limited. Additionally, in patients with mild dementia, no differences in the distribution of c_1 , c_2 , and sample entropy compared to more severe patients appeared in the repeated measures ANOVA. Therefore, the classification accuracy may not change in case of a classification between HC and patients with mild dementia, which corresponds to the condition assumed for early diagnosis.

Finally, we must consider the limitations of this study. First, EEG signals do not always reflect the neural activity directly under the electrode. In this study, 16 electrodes were used to measure EEG, but the spatial resolution was too low to identify AD's complex functional connection structure. However, it is possible to use MEGs with a high spatial resolution and cortical positioning to solve this problem. Second, pre-processing for EEG signals was not adopted except for a band-pass filter. However, a recent study by Racz et al. (2018) indicated that appropriate pre-processing is needed for complexity analysis. Artifacts and noise are to be avoided, especially at the stage of clinical application. Therefore, this pre-processing for complexity analysis must be developed and adopted in future studies. Third, we consider that for our EEG data set, the multifractal analysis method proposed by Jaffard et al. (2006) and Wendt and Abry (2007) is sufficient, because a corrupted/inversed $D(h)$ distribution did not arise (see **Figure 2**). Additionally,



this study was conducted on the assumption of multifractality in EEG signals (Takahashi, 2013; Yang and Tsai, 2013; Sikdar et al., 2018). However, several studies highlighted the issues of incorrect estimation of multifractal indexes in time-series without multifractality (Grech and Pamula, 2012; Mukli et al., 2015). Therefore, multifractal analysis methods with higher robustness (Mukli et al., 2015) are desired at the stage of clinical application, since proper validation of EEG multifractality (Mukli et al., 2015; Racz et al., 2018) is an important issue. Fourth, the AD group had high heterogeneity of severity, and the sample size of the AD group was small, which could have influenced the classification accuracy. Therefore, the classification ability of our proposed method must be evaluated in larger AD groups. Additionally, a Bayesian statistic approach is more suitable for small size and high sample heterogeneity than that based on frequentist inference.

5. CONCLUSION

In this study, both MSE and MF analysis showed a reduction in EEG complexity in AD patients. Classification accuracy is better by combining MSE analysis and MF analysis than when

applying each one individually. Despite its limitations, this study shows that MSE and MF analysis play complementary roles in detecting the alteration of neural activity in AD. The use of both MSE and MF analysis may facilitate the development of AD diagnostic tools.

DATA AVAILABILITY STATEMENT

The datasets presented in this article are not readily available because the informed consent did not include the declaration regarding publicity of clinical data. Requests to access the datasets should be directed to Sou Nobukawa, nobukawa@cs.it-chiba.ac.jp.

ETHICS STATEMENT

The studies involving human participants were reviewed and approved by Ethics Committee of Kanazawa University. The patients/participants provided their written informed consent to participate in this study.

AUTHOR CONTRIBUTIONS

MA, SN, MK, and TT conceived the methods. MA and SN analyzed the results, wrote the main manuscript text, and prepared all the figures. MK conducted the experiments. All authors reviewed the manuscript.

REFERENCES

- Abásolo, D., Escudero, J., Hornero, R., Gómez, C., and Espino, P. (2008). Approximate entropy and auto mutual information analysis of the electroencephalogram in Alzheimer's disease patients. *Med. Biol. Eng. Comput.* 46, 1019–1028. doi: 10.1007/s11517-008-0392-1
- Ahmadlou, M., Adeli, H., and Adeli, A. (2011). Fractality and a wavelet-chaos-methodology for EEG-based diagnosis of Alzheimer disease. *Alzheimer Dis. Assoc. Disord.* 25, 85–92. doi: 10.1097/WAD.0b013e3181ed1160
- Al-Nuaimi, A. H., Jammeh, E., Sun, L., and Ifeakor, E. (2017). "Higuchi fractal dimension of the electroencephalogram as a biomarker for early detection of Alzheimer's disease," in *2017 39th Annual International Conference of the IEEE Engineering in Medicine and Biology Society (EMBC)* (Jeju: IEEE), 2320–2324. doi: 10.1109/EMBC.2017.8037320
- Besthorn, C., Sattel, H., Geiger-Kabisch, C., Zerfass, R., and Förstl, H. (1995). Parameters of eeg dimensional complexity in Alzheimer's disease. *Electroencephalogr. Clin. Neurophysiol.* 95, 84–89. doi: 10.1016/0013-4694(95)00050-9
- Brookmeyer, R., Johnson, E., Ziegler-Graham, K., and Arrighi, H. M. (2007). Forecasting the global burden of Alzheimer's disease. *Alzheimer's Dement.* 3, 186–191. doi: 10.1016/j.jalz.2007.04.381
- Calvo-Flores Guzmán, B., Vinnakota, C., Govindpani, K., Waldvogel, H. J., Faull, R. L., and Kwakowsky, A. (2018). The gabaergic system as a therapeutic target for Alzheimer's disease. *J. Neurochem.* 146, 649–669. doi: 10.1111/jnc.14345
- Costa, M., Goldberger, A. L., and Peng, C.-K. (2002). Multiscale entropy analysis of complex physiologic time series. *Phys. Rev. Lett.* 89, 068102. doi: 10.1103/PhysRevLett.89.068102
- Cukic, M. B., Platisa, M. M., Kalauzi, A., Oommen, J., and Ljubisavljevic, M. R. (2018). The comparison of Higuchi fractal dimension and Sample Entropy analysis of sEMG: effects of muscle contraction intensity and TMS. *arXiv [Preprint]* arXiv:1803.10753.
- Dickerson, B. C., and Sperling, R. A. (2008). Functional abnormalities of the medial temporal lobe memory system in mild cognitive impairment and Alzheimer's disease: insights from functional MRI studies. *Neuropsychologia* 46, 1624–1635. doi: 10.1016/j.neuropsychologia.2007.11.030
- Ewers, M., Sperling, R. A., Klunk, W. E., Weiner, M. W., and Hampel, H. (2011). Neuroimaging markers for the prediction and early diagnosis of Alzheimer's disease dementia. *Trends Neurosci.* 34, 430–442. doi: 10.1016/j.tins.2011.05.005
- Gómez, C., Vaquerizo-Villar, F., Poza, J., Ruiz, S. J., Tola-Arribas, M. A., Cano, M., et al. (2017). "Bispectral analysis of spontaneous EEG activity from patients with moderate dementia due to Alzheimer's disease," in *2017 39th Annual International Conference of the IEEE Engineering in Medicine and Biology Society (EMBC)* (Jeju: IEEE), 422–425. doi: 10.1109/EMBC.2017.8036852
- Govindpani, K., Calvo-Flores Guzmán, B., Vinnakota, C., Waldvogel, H. J., Faull, R. L., and Kwakowsky, A. (2017). Towards a better understanding of gabaergic remodeling in Alzheimer's disease. *Int. J. Mol. Sci.* 18, 1813. doi: 10.3390/ijms18081813
- Grech, D., and Pamula, G. (2012). Multifractal background noise of monofractal signals. *Acta Phys. Pol. A* 121, 34–39. doi: 10.12693/APhysPolA.121.B-34
- Greicius, M. D., Srivastava, G., Reiss, A. L., and Menon, V. (2004). Default-mode network activity distinguishes Alzheimer's disease from healthy aging: evidence from functional mri. *Proc. Natl. Acad. Sci. U.S.A.* 101, 4637–4642. doi: 10.1073/pnas.0308627101
- Ieracitano, C., Mammone, N., Hussain, A., and Morabito, F. C. (2020). A novel multi-modal machine learning based approach for automatic classification of EEG recordings in dementia. *Neural Netw.* 123, 176–190. doi: 10.1016/j.neunet.2019.12.006
- Ihlen, E. A. F. E. (2012). Introduction to multifractal detrended fluctuation analysis in matlab. *Front. Physiol.* 3:141. doi: 10.3389/fphys.2012.00141
- Jaffard, S., Lashermes, B., and Abry, P. (2006). "Wavelet leaders in multifractal analysis," in *Wavelet Analysis and Applications* (Basel: Springer), 201–246.
- Jelles, B., Van Birgelen, J., Slaets, J., Hekster, R., Jonkman, E., and Stam, C. (1999). Decrease of non-linear structure in the EEG of Alzheimer patients compared to healthy controls. *Clin. Neurophysiol.* 110, 1159–1167. doi: 10.1016/S1388-2457(99)00013-9
- Jeong, J. (2004). Eeg dynamics in patients with Alzheimer's disease. *Clin. Neurophysiol.* 115, 1490–1505. doi: 10.1016/j.clinph.2004.01.001
- Kantz, H., and Schreiber, T. (2004). *Nonlinear Time Series Analysis* Vol. 7, Cambridge: Cambridge University Press. doi: 10.1017/CBO9780511755798
- Klimesch, W., Sauseng, P., Hanslmayr, S., Gruber, W., and Freunberger, R. (2007). Event-related phase reorganization may explain evoked neural dynamics. *Neurosci. Biobehav. Rev.* 31, 1003–1016. doi: 10.1016/j.neubiorev.2007.03.005
- Kulkarni, N. (2018). Use of complexity based features in diagnosis of mild Alzheimer disease using EEG signals. *Int. J. Inf. Technol.* 10, 59–64. doi: 10.1007/s41870-017-0057-0
- Kulkarni, N., and Bairagi, V. (2018). *EEG-Based Diagnosis of Alzheimer Disease: A Review and Novel Approaches for Feature Extraction and Classification Techniques*. London; San Diego, CA; Cambridge, MA; Oxford: Academic Press.
- Liu, S., Liu, S., Cai, W., Pujol, S., Kikinis, R., and Feng, D. (2014). "Early diagnosis of Alzheimer's disease with deep learning," in *2014 IEEE 11th International Symposium on Biomedical Imaging (ISBI)* (IEEE), 1015–1018. doi: 10.1109/ISBI.2014.6868045
- McKhann, G. M., Knopman, D. S., Chertkow, H., Hyman, B. T., Jack Jr, C. R., Kawas, C. H., et al. (2011). The diagnosis of dementia due to Alzheimer's disease: recommendations from the national institute on aging-Alzheimer's association workgroups on diagnostic guidelines for Alzheimer's disease. *Alzheimer's Dement.* 7, 263–269. doi: 10.1016/j.jalz.2011.03.005
- Mizuno, T., Takahashi, T., Cho, R. Y., Kikuchi, M., Murata, T., Takahashi, K., et al. (2010). Assessment of eeg dynamical complexity in Alzheimer's disease using multiscale entropy. *Clin. Neurophysiol.* 121, 1438–1446. doi: 10.1016/j.clinph.2010.03.025
- Mukli, P., Nagy, Z., and Eke, A. (2015). Multifractal formalism by enforcing the universal behavior of scaling functions. *Phys. A Stat. Mech. Appl.* 417, 150–167. doi: 10.1016/j.physa.2014.09.002
- Nava-Mesa, M. O., Jiménez-Díaz, L., Yajeya, J., and Navarro-Lopez, J. D. (2014). Gabaergic neurotransmission and new strategies of neuromodulation to compensate synaptic dysfunction in early stages of Alzheimer's disease. *Front. Cell. Neurosci.* 8:167. doi: 10.3389/fncel.2014.00167
- Ni, H., Zhou, L., Ning, X., Wang, L., and (ADNI), A. D. N. I. (2016). Exploring multifractal-based features for mild Alzheimer's disease classification. *Magn. Reson. Med.* 76, 259–269. doi: 10.1002/mrm.25853
- Nobukawa, S., Yamanishi, T., Kasakawa, S., Nishimura, H., Kikuchi, M., and Takahashi, T. (2020). Classification methods based on complexity and synchronization of electroencephalography signals in Alzheimer's disease. *Front. Psychiatry* 11:255. doi: 10.3389/fpsyt.2020.00255
- Nobukawa, S., Yamanishi, T., Nishimura, H., Wada, Y., Kikuchi, M., and Takahashi, T. (2019). Atypical temporal-scale-specific fractal changes in Alzheimer's disease EEG and their relevance to cognitive decline. *Cogn. Neurodyn.* 13, 1–11. doi: 10.1007/s11571-018-9509-x
- Racz, F. S., Stylianou, O., Mukli, P., and Eke, A. (2018). Multifractal dynamic functional connectivity in the resting-state brain. *Front. Physiol.* 9:1704. doi: 10.3389/fphys.2018.01704
- Sikdar, D., Roy, R., and Mahadevappa, M. (2018). Epilepsy and seizure characterisation by multifractal analysis of EEG subbands. *Biomed. Signal Proc. Control* 41, 264–270. doi: 10.1016/j.bspc.2017.12.006

FUNDING

This work was supported by JSPS KAKENHI for Early-Career Scientists (grant no. 18K18124) (SN) and the OKAWA FOUNDATION for information and telecommunications (grant no. 20–20) (SN).

- Sims, R., Van Der Lee, S. J., Naj, A. C., Bellenguez, C., Badarinarayan, N., Jakobsdottir, J., et al. (2017). Rare coding variants in *PLCG2*, *ABI3*, and *TREM2* implicate microglial-mediated innate immunity in Alzheimer's disease. *Nat. Genet.* 49, 1373–1384. doi: 10.1038/ng.3916
- Smailovic, U., Koenig, T., Laukka, E. J., Kalpouzos, G., Andersson, T., Winblad, B., et al. (2019). Eeg time signature in Alzheimer's disease: functional brain networks falling apart. *Neuroimage Clin.* 24:102046. doi: 10.1016/j.nicl.2019.102046
- Smits, F. M., Porcaro, C., Cottone, C., Cancelli, A., Rossini, P. M., and Tecchio, F. (2016). Electroencephalographic fractal dimension in healthy ageing and Alzheimer's disease. *PLoS ONE* 11:e0149587. doi: 10.1371/journal.pone.0149587
- Sperling, R. A., Aisen, P. S., Beckett, L. A., Bennett, D. A., Craft, S., Fagan, A. M., et al. (2011). Toward defining the preclinical stages of Alzheimer's disease: Recommendations from the national institute on aging-Alzheimer's association workgroups on diagnostic guidelines for Alzheimer's disease. *Alzheimers Dement.* 7, 280–292. doi: 10.1016/j.jalz.2011.03.003
- Stam, C. J. (2005). Nonlinear dynamical analysis of EEG and MEG: review of an emerging field. *Clin. Neurophysiol.* 116, 2266–2301. doi: 10.1016/j.clinph.2005.06.011
- Takahashi, T. (2013). Complexity of spontaneous brain activity in mental disorders. *Prog. Neuropsychopharmacol. Biol. Psychiatry* 45, 258–266. doi: 10.1016/j.pnpbp.2012.05.001
- Vecchio, F., Babiloni, C., Lizio, R., Fallani, F. D. V., Blinowska, K., Verrienti, G., et al. (2013). Resting state cortical EEG rhythms in Alzheimer's disease: toward eeg markers for clinical applications: a review. *Suppl. Clin. Neurophysiol.* 62, 223–236. doi: 10.1016/B978-0-7020-5307-8.00015-6
- Wada, Y., Nanbu, Y., Koshino, Y., Shimada, Y., and Hashimoto, T. (1996). Inter- and intrahemispheric EEG coherence during light drowsiness. *Clin. EEG Neurosci.* 27, 84–88. doi: 10.1177/155005949602700207
- Wang, B., Niu, Y., Miao, L., Cao, R., Yan, P., Guo, H., et al. (2017). Decreased complexity in Alzheimer's disease: resting-state fMRI evidence of brain entropy mapping. *Front. Aging Neurosci.* 9:378. doi: 10.3389/fnagi.2017.00378
- Wang, R., Wang, J., Li, S., Yu, H., Deng, B., and Wei, X. (2015). Multiple feature extraction and classification of electroencephalograph signal for Alzheimer's with spectrum and bispectrum. *Chaos* 25, 013110. doi: 10.1063/1.4906038
- Wendt, H., and Abry, P. (2007). Multifractality tests using bootstrapped wavelet leaders. *IEEE Trans. Signal Proc.* 55, 4811–4820. doi: 10.1109/TSP.2007.896269
- Wickramasinghe, N., and Geisler, E. (2008). *Encyclopedia of Healthcare Information Systems*. London; Pennsylvania, PA: IGI Global. doi: 10.4018/978-1-59904-889-5
- Woysville, M. J., and Calabrese, J. R. (1994). Quantification of occipital eeg changes in Alzheimer's disease utilizing a new metric: the fractal dimension. *Biol. Psychiatry* 35, 381–387. doi: 10.1016/0006-3223(94)90004-3
- Yamaguchi-Kabata, Y., Morihara, T., Ohara, T., Ninomiya, T., Takahashi, A., Akatsu, H., et al. (2018). Integrated analysis of human genetic association study and mouse transcriptome suggests *lbh* and *shf* genes as novel susceptible genes for amyloid- β accumulation in Alzheimer's disease. *Hum. Genet.* 137, 521–533. doi: 10.1007/s00439-018-1906-z
- Yang, A. C., and Tsai, S.-J. (2013). Is mental illness complex? from behavior to brain. *Progr. Neuropsychopharmacol. Biol. Psychiatry* 45, 253–257. doi: 10.1016/j.pnpbp.2012.09.015
- Zorick, T., Landers, J., Leuchter, A., and Mandelkern, M. A. (2020). Eeg multifractal analysis correlates with cognitive testing scores and clinical staging in mild cognitive impairment. *J. Clin. Neurosci.* 76, 195–200. doi: 10.1016/j.jocn.2020.04.003

Conflict of Interest: The authors declare that the research was conducted in the absence of any commercial or financial relationships that could be construed as a potential conflict of interest.

Copyright © 2021 Ando, Nobukawa, Kikuchi and Takahashi. This is an open-access article distributed under the terms of the Creative Commons Attribution License (CC BY). The use, distribution or reproduction in other forums is permitted, provided the original author(s) and the copyright owner(s) are credited and that the original publication in this journal is cited, in accordance with accepted academic practice. No use, distribution or reproduction is permitted which does not comply with these terms.



Differences in Multimodal Electroencephalogram and Clinical Correlations Between Early-Onset Alzheimer's Disease and Frontotemporal Dementia

Nan Lin[†], Jing Gao[†], Chenhui Mao, Heyang Sun, Qiang Lu* and Liying Cui*

Department of Neurology, Peking Union Medical College Hospital, Beijing, China

OPEN ACCESS

Edited by:

Kin Ying Mok,
University College London,
United Kingdom

Reviewed by:

András Horváth,
National Institute of Clinical
Neurosciences, Hungary
Frederic Von Wegner,
University of New South Wales,
Australia
Siti Anom Ahmad,
Putra Malaysia University, Malaysia

*Correspondence:

Qiang Lu
luqiang@pumch.cn
Liying Cui
pumchcuily@sina.com

[†] These authors have contributed
equally to this work

Specialty section:

This article was submitted to
Neurodegeneration,
a section of the journal
Frontiers in Neuroscience

Received: 28 March 2021

Accepted: 02 July 2021

Published: 05 August 2021

Citation:

Lin N, Gao J, Mao C, Sun H, Lu Q
and Cui L (2021) Differences
in Multimodal Electroencephalogram
and Clinical Correlations Between
Early-Onset Alzheimer's Disease
and Frontotemporal Dementia.
Front. Neurosci. 15:687053.
doi: 10.3389/fnins.2021.687053

Background: Alzheimer's disease (AD) and frontotemporal dementia (FTD) are the two main types of dementia. We investigated the electroencephalogram (EEG) difference and clinical correlation in early-onset Alzheimer's disease (EOAD), and FTD using multimodal EEG analyses. EOAD had more severe EEG abnormalities than late-onset AD (LOAD). Group comparisons between EOAD and LOAD were also performed.

Methods: Thirty patients diagnosed with EOAD, nine patients with LOAD, and 14 patients with FTD (≤ 65 y) were recruited (2008.1–2020.2), along with 24 healthy controls (≤ 65 y, $n = 18$; > 65 y, $n = 6$). Clinical data were reviewed. Visual EEG, EEG microstate, and spectral analyses were performed.

Results: Compared to controls, markedly increased mean microstate duration, reduced mean occurrence, and reduced global field power (GFP) peaks per second were observed in EOAD and FTD. We found increased durations of class B in EOAD and class A in FTD. EOAD had reduced occurrences in classes A, B, and C, while only class C occurrence was reduced in FTD. The visual EEG results did not differ between AD and FTD. Microstate B showed correlations with activities of daily living score ($r = 0.780$, $p = 0.008$) and cerebrospinal fluid (CSF) A β 42 ($r = -0.833$, $p = 0.010$) in EOAD. Microstate D occurrence was correlated with the CSF A β 42 level in FTD ($r = 0.786$, $p = 0.021$). Spectral analysis revealed a general slowing EEG, which may contribute to microstate dynamic loss. Power in delta was significantly higher in EOAD than in FTD all over the head. In addition, EOAD had a marked increased duration and decreased occurrence than late-onset AD (LOAD), with no group differences in visual EEG results.

Conclusion: The current study found that EOAD and FTD had different EEG changes, and microstate had an association with clinical severity and CSF biomarkers. EEG microstate is more sensitive than visual EEG and may be useful for the differentiation between AD and FTD. The observations support that EEG can be a potential biomarker for the diagnosis and assessment of early-onset dementias.

Keywords: EEG microstate, early onset Alzheimer's disease, frontotemporal dementia, CSF biomarkers, spectral analysis

INTRODUCTION

Alzheimer's disease (AD) is the most common form of dementia, accounting for 60–80% of cases (Scheltens et al., 2016). A diagnosis of AD below the age of 65 is classed as early-onset AD (EOAD). EOAD accounts for only 5%–10% of all AD cases (Dai et al., 2018). Accumulation of abnormally folded amyloid beta ($A\beta$) and hyperphosphorylated tau proteins in amyloid plaques and neural tangles is causally related to neurodegenerative processes (Karran et al., 2011). Low $A\beta_{42}$ levels, high concentrations of t-tau and p-tau, and the ratio of tau/ $A\beta_{42}$ help to discriminate AD from healthy controls and other dementias (Shaw et al., 2009; Casoli et al., 2019). Patients with EOAD display greater cerebrospinal fluid (CSF) anomalies (Dumurgier et al., 2013) and more severe electroencephalogram (EEG) abnormalities (Micanovic and Pal, 2014).

Frontotemporal dementia (FTD) accounts for approximately 10% of all dementias (Hogan et al., 2016), characterized by prominent changes in social behavior and personality or aphasia accompanied by pathological changes in the frontal and temporal lobes. TAR (*trans*-active response) DNA-binding protein 43, tau, and fused-in-sarcoma protein were the three major disease proteins in the neuropathology of FTD (Wang et al., 2013). It can be difficult to distinguish clinically FTD from AD, especially EOAD, as EOAD may more commonly manifest with non-memory presentations, like language problems (Koedam et al., 2010).

Electroencephalogram is a relatively cost-effective, non-invasive technique, increasingly considered to be a potential biomarker for dementia differentiation recently. Several characteristics of the EEG have been put forward as biomarkers in AD and might be useful in the early recognition of neural signatures of dementias and differential diagnosis. Spectral EEG measures in AD showed a reduction of alpha and beta spectral powers and an increase in theta and delta spectral powers. The changes were associated with disease severity (Horvath et al., 2018). Recently, EEG microstate analyses were used in dementia. EEG microstates are defined as quasi-stable brief patterns of coordinated electrical activity on the scalp surface, which was first described by Lehmann et al. (1987) (Schumacher et al., 2019). The topographies remained transiently stable for 60–150 ms before rapidly transitioning into a new state.

Electroencephalogram microstates have been shown to be associated with cognition and perception (Milz et al., 2016; Santarnecchi et al., 2017). Previous studies observed microstate changes in cognitive disorders (Stevens and Kircher, 1998; Nishida et al., 2013; Hatz et al., 2015; Musaeus et al., 2019; Schumacher et al., 2019; Smailovic et al., 2019; Tait et al., 2020). However, microstate characteristics and correlation with CSF biomarkers in early-onset dementias, including AD and FTD, have not been well studied. The current study was set to investigate the EEG microstate in EOAD and FTD, along with EEG spectral analysis, and the correlations with clinical data and CSF biomarkers. The differences in EEG data were then analyzed to test the utility of EEG as a biomarker for clinical evaluations and differential diagnosis. Comparisons between EOAD, late-onset AD (LOAD), and healthy controls were also performed to

investigate the difference between microstate and visual EEG and the effect of age.

MATERIALS AND METHODS

Patients

The study population consisted of patients with cognition impairment in Peking Union Medical College Hospital between June 2015 and October 2019. Patients were diagnosed based on information obtained from an extensive clinical history, physical examinations, and lab examinations and excluded mood disorders and schizophrenia. All patients diagnosed with AD met the IWG-II criteria (Dubois et al., 2014) with cognitive scales, brain MRI, and CSF biomarker results. For FTD diagnosis, the Neary et al. (1998) or the McKhann et al. (2001) criteria were employed with brain MRI and CSF biomarker results for differentiation from AD. Dementia diagnoses were performed independently by two experienced clinicians. Patients who had complications of other neurological or psychiatric disorders, and severe systemic diseases that may influence the central nervous system, were excluded. Patients with AD were divided into EOAD and LOAD by age 65. Patients with FTD who were older than 65 years were further excluded. Clinical assessment scales included the Mini-Mental State Examination (MMSE) (Folstein et al., 1975), the Montreal Cognitive Assessment (MoCA) (Nasreddine et al., 2005), and activities of daily living (ADL) score. The data of CSF biomarkers and cognitive assessments undergone at the same time with EEG recordings were used for further analyses.

Biomarkers Assessments

Cerebrospinal fluid t-tau, p-tau, and $A\beta_{42}$ were measured using an enzyme-linked immunosorbent assay (Fujirebio, Ghent, Belgium). Samples were handled by experienced senior laboratory technicians blinded to patients' information.

EEG Examination and Data Preprocessing

Video EEG monitoring was performed using a 19-channel video-EEG monitoring system (EEG-1200C, Nihon Kohden, Tokyo, Japan) in hospital for more than 2 h. Recording electrodes were placed according to the international 10–20 system with a sampling frequency of 500 Hz. The visual EEG results were evaluated by at least one experienced epilepsy specialist. The degree of visual EEG abnormality was scored as follows: (1) 0 = normal; (2) 1 = mildly abnormal; (3) 2 = moderately abnormal; and (4) 3 = severely abnormal (Table 1).

Resting-state EEG data without excessive noise, artifacts, and epileptiform discharges were preprocessed with EEGLAB (R13_6_5b) in MATLAB R2017a. An independent component analysis was used for further artifact removal. Data were bandpass filtered into the range of 0.1–40 Hz and were recomputed against the average reference. EEG data were split into non-overlapping epochs of 2 s. Patients with less than 25 epochs were excluded. It resulted in 30 patients with EOAD, 14 with FTD, and 18 healthy

TABLE 1 | Definitions of visual EEG abnormality scores.

Visual EEG scores	Definitions
1 = mildly abnormal	At least one of the following EEG patterns: <ul style="list-style-type: none"> • <50% asymmetrical background activity; • Irregular alpha rhythm; • Excess beta activity with amplitude >50 μV, • Excessive theta activity mainly over the frontal region • Mildly excessive delta activity
2 = moderately abnormal	At least one of the following EEG patterns: <ul style="list-style-type: none"> • Occipital 7–8-Hz frequency band • No obvious occipital alpha rhythm • Asymmetry [>50%] moderately high delta activities • Sporadic epileptiform discharges
3 = severely abnormal	At least one of the following EEG patterns: <ul style="list-style-type: none"> • Persistent low-voltage or electrical silence • Periodic phenomenon • Dominant background delta or theta activity • Rhythmic epileptiform discharges

controls (≤ 65 y) for further analyses. Moreover, nine patients with LOAD and six healthy controls (> 65 y) were included in the current study. Frequency spectral analysis was performed in the following frequency bands: delta (1–4 Hz), theta (4–8 Hz), alpha (8–12 Hz), and beta (12–30 Hz).

Microstate Analysis

The microstate analysis was conducted using the EEGLAB plugin Microstate 1.1 in MATLAB R2017a. EEG data were further bandpass filtered into the 1–20-Hz range for microstate analysis. The overall variances across all electrodes were quantified by measuring the global field power (GFP). GFP was calculated as the standard deviation of the data at each time point (Wackermann et al., 1993; Hatz et al., 2015):

$$GFP_t = \sqrt{\frac{\sum_{i=1}^n u_i^2}{n}}$$

(n = number of channels)

u = amplitude in μ V at time point t)

Electroencephalogram topographies tend to be stable during periods of high GFP (Lehmann et al., 1987). The scalp maps at the momentary peaks of the GFP were extracted and clustered using a k-means cluster analysis (Hatz et al., 2015). Previous studies revealed that the optimal number of microstate classes belonged to two to six classes (mean 3.7 classes), according to the agglomerative clustering procedure (Lehmann et al., 1993; Khanna et al., 2015; Michel and Koenig, 2018). The current study used a cross-validation criterion and the Krzanowski–Lai criterion by the Cartool software (Brunet et al., 2011) to determine the optimal number of microstate classes, testing the entire range of 1–12 classes.

The cluster analysis resulted in mean microstate topographies for each class. Each group model maps were created based on individual model maps. The resulting class-labeled group microstate maps were then fit back to the templates to assign model maps to each participant.

Microstate topographies of each microstate class were compared between groups using a non-parametric randomization test (TANOVA, topographical analysis of variance), as implemented in the Ragu software (Koenig et al., 2011). GFP peaks per second (PPS), microstate duration (ms), frequency of occurrence of each microstate (/s), the percentage of total analysis time covered by each microstate (%), and transition probabilities were calculated.

Frequency Spectral Analysis

Frequency spectral analysis was performed using a fast Fourier transform (FFT, 1,000-point) algorithm. The absolute power spectral density [PSD, dB, $10 \log_{10}(V^2/Hz)$] for each channel based on the periodogram was calculated. The relative PSD (rPSD) was computed by normalizing the total power in the whole frequency range. The absolute and relative PSDs were averaged across channels within groups to measure global comparisons between groups in each frequency band.

Statistics Analyses

The relatively symmetrical data distribution of microstate, rPSD, and absolute PSD is shown in the box plots (**Supplementary Material 1**). Although there were outliers, it intuitively conformed to the normal assumption. Multivariate analysis of variance (MANOVA) was therefore performed to assess group differences of microstate variables. When overall significant effects were found, univariate ANOVAs followed by *post hoc* analyses with Bonferroni correction were performed. A Spearman correlation test was used for the correlation analysis. Continuous non-normal data were examined using the Kruskal–Wallis test or Mann–Whitney *U* test for group comparisons. The chi-square test was used for group comparison of categorical data. The level of significance was set at 0.05. Statistics analyses were performed using IBM SPSS Statistics v22.

RESULTS

Clinical and demographic data between dementia and control groups are presented in **Table 2**. Controls, EOAD, and FTD participants had no significant differences in age and gender. The FTD group was significantly less impaired in the MMSE than EOAD group ($p = 0.015$). Additionally, the two dementia groups did not differ significantly in terms of dementia duration, ADL, and MoCA. The percentage of patients taking acetylcholinesterase inhibitors (AChEIs) at the same time of EEG recordings did not differ between the two dementia groups.

Cerebrospinal fluid biomarker results were available in eight patients with EOAD and eight with FTD at the time of EEG recordings. The levels of $A\beta_{42}$, t-tau, and p-tau did not differ between the EOAD and FTD groups. However, the ratio of p-tau to $A\beta_{42}$ was shown to be significantly higher in EOAD, compared to FTD ($p = 0.028$). A percentage of 36.4% (4/11) subjects in the EOAD group were APOE $\epsilon 4$ carriers, of which one patient (11.1%) had two copies. For the FTD group, 42.9% (3/7) of patients were carriers of the APOE $\epsilon 4$ genotype, and no one had APOE $\epsilon 4$ homozygotes.

TABLE 2 | Demographic, clinical data, and CSF biomarkers in dementia and control groups.

	HC (<i>n</i> = 18)	EOAD (<i>n</i> = 30)	FTD (<i>n</i> = 14)	<i>p</i>
Age (mean, range)	54 (44–64)	55 (41–64)	57 (47–64)	<i>p</i> = 0.112
Gender (M:F)	10:8	11:19	8:6	<i>p</i> = 0.476
Disease course (mean, range, /y)	–	3.4 (0.25–13)	3.1 (0.75–6)	<i>P</i> _{AD-FTD} = 0.603
AChEI	–	16 (53.3%)	5 (35.7%)	<i>P</i> _{AD-FTD} = 0.342
MMSE (mean, range)	–	12 (1–25, <i>n</i> = 29)	19 (6–27, <i>n</i> = 9)	<i>P</i> _{AD-FTD} = 0.010
MoCA (mean, range)	–	13 (8–21, <i>n</i> = 7)	17 (12–19, <i>n</i> = 6)	<i>P</i> _{AD-FTD} = 0.234
ADL (mean, range)	–	33 (20–50, <i>n</i> = 10)	25 (0–39, <i>n</i> = 6)	<i>P</i> _{AD-FTD} = 0.313
CSF biomarkers (pg/ml, mean, range)	–	<i>n</i> = 8	<i>n</i> = 8	
Aβ ₄₂		420 (281–550)	658 (287–870)	<i>P</i> _{AD-FTD} = 0.065
T-tau		445 (94–1573)	261 (117–587)	<i>P</i> _{AD-FTD} = 0.505
P-tau		69.2 (40.9–122)	47.3 (26.7–71)	<i>P</i> _{AD-FTD} = 0.13
T-tau/Aβ ₄₂		1.18 (0.20–4.59)	0.46 (0.15–1.09)	<i>P</i> _{AD-FTD} = 0.083
P-tau/Aβ ₄₂		0.18 (0.11–0.36)	0.09 (0.03–0.20)	<i>P</i> _{AD-FTD} = 0.028
APOE ε4	–			<i>P</i> _{AD-FTD} = 0.782
0		7/11 (63.6%)	4/7 (57.1%)	
1		3/11 (27.3%)	3/7 (42.9%)	
2		1/11 (9.1%)	0	
Visual EEG score				<i>P</i> _{AD-FTD} = 0.304
0	24 (100%)	13 (43.3%)	8 (57.1%)	
1		3 (10.0%)	2 (14.3%)	
2		14 (46.7%)	4 (28.6%)	
3		0	0	

HC, healthy controls; EOAD, early-onset Alzheimer disease; FTD, frontotemporal dementia.

Overall, 17 EOAD patients had abnormal EEG results, including three patients with scores of 1, and 14 with scores of 2. For the FTD group, eight patients had scores of 0, two had scores of 1, and four had scores of 2. No participants had severe abnormal EEG results. The main EEG visual signs were abnormal or disappeared posterior dominant alpha rhythm and anterior dominant or diffuse slowing. Only one patient with EOAD had epileptiform discharges. The Mann–Whitney *U* test showed no significant group difference in visual EEG severity.

EEG Microstates

The median optimal number of microstate classes in the EOAD and control groups was four, while the median in FTD was five. The overall median optimal number in the entire dataset was four. Therefore, the number of microstate classes was therefore set to four for further analyses, commonly used in most studies, labeled as A, B, C, and D (Koenig et al., 1999; Michel and Koenig, 2018). The mean global explained variance (standard deviation, SD) of four microstates in each group was 79.8% (3.3%) for controls, 74.1% (2.3%) for EOAD, and 77.0% (4.4%) for FTD.

Group microstate maps are illustrated in **Figure 1**. After application of the Bonferroni correction, TANOVAs for each microstate class showed that the EOAD maps were different from control maps for classes B and C, and FTD maps were different from EOAD and control maps for class A. There were no significant group differences between FTD and controls in model map topography for classes B, C, and D.

Across all microstate classes, the mean microstate duration was 66.9 ms in controls, 77.8 ms in EOAD patients, and 76.6 ms in FTD patients. The mean duration in dementia groups was increased significantly compared to controls (*P*_{HC-EOAD} = 0.002; *P*_{HC-FTD} = 0.028) (**Table 3**). The mean number of unique microstate occurrences per second and PPS was reduced in EOAD and FTD, compared to HC (mean occurrence: *P*_{HC-EOAD} < 0.001, *P*_{HC-FTD} = 0.035; PPS: *P*_{HC-EOAD} < 0.001, *P*_{HC-FTD} = 0.001) (**Figure 2**).

Microstate analysis results are presented in **Table 3** and **Figure 2**. There were no significant differences between the EOAD and FTD groups. Compared to controls, microstate A duration in FTD and microstate B and D durations in EOAD were increased. Microstate C occurrence was reduced in both dementia groups compared to controls, with no significant difference between EOAD and FTD groups. Microstate A and B occurrences were significantly reduced in EOAD, compared to controls. No significant group differences were observed in microstate coverage and transition probabilities (**Supplementary Material 2**).

Relation Between Microstate and Clinical/CSF Biomarker Data

We found that the degree of visual EEG abnormality was negatively correlated with MMSE score (*r* = −0.380, *p* = 0.042) in EOAD. Visual EEG scores were positively correlated with disease course (*r* = 0.631, *p* = 0.021), p-tau (*r* = 0.756, *p* = 0.030), and the ratio of t-tau to Aβ₄₂ (*r* = 0.756, *p* = 0.030) in FTD.

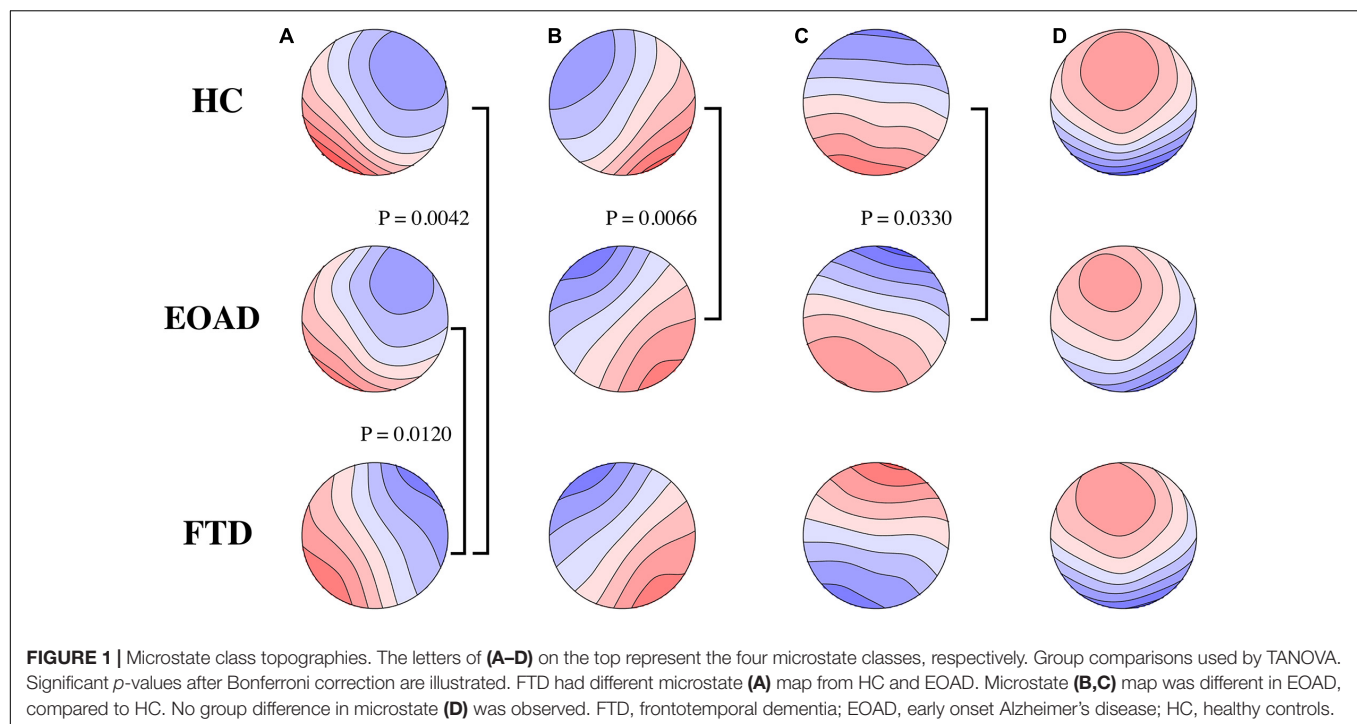


TABLE 3 | EEG microstate data in dementia and control groups.

Duration /ms (Std)	HC(<i>n</i> = 18)	EOAD(<i>n</i> = 30)	FTD(<i>n</i> = 14)	ANOVA(2,59)	<i>P</i> _{HC-EOAD}	<i>P</i> _{EOAD-FTD}	<i>P</i> _{HC-FTD}
A	64.7 (9.1)	70.3 (6.9)	74.1 (14.8)	$F = 3.805p = 0.028$	0.181	0.703	0.028
B	64.6 (8.1)	75.7 (10.7)	70.4 (16.6)	$F = 5.140p = 0.009$	0.007	0.493	0.510
C	66.8 (9.7)	78.3 (13.9)	75.3 (25.2)	$F = 2.913p = 0.062$			
D	63.0 (14.3)	77.5 (21.8)	74.6 (19.5)	$F = 3.279p = 0.045$	0.043	1.000	0.290
Mean duration	66.9 (5.8)	77.8 (9.3)	76.6 (15.0)	$F = 7.008p = 0.002$	0.002	1.000	0.028
Occurrence /s (Std)	HC	EOAD	FTD	ANOVA(2,59)	<i>P</i> _{HC-EOAD}	<i>P</i> _{EOAD-FTD}	<i>P</i> _{HC-FTD}
A	3.82 (0.64)	3.18 (0.57)	3.62 (0.97)	$F = 5.219p = 0.008$	0.009	0.167	1.000
B	3.95 (0.79)	3.35 (0.47)	3.57 (0.72)	$F = 4.981p = 0.010$	0.008	0.889	0.292
C	4.31 (0.72)	3.62 (0.71)	3.36 (0.42)	$F = 9.439p \leq 0.001$	0.003	0.682	<0.001
D	3.38 (0.65)	3.21 (0.76)	3.42 (1.14)	$F = 0.391p = 0.678$			
Mean occurrence	3.87 (0.31)	3.34 (0.36)	3.49 (0.57)	$F = 9.757p \leq 0.001$	<0.001	0.724	0.035
PPS	22 (1.4)	18 (1.7)	19 (3.0)	$F = 25.879p \leq 0.001$	<0.001	0.085	0.001

HC, healthy controls; EOAD, early-onset Alzheimer disease; FTD, frontotemporal dementia; PPS, global field power peaks per second.

In the EOAD group, microstate B coverage was negatively correlated with the concentration of CSF $A\beta_{42}$ ($r = -0.833$, $p = 0.010$) and was positively correlated with the ADL score ($r = 0.780$, $p = 0.008$). Additionally, the transition probability from A to B was positively related to the ADL score ($r = 0.657$, $p = 0.039$) and negatively related to the CSF $A\beta_{42}$ concentration ($r = -0.714$, $p = 0.047$). The P-tau concentration was negatively related to the transition probability from A to C ($r = -0.738$, $p = 0.037$).

In the FTD group, the CSF $A\beta_{42}$ level was positively related to microstate D occurrence ($r = 0.786$, $p = 0.021$) and transition probability from D to A ($r = 0.714$, $p = 0.047$). There was a negative correlation between the mean occurrence and CSF t-tau concentration ($r = -0.714$, $p = 0.047$). ADL was negatively

related to transition probability from D to B ($r = -0.886$, $p = 0.019$).

The microstate variables were not significantly correlated with MoCA scores, ratios of p-tau to $A\beta_{42}$, and the number of APOE $\epsilon 4$ copies in both groups. PPS showed no correlation with cognitive scores and CSF biomarkers. The Spearman correlations with a relatively high significance level ($p < 0.040$) are illustrated in Figure 3. The correlations with p -value > 0.040 required a larger sample to be confirmed.

EEG Microstate in Early- and Late-Onset AD

Group comparisons in EOAD ($n = 30$), LOAD ($n = 9$), and age-matched controls (young: $n = 18$, old: $n = 6$) were performed.

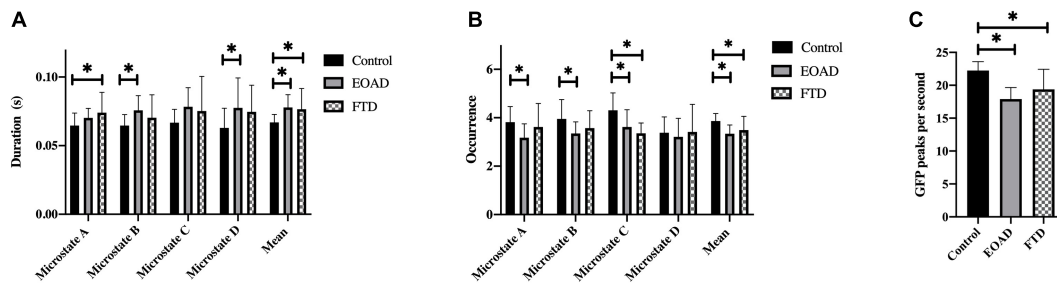


FIGURE 2 | Microstate characteristics. Group comparison of microstate duration (A), occurrence (B), and GFP peaks per second (C). *p*-values result from pairwise *post hoc* tests following univariate ANOVAs. **p* < 0.05. FTD, frontotemporal dementia; EOAD, early-onset Alzheimer's disease; HC, healthy controls; GFP, global field power.

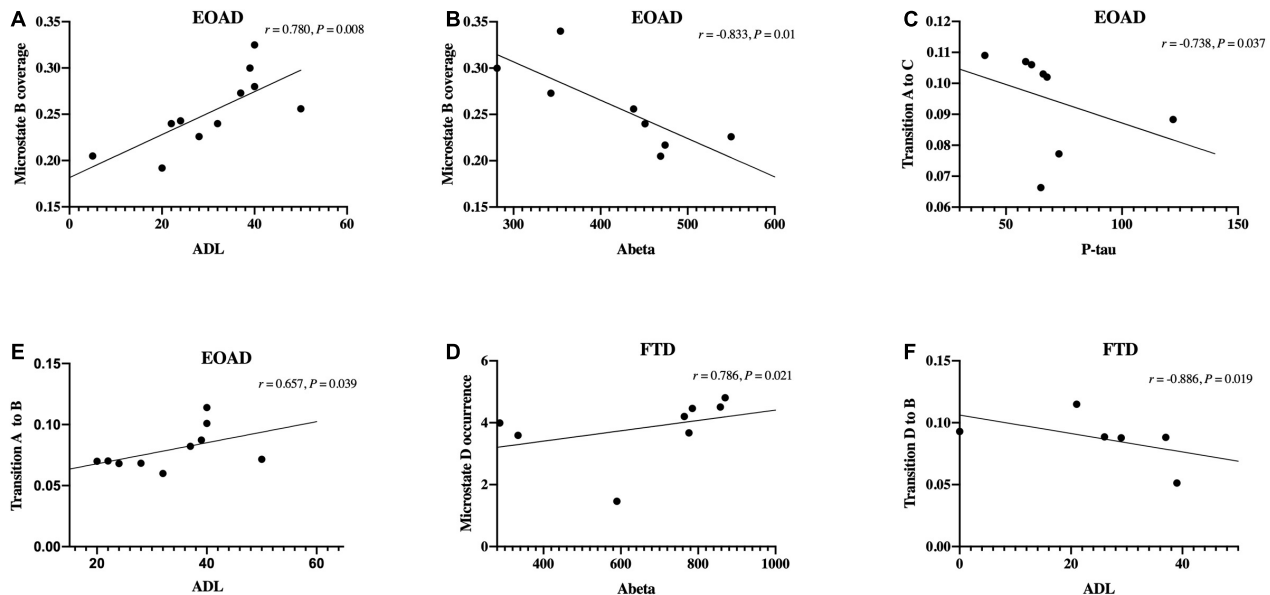


FIGURE 3 | Correlations between microstate and clinical data. (A–F) Spearman's correlations between microstate variables and clinical data, including cognitive scores and cerebrospinal fluid biomarkers levels. FTD, frontotemporal dementia; EOAD, early-onset Alzheimer's disease; ADL, activities of daily living.

Demographic data and clinical assessment scales are presented in Table 4. There are no significant differences between the AD subgroups in terms of gender, MMSE, MoCA, ADL, and visual EEG score.

The differences between HC and EOAD groups were consistent with the above observations. Moreover, we found that microstate B duration and the mean duration were significantly increased in EOAD, compared with LOAD. Microstate A occurrence, the mean occurrence, and PPS were reduced in EOAD, compared with LOAD. Additionally, a preferential transition to microstates A from D was revealed in LOAD, compared to age matched controls (0.090 vs. 0.047, $p = 0.02$). No significant group differences were observed in LOAD and age-matched controls in other microstate analyses.

Frequency Spectral Analysis

The across-channel grand average of global EEG PSD in each group is illustrated in Figures 4A,C. The means of the absolute

PSD in the control group were higher than in the dementia groups in alpha and beta bands with significance (Figure 4A and Table 5). As shown in Figure 4C and Table 5, the global rPSD in dementia groups was significantly reduced in alpha and beta bands and increased in delta bands, compared to controls. Moreover, rPSD in the theta band was higher in EOAD, compared to the control group. The topographies calculated from the global absolute and relative PSDs over frequency bands were illustrated in Figures 4B,D. The topographies revealed that PSD changes were presented in the whole scalp regions.

Early-onset Alzheimer's disease had a higher rPSD in the delta band, compared to FTD. The rPSD of three separated scalp regions (anterior: Fp1, Fp2, F3, F4, C3, C4, Fz, Cz; posterior: P3, P4, O1, O2, Pz; temporal: F7, F8, T3, T4, T5, T6) was calculated and compared among groups. The group comparison results in rPSD of each scalp region were the same with results in global rPSD (Supplementary Material 3).

TABLE 4 | Clinical and EEG microstate data in early- and late-onset AD and age-matched controls.

	HC		AD		
	Younger (1) <i>n</i> = 18	Older (2) <i>n</i> = 6	EOAD (3) <i>n</i> = 30	LOAD (4) <i>n</i> = 9	
Age (mean, range)	54 (44–64)	71 (68–74)	55 (41–64)	69 (65–75)	
Gender (M:F)	10:8	4:2	11:19	5:4	$P_{EOAD-LOAD} = 0.398$
Disease course (mean, range, /y)			3.4 (0.25–13.0)	3.0 (1.0–6.0)	$P_{EOAD-LOAD} = 0.844$
AChEI			16:14	3:6	$P_{EOAD-LOAD} = 0.451$
MMSE (mean, range)			12 (1–25)	14 (3–27)	$P_{EOAD-LOAD} = 0.493$
MoCA (mean, range)			13 (8–21)	11 (6–15)	$P_{EOAD-LOAD} = 0.831$
ADL (mean, range)			33 (20–50)	35 (22–54)	$P_{EOAD-LOAD} = 0.524$
Visual EEG score			0 (<i>n</i> = 13) 1 (<i>n</i> = 3) 2 (<i>n</i> = 14)	0 (<i>n</i> = 5) 1 (<i>n</i> = 2) 2 (<i>n</i> = 2)	$P_{EOAD-LOAD} = 0.327$
Duration/ms (Std)	1	2	3	4	ANOVA (3,59)
A	64.7 (9.1)	64.9 (6.7)	70.3 (6.9)	64.9 (6.7)	$F = 2.913 p = 0.042$
B	64.6 (8.1)	66.45 (5.3)	75.7 (10.7)	64.9 (10.6)	$F = 7.042 p < 0.001$ $P_{1-3} = 0.001, P_{3-4} = 0.024$
C	66.8 (9.7)	86.0 (28.6)	78.3 (13.9)	63.5 (10.5)	$F = 3.322 p = 0.026$
D	63.0 (14.3)	64.8 (17.9)	77.5 (21.8)	65.7 (12.5)	$F = 2.999 p = 0.038$ $P_{1-3} = 0.043$
Mean duration	66.9 (5.8)	74.1 (14.4)	77.8 (9.3)	66.0 (7.9)	$F = 7.401 p < 0.001$ $P_{1-3} = 0.001, P_{3-4} = 0.005$
Occurrence/s (Std)	1	2	3	4	ANOVA (3,59)
A	3.82 (0.64)	3.52 (1.23)	3.18 (0.57)	4.19 (0.73)	$F = 6.899 p < 0.001$ $P_{1-3} = 0.008, P_{3-4} = 0.002$
B	3.95 (0.79)	3.72 (0.96)	3.35 (0.47)	3.99 (0.43)	$F = 4.316 p = 0.008$ $P_{1-3} = 0.032$
C	4.31 (0.72)	4.47 (0.54)	3.62 (0.71)	3.79 (0.70)	$F = 4.961 p = 0.004$ $P_{1-3} = 0.005$
D	3.38 (0.65)	2.75 (0.38)	3.21 (0.76)	3.75 (0.59)	$F = 1.746 p = 0.167$
Mean occurrence	3.87 (0.31)	3.61 (0.59)	3.34 (0.36)	3.93 (0.46)	$F = 9.435 p < 0.001$ $P_{1-3} < 0.001, P_{3-4} = 0.001$
Coverage (Std)	1	2	3	4	ANOVA (3,59)
A	0.25 (0.06)	0.22 (0.07)	0.22 (0.04)	0.26 (0.04)	$F = 3.2 p = 0.030$
B	0.25 (0.07)	0.25 (0.06)	0.25 (0.04)	0.25 (0.04)	$F = 0.16 p = 0.923$
C	0.28 (0.07)	0.35 (0.07)	0.28 (0.07)	0.24 (0.05)	$F = 1.867 p = 0.145$
D	0.22 (0.08)	0.18 (0.06)	0.25 (0.11)	0.24 (0.06)	$F = 0.999 p = 0.400$
PPS (Std)	22 (1.4)	21 (2.7)	18 (1.7)	21 (2.6)	$F = 21.441 p < 0.001$ $P_{1-3} < 0.001, P_{3-4} = 0.003$

HC, healthy controls; EOAD, early-onset Alzheimer disease; LOAD, late-onset Alzheimer disease; PPS, global field power peaks per second.

DISCUSSION

The current study investigated the EEG microstate's changes, PSD, and visual EEG in EOAD and FTD. Comparison results between EOAD and LOAD were also presented. The correlations between EEG microstate and clinical severity and CSF biomarkers in AD and FTD were observed.

Cognitive scores and CSF biomarkers were different between FTD and EOAD, as expected. A previous study reported that FTD was associated with greater impairments in ADLs than AD (Mioshi et al., 2007). We found that the two groups had similar ADL scores, but significantly higher MMSE scores in FTD than in EOAD were revealed. It indicated that FTD needs a higher

MMSE score to get the same ADL with EOAD. The present study revealed that the ratio of p-tau to Aβ₄₂ was significantly increased in EOAD compared to FTD, which is in line with previous studies on AD and FTD (Visser et al., 2009; Vergallo et al., 2017).

The visual EEG severity was correlated with the MMSE score negatively in EOAD and disease course positively in FTD. Previous studies reported the positive correlation between visual EEG scores and clinical severity (Kowalski et al., 2001; de Waal et al., 2011), which was also supported in the present study. We found that visual EEG severity was correlated with CSF biomarkers in FTD. Previous studies observed an inverse correlation between Aβ levels and with the MMSE score (Lewczuk et al., 2020). However, another study also reported

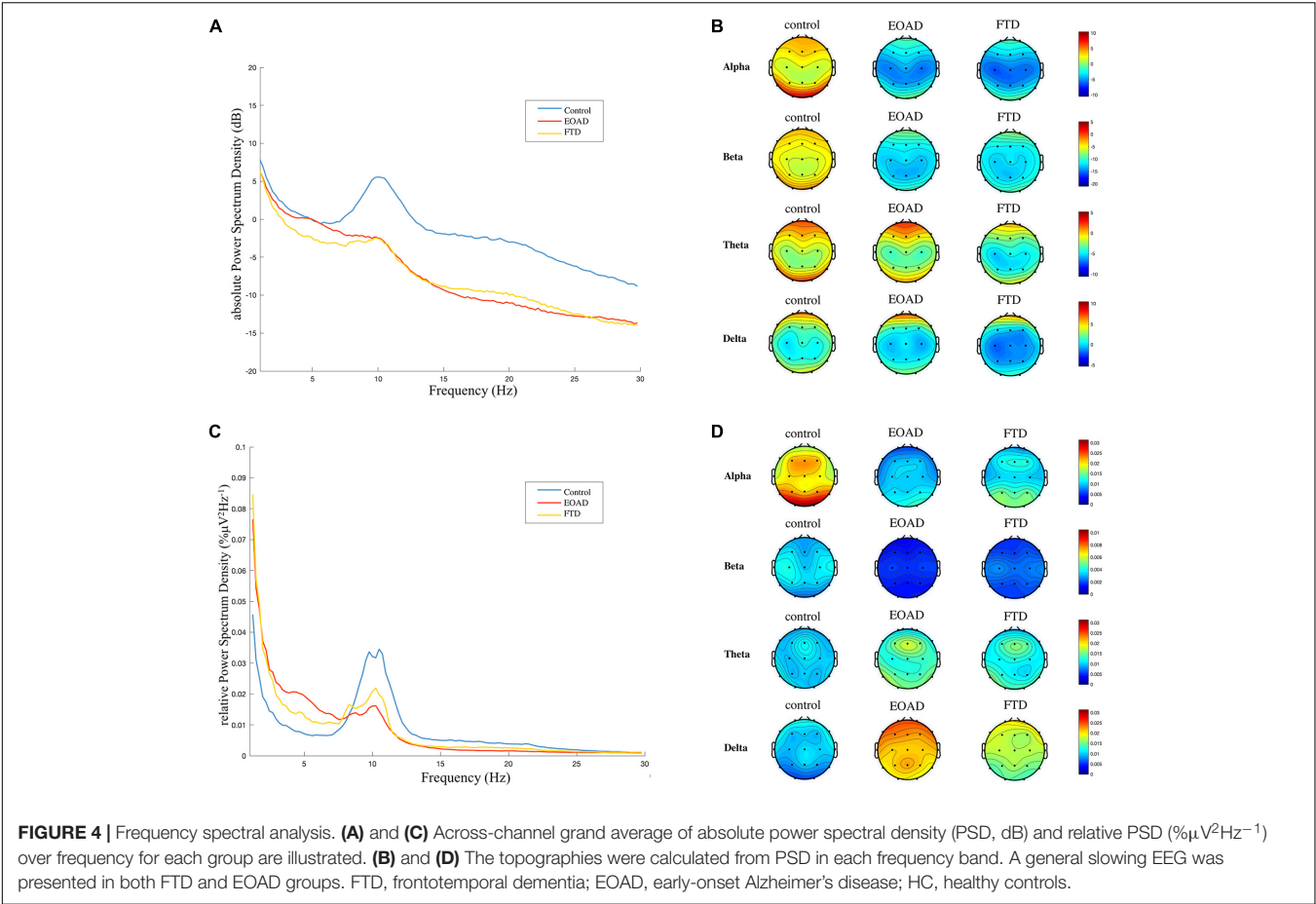


TABLE 5 | Power spectral density in dementia and control groups.

PSD (dB) (mean, std)	HC <i>n</i> = 18	EOAD <i>n</i> = 30	FTD <i>n</i> = 14	MANOVA (2, 59)	<i>P</i> _{HC-EOAD}	<i>P</i> _{EOAD-FTD}	<i>P</i> _{HC-FTD}
1–4 Hz	2.90 (8.1)	1.91 (2.88)	0.74 (3.32)	<i>F</i> = 0.716 <i>p</i> = 0.493			
4–8 Hz	−0.07 (8.54)	−0.91 (2.72)	−2.90 (2.98)	<i>F</i> = 1.231 <i>p</i> = 0.299			
8–12 Hz	3.73 (8.65)	−3.21 (3.69)	−3.53 (3.81)	<i>F</i> = 10.085 <i>p</i> ≤ 0.001	<0.001	1.000	0.002
12–30 Hz	−4.15 (8.38)	−11.19 (2.40)	−10.73 (2.54)	<i>F</i> = 12.445 <i>p</i> ≤ 0.001	<0.001	1.000	0.001
rPSD (% , mean, std)	HC	EOAD	FTD	MANOVA(2,59)	<i>P</i> _{HC-EOAD}	<i>P</i> _{EOAD-FTD}	<i>P</i> _{HC-FTD}
1–4 Hz	0.98 (0.4)	2.26 (0.54)	1.70 (0.81)	<i>F</i> = 25.725 <i>p</i> ≤ 0.001	<0.001	0.025	0.003
4–8 Hz	1.01 (0.4)	1.39 (0.37)	1.24 (0.62)	<i>F</i> = 4.159 <i>p</i> = 0.020	0.016	0.861	0.469
8–12 Hz	2.14 (0.72)	0.95 (0.69)	1.19 (0.94)	<i>F</i> = 14.167 <i>p</i> ≤ 0.001	<0.001	1.000	0.003
12–30 Hz	0.32 (0.10)	0.15 (0.06)	0.21 (0.09)	<i>F</i> = 28.330 <i>p</i> ≤ 0.001	<0.001	0.087	<0.001

HC, healthy controls; EOAD, early-onset Alzheimer disease; FTD, frontotemporal dementia.

that CSF biomarkers had no association with cognition scales (Vemuri et al., 2010). In the current study, we found no correlation between CSF biomarkers and cognition scales, which might be explained with the small sample.

Electroencephalogram microstate topographies in EOAD and FTD significantly deviate from controls. Microstate B and C maps were different between EOAD and control, while the class A map differed between FTD and control. Previous studies on patients with dementias revealed very different results. Two studies revealed no topography differences between AD (mean

age 65–70 y) and controls (Stevens and Kircher, 1998; Nishida et al., 2013; Grieder et al., 2016), but topographies of classes B and C in semantic dementia, a variant of FTD, were different from maps in control (Grieder et al., 2016). Schumacher et al. (2019) reported that all five classes (A–E) maps were different between AD (mean age 75 y) and control groups. Another study reported that AD (mean age 68 y) had different topographies of classes A and D compared to the control group (Smailovic et al., 2019). Microstate topography showed poor consistence in all these studies. Age may be one of the factors that influenced the results.

Both FTD and EOAD groups showed increased mean microstate duration and reduced mean occurrence. The increased duration, reduced occurrence, and PPS reflect the loss of microstate dynamics, which may be related to the EEG slowing (Schumacher et al., 2019). Tait et al. also reported that microstate transitions were slower in AD, compared to healthy controls (Tait et al., 2020). Some studies revealed that microstate durations were decreased in patients with dementia or cognitive impairment (Dierks et al., 1997; Strik et al., 1997; Stevens and Kircher, 1998; Nishida et al., 2013). However, more recent studies reported increased durations (Musaeus et al., 2019; Schumacher et al., 2019; Smailovic et al., 2019) and reduced occurrences (Schumacher et al., 2019; Smailovic et al., 2019) in AD, all based on the clustering algorithms, like topographic atomize and agglomerate hierarchical clustering (TAAHC) and k-means. The microstate map classification methods which differed in these studies may be one of the reasons for the different results. We also found that PPS was reduced in AD and FTD, compared to controls. PPS was easier to be calculated, compared to microstate which requires clustering. It showed the same change tendency with mean occurrence, indicating a good simple marker for EEG slowing and microstate dynamics loss.

In addition, microstate variables changes were different in EOAD and FTD. We found increased durations of class B in EOAD and class A in FTD. Microstate C occurrence was decreased in both dementia groups, and microstate A and B occurrences were reduced only in the EOAD group. EOAD had more microstate classes changes, compared to FTD.

Microstate B was significantly different in EOAD for topography and duration and correlated with CSF A β ₄₂ and ADL score, with a high Spearman's rank coefficient. These class B alterations were not presented in FTD. Previous studies revealed that microstate B was associated with the bilateral occipital cortex (Britz et al., 2010). AD patients have more atrophy in the occipital gyrus and precuneus than FTD patients (Zhang et al., 2011), which may partially explain the difference of microstate B alteration between EOAD and FTD. For microstate A change in FTD, class A was associated with superior and middle temporal lobes (Britz et al., 2010), consistent with the frontotemporal pathologic abnormalities in FTD. These results indicated that microstate may be helpful to differentiate EOAD and FTD.

Cerebrospinal fluid biomarkers were related to microstate in both dementia groups. The A β ₄₂ level was related to microstate B coverage negatively in EOAD and to microstate D occurrence positively in FTD, with high Spearman's rank coefficient. Smailovic et al. (2019) reported microstate B coverage negatively associated with the A β ₄₂ level in patients with AD (mean age 68 y), but with low Spearman's rank coefficient. The associations with A β ₄₂ level were also observed in other classes (Smailovic et al., 2019). The current study demonstrated a stronger correlation between microstate and CSF biomarkers in patients with EOAD. CSF A β ₄₂ and tau have high diagnostic accuracy. The correlation between biomarkers and EEG microstate and visual scores indicated that EEG could be a potential diagnostic method for early-onset dementia. Since EEG is a non-invasive and convenient examination, the diagnostic value of microstate for early-onset dementia is worthy of further work.

For EOAD and LOAD group comparisons, earlier studies reported that visual EEG abnormalities were more severe in EOAD (Schreiter-Gasser et al., 1993; de Waal et al., 2011). Since visual EEG results showed no difference between the two AD groups, the microstate differences between EOAD and LOAD indicate that loss of microstate dynamics may be more sensitive than visual EEG slowing. EOAD also showed more microstate changes than LOAD. Moreover, microstate analyses showed that no significant differences in microstate duration and occurrence were observed between LOAD and age-matched controls, which may due to the small sample size. A larger sample study is required.

The spectral analysis demonstrated that FTD and EOAD had lower rPSD in alpha and beta bands, and higher rPSD in delta bands, indicating that the general EEG was slowing. It further suggests that loss of microstate dynamics may be attributed to EEG slowing. A diffuse slowing with reduction of power in faster rhythm and increased power in slow rhythm has been observed in AD (Bennys et al., 2001; Malek et al., 2017) and FTD (Lindau et al., 2003). Additionally, the power in the delta band was increased in AD compared to FTD (Lindau et al., 2003; Caso et al., 2012), which was consistent with findings in the current study. We found delta band rPSD in EOAD was higher than rPSD in FTD all over the head, indicating a more diffuse slowing in EOAD than FTD.

LIMITATIONS

The present study has some limitations. First, the sample size of EOAD and FTD patients with CSF biomarker results was small. Therefore, the correlation analysis results with low Spearman's rank coefficient and significance level were not strong enough. A larger sample will draw more convincing conclusions. Second, the sample size of LOAD was small, and patients with late-onset FTD (>65 y) were lacked. In addition, part of patients with dementia were taking AChEIs which may influence EEG data (Babiloni et al., 2013). There was no difference in the number of patients taking AChEIs between FTD and EOAD. However, group comparisons between dementia and control groups may be influenced by the use of AChEIs. Further work, like better statistical analysis, or the set of prospective studies, may help to solve the effect.

CONCLUSION

The current study demonstrated that EOAD and FTD both had EEG slowing and loss of microstate dynamics, compared to controls. Moreover, EOAD and FTD had different microstate class changes, with no differences in visual EEG results. Similar results were also observed in-group comparisons between EOAD and LOAD. It indicated that microstate is more sensitive than visual EEG and may be useful for differentiation between EOAD and FTD. Correlations with clinical severity and CSF biomarkers were observed in EOAD and FTD, suggesting that microstate could be a potential marker for dementia diagnosis and clinical

severity evaluations. However, microstate analyses can produce numerous variables. Some variables, like topography, had poor consistency, while some variables, like durations, which were not specific to one class, showed similar characteristics in recent studies. Age and clustering methods may be the reasons, but more work is required to identify which EEG variables are useful for disease diagnosis and evaluations.

DATA AVAILABILITY STATEMENT

The original contributions presented in the study are included in the article/**Supplementary Material**, further inquiries can be directed to the corresponding author/s.

ETHICS STATEMENT

The studies involving human participants were reviewed and approved by The Ethics Committee of Peking Union Medical College Hospital (No. JS-2089). The patients/participants provided their written informed consent to participate in this study.

AUTHOR CONTRIBUTIONS

NL analyzed and interpreted the data and wrote the original manuscript. JG analyzed the data, diagnosed the patients, and

revised the manuscript. QL and LC conceived the study and revised the manuscript. CM acquired the data and diagnosed the patients. HS performed the EEG recordings and analyzed visual EEG data. All authors read and approved the final manuscript. All authors agreed to be accountable for the content of the work.

FUNDING

This study was funded by the Chinese Academy of Medical Sciences (CAMS) Innovation Fund for Medical Sciences (CIFMS) (grant number: 2016-I2M-1-004) and the National Key Research and Development Project (grant number: SQ2018YFC200148).

ACKNOWLEDGMENTS

We would like to thank all the participants and their family members who took part in the study.

SUPPLEMENTARY MATERIAL

The Supplementary Material for this article can be found online at: <https://www.frontiersin.org/articles/10.3389/fnins.2021.687053/full#supplementary-material>

REFERENCES

- Babiloni, C., Del Percio, C., Bordet, R., Bourriez, J. L., Bentivoglio, M., Payoux, P., et al. (2013). Effects of acetylcholinesterase inhibitors and memantine on resting-state electroencephalographic rhythms in Alzheimer's disease patients. *Clin. Neurophysiol.* 124, 837–850. doi: 10.1016/j.clinph.2012.09.017
- Bennys, K., Rondouin, G., Vergnes, C., and Touchon, J. (2001). Diagnostic value of quantitative EEG in Alzheimer's disease. *Neurophysiol. Clin.* 31, 153–160. doi: 10.1016/s0987-7053(01)00254-4
- Britz, J., Van De Ville, D., and Michel, C. M. (2010). BOLD correlates of EEG topography reveal rapid resting-state network dynamics. *NeuroImage* 52, 1162–1170. doi: 10.1016/j.neuroimage.2010.02.052
- Brunet, D., Murray, M. M., and Michel, C. M. (2011). Spatiotemporal analysis of multichannel EEG: CARTOOL. *Comput. Intell. Neurosci.* 2011:813870.
- Caso, F., Cursi, M., Magnani, G., Fanelli, G., Falautano, M., Comi, G., et al. (2012). Quantitative EEG and LORETA: valuable tools in discerning FTD from AD? *Neurobiol. Aging* 33, 2343–2356. doi: 10.1016/j.neurobiolaging.2011.12.011
- Casoli, T., Paolini, S., Fabbietti, P., Fattoretti, P., Pacioni, L., Fabb, K., et al. (2019). Cerebrospinal fluid biomarkers and cognitive status in differential diagnosis of frontotemporal dementia and Alzheimer's disease. *J. Int. Med. Res.* 47, 4968–4980. doi: 10.1177/0300060519860951
- Dai, M. H., Zheng, H., Zeng, L. D., and Zhang, Y. (2018). The genes associated with early-onset Alzheimer's disease. *Oncotarget* 9, 15132–15143.
- de Waal, H., Stam, C. J., Blankenstein, M. A., Pijnenburg, Y. A., Scheltens, P., and van der Flier, W. M. (2011). EEG abnormalities in early and late onset Alzheimer's disease: understanding heterogeneity. *J. Neurol. Neurosurg. Psychiatry* 82, 67–71. doi: 10.1136/jnnp.2010.216432
- Dierks, T., Jelic, V., Julin, P., Maurer, K., Wahlund, L. O., Almkvist, O., et al. (1997). EEG-microstates in mild memory impairment and Alzheimer's disease: possible association with disturbed information processing. *J. Neural. Transm. (Vienna)* 104, 483–495. doi: 10.1007/bf01277666
- Dubois, B., Feldman, H. H., Jacova, C., Hampel, H., Molinuevo, J. L., Blennow, K., et al. (2014). Advancing research diagnostic criteria for Alzheimer's disease: the IWG-2 criteria. *Lancet Neurol.* 13, 614–629.
- Dumurgier, J., Gabelle, A., Vercruysse, O., Bombois, S., Laplanche, J. L., Peoc'h, K., et al. (2013). Exacerbated CSF abnormalities in younger patients with Alzheimer's disease. *Neurobiol. Dis.* 54, 486–491. doi: 10.1016/j.nbd.2013.01.023
- Folstein, M. F., Folstein, S. E., and McHugh, P. R. (1975). "Mini-mental state". A practical method for grading the cognitive state of patients for the clinician. *J. Psychiatr. Res.* 12, 189–198.
- Grieder, M., Koenig, T., Kinoshita, T., Utsunomiya, K., Wahlund, L. O., Dierks, T., et al. (2016). Discovering EEG resting state alterations of semantic dementia. *Clin. Neurophysiol.* 127, 2175–2181. doi: 10.1016/j.clinph.2016.01.025
- Hatz, F., Hardmeier, M., Benz, N., Ehrensperger, M., Gschwandtner, U., Rüegg, S., et al. (2015). Microstate connectivity alterations in patients with early Alzheimer's disease. *Alzheimers Res. Ther.* 7:78.
- Hogan, D. B., Jetté, N., Fiest, K. M., Roberts, J. I., Pearson, D., Smith, E. E., et al. (2016). The Prevalence and Incidence of Frontotemporal Dementia: a Systematic Review. *Can. J. Neurol. Sci.* 43, S96–S109.
- Horvath, A., Szucs, A., Csukly, G., Sakovics, A., Stefanics, G., and Kamondi, A. (2018). EEG and ERP biomarkers of Alzheimer's disease: a critical review. *Front. Biosci. (Landmark Ed)* 23, 183–220. doi: 10.2741/4587
- Karran, E., Mercken, M., and De Strooper, B. (2011). The amyloid cascade hypothesis for Alzheimer's disease: an appraisal for the development of therapeutics. *Nat. Rev. Drug Discov.* 10, 698–712. doi: 10.1038/nrd3505
- Khanna, A., Pascual-Leone, A., Michel, C. M., and Farzan, F. (2015). Microstates in resting-state EEG: current status and future directions. *Neurosci. Biobehav. Rev.* 49, 105–113. doi: 10.1016/j.neubiorev.2014.12.010
- Koedam, E. L., Lauffer, V., van der Vlies, A. E., van der Flier, W. M., Scheltens, P., and Pijnenburg, Y. A. (2010). Early-versus late-onset Alzheimer's disease: more than age alone. *J. Alzheimers Dis.* 19, 1401–1408. doi: 10.3233/jad-2010-1337

- Koenig, T., Kottlow, M., Stein, M., and Melie-Garcia, L. (2011). Ragu: a free tool for the analysis of EEG and MEG event-related scalp field data using global randomization statistics. *Comput. Intell. Neurosci.* 2011:938925.
- Koenig, T., Lehmann, D., Merlo, M. C., Kochi, K., Hell, D., and Koukkou, M. (1999). A deviant EEG brain microstate in acute, neuroleptic-naïve schizophrenics at rest. *Eur. Arch. Psychiatry Clin. Neurosci.* 249, 205–211. doi: 10.1007/s004060050088
- Kowalski, J. W., Gawel, M., Pfeffer, A., and Barcikowska, M. (2001). The diagnostic value of EEG in Alzheimer disease: correlation with the severity of mental impairment. *J. Clin. Neurophysiol.* 18, 570–575. doi: 10.1097/00004691-200111000-00008
- Lehmann, D., Ozaki, H., and Pal, I. (1987). EEG alpha map series: brain micro-states by space-oriented adaptive segmentation. *Electroencephalogr. Clin. Neurophysiol.* 67, 271–288. doi: 10.1016/0013-4694(87)90025-3
- Lehmann, D., Wackermann, J., Michel, C. M., and Koenig, T. (1993). Space-oriented EEG segmentation reveals changes in brain electric field maps under the influence of a nootropic drug. *Psychiatry Res.* 50, 275–282. doi: 10.1016/0925-4927(93)90005-3
- Lewczuk, P., Łukaszewicz-Zajac, M., Mroczko, P., and Kornhuber, J. (2020). Clinical significance of fluid biomarkers in Alzheimer's Disease. *Pharmacol. Rep.* 72, 528–542. doi: 10.1007/s43440-020-00107-0
- Lindau, M., Jelic, V., Johansson, S. E., Andersen, C., Wahlund, L. O., and Almkvist, O. (2003). Quantitative EEG abnormalities and cognitive dysfunctions in frontotemporal dementia and Alzheimer's disease. *Dement. Geriatr. Cogn. Disord.* 15, 106–114. doi: 10.1159/000067973
- Malek, N., Baker, M. R., Mann, C., and Greene, J. (2017). Electroencephalographic markers in dementia. *Acta Neurol. Scand.* 135, 388–393. doi: 10.1111/ane.12638
- McKhann, G. M., Albert, M. S., Grossman, M., Miller, B., Dickson, D., and Trojanowski, J. Q. (2001). Clinical and pathological diagnosis of frontotemporal dementia: report of the Work Group on Frontotemporal Dementia and Pick's Disease. *Arch. Neurol.* 58, 1803–1809. doi: 10.1001/archneur.58.11.1803
- Micanovic, C., and Pal, S. (2014). The diagnostic utility of EEG in early-onset dementia: a systematic review of the literature with narrative analysis. *J. Neural. Transm. (Vienna)* 121, 59–69. doi: 10.1007/s00702-013-1070-5
- Michel, C. M., and Koenig, T. (2018). EEG microstates as a tool for studying the temporal dynamics of whole-brain neuronal networks: a review. *NeuroImage* 180, 577–593. doi: 10.1016/j.neuroimage.2017.11.062
- Milz, P., Faber, P. L., Lehmann, D., Koenig, T., Kochi, K., and Pascual-Marqui, R. D. (2016). The functional significance of EEG microstates—Associations with modalities of thinking. *NeuroImage* 125, 643–656. doi: 10.1016/j.neuroimage.2015.08.023
- Mioshi, E., Kipps, C. M., Dawson, K., Mitchell, J., Graham, A., and Hodges, J. R. (2007). Activities of daily living in frontotemporal dementia and Alzheimer disease. *Neurology* 68, 2077–2084. doi: 10.1212/01.wnl.0000264897.13722.53
- Musaeus, C. S., Nielsen, M. S., and Hogh, P. (2019). Microstates as Disease and Progression Markers in Patients With Mild Cognitive Impairment. *Front. Neurosci.* 13:563. doi: 10.3389/fnins.2019.00563
- Nasreddine, Z. S., Phillips, N. A., Bédirian, V., Charbonneau, S., Whitehead, V., Collin, I., et al. (2005). The Montreal Cognitive Assessment, MoCA: a brief screening tool for mild cognitive impairment. *J. Am. Geriatr. Soc.* 53, 695–699. doi: 10.1111/j.1532-5415.2005.53221.x
- Neary, D., Snowden, J. S., Gustafson, L., Passant, U., Stuss, D., Black, S., et al. (1998). Frontotemporal lobar degeneration: a consensus on clinical diagnostic criteria. *Neurology* 51, 1546–1554. doi: 10.1212/wnl.51.6.1546
- Nishida, K., Morishima, Y., Yoshimura, M., Isotani, T., Irisawa, S., Jann, K., et al. (2013). EEG microstates associated with salience and frontoparietal networks in frontotemporal dementia, schizophrenia and Alzheimer's disease. *Clin. Neurophysiol.* 124, 1106–1114. doi: 10.1016/j.clinph.2013.01.005
- Santarnecchi, E., Khanna, A. R., Musaeus, C. S., Benwell, C. S. Y., Davila, P., Farzan, F., et al. (2017). EEG Microstate Correlates of Fluid Intelligence and Response to Cognitive Training. *Brain Topogr.* 30, 502–520. doi: 10.1007/s10548-017-0565-z
- Scheltens, P., Blennow, K., Breteler, M. M., de Strooper, B., Frisoni, G. B., Salloway, S., et al. (2016). Alzheimer's disease. *Lancet* 388, 505–517.
- Schreier-Gasser, U., Gasser, T., and Ziegler, P. (1993). Quantitative EEG analysis in early onset Alzheimer's disease: a controlled study. *Electroencephalogr. Clin. Neurophysiol.* 86, 15–22. doi: 10.1016/0013-4694(93)90063-2
- Schumacher, J., Peraza, L. R., Firbank, M., Thomas, A. J., Kaiser, M., Gallagher, P., et al. (2019). Dysfunctional brain dynamics and their origin in Lewy body dementia. *Brain* 142, 1767–1782. doi: 10.1093/brain/awz069
- Shaw, L. M., Vanderstichele, H., Knapiak-Czajka, M., Clark, C. M., Aisen, P. S., Petersen, R. C., et al. (2009). Cerebrospinal fluid biomarker signature in Alzheimer's disease neuroimaging initiative subjects. *Ann. Neurol.* 65, 403–413. doi: 10.1002/ana.21610
- Smailovic, U., Koenig, T., Laukka, E. J., Kalpouzos, G., Andersson, T., Winblad, B., et al. (2019). EEG time signature in Alzheimer's disease: functional brain networks falling apart. *Neuroimage Clin.* 24:102046. doi: 10.1016/j.nicl.2019.102046
- Stevens, A., and Kircher, T. (1998). Cognitive decline unlike normal aging is associated with alterations of EEG temporo-spatial characteristics. *Eur. Arch. Psychiatry Clin. Neurosci.* 248, 259–266. doi: 10.1007/s004060050047
- Strik, W. K., Chiaramonti, R., Muscas, G. C., Paganini, M., Mueller, T. J., Fallgatter, A. J., et al. (1997). Decreased EEG microstate duration and anteriorisation of the brain electrical fields in mild and moderate dementia of the Alzheimer type. *Psychiatry Res.* 75, 183–191. doi: 10.1016/s0925-4927(97)00054-1
- Tait, L., Tamagnini, F., Stothart, G., Barvas, E., Monaldini, C., Frusciante, R., et al. (2020). EEG microstate complexity for aiding early diagnosis of Alzheimer's disease. *Sci. Rep.* 10:17627. doi: 10.1038/s41598-020-74790-7
- Vemuri, P., Wiste, H. J., Weigand, S. D., Knopman, D. S., Trojanowski, J. Q., Shaw, L. M., et al. (2010). Serial MRI and CSF biomarkers in normal aging, MCI, and AD. *Neurology* 75, 143–151. doi: 10.1212/wnl.0b013e3181e7ca82
- Vergallo, A., Carlesi, C., Pagni, C., Giorgi, F. S., Baldacci, F., Petrozzi, L., et al. (2017). A single center study: Aβ42/p-Tau(181) CSF ratio to discriminate AD from FTD in clinical setting. *Neurol. Sci.* 38, 1791–1797. doi: 10.1007/s10072-017-3053-z
- Visser, P. J., Verhey, F., Knol, D. L., Scheltens, P., Wahlund, L. O., Freund-Levi, Y., et al. (2009). Prevalence and prognostic value of CSF markers of Alzheimer's disease pathology in patients with subjective cognitive impairment or mild cognitive impairment in the DESCRIPA study: a prospective cohort study. *Lancet Neurol.* 8, 619–627. doi: 10.1016/s1474-4422(09)70139-5
- Wang, X., Shen, Y., and Chen, W. (2013). Progress in frontotemporal dementia research. *Am. J. Alzheimers Dis. Other Dement.* 28, 15–23.
- Wackermann, J., Lehmann, D., Michel, C. M., and Strik, W. K. (1993). Adaptive segmentation of spontaneous EEG map series into spatially defined microstates. *Int. J. Psychophysiol.* 14, 269–283. doi: 10.1016/0167-4998760(93)90041-m
- Zhang, Y., Schuff, N., Ching, C., Tosun, D., Zhan, W., Nezamzadeh, M., et al. (2011). Joint assessment of structural, perfusion, and diffusion MRI in Alzheimer's disease and frontotemporal dementia. *Int. J. Alzheimers Dis.* 2011:546871.

Conflict of Interest: The authors declare that the research was conducted in the absence of any commercial or financial relationships that could be construed as a potential conflict of interest.

Publisher's Note: All claims expressed in this article are solely those of the authors and do not necessarily represent those of their affiliated organizations, or those of the publisher, the editors and the reviewers. Any product that may be evaluated in this article, or claim that may be made by its manufacturer, is not guaranteed or endorsed by the publisher.

Copyright © 2021 Lin, Gao, Mao, Sun, Lu and Cui. This is an open-access article distributed under the terms of the Creative Commons Attribution License (CC BY). The use, distribution or reproduction in other forums is permitted, provided the original author(s) and the copyright owner(s) are credited and that the original publication in this journal is cited, in accordance with accepted academic practice. No use, distribution or reproduction is permitted which does not comply with these terms.



Blood–Brain Barrier Breakdown: An Emerging Biomarker of Cognitive Impairment in Normal Aging and Dementia

Basharat Hussain^{1,2†}, Cheng Fang^{1†} and Junlei Chang^{1*}

¹ Shenzhen Key Laboratory of Biomimetic Materials and Cellular Immunomodulation, Institute of Biomedicine and Biotechnology, Shenzhen Institute of Advanced Technology, Chinese Academy of Sciences, Shenzhen, China, ² University of Chinese Academy of Sciences, Beijing, China

OPEN ACCESS

Edited by:

Kin Ying Mok,
University College London,
United Kingdom

Reviewed by:

Berislav Zlokovic,
University of Southern California,
United States
Vinod Kumar,
The University of
Queensland, Australia
Zhen Zhao,
University of Southern California,
United States

*Correspondence:

Junlei Chang
jl.chang@sia.ac.cn

[†]These authors have contributed
equally to this work

Specialty section:

This article was submitted to
Neurodegeneration,
a section of the journal
Frontiers in Neuroscience

Received: 30 March 2021

Accepted: 14 July 2021

Published: 19 August 2021

Citation:

Hussain B, Fang C and Chang J
(2021) Blood–Brain Barrier
Breakdown: An Emerging Biomarker
of Cognitive Impairment in Normal
Aging and Dementia.
Front. Neurosci. 15:688090.
doi: 10.3389/fnins.2021.688090

The blood–brain barrier (BBB) plays a vital role in maintaining the specialized microenvironment of the neural tissue. It separates the peripheral circulatory system from the brain parenchyma while facilitating communication. Alterations in the distinct physiological properties of the BBB lead to BBB breakdown associated with normal aging and various neurodegenerative diseases. In this review, we first briefly discuss the aging process, then review the phenotypes and mechanisms of BBB breakdown associated with normal aging that further cause neurodegeneration and cognitive impairments. We also summarize dementia such as Alzheimer's disease (AD) and vascular dementia (VaD) and subsequently discuss the phenotypes and mechanisms of BBB disruption in dementia correlated with cognition decline. Overlaps between AD and VaD are also discussed. Techniques that could identify biomarkers associated with BBB breakdown are briefly summarized. Finally, we concluded that BBB breakdown could be used as an emerging biomarker to assist to diagnose cognitive impairment associated with normal aging and dementia.

Keywords: blood-brain barrier, biomarkers, cognitive impairment, aging, dementia

INTRODUCTION

The central nervous system (CNS) comprises the brain and spinal cord that control all the essential functions of the body. The distinctive physiological and anatomical structure of the brain and spinal cord makes the CNS a largely immune-privileged organ (Engelhardt and Coisne, 2011; Ransohoff and Engelhardt, 2012). Blood vessels are essential to transport oxygen and nutrients, remove CO₂ and other waste products, and, thus, maintain homeostasis in the body. Blood vessels that vascularize the CNS acquire specific anatomical and functional characteristics that collectively form the blood–brain barrier (BBB) (Obermeier et al., 2013; Zhao et al., 2015).

At the cellular level, the BBB is developed by continuous non-fenestrated endothelial cells (ECs) encompassed by pericytes, smooth muscle cells, astrocytes, microglia, oligodendroglia, and neurons that are altogether called the neurovascular unit (NVU) (Zlokovic, 2011; Blanchette and Daneman, 2015; Chow and Gu, 2015). At the molecular level, the BBB ECs are compacted by claudins, occludins, and ZO-1 [tight junction (TJ) proteins] and junction adhesion molecules (JAM) proteins to restrict the paracellular and transcellular diffusion of molecules in the CNS. In addition, the BBB ECs mediate influx transporters to select metabolite uptake from the blood and efflux transporters

to remove toxins and waste products from the brain into the blood. In BBB ECs, leukocyte adhesion molecules (LAMs) express very low to suppress immune surveillance in the brain (Quaeghebeur et al., 2011; Engelhardt and Ransohoff, 2012; Chow and Gu, 2015; Xiao et al., 2020). Thus, the BBB confines the access of neurotoxic compounds, blood cells, and pathogens to the brain (Winkler et al., 2011). In addition, the BBB sustains the homeostasis of the brain through tight regulation of the transport of molecules between the brain parenchyma and peripheral circulation (Abbott, 2013). **Figure 1A** shows the normal BBB.

Hence, the BBB is a fundamental and crucial element of normal and healthy brain function. Any impairment in the cellular or molecular components causes BBB breakdown that results in BBB dysfunction. Aging is one of several factors involved in the breaking of the BBB and was first observed in aged patients reported in the 1970s (Tibbling et al., 1977). In dysfunctional BBBs, the possibility of permeability increases; thus, toxic and blood-borne inflammatory substances that infiltrate the brain could change the biochemical microenvironment of the neurons, thus leading to neurodegenerative diseases and dementia (Abbott et al., 2010; Zeevi et al., 2010; Zlokovic, 2011; Rosenberg, 2014; Sweeney et al., 2018b). It has been reported that BBB disruption in aged people is strongly related to Alzheimer's disease (AD) and cognitive impairment (Farrall and Wardlaw, 2009; Van De Haar et al., 2016; Skillbäck et al., 2017; Zenaro et al., 2017; Sweeney et al., 2018b; Nation et al., 2019). **Figure 1B** shows the impaired BBB.

In this review, we first briefly discuss the aging process, and then review the phenotypes and mechanisms of BBB breakdown associated with normal aging that further cause neurodegeneration and cognitive impairments. We also summarize dementia such as AD and vascular dementia (VaD); then, we discuss the phenotypes and mechanisms of BBB disruption in dementia correlated with cognition decline. Subsequently, we also discuss the overlap between AD and VaD. Furthermore, we mention biomarkers associated with BBB breakdown during aging and dementia; additionally, we also briefly discuss various techniques to identify BBB biomarkers. Finally, we conclude that BBB breakdown could be used as a novel biomarker to diagnose cognitive impairment associated with normal aging and dementia.

BBB BREAKDOWN IN NORMAL AGING

The universal process in an organism leads to the cumulation of biological variations responsible for progressively diminishing bodily functions over time, which is known as aging (Kritsilis et al., 2018). Because of the advancement in medicine and the living standard of humans, life expectancy has doubled worldwide (Aw et al., 2007). Aged people are estimated to make up approximately 20% of the world population in the next 50 years (Ellison et al., 2015). In terms of the brain and the BBB, normal aging can be defined as a retrogression in the activities of the body with no cognitive ailment and dementia. Although ailments do not occur in this case, the frequency of age-related diseases increases with the aging process. Alzheimer's,

cardiovascular, Parkinson's disease, stroke, and various other neurological diseases commonly occur in aged people (Erdo et al., 2017). A recent study demonstrated that BBB breakdown could be considered a biomarker for the normal aging process (Verheggen et al., 2020). Furthermore, BBB breakdown also impairs the influx of nutrients (glucose) and oxygen and efflux of waste products, which may cause hypoxia-associated inflammation (Elahy et al., 2015; Raja et al., 2018). Subsequently, age-related BBB pathology makes the brain more susceptible to neuronal impairment and even causes neurodegeneration (Levit et al., 2020; Banks et al., 2021). It has been reported that aged people with prior cognitive impairment were more vulnerable to BBB disruption than people with no cognitive dysfunction of the same age; hence, BBB disruption can be considered an early biomarker related to declines in human cognition (Nation et al., 2019). All these studies show that the way alterations in BBB components progress with time might be an interesting research topic to explore in association with the normal aging brain.

Phenotypes of BBB Breakdown in Normal Aging

During aging, various changes occur in the structure and function of brain vasculature. In the aged brain, the BBB becomes broken; hence, the permeability of the BBB elevates (Villeda et al., 2011; Hyman et al., 2012) and declines in the cerebral blood flow (CBF) occur (Tarumi and Zhang, 2018). The potency of neovascularization diminishes (Rivard et al., 2000; Gao et al., 2009) and the density of capillary of brain vasculature reduces with age (Reeson et al., 2018). It has been observed that, during aging, BBB breakdown is the first incident that starts in the hippocampus, which may lead to declines in cognition (Montagne et al., 2015). In normal aging, the main changes that are strongly correlated to BBB breakdown are presented in **Table 1**.

It has been reported that, in aging, the brain endothelium becomes progressively dysfunctional, which is correlated with aberrant changes in the BBB (Cai W. et al., 2017; Edwards et al., 2019). The extracellular matrix (ECM) of the basal membrane or basal lamina covers the brain endothelium and is considered uniform and thin. In normal aging, the thickness of the ECM increases with the increase in collagen IV and argin but decreases in laminin concentrations (Candiello et al., 2010). Although the ECM has a role in maintaining BBB integrity by inducing TJ (occludin) protein expression, changes in the ECM cause BBB disruption, and thus result in increased BBB permeability (Hawkins and Davis, 2005; Candiello et al., 2010; Sanchez-Covarrubias et al., 2014).

In the CNS BBB, ECs associated with pericytes, astrocytes, neurons, and glial cells that develop and maintain their specific phenotype led to BBB integrity (Erickson and Banks, 2018). However, with aging, this association caused BBB breakdown. During aging, physiological ultrastructure changes have been reported in pericytes, such as an increase in mitochondria size (Hicks et al., 1983), vesicular and lipofuscin-like inclusions

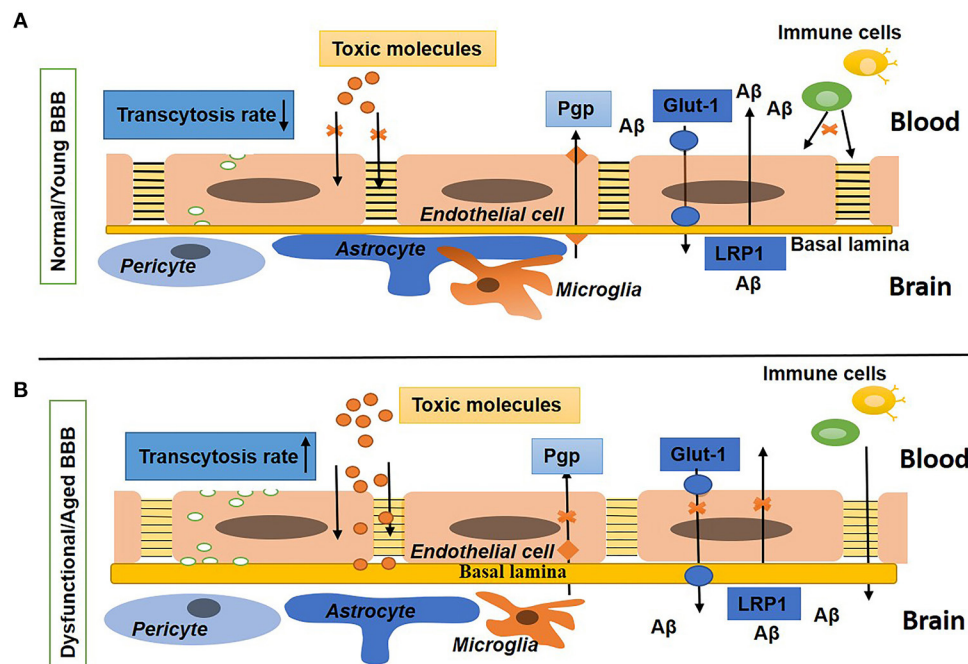


FIGURE 1 | Schematic diagram shows the normal/young blood–brain barrier (BBB) and dysfunctional/aged BBB. **(A)** Shows BBB in a young or normal state with tight and adherens junctions, a low rate of transcytosis, no diffusion of toxins, the presence of influx (Glut-1) and efflux (P-gp) transporters, and a low expression of leukocytes adhesion molecules (LAMs). The basal lamina is thin and surrounded by pericytes, astrocyte endfeet, and microglia. **(B)** Shows BBB in an aged or disease state with a high rate of transcytosis and diffusion of toxins, repression in influx and efflux transporters, upregulated expression of LAMs, and increased density of the extracellular matrix (ECM). Pericytes, astrocytes, and microglia are not associated with the basal lamina.

(Rascher and Wolburg, 2002), and foamy transformations (Sturrock, 1980). In addition, the protrusions on the basal lamina or the ECM membrane of the microvessels have been observed to result in the degeneration of pericytes (Ueno et al., 1998). A loss of pericytes has also been reported in aging mice, rats, and the human brain (Stewart et al., 1987; De Jong et al., 1990; Bell et al., 2010; Duncombe et al., 2017; Goodall et al., 2018) but some studies observed that the number of pericytes increases in aged rat brains (Heinsen and Heinsen, 1983; Peinado et al., 1998). However, no change was observed in the number of pericytes in aged monkey brains (Peters et al., 1991).

Platelet-derived growth factor receptor beta (PDGFRβ) maintains the phenotype of pericytes in the brains of aged mice with *PDGFRβ*^{+/−}, which shows that the loss of pericytes leads to BBB breakdown and increased BBB permeability (Bell et al., 2010). It has been reported, in the aged human brain, the level of soluble PDGFRβ in cerebrospinal fluid (CSF) increases, showing damage to the pericyte associated with BBB disruption (Montagne et al., 2015; Sagare et al., 2015; Nation et al., 2019). In addition, it has been reported that, in APOE4 carriers, the elevated PDGFRβ in the CSF may be used as a biomarker of cognitive impairment (Montagne et al., 2020).

The endfeet of astrocytes that ensheath the pericytes have a contribution to BBB development and maintenance. With

the age, vascular coverage and aquaporin-4 (AQP4) expression of astrocyte endfeet are reduced whereas glial fibrillary acidic protein (GFAP) expression and endfeet sizes are increased (Middeldorp and Hol, 2011; Duncombe et al., 2017; Goodall et al., 2018), leading to increase in reactive astrogliosis.

Microglia are distributed ubiquitously in the CNS and activated during aging and pathology (Kettenmann et al., 2011; Kofler and Wiley, 2011; Harry, 2013; Sanchez-Covarrubias et al., 2014). Microglia have a ramified structure in the resting state, but when activated, this structure changes into an amoeboid morphology during aging or a pathophysiological state (Kettenmann et al., 2011). During aging or stress, the activated microglia produce tumor necrosis factor-α (TNF-α), proteases, nitric oxide (NO), and peroxide (Ronaldson and Davis, 2012), which are associated with an alteration in the TJ protein. This alteration induces BBB leakage (Huber et al., 2006), which, in turn, leads to cell injury and neurodegeneration (Ronaldson and Davis, 2012).

Studies have shown that neurons directly connect with brain ECs and astrocytes (Ben-Menachem et al., 1982; Cohen et al., 1996, 1997; Tong and Hamel, 1999; Vaucher et al., 2000; Sanchez-Covarrubias et al., 2014). Impairment in this association results in BBB breakdown and leads to an increase in BBB permeability to albumin (Berezowski et al., 2004). **Figure 1** shows the difference between young or normal BBB and aged or dysfunctional BBB.

TABLE 1 | Changes associated with blood–brain barrier (BBB) breakdown in normal aging, Alzheimer's disease (AD), and vascular dementia (VaD).

BBB elements	Characteristics	Aging	References	AD	References	VaD	References
ECs	<ul style="list-style-type: none"> Endothelium degeneration, Mitochondrial content decrease, pinocytotic vesicle increase Microvessel density decrease 	Yes	(Bell and Zlokovic, 2009; Grinberg and Thal, 2010; Richardson et al., 2012; Rouhl et al., 2012; Sagare et al., 2012)	Yes	(Salmina et al., 2010; Villar-Vesga et al., 2020; Chacón-Quintero et al., 2021; González-Molina et al., 2021)	Yes	(Wardlaw et al., 2003; Zhang et al., 2014; Rajani et al., 2018; Wang et al., 2018; Tayler et al., 2021; Zhu et al., 2021)
Extracellular components	<ul style="list-style-type: none"> Increase (accumulation) 	Yes	(Brown and Thore, 2011)	Yes	(Zlokovic, 2011; Hawkes et al., 2013; Morris et al., 2014; Howe et al., 2020)	Yes	(Ueno et al., 2002; Rosenberg, 2017)
Basal lamina	<ul style="list-style-type: none"> Thickness increase 	Yes	(Grinberg and Thal, 2010; Richardson et al., 2012; Rouhl et al., 2012)	Yes	(Zlokovic, 2011; Morris et al., 2014)	Yes	(Ueno et al., 2002; Iadecola, 2013; Rosenberg, 2017)
Pericytes	<ul style="list-style-type: none"> Pericytes number decrease PDGFRβ in CSF increase 	Yes	(Bell et al., 2010; Montagne et al., 2015; Sagare et al., 2015; Duncombe et al., 2017; Erdo et al., 2017; Goodall et al., 2018; Nation et al., 2019)	Yes	(Sengillo et al., 2013; Halliday et al., 2016; Montagne et al., 2018; Miners et al., 2019; Uemura et al., 2020)	Yes	(Iadecola, 2013; Montagne et al., 2018; Yang et al., 2018; Uemura et al., 2020)
Astrocytes	<ul style="list-style-type: none"> Vascular coverage reduction GFAP upregulation AQP4 downregulation 	Yes	(Middeldorp and Hol, 2011; Duncombe et al., 2017; Goodall et al., 2018; Heithoff et al., 2021)	Yes	(Abbott et al., 2006; Yang Y. et al., 2011; Kimbrough et al., 2015; Ahmad et al., 2019)	Yes	(Wardlaw et al., 2003; Iadecola, 2013; Saggu et al., 2016; Price et al., 2018; Wang et al., 2018; Tayler et al., 2021)
Microglia	<ul style="list-style-type: none"> Release of neurotoxins Changes to amoeboid morphology 	Yes	(Kettenmann et al., 2011; Ronaldson and Davis, 2012)	Yes	(Zotova et al., 2011; Hansen et al., 2018; Ahmad et al., 2019; Hemonnot et al., 2019; Leng and Edison, 2020)	Yes	(Wu et al., 2016; Wang et al., 2018; Tayler et al., 2021)
Neurons	<ul style="list-style-type: none"> Synaptic plasticity diminishment Impaired long-term potentiation Dysfunctional neurogenesis Elevation in apoptosis Neurodegeneration 	Yes	(Buschini et al., 2011; Blau et al., 2012; Cerbai et al., 2012; Lucke-Wold et al., 2014)	Yes	(Crews and Masliah, 2010; Arendt et al., 2015; Vasic et al., 2019; Bartels et al., 2020)	Yes	(Saggu et al., 2016; Montagne et al., 2018; Wang et al., 2018; Tayler et al., 2021; Zhu et al., 2021)
Tight junctions Proteins	<ul style="list-style-type: none"> CLDN5, OCLN, ZO-1 expression decreases and BBB integrity reduction, BBB permeability increase 	Yes	(Bake et al., 2009; Wang et al., 2011; Lassman et al., 2012; Elahy et al., 2015)	Yes	(Biron et al., 2011; Cuevas et al., 2019; Yamazaki et al., 2019)	Yes	(Wang et al., 2018; Yang et al., 2018)
Transporter dysfunctions	<ul style="list-style-type: none"> Influx transporter: Glut1 expression decrease, glucose uptake reduction Efflux Transporter: LRP-1 (human) and P-gp expression decrease (mouse) 	Yes	(van Assema et al., 2012; Ding et al., 2013; Jiang et al., 2013; Chiu et al., 2015; Ramanathan et al., 2015; Hoffman et al., 2017; Patching, 2017; Sweeney et al., 2019a)	Yes	(Owen et al., 2010; Jaeger et al., 2011; Ding et al., 2013; Chiu et al., 2015; Ramanathan et al., 2015; Winkler et al., 2015; Halliday et al., 2016; Patching, 2017; Yu et al., 2020; Kyrтата et al., 2021)	Yes	(Hase et al., 2019)
Circulating factors	<ul style="list-style-type: none"> ASM (acid sphingomyelinase), sphingomyelin phosphodiesterase 1 (Smpd1) upregulation 	Yes	(Park et al., 2018; Wangb et al., 2019)	*		*	
Other factors	<ul style="list-style-type: none"> SIRT1 expression decrease 	Yes	(Chang and Guarente, 2014; Imai and Guarente, 2014; Stamatovic et al., 2019)	*		*	

“*” shows no obvious research studies are found related to AD and VaD.

Mechanisms of BBB Breakdown During Normal Aging

During aging, various mechanisms cause BBB breakdown and increase BBB permeability. For example, in aging, oxidative stress

induces ECs to produce TNF- α that cause the degradation of the basement membrane, and TJs (Occludin, Zonula occludins-1), which, in turn, results in BBB disruption and an increase in BBB permeability (Donato et al., 2007; Bake et al., 2009; Lee

et al., 2012; Elahy et al., 2015; Cai W. et al., 2017). In addition, the activity of caspase 3/7 in the aged brain increases, which causes the suppression of cell viability and the upregulation of apoptosis in pericytes (Schultz et al., 2018), resulting in the reduction of the number of pericytes in the BBB (Bell et al., 2010). The senile pericytes produce NO and react with O₂, causing increased oxidative stress and compromised BBB integrity (Hughes et al., 2006; Sweeney et al., 2016; Cai W. et al., 2017). Similarly, in aging, oxidative stress enhances astrocytes to upregulate the expression of cytokines and chemokines, such as matrix metalloproteinase 3 (MMP3) and p16INK4A [senescence-associated secretory phenotype (SASP)], that induce BBB disruption, neuroinflammation, and cognitive impairments (Simpson et al., 2010; Salminen et al., 2011; Cai Z. et al., 2017; Bussian et al., 2018). In aging, oxidative stress also activates the microglia to release cytokines, chemokines IL-6, IL1 β , and TNF- α , which results in the elevation of reactive oxygen and nitrogen species; this ultimately causes the breakdown of the BBB (Gredilla et al., 2010; Choi et al., 2014; Fivenson et al., 2017). With age, oxidative stress causes the production of reactive oxygen species (ROS) to elevate in the CNS, but the capability of neurons to clear ROS decreases, resulting in neurodegeneration (Nicholls and Budd, 2000; Mattson and Magnus, 2006). Furthermore, with age, calcium dysregulation in neurons occurs, which represses calcium-binding proteins correlated with the elevation of ROS. This results in BBB degradation and neuronal loss (He et al., 1997) as shown (Figure 2).

Once the BBB integrity becomes compromised, blood-derived proteins such as fibrinogen and plasminogen cross the BBB, and the pro-inflammatory fibrin aggregates in the brain (Cortes-Canteli et al., 2015). A study using a mouse model showed that accumulated fibrin bind with CD11b/CD18 and activate microglia, which then triggers a decline in cognition (Merlini et al., 2019). Accumulated fibrin in brain also induce increased ROS level and activates nicotinamide adenine dinucleotide phosphate (NADPH oxidase), which upregulates pro-inflammatory gene expression and causes damage to neuronal axons (Ryu et al., 2018; Merlini et al., 2019). In addition, fibrinogen phosphorylates Smad 1/5/8 represses oligodendrocyte progenitor cells (OPCs) (Ryu et al., 2015). Furthermore, the complex of A β -fibrinogen activates microglia *via* CD11b/CD18, which inhibits the breakdown of fibrinogen and promotes neuronal degeneration (Cortes-Canteli et al., 2010; Zhao et al., 2017) as shown (Figure 3A).

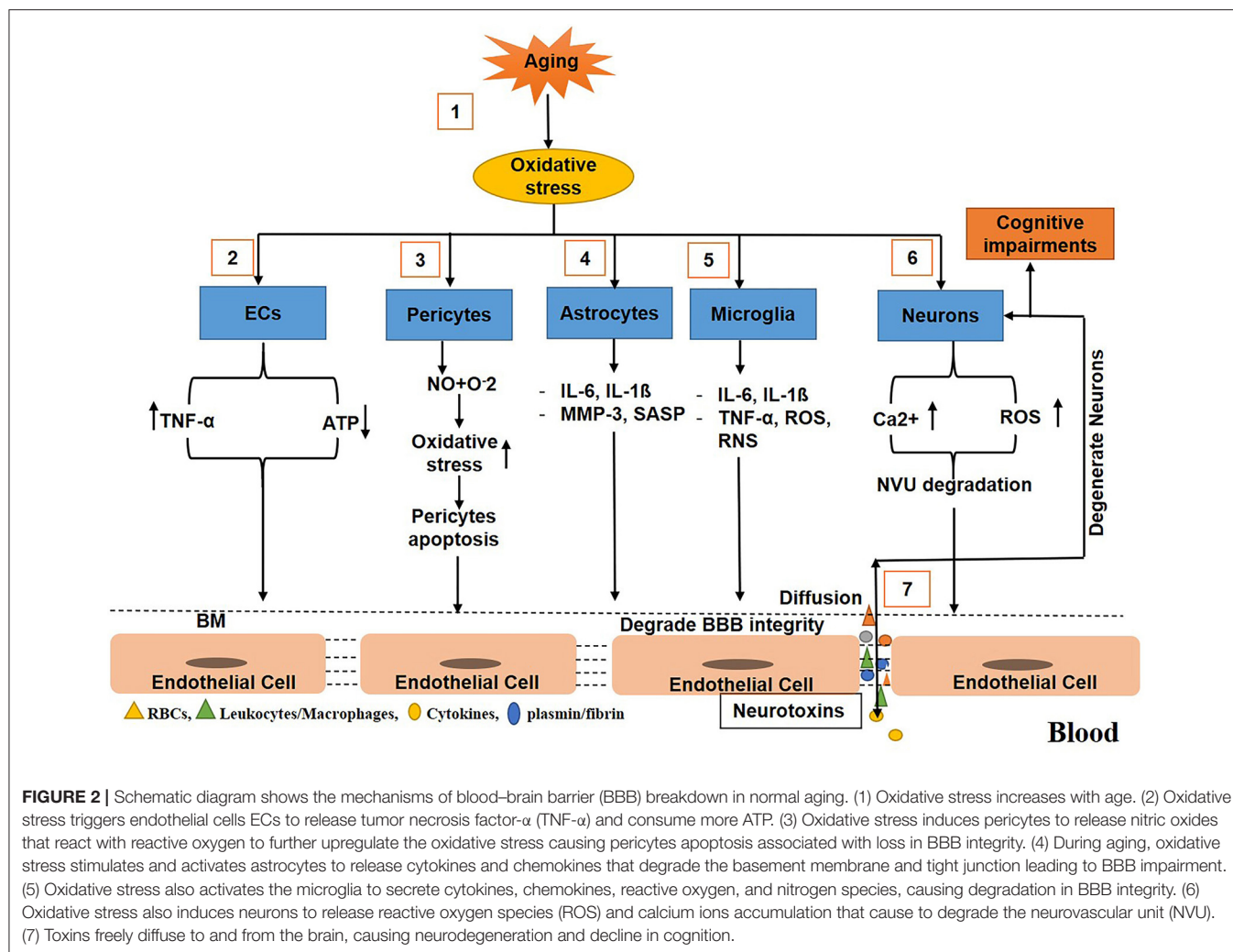
The tissue-type plasminogen activator (tPA) binds and activates low-density lipoprotein receptor-related protein-1 (LRP-1) on ECs. In turn, these ECs produce pro-MMPs (MMP-2, MMP-3, and MMP-9) (Wang et al., 2003; Cheng et al., 2006; Suzuki et al., 2009). Subsequently, tPA converts the surface-bound inactive plasminogen (Plg) into active plasmin (Plm) (Doeuvre et al., 2010; Yepes et al., 2021). Plasmin, in turn, activates the MMPs, leading to the degradation of TJs and basal lamina (Mazzieri et al., 1997; Ramos-DeSimone et al., 1999; Monea et al., 2002; Rosenberg and Yang, 2007; Yang Y. et al., 2011). Furthermore, tPA also binds with LRP-1 on astrocytes,

which induces plasmin-mediated activation of Rho kinases and retracts the endfeet of the astrocytes from the blood vessel wall, thus resulting in BBB dysfunction (Niego et al., 2012). In addition, a study suggested that plasminogen might regulate brain inflammation during AD (Baker et al., 2018) as shown (Figure 3B).

Human brain ECs continuously produce complement regulatory proteins and components (Wu et al., 2016), which are elevated by CNS injury or infiltration into the brain when the BBB is dysfunctional. However, at a young age or in a normal state, complement proteins mostly do not cross the BBB (Hoarau et al., 2011; Veerhuis et al., 2011). Once the complement proteins cross the compromised BBB, they could alter the functions of the microglia, oligodendrocytes, and neurons (Orsini et al., 2014). Complement activation produces C3a and C5a that interact with C3aR and C5aR1, respectively, which play a significant role in the infiltration of inflammatory cells into the brain and the induction of cytokine cascades (IL-1, TNF- α , IL-6, IL-8, IL-17) subsequently leading to neurodegeneration (Jacob and Alexander, 2014; Alexander, 2018). In AD, amyloid-beta (A β) activates the complement signaling by binding to C1q. Inhibition of the C5/C5aR1 pathway was also reported to be a protective therapeutic target in AD (Fonseca et al., 2009) as shown (Figure 3C).

BBB BREAKDOWN IN DEMENTIA (INCLUDING AD AND VASCULAR DEMENTIA)

Dementia is a group of conditions or disorders that affect the functions of the brain. It is a progressive neurological disease associated with impairments in cognition and deterioration of the everyday life activities of an affected individual (Mills et al., 2007; Kirshner, 2009). In dementia, BBB breakdown and cerebral hypoperfusion cause brain damage and a decline in cognition (Nation et al., 2019; Tayler et al., 2021). Dementia is a considerable health complication affecting millions of people worldwide. In developed countries, AD and VaD are two significant types of dementia with a prevalence of about 4.4 and 1–2%, respectively (Ray et al., 2013), with AD being the most common type of dementia in aged people (Ballad et al., 2011; Hyman et al., 2012). The World Alzheimer Report 2018 estimated that approximately 50 million people of the global population suffer from dementia, which can increased to 82 million in 2030 and triple to 152 million by 2050 (Patterson, 2018). Alzheimer's is considered to account for 60–70% of all dementia cases worldwide (Leng and Edison, 2020). As the BBB has vital contributions to maintaining the microenvironment of the CNS, any impairment in the cellular or molecular components of the BBB can cause various neurodegenerative diseases, including AD (Zlokovic, 2005; Erickson and Banks, 2013; Zenaro et al., 2017). After AD, VaD is the second most common type of dementia, accounting for 15% of all dementia cases worldwide (O'Brien and Thomas, 2015). Vascular dementia is a type of neurological disease with a defect in cognition caused by impairment in the vascular system, such



as a reduction in CBF (Sabayan et al., 2012). Various vascular pathologies are associated with VaD, such as infarcts and white matter (WM) alterations (O'Brien and Thomas, 2015). In addition, brain hemorrhage, ischemia, and hypoxia may be the causing factors of VaD (Kirshner, 2009; Grinberg and Heinsen, 2010).

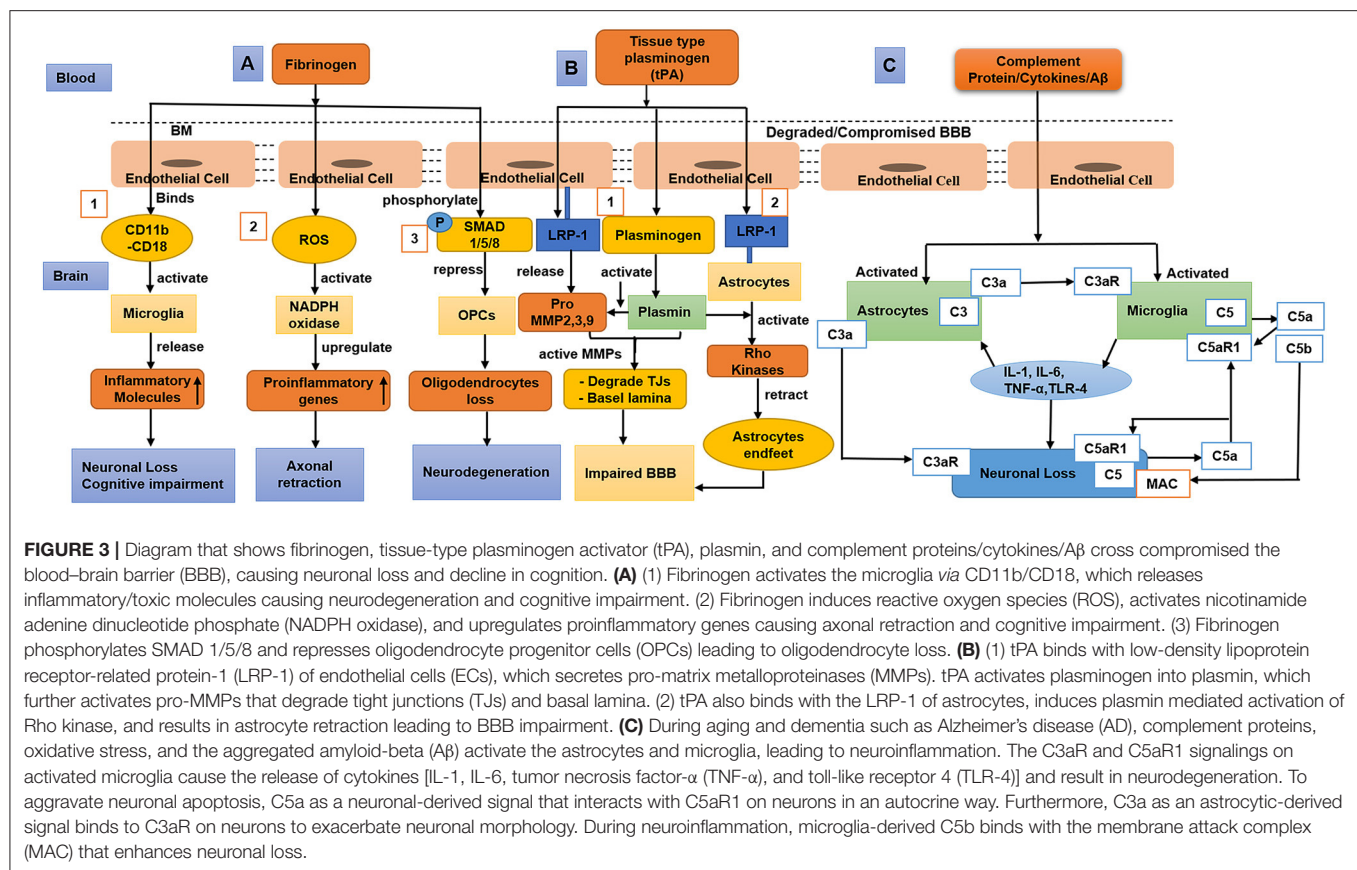
BBB Breakdown in AD

Pathophysiology of AD

Aging is responsible for pathophysiological changes that aggravate neurological diseases. It causes the thickening of the wall of the blood vessel and increases blood vessel tortuosity, which may lead to BBB disruption (Rosenberg, 2012). The BBB breakdown in AD results in the accumulation of insoluble extracellular plaques of β -amyloid ($A\beta$) along the walls of blood vessels and causes inflammation in the NVU (Kinnecom et al., 2007; Kang et al., 2017). In neuronal cytoplasm, the accumulation of neurofibrillary tangles (NFT) of P-tau is also associated with AD (Kang et al., 2017). It has been observed that, in AD, the reduction of $A\beta$ clearance is correlated with declines in CBF and cognitive impairment (Sagare et al., 2012). These

pathological markers are associated with BBB impairment, which causes microglial activation, neuroinflammation, degeneration of neurons, and cognitive impairment (Bhaskar et al., 2010; Iadecola, 2013). As pericytes have a crucial role in the development and maintenance of BBB, their number and density decreased in the cortex and hippocampus of AD patients (Sengillo et al., 2013), subsequently leading to the upregulation of the expression of $A\beta$ and p-tau protein (Sagare et al., 2013).

Vascular (stroke, hypertension, diabetes, etc.) and genetic factors (*APOE4*) are two pathways that cause BBB impairment and oligemia (reduced CBF) that result in dementia. In the $A\beta$ -independent pathway (blue), the BBB breakdown causes a release of neurotoxins from one side and leads to CBF reduction on another side. In the $A\beta$ -dependent pathway (green), the BBB breakdown impairs the clearance of $A\beta$ and APP (amyloid precursor protein), leading to the aggregation of $A\beta$ in the brain. The accumulated $A\beta$ and vascular hypoperfusion phosphorylate tau, leading to the formation of NFTs. In addition, the deposited $A\beta$ also cause inflammation in the brain. In conclusion, both factors and pathways cause neurodegeneration



leading to dementia (AD) (Iadecola and Davisson, 2008; Jack, 2010; Winkler et al., 2011; Sagare et al., 2013; Edwards et al., 2019) as shown (Figure 4).

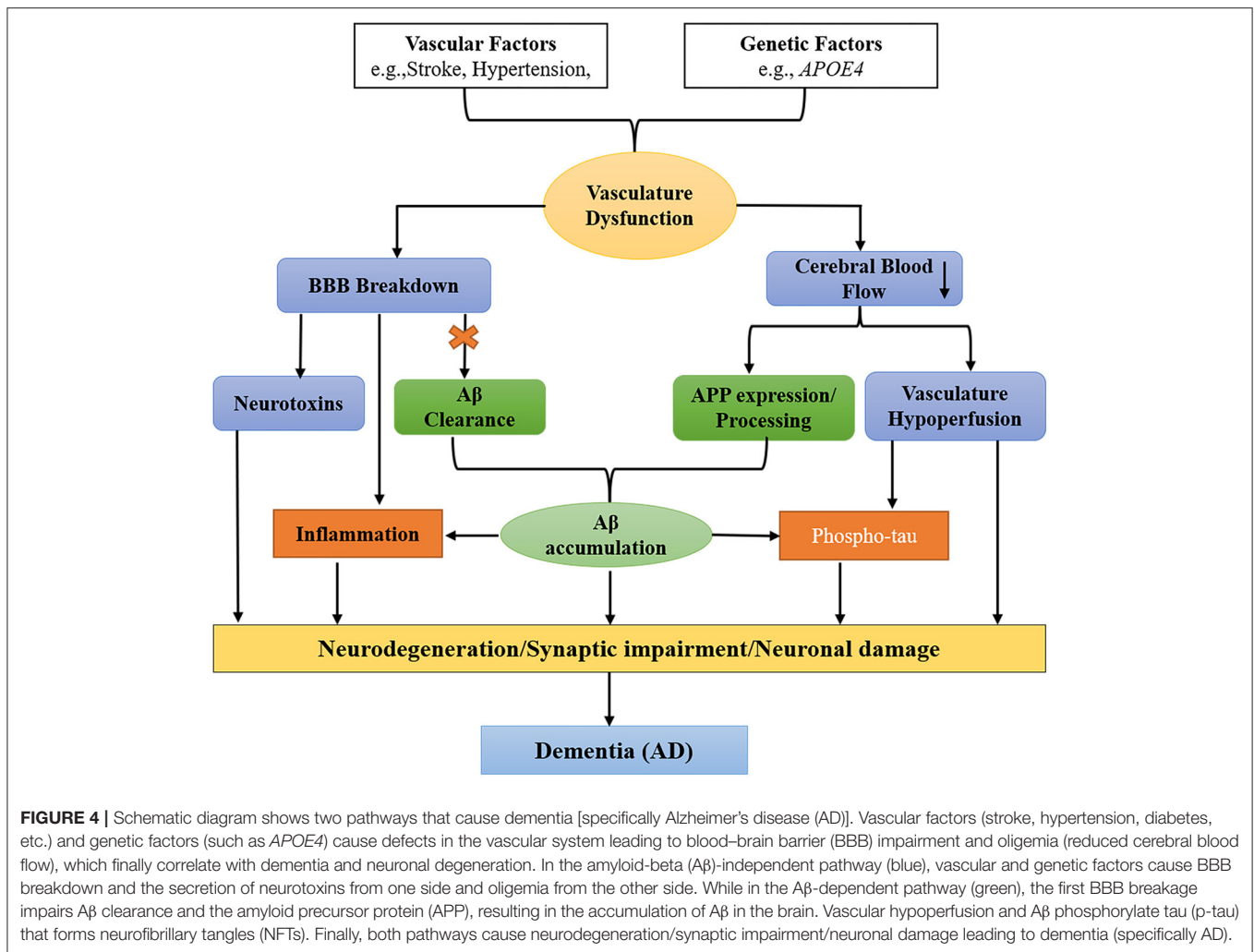
Phenotypes of BBB Breakdown in AD

In AD patients, the BBB is shown as leakages in brain vasculature, the perivascular aggregation of fibrinogen, albumin, thrombin, and immunoglobulin (IgG), the loss of TJs, and the degeneration of ECs and pericytes (Nelson et al., 2016). Furthermore, identical phenotypes were also observed in *ApoE*^{-/-} mice due to BBB impairment (Nishitsuji et al., 2011; Bell et al., 2012; Hammer et al., 2014; Soto et al., 2015; Castillo-Gomez et al., 2016; Di Cataldo et al., 2016), indicating that ApoE is vital for maintaining BBB integrity.

As pericytes are crucial for maintaining the BBB, any dysfunction in the signaling pathways of pericytes results in the breakdown of BBB, which causes dementia and other neurodegenerative diseases (Sagare et al., 2013; Nikolakopoulou et al., 2019). Brain microvascular endothelial cells (BMEC) secrete platelet-derived growth factor BB (PDGF-BB) and activate PDGFR β signaling, which is essential for the proliferation, migration, and survival of pericytes (Stratman et al., 2010). An impairment in PDGFR β signaling leads to pericyte degeneration (Stratman et al., 2010; Nation et al., 2019). According to a previous study, PDGFR β signaling was decreased in adult *Foxf2* deficient mice, thus resulting in high

BBB permeability (Reyahi et al., 2015). Impairment in the BBB was also reported in *Pdgfr β* ^{+/-} pericyte-deficient mice, which subsequently caused neuronal degeneration (Bell et al., 2010). In the AD murine model (*APP*^{SW/0}), the deterioration of pericytes results in the dysfunction of the BBB, leading to amyloid β accumulation and tau protein (p-tau) phosphorylation (Sagare et al., 2013). The breakdown of the BBB was also reported in AD patients associated with the reduction in pericytes (Sengillo et al., 2013). Studies also showed that the leakage of the BBB in AD patients starts at the hippocampus, resulting in an increase of soluble PDGFR β (sPDGFR β) in the CSF (Montagne et al., 2015; Miners et al., 2019). Additionally, the level of sPDGFR β in the CSF can be used as a biomarker to predict dementia and other neurodegenerative diseases such as AD (Nation et al., 2019).

Astrocytes are one of the main components of the NVU and are essential for the integrity of the BBB. In an *in vitro* study, it was observed that Sonic hedgehog (Shh) signaling released from astrocytes plays a vital role in the maintenance of BBB integrity by upregulation of *CLDN5* and *OCN* (Alvarez et al., 2011; Wang et al., 2014). Recently, it was also reported that, in the stroke mouse model, ischemia-induced astrogliosis led to the downregulation of the expression of TJ protein claudin-5 and occludin (Matthes et al., 2021), suggesting that astrocytes have a role in the regulation of TJ proteins. Another recent study reported that, in the tamoxifen-induced astrocyte ablation adult mouse model, the expression of TJ protein ZO-1 was

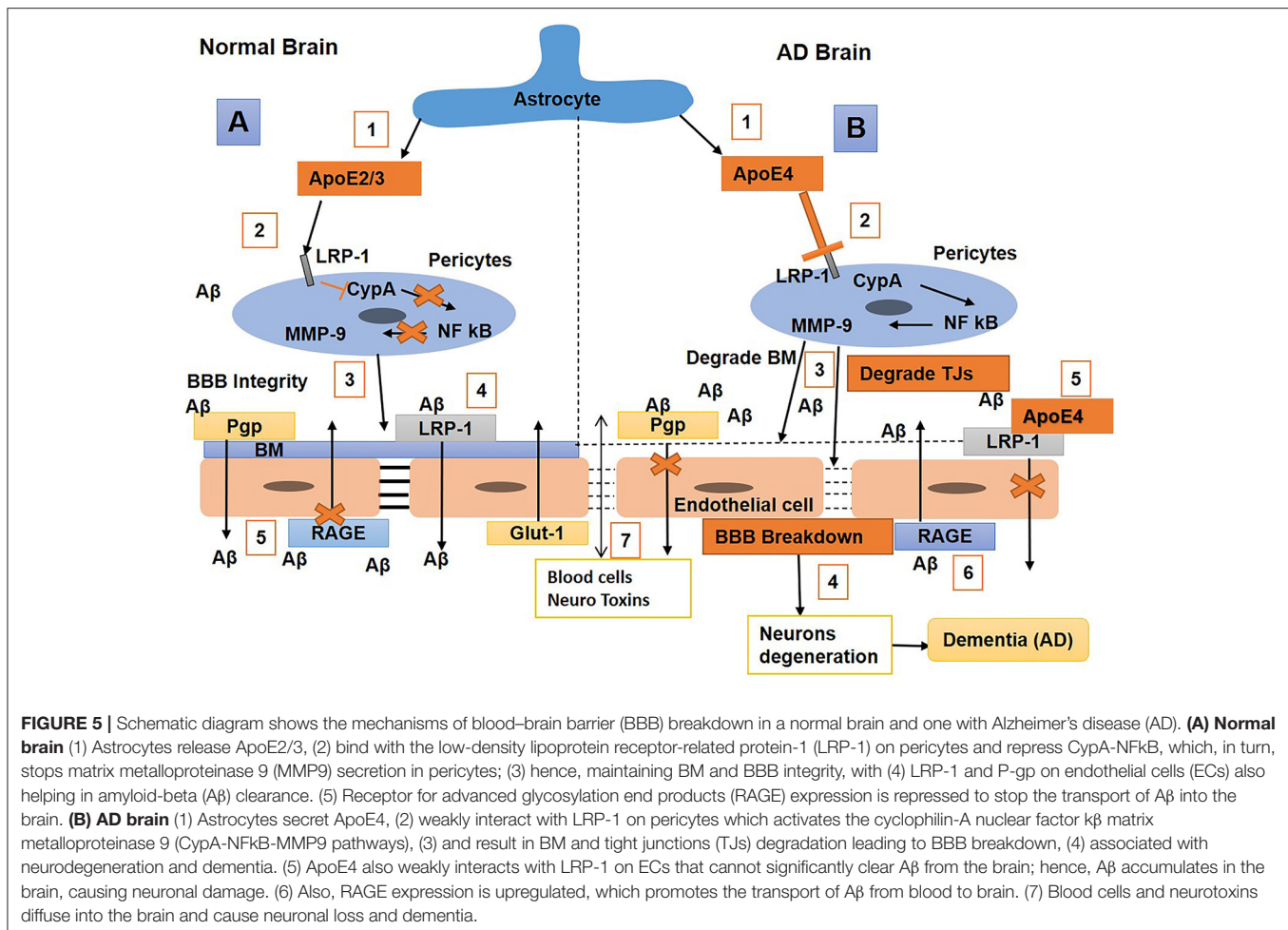


downregulated in vessel regions where astrocyte loss occurred, which may show the role of astrocytes in maintaining the integrity of the BBB in adult brains (Heithoff et al., 2021). A conditional knockout mouse study also showed that the deletion of laminins in astrocytes caused a decline in astrocytic AQP4 (Aquaporin4) expression, thus leading to a loss of TJ in ECs (Yao et al., 2014). In the AD brain, various changes in the morphology of astrocytes have been reported to cause BBB breakdown (Cai Z. et al., 2017). The depolarization of astrocyte endfeet may diminish the integrity of BBB, which was reported in the tg-ArcSwe mouse model of AD (Yang J. et al., 2011). In AD models, researchers also identified several changes in the morphology of astrocytes endfeet near aggregated vascular $A\beta$ (Kimbrough et al., 2015).

A mouse study showed that microglia stimulate TJ protein claudin-5 expression and maintain BBB integrity (Haruwaka et al., 2019). However, the BBB integrity becomes compromised with prolonged inflammation through the changing of the morphology of microglia (Lassman et al., 2012; Haruwaka et al., 2019). In the AD brain, due to the accumulation of $A\beta$, microglia

activate and secrete inflammatory cytokines, such as interleukins (IL-1 and IL-6) and tumor necrosis factor (TNF- α , and TNF- β) (Zhou et al., 2012) that cause BBB impairment (Wang et al., 2014). As a result, the trafficking of neutrophils through the BBB becomes elevated due to BBB breakdown (Allen et al., 2012; Wang et al., 2014; Zenaro et al., 2015). Furthermore, it has been observed that, in the tamoxifen-induced astrocyte knockout adult mouse model, the loss of astrocytes causes the activation of microglia (Heithoff et al., 2021); in turn, the activated microglia produce reactive oxygen and reactive nitrogen species (RNS), leading to BBB dysfunction and neurodegeneration (Block, 2008; Sumi et al., 2010).

In the physiological state, perivascular macrophages (PVMs) have a significant role in the maintenance of TJs between ECs. They also decrease vessel leakage, degrade pathogens, and limit inflammation (Lapenna et al., 2018) while contributing to BBB breakdown in the disease state (Boyle et al., 2018). These PVMs are enriched with scavenger receptors, might be involved in the clearance of toxin products from the brain parenchyma (Faraco et al., 2017), and have a diverse role in disease states such



as AD (Lapenna et al., 2018). Perivascular macrophages have been shown to phagocytose and alleviate Aβ plaques, and the PVM-deficient mouse model showed an increased aggregation of Aβ42 and cerebral amyloid angiopathy (CAA) related with AD (Yang et al., 2019). Another study showed that PVMs that are deficient in CD36 and Nox2 abrogated the production of ROS and Aβ cerebrovascular impairment compared with wild-type mice (Park et al., 2017).

In addition, perivascular fibroblasts (FBs) express the ECM genes *col1a2* and *col5a1* and are considered to mediate blood vessel integrity. Zebrafish deficient with *col5a1* showed spontaneous hemorrhage in the presence of the additional genetic ablation of the *col1a2* gene, suggesting the role of perivascular FBs in stabilizing vascular integrity (Rajan et al., 2020). Perivascular FBs also express *Lama2*, *Lamb1*, and *Lamc1*, which encode laminin 211 that interacts with astrocytic dystrophin, resulting in the regulation of AQP4 in astrocytic endfeet. This study suggests that any impairment in perivascular FBs result in the dysregulation of AQP4, which may cause Aβ aggregation and AD as reviewed by Lendahl et al. (2019). Furthermore, it has been reported that alteration in the activity of perivascular FBs also leads to other neurological disorders (Månberg et al., 2021).

Mechanisms of BBB Breakdown in AD

Various pathological and aberrant events such as oxidative stress, inflammation, and the ApoE4 genotype cause BBB breakdown associated with AD. Research has shown that, in AD, the activation of the inflammatory and oxidative stress signaling pathways is the primary event that causes BBB disruption (Perry et al., 2002; Candore et al., 2010; Eikelenboom et al., 2012). Cytokines (Pan et al., 2011), Aβ (Gonzalez-Velasquez et al., 2008; Deli et al., 2010; Carrano et al., 2011), LPS (Bannerman and Goldblum, 1999; Verma et al., 2006), and p-tau proteins (Kovac et al., 2009) are the stimulus of inflammation for the activation of inflammatory pathways in BBB ECs. Hence, increases of the pro-inflammatory mediators and ROS/RNS in BBB ECs, astrocytes (Tada et al., 1994), and pericytes (Kovac et al., 2011; Takata et al., 2011) ultimately cause BBB breakdown. Recently we reviewed the role of peripheral inflammation in BBB breakdown (Huang et al., 2021). Glucose transporter protein (GLUT1) is repressed in the endothelium of AD, which causes a decline in the glucose level of the CNS (Mooradian et al., 1997; Winkler et al., 2015). In human AD, LRP1, which is a primary receptor for the clearance of amyloid-β, is downregulated with an increase in oxidative stress (Deane et al., 2004; Donahue et al., 2006; Sagare et al., 2007; Miller et al., 2008; Owen et al., 2010;

Halliday et al., 2016); as a result, the transport of A β from the brain becomes reduced and leads to amyloid- β accumulation in the brain (Deane et al., 2004, 2008; Storck et al., 2016). In mice, systemic inflammation with LPS has been observed to downregulate both LRP-1 and P-gp efflux transporters and block the A β clearance from the brain (Jaeger et al., 2011; Erickson et al., 2012). Furthermore, it has been reported that the expression levels of the receptor for advanced glycosylation end products (RAGE) in both mural cells and brain endothelium were elevated (Deane et al., 2003; Donahue et al., 2006; Miller et al., 2008). The function of the RAGE is to transfer A β from blood to the brain (opposite to LRP1), which enhances neuronal inflammation. In AD patients, the RAGE is observed as a significant therapeutic target (Bell et al., 2012). A transgenic mouse with overexpressed APP (amyloid precursor protein) has been reported to show vascular impairment due to the elevation of A β 40 (Niwa et al., 2000).

Aquaporin-4 (AQP4) is the prime water channel expressed in the CNS and is primarily expressed in astrocytes, thus playing a vital role in normal brain homeostasis and various neurological diseases (Lan et al., 2016b). Specifically, AQP4 facilitates the clearance of A β , and alteration in AQP4 expression leads to the accumulation of amyloid- β in the brain (Hoshi et al., 2012; Yang et al., 2012). Furthermore astrocytic AQP4-deficient animals cannot efficiently remove A β from the brain (Iliff et al., 2012). A study showed that AQP4 is crucial to regulate fluid flow in the brain interstitial required to maintain the microenvironment for neurons to function properly. The perturbed AQP4 expression has been observed to cause A β deposition and inflammation in the human brain, which leads to AD (Rasmussen et al., 2018). In AD patients and animal models, the expression and distribution of AQP4 were altered, leading to amyloid- β accumulation, which plays a vital role in the pathogenesis of AD as reviewed by Yang et al. (2016). Furthermore, it has been observed that, in AD patients, the localization of AQP4 in the perivascular space was reduced and is associated with an increase in neurofibrillary and amyloid- β pathology (Zeppenfeld et al., 2017). In addition, AQP4 facilitates the transport of potassium and calcium ions, which plays an essential role in the pathogenesis of AD as reviewed by Lan et al. (2016a). In AD, the chronic activation of microglia leads to the release of abundant pro-inflammatory cytokines and abolishes phagocytosis, thus causing the deposition of A β and neuroinflammation (Krabbe et al., 2013; Heneka et al., 2015) and subsequently producing ROS that causes BBB dysfunction and neurotoxicity (Block, 2008; Sumi et al., 2010). The activated microglia also release IL-1 β (a pro-inflammatory cytokine) that amplify the BBB leakage and diminish the ability of the astrocytes to maintain the BBB (Wang et al., 2014). Therefore, AQP4 can be a fascinating therapeutic target for AD and other CNS diseases.

Apolipoprotein E (ApoE) is a protein encoded by the *APOE* gene, located on chromosome 9 and associated with lipid transport. *APOE* consists of three alleles, namely, ϵ 2, ϵ 3, and ϵ 4, translated to ApoE2, ApoE3, and ApoE4 isoforms. The *APOE* isoform distributed as *APOE3* is the most abundant in humans at approximately 77.9%, while *APOE4* and *APOE2* distributions are 13.7 and 8.4%, respectively (Farrer et al., 1997). In the CNS,

astrocytes produce ApoE, whereas, in peripheral tissue, ApoE production occurs in the liver (Liu et al., 2013).

Studies reported that ApoE plays an essential role in maintaining BBB integrity (Nishitsuji et al., 2011). An *in vivo* study showed that ApoE2/3 induces BBB integrity by interacting with LRP-1 on pericytes to block the cyclophilin-A nuclear factor κ B matrix metalloproteinase 9 (CypA-NF- κ B-MMP-9) pathway, thus resulting in the inhibition of MMPs (Bell et al., 2012). Researchers also observed that the *APOE4* isoform is a major risk factor for AD, and that the binding of A β with apoE4 shifts fast clearance of soluble A β 40/42 from LRP1 to VLDLR; hence, A β -apoE4 complexes at the BBB are cleared with a slower rate than LRP1 (Deane et al., 2008; Tachibana et al., 2019). The expression of *APOE4* causes a reduction in BBB integrity by promoting pericyte degeneration in AD (Bell et al., 2012), which is correlated with high BBB permeability to IgG and fibrin (Halliday et al., 2016). In a transgenic mouse study, the mice that had *ApoE* replaced with human *APOE* (*TR-APOE*) showed astrocytes that secreted ApoE4 blocks pericytic LRP-1, resulting in the activation of the proinflammatory CypA-NF- κ B MMP9 pathway, BBB disruption, and brain hemorrhage through the enzymatic breakdown of the TJ and basement membrane (Nishitsuji et al., 2011; Bell et al., 2012). A study showed that an LRP1 endothelial knockout caused the activation of the CypA-MMP9 pathway in the endothelium, which led to damage to TJs and BBB breakdown (Nikolakopoulou et al., 2021). In *TR-APOE4* mice, the repression of Glut1 and upregulation of RAGE expression were also observed compared with *TR-APOE3* or *TR-APOE2* (Alata et al., 2015). It has been reported that humans carrying *APOE4* are more prone to breakdown in the BBB and loss of pericytes than non-*APOE4* carriers (Hultman et al., 2013; Zonneveld et al., 2014; Halliday et al., 2016). Furthermore, CypA and MMP-9 levels increase in *APOE4* carriers, leading to the elevation of IgG and fibrinogen leakages (Halliday et al., 2016). Overall, these results suggest that ApoE2/3 represses inflammation by interacting with pericyte LRP-1, subsequently inducing BBB integrity. In contrast, the ApoE4 might have BBB impairment properties or cause a higher risk of BBB breakdown. The repression of ApoE4 or inhibition of the CypA-MMP9 pathway in humans with AD might be an exciting topic in the future for the reduction the neurodegenerative process (Figure 5).

BBB Breakdown in VaD

Vascular dementia is a neurodegenerative disease caused by reduced CBF to the brain resulting in cognitive dysfunction. After AD, VaD is considered the second most common dementia, accounting for ~15–30% of all dementia (Sloane et al., 2002; Abou-Saleh et al., 2011; Gorelick et al., 2011; Goodman et al., 2017).

Pathophysiology of VaD

Chronic hypoperfusion and thrombosis are the main factors in VaD that cause reduced CBF and promote oxidative stress, hypoxia, and inflammatory molecule expression (cytokines/chemokines). These chronic events cause damage to the periventricular WM, basal ganglia, and hippocampus.

Cerebrovascular pathology has a significant contribution to the pathogenesis of VaD by damaging the brain. Vascular impairments include large vessel atherosclerosis (AS), small vessel AS, and CAA. These cerebrovascular pathologies cause microinfarcts in gray matter, WM lesions, and microbleeds (Thal et al., 2012). These vascular abnormalities can occur throughout the brain, resulting in VaD (Grinberg and Heinsen, 2010).

Phenotypes of BBB Breakdown in VaD

Hypertension is one of the factors that cause BBB breakdown in VaD with the accumulation of perivascular collagen in the hippocampus and WM lesions (Verhaaren et al., 2013). Toxic molecules or high blood pressure cause damage to the BBB endothelium. Hypertension also causes a reduction in the integrity of ECs and pericytes, astrocytes endfeet swelling, and retraction from the vessel wall, which results in BBB breakdown and subsequently leading to a reduction in CBF (Wardlaw et al., 2003). Studies reported that acute ischemia induces BBB permeability by the secretion of ROS (Abboud et al., 2007; Simpkins et al., 2016). A study also showed that, during vascular pathology, chronic hypoperfusion causes BBB disruption in WM lesions (Tomimoto et al., 1996). Another study showed that BBB disruption due to the degeneration of pericytes results in the disruption of WM circulation, deposition of fibrinogen, and reduction of CBF that further induces damage to the myelin, axons, and oligodendrocytes (Montagne et al., 2018) (Figure 6). Furthermore, animal experiments showed that chronic cerebral hypoperfusion (CCH) increases BBB leakage to intravenously injected horseradish peroxidase (HRP) in the corpus callosum. In animals, perivascular collagen was also accumulated in the corpus callosum associated with WM lesion formation and elevated BBB permeability (Ueno et al., 2002). In VaD, PVMs have been reported to induce oxidative stress leading to hypertension (Yang et al., 2019).

Mechanisms of BBB Breakdown in VaD

Hypoxia upregulates oxidative stress, which produces NO, ROS, and free radicals (Li et al., 2013; Ma et al., 2013; Zhang et al., 2014). In addition, oxidative stress disrupts the ratio of antioxidants, NO, and ROS and causes damage to the endothelial, glial, and neuronal cells, resulting in the impairment of the NVU, BBB disruption, and mediation of a reduction in CBF (Liu and Zhang, 2012). In particular, ROS can further lead to mitochondrial dysfunction resulting in cerebral hypoxia that induces oxidative stress (Zhang et al., 2014). Cerebral vascular hypoxia produces inflammatory molecules that cause apoptosis and impairments in the function of microvessels. The cytokines/chemokines cause damage to the endothelium, glial, and neurons cells and, hence, enhance BBB permeability (Gill et al., 2010). The inflammatory molecules such as IL-1, IL-6, MMPs (MMP-2, MMP-9), TNF α , and TLR4 (toll-like receptor 4) infiltrate the brain (Li and Lai, 2007; Gill et al., 2010; Candelario-Jalil et al., 2011; Reuter et al., 2015), cause demyelination, and damage the axons and oligodendrocytes associated with the hippocampus and WM lesions (Chen et al., 2011).

Damage to oligodendrocytes represses remyelination (Ihara et al., 2010), and demyelination retains the transmission of

neural signals, thus resulting in cognitive impairment. Overall, hypoxia, oxidative stress, and inflammation cause defects in neurogenesis, impairment in the proliferation of neuronal progenitor cell, synaptic plasticity, and reduced spine density in the hippocampus, thus resulting in cognitive impairment (Stranahan et al., 2008; Park et al., 2010) (Figure 6). Furthermore, several studies reported that CCH causes AD and VaD (Du et al., 2017). It has also been reported that intercellular adhesion molecule 1 (ICAM-1) and vascular adhesion molecule 1 (VCAM-1) were significantly upregulated in the vascular ECs of the CCH animal model associated with cognitive impairment (Won et al., 2013; Khan et al., 2015).

Overlap Between Alzheimer's and Vascular Dementia

As discussed above and in other studies, significant clinical heterogeneity has been shown between AD and VaD (Sachdev et al., 2014; Chui and Ramirez-Gomez, 2015); however, recent studies reported that these two diseases co-occur in what is called mixed dementia (Emrani et al., 2020). In mixed dementia, vascular pathology not only mediates AD progression, but the pathology of AD also potentiates vascular impairments, suggesting that pure AD or VaD rarely occur (Emrani et al., 2020). In addition, another study reported that, in aged individuals, there is genetic overlap between vascular dysfunction and AD that is primarily associated with apolipoprotein E (Lin et al., 2019).

Community and epidemiological studies reported the mixed neuropathology that is quite common in both AD and VaD (Schneider et al., 2009; Wharton et al., 2011). The clinical study observed that only 9% of 1,000 patients with cognitive impairments have pure AD pathology; however, AD pathology is mainly associated with vascular dysfunction or other neurodegenerative diseases (Boyle et al., 2018). Another clinical study examined 63 patients with mild cognitive impairment (MCI), in which only 28% were reported as pure AD and approximately 24% were diagnosed with mixed dementia (AD and VaD) (Silbert et al., 2012). Researchers observed that frontal lobe lesions and vascular pathology, e.g., white matter hyperintensities (WMH), are associated with neuropsychiatric symptoms and are common in both AD and VaD (Anor et al., 2017). Alzheimer's disease and VaD share many similar clinical pathologies that lead to cognitive impairment and neuropsychiatric symptoms associated with behavioral alterations (Kalara, 2002) as shown in Table 2. Hence, these studies suggest that there might be considerable overlaps between AD and VaD, and comprehensive studies should be considered to understand the pathophysiology of dementia instead of segregating AD from VaD.

BIOMARKERS ASSOCIATED WITH BBB BREAKDOWN

Various imaging techniques and other methods are currently being used to identify biomarkers associated with BBB breakdown in different neurological disorders, which are

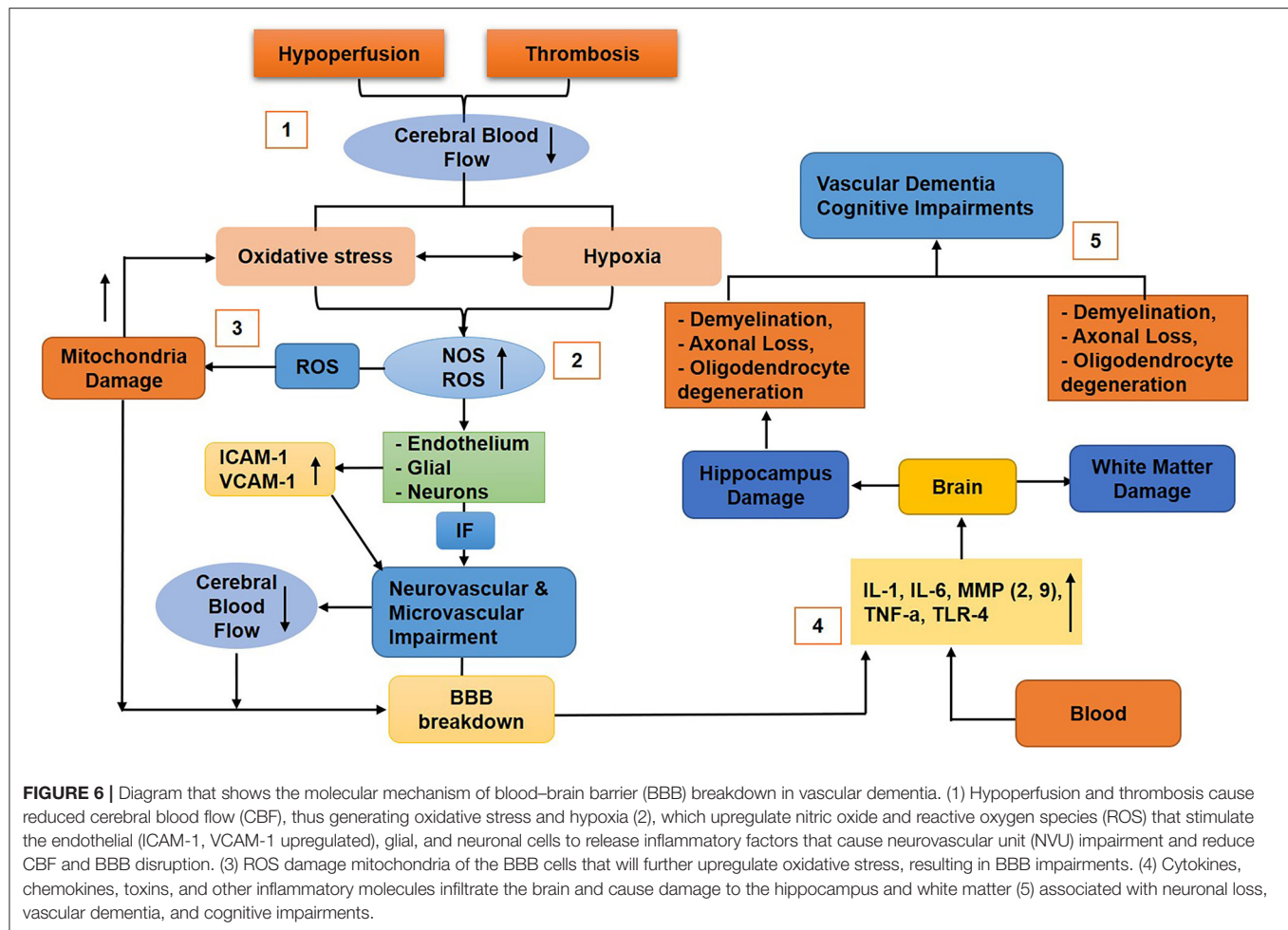


TABLE 2 | Pathologies associated to both Alzheimer's disease and vascular dementia.

Clinical pathologies	Alzheimer's disease (%)	Vascular dementia (%)
Cerebral amyloid angiopathy	98	30
Microvascular degeneration	100	30
Total infarctions	36	100
Micro-infarcts	31	65
Intracerebral hemorrhage	7	15
White matter lesions	35	70
Loss of cholinergic neurones	70	40
Cardiovascular disease	77	60

helpful in healthcare decisions. However, during the acute phase of BBB disruption, some of the clinical care places may lack the facilities to perform MRIs; hence, the detection of peripheral blood biomarkers is the best approach to identifying the status of BBB.

Studies showed that, while the blood/CSF albumin ratio can be used as a biomarker to detect BBB permeability, it cannot distinguish BBB and blood-CSF permeability nor locate leakage

as reviewed by Farrall and Wardlaw (2009). Hence, nowadays, the dynamic contrast-enhanced MRI (DCE-MRI) technique is used to directly identify and localize these elusive permeability values (Raja et al., 2018). A study in healthy, aged individuals using DCE-MRI with a gadolinium-based contrast agent injected intravenously identified that BBB leakage was high and localized in the brain regions most vulnerable to damage from aging (Verheggen et al., 2020). It has been observed that, by using DCE-MRI, the BBB permeability index K_{trans} was increased in the hippocampus and some of its sub-regions, CA1 and dentate gyrus (DG), but not in CA3. This study showed that, in the hippocampus, the BBB integrity was lost progressively with age. Still, no significant BBB leakage was observed in the cortical and sub-cortical regions (Montagne et al., 2015), suggesting that, in terms of aging, the BBB breakdown starts in the hippocampus. A study using CSF biomarkers and the DCE-MRI technique reported that aged people with prior cognitive impairment had higher BBB permeability than healthy individuals (Nation et al., 2019). These studies suggest that it is possible to detect and localize BBB leakage by using DCE-MRI.

It has been observed that, in epileptic patients, the levels of serum Visinin-like protein 1 (sVILIP-1) and serum caveolin 1 (sCAV-1) are higher, which may be used as biomarkers for the

diagnosis of BBB breakdown (Tan et al., 2020). Another protein biomarker is s100 β , which is produced by astrocyte endfeet; when the BBB becomes compromised, s100 β is immediately released into the peripheral blood (Kadry et al., 2020). Furthermore, a study identified that the expression levels of A-kinase anchoring protein 7 (AKAP7) were high in the peripheral blood (lymphocyte), and thus might be considered to identify BBB breakdown during ischemic stroke or post-stroke (O'Connell et al., 2017). Neuron-specific enolase (NSE) and GFAP are also promising biomarkers that can be detected in the CSF to identify BBB breakdown (Kadry et al., 2020). A study reported that the elevated level of sPDGFR β is associated with damage to the pericytes and BBB disruption leading to a decline in cognition (Sweeney et al., 2020). Soluble PDGFR β as a biomarker was also observed in VaD (Iadecola, 2017; Sweeney et al., 2019a) and various other neurological diseases (Sweeney et al., 2018a, 2019b). Soluble cell adhesion molecules (CAMs), zonulin, and soluble 4-1BBL (transmembrane protein receptor) have also been identified to be associated with BBB damage. PECAM-1, P-selectin, and E-selectin are soluble adhesion molecules reported to be upregulated in individuals with compromised BBB and can be used as biomarkers for BBB breakdown (D'Ambrosio et al., 2015). Increased leakage of gadolinium (DCE-MRI; *Ktrans*), microbleeds (T2*-weighted and SWI-MRI), reduced glucose transport (FDG-PET), diminished P-glycoprotein 1 function (verapamil-PET), and CNS leukocyte infiltration (MMP inhibitor-PET) are some of the techniques that can be used to identify biomarkers associated with BBB damages in various CNS diseases (Sweeney et al., 2018b).

CONCLUSIONS AND FUTURE DIRECTIONS

The BBB consists of a set of physiological properties that tightly regulate the normal microenvironment essential for proper neuronal activities. Any impairment in these properties either at the cellular or molecular level causes BBB breakdown. Aging is one of the factors that contribute to BBB disruption. During aging, the various physiological properties of the BBB are impaired, leading to BBB dysfunction. The neurotoxins infiltrating the brain can also cause cognitive impairments and neurodegeneration. Furthermore, BBB breakdown also contributes to dementia that includes ADs and VaD. In AD with disruption of BBB, A β and NFT of p-tau accumulate in the blood vessel, causing further inflammation in the NVU that, in turn, induces the release inflammatory factors to degenerate neurons associated with a decline in cognition. Another factor that degrades the integrity of BBB associated with AD is *APOE4*. In dementia, VaD accounts for the most cases next to AD caused by BBB breakdown. In VaD, the CBF is reduced and inflammatory molecules infiltrate the brain due to BBB impairment, subsequently causing neuronal loss and, thus, cognitive impairment. Hence, BBB breakdown can be used as a novel biomarker to study various neurological impairments such as AD, VaD, and other associated declines in cognition.

Recently, RepSox was identified to inhibit TGF- β , VEGFA, and inflammatory gene networks (Roudnicky et al., 2020). Furthermore, RepSox significantly elevated BBB resistance, induced TJ and transporters, reduced paracellular permeability by activating Notch and Wnt pathways, and, thus, might be used as an emerging BBB therapeutics to treat neurological diseases such as AD (Roudnicky et al., 2020). In addition, secreted protein acidic and rich in cysteine (SPARC) was identified to decrease transendothelial electrical resistance (TEER) and TJ proteins (ZO-1, OCLN) and increase paracellular permeability by regulating the tyrosine kinase pathway (Alkabie et al., 2016). Hence, the SPARC-collagen binding domain might be a potential therapeutic target to treat AD (Piloizzi et al., 2020). Furthermore, SPARC/Hevin normalization may also be considered as a novel therapeutic target for the modulation of AD progression (Strunz et al., 2019).

Although researchers have reported the contributions of BBB disruption to the pathogenesis of cognitive impairment associated with normal aging and dementia, more research is needed to elucidate the precisely causing factors and the cellular and molecular mechanisms of BBB maintenance, breakdown, and repair correlated with neurodegeneration and cognition decline. In the future, how aging and dementia affect BBB function in health and disease state, thus leading to neurodegeneration and cognitive impairment, should be explored in living organisms. Clinical research pertaining to this will boost our knowledge and help us better understand the association between BBB breakdown and cognitive decline. Such studies pave the way for the use of the BBB as a novel biomarker and therapeutic target to treat dementia and other neurological diseases associated with cognitive impairment. Furthermore, these studies suggest that amelioration in the cerebrovascular pathways (particularly BBB breakdown) can alleviate neurodegeneration in dementia (particularly AD) associated with cognitive impairment. Hence, the characterization of the cellular and molecular constituents of the cerebrovascular systems that contribute to the pathophysiology of dementia will provide a systematic methodology of dementia diagnosis. More profound knowledge of the vascular system will also help design emerging efficient strategies that can be used for the therapeutic interventions of cognitive impairment and dementia.

AUTHOR CONTRIBUTIONS

BH drafted the manuscript and made the figures and table. CF and JC discussed and revised the manuscript. All authors contributed to the article and approved the final manuscript.

FUNDING

This study was supported by the National Natural Science Foundation of China (81771293), the Science Technology and Innovation Commission of Shenzhen Municipality (ZDSYS20190902093409851 and SGLH20180625142404672),

the international collaboration project of the Chinese Academy of Sciences (172644KYSB20200045), the CAS-Croucher Funding Scheme for Joint Laboratories, and the Guangdong Innovation

Platform of Translational Research for Cerebrovascular Diseases. BH is supported by the Chinese Government Scholarship (CSC No. 2018SLJ023241) for International Students.

REFERENCES

- Abbott, N. J. (2013). Blood-brain barrier structure and function and the challenges for CNS drug delivery. *J. Inherit. Metab. Dis.* 36, 437–449. doi: 10.1007/s10545-013-9608-0
- Abbott, N. J., Patabendige, A. A., Dolman, D. E., Yusof, S. R., and Begley, D. J. (2010). Structure and function of the blood-brain barrier. *Neurobiol. Dis.* 37, 13–25. doi: 10.1016/j.nbd.2009.07.030
- Abbott, N. J., Rönnbäck, L., and Hansson, E. (2006). Astrocyte-endothelial interactions at the blood-brain barrier. *Nat. Rev. Neurosci.* 7, 41–53. doi: 10.1038/nrn1824
- Abboud, H., Labrecque, J., Meseguer, E., Lavalley, P. C., Simon, O., Olivot, J.-M., et al. (2007). Ischemia-modified albumin in acute stroke. *Cerebrovasc. Dis.* 23, 216–220. doi: 10.1159/000097644
- Abou-Saleh, M. T., Katona, C. L., and Kumar, A. (2011). *Principles and Practice of Geriatric Psychiatry*. Hoboken, NJ: Wiley-Blackwell.
- Ahmad, M. H., Fatima, M., and Mondal, A. C. (2019). Influence of microglia and astrocyte activation in the neuroinflammatory pathogenesis of Alzheimer's disease: rational insights for the therapeutic approaches. *J. Clin. Neurosci.* 59, 6–11. doi: 10.1016/j.jocn.2018.10.034
- Alata, W., Ye, Y., St-Amour, I., Vandal, M., and Calon, F. (2015). Human apolipoprotein E $\epsilon 4$ expression impairs cerebral vascularization and blood-brain barrier function in mice. *J. Cereb. Blood Flow Metab.* 35, 86–94. doi: 10.1038/jcbfm.2014.172
- Alexander, J. J. (2018). Blood-brain barrier (BBB) and the complement landscape. *Mol. Immunol.* 102, 26–31. doi: 10.1016/j.molimm.2018.06.267
- Alkabbie, S., Basivireddy, J., Zhou, L., Roskams, J., Rieckmann, P., and Quandt, J. A. (2016). SPARC expression by cerebral microvascular endothelial cells *in vitro* and its influence on blood-brain barrier properties. *J. Neuroinflammation* 13, 1–17. doi: 10.1186/s12974-016-0657-9
- Allen, C., Thornton, P., Denes, A., McColl, B. W., Pierozynski, A., Monestier, M., et al. (2012). Neutrophil cerebrovascular transmigration triggers rapid neurotoxicity through release of proteases associated with decondensed DNA. *J. Immunol.* 189, 381–392. doi: 10.4049/jimmunol.1200409
- Alvarez, J. I., Dodelet-Devillers, A., Kebir, H., Ifergan, I., Fabre, P. J., Terouz, S., et al. (2011). The Hedgehog pathway promotes blood-brain barrier integrity and CNS immune quiescence. *Science* 334, 1727–1731. doi: 10.1126/science.1206936
- Anor, C. J., O'Connor, S., Saund, A., Tang-Wai, D. F., Keren, R., and Tartaglia, M. C. (2017). Neuropsychiatric symptoms in Alzheimer disease, vascular dementia, and mixed dementia. *Neurodegener. Dis.* 17, 127–134. doi: 10.1159/000455127
- Arendt, T., Brückner, M. K., Morawski, M., Jäger, C., and Gertz, H.-J. (2015). Early neurone loss in Alzheimer's disease: cortical or subcortical? *Acta Neuropathol. Commun.* 3, 1–11. doi: 10.1186/s40478-015-0187-1
- Aw, D., Silva, A. B., and Palmer, D. B. (2007). Immunosenescence: emerging challenges for an ageing population. *Immunology* 120, 435–446. doi: 10.1111/j.1365-2567.2007.02555.x
- Bake, S., Friedman, J. A., and Sohrabji, F. (2009). Reproductive age-related changes in the blood brain barrier: expression of IgG and tight junction proteins. *Microvasc. Res.* 78, 413–424. doi: 10.1016/j.mvr.2009.06.009
- Baker, S. K., Chen, Z.-L., Norris, E. H., Revenko, A. S., MacLeod, A. R., and Strickland, S. (2018). Blood-derived plasminogen drives brain inflammation and plaque deposition in a mouse model of Alzheimer's disease. *Proc. Natl. Acad. Sci. U.S.A.* 115, E9687–E9696. doi: 10.1073/pnas.1811172115
- Ballaed, C., Gauthier, S., Corbett, A., Brayne, C., and Aarsland, D. (2011). Jones e. Alzheimer's disease. *Lancet* 377, 1019–1031. doi: 10.1016/S0140-6736(10)61349-9
- Banks, W. A., Reed, M. J., Logsdon, A. F., Rhea, E. M., and Erickson, M. A. (2021). Healthy aging and the blood-brain barrier. *Nature Aging* 1, 243–254. doi: 10.1038/s43587-021-00043-5
- Bannerman, D. D., and Goldblum, S. E. (1999). Direct effects of endotoxin on the endothelium: barrier function and injury. *Lab. Invest.* 79, 1181–1199.
- Bartels, T., De Schepper, S., and Hong, S. (2020). Microglia modulate neurodegeneration in Alzheimer's and Parkinson's diseases. *Science* 370, 66–69. doi: 10.1126/science.abb8587
- Bell, R. D., Winkler, E. A., Sagare, A. P., Singh, I., LaRue, B., Deane, R., et al. (2010). Pericytes control key neurovascular functions and neuronal phenotype in the adult brain and during brain aging. *Neuron* 68, 409–427. doi: 10.1016/j.neuron.2010.09.043
- Bell, R. D., Winkler, E. A., Singh, I., Sagare, A. P., Deane, R., Wu, Z., et al. (2012). Apolipoprotein E controls cerebrovascular integrity via cyclophilin A. *Nature* 485, 512–516. doi: 10.1038/nature11087
- Bell, R. D., and Zlokovic, B. V. (2009). Neurovascular mechanisms and blood-brain barrier disorder in Alzheimer's disease. *Acta Neuropathol.* 118, 103–113. doi: 10.1007/s00401-009-0522-3
- Ben-Menachem, E., Johansson, B. B., and Svensson, T. (1982). Increased vulnerability of the blood-brain barrier to acute hypertension following depletion of brain noradrenaline. *J. Neural Transm.* 53, 159–167. doi: 10.1007/BF01243407
- Berezowski, V., Landry, C., Dehouck, M.-P., Cecchelli, R., and Fenart, L. (2004). Contribution of glial cells and pericytes to the mRNA profiles of P-glycoprotein and multidrug resistance-associated proteins in an *in vitro* model of the blood-brain barrier. *Brain Res.* 1018, 1–9. doi: 10.1016/j.brainres.2004.05.092
- Bhaskar, K., Konerth, M., Kokiko-Cochran, O. N., Cardona, A., Ransohoff, R. M., and Lamb, B. T. (2010). Regulation of tau pathology by the microglial fractalkine receptor. *Neuron* 68, 19–31. doi: 10.1016/j.neuron.2010.08.023
- Biron, K. E., Dickstein, D. L., Gopaul, R., and Jefferies, W. A. (2011). Amyloid triggers extensive cerebral angiogenesis causing blood brain barrier permeability and hypervascularity in Alzheimer's disease. *PLoS ONE* 6:e23789. doi: 10.1371/journal.pone.0023789
- Blanchette, M., and Daneman, R. (2015). Formation and maintenance of the BBB. *Mech. Dev.* 138, 8–16. doi: 10.1016/j.mod.2015.07.007
- Blau, C. W., Cowley, T. R., O'Sullivan, J., Grehan, B., Browne, T. C., Kelly, L., et al. (2012). The age-related deficit in LTP is associated with changes in perfusion and blood-brain barrier permeability. *Neurobiol. Aging* 33, 1005.e1023–1005.e1035. doi: 10.1016/j.neurobiolaging.2011.09.035
- Block, M. L. (2008). NADPH oxidase as a therapeutic target in Alzheimer's disease. *BMC Neurosci.* 9:S8. doi: 10.1186/1471-2202-9-S2-S8
- Boyle, P. A., Yu, L., Wilson, R. S., Leurgans, S. E., Schneider, J. A., and Bennett, D. A. (2018). Person-specific contribution of neuropathologies to cognitive loss in old age. *Ann. Neurol.* 83, 74–83. doi: 10.1002/ana.25123
- Brown, W. R., and Thore, C. R. (2011). Cerebral microvascular pathology in ageing and neurodegeneration. *Neuropathol. Appl. Neurobiol.* 37, 56–74. doi: 10.1111/j.1365-2990.2010.01139.x
- Buschini, E., Piras, A., Nuzzi, R., and Vercelli, A. (2011). Age related macular degeneration and drusen: neuroinflammation in the retina. *Prog. Neurobiol.* 95, 14–25. doi: 10.1016/j.pneurobio.2011.05.011
- Bussian, T. J., Aziz, A., Meyer, C. F., Swenson, B. L., van Deursen, J. M., and Baker, D. J. (2018). Clearance of senescent glial cells prevents tau-dependent pathology and cognitive decline. *Nature* 562, 578–582. doi: 10.1038/s41586-018-0543-y
- Cai, W., Zhang, K., Li, P., Zhu, L., Xu, J., Yang, B., et al. (2017). Dysfunction of the neurovascular unit in ischemic stroke and neurodegenerative diseases: an aging effect. *Ageing Res. Rev.* 34, 77–87. doi: 10.1016/j.arr.2016.09.006
- Cai, Z., Wan, C.-Q., and Liu, Z. (2017). Astrocyte and Alzheimer's disease. *J. Neurol.* 264, 2068–2074. doi: 10.1007/s00415-017-8593-x

- Candelario-Jalil, E., Thompson, J., Taheri, S., Grossetete, M., Adair, J. C., Edmonds, E., et al. (2011). Matrix metalloproteinases are associated with increased blood-brain barrier opening in vascular cognitive impairment. *Stroke* 42, 1345–1350. doi: 10.1161/STROKEAHA.110.600825
- Candiello, J., Cole, G. J., and Halfter, W. (2010). Age-dependent changes in the structure, composition and biophysical properties of a human basement membrane. *Matrix Biol.* 29, 402–410. doi: 10.1016/j.matbio.2010.03.004
- Candore, G., Bulati, M., Caruso, C., Castiglia, L., Colonna-Romano, G., Di Bona, D., et al. (2010). Inflammation, cytokines, immune response, apolipoprotein E, cholesterol, and oxidative stress in Alzheimer disease: therapeutic implications. *Rejuvenation Res.* 13, 301–313. doi: 10.1089/rej.2009.0993
- Carrano, A., Hoozemans, J. J., van der Vies, S. M., Rozemuller, A. J., van Horsen, J., and de Vries, H. E. (2011). Amyloid beta induces oxidative stress-mediated blood-brain barrier changes in capillary amyloid angiopathy. *Antioxid. Redox Signal.* 15, 1167–1178. doi: 10.1089/ars.2011.3895
- Castillo-Gomez, E., Kästner, A., Steiner, J., Schneider, A., Hettling, B., Poggi, G., et al. (2016). The brain as immunoprecipitator of serum autoantibodies against N-Methyl-D-aspartate receptor subunit NR1. *Ann. Neurol.* 79, 144–151. doi: 10.1002/ana.24545
- Cerbai, F., Lana, D., Nosi, D., Petkova-Kirova, P., Zecchi, S., Brothers, H. M., et al. (2012). The neuron-astrocyte-microglia triad in normal brain ageing and in a model of neuroinflammation in the rat hippocampus. *PLoS ONE* 7:e45250. doi: 10.1371/journal.pone.0045250
- Chacón-Quintero, M. V., Pineda-López, L. G., Villegas-Lanau, C. A., Posada-Duque, R., and Cardona-Gómez, G. P. (2021). Beta-secretase 1 underlies reactive astrocytes and endothelial disruption in neurodegeneration. *Front. Cell. Neurosci.* 15:656832. doi: 10.3389/fncel.2021.656832
- Chang, H.-C., and Guarente, L. (2014). SIRT1 and other sirtuins in metabolism. *Trends Endocrinol. Metab.* 25, 138–145. doi: 10.1016/j.tem.2013.12.001
- Chen, J., Cui, X., Zacharek, A., Cui, Y., Roberts, C., and Chopp, M. (2011). White matter damage and the effect of matrix metalloproteinases in type 2 diabetic mice after stroke. *Stroke* 42, 445–452. doi: 10.1161/STROKEAHA.110.596486
- Cheng, T., Petraglia, A. L., Li, Z., Thiagarajan, M., Zhong, Z., Wu, Z., et al. (2006). Activated protein C inhibits tissue plasminogen activator-induced brain hemorrhage. *Nat. Med.* 12, 1278–1285. doi: 10.1038/nm1498
- Chiu, C., Miller, M. C., Monahan, R., Osgood, D. P., Stopa, E. G., and Silverberg, G. D. (2015). P-glycoprotein expression and amyloid accumulation in human aging and Alzheimer's disease: preliminary observations. *Neurobiol. Aging* 36, 2475–2482. doi: 10.1016/j.neurobiolaging.2015.05.020
- Choi, D.-H., Kim, J.-H., Seo, J.-H., Lee, J., Choi, W. S., and Kim, Y.-S. (2014). Matrix metalloproteinase-3 causes dopaminergic neuronal death through Nox1-regenerated oxidative stress. *PLoS ONE* 9:e115954. doi: 10.1371/journal.pone.0115954
- Chow, B. W., and Gu, C. (2015). The molecular constituents of the blood-brain barrier. *Trends Neurosci.* 38, 598–608. doi: 10.1016/j.tins.2015.08.003
- Chui, H. C., and Ramirez-Gomez, L. (2015). Clinical and imaging features of mixed Alzheimer and vascular pathologies. *Alzheimers Res. Ther.* 7:21. doi: 10.1186/s13195-015-0104-7
- Cohen, Z., Bonvento, G., Lacombe, P., and Hamel, E. (1996). Serotonin in the regulation of brain microcirculation. *Prog. Neurobiol.* 50, 335–362. doi: 10.1016/S0304-0082(96)00033-0
- Cohen, Z., Molinatti, G., and Hamel, E. (1997). Astroglial and vascular interactions of noradrenaline terminals in the rat cerebral cortex. *J. Cereb. Blood Flow Metab.* 17, 894–904. doi: 10.1097/00004647-199708000-00008
- Cortes-Canteli, M., Mattei, L., Richards, A. T., Norris, E. H., and Strickland, S. (2015). Fibrin deposited in the Alzheimer's disease brain promotes neuronal degeneration. *Neurobiol. Aging* 36, 608–617. doi: 10.1016/j.neurobiolaging.2014.10.030
- Cortes-Canteli, M., Paul, J., Norris, E. H., Bronstein, R., Ahn, H. J., Zamołodchikov, D., et al. (2010). Fibrinogen and β -amyloid association alters thrombosis and fibrinolysis: a possible contributing factor to Alzheimer's disease. *Neuron* 66, 695–709. doi: 10.1016/j.neuron.2010.05.014
- Crews, L., and Masliah, E. (2010). Molecular mechanisms of neurodegeneration in Alzheimer's disease. *Hum. Mol. Genet.* 19, R12–R20. doi: 10.1093/hmg/ddq160
- Cuevas, E., Rosas-Hernandez, H., Burks, S. M., Ramirez-Lee, M. A., Guzman, A., Imam, S. Z., et al. (2019). Amyloid Beta 25-35 induces blood-brain barrier disruption *in vitro*. *Metab. Brain Dis.* 34, 1365–1374. doi: 10.1007/s11011-019-00447-8
- D'Ambrosio, A., Pontecorvo, S., Colasanti, T., Zamboni, S., Francia, A., and Margutti, P. (2015). Peripheral blood biomarkers in multiple sclerosis. *Autoimmun. Rev.* 14, 1097–1110. doi: 10.1016/j.autrev.2015.07.014
- De Jong, G., Horvath, E., and Luiten, P. (1990). Effects of early onset of nimodipine treatment on microvascular integrity in the aging rat brain. *Stroke* 21(12 Suppl), IV113–IV116.
- Deane, R., Du Yan, S., Subramanyam, R. K., LaRue, B., Jovanovic, S., Hogg, E., et al. (2003). RAGE mediates amyloid- β peptide transport across the blood-brain barrier and accumulation in brain. *Nat. Med.* 9, 907–913. doi: 10.1038/nm890
- Deane, R., Sagare, A., Hamm, K., Parisi, M., Lane, S., Finn, M. B., et al. (2008). apoE isoform-specific disruption of amyloid β peptide clearance from mouse brain. *J. Clin. Invest.* 118, 4002–4013. doi: 10.1172/JCI36663
- Deane, R., Wu, Z., Sagare, A., Davis, J., Du Yan, S., Hamm, K., et al. (2004). LRP/amyloid β -peptide interaction mediates differential brain efflux of A β isoforms. *Neuron* 43, 333–344. doi: 10.1016/j.neuron.2004.07.017
- Deli, M. A., Veszelka, S., Csiszár, B., Tóth, A., Kittel, A., Csete, M., et al. (2010). Protection of the blood-brain barrier by pentosan against amyloid- β -induced toxicity. *J. Alzheimers Dis.* 22, 777–794. doi: 10.3233/JAD-2010-100759
- Di Cataldo, V., Gélöen, A., Langlois, J.-B., Chauveau, F., Thézé, B., Hubert, V., et al. (2016). Exercise does not protect against peripheral and central effects of a high cholesterol diet given *ad libitum* in old ApoE $^{-/-}$ mice. *Front. Physiol.* 7:453. doi: 10.3389/fphys.2016.00453
- Ding, F., Yao, J., Rettberg, J. R., Chen, S., and Brinton, R. D. (2013). Early decline in glucose transport and metabolism precedes shift to ketogenic system in female aging and Alzheimer's mouse brain: implication for bioenergetic intervention. *PLoS ONE* 8:e79977. doi: 10.1371/journal.pone.0079977
- Doeuvre, L., Plawinski, L., Goux, D., Vivien, D., and Anglés-Cano, E. (2010). Plasmin on adherent cells: from microvesiculation to apoptosis. *Biochem. J.* 432, 365–373. doi: 10.1042/BJ20100561
- Donahue, J. E., Flaherty, S. L., Johanson, C. E., Duncan, J. A., Silverberg, G. D., Miller, M. C., et al. (2006). RAGE, LRP-1, and amyloid-beta protein in Alzheimer's disease. *Acta Neuropathol.* 112, 405–415. doi: 10.1007/s00401-006-0115-3
- Donato, A. J., Eskurza, I., Silver, A. E., Levy, A. S., Pierce, G. L., Gates, P. E., et al. (2007). Direct evidence of endothelial oxidative stress with aging in humans: relation to impaired endothelium-dependent dilation and upregulation of nuclear factor- κ B. *Circ. Res.* 100, 1659–1666. doi: 10.1161/01.RES.0000269183.13937.e8
- Du, S.-Q., Wang, X.-R., Xiao, L.-Y., Tu, J.-F., Zhu, W., He, T., et al. (2017). Molecular mechanisms of vascular dementia: what can be learned from animal models of chronic cerebral hypoperfusion? *Mol. Neurobiol.* 54, 3670–3682. doi: 10.1007/s12035-016-9915-1
- Duncombe, J., Lennen, R. J., Jansen, M. A., Marshall, I., Wardlaw, J. M., and Horsburgh, K. (2017). Ageing causes prominent neurovascular dysfunction associated with loss of astrocytic contacts and gliosis. *Neuropathol. Appl. Neurobiol.* 43, 477–491. doi: 10.1111/nan.12375
- Edwards, G. A. III, Gamez, N., Escobedo Jr, G., Calderon, O., and Moreno-Gonzalez, I. (2019). Modifiable risk factors for Alzheimer's disease. *Front. Aging Neurosci.* 11:146. doi: 10.3389/fnagi.2019.00146
- Eikelenboom, P., Van Exel, E., Veerhuis, R., Rozemuller, A. J., Van Gool, W. A., and Hoozemans, J. J. (2012). Innate immunity and the etiology of late-onset Alzheimer's disease. *Neurodegener. Dis.* 10, 271–273. doi: 10.1159/000334287
- Elahy, M., Jackaman, C., Mamo, J. C., Lam, V., Dhaliwal, S. S., Giles, C., et al. (2015). Blood-brain barrier dysfunction developed during normal aging is associated with inflammation and loss of tight junctions but not with leukocyte recruitment. *Immunity Ageing* 12, 1–9. doi: 10.1186/s12979-015-0029-9
- Ellison, D., White, D., and Farrar, F. C. (2015). Aging population. *Nurs. Clin.* 50, 185–213. doi: 10.1016/j.cnur.2014.10.014
- Emrani, S., Lamar, M., Price, C. C., Wasserman, V., Matusz, E., Au, R., et al. (2020). Alzheimer's/vascular spectrum dementia: classification in addition to diagnosis. *J. Alzheimers Dis.* 73, 63–71. doi: 10.3233/JAD-190654
- Engelhardt, B., and Coisne, C. (2011). Fluids and barriers of the CNS establish immune privilege by confining immune surveillance to a two-walled castle moat surrounding the CNS castle. *Fluids Barriers CNS* 8, 1–9. doi: 10.1186/2045-8118-8-4
- Engelhardt, B., and Ransohoff, R. M. (2012). Capture, crawl, cross: the T cell code to breach the blood-brain barriers. *Trends Immunol.* 33, 579–589. doi: 10.1016/j.it.2012.07.004

- Erdo, F., Denes, L., and de Lange, E. (2017). Age-associated physiological and pathological changes at the blood-brain barrier: a review. *J. Cereb. Blood Flow Metab.* 37, 4–24. doi: 10.1177/0271678X16679420
- Erickson, M. A., and Banks, W. A. (2013). Blood-brain barrier dysfunction as a cause and consequence of Alzheimer's disease. *J. Cereb. Blood Flow Metab.* 33, 1500–1513. doi: 10.1038/jcbfm.2013.135
- Erickson, M. A., and Banks, W. A. (2018). Neuroimmune axes of the blood-brain barriers and blood-brain interfaces: bases for physiological regulation, disease states, and pharmacological interventions. *Pharmacol. Rev.* 70, 278–314. doi: 10.1124/pr.117.014647
- Erickson, M. A., Hansen, K., and Banks, W. A. (2012). Inflammation-induced dysfunction of the low-density lipoprotein receptor-related protein-1 at the blood-brain barrier: protection by the antioxidant N-acetylcysteine. *Brain Behav. Immun.* 26, 1085–1094. doi: 10.1016/j.bbi.2012.07.003
- Faraco, G., Park, L., Anrather, J., and Iadecola, C. (2017). Brain perivascular macrophages: characterization and functional roles in health and disease. *J. Mol. Med.* 95, 1143–1152. doi: 10.1007/s00109-017-1573-x
- Farrall, A. J., and Wardlaw, J. M. (2009). Blood-brain barrier: ageing and microvascular disease-systematic review and meta-analysis. *Neurobiol. Aging* 30, 337–352. doi: 10.1016/j.neurobiolaging.2007.07.015
- Farrer, L. A., Cupples, L. A., Haines, J. L., Hyman, B., Kukull, W. A., Mayeux, R., et al. (1997). Effects of age, sex, and ethnicity on the association between apolipoprotein E genotype and Alzheimer disease: a meta-analysis. *JAMA* 278, 1349–1356. doi: 10.1001/jama.1997.03550160069041
- Fivenson, E. M., Lautrup, S., Sun, N., Scheibye-Knudsen, M., Stevnsner, T., Nilsen, H., et al. (2017). Mitophagy in neurodegeneration and aging. *Neurochem. Int.* 109, 202–209. doi: 10.1016/j.neuint.2017.02.007
- Fonseca, M. I., Ager, R. R., Chu, S.-H., Yazan, O., Sanderson, S. D., LaFerla, F. M., et al. (2009). Treatment with a C5aR antagonist decreases pathology and enhances behavioral performance in murine models of Alzheimer's disease. *J. Immunol.* 183, 1375–1383. doi: 10.4049/jimmunol.0901005
- Gao, T., Lin, Z., and Jin, X. (2009). Hydrocortisone suppression of the expression of VEGF may relate to toll-like receptor (TLR) 2 and 4. *Curr. Eye Res.* 34, 777–784. doi: 10.1080/02713680903067919
- Gill, R., Tsung, A., and Billiar, T. (2010). Linking oxidative stress to inflammation: Toll-like receptors. *Free Radic. Biol. Med.* 48, 1121–1132. doi: 10.1016/j.freeradbiomed.2010.01.006
- González-Molina, L. A., Villar-Vesga, J., Henao-Restrepo, J., Villegas, A., Lopera, F., Cardona-Gómez, G. P., et al. (2021). Extracellular vesicles from 3xTg-AD mouse and Alzheimer's disease patient astrocytes impair neuroglial and vascular components. *Front. Aging Neurosci.* 13:593927. doi: 10.3389/fnagi.2021.593927
- Gonzalez-Velasquez, F. J., Kotarek, J. A., and Moss, M. A. (2008). Soluble aggregates of the amyloid- β protein selectively stimulate permeability in human brain microvascular endothelial monolayers. *J. Neurochem.* 107, 466–477. doi: 10.1111/j.1471-4159.2008.05618.x
- Goodall, E. F., Wang, C., Simpson, J. E., Baker, D. J., Drew, D. R., Heath, P. R., et al. (2018). Age-associated changes in the blood-brain barrier: comparative studies in human and mouse. *Neuropathol. Appl. Neurobiol.* 44, 328–340. doi: 10.1111/nan.12408
- Goodman, R. A., Lochner, K. A., Thambisetty, M., Wingo, T. S., Posner, S. F., and Ling, S. M. (2017). Prevalence of dementia subtypes in United States Medicare fee-for-service beneficiaries, 2011–2013. *Alzheimers Dement.* 13, 28–37. doi: 10.1016/j.jalz.2016.04.002
- Gorelick, P. B., Scuteri, A., Black, S. E., DeCarli, C., Greenberg, S. M., Iadecola, C., et al. (2011). Vascular contributions to cognitive impairment and dementia: a statement for healthcare professionals from the American Heart Association/American Stroke Association. *Stroke* 42, 2672–2713. doi: 10.1161/STR.0b013e3182299496
- Gredilla, R., Bohr, V. A., and Stevnsner, T. (2010). Mitochondrial DNA repair and association with aging-an update. *Exp. Gerontol.* 45, 478–488. doi: 10.1016/j.exger.2010.01.017
- Grinberg, L. T., and Heinsen, H. (2010). Toward a pathological definition of vascular dementia. *J. Neurol. Sci.* 299, 136–138. doi: 10.1016/j.jns.2010.08.055
- Grinberg, L. T., and Thal, D. R. (2010). Vascular pathology in the aged human brain. *Acta Neuropathol.* 119, 277–290. doi: 10.1007/s00401-010-0652-7
- Halliday, M. R., Rege, S. V., Ma, Q., Zhao, Z., Miller, C. A., Winkler, E. A., et al. (2016). Accelerated pericyte degeneration and blood-brain barrier breakdown in apolipoprotein E4 carriers with Alzheimer's disease. *J. Cereb. Blood Flow Metab.* 36, 216–227. doi: 10.1038/jcbfm.2015.44
- Hammer, C., Stepniak, B., Schneider, A., Papiol, S., Tantra, M., Begemann, M., et al. (2014). Neuropsychiatric disease relevance of circulating anti-NMDA receptor autoantibodies depends on blood-brain barrier integrity. *Mol. Psychiatry* 19, 1143–1149. doi: 10.1038/mp.2013.110
- Hansen, D. V., Hanson, J. E., and Sheng, M. (2018). Microglia in Alzheimer's disease. *J. Cell Biol.* 217, 459–472. doi: 10.1083/jcb.201709069
- Harry, G. J. (2013). Microglia during development and aging. *Pharmacol. Therapeut.* 139, 313–326. doi: 10.1016/j.pharmthera.2013.04.013
- Haruwaka, K., Ikegami, A., Tachibana, Y., Ohno, N., Konishi, H., Hashimoto, A., et al. (2019). Dual microglia effects on blood brain barrier permeability induced by systemic inflammation. *Nat. Commun.* 10, 1–17. doi: 10.1038/s41467-019-13812-z
- Hase, Y., Ding, R., Harrison, G., Hawthorne, E., King, A., Gettings, S., et al. (2019). White matter capillaries in vascular and neurodegenerative dementias. *Acta Neuropathol. Commun.* 7, 1–12. doi: 10.1186/s40478-019-0666-x
- Hawkes, C. A., Gatherer, M., Sharp, M. M., Dorr, A., Yuen, H. M., Kalaria, R., et al. (2013). Regional differences in the morphological and functional effects of aging on cerebral basement membranes and perivascular drainage of amyloid- β from the mouse brain. *Aging Cell* 12, 224–236. doi: 10.1111/ace.12045
- Hawkins, B. T., and Davis, T. P. (2005). The blood-brain barrier/neurovascular unit in health and disease. *Pharmacol. Rev.* 57, 173–185. doi: 10.1124/pr.57.2.4
- He, H., Lam, M., McCormick, T. S., and Distelhorst, C. W. (1997). Maintenance of calcium homeostasis in the endoplasmic reticulum by Bcl-2. *J. Cell Biol.* 138, 1219–1228. doi: 10.1083/jcb.138.6.1219
- Heinsen, H., and Heinsen, Y. (1983). Cerebellar capillaries. *Anat. Embryol.* 168, 101–116. doi: 10.1007/BF00305402
- Heithoff, B. P., George, K. K., Phares, A. N., Zuidhoek, I. A., Munoz-Ballester, C., and Robel, S. (2021). Astrocytes are necessary for blood-brain barrier maintenance in the adult mouse brain. *Glia* 69, 436–472. doi: 10.1002/glia.23908
- Hemmonot, A.-L., Hua, J., Ulmann, L., and Hirbec, H. (2019). Microglia in Alzheimer disease: well-known targets and new opportunities. *Front. Aging Neurosci.* 11:233. doi: 10.3389/fnagi.2019.00233
- Heneka, M. T., Carson, M. J., El Khoury, J., Landreth, G. E., Brosseron, F., Feinstein, D. L., et al. (2015). Neuroinflammation in Alzheimer's disease. *Lancet Neurol.* 14, 388–405. doi: 10.1016/S1474-4422(15)70016-5
- Hicks, P., Rolsten, C., Brizzee, D., and Samorajski, T. (1983). Age-related changes in rat brain capillaries. *Neurobiol. Aging* 4, 69–75. doi: 10.1016/0197-4580(83)90057-X
- Hoarau, J.-J., Krejbich-Trotot, P., Jaffar-Bandjee, M.-C., Das, T., Thon-Hon, G.-V., Kumar, S., et al. (2011). Activation and control of CNS innate immune responses in health and diseases: a balancing act finely tuned by neuroimmune regulators (NIReg). *CNS Neurol. Disord. Drug Targets* 10, 25–43. doi: 10.2174/187152711794488601
- Hoffman, J. D., Parikh, I., Green, S. J., Chlipala, G., Mohnsey, R. P., Keaton, M., et al. (2017). Age drives distortion of brain metabolic, vascular and cognitive functions, and the gut microbiome. *Front. Aging Neurosci.* 9:298. doi: 10.3389/fnagi.2017.00298
- Hoshi, A., Yamamoto, T., Shimizu, K., Ugawa, Y., Nishizawa, M., Takahashi, H., et al. (2012). Characteristics of aquaporin expression surrounding senile plaques and cerebral amyloid angiopathy in Alzheimer disease. *J. Neuropathol. Exp. Neurol.* 71, 750–759. doi: 10.1097/NEN.0b013e3182632566
- Howe, M. D., McCullough, L. D., and Urayama, A. (2020). The role of basement membranes in cerebral amyloid angiopathy. *Front. Physiol.* 11:601320. doi: 10.3389/fphys.2020.601320
- Huang, X., Hussain, B., and Chang, J. (2021). Peripheral inflammation and blood-brain barrier disruption: effects and mechanisms. *CNS Neurosci. Therapeut.* 27, 36–47. doi: 10.1111/cns.13569
- Huber, J. D., Campos, C. R., Mark, K. S., and Davis, T. P. (2006). Alterations in blood-brain barrier ICAM-1 expression and brain microglial activation after λ -carrageenan-induced inflammatory pain. *Am. J. Physiol. Heart Circ. Physiol.* 290, H732–H740. doi: 10.1152/ajpheart.00747.2005
- Hughes, S., Gardiner, T., Hu, P., Baxter, L., Rosinova, E., and Chan-Ling, T. (2006). Altered pericyte-endothelial relations in the rat retina during aging: implications for vessel stability. *Neurobiol. Aging* 27, 1838–1847. doi: 10.1016/j.neurobiolaging.2005.10.021

- Hultman, K., Strickland, S., and Norris, E. H. (2013). The APOE $\epsilon 4/\epsilon 4$ genotype potentiates vascular fibrin (ogen) deposition in amyloid-laden vessels in the brains of Alzheimer's disease patients. *J. Cereb. Blood Flow Metab.* 33, 1251–1258. doi: 10.1038/jcbfm.2013.76
- Hyman, B. T., Phelps, C. H., Beach, T. G., Bigio, E. H., Cairns, N. J., Carrillo, M. C., et al. (2012). National Institute on Aging-Alzheimer's Association guidelines for the neuropathologic assessment of Alzheimer's disease. *Alzheimers Dement.* 8, 1–13. doi: 10.1016/j.jalz.2011.10.007
- Iadecola, C. (2013). The pathobiology of vascular dementia. *Neuron* 80, 844–866. doi: 10.1016/j.neuron.2013.10.008
- Iadecola, C. (2017). The neurovascular unit coming of age: a journey through neurovascular coupling in health and disease. *Neuron* 96, 17–42. doi: 10.1016/j.neuron.2017.07.030
- Iadecola, C., and Davisson, R. L. (2008). Hypertension and cerebrovascular dysfunction. *Cell Metab.* 7, 476–484. doi: 10.1016/j.cmet.2008.03.010
- Ihara, M., Polvikoski, T. M., Hall, R., Slade, J. Y., Perry, R. H., Oakley, A. E., et al. (2010). Quantification of myelin loss in frontal lobe white matter in vascular dementia, Alzheimer's disease, and dementia with Lewy bodies. *Acta Neuropathol.* 119, 579–589. doi: 10.1007/s00401-009-0635-8
- Iliff, J. J., Wang, M., Liao, Y., Plogg, B. A., Peng, W., Gundersen, G. A., et al. (2012). A paravascular pathway facilitates CSF flow through the brain parenchyma and the clearance of interstitial solutes, including amyloid β . *Sci. Transl. Med.* 4:147ra111. doi: 10.1126/scitranslmed.3003748
- Imai, S.-I., and Guarente, L. (2014). NAD⁺ and sirtuins in aging and disease. *Trends Cell Biol.* 24, 464–471. doi: 10.1016/j.tcb.2014.04.002
- Jack, C. (2010). Vascular risk factor detection and control may prevent Alzheimer's disease. *Ageing Res. Rev.* 9, 218–225. doi: 10.1016/j.arr.2010.04.002
- Jacob, A., and Alexander, J. J. (2014). Complement and blood-brain barrier integrity. *Mol. Immunol.* 61, 149–152. doi: 10.1016/j.molimm.2014.06.039
- Jaeger, L., Dohgu, S., Sultana, R., Lynch, J., Owen, J., Erickson, M., et al. (2011). Lipopolysaccharide alters the blood-brain barrier transport of amyloid β protein: a mechanism for inflammation in the progression of Alzheimer's disease. *Brain Behav. Immun.* 23, 507–517. doi: 10.1016/j.bbi.2010.11.019
- Jiang, T., Yin, F., Yao, J., Brinton, R. D., and Cadenas, E. (2013). Lipoic acid restores age-associated impairment of brain energy metabolism through the modulation of A kt/JNK signaling and PGC 1 α transcriptional pathway. *Ageing Cell* 12, 1021–1031. doi: 10.1111/acel.12127
- Kadry, H., Noorani, B., and Cucullo, L. (2020). A blood-brain barrier overview on structure, function, impairment, and biomarkers of integrity. *Fluids Barriers CNS* 17, 1–24. doi: 10.1186/s12987-020-00230-3
- Kalaria, R. (2002). Similarities between Alzheimer's disease and vascular dementia. *J. Neurol. Sci.* 203, 29–34. doi: 10.1016/S0022-510X(02)00256-3
- Kang, S., Lee, Y.-H., and Lee, J. E. (2017). Metabolism-centric overview of the pathogenesis of Alzheimer's disease. *Yonsei Med. J.* 58, 479–488. doi: 10.3349/ymj.2017.58.3.479
- Kettenmann, H., Hanisch, U.-K., Noda, M., and Verkhratsky, A. (2011). Physiology of microglia. *Physiol. Rev.* 91, 461–553. doi: 10.1152/physrev.00011.2010
- Khan, M. B., Hoda, M. N., Vaibhav, K., Giri, S., Wang, P., Waller, J. L., et al. (2015). Remote ischemic postconditioning: harnessing endogenous protection in a murine model of vascular cognitive impairment. *Transl. Stroke Res.* 6, 69–77. doi: 10.1007/s12975-014-0374-6
- Kimbrough, I. F., Robel, S., Roberson, E. D., and Sontheimer, H. (2015). Vascular amyloidosis impairs the gliovascular unit in a mouse model of Alzheimer's disease. *Brain* 138, 3716–3733. doi: 10.1093/brain/awv327
- Kinnecom, C., Lev, M., Wendell, L., Smith, E., Rosand, J., Frosch, M., et al. (2007). Course of cerebral amyloid angiopathy-related inflammation. *Neurology* 68, 1411–1416. doi: 10.1212/01.wnl.0000260066.98681.2e
- Kirshner, H. S. (2009). Vascular dementia: a review of recent evidence for prevention and treatment. *Curr. Neurol. Neurosci. Rep.* 9, 437–442. doi: 10.1007/s11910-009-0065-y
- Kofler, J., and Wiley, C. A. (2011). Microglia: key innate immune cells of the brain. *Toxicol. Pathol.* 39, 103–114. doi: 10.1177/0192623310387619
- Kovac, A., Erickson, M. A., and Banks, W. A. (2011). Brain microvascular pericytes are immunoactive in culture: cytokine, chemokine, nitric oxide, and LRP-1 expression in response to lipopolysaccharide. *J. Neuroinflammation* 8, 1–9. doi: 10.1186/1742-2094-8-139
- Kovac, A., Zilkova, M., Deli, M. A., Zilka, N., and Novak, M. (2009). Human truncated tau is using a different mechanism from amyloid- β to damage the blood-brain barrier. *J. Alzheimers Dis.* 18, 897–906. doi: 10.3233/JAD-2009-1197
- Krabbe, G., Halle, A., Matyash, V., Rinnenthal, J. L., Eom, G. D., Bernhardt, U., et al. (2013). Functional impairment of microglia coincides with Beta-amyloid deposition in mice with Alzheimer-like pathology. *PLoS ONE* 8:e60921. doi: 10.1371/journal.pone.0060921
- Kritsilis, M., V., Rizou, S., Koutsoudaki, P. N., Evangelou, K., Gorgoulis, V. G., et al. (2018). Ageing, cellular senescence and neurodegenerative disease. *Int. J. Mol. Sci.* 19:2937. doi: 10.3390/ijms19102937
- Kyrtata, N., Emsley, H. C., Sparasci, O., Parkes, L. M., and Dickie, B. R. (2021). A Systematic review of glucose transport alterations in Alzheimer's disease. *Front. Neurosci.* 15:626636. doi: 10.3389/fnins.2021.626636
- Lan, Y.-L., Zhao, J., Ma, T., and Li, S. (2016a). The potential roles of aquaporin 4 in Alzheimer's disease. *Mol. Neurobiol.* 53, 5300–5309. doi: 10.1007/s12035-015-9446-1
- Lan, Y.-L., Zou, S., Chen, J.-J., Zhao, J., and Li, S. (2016b). The neuroprotective effect of the association of aquaporin-4/glutamate transporter-1 against Alzheimer's disease. *Neural Plast.* 2016:4626593. doi: 10.1155/2016/4626593
- Lapenna, A., De Palma, M., and Lewis, C. E. (2018). Perivascular macrophages in health and disease. *Nat. Rev. Immunol.* 18, 689–702. doi: 10.1038/s41577-018-0056-9
- Lassman, M. E., McLaughlin, T. M., Somers, E. P., Stefanni, A. C., Chen, Z., Murphy, B. A., et al. (2012). A rapid method for cross-species quantitation of apolipoproteins A1, B48 and B100 in plasma by ultra-performance liquid chromatography/tandem mass spectrometry. *Rapid Commun. Mass Spectrom.* 26, 101–108. doi: 10.1002/rcm.5296
- Lee, P., Kim, J., Williams, R., Sandhir, R., Gregory, E., Brooks, W. M., et al. (2012). Effects of aging on blood brain barrier and matrix metalloproteases following controlled cortical impact in mice. *Exp. Neurol.* 234, 50–61. doi: 10.1016/j.expneurol.2011.12.016
- Lendahl, U., Nilsson, P., and Betsholtz, C. (2019). Emerging links between cerebrovascular and neurodegenerative diseases—a special role for pericytes. *EMBO Rep.* 20:e48070. doi: 10.15252/embr.201948070
- Leng, F., and Edison, P. (2020). Neuroinflammation and microglial activation in Alzheimer disease: where do we go from here? *Nat. Rev. Neurol.* 17, 157–172. doi: 10.1038/s41582-020-00435-y
- Levit, A., Hachinski, V., and Whitehead, S. N. (2020). Neurovascular unit dysregulation, white matter disease, and executive dysfunction: the shared triad of vascular cognitive impairment and Alzheimer disease. *GeroScience* 42, 445–465. doi: 10.1007/s11357-020-00164-6
- Li, W., and Lai, X.-S. (2007). Changes of interleukin-1 β and TNF- α contents in the hippocampus and the interventional effect of electroacupuncture in vascular dementia rats. *Zhen Ci Yan Jiu* 32, 34–37.
- Li, W. Z., Wu, W. Y., Huang, H., Wu, Y. Y., and Yin, Y. Y. (2013). Protective effect of bilobalide on learning and memory impairment in rats with vascular dementia. *Mol. Med. Rep.* 8, 935–941. doi: 10.3892/mmr.2013.1573
- Lin, Y.-F., Smith, A. V., Aspelund, T., Betensky, R. A., Smoller, J. W., Gudnason, V., et al. (2019). Genetic overlap between vascular pathologies and Alzheimer's dementia and potential causal mechanisms. *Alzheimers Dement.* 15, 65–75. doi: 10.1016/j.jalz.2018.08.002
- Liu, C.-C., Kanekiyo, T., Xu, H., and Bu, G. (2013). Apolipoprotein E and Alzheimer disease: risk, mechanisms and therapy. *Nat. Rev. Neurol.* 9, 106–118. doi: 10.1038/nrneurol.2012.263
- Liu, H., and Zhang, J. (2012). Cerebral hypoperfusion and cognitive impairment: the pathogenic role of vascular oxidative stress. *Int. J. Neurosci.* 122, 494–499. doi: 10.3109/00207454.2012.686543
- Lucke-Wold, B. P., Logsdon, A. F., Turner, R. C., Rosen, C. L., and Huber, J. D. (2014). Aging, the metabolic syndrome, and ischemic stroke: redefining the approach for studying the blood-brain barrier in a complex neurological disease. *Adv. Pharmacol.* 71, 411–449. doi: 10.1016/bs.apha.2014.07.001
- Månberg, A., Skene, N., Sanders, F., Trusohamn, M., Remnestrål, J., Szczepińska, A., et al. (2021). Altered perivascular fibroblast activity precedes ALS disease onset. *Nat. Med.* 27, 640–646. doi: 10.1038/s41591-021-01295-9

- Ma, X., Sun, Z., Liu, Y., Jia, Y., Zhang, B., and Zhang, J. (2013). Resveratrol improves cognition and reduces oxidative stress in rats with vascular dementia. *Neural Regen. Res.* 8, 2050–2059. doi: 10.3969/j.issn.1673-5374.2013.22.004
- Matthes, F., Matuskova, H., Arkelius, K., Ansar, S., Lundgaard, I., and Meissner, A. (2021). An improved method for physical separation of cerebral vasculature and parenchyma enables detection of blood-brain-barrier dysfunction. *NeuroSci* 2, 59–74. doi: 10.3390/neurosci2010004
- Mattson, M. P., and Magnus, T. (2006). Ageing and neuronal vulnerability. *Nat. Rev. Neurosci.* 7, 278–294. doi: 10.1038/nrn1886
- Mazzieri, R., Masiero, L., Zanetta, L., Monea, S., Onisto, M., Garbisa, S., et al. (1997). Control of type IV collagenase activity by components of the urokinase-plasmin system: a regulatory mechanism with cell-bound reactants. *EMBO J.* 16, 2319–2332. doi: 10.1093/emboj/16.9.2319
- Merlini, M., Rafalski, V. A., Coronado, P. E. R., Gill, T. M., Ellisman, M., Muthukumar, G., et al. (2019). Fibrinogen induces microglia-mediated spine elimination and cognitive impairment in an Alzheimer's disease model. *Neuron* 101, 1099.e6–1108.e6. doi: 10.1016/j.neuron.2019.01.014
- Middelkamp, J., and Hol, E. (2011). GFAP in health and disease. *Prog. Neurobiol.* 93, 421–443. doi: 10.1016/j.pneurobio.2011.01.005
- Miller, M. C., Tavares, R., Johanson, C. E., Hovanesian, V., Donahue, J. E., Gonzalez, L., et al. (2008). Hippocampal RAGE immunoreactivity in early and advanced Alzheimer's disease. *Brain Res.* 1230, 273–280. doi: 10.1016/j.brainres.2008.06.124
- Mills, S., Cain, J., Purandare, N., and Jackson, A. (2007). Biomarkers of cerebrovascular disease in dementia. *Brit. J. Radiol.* 80, S128–S145. doi: 10.1259/bjr/79217686
- Miners, J., Kehoe, P., Love, S., Zetterberg, H., and Blennow, K. (2019). CSF evidence of pericyte damage in Alzheimer's disease is associated with markers of blood-brain barrier dysfunction and disease pathology. *Alzheimers Res. Ther.* 11, 1–6. doi: 10.1186/s13195-019-0534-8
- Monea, S., Lehti, K., Keski-Oja, J., and Mignatti, P. (2002). Plasmin activates pro-matrix metalloproteinase-2 with a membrane-type 1 matrix metalloproteinase-dependent mechanism. *J. Cell. Physiol.* 192, 160–170. doi: 10.1002/jcp.10126
- Montagne, A., Barnes, S. R., Sweeney, M. D., Halliday, M. R., Sagare, A. P., Zhao, Z., et al. (2015). Blood-brain barrier breakdown in the aging human hippocampus. *Neuron* 85, 296–302. doi: 10.1016/j.neuron.2014.12.032
- Montagne, A., Nation, D. A., Sagare, A. P., Barisano, G., Sweeney, M. D., Chakhoyan, A., et al. (2020). APOE4 leads to blood-brain barrier dysfunction predicting cognitive decline. *Nature* 581, 71–76. doi: 10.1038/s41586-020-2247-3
- Montagne, A., Nikolakopoulou, A. M., Zhao, Z., Sagare, A. P., Si, G., Lazic, D., et al. (2018). Pericyte degeneration causes white matter dysfunction in the mouse central nervous system. *Nat. Med.* 24, 326–337. doi: 10.1038/nm.4482
- Mooradian, A., Chung, H., and Shah, G. (1997). GLUT-1 expression in the cerebra of patients with Alzheimer's disease. *Neurobiol. Aging* 18, 469–474. doi: 10.1016/S0197-4580(97)00111-5
- Morris, A. W., Carare, R. O., Schreiber, S., and Hawkes, C. A. (2014). The cerebrovascular basement membrane: role in the clearance of β -amyloid and cerebral amyloid angiopathy. *Front. Aging Neurosci.* 6:251. doi: 10.3389/fnagi.2014.00251
- Nation, D. A., Sweeney, M. D., Montagne, A., Sagare, A. P., D'Orazio, L. M., Pachicano, M., et al. (2019). Blood-brain barrier breakdown is an early biomarker of human cognitive dysfunction. *Nat. Med.* 25, 270–276. doi: 10.1038/s41591-018-0297-y
- Nelson, A. R., Sweeney, M. D., Sagare, A. P., and Zlokovic, B. V. (2016). Neurovascular dysfunction and neurodegeneration in dementia and Alzheimer's disease. *Biochim. Biophys. Acta* 1862, 887–900. doi: 10.1016/j.bbdis.2015.12.016
- Nicholls, D. G., and Budd, S. L. (2000). Mitochondria and neuronal survival. *Physiol. Rev.* 80, 315–360. doi: 10.1152/physrev.2000.80.1.315
- Niego, B. E., Freeman, R., Puschmann, T. B., Turnley, A. M., and Medcalf, R. L. (2012). t-PA-specific modulation of a human blood-brain barrier model involves plasmin-mediated activation of the Rho kinase pathway in astrocytes. *Blood* 119, 4752–4761. doi: 10.1182/blood-2011-07-369512
- Nikolakopoulou, A. M., Montagne, A., Kisler, K., Dai, Z., Wang, Y., Huuskonen, M. T., et al. (2019). Pericyte loss leads to circulatory failure and pleiotrophin depletion causing neuron loss. *Nat. Neurosci.* 22, 1089–1098. doi: 10.1038/s41593-019-0434-z
- Nikolakopoulou, A. M., Wang, Y., Ma, Q., Sagare, A. P., Montagne, A., Huuskonen, M. T., et al. (2021). Endothelial LRP1 protects against neurodegeneration by blocking cyclophilin A. *J. Exp. Med.* 218:e20202207. doi: 10.1084/jem.20202207
- Nishitsuji, K., Hosono, T., Nakamura, T., Bu, G., and Michikawa, M. (2011). Apolipoprotein E regulates the integrity of tight junctions in an isoform-dependent manner in an *in vitro* blood-brain barrier model. *J. Biol. Chem.* 286, 17536–17542. doi: 10.1074/jbc.M111.225532
- Niwa, K., Younkin, L., Ebeling, C., Turner, S. K., Westaway, D., Younkin, S., et al. (2000). A β 1-40-related reduction in functional hyperemia in mouse neocortex during somatosensory activation. *Proc. Nat. Acad. Sci. U.S.A.* 97, 9735–9740. doi: 10.1073/pnas.97.17.9735
- Obermeier, B., Daneman, R., and Ransohoff, R. M. (2013). Development, maintenance and disruption of the blood-brain barrier. *Nat. Med.* 19, 1584–1596. doi: 10.1038/nm.3407
- O'Brien, T., and Thomas, J. A. (2015). Vascular dementia. *Lancet* 386, 1698–1706. doi: 10.1016/S0140-6736(15)00463-8
- O'Connell, G. C., Treadway, M. B., Petrone, A. B., Tennant, C. S., Lucke-Wold, N., Chantler, P. D., et al. (2017). Peripheral blood AKAP7 expression as an early marker for lymphocyte-mediated post-stroke blood brain barrier disruption. *Sci. Rep.* 7, 1–13. doi: 10.1038/s41598-017-01178-5
- Orsini, F., De Blasio, D., Zangari, R., Zanier, E. R., and De Simoni, M.-G. (2014). Versatility of the complement system in neuroinflammation, neurodegeneration and brain homeostasis. *Front. Cell. Neurosci.* 8:380. doi: 10.3389/fncel.2014.00380
- Owen, J. B., Sultana, R., Aluise, C. D., Erickson, M. A., Price, T. O., Bu, G., et al. (2010). Oxidative modification to LDL receptor-related protein 1 in hippocampus from subjects with Alzheimer disease: implications for A β accumulation in AD brain. *Free Radic. Biol. Med.* 49, 1798–1803. doi: 10.1016/j.freeradbiomed.2010.09.013
- Pan, W., P., Stone, K., Hsueh, H., K., Manda, V., et al. (2011). Cytokine signaling modulates blood-brain barrier function. *Curr. Pharm. Des.* 17, 3729–3740. doi: 10.2174/138161211798220918
- Park, H. R., Park, M., Choi, J., Park, K.-Y., Chung, H. Y., and Lee, J. (2010). A high-fat diet impairs neurogenesis: involvement of lipid peroxidation and brain-derived neurotrophic factor. *Neurosci. Lett.* 482, 235–239. doi: 10.1016/j.neulet.2010.07.046
- Park, L., Uekawa, K., Garcia-Bonilla, L., Koizumi, K., Murphy, M., Pistik, R., et al. (2017). Brain perivascular macrophages initiate the neurovascular dysfunction of Alzheimer A β peptides. *Circ. Res.* 121, 258–269. doi: 10.1161/CIRCRESAHA.117.311054
- Park, M. H., Lee, J. Y., Park, K. H., Jung, I. K., Kim, K.-T., Lee, Y.-S., et al. (2018). Vascular and neurogenic rejuvenation in aging mice by modulation of ASM. *Neuron* 100, 167.e9–182.e9. doi: 10.1016/j.neuron.2018.09.010
- Patching, S. G. (2017). Glucose transporters at the blood-brain barrier: function, regulation and gateways for drug delivery. *Mol. Neurobiol.* 54, 1046–1077. doi: 10.1007/s12035-015-9672-6
- Patterson, C. (2018). *World Alzheimer Report 2018*.
- Peinado, M. A., Quesada, A., Pedrosa, J. A., Torres, M. I., Martinez, M., Esteban, F. J., et al. (1998). Quantitative and ultrastructural changes in glia and pericytes in the parietal cortex of the aging rat. *Microsc. Res. Tech.* 43, 34–42. doi: 10.1002/(SICI)1097-0029(19981001)43:1<34::AID-JEMT6>3.0.CO;2-G
- Perry, G., Cash, A. D., and Smith, M. A. (2002). Alzheimer disease and oxidative stress. *J. Biomed. Biotechnol.* 2, 120–123. doi: 10.1155/S1110724302203010
- Peters, A., Josephson, K., and Vincent, S. L. (1991). Effects of aging on the neuroglial cells and pericytes within area 17 of the rhesus monkey cerebral cortex. *Anat. Rec.* 229, 384–398. doi: 10.1002/ar.1092290311
- Pilozzi, A., Carro, C., Whalen, M., and Huang, X. (2020). "Blood-brain barrier degradation and the implication of SPARC protein as a potential therapeutic target for Alzheimer's disease," in *Alzheimer's Disease: Drug Discovery*, ed X. Huang (Brisbane, QLD: Exon Publications), 135–149. doi: 10.36255/exonpublications.alzheimersdisease.2020.ch8
- Price, B. R., Norris, C. M., Sompol, P., and Wilcock, D. M. (2018). An emerging role of astrocytes in vascular contributions to cognitive impairment and dementia. *J. Neurochem.* 144, 644–650. doi: 10.1111/jnc.14273

- Quaegelbeur, A., Lange, C., and Carmeliet, P. (2011). The neurovascular link in health and disease: molecular mechanisms and therapeutic implications. *Neuron* 71, 406–424. doi: 10.1016/j.neuron.2011.07.013
- Raja, R., Rosenberg, G. A., and Caprihan, A. (2018). MRI measurements of blood-brain barrier function in dementia: a review of recent studies. *Neuropharmacology* 134, 259–271. doi: 10.1016/j.neuropharm.2017.10.034
- Rajan, A. M., Ma, R. C., Kocha, K. M., Zhang, D. J., and Huang, P. (2020). Dual function of perivascular fibroblasts in vascular stabilization in zebrafish. *PLoS Genet.* 16:e1008800. doi: 10.1371/journal.pgen.1008800
- Rajani, R. M., Quick, S., Ruigrok, S. R., Graham, D., Harris, S. E., Verhaaren, B. F., et al. (2018). Reversal of endothelial dysfunction reduces white matter vulnerability in cerebral small vessel disease in rats. *Sci. Transl. Med.* 10:eam9507. doi: 10.1126/scitranslmed.aam9507
- Ramanathan, A., Nelson, A. R., Sagare, A. P., and Zlokovic, B. V. (2015). Impaired vascular-mediated clearance of brain amyloid beta in Alzheimer's disease: the role, regulation and restoration of LRP1. *Front. Aging Neurosci.* 7:136. doi: 10.3389/fnagi.2015.00136
- Ramos-DeSimone, N., Hahn-Dantona, E., Siple, J., Nagase, H., French, D. L., and Quigley, J. P. (1999). Activation of matrix metalloproteinase-9 (MMP-9) via a converging plasmin/stromelysin-1 cascade enhances tumor cell invasion. *J. Biol. Chem.* 274, 13066–13076. doi: 10.1074/jbc.274.19.13066
- Ransohoff, R. M., and Engelhardt, B. (2012). The anatomical and cellular basis of immune surveillance in the central nervous system. *Nat. Rev. Immunol.* 12, 623–635. doi: 10.1038/nri3265
- Rascher, G., and Wolburg, H. (2002). "The blood-brain barrier in the aging brain." in *Neuroglia in the Aging Brain*, ed J. S. de Vellis (Totowa, NJ: Humana Press), 305–320. doi: 10.1385/1-59259-105-1:305
- Rasmussen, M. K., Mestre, H., and Nedergaard, M. (2018). The glymphatic pathway in neurological disorders. *Lancet Neurol.* 17, 1016–1024. doi: 10.1016/S1474-4422(18)30318-1
- Ray, L., Khemka, V. K., Behera, P., Bandyopadhyay, K., Pal, S., Pal, K., et al. (2013). Serum homocysteine, dehydroepiandrosterone sulphate and lipoprotein (a) in Alzheimer's disease and vascular dementia. *Aging Dis.* 4, 57–64.
- Reeson, P., Choi, K., and Brown, C. E. (2018). VEGF signaling regulates the fate of obstructed capillaries in mouse cortex. *Elife* 7:e33670. doi: 10.7554/eLife.33670.029
- Reuter, B., Rodemer, C., Grudzenski, S., Meairs, S., Bugert, P., Hennerici, M. G., et al. (2015). Effect of simvastatin on MMPs and TIMPs in human brain endothelial cells and experimental stroke. *Transl. Stroke Res.* 6, 156–159. doi: 10.1007/s12975-014-0381-7
- Reyahi, A., Nik, A. M., Ghiami, M., Gritli-Linde, A., Pontén, F., Johansson, B. R., et al. (2015). Foxf2 is required for brain pericyte differentiation and development and maintenance of the blood-brain barrier. *Dev. Cell* 34, 19–32. doi: 10.1016/j.devcel.2015.05.008
- Richardson, K., C. M., Stephan, B., G., Ince, P., Brayne, C., et al. (2012). The neuropathology of vascular disease in the medical research council cognitive function and ageing study (MRC CFAS). *Curr. Alzheimer Res.* 9, 687–696. doi: 10.2174/156720512801322654
- Rivard, A., Berthou-Soulie, L., Principe, N., Kearney, M., Curry, C., Branellec, D., et al. (2000). Age-dependent defect in vascular endothelial growth factor expression is associated with reduced hypoxia-inducible factor 1 activity. *J. Biol. Chem.* 275, 29643–29647. doi: 10.1074/jbc.M001029200
- Ronaldson, T., and Davis, P. (2012). Blood-brain barrier integrity and glial support: mechanisms that can be targeted for novel therapeutic approaches in stroke. *Curr. Pharm. Des.* 18, 3624–3644. doi: 10.2174/138161212802002625
- Rosenberg, G. (2014). Blood-brain barrier permeability in aging and Alzheimer's disease. *J. Prevent. Alzheimers Dis.* 1, 138–139. doi: 10.14283/jpad.2014.25
- Rosenberg, G. A. (2012). Neurological diseases in relation to the blood-brain barrier. *J. Cereb. Blood Flow Metab.* 32, 1139–1151. doi: 10.1038/jcbfm.2011.197
- Rosenberg, G. A. (2017). Extracellular matrix inflammation in vascular cognitive impairment and dementia. *Clin. Sci.* 131, 425–437. doi: 10.1042/CS20160604
- Rosenberg, G. A., and Yang, Y. (2007). Vasogenic edema due to tight junction disruption by matrix metalloproteinases in cerebral ischemia. *Neurosurg. Focus* 22, 1–9. doi: 10.3171/foc.2007.22.5.5
- Roudnicky, F., Zhang, J. D., Kim, B. K., Pandya, N. J., Lan, Y., Sach-Peltason, L., et al. (2020). Inducers of the endothelial cell barrier identified through chemogenomic screening in genome-edited hPSC-endothelial cells. *Proc. Nat. Acad. Sci. U.S.A.* 117, 19854–19865. doi: 10.1073/pnas.1911532117
- Rouhl, R. P., Damoiseaux, J. G., Lodder, J., Theunissen, R. O., Knottnerus, I. L., Staals, J., et al. (2012). Vascular inflammation in cerebral small vessel disease. *Neurobiol. Aging* 33, 1800–1806. doi: 10.1016/j.neurobiolaging.2011.04.008
- Ryu, J. K., Petersen, M. A., Murray, S. G., Baeten, K. M., Meyer-Franke, A., Chan, J. P., et al. (2015). Blood coagulation protein fibrinogen promotes autoimmunity and demyelination via chemokine release and antigen presentation. *Nat. Commun.* 6, 1–15. doi: 10.1038/ncomms9164
- Ryu, J. K., Rafalski, V. A., Meyer-Franke, A., Adams, R. A., Poda, S. B., Coronado, P. E. R., et al. (2018). Fibrin-targeting immunotherapy protects against neuroinflammation and neurodegeneration. *Nat. Immunol.* 19, 1212–1223. doi: 10.1038/s41590-018-0232-x
- Sabayan, B., Jansen, S., Oleksik, A. M., van Osch, M. J., van Buchem, M. A., van Vliet, P., et al. (2012). Cerebrovascular hemodynamics in Alzheimer's disease and vascular dementia: a meta-analysis of transcranial Doppler studies. *Ageing Res. Rev.* 11, 271–277. doi: 10.1016/j.arr.2011.12.009
- Sachdev, P., Kalaria, R., O'Brien, J., Skoog, I., Alladi, S., Black, S. E., et al. (2014). Diagnostic criteria for vascular cognitive disorders: a VASCOG statement. *Alzheimer Dis. Assoc. Disord.* 28, 206–218. doi: 10.1097/WAD.0000000000000034
- Sagare, A., Deane, R., Bell, R. D., Johnson, B., Hamm, K., Pendu, R., et al. (2007). Clearance of amyloid- β by circulating lipoprotein receptors. *Nat. Med.* 13, 1029–1031. doi: 10.1038/nm1635
- Sagare, A. P., Bell, R. D., Zhao, Z., Ma, Q., Winkler, E. A., Ramanathan, A., et al. (2013). Pericyte loss influences Alzheimer-like neurodegeneration in mice. *Nat. Commun.* 4, 1–14. doi: 10.1038/ncomms3932
- Sagare, A. P., Bell, R. D., and Zlokovic, B. V. (2012). Neurovascular dysfunction and faulty amyloid β -peptide clearance in Alzheimer disease. *Cold Spring Harb. Perspect. Med.* 2:a011452. doi: 10.1101/cshperspect.a011452
- Sagare, A. P., Sweeney, M. D., Makshannoff, J., and Zlokovic, B. V. (2015). Shedding of soluble platelet-derived growth factor receptor- β from human brain pericytes. *Neurosci. Lett.* 607, 97–101. doi: 10.1016/j.neulet.2015.09.025
- Saggu, R., Schumacher, T., Gerich, F., Rakers, C., Tai, K., Delekate, A., et al. (2016). Astroglial NF- κ B contributes to white matter damage and cognitive impairment in a mouse model of vascular dementia. *Acta Neuropathol. Commun.* 4, 1–10. doi: 10.1186/s40478-016-0350-3
- Salmina, A. B., Inzhutova, A. I., Malinovskaya, N. A., and Petrova, M. M. (2010). Endothelial dysfunction and repair in Alzheimer-type neurodegeneration: neuronal and glial control. *J. Alzheimers Dis.* 22, 17–36. doi: 10.3233/JAD-2010-091690
- Salminen, A., Ojala, J., Kaarniranta, K., Haapasalo, A., Hiltunen, M., and Soininen, H. (2011). Astrocytes in the aging brain express characteristics of senescence-associated secretory phenotype. *Eur. J. Neurosci.* 34, 3–11. doi: 10.1111/j.1460-9568.2011.07738.x
- Sanchez-Covarrubias, L., Slosky, L. M., Thompson, B. J., Davis, T. P., and Ronaldson, P. T. (2014). Transporters at CNS barrier sites: obstacles or opportunities for drug delivery? *Curr. Pharm. Des.* 20, 1422–1449. doi: 10.2174/13816128113199990463
- Schneider, J. A., Arvanitakis, Z., Leurgans, S. E., and Bennett, D. A. (2009). The neuropathology of probable Alzheimer disease and mild cognitive impairment. *Ann. Neurol.* 66, 200–208. doi: 10.1002/ana.21706
- Schultz, N., Brännström, K., Byman, E., Moussaud, S., Nielsen, H. M., Bank, N. B., et al. (2018). Amyloid-beta 1-40 is associated with alterations in NG2+ pericyte population *ex vivo* and *in vitro*. *Aging Cell* 17:e12728. doi: 10.1111/accel.12728
- Sengillo, J. D., Winkler, E. A., Walker, C. T., Sullivan, J. S., Johnson, M., and Zlokovic, B. V. (2013). Deficiency in mural vascular cells coincides with blood-brain barrier disruption in Alzheimer's disease. *Brain Pathol.* 23, 303–310. doi: 10.1111/bpa.12004
- Silbert, L. C., Dodge, H. H., Perkins, L. G., Sherbakov, L., Lahna, D., Erten-Lyons, D., et al. (2012). Trajectory of white matter hyperintensity burden preceding mild cognitive impairment. *Neurology* 79, 741–747. doi: 10.1212/WNL.0b013e3182661f2b
- Simpkins, A. N., Dias, C., Leigh, R., Benson, R. T., Hsia, A. W., Latour, L. L., et al. (2016). Identification of reversible disruption of the human

- blood-brain barrier following acute ischemia. *Stroke* 47, 2405–2408. doi: 10.1161/STROKEAHA.116.013805
- Simpson, J., Ince, P., Haynes, L., Theaker, R., Gelsthorpe, C., Baxter, L., et al. (2010). Population variation in oxidative stress and astrocyte DNA damage in relation to Alzheimer-type pathology in the ageing brain. *Neuropathol. Appl. Neurobiol.* 36, 25–40. doi: 10.1111/j.1365-2990.2009.01030.x
- Skillbäck, T., Delsing, L., Synnergren, J., Mattsson, N., Janelidze, S., Nägga, K., et al. (2017). CSF/serum albumin ratio in dementias: a cross-sectional study on 1861 patients. *Neurobiol. Aging* 59, 1–9. doi: 10.1016/j.neurobiolaging.2017.06.028
- Sloane, P. D., Zimmerman, S., Suchindran, C., Reed, P., Wang, L., Boustani, M., et al. (2002). The public health impact of Alzheimer's disease, 2000–2050: potential implication of treatment advances. *Annu. Rev. Public Health* 23, 213–231. doi: 10.1146/annurev.publhealth.23.100901.140525
- Soto, I., Graham, L. C., Richter, H. J., Simeone, S. N., Radell, J. E., Grabowska, W., et al. (2015). APOE stabilization by exercise prevents aging neurovascular dysfunction and complement induction. *PLoS Biol.* 13:e1002279. doi: 10.1371/journal.pbio.1002279
- Stamatovic, S. M., Martinez-Revollar, G., Hu, A., Choi, J., Keep, R. F., and Andjelkovic, A. V. (2019). Decline in Sirtuin-1 expression and activity plays a critical role in blood-brain barrier permeability in aging. *Neurobiol. Dis.* 126, 105–116. doi: 10.1016/j.nbd.2018.09.006
- Stewart, P., Magliocco, M., Hayakawa, K., Farrell, C., Del Maestro, R., Girvin, J., et al. (1987). A quantitative analysis of blood-brain barrier ultrastructure in the aging human. *Microvasc. Res.* 33, 270–282. doi: 10.1016/0026-2862(87)90022-7
- Storck, S. E., Meister, S., Nahrath, J., Meißner, J. N., Schubert, N., Di Spiezio, A., et al. (2016). Endothelial LRP1 transports amyloid- β 1–42 across the blood-brain barrier. *J. Clin. Invest.* 126, 123–136. doi: 10.1172/JCI81108
- Stranahan, A. M., Norman, E. D., Lee, K., Cutler, R. G., Telljohann, R. S., Egan, J. M., et al. (2008). Diet-induced insulin resistance impairs hippocampal synaptic plasticity and cognition in middle-aged rats. *Hippocampus* 18, 1085–1088. doi: 10.1002/hipo.20470
- Stratman, A. N., Schwindt, A. E., Malotte, K. M., and Davis, G. E. (2010). Endothelial-derived PDGF-BB and HB-EGF coordinately regulate pericyte recruitment during vasculogenic tube assembly and stabilization. *Blood* 116, 4720–4730. doi: 10.1182/blood-2010-05-286872
- Strunz, M., Jarrell, J. T., Cohen, D. S., Rosin, E. R., Vanderburg, C. R., and Huang, X. (2019). Modulation of SPARC/Hevin proteins in Alzheimer's disease brain injury. *J. Alzheimers Dis.* 68, 695–710. doi: 10.3233/JAD-181032
- Sturrock, R. (1980). A comparative quantitative and morphological study of ageing in the mouse neostriatum, indusium griseum and anterior commissure. *Neuropathol. Appl. Neurobiol.* 6, 51–68. doi: 10.1111/j.1365-2990.1980.tb00204.x
- Sumi, N., Nishioku, T., Takata, F., Matsumoto, J., Watanabe, T., Shuto, H., et al. (2010). Lipopolysaccharide-activated microglia induce dysfunction of the blood-brain barrier in rat microvascular endothelial cells co-cultured with microglia. *Cell. Mol. Neurobiol.* 30, 247–253. doi: 10.1007/s10571-009-9446-7
- Suzuki, Y., Nagai, N., Yamakawa, K., Kawakami, J., Lijnen, H. R., and Umemura, K. (2009). Tissue-type plasminogen activator (t-PA) induces stromelysin-1 (MMP-3) in endothelial cells through activation of lipoprotein receptor-related protein. *Blood* 114, 3352–3358. doi: 10.1182/blood-2009-02-203919
- Sweeney, M. D., Ayyadurai, S., and Zlokovic, B. V. (2016). Pericytes of the neurovascular unit: key functions and signaling pathways. *Nat. Neurosci.* 19, 771–783. doi: 10.1038/nn.4288
- Sweeney, M. D., Kisler, K., Montagne, A., Toga, A. W., and Zlokovic, B. V. (2018a). The role of brain vasculature in neurodegenerative disorders. *Nat. Neurosci.* 21, 1318–1331. doi: 10.1038/s41593-018-0234-x
- Sweeney, M. D., Montagne, A., Sagare, A. P., Nation, D. A., Schneider, L. S., Chui, H. C., et al. (2019a). Vascular dysfunction—the disregarded partner of Alzheimer's disease. *Alzheimers Dement.* 15, 158–167. doi: 10.1016/j.jalz.2018.07.222
- Sweeney, M. D., Sagare, A. P., Pachicano, M., Harrington, M. G., Joe, E., Chui, H. C., et al. (2020). A novel sensitive assay for detection of a biomarker of pericyte injury in cerebrospinal fluid. *Alzheimers Dement.* 16, 821–830. doi: 10.1002/alz.12061
- Sweeney, M. D., Sagare, A. P., and Zlokovic, B. V. (2018b). Blood-brain barrier breakdown in Alzheimer disease and other neurodegenerative disorders. *Nat. Rev. Neurol.* 14, 133–150. doi: 10.1038/nrnneurol.2017.188
- Sweeney, M. D., Zhao, Z., Montagne, A., Nelson, A. R., and Zlokovic, B. V. (2019b). Blood-brain barrier: from physiology to disease and back. *Physiol. Rev.* 99, 21–78. doi: 10.1152/physrev.00050.2017
- Tachibana, M., Holm, M.-L., Liu, C.-C., Shinohara, M., Aikawa, T., Oue, H., et al. (2019). APOE4-mediated amyloid- β pathology depends on its neuronal receptor LRP1. *J. Clin. Invest.* 129, 1272–1277. doi: 10.1172/JCI124853
- Tada, M., Diserens, A.-C., Desbaillets, I., and de Tribolet, N. (1994). Analysis of cytokine receptor messenger RNA expression in human glioblastoma cells and normal astrocytes by reverse-transcription polymerase chain reaction. *J. Neurosurg.* 80, 1063–1073. doi: 10.3171/jns.1994.80.6.1063
- Takata, F., Dohgu, S., Matsumoto, J., Takahashi, H., Machida, T., Wakigawa, T., et al. (2011). Brain pericytes among cells constituting the blood-brain barrier are highly sensitive to tumor necrosis factor- α , releasing matrix metalloproteinase-9 and migrating *in vitro*. *J. Neuroinflammation* 8, 1–12. doi: 10.1186/1742-2094-8-106
- Tan, Z., Jiang, J., Tian, F., Peng, J., Yang, Z., Li, S., et al. (2020). Serum visinin-like protein 1 is a better biomarker than neuron-specific enolase for seizure-induced neuronal injury: a prospective and observational study. *Front. Neurol.* 11:567587. doi: 10.3389/fneur.2020.567587
- Tarumi, T., and Zhang, R. (2018). Cerebral blood flow in normal aging adults: cardiovascular determinants, clinical implications, and aerobic fitness. *J. Neurochem.* 144, 595–608. doi: 10.1111/jnc.14234
- Taylor, H., Miners, J. S., Güzel, Ö., MacLachlan, R., and Love, S. (2021). Mediators of cerebral hypoperfusion and blood-brain barrier leakiness in Alzheimer's disease, vascular dementia and mixed dementia. *Brain Pathol.* 31:e12935. doi: 10.1111/bpa.12935
- Thal, D. R., Grinberg, L. T., and Attems, J. (2012). Vascular dementia: different forms of vessel disorders contribute to the development of dementia in the elderly brain. *Exp. Gerontol.* 47, 816–824. doi: 10.1016/j.exger.2012.05.023
- Tibblin, G., Link, H., and Öhman, S. (1977). Principles of albumin and IgG analyses in neurological disorders. I. Establishment of reference values. *Scand. J. Clin. Lab. Invest.* 37, 385–390. doi: 10.3109/00365517709091496
- Tomimoto, H., Aikiguchi, I., Suenaga, T., Nishimura, M., Wakita, H., Nakamura, S., et al. (1996). Alterations of the blood-brain barrier and glial cells in white-matter lesions in cerebrovascular and Alzheimer's disease patients. *Stroke* 27, 2069–2074. doi: 10.1161/01.STR.27.11.2069
- Tong, X., and Hamel, E. (1999). Regional cholinergic denervation of cortical microvessels and nitric oxide synthase-containing neurons in Alzheimer's disease. *Neuroscience* 92, 163–175. doi: 10.1016/S0306-4522(98)00750-7
- Uemura, M. T., Maki, T., Ihara, M., Lee, V. M., and Trojanowski, J. Q. (2020). Brain microvascular pericytes in vascular cognitive impairment and dementia. *Front. Aging Neurosci.* 12:80. doi: 10.3389/fnagi.2020.00080
- Ueno, M., Aikiguchi, I., Hosokawa, M., Shinnou, M., Sakamoto, H., Takemura, M., et al. (1998). Ultrastructural and permeability features of microvessels in the olfactory bulbs of SAM mice. *Acta Neuropathol.* 96, 261–270. doi: 10.1007/s004010050893
- Ueno, M., Tomimoto, H., Aikiguchi, I., Wakita, H., and Sakamoto, H. (2002). Blood-brain barrier disruption in white matter lesions in a rat model of chronic cerebral hypoperfusion. *J. Cereb. Blood Flow Metab.* 22, 97–104. doi: 10.1097/00004647-200201000-00012
- van Assema, D. M., Lubberink, M., Boellaard, R., Schuit, R. C., Windhorst, A. D., Scheltens, P., et al. (2012). P-glycoprotein function at the blood-brain barrier: effects of age and gender. *Mol. Imaging Biol.* 14, 771–776. doi: 10.1007/s11307-012-0556-0
- Van De Haar, H. J., Burgmans, S., Jansen, J. F., Van Osch, M. J., Van Buchem, M. A., Muller, M., et al. (2016). Blood-brain barrier leakage in patients with early Alzheimer disease. *Radiology* 281, 527–535. doi: 10.1148/radiol.2016152244
- Vasic, V., Barth, K., and Schmidt, M. H. (2019). Neurodegeneration and neuro-regeneration—Alzheimer's disease and stem cell therapy. *Int. J. Mol. Sci.* 20, 4272. doi: 10.3390/ijms20174272
- Vaucher, E., Tong, X. K., Cholet, N., Lantin, S., and Hamel, E. (2000). GABA neurons provide a rich input to microvessels but not nitric oxide neurons in the rat cerebral cortex: a means for direct regulation of local cerebral blood flow. *J. Compar. Neurol.* 421, 161–171. doi: 10.1002/(SICI)1096-9861(20000529)421:2<161::AID-CNE3>3.0.CO;2-F

- Veerhuis, R., Nielsen, H. M., and Tenner, A. J. (2011). Complement in the brain. *Mol. Immunol.* 48, 1592–1603. doi: 10.1016/j.molimm.2011.04.003
- Verhaaren, B. F., Vernooij, M. W., de Boer, R., Hofman, A., Niessen, W. J., van der Lugt, A., et al. (2013). High blood pressure and cerebral white matter lesion progression in the general population. *Hypertension* 61, 1354–1359. doi: 10.1161/HYPERTENSIONAHA.111.00430
- Verheggen, I. C., de Jong, J. J., van Bortel, M. P., Gronenschild, E. H., Palm, W. M., Postma, A. A., et al. (2020). Increase in blood-brain barrier leakage in healthy, older adults. *GeroScience* 42, 1183–1193. doi: 10.1007/s11357-020-00211-2
- Verma, S., Nakaoka, R., Dohgu, S., and Banks, W. A. (2006). Release of cytokines by brain endothelial cells: a polarized response to lipopolysaccharide. *Brain Behav. Immun.* 20, 449–455. doi: 10.1016/j.bbi.2005.10.005
- Villar-Vesga, J., Henao-Restrepo, J., Voshart, D. C., Aguillon, D., Villegas, A., Castaño, D., et al. (2020). Differential profile of systemic extracellular vesicles from sporadic and familial Alzheimer's disease leads to neuroglial and endothelial cell degeneration. *Front. Aging Neurosci.* 12:587989. doi: 10.3389/fnagi.2020.587989
- Villeda, S. A., Luo, J., Mosher, K. I., Zou, B., Britschgi, M., Bieri, G., et al. (2011). The ageing systemic milieu negatively regulates neurogenesis and cognitive function. *Nature* 477, 90–94. doi: 10.1038/nature10357
- Wang, F., Cao, Y., Ma, L., Pei, H., Rausch, W. D., and Li, H. (2018). Dysfunction of cerebrovascular endothelial cells: prelude to vascular dementia. *Front. Aging Neurosci.* 10:376. doi: 10.3389/fnagi.2018.00376
- Wang, W., Lv, S., Zhou, Y., Fu, J., Li, C., and Liu, P. (2011). Tumor necrosis factor- α affects blood-brain barrier permeability in acetaminophen-induced acute liver failure. *Eur. J. Gastroenterol. Hepatol.* 23, 552–558. doi: 10.1097/MEG.0b013e3283470212
- Wang, X., Lee, S.-R., Arai, K., Lee, S.-R., Tsuji, K., Rebeck, G. W., et al. (2003). Lipoprotein receptor-mediated induction of matrix metalloproteinase by tissue plasminogen activator. *Nat. Med.* 9, 1313–1317. doi: 10.1038/nm926
- Wang, Y., Jin, S., Sonobe, Y., Cheng, Y., Horiuchi, H., Parajuli, B., et al. (2014). Interleukin-1 β induces blood-brain barrier disruption by downregulating sonic hedgehog in astrocytes. *PLoS ONE* 9:e110024. doi: 10.1371/journal.pone.0110024
- Wang, C. L. A., Wuc, Y., Gulbins, E., Grassméc, H., and Zhao, Z. (2019). Acid sphingomyelinase-ceramide system in bacterial infections. *Cell. Physiol. Biochem.* 52, 280–301. doi: 10.33594/0000000021
- Wardlaw, J., Sandercock, P., Dennis, M., and Starr, J. (2003). Is breakdown of the blood-brain barrier responsible for lacunar stroke, leukoaraiosis, and dementia? *Stroke* 34, 806–812. doi: 10.1161/01.STR.0000058480.77236.B3
- Wharton, S. B., Brayne, C., Sava, G. M., Matthews, F. E., Forster, G., Simpson, J., et al. (2011). Epidemiological neuropathology: the MRC cognitive function and aging study experience. *J. Alzheimers Dis.* 25, 359–372. doi: 10.3233/JAD-2011-091402
- Winkler, E. A., Bell, R. D., and Zlokovic, B. V. (2011). Central nervous system pericytes in health and disease. *Nat. Neurosci.* 14, 1398–1405. doi: 10.1038/nn.2946
- Winkler, E. A., Nishida, Y., Sagare, A. P., Rege, S. V., Bell, R. D., Perlmutter, D., et al. (2015). GLUT1 reductions exacerbate Alzheimer's disease vasculo-neuronal dysfunction and degeneration. *Nat. Neurosci.* 18, 521–530. doi: 10.1038/nn.3966
- Won, J.-S., Kim, J., Annamalai, B., Shunmugavel, A., Singh, I., and Singh, A. K. (2013). Protective role of S-nitrosoglutathione (GSNO) against cognitive impairment in rat model of chronic cerebral hypoperfusion. *J. Alzheimers Dis.* 34, 621–635. doi: 10.3233/JAD-121786
- Wu, F., Zou, Q., Ding, X., Shi, D., Zhu, X., Hu, W., et al. (2016). Complement component C3a plays a critical role in endothelial activation and leukocyte recruitment into the brain. *J. Neuroinflammation* 13, 1–14. doi: 10.1186/s12974-016-0485-y
- Xiao, M., Xiao, Z. J., Yang, B., Lan, Z., and Fang, F. (2020). Blood-brain barrier: more contributor to disruption of central nervous system homeostasis than victim in neurological disorders. *Front. Neurosci.* 14:764. doi: 10.3389/fnins.2020.00764
- Yamazaki, Y., Shinohara, M., Shinohara, M., Yamazaki, A., Murray, M. E., Liesinger, A. M., et al. (2019). Selective loss of cortical endothelial tight junction proteins during Alzheimer's disease progression. *Brain* 142, 1077–1092. doi: 10.1093/brain/awz011
- Yang, C., Huang, X., Huang, X., Mai, H., Li, J., Jiang, T., et al. (2016). Aquaporin-4 and Alzheimer's disease. *J. Alzheimers Dis.* 52, 391–402. doi: 10.3233/JAD-150949
- Yang, J., Lunde, L. K., Nuntagij, P., Oguchi, T., Camassa, L., Nilsson, L. N., et al. (2011). Loss of astrocyte polarization in the tg-ArcSwe mouse model of Alzheimer's disease. *J. Alzheimers Dis.* 27, 711–722. doi: 10.3233/JAD-2011-110725
- Yang, T., Guo, R., and Zhang, F. (2019). Brain perivascular macrophages: recent advances and implications in health and diseases. *CNS Neurosci. Therapeut.* 25, 1318–1328. doi: 10.1111/cns.13263
- Yang, W., Wu, Q., Yuan, C., Gao, J., Xiao, M., Gu, M., et al. (2012). Aquaporin-4 mediates astrocyte response to β -amyloid. *Mol. Cell. Neurosci.* 49, 406–414. doi: 10.1016/j.mcn.2012.02.002
- Yang, Y., Hill, J. W., and Rosenberg, G. A. (2011). Multiple roles of metalloproteinases in neurological disorders. *Prog. Mol. Biol. Transl. Sci.* 99, 241–263. doi: 10.1016/B978-0-12-385504-6.00006-3
- Yang, Y., Kimura-Ohba, S., Thompson, J. F., Salayandia, V. M., Cosse, M., Raz, L., et al. (2018). Vascular tight junction disruption and angiogenesis in spontaneously hypertensive rat with neuroinflammatory white matter injury. *Neurobiol. Dis.* 114, 95–110. doi: 10.1016/j.nbd.2018.02.012
- Yao, Y., Chen, Z.-L., Norris, E. H., and Strickland, S. (2014). Astrocytic laminin regulates pericyte differentiation and maintains blood brain barrier integrity. *Nat. Commun.* 5, 1–12. doi: 10.1038/ncomms4413
- Yepes, M., Woo, Y., and Martin-Jimenez, C. (2021). Plasminogen activators in neurovascular and neurodegenerative disorders. *Int. J. Mol. Sci.* 22:4380. doi: 10.3390/ijms22094380
- Yu, X., Ji, C., and Shao, A. (2020). Neurovascular unit dysfunction and neurodegenerative disorders. *Front. Neurosci.* 14:334. doi: 10.3389/fnins.2020.00334
- Zeevi, N., Pachter, J., McCullough, L. D., Wolfson, L., and Kuchel, G. A. (2010). The blood-brain barrier: geriatric relevance of a critical brain-body interface. *J. Am. Geriatr. Soc.* 58, 1749–1757. doi: 10.1111/j.1532-5415.2010.03011.x
- Zenaro, E., Piacentino, G., and Constantini, G. (2017). The blood-brain barrier in Alzheimer's disease. *Neurobiol. Dis.* 107, 41–56. doi: 10.1016/j.nbd.2016.07.007
- Zenaro, E., Pietronigro, E., Della Bianca, V., Piacentino, G., Marongiu, L., Budui, S., et al. (2015). Neutrophils promote Alzheimer's disease-like pathology and cognitive decline via LFA-1 integrin. *Nat. Med.* 21, 880–886. doi: 10.1038/nm.3913
- Zeppenfeld, D. M., Simon, M., Haswell, J. D., D'Abreo, D., Murchison, C., Quinn, J. F., et al. (2017). Association of perivascular localization of aquaporin-4 with cognition and Alzheimer disease in aging brains. *JAMA Neurol.* 74, 91–99. doi: 10.1001/jamaneurol.2016.4370
- Zhang, X., Wu, B., Nie, K., Jia, Y., and Yu, J. (2014). Effects of acupuncture on declined cerebral blood flow, impaired mitochondrial respiratory function and oxidative stress in multi-infarct dementia rats. *Neurochem. Int.* 65, 23–29. doi: 10.1016/j.neuint.2013.12.004
- Zhao, Z., Nelson, A. R., Betsholtz, C., and Zlokovic, B. V. (2015). Establishment and dysfunction of the blood-brain barrier. *Cell* 163, 1064–1078. doi: 10.1016/j.cell.2015.10.067
- Zhao, Z., Ong, L. K., Johnson, S., Nilsson, M., and Walker, F. R. (2017). Chronic stress induced disruption of the peri-infarct neurovascular unit following experimentally induced photothrombotic stroke. *J. Cereb. Blood Flow Metab.* 37, 3709–3724. doi: 10.1177/0271678X17696100
- Zhou, X., Spittau, B., and Kriegstein, K. (2012). TGF β signalling plays an important role in IL4-induced alternative activation of microglia. *J. Neuroinflammation* 9, 1–14. doi: 10.1186/1742-2094-9-210
- Zhu, H.-Y., Hong, F.-F., and Yang, S.-L. (2021). The roles of nitric oxide synthase/nitric oxide pathway in the pathology of vascular dementia and related therapeutic approaches. *Int. J. Mol. Sci.* 22:4540. doi: 10.3390/ijms22094540
- Zlokovic, B. V. (2005). Neurovascular mechanisms of Alzheimer's neurodegeneration. *Trends Neurosci.* 28, 202–208. doi: 10.1016/j.tins.2005.02.001
- Zlokovic, B. V. (2011). Neurovascular pathways to neurodegeneration in Alzheimer's disease and other disorders. *Nat. Rev. Neurosci.* 12, 723–738. doi: 10.1038/nrn3114

- Zonneveld, H. I., Goos, J. D., Wattjes, M. P., Prins, N. D., Scheltens, P., van der Flier, W. M., et al. (2014). Prevalence of cortical superficial siderosis in a memory clinic population. *Neurology* 82, 698–704. doi: 10.1212/WNL.0000000000000150
- Zotova, E., Holmes, C., Johnston, D., Neal, J. W., Nicoll, J. A., and Boche, D. (2011). Microglial alterations in human Alzheimer's disease following A β 42 immunization. *Neuropathol. Appl. Neurobiol.* 37, 513–524. doi: 10.1111/j.1365-2990.2010.01156.x

Conflict of Interest: The authors declare that the research was conducted in the absence of any commercial or financial relationships that could be construed as a potential conflict of interest.

Publisher's Note: All claims expressed in this article are solely those of the authors and do not necessarily represent those of their affiliated organizations, or those of the publisher, the editors and the reviewers. Any product that may be evaluated in this article, or claim that may be made by its manufacturer, is not guaranteed or endorsed by the publisher.

Copyright © 2021 Hussain, Fang and Chang. This is an open-access article distributed under the terms of the Creative Commons Attribution License (CC BY). The use, distribution or reproduction in other forums is permitted, provided the original author(s) and the copyright owner(s) are credited and that the original publication in this journal is cited, in accordance with accepted academic practice. No use, distribution or reproduction is permitted which does not comply with these terms.

Advantages of publishing in Frontiers



OPEN ACCESS

Articles are free to read
for greatest visibility
and readership



FAST PUBLICATION

Around 90 days
from submission
to decision



HIGH QUALITY PEER-REVIEW

Rigorous, collaborative,
and constructive
peer-review



TRANSPARENT PEER-REVIEW

Editors and reviewers
acknowledged by name
on published articles

Frontiers

Avenue du Tribunal-Fédéral 34
1005 Lausanne | Switzerland

Visit us: www.frontiersin.org

Contact us: frontiersin.org/about/contact



REPRODUCIBILITY OF RESEARCH

Support open data
and methods to enhance
research reproducibility



DIGITAL PUBLISHING

Articles designed
for optimal readership
across devices



FOLLOW US

@frontiersin



IMPACT METRICS

Advanced article metrics
track visibility across
digital media



EXTENSIVE PROMOTION

Marketing
and promotion
of impactful research



LOOP RESEARCH NETWORK

Our network
increases your
article's readership